

~~UNCLASSIFIED~~

AD 260 564

Best Available Copy

*Reproduced
by the*

ARMED SERVICES TECHNICAL INFORMATION AGENCY
ARLINGTON HALL STATION
ARLINGTON 12, VIRGINIA



20030707001

~~UNCLASSIFIED~~

NOTICE: When government or other drawings, specifications or other data are used for any purpose other than in connection with a definitely related government procurement operation, the U. S. Government thereby incurs no responsibility, nor any obligation whatsoever; and the fact that the Government may have formulated, furnished, or in any way supplied the said drawings, specifications, or other data is not to be regarded by implication or otherwise as in any manner licensing the holder or any other person or corporation, or conveying any rights or permission to manufacture, use or sell any patented invention that may in any way be related thereto.

1907000002

BULLETIN No. 28

**SHOCK, VIBRATION
AND
ASSOCIATED ENVIRONMENTS**

PART III

JULY 1961

CATALOGED BY ASTIA

AS AD NO. 260534

**OFFICE OF
THE SECRETARY OF DEFENSE**

Research and Engineering



Washington, D. C.

BULLETIN No. 29

**SHOCK, VIBRATION
AND
ASSOCIATED ENVIRONMENTS**

PART III

JULY 1961

**OFFICE OF
THE SECRETARY OF DEFENSE
Research and Engineering**

The 29th Symposium on Shock, Vibration and Associated Environments was held at the U.S. Naval Supply Center, Oakland, California on November 15-17, 1960. The Department of the Navy was host.

Washington, D. C.

**INTERSERVICE TECHNICAL GROUP FOR SHOCK,
VIBRATION, AND ASSOCIATED ENVIRONMENTS**

ARMY MEMBERS

Mr. A. O. Crobaugh
Director
Electro-Mechanical Laboratories
White Sands Missile Range
Las Cruces, New Mexico

Dr. Joseph S. diRende
Scientific Director
U.S. Army Transportation
Research Command
Fort Eustis, Virginia

Mr. Joseph Kaufman
Office of the Chief of Ordnance
U.S. Army
Pentagon Annex No. 2
Washington 25, D.C.

Mr. Frederick J. Lindner
Packaging Development Branch
U.S. Army Engineer Research and
Development Laboratories
Fort Belvoir, Virginia

Mr. Joseph J. Oliveri
Engineering Science Department
U.S. Army Signal Research and
Development Laboratories
Fort Monmouth, New Jersey

NAVY MEMBERS

Mr. J. M. Crowley
Code 439
Office of Naval Research
Washington 25, D.C.

Mr. E. R. Mullen
U.S. Naval Air Development Center
Johnsville, Pennsylvania

Mr. R. H. Oliver
Code 423
Bureau of Ships
Washington 25, D.C.

Mr. Harry Rich
David Taylor Model Basin
Washington 7, D.C.

Mr. Theodore Soo-Hoo
Office of the Chief of Naval Operations
Pentagon
Washington 25, D.C.

Mr.
Mr. George Stathopoulos
U.S. Naval Ordnance Laboratory
White Oak
Silver Spring, Maryland

AIR FORCE MEMBERS

Mr. E. A. Catenaro
rome Air Development Center
Attn: RCSSM
Griffiss Air Force Base, New York

Mr. C. Golueke
Wright Air Development Division
Attn: WFFEVD
Wright-Patterson Air Force Base
Ohio

Mr. D. C. Kennard
Wright Air Development Division
Attn: WFFE
Wright-Patterson Air Force Base
Ohio

Mr. H. A. McCall
Wright-Air Development Division
Attn: WWRMD
Wright-Patterson Air Force Base
Ohio

Dr. L. L. W. Wosko
Air Force Office of Scientific Research
Tempo D Building
Washington 25, D.C.

Dr. George A. Young
Air Force Special Weapons Center
Kirtland Air Force Base
New Mexico

DEFENSE ATOMIC SUPPORT AGENCY MEMBER

Mr. John Lewis
Defense Atomic Support Agency
Pentagon
Washington 25, D.C.

NATIONAL AERONAUTICS AND SPACE ADMINISTRATION MEMBER

Mr. John C. New
Code 320
National Aeronautics and Space
Administration
Goddard Space Flight Center
Greenbelt, Maryland

DISTRIBUTION

Aberdeen Proving Ground, Md.		Att: Mr. G. Sisson	1
Att: Ballistic Research Lab.	1	Att: Mr. W.R. Perret	1
Att: Development & Proof Services	1		
Att: Physical Test Lab.	1		
Aeronautical Standards Group, D.C.	1	Air Proving Ground Ctr., Eglin AFB	
Air Defens. Command, Ft. AFB		Att: Weapons & Missiles Br.	1
Att: Deputy for Civil Engineering	1	Att: 3208th Test Group (TF)	
Att: ADIRP	1	Lab. Div., Chief, Airborne	
Instr. Br.		Instr. Br.	1
Air Force Ballistic Missile Division, L.A.		Att: PGTRI, Tech. Library	1
Att: Technical Data Division	3		
Air Force Flight Test Ctr., Edwards AFB		Air Material Command, Wright-	
Att: FTOTL	1	Patterson AFB	
Att: FTRLG (A. C. Davies)	1	Att: Civil Engineer	1
Air Force Flight Test Ctr., El Centro		Air Research & Dev. Cd., Andrews AFB	
Att: Mr. E. C. Myers, Tech. Dir.,		Att: Aerodynamics Br.	1
6511th Test Group (Parachute)	1	Att: Directorate of Equipment	1
Att: RDTAEF		Att: RDTAEF	1
Att: Dir/AI			1
Air Force Headquarters, D.C.		Air Research & Dev. Cd., Wright-	
Att: AFCOA Library	2	Patterson AFB	
Att: AFCIN-3V	2	Att: WWD	?
Att: AFDRD-GW, Capt. A.R. Deptula	1	Air Training Command, Randolph AFB	
Att: AFROCE-ES	6	Att: DCS/CE	1
Air Force Missile Dev. Ctr., Holloman AFB		Alaskan Air Command, Seattle	
Att: MTHTP	2	Att: DCS/CE	1
Att: HDOIL	1	Armed Services Tech. Info. Ag.,	
Att: MDWTE, Lt. C.R. Kowal	1	Arlington	10
Air Force Missile Test Ctr., Patrick AFB		Army Air Defense Ctr., Ft. Bliss	
Att: Chief, Tech. Systems Lab.	2	Att: AKBAAC 337	1
Air Force Office of Scientific Research, D.C.		Army Ballistic Missile Agency, Ala.	
Att: Library	1	Att: ORL AB-HST	1
Att: Dr. H.W. Wolko, SRHM	1	Army Chemical Ctr., Md.	
Air Force Regional Civil Engineer		Att: Mr. H.L. Solomonson	1
Att: Mediterranean Region	1	Att: CMLEN-CE-S	1
Att: Missouri River Region	1	Army Engineer District, N.Y.	
Att: New England Region	1	Att: NANGD	1
Att: North Atlantic Region	1	Army Engineer District, Omaha	2
Att: North Pacific Region	1	Army Engineer Division, Missouri River	1
Att: Ohio River Region	1	Army Engineer R&D Labs., Ft. Belvoir	
Att: South Atlantic Region,		Att: Director of Research	1
AFRCE-A-E		Att: Package Development Br.	1
Att: South Pacific Region	1	Att: Mr. F.J. Lindner	1
Att: Southwest Region	1	Att: Dr. T.A. Walsh, Chief, Spec.	
Air Force Research Division,		Proj. Br.	4
ARDC, Mass.			
Att: Library	1	Army Engineer Waterways Exp. Sta.,	
Air Force Special Weapons Ctr.,		Vicksburg	
Kirtland AFB		Att: Mr. J.M. Strange	1
Att: Development Test Div.	1		
Att: Dr. G. Young, SWRS	1		
Att: Mr. H.R.J. Walsh	1		

Army Field Forces, Ft. Bragg	1	Boston Naval Shipyard Att: Code 259c	1
Army Field Forces, Ft. Monroe Att: ATDEV-9	1	Bureau of Medicine & Surgery, D.C. Att: Research Div.	1
Army, Off. Chief of Engineers Att: Asst. Chief for Military Operations, Engineer R&D Division	2	Bureau of Naval Weapons, D.C. Att: DLI-3	15
Att: ENGEB	1	Att: FWAA, C.H. Barr	1
Att: ENGMG-EB	1	Att: RREN-5	5
		Att: RRMA	1
Army, Off. Chief of Ordnance Att: ORDFA-T	1	Att: RAAE-2	1
Att: ORDFM	1	Att: RM-3	2
Att: ORDTB, M1. J. Kaufman	1	Att: RM-2	1
		Att: RSSH	2
		Att: FWAE	1
Army, Off. Chief of Res. & Dev. Att: Mr. A.L. Tarr	1	Bureau of Naval Weapons Rep., E. Hartford	2
Army, Off. Chief of Staff Att: Surface-to-Surface Missiles Div.	1	Bureau of Naval Weapons Rep., Pomona Att: Chief Engineer	1
Army Off. Chief of Transportation Att: Executive for R&D	1	Att: Metrology Dept., Code 60	1
Army Ordnance Missile Command, Ala. Att: Chief Engineer	1	Bureau of Naval Weapons Rep., Sunnyvale Att: Mr. C.M. Fitch	1
Army Security Agency, Md.	1	Bureau of Ships, D.C. Att: Code 423	20
Army Signal Equipment Support Ag., N.J. Att: SIGFM/ES-PFM-4	1	Bureau of Supplies & Accounts, D.C. Att: Code H43	1
Army Signal R&D Labs., N.J. Att: SIGRA/SL-ADTE Technical Document Center	1	Bureau of Yards & Docks, D.C. Att: Code D-440	1
Att: SIGRA/SL-PEE Electronic Components Research Dept.	1	Att: Code D-220	1
Att: SIGRA/SL-PRT Electronic Components Research Dept.	1	Att: Code D-220 (Unclassified Parts)	6
Att: SIGRA/SL-GDM Engineering Sciences Dept.	1	Civil Engineering Ctr., Wright-Patterson AFB Att: AFIT	2
Att: SIGRA/SL-GTF Engineering Sciences Dept.	1	Coast Guard Headquarters, D.C.	1
Att: Mr. J.J. Oliveri	1	David Taylor Model Basin, D.C. Att: Library	3
Army Transportation Research Ctr., Ft. Eustis Att: Library	1	Att: Mr. Harry Rich	1
Att: Dr. J. diRende, Sci. Director	1	Att: Contract Research Administrator, 513	1
Arnold Engineering Dev. Ctr., Tenn. Att: AEOIM	1	Att: Mr. R.E. Conaverse	1
Atomic Energy Commission, Oak Ridge	6	Att: Mr. E. Buchmann	1
Atomic Energy Commission, D.C. Att: Library	1	Att: Mr. J.A. Luistro, Code 501L	1
Att: Div. of Reactor Development, Tech. Evaluation Br. (Army Reactors)	1	Dayton Air Force Depot, Gentile AFB Att: MDMG	1
		Defense Atomic Support Agency, D.C. Att: Technical Director	1
		Att: Weapons Development Dir.	1
		Att: Mr. John G. Lewis	1
		Defense Atomic Support Agency, Livermore Att: Administrative Officer	1

Detroit Arsenal, Michigan	NASA, High Speed Flight Sta., Edwards AFB	1
Att: Technical Library		
Att: Engineering Standards Unit		
Dept. of Interior, Bureau of Mines, D.C.	NASA, Goddard Space Flight Ctr., Beltsville	1
Att: Dr. L. Obert, Applied Physics Res. Lab.	Att: Mr. J.C. New, Code 320 Att: Mr. Neal Ganick, Code 320	1 1
Diamond Ord. Fuze Lab., D.C.	NASA, Langley Research Ctr., Va.	1
Att: Mr. W.S. Hinman, Jr.	Att: Mr. E.I. Garrick	1
Att: Components Lab., 300	Att: Mr. G.W. Brooks	1
Att: Industrial Div. 700		
Att: Mr. R.G. Barclay, Br. 420	NASA, Lewis Flight Propulsion Lab., Cleveland	1
Att: Tech. Ref. Ctr., .012	Att: Library	1
Electronics Supply Office, Great Lakes	NASA, Marshall Space Flight Ctr., Huntsville	1
Federal Aviation Agency, D.C.	Att: Mr. R.M. Hunt, Structures & Mech. Div.	1
Att: Emergency Readiness Div., Off. of Plans & Requirements		
Frankford Arsenal, Phila.	NASA, Washington, D.C.	1
Att: Fire Control Lab.	Att: Library	1
Att: Physics Research Lab.		
Att: Electronic VT Fuze Dept.	National Bur. of Standards, Colorado	1
Att: Mr. A.L. Jamieson	Att: AEC Cryogenic Engr. Lab.	1
InsMat San Francisco	National Bur. of Standards, D.C.	1
Long Beach Naval Shipyard, Cal.	Att: Mr. E.L. Wilson	2
Att: Code 240	Att: Mr. W.A. Wildhack	1
Los Alamos Scientific Laboratory, N.M.	Att: Mr. S. Edelman, Mech. Div.	1
Att: Report Librarian		
Los Angeles Air Procurement District, Cal.	Naval Air Development Ctr., Johnsville	1
Att: Quality Control Division	Att: Mr. E.R. Mullin	1
Los Angeles Ordnance District, USA, Cal.	Att: Aviation Armament Lab.	1
Att: ORDEV	Att: Materials & Components Br.	1
Mare Island Naval Shipyard	Att: Aeronautical Instruments Lab.	1
Att: Electronics Officer		
Att: Industrial Laboratory	Naval Air Engrg. Facility, Phila.	1
Marine Corps Equipment Board, Quantico	Att: Library	1
Marine Corps Headquarters, D.C.	Naval Air Material Ctr., Phila.	1
Att: Research & Dev. Section	Att: Library	1
Att: Code AO4E	Naval Air Station, Alameda	1
Maxwell Air Force Base, Ala.	Att: Aeronautical Engrg. Group	1
Att: Air Command & Staff School		
Att: USAF Institute of Tech.	Naval Air Station, Patuxent River	3
Military Air Transport Service, Scott AFB	Att: Armament Test Div. (M. Regan)	1
Att: Chief, C.E.D.	Naval Air Test Center, Patuxent River	1
Mobile Air Materiel Area, Brookley AFB	Att: Electronics Test Div.	1
Att: MONPRR		
Att: MONE	Naval Ammunition Depot, Earle	1
NASA, Ames Research Ctr., Moffett Field	Att: Mr. J.E. Kally, Chief Engr., Materials Handling Lab.	1
Att: Dr. S.J. DeFrance, Dir.	Naval Ammunition Dep., Crdn	1
	Att: Weapons Tech. Library	1
	Naval Attache, Navy 100	1
	Att: Logistics Division	1
	Naval Civil Engineering Lab., Pt. Hueneme	1
	Att: Library	1

Naval Construction Battalion Ctr., Pt. Hueneme	Naval Research Laboratory, D.C.
Att: OIC, USN School, Civil Engineer Corps Officers	Att: Code 6250 1 Att: Code 6260 1 Att: Code 6201 1 Att: Code 4021 2
Naval Engrg. Experiment Sta. Annapolis	Naval Supply R&D Facility, Bayonne
Att: Code 705	Att: Library 1
Naval Medical Field Res. Lab., Camp Lejeune	Naval Torpedo Station, Keyport
Att: QEL. Technical Library	Att: QEL. Technical Library 1
Naval Medical Research Inst., Bethesda	Naval Training Device Ctr., N.Y.
Att: Dr. David Goldman	Att: Library Branch 1
Naval Mine Engrg. Facility, Yorktown	Naval Underwater Ord. Sta., Newport
Naval Missile Ctr., Pt. Mugu	Att: Tech. Documents Library 1
Att: Library	Naval Weapons Laboratory, Dahlgren
Att: Launcher & Environment Div.	Att: Technical Library 1
Naval Nuclear Ord. Eval. Unit, Albuquerque	Naval Weapons Plant, D.C.
Att: Op 31	Att: Aviation Ordnance Unit 6
Att: Op 34	Att: Design Dept. Code DE-740 4
Att: Op 75	Att: Engng. Dept. Code 733.2 1
Att: Op07-G	Att: Missile Sys. Sys. Engrg. Div., Code 760 2
Att: Op07T6, Mr. T. Soo-Hoo	Navy Central Torpedo Office, Newport
Att: Quality Eval. Lab.	Att: Quality Evaluation Lab. 1
Att: Code 56, Sys. Eval. Div.	Navy Electronics Lab., San Diego
Naval Ordnance Lab., Corona	Att: Library 1
Att: Shock Branch	Navy Mine Defense Lab., Panama City
Att: Vibration Branch	Att: Library 1
Att: Environmental Evaluation Div.	Navy ROTC & Admin. Unit, MIT
Att: Mr. G. Stathopoulos	Navy Underwater Sound Lab., New London
Naval Ordnance Test Sta., China Lake	Att: Dr. J.M. Ide 1
Att: Code 55514	Att: Mr. J.G. Powell 1
Att: Technical Library	Navy Underwater Sound Ref. Lab., Orlando
Att: Mr. J.M. Taylor	Att: Mr. J.M. Taylor 1
Naval Ordnance Test Sta., Pasadena	New York Naval Shipyard
Att: P8087	Att: OinC, Naval Material, Lab., Code 912b 3
Att: P8092	Norfolk Naval Shipyard, Va.
Att: P8073	Att: Design Superintendent 1
Att: P80962	Att: Underwater Explosions Res. Div., Code 281A(2) 1
Naval Postgraduate School, Monterey	Att: Mr. J.K. Fleming 1
Att: Library	Norton AFB, Calif.
Naval Propellant Plant, Indian Head	Att: 3002d IC, D/RML, Suppy Services and Transportation 1
Att: Mr. K.M. Carr, Code R5R	Off. Civil & Defense Mobilization, Battle Creek 11
Naval Radiobiological Def. Lab., San Fran.	Off. Naval Material, D.C. 1
Att: Library	
Att: Mr. R. Cole	
Naval Repair Facility, San Diego	
Att: Tech. Library, Bldg. 38	

Off. Naval Research, D.C. Att: Code 439 Att: Code 104	6 1	Randolph AFB, Texas Att: USAF School of Aviation Medicine	1
Off. Naval Research Branch Off., Boston	1	Redstone Arsenal, Ala. Att: Technical Library	4
Off. Naval Research Branch Off., Pasadena	1	Att: Mission Planning & Coor. Off.	1
Off. Naval Research Branch Off., San Francisco	1	Att: Guided Missile Dev. Div.	1
Off. Secretary of Defense, Dir. of Defense R&E Att: Technical Library Att: Mr. G.B. Wareham	3 1	Att: Mech. Branch, T&E Div.	1
Off. Secretary of Defense, Dir. of Defense R&E, Advisory Group on Electron Tubes, N.Y. Att: Secretary	1	Att: Rocket Development Div.	1
Oklahoma City Air Materiel Area, Tinker AFB Att: Engineering Div.	1	Att: James M. Taylor, RDL-Bldg. 855	1
Ordnance Ammunition Ctr., USA, Joliet Att: ORDLY-M-P, H.S. Stein Att: NNOC/A	1	Att: ORDDW-GMTP	1
Pacific Air Force Att: ACS/CE	1	Att: ORDDW-IDES-J	1
Portland Harbor Naval Shipyard Att: Code 264	1	Rome Air Development Center, N.Y. Att: Mr. E.A. Catena, RCSSM	3
Philadelphia Naval Shipyard Att: Ship Design Section	1	Rossford Ordnance Depot, Ohio Att: Ordnance Packaging Cff.	1
Picatinny Arsenal, Dover Att: Library Att: Packaging Sec., Tech. Div.	1	San Francisco Naval Shipyard Att: Code 251 Att: Code 254-T	1 1
Portsmouth Naval Shipyard Att: Code 251b Mr. E.C. Taylor	1 1	Savanna Ordnance Depot, Illinois Att: Ammunition Instructor's School	1
Puget Sound Naval Shipyard Att: Design Supt., Code 251 Att: Material Labs. Att: K.G. Johnson, Design Div., Planning Dept.	1 1 1	Signal Corps Supply Agency, Phila.	1
Quartermaster Food & Container Inst., Chicago Att: Dir., Container Lab. Att: Technical Library	1 1	Signal Officer, Off. of Chief, Arlington Att: Engineering Control Div.	1
Quartermaster General, Off. of, D.C. Att: Military Planning Div.	1	Signal Officer, Off. of Chief, D.C. Att: R&D Division	1
Quartermaster Res. & Dev. Ctr., Natick Att: Technical Library	2	Special Projects, USN, D.C. Att: SP Tech. Library	1
Radford Arsenal, Va. Att: ORDCB, W.B. Helbert	1	Springfield Armory, Mass. Att: Library	2
		Strategic Air Command, Offutt AFB Att: Operations Analysis Off. Att: Director of Civil Engineering	1 1
		Tactical Air Command, Langley AFB Att: Director of Installations	1
		U.S. Air Forces in Europe Att: DCS/I	1
		Watertown Arsenal, Mass. Att: Dr. R. Beeuwkes, Jr., Ord. Mats. Res. Off. Att: Technical Information Sec.	2 1
		Watervliet Arsenal, N.Y. Att: ORDBF-RR	1
		White Sands Missile Range, N.M. Att: Electro Mechanical Div. Att: ORDIES-TS-TJL Att: Mr. A.J. Crobaugh	1 3 1

Wright Air Development Division,
Ohio

Att: WWRC
Att: WWRMC (H.E. VonGierke)
Att: WWRMD
Att: WWRMV

Att: Wv. RMF
Att: WWDM
Att: WWMFE
Att: WWRMD (H.A. Magrath)
Att: WWFEV (D.C. Kennard)
Att: WWFEVD (C. Golueke)

1

1

FOREWORD

In this section of the Bulletin are unclassified papers on free-field phenomena, interaction of soils with structures, structural design, and effects on equipment in hardsites. A table of contents of all four Parts of the Bulletin and an attendance list for the 29th Symposium may be found in Part I.

The attention of all holders of past Bulletins is directed to the notice on the following page concerning declassification action on some of the early issues. Further information on later Bulletins will be promulgated in due course.

H.D. Match.

July 3, 1961

**NOTICE OF REGRADING OR
CLASSIFICATION CHANGE ACTION**

1. The following classification actions have been taken on
Shock and Vibration Bulletins:

<u>S & V BUL. NO.</u>	<u>ACTION</u>
4	DECLASSIFIED
5	DECLASSIFIED
6	DECLASSIFIED
7	DECLASSIFIED
9	DECLASSIFIED
10	DECLASSIFIED
11	DECLASSIFIED

2. All holders are requested to reclassify copies in their
possession. This publication may be cited as the authority
for the action.

CONTENTS

PART III

Distribution	iii
Foreword	ix

Section 1 Free-Field Phenomena

Cratering from a Megaton Surface Burst	1
H. L. Brode and R. L. Bjork, The Rand Corporation, Santa Monica, California	
Analytical and Experimental Studies on Locking Media	30
Paul Weidlinger, Weidlinger Consultants, New York, New York	
An Experiment on Soils Loaded Dynamically by a Shock Tube	40
H. R. J. Walsh, Air Force Special Weapons Center, Kirtland Air Force Base, New Mexico	
Motions Produced by an Explosion Above a Nonhomogeneous Elastic Medium	57
C. M. Ablow, R. C. Alverson, F. Gair, and F. M. Sauer, Stanford Research Institute, Menlo Park, California	
A Device for Determining Dynamic Stress-Strain Relationships of Soils	65
K. Kaplan, J. V. Zaccor, and A. B. Willoughby, Broadview Research Corporation, Burlingame, California	
Impact Wave Propagation in Columns of Sand	75
B. R. Parkin, The Rand Corporation, Santa Monica, California	
Equations of State Studies for Soil	76
M. A. Chasseyka, Armour Research Foundation, Chicago, Illinois	
Comments of the Chairman	89
H. L. Brode, The Rand Corporation	

Section 2 Interaction of Soils with Structures

Introductory Remarks by the Chairman	91
G. A. Young, Air Force Special Weapons Center, Kirtland Air Force Base, New Mexico	
Present Role of Soil Dynamics in the Design of Underground Protective Structures	93
G. N. Sirson, Air Force Special Weapons Center, Kirtland Air Force Base, New Mexico	
A Concept for Soil-Structure Interaction Due to Ground Shock Waves	100
A. H. Wiedermann, Armour Research Foundation, Chicago, Illinois	
The Effects of Nuclear Explosions on Deep Underground Cylindrical Tunnels in Elastic Media	1
M. L. Baron, Weidlinger Consultants, New York, New York	
A Simplified Theory of the Interaction of Shell Structures with Soil	126
T. G. Morrison, American Machine and Foundry Company, Niles, Illinois	
Dynamic Strength of Rocks	136
D. R. Grine, Stanford Research Institute, Menlo Park, California	

Soil Displacement Induced by Air Blast	145
W. R. Perret, Sandia Corporation, Albuquerque, New Mexico	

Section 3 Structural Design

The Earthquake Ground Shock Problem and its Relation to the Explosive-Generated Ground Shock Problem	157
C. W. Housner, California Institute of Technology, Pasadena, California	
Model Experiments Pertaining to the Design of Underg. and Openings Subjected to Intense Ground Shocks	169
J. S. Rinehart, Colorado School of Mines	
Design of Below Ground Arch and Dome Type Structures Exposed to Nuclear Blast	188
E. B. Laing and E. Cohen, Ammann and Whitney, New York, New York	
Antennas for Hard Radio Communications Systems - A Preliminary Study	224
S. P. Morgan and E. E. Zajac, Bell Telephone Laboratories, Inc., Murray Hill, New Jersey	
Review of Blast Closure Systems	233
M. Hassman and E. Cohen, Ammann and Whitney, New York, New York	
Foundations for Protective Structures	275
K. E. McKee, Armour Research Foundation, Chicago, Illinois	
Protective Construction by Proven Components	289
Capt. R. H. Sievers, Jr., USAERDL	
Consideration of Costs and Capabilities of Protective Structures	299
R. B. Valie, Jr., Stanford Research Institute, Menlo Park, California	

Section 4 Effects on Equipment in Hardsites

Nuclear Ground Shocks Environment	305
R. V. Dowdy, Daniel, Mann, Johnson, and Mendenhall and Associates, Los Angeles, California	
Nuclear Weapon Blast and Ground Shock Effects on Dynamic Response of Interior Components and Equipment in Underground Structures	324
S. Weissman, E. Cohen, and N. Dobbs, Ammann and Whitney, New York, New York	
A Free-Field Stress Gage and Test Results in a New 1000-psi Dynamic Pressure Tank	338
T. Winston and J. R. Stagner, United Electrodynamics, Inc., Pasadena, California	
Test Planning for Shock Tests of a Hardened Weapon System	348
H. M. Salisbury, Convair, Astronautics, San Diego, California	
Ground Shock Loads Imposed on the Silo Stored ICBM	353
A. F. Winemiller, The Martin Company, Denver, Colorado	

K O D A K E S E

Section 1 FREE-FIELD PHENOMENA

CRATERING FROM A MEGATON SURFACE BURST

H. L. Brode and R. L. Bjork
The RAND Corporation
Santa Monica, California

Assuming a hydrodynamic model, the authors have calculated the stresses and early motions associated with the cratering of a rock medium (tufa) from a 2-megaton (2-MT) surface burst. The results demonstrate the basically two-dimensional geometry of such an explosion and offer preliminary values of the pressures and motions involved. The excavating action is found to be associated with the direct shock from the bomb and not due to the loading, developed by the air overpressures in the early fireball. A limited description of the method, inputs, and equation of state of rock is included. Graphic results, together with some discussion of the salient features and the various physical assumptions and limitations associated with the calculations, make up the body of this report.

INTRODUCTION

The cratering action of large-yield explosions is an important part of both peaceful and war-like applications of nuclear weapons effects. It is a dominant feature in any earth-moving application, such as in the proposed harbor and canal digging (Plowshare) operations. In protective construction for the military, the crater boundaries define a sensible if perhaps extreme limit inside which survival cannot be expected. For an increasing number of applications more exact knowledge of expected craters and the associated ground shocks has become a vital factor.

An improved understanding of cratering must come from theoretical work coupled with field work using scaled or small-yield explosions. Ideally, theory and experiment should be combined at the yields of interest, but for several overriding reasons, no large yield surface (or shallow-buried) bursts have been

shot or are contemplated in a site of dry soil or rock, and it is necessary to rely on extrapolation from small nuclear shots and from chemical explosive work for the experimental aspects. Without benefit of adequate theoretical work, the extension of small-yield field data to large-yield situations is at best approximate and at worst may be quite wrong. A clear physical basis for predictions and scaling is particularly desirable at this time, and it is toward that goal that the calculations covered in this report were aimed.

In constructing a reasonable theoretical model of the cratering action, several factors stand out as being immediately necessary: Because the early phases of either chemical or nuclear explosions involve pressures far in excess of the shear or tensile stresses characteristic of any natural materials, and because the resulting strong shocks induce appreciable compression and heating in the surrounding matter, a hydrodynamic model is

not only reasonable but is a necessity at early stages. Furthermore, because the geometry of the burst relative to the interface separating ground and air figures dominantly in the formation of any crater, the hydrodynamics must be carried out in two space dimensions (i.e., must include vertical and radial motions). A program for numerical computation of hydrodynamic motions in two dimensions has existed at RAND for some time, and is particularly appropriate for use on the nuclear cratering problems. The scheme was originally generated by Bjork [1] in an investigation of high-speed impact craters in metals. The programming was due to N. J. Brode.

Although the hydrodynamic assumption is basic to the model, two further features are of importance, if less obviously so. In order to properly follow the cratering action of a surface burst nuclear explosion, it is necessary to know with considerable precision the early history of a nuclear bomb explosion. The exact amount of energy (and its form) that enters the ground and also how much energy goes in or out across the surface of the ground at later times will depend critically on the bomb energetics and the early fireball and air-blast history. Recent detailed calculations by Brode [2] have made easy the definition of initial and boundary conditions to approximate the influence of the complex dynamic loading induced by a surface-burst nuclear weapon.

One further factor of prime importance involves the equation of state-of-the-earth material. A cratering problem is sensitive to the relation between energies and sound speeds in the two media on either side of the interface. In the air above, the ambient sound speed is about 330 meters per second (330 m per sec), while seismic velocities in natural earth materials vary from typical soil seismic speeds around 600 m per sec to a speed in granite near 3700 m per sec. Air is quite compressible and very heat absorbent at the high pressures in a nuclear explosion while solid materials are much less compressible and tend to be much less dissipative at comparable stress levels. The extent to which these inequalities matter in such a cratering calculation can easily be appreciated.

As the stress level in the soil or rock sinks below a level where hydrodynamics can properly be considered the dominant force in producing motions and transporting energy, the calculation should embrace such physical features as plasticity and elasticity and should then deal with real solid-state features of the

material. Although something of this sort has been done in the simpler case of spherically symmetric explosions by Nuckolls [3], it was not attempted in any comparable sense here in connection with the two-dimensional cratering calculations. Furthermore, since the forces far exceed the force of gravity in the pressure regime where the model is considered valid, gravitational forces were not carried in this program.

NUMERICAL METHOD

The motion of the ground itself is assumed to be governed by the compressible, hydrodynamic equations. Written in terms of Eulerian variables, these are

$$\rho \frac{\partial \bar{u}}{\partial t} + \rho \bar{u} \cdot \text{grad } \bar{u} + \text{grad } P = 0 \quad (1)$$

$$\frac{\partial \rho}{\partial t} + \bar{u} \cdot \text{grad } \rho + \beta \text{div } \bar{u} = 0 \quad (2)$$

$$\rho \frac{\partial e}{\partial t} + \rho \bar{u} \cdot \text{grad } e + P \text{div } \bar{u} = 0 \quad (3)$$

$$P = P(\rho, e) \quad (4)$$

where the variables are

\bar{u} particle velocity

P pressure

e specific internal energy

ρ density

t time.

The effects of viscosity and heat conduction are neglected in these equations. It is possible to show by order-of-magnitude arguments that neglecting heat conduction is a good approximation. However, not enough is known of the viscous properties of materials under high pressures and densities to make such a positive statement relative to neglecting viscosity. Viscosity is really omitted from the framework of these calculations for the practical reason that no good estimates of it are available.

The nature of the problem renders the solution of these equations particularly difficult. Portions of the ground suffer large distortions, so that a Lagrangian description fails after a short time. The Eulerian formulation suffers from the continual inclusion across interfaces.

The numerical technique employed was one previously developed by Bjork [1] to treat

problems of high-velocity impact, where similar difficulties occur. Briefly, the method treats mass points moving through an Eulerian mesh. Integration is carried out on time, starting from the initial conditions (described later) and imposing the appropriate boundary conditions. The advance over Δt is carried out in two steps. In the first step, the transport terms in Eqs. (1) through (4) are neglected, and the integration is performed by solving the difference analog of the resulting differential equations. In the second step, the transport terms are accounted for by noting which masses change cells in the first step.

To get the new mass of the cells affected, one merely sums the masses now present in each cell, which accounts for the mass transport term in Eq. (2). A mass which changes cells is assumed to carry with it an increment of internal energy given by the product of the mass in question and the specific internal energy of the cell which it left. This accounts for the internal energy transport term in Eq. (3).

A mass, in changing cells, also brings with it an increment of momentum given by the product of the mass and the velocity present in the cell which it left. This momentum is added to the cell entered by the mass, and that cell is given a new velocity equal to the new momentum divided by the new total mass. Thus the momentum transport term of Eq. (4) is taken into account.

The process described conserves mass, internal energy, and momentum. It is easily shown, however, that kinetic energy is always lost in this repartitioning, unless the velocities of the two cells involved are equal. This is accounted for by arbitrarily adding the loss in kinetic energy of the two cells to the internal energy of the entered cell. Thus, total energy is conserved, but a small fraction of the kinetic energy is converted to internal energy in the process. This conversion may be shown to be equivalent to an artificial viscosity of the Landshoff type [4], and its presence precludes the necessity of adding any further artificial viscosity to the problem.

In both of the previously treated impact problems and the present ground motion calculations, the magnitude of the viscosity is ideal in the sense that it spreads the shock jumps over about three mesh spaces.

The method was tested in two ways. The first was to compare the solution generated for one-dimensional impacts with analytical

solutions which are available in this case. This test showed that the method gave correctly the jumps in pressure, density, and velocity across a shock, and also the velocities of the shocks themselves. This means that the jump in entropy across the shock is given correctly, placing the final state on the Hugoniot rather than the adiabat connecting the initial and final states. The second test was to calculate with the two-dimensional code a spherically symmetric nuclear air burst previously calculated by Brode [5] with a one-dimensional code. The agreement was checked in the vertical direction, the horizontal direction, and at an angle of 45 degrees between the two, and found to be satisfactory in all cases.

The calculations were performed by an IBM 704, possessing a 32,000-word fast memory. The memory size was the limiting factor in the resolution. To obtain an adequate mass resolution, 20 mass points per cell were used. This meant that on the average, a cell's density could change in 5-percent increments. This choice of the number of mass points restricted the number of space grid points to 400, which were arranged in a 20 by 20 rectangular array. Using fewer mass points per cell would have resulted in a larger number of space grid points, but it was not deemed feasible to coarsen further the mass resolution.

By an artifice known as "grid changing," the 400 grid points were always arranged to encompass only the region of activity and its immediate environs. In a "grid change," the points were laid down in such a manner as to encompass the shock front plus about an equal extent of undisturbed media. Within the shock, the dependent variables were given the values existing at the end of the previous grid, and outside they were assigned values appropriate to the undisturbed media. The new grid was then used until the program detected the first faint movement on the grid's boundary caused by the approaching shock, at which time a new grid change was effected.

In the present calculation, it is possible to gain only a very rough idea of the crater dimensions, as the forming crater is covered only by very few space grid points. The reason for this is that the ground shock is several times as deep as the crater bottom and the grid spacing is uniform in the vertical direction. In this sense the present calculation emphasizes the information relative to the deep ground motion. It will be possible to emphasize the cratering information by using

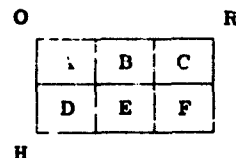
a gradation of grid sizes in the vertical direction, so that there will be many points near the surface and only a few deep underground.

INITIAL AND BOUNDARY CONDITIONS

The problem to which we address ourselves is that of calculating the crater and ground motion due to a two megaton surface burst. The nature of the problem is contained in the specification of the boundary conditions.

se initial and boundary conditions were based on results of calculations by Brode [2] on the early phases of a nuclear explosion. From these calculations at 1 msec after initiation, one finds that approximately half the bomb energy has radiated out of the bomb into the surrounding air, and most of the energy remaining in the bomb is in directed kinetic energy of the bomb materials. At this time it is reasonable to characterize the explosive input to the ground as due to both the impact of the bomb mass on the ground directly below it and to the pressure on the surface from the initially extended and rapidly growing fireball or strong shock in air. The pressures generated by this air blast are initially several orders of magnitude less than the pressures created directly by the bomb vapors, since the energies in the air and in the bomb are comparable, but the volume of air is many times larger than that occupied by the bomb itself.

These initial conditions lead to a specification of velocities of the order of 1700 meters per millisecond (1700 m per msec) in the first few zones of the rock, representing the mass and kinetic energy of the lower half of the bomb. In these zones an appropriate internal energy was included. These conditions, together with the initial choice of grid spacings lead to the following initial configuration:



In the grid, each initial zone was $1/4$ meter ($.25$ m) both across and deep, representing rings of mass in the cylindrical coordinates used. Each of the six "bomb" zones had a specific internal energy (and a pressure associated with it) corresponding to 8.05×10^5 in the meter-millisecond-megagram system of units used here (i.e., in 10^{16} ergs per 10^6 gms). Each of these zones also had an initial velocity of 1670 meters per millisecond (1670 m per msec), directed radially, so that the initial velocity components were as in Table 1.

Energies, pressures, and velocities were all initially zero outside of the six bomb zones. These bomb zones represented only the lower half of the bomb in a "true" surface burst position (i.e., with the center of gravity located on the plane of the surface between rock and air). The upper half of the bomb had been carried in the calculations in an early version, but proved to have an entirely negligible effect on the subsurface behavior. Since it added to the complexity of the problem to follow the upper masses as they flew off at high velocity, they were omitted from subsequent computations.

The surface pressures due to the air blast were included in the form of a boundary condition on the uppermost masses. An analytical form representing the air pressures as a function of time and radius was developed from the detailed calculations of an air-burst megaton explosion [2]. The fit is approximately

TABLE 1
Initial Velocity Components

Zone	Vertical Velocity		Horizontal Velocity		E	ρ_0
	V	U				
A	1181	1181			8.05×10^5	1.7
B	528	1584			"	"
C	327	1638			"	"
D	1584	528			"	"
E	1181	1181			"	"
F	859	1432			"	"

correct from earliest times until around 1/2 sec, after which it increasingly overestimates the pressures. At 1/2 sec, the peak overpressure in the air shock should be about 145 psi (at a shock radius of more than 1 kilometer (1 km)) while the fit gives about 180 psi. A comparison between the detailed calculation overpressures and the fit used is presented in Fig. 1. The impulse from this overpressure in its positive phase is generally too high.

factor of 1.5 over the applicable range of distances. Since nearly all of the observed ground motions were directly attributable to the direct impulse from the bomb vapors and not at all from the air blast impulse, the use of an air overpressure formula which over-emphasizes the air impulse is conservative in the present calculations, and emphasizes that no appreciable change would have resulted had the air overpressure been completely ignored.

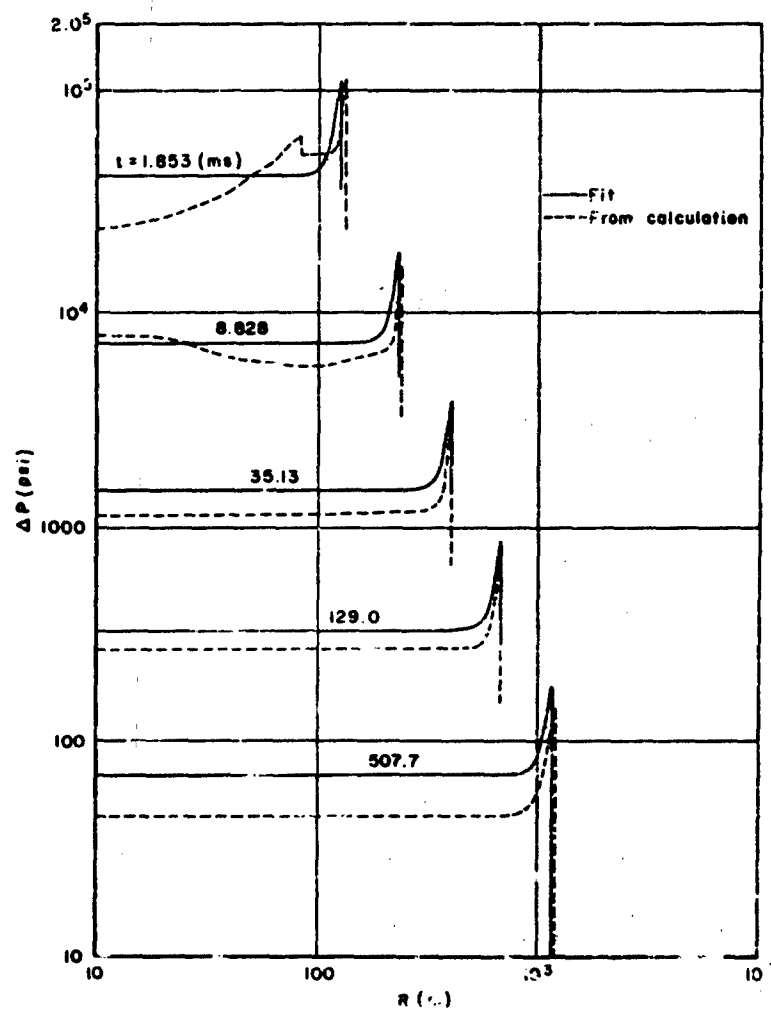


Fig. 1 - Comparison of air overpressure from approximate analytical form (—) with detail numerical results (----)

The formula employed for the air over-pressure boundary condition is the following:

$$\Delta P = \frac{.62}{1 + t^{1.15}} \left[1 + 1.6 \left(\frac{t_s}{t} \right)^6 \right] 10^{10} \text{ dyne per cm}^2$$

where t_s is the time of shock arrival, t is the time (both in milliseconds) and $t \geq t_s$.

$$t_s = 7 \times 10^{-5} + 7.24 \times 10^{-20} R_s^{10} \quad \text{for } R_s \leq 56$$

$$= \frac{7.24 \times 10^{-20} R_s^2}{1 + .637 \times 10^{-14} R_s^{7.5}} \quad \text{for } 56 < R_s < 200$$

$$= \left(\frac{R_s}{95} \right)^{2.5} \quad \text{for } R_s \geq 200 \text{ m}$$

in which R_s is the shock radius in meters. At times before shock arrival the overpressure is zero.

For a low air burst, in which the bomb materials do not get close enough to the ground to shock it strongly the main mechanism for inducing ground motion would be just the air blast. The form just presented could also represent the approximate pressure history on the surface from a burst at about 100 m above the surface. At that burst height, the direct bomb shock would be negligible, but the air shock would be quite similar to that from a true surface burst for horizontal ranges greater than about 100 m.

Since the compressions in the ground from such a low air burst would be quite small, the particular numerical scheme used here is not appropriate. It may be more reasonable to carry out such a calculation using a Lagrangian scheme, more adapted to propagations with small density changes. It is fairly clear that the nature of the air-slap loading is such that no conventional crater will occur from it alone in rock or in most soils. Its load is applied so rapidly over such a wide area and is relieved so rapidly that the main response is a tendency to compact, and very little excavating motion would be generated. On the other hand, the induced ground shock will not be entirely in the vertical direction, and will be quite divergent (i.e., will not be a plane wave). These trends as stated here were substantiated by two calculations which used only the air-slap input. Unfortunately these same calculations used unreal equations of state,

and so are not useful beyond their indications of a general geometric nature.*

EQUATION OF STATE

The influence of the equation of state on the results of such calculations has been only partially explored. A preliminary problem using an ideal gas of specific heat ratio three ($\gamma = 3$) was run; but at the lower pressures, it suffered most from the fact that the computation treated all shocks as strong shocks. In the region where the ground shock is properly strong, the comparison with a more nearly correct equation of state shows an expected greater effective explosive energy for the ideal gas case. Since, for real gases, much more energy is involved in the ionization and dissociation of the hot gas behind the shock front, the shock in a real gas very quickly drops to a lower strength than the corresponding shock in an ideal gas of high specific heat ratio.

The best equation of state used so far represents a soft volcanic rock called tuff (the rock in which some underground nuclear explosions at the Nevada test site were shot). This equation of state was represented by an analytical formula fitting three general regions of information. At the high-temperature end, the fit was to data from a Fermi-Thomas-D'Rac calculation for an appropriate mixture of elements representing the chemical constituents of tuff. We are indebted to Bill McMillan of RAND for this data and to Forrest Gilmore and Arthur Smith of RAND for some thermodynamic interpretation. In the region between 80 and 300 kilobars (kbar), the Hugoniot data from high explosive experiments on tuff were used as guidance for the fitting. These data, a part of experimental work carried out by a group at the Livermore Laboratory of the AEC, were called to our attention by Arthur Smith.

In carrying the fit to lower pressures, the observed speed of sound in tuff was used as a

* The first was an ideal gas, strong shock case, and the second used an unusually "soft" fluid. The second problem was not restricted to the strong shock limitation and did have a reasonable seismic speed (~ 2000 ft per sec), but was too compressible to be realistic. (A pressure of 20 kbar would cause a compression to twice the original density.) A more appropriate problem will be carried out soon.

limiting condition. The fit, while only approximately satisfying all of these restrictions is considered compatible with the accuracy limits imposed by other physical approximations involved in the calculations.

Expressed in terms of the specific internal energy (Σ) and the density relative to the standard density for tuff ($\eta = \rho/\rho_0$), the pressure, according to the resulting fit, was defined as

$$P = .425 \cdot F + .113 \cdot \eta^{3/2} \cdot \Sigma + 5 \cdot 10^{-7} \cdot \Sigma^{1/2}$$

$$+ .707 \cdot \Sigma^2 / (10^3 + \Sigma) \quad (10^{10} \text{ dyne/cm}^2)$$

Σ in 10^{10} erg/gm. $\eta = \rho/\rho_0$. $\rho_0 = 1.7$ gm/cc.

Of course, the solid-state properties of the rock which become important at stress levels below about 10 kbar are not realistically covered by the concepts of thermodynamic equilibrium implicit in the equation of state, but further, this equation includes no special consideration for phase changes—melting and vaporizing. It appears unlikely that the inclusion of phase changes would cause the equation-of-state behavior to be radically different from that assumed, however. In the first place, both the melting and vaporization points occur in about the same temperature range, and neither would occur at a precise temperature but would be spread over a factor of two or so in temperature. It is questionable that a melting point would even exist under explosive loading. The shock pressure at the melting temperature should be somewhat less than 100 kbar, and the above fit covers this region by bridging smoothly the gap between Thomas-Fermi-Dirac results and high-explosive experimental results.

Tuff is a rock which contains an unusually high amount of voids. It is not likely that the collapse of the voids creates a permanent change in the tuff density at the high pressures because at the highest temperatures the material is violently excavated and at more modest temperatures (near melting) the voids seem to reconstitute themselves. At the lowest stress levels (below 10 kbar), where this hydrodynamic model is already inapplicable, permanent void collapsing is likely. No such hysteresis was included in the treatment here. The equation of state for tuff used in these calculations is shown in Fig. 2.

THE RESULTS

Although the boundary and initial conditions specified accurately both the bomb-vapor

residual energies and the impulse from the air-blast slap, it is a striking feature of the result that only the former plays an important role in the excavation process. The air slap does indeed send a shock into the ground, but over a wide area and at pressures several orders of magnitude less than those at the same time in the direct bomb shock. Out along the surface beyond the region of the crater, of course, the air-blast slap exceeds the direct shock (which arrives later), but for the cratering action, and for shocks immediately below the crater, one could validly omit the air slap.

In Fig. 3, the early pressure field is displayed as a map of isobars (at 0.1026 msec). The bomb shock has created a nearly hemispheric shock front with peak pressures of around 7000 kbar in the 90-degree solid angle downward about the vertical axis (darkened area). The lack of a sharp front to the shock at this stage is due to the nature of the computation scheme which spreads shock discontinuities over about three zones of the chosen space grid. Such spreading does not seriously affect the Hugoniot or shock values of the various hydrodynamic variables. At this time, about 1/10 msec., the direct shock has progressed only some 7 m while the air shock aided by radiation diffusion has gone out more than 50 m. The 7-megabar, ground-shock pressures are to be compared with the peak overpressure in the air shock at this time of some 30 kbar. The shaded box at the origin represents the volume of rock in which the initial kinetic and internal energy was put, to approximate the bomb. It is already clear at this time that the ground shock is no longer dependent on the geometrical details of the source.

Figure 4 displays the velocity vectors of various rock masses at this same early time. Here, the symmetrical nature of the strong shock generated by the bomb energy becomes even more evident. All the compressed region of the shock front is rapidly expanding spherically. The topmost rock is being blown off into the air (in this case into the fireball above) at extreme velocities. This upward flying rock is of course not a true vapor and is already at fairly low density. The same is true of that material below the surface and well behind the shock front, although the motions are more nearly random below a couple of meters depth.

At 10 time, this early time, at 1 msec, the shock has advanced to some 18 m deep and has dropped to a peak pressure (in the vertical

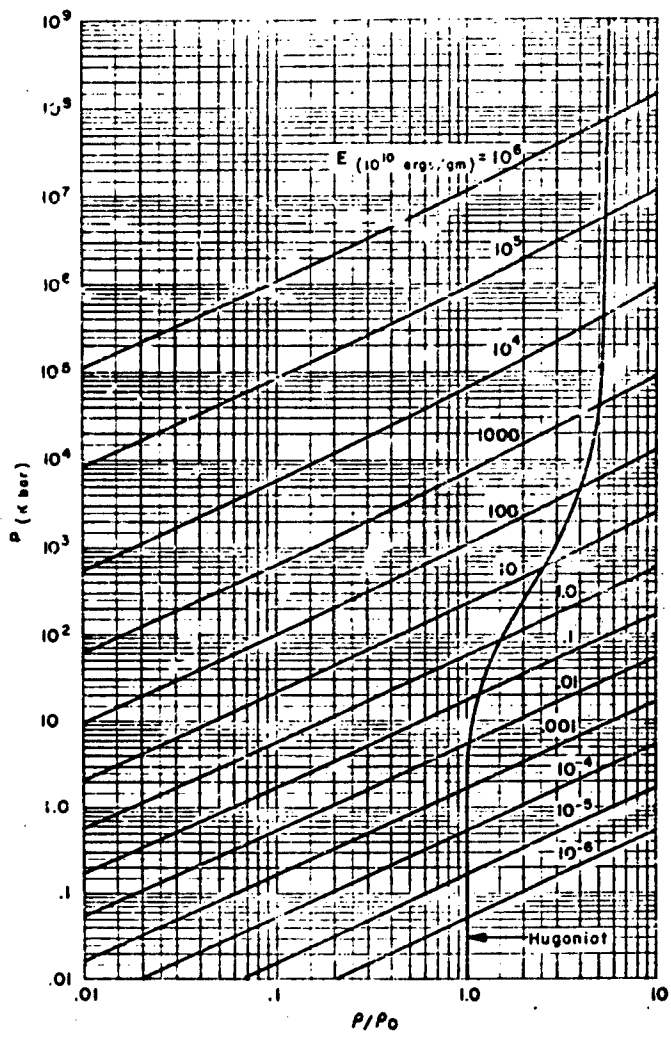


Fig. 2 - Equation of state for tuff

cone) of the order of 500 kbar (Fig. 5). The shock front is still fairly uniformly spherical out to 45 degrees from the vertical, dropping an order of magnitude from there to the surface. The pressure behind the shock appears more chaotic.

Later, at 3.4 msec the shock has progressed down to 32 m and fallen to a peak pressure of around 125 kbar in the same 90-degree vertical cone (Fig. 6).

The subsequent progress is shown at various times (at about 10, 21, 50, 80, and 100 ms) in Figs. 7 through 14. Throughout these figures one can follow the hemispherical shape of the shock. At all times the peak pressures along the vertical are largest and extend fairly uniformly out to a point 45 degrees from the vertical before a serious drop in pressure begins as one follows the shock front further toward the surface. At the later times (> 40 msec) the calculation has

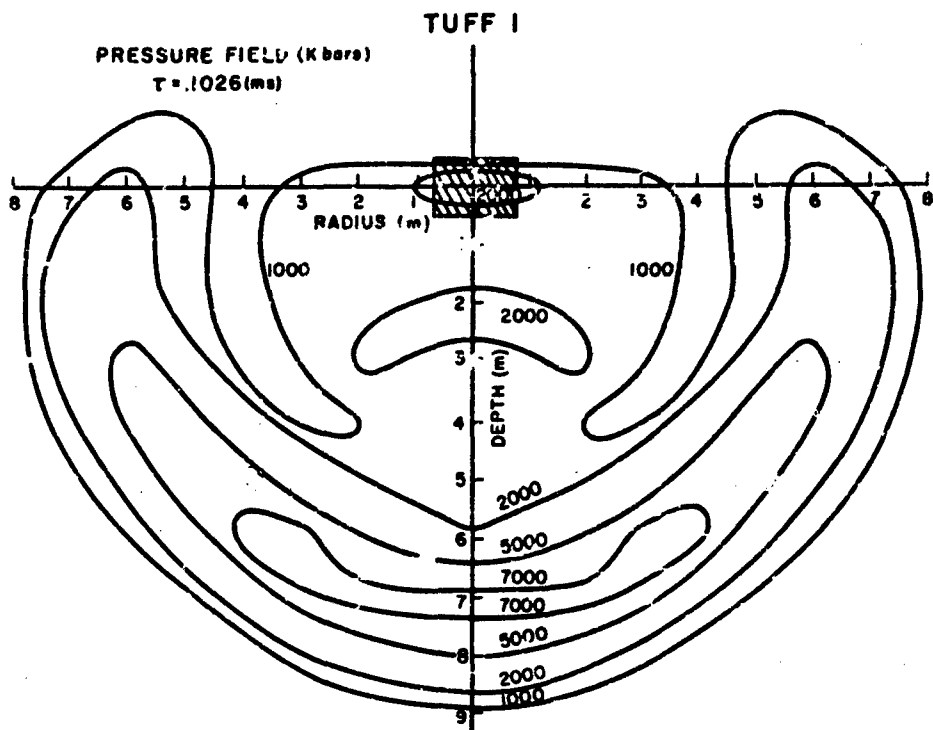


Fig. 3 - The early pressure field (kbar) at $t = 0.1026$ msec

been illustrated beyond a point where all pressures are below 10 kbar, and so beyond a time when the hydrodynamic assumption is reasonably rigorous. It is interesting to note that at these late times, when the shock is no longer strong enough to make a fluid of the rock, the velocity maps (Figs. 10, 12, and 14) indicate a fairly sharp cleavage at around 70 m deep. Above that point the material is moving up and continues to go up. Below that depth the material continues to move down. This "crater bottom" persists at the same depth after the 50-msec time. Since this is a fluid model and since we have claimed no rigor for the model at late times and low pressures, this evidence of a crater depth approximately equal to that predicted by conventional scaling laws [6] can be considered at least in part as a gratifying coincidence. It should be noted however that conservation of mass, momentum, and energy in the correct geometry are still appropriate and are in fact responsible for the motions illustrated, and it may well be that the plastic and elastic properties of the

rock play secondary roles in determining crater depths.

Pressures, as a function of time at fixed vertical positions fairly close beneath the source, display the usual strong shock-type bimodal decay in which the pressure, after rising to a peak and falling rapidly for a time, follows a more gradual decay rate (Fig. 15). At greater distance, less structure is evident in the pressure histories (Fig. 16), and only rough values of peak stress and total impulse are derivable from them. A similar description applies to the pressure histories at positions along the line inclined at 45 degrees from the horizontal (Figs. 17 and 18), but the pressure-time relations at points along the surface are quite different. Along the surface, air pressures arrive first (Figs. 19 and 20), dropping from a peak air or ground pressure (not shown in Figs. 19 and 20) to a "slowly" decaying fireball pressure. Later the direct ground shock arrives, driving the pressure up one or more orders of magnitude for a short time.

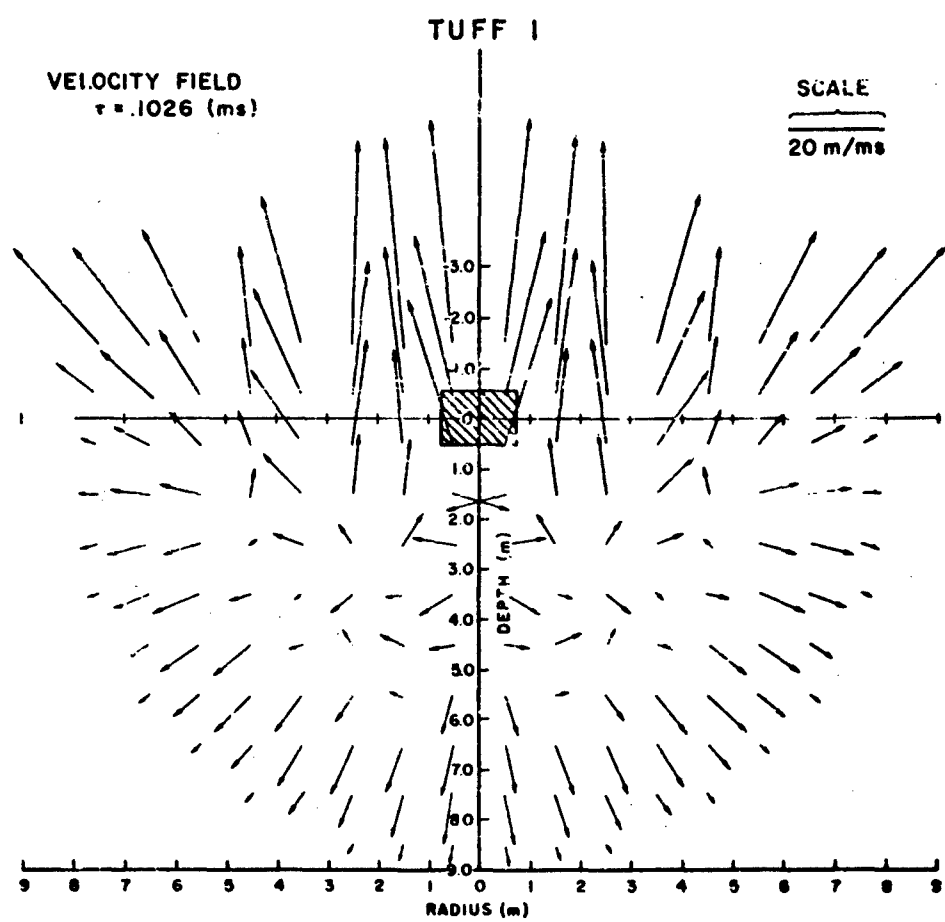


Fig. 4 - The velocity field—velocity meters of rock mass at $t = 0.1026 \text{ msec}$

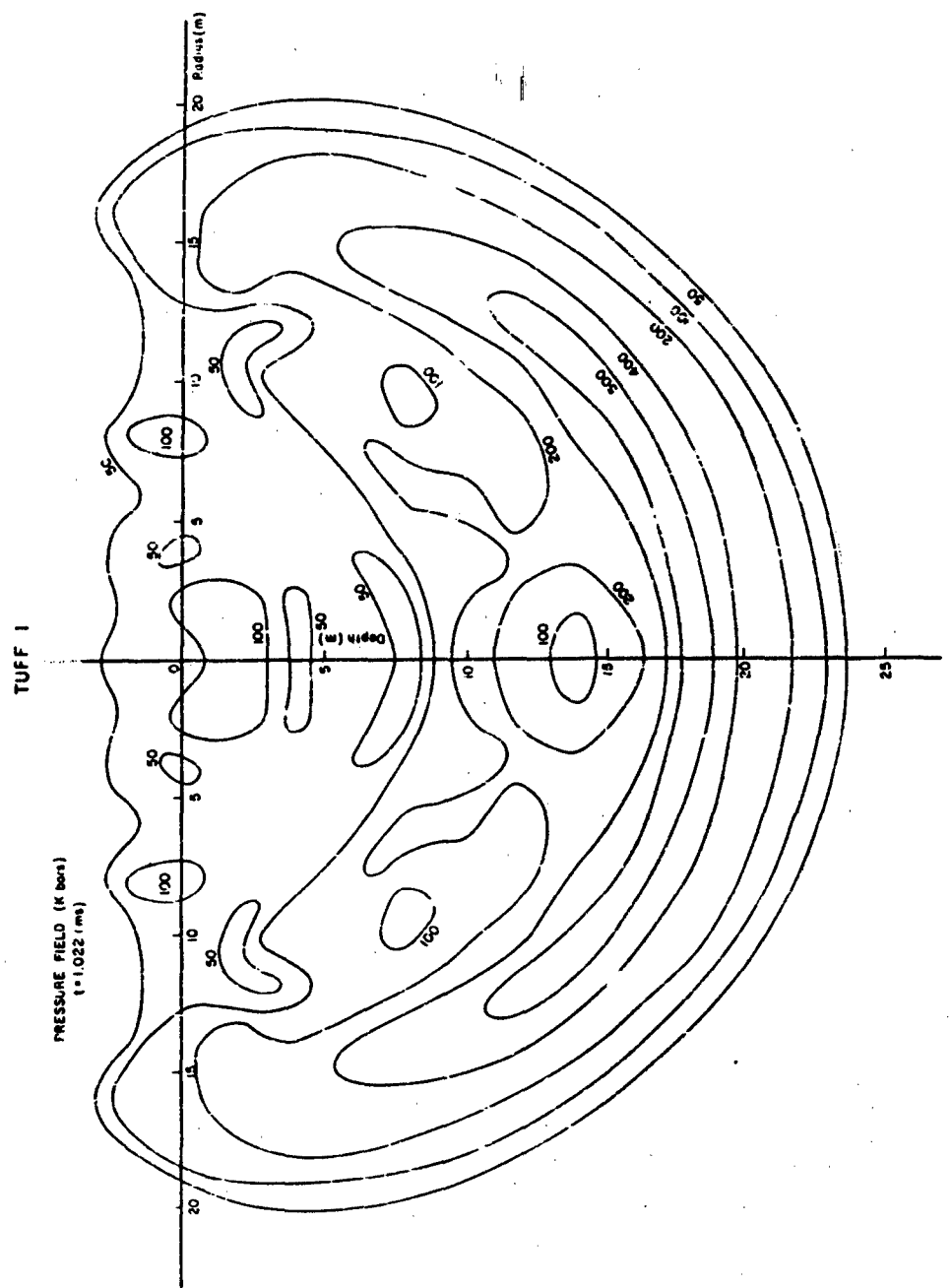


Fig. 5 - The pressure field (kbar) at 1.022 msec.

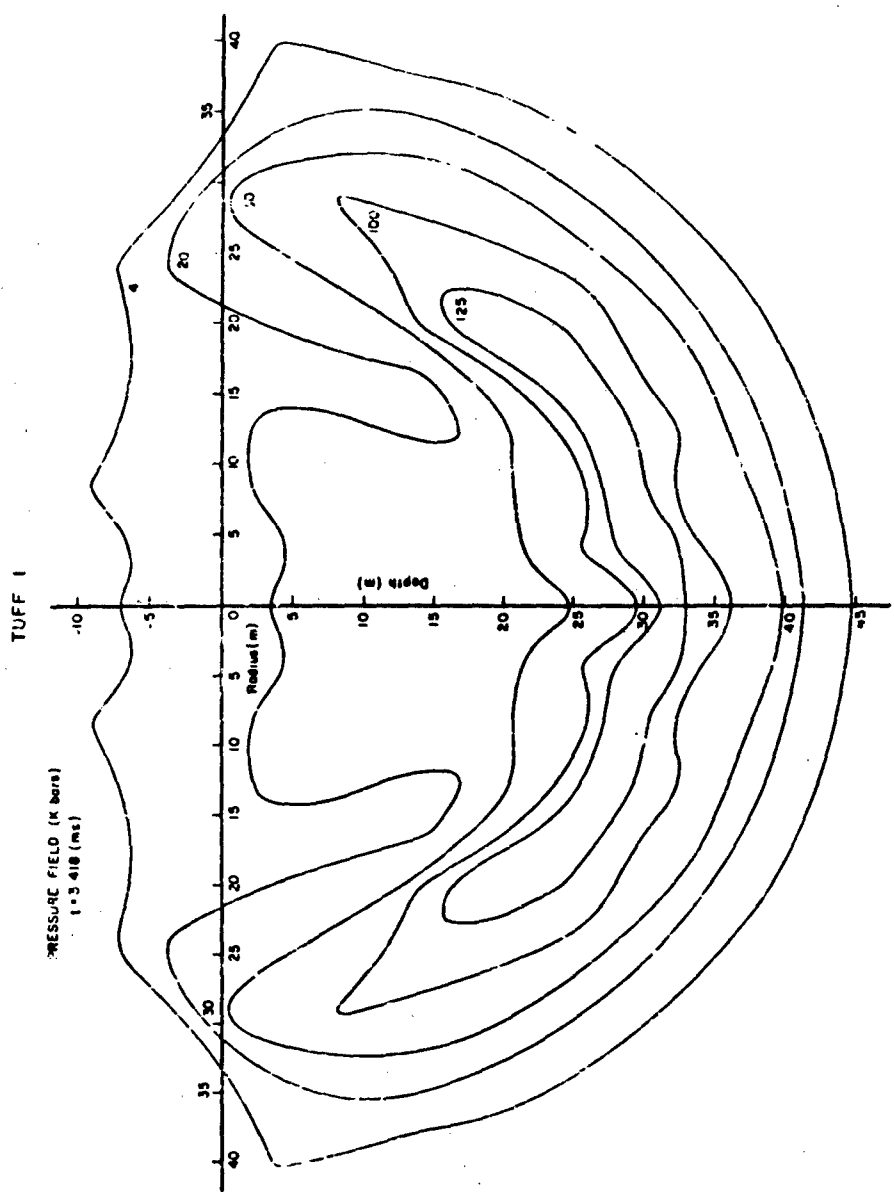


Fig. 6 - The pressure field (kbar) at 3.418 msec

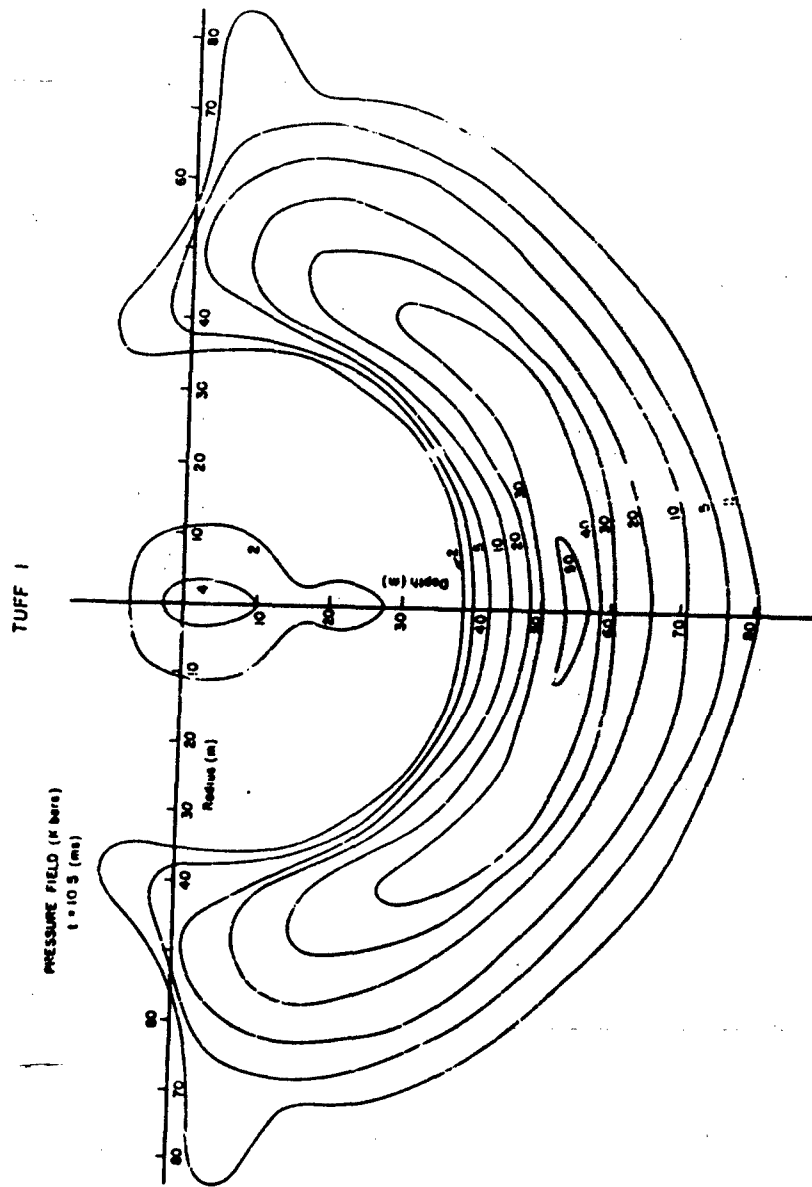


Fig. 7 - The pressure field ($t = 1.0 \times 10^{-4}$ sec.)

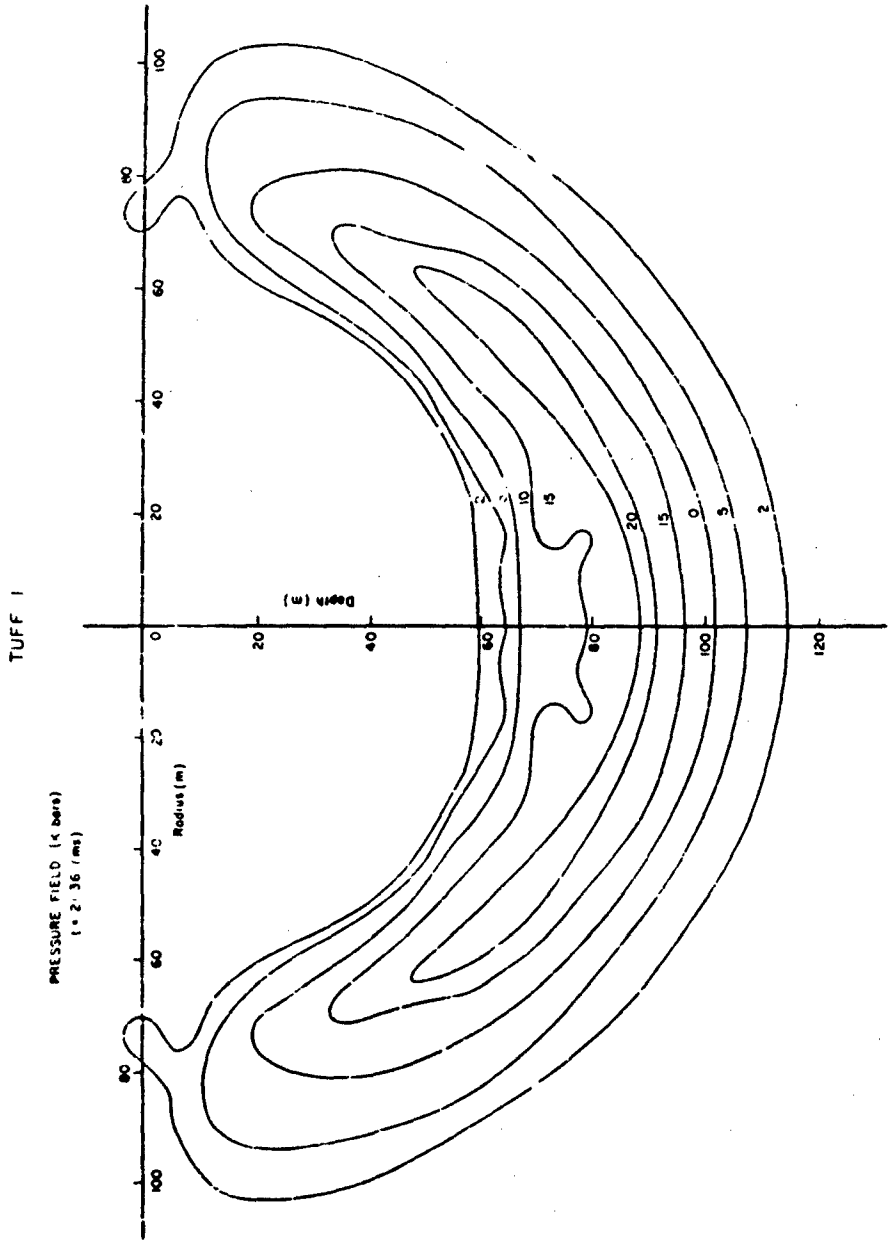


Fig. 8 - The pressure field (kbar) at 21.36 msec

TUFF I

PRESSURE FIELD (K bars)
 $\tau = 52.49$ (ms)

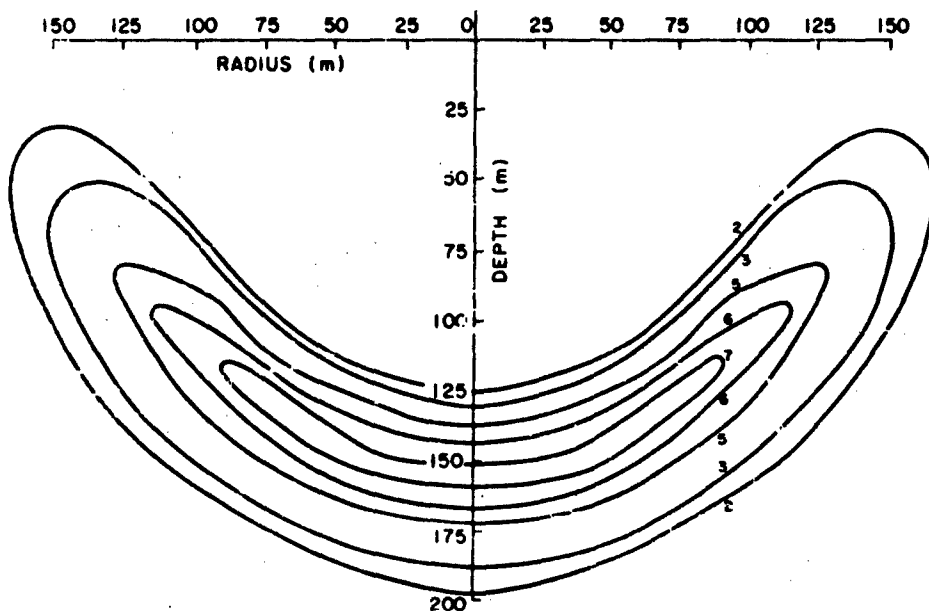


Fig. 9 - The pressure field (kbar) at 52.49 mscc

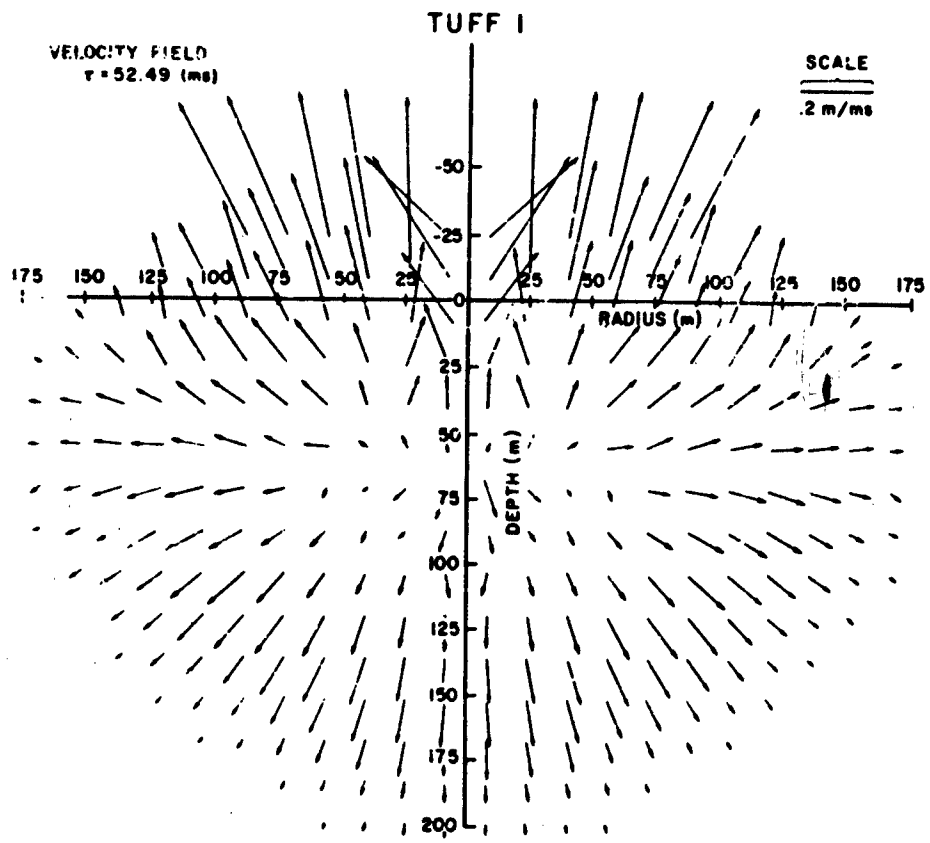


Fig. 10 - The velocity field—velocity meters of rock mass at $t = 52.49 \text{ msec}$

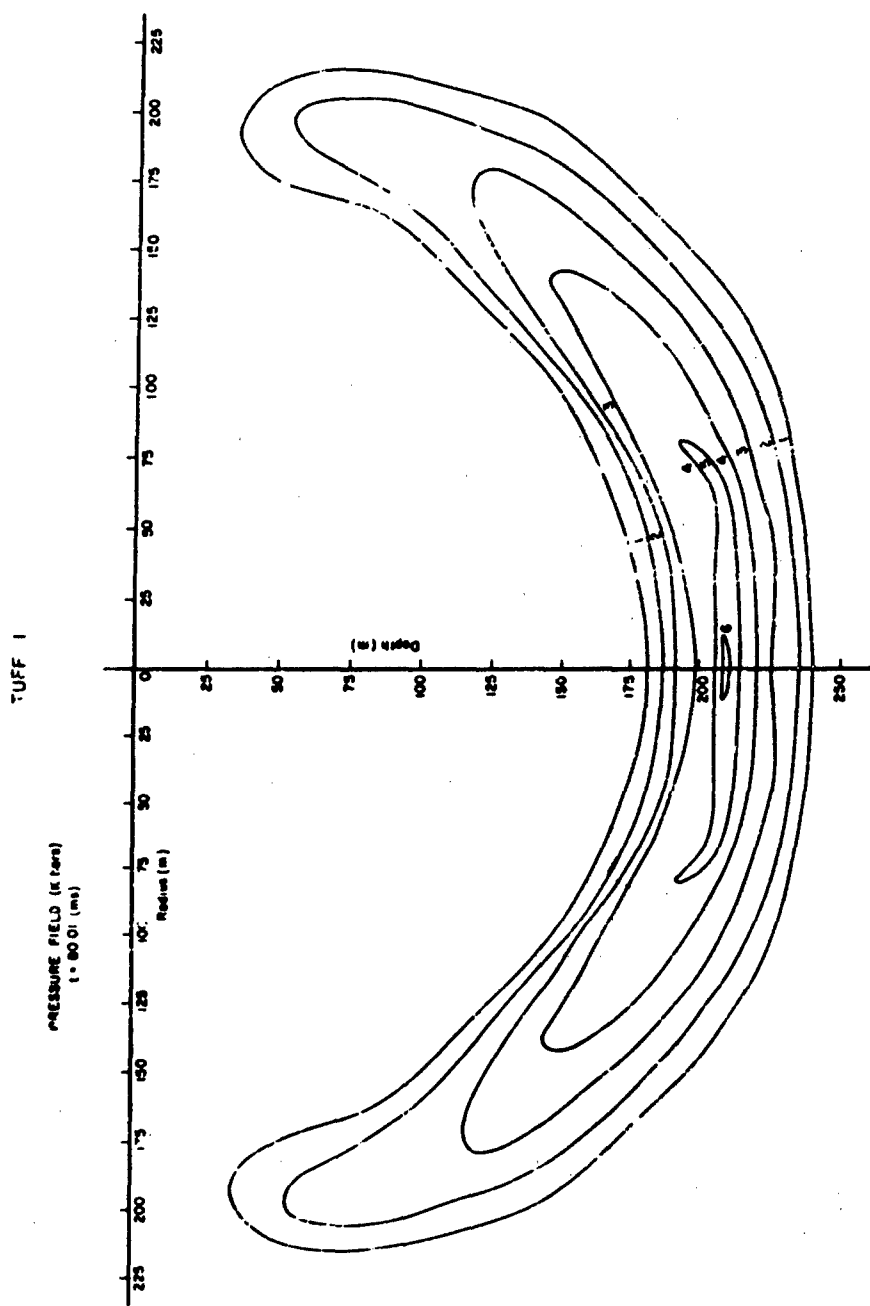


Fig. 11 - The pressure field (kbar) at 80.01 msec

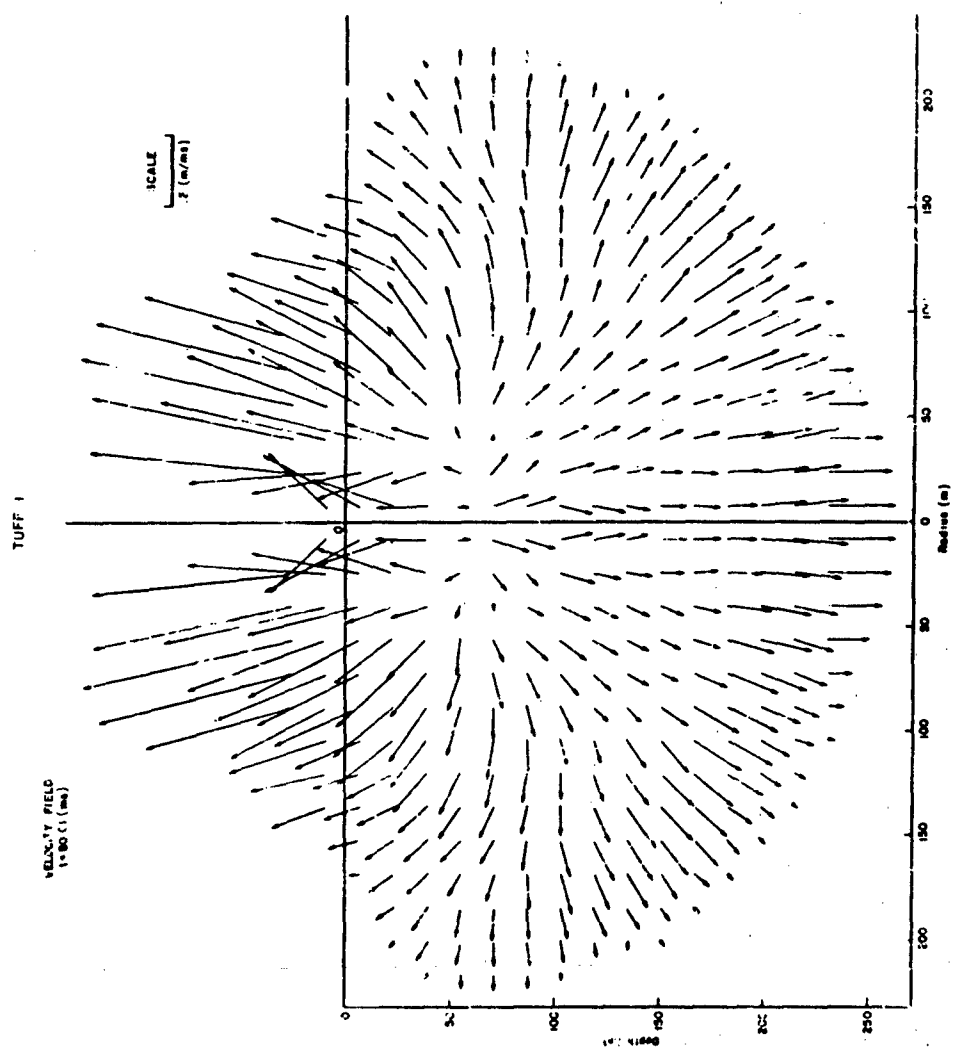


Fig. 12 - The velocity field--velocity meters of rock mass at $t = 80.1$ msec

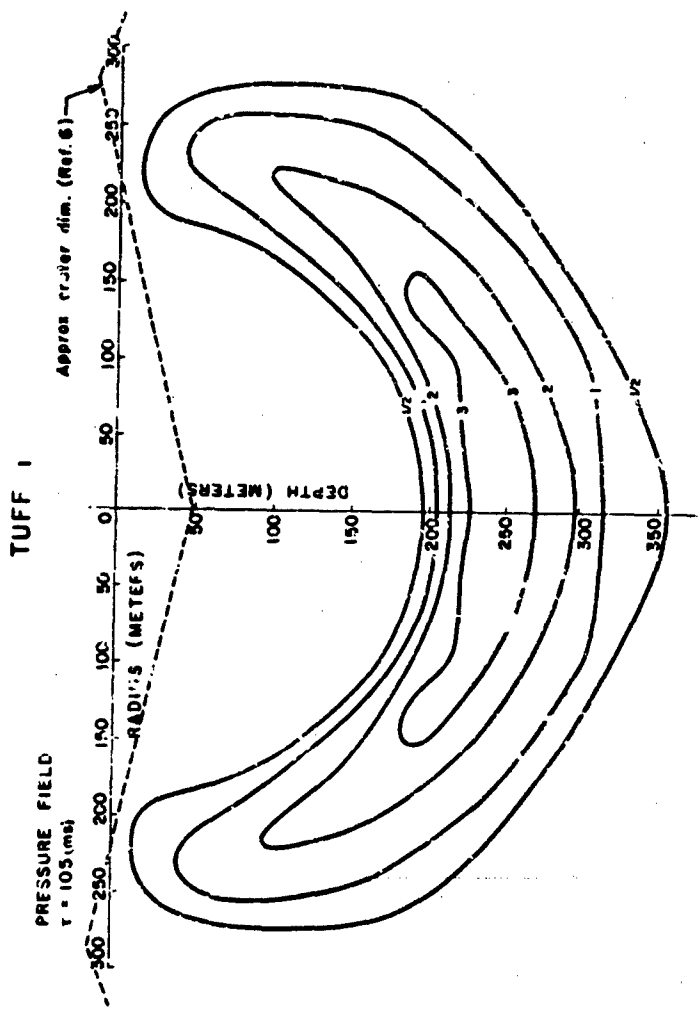


Fig. 13 - The pressure field (kbar) at 105 msec

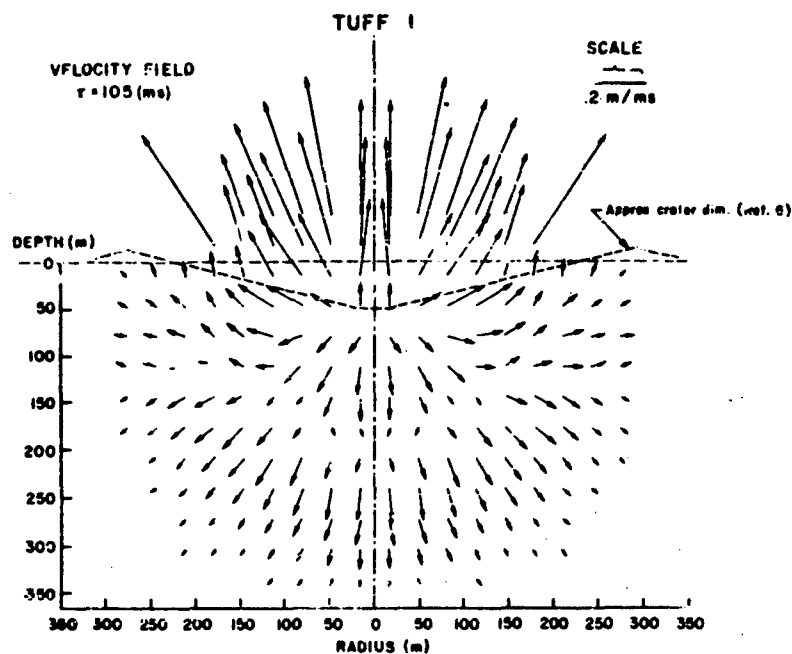


Fig. 14 - The velocity field—velocity meters of rock mass at $t = 105$ msec

At distances beyond a few 10's of meters (Fig. 20), it is clear that in surface-pressure histories the direct shock rapidly drops out of importance, and at horizontal distances much greater than 100 m, the direct shock can be ignored. But it does not follow that the direct shock can be ignored at depths below the surface at the same horizontal distances.

Referring to Fig. 13, it is evident that the direct shock brings pressures up to 2 kbar out to a distance larger than 200 m, but at depth of some 100 m. Even at a 50-m depth one would expect 1 kbar and perhaps 1/2 kbar (> 7000 psi) at depths less than 20 m and at ranges better than 200 m. At distances much beyond 200 m, however, and at depths of less than 100 m (or more nearly correctly, at depths such that a direct line to the point of explosion makes an inclination from the horizontal of less than about 20 degrees), it is the air blast alone which creates the pressure pulse. The peak overpressure from the air blast will be almost an order of magnitude higher than that from the direct shock at 100 m, while the air blast impulse is already a little larger than the impulse in the direct shock at the surface at that distance.

In Fig. 21, the peak pressures in the direct shock are shown versus the radial distance from the point of burst for the three directions, as solid curves labeled vertical (v), horizontal (H), and diagonal (D). In the early, strong shock region the decay of pressure is approximately like the inverse cube of distance while at lower pressures, the decay is less rapid, approaching a slope like the inverse three-halves power of the radial distance. The pressures along the surface (H) continue to drop rapidly even at large distances, since a rarefaction wave propagates downward from the surface on which the air pressure is at every instant much lower than the vertical ground shock pressures. The air was not always at a lower pressure, since at an earlier time the air shock created surface pressures much higher—out as indicated by the small circles. The dashed curves are from the ideal gas calculation; these begin at higher pressures but continue to drop rapidly at low pressures because of the strong shock restriction involved in the ideal gas calculations. The shock compression in the vertical and horizontal directions is indicated by the curves labeled $10(\eta-1)$ (where $\eta = \rho/\rho_0$). Thus at 10 m, the vertical shock has a density

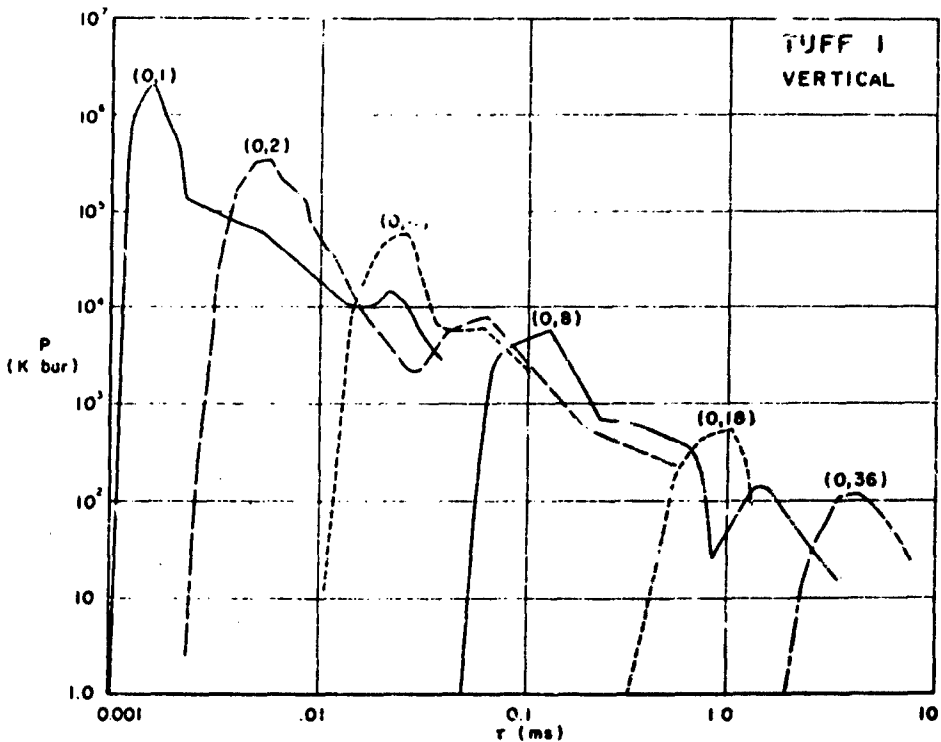


Fig. 15 - Pressure versus time at indicated depths (m) below burst point

of $2\rho_0$ and the horizontal shock a density of $\sim 1.5 \rho_0$.

Figure 22 shows the maximum components of velocity as a function of distance down the vertical and also horizontally. From this one observes that the velocities along the vertical are dominantly vertical (v_v) but have some slight radial component (v_r) indicating some hemispherical divergence. The velocities along the horizontal are both upward ($-v_u$) and outward (v_w), and of comparable magnitudes at most distances.

As the problem progressed and as it was necessary to include more material into which the shock could run, new and larger sets of zones were arranged, and the hydrodynamic variables were adjusted to the new grid, according to the conservation laws. When such new grids were introduced, those masses above the initial surface, having high-speed motions upward, were omitted. In excluding

these jettisoned materials some energy and mass is lost to the system. Slightly less than 50 kilotons (50 KT) of mass were ejected by this procedure (in the 100 msec covered). (It is estimated that altogether something on the order of megatons of material are carried aloft and tossed out of the crater from such an explosion.) Figure 23 shows this mass loss as a function of time along with the energy changes.

A study of the energy-time relations shown in Fig. 23, leads to the following observations: The downward kinetic energy, initially half a megaton, decreases rapidly as the shock develops in the surrounding rock. The heat or internal energy builds up rapidly at the expense of the initial kinetic energy, but begins to return to kinetic energy as surface material blows off. The sharp drops in energy occur as blow-off masses and their associated energies are eliminated at grid changes. Note in Fig. 23 that the biggest drop

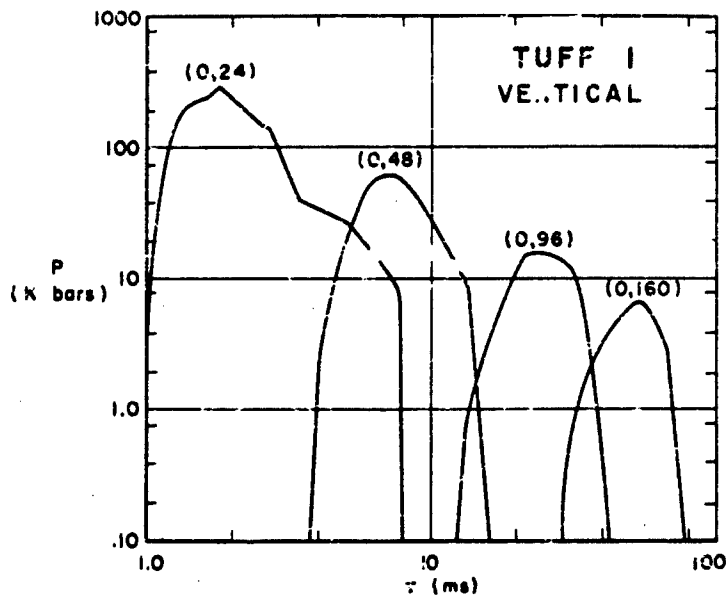


Fig. 16 - Pressure versus time at indicated depths (m) below burst point

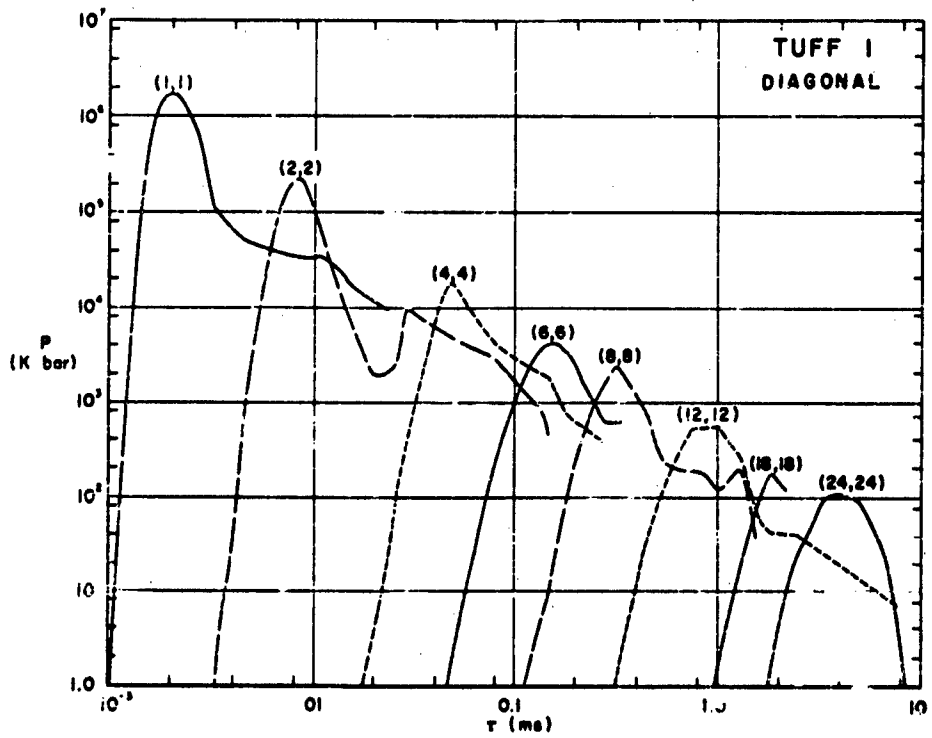


Fig. 17 - Pressure versus time at points with radii and depths indicated in meters

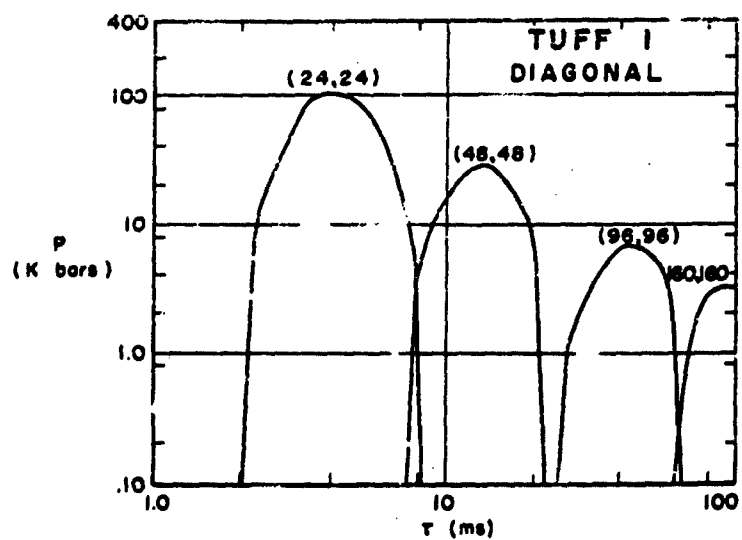


Fig. 18 - Pressure versus time at indicated position (m)

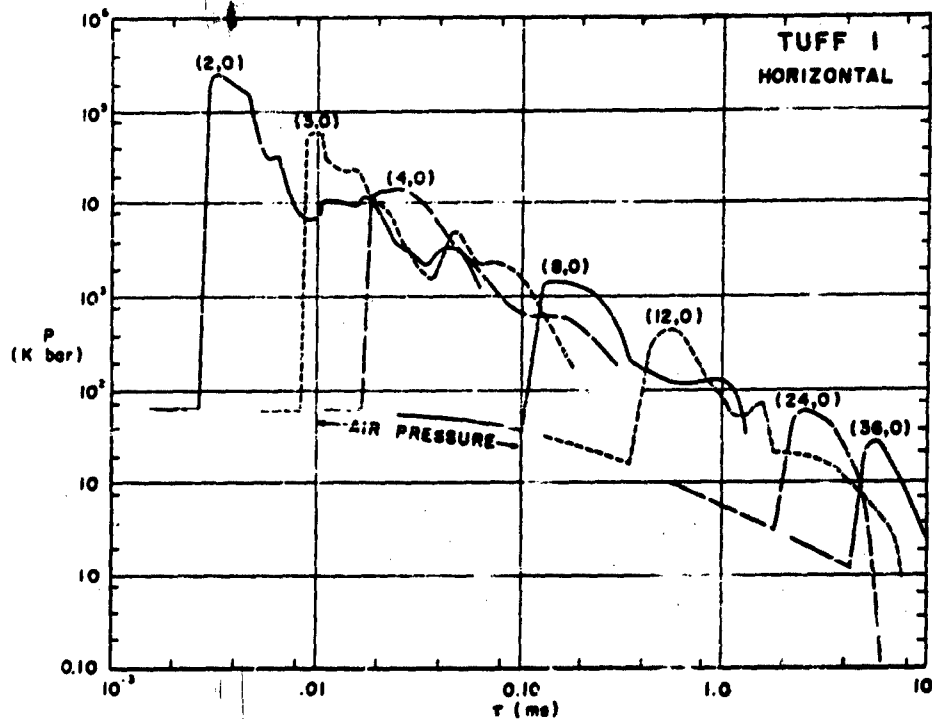


Fig. 19 - Pressure versus time at indicated radial distances (m) at the surface

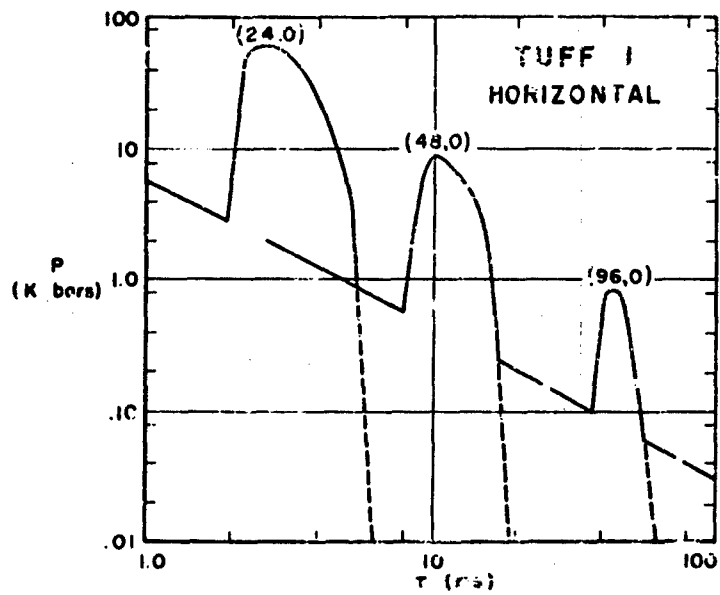


Fig. 20 - Pressure versus time at indicated radii (m) along the surface

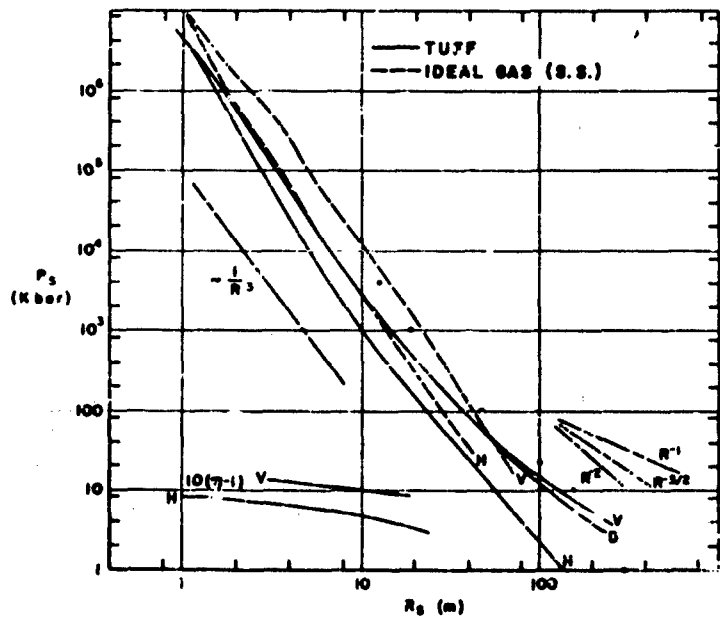


Fig. 21 - Peak pressures and compressions (η) versus range along vertical (V), horizontal (H), and diagonal (D), from burst point

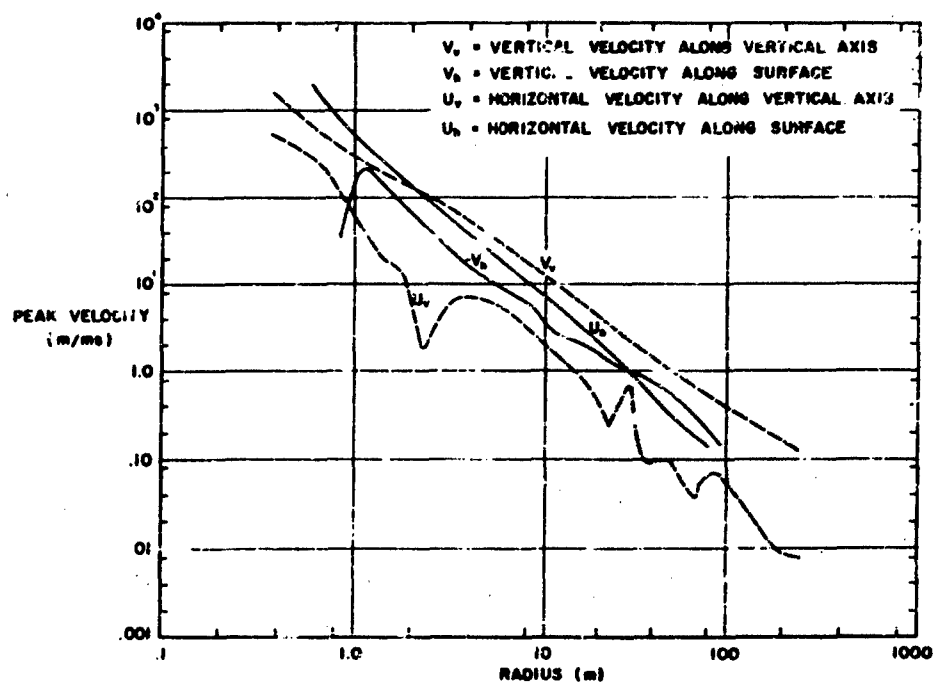


Fig. 22 - Maximum components of velocity as a function of distance down the vertical, and horizontally

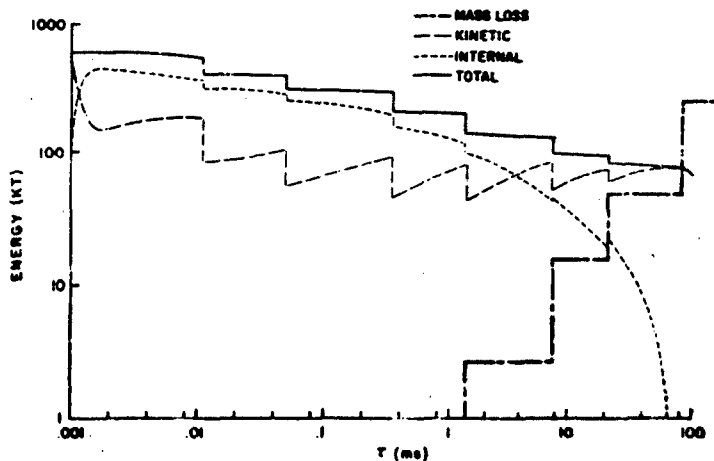


Fig. 23 - Energy and mass loss versus time

is in the kinetic energy. The total energy drops because of such periodic (and arbitrary) mass losses and because of the work done continuously against the high-pressure air of the fireball above. At the beginning, the total energy is 800 KT or 30 percent of 2 MT, but by the time the direct shock is out some 50 m, the energy is down to less than 100 KT (< 5 percent) and must drop further by both mechanisms.

The seemingly strange behavior of the internal energy at late times (Fig. 23) is an unfortunate consequence of the treatment of energies and pressures at low densities. Although negative pressures were not allowed (replaced as zero) in the calculation, negative internal energies did arise in low-pressure, low-density zones as these zones did work on their surrounding zones. The lack of consistency here is considered to be due to undamped and nearly random kinetic motions which absorb the energy and thus cause it to be recorded as kinetic rather than as internal. It is perhaps only a misidentification which makes the energy partition motions artificial; but it may also be a source of real error since—if energies were allowed to become consistent with a simple gas pressure—the pressures might well have been higher, causing further accelerations. This effective transfer of energy did not become seriously "out of line" until times after 10 msec, so that—although late-time information may be of doubtful accuracy—the early history should still be correct.

An investigation of ways to avoid this trouble is still in progress, although it is currently expected that the general features of the present calculation will remain unaltered by the correction of this inconsistency.

CONCLUSIONS

Perhaps the most significant result to come out of these preliminary calculations, aside from the general observation that the method seems capable of offering an interpretation of the cratering phenomena, is that the kinetic energy in the bomb debris when it reaches the ground is the most important mechanism in inducing the ground motion below the crater, as well as in the formation of the crater itself.

This fact implies that the crater size should be very sensitive to the height of burst near the ground. For if the debris must travel even a short distance through air

before contacting the ground, its energy may be seriously reduced as it drives a strong air shock. This energy is quickly radiated away to the periphery of the fireball and contributes to increasing the air blast at the expense of cratering efficiency.

Moreover, it implies that the cratering is sensitive to the details of the bomb disassembly in that this process determines the partitioning of bomb energy between the debris' internal and kinetic energy and that radiated away to air. This indicates that shallow burial or denser case should enhance cratering efficiency.

It also shows that comparisons with high-explosive bursts in this regime would seem particularly unfruitful because the early energy partitions between explosive gases, air, and earth are vastly different.

It is a further remarkable quality that the presence of a nearly free surface causes the stress patterns below the burst to be elongated along the vertical axis. The fact that the pressures along the shock front are far from uniform at any given time is understandable in terms of the geometry of the surface burst, but is not always a recognized factor in previous analysis of ground shocks generated by low air, surface or shallow-buried nuclear bursts.

A further feature worthy of reiteration is the nature of the continuous loss of effective energy in the ground medium due both to the work done by the expanding ground against air overpressure and to the essential disassociation of jetting material from the main body of soil or rock.

It would appear that further investigations should include studies of

1. Subsurface bursts.

2. Bursts in other materials, both hard rock and dry soil. (It may prove interesting to consider some cases of bursts on wet soils or even water.)

3. High explosive bursts for the sake of comparison and to illustrate more clearly the differences in the action between nuclear and chemical explosions.

4. Special geometries of high explosive charges with a view to modeling the stress wave history of a nuclear explosion (an investigation of this possibility is currently under study at SRI with DASA sponsorship).

These preliminary calculations were intended to reveal the basic nature of the cratering process and the formation of ground shocks. That the hydrodynamic model was used should always be kept in mind. This limits the strict applicability of these results to pressures greater than 8 kbar (which corresponds to compressions of greater than 10 percent) for the soft rock, tuff, which was the only material considered. It is believed that above this compression and pressure, the results are substantially correct, although the various uncertainties could easily lead to errors of about a factor of two.

Even recognizing this, it is of interest to examine the results of the present model beyond the region of its strict applicability, for it is not unreasonable to expect that at least the first motions are given correctly by it, leading to roughly correct values of peak pressure and peak velocity. However, the energetics at late times are questionable, and are subject to further interpretation.

It is hoped that the results presented here will furnish useful guidance and inputs to further studies at lower stress levels, which are very important to the design of protective structures. At these lower stress levels, the present hydrodynamic model must be replaced

by one which considers the tensor nature of the equation of state.

ACKNOWLEDGMENTS

The authors wish to credit Mrs. Nancy J. Brooks (Computer Sciences Department, the RAND Corporation) with recognition for her truly professional management of the entire computing program of this problem. In addition to her competent organization of the numerical work, Mrs. Brooks participated enthusiastically in discussions and decisions concerning the progress of the over-all effort. Our appreciation extends also to Miss Linda Larson, Mrs. Margaret Cohen, and Mrs. Rosemary Fue for aid in the analysis and preparation of report graphs.

Although this study was initiated primarily to satisfy a need in military applications, the method and some results are of significance to several proposals for peaceful uses of nuclear explosions under the PLOWSHARE program of the Atomic Energy Commission. For this reason the study was funded in a small part under Contract No. AT(11-1)-135 with the University of California Lawrence Radiation Laboratory, Livermore, California.

REFERENCES

- [1] R. L. Bjork and N. J. Brooks, A Numerical Technique for Solution of Multi-Dimension Hydrodynamic Problems, The RAND Corporation, Research Memorandum RM-2628 (to be published).
- [2] H. L. Brode, Weapon Effects for Protective Design, The RAND Corporation, Paper P-1931, 31 March 1960.
- [3] Nuckolic, Second Pliowshare Symposium, San Francisco, AEC, May 13-15, 1959.
- [4] Rolf Landshoff, A Numerical Method for Treating Fluid Flow in the Presence of Shocks, Los Alamos Scientific Laboratory (1955).
- [5] H. L. Brode, "Numerical Solutions of Spherical Blast Waves," J. Appl. Phys., Vol. 26, No. 6, June 1955, pp. 766-775.
- [6] Ed. Glasstone, The Effects of Nuclear Weapons, AEC and DOD, pp. 309-213, June 1957.

DISCUSSION

Mr. Chasseyka (Armour Research Foundation): At what soil pressure did you find that the soil stopped going into the air?

Mr. Bjork: The soil was flying into the air as far as we carried the calculation.

Unfortunately I don't have that pressure listed here.

Mr. Chasseyka: Approximately what soil pressure do you think that was?

Dr. Brode (Chairman, Rand Corporation): At the last time, roughly 100 ms, part of it was still streaming from the surface. There was still, in other words, a pressure gradient upward.

Mr. Chasseyka: Well, the soil vaporizes at well over 100 kbar; and if the soil is not vaporized, I just wonder how it could be going up in the air?

Mr. Bjork: In Fig. 13, we have the solution for the pressure field out to about 225 m which is the crater radius. The outer contour is 1/2 kbar and the next is 1 kbar. So the pressure gradient is 1/2 kbar. This kind of pressure gradient is obviously sufficient to hurl the ground into the air. Now this behavior persisted out to about 350 m. I don't happen to have the exact pressures that existed near the ground surface at that time. I might add that the streaming of these upper particles is most strikingly like the streaming out jets from a surface burst, either nuclear or from high explosives. From the high-speed motion pictures one notices the same kind of jetting of both vapors and crushed or powdered materials and in some cases even blocks of materials depending on the medium.

Mr. Chasseyka: Yes, this is a phenomena that one observes close in where the pressures are extremely high, or certainly much higher than 500 kbar. (Five hundred kilobars is way below the vaporization.) It occurs to me that the pressures at a considerable depth in the ocean, or ground, are much higher than they are on the surface, yet you find no streaming into the air.

Mr. Bjork: Oh, yes. We're not maintaining that the material out here is vaporized or even left in a liquid form. We just notice a mechanical pressure gradient that will physically throw large portions of the rock into the air. Now it might be that at this low-pressure level we should put in the strength of the tuff. It might be that it won't be overcome. In fact it's probable because this represents about the periphery of the crater and you know from experiment you don't get material thrown into the air. If this were a fluid it would be thrown into the air, but putting in the strength effects will probably kill the motion about this point—at about this radius, that is.

Mr. Chasseyka: Is this verified by experiment?

Dr. Brode: At the stage of the last calculation the ground shock, as shown in Fig. 13, is slightly beyond the edge of the crater, for a hardrock crater. In fact, it's slightly beyond that for a dry-soil crater. In any case, one could hardly expect in a fluid model such as this to be doing much more than indicating the direction of forces. However, if this were an incompetent rock or a soil for which this model would be undoubtedly as good as it is for tuff, then you would expect—if you put these kinds of accelerations to the material—that it will move. You are in the region where material does move in the lip of the crater and in the crater edges. There isn't much strength to overcome in shear if we're dealing with, say, a soil. The model isn't so good that we can distinguish between soil and rock because after all it's still a fluid model.

Mr. Chasseyka: What you're saying is that pressure is better defined as kinetic energy. Is this what you mean?

Mr. Bjork: No, we mean a pressure that's generated by a compression in the material.

Mr. Morrison (AMF): Were any computations made comparing the impulse of the ground pressure with the impulse of the air pressure immediately above?

Dr. Brode: The pressures and the durations of pressures are such in the air above that the total impulse at almost all distances are greater from the air pressures. The impulse, at any point below the surface from this ground shock is less than the impulse over a comparable area from the air blast. Now the significance of this is questionable in my mind. After all, the impulse on the surface over a week is every bit as great, just from the ambient pressure. What is important is the spectral character, the time history of this impulse and, in fact, the peak pressures. As was pointed out the peak pressures are much higher than any pressure delivered by the air shock which, after all is limited to, in the very highest regions, pressures like 10^6 psi but not nearly as high as these pressures in the ground. The pulse is shorter in this ground shock; therefore, although the pressures are much higher, the impulse is not as impressive.

Mr. Morrison: Am I correct in assuming that, in the ground, the impulse of the pressure at a given distance from ground zero and

fairly close to the surface is actually greater than the impulse of the air pressure at the same point or the overpressure at the same point?

Dr. Brode: Let me say we should be more specific and more careful about this. Obviously if we get close enough to the crater region, to the bomb itself, the impulse delivered from this direct shock is larger than that from the air shock. But if we take

an area comparable to the size of the crater and consider the average impulse on that area from the air shock and the impulse at any point due to this direct ground shock, then the air impulse is greater. The stresses in the soil, however, are greater at any time than those delivered by the air shock. Am I reading your question right?

Mr. Morrison: Yes, I think I have the point now, thanks.

ANALYTICAL AND EXPERIMENTAL STUDIES ON LOCKING MEDIA

Paul Weidlinger
Weidlinger Consultants, New York, New York

A summary of recent researches on stress wave propagation in locking media are presented. Results of analytical and of some experimental work are given and their implication on groundshock phenomena is discussed.

INTRODUCTION

The current interest and research activity in wave propagation in locking and other dissipative media is of such recent origin that it may be useful to provide a brief account of the history of these activities.

The work of our group in this field was started about 4 years ago to provide a theoretical basis for the prediction of groundshock effects. It was already apparent at that time that the data which were obtained from measurements of ground displacements and accelerations during weapons tests were not explicable under simple linear elastic assumptions. In considering this problem, the first significant observation is that the macroscopic granular structure of sand and of similar materials implies a behavior which is different from that of other solids. A review of the literature shows that the problem of a granular mass, consisting of elastic grains, has been extensively studied. These researches were probably primarily motivated by seismological problems, and have been pursued by Japanese and American scientists [1-4]. These investigations were restricted to the range of elastic behavior, and it turns out that the slight nonlinearity found in the stress-strain relation is insufficient to account for the large permanent deformations and other phenomena which are manifested by soil masses under intense pressure. Some of the experimental work, however, which has been carried out at Columbia University [3,4], on compression tests of granular columns, constructed of

ball-bearings, provides an important clue. High-speed photographs taken during the collapse of such granular columns indicate that the collapse mechanism consists of a rearrangement of grains from a loose to a dense packed or compacted state, and during the collapse a well-defined front, consisting of densely packed grains advances into the as-yet undisturbed, loose-packed medium. This phenomenon seems to indicate that at least a part of the essential mechanism consists of irreversible compaction of the medium, into a denser state, accompanied by large volumetric changes.

From these considerations we arrive at a tentative hypothesis regarding the character of the stress-strain relation of granular masses under uniaxial pressure which may be described as follows:

First Stage: On initial compression, we find a slightly nonlinear elastic behavior.

Second Stage: Further compression may produce a plastic flow and some gradual breaking of grains which produces a softening or plastic response.

Third Stage: Additional pressure produces a rather sudden rearrangement of granules into a less compressible state accompanied by large volumetric changes accompanied by permanent strains, manifested by the up-turning of the stress-strain curve.

This hypothesis can be made plausible by noting that the observed range of the void

ratios of sand in the loose and densely packed state is in the range of 0.3 to 1.00 while the void ratio of tangent spheres of equal diameter is computed to be 0.35 in loose packed and 0.91 in the densest state, corresponding to cubic packing.

The general form of the stress-strain curve may be of the form shown in Fig. 1, and it is similar to the behavior of solids under very high-hydrostatic pressure. Wave phenomena in materials which exhibit this type of stress-strain relation has been considered in the past [5,6,7], but mathematical difficulties prevent the formulation of closed form solutions needed for the assessment of its effects.

The difficulties can be overcome to some extent by representing the stress-strain relation by various idealized curves as shown on Figs. 2, 3, and 4. The simplest form is that of Fig. 2a where the stress-strain curve is that of a single vertical line parallel to the

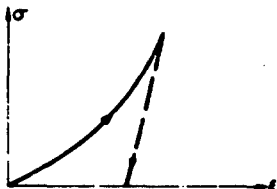


Fig. 1 - Possible form of stress-strain curve for granular media

stress axis. (This simplification is a counterpart of the rigid-plastic medium which is used to approximate the general elasto-plastic behavior of some materials.) This stress-strain diagram implies that upon initial loading the medium exerts no resistance until a critical value of the strain (or density) is reached. Beyond this critical strain the material becomes incompressible. Besides this simplest assumption one may construct other stress-strain diagrams such as shown on Figs. 2b, 2c, 3, and 4. These modifications affect either the initial behavior of the material, making it initially elastic (Fig. 2b) or initially elasto-plastic (Fig. 2c) or they influence the behavior after the critical strain is reached by permitting a certain amount of residual elasticity, leading to the bilinear model of Fig. 3. Finally, if we are interested in more details at lower levels of compression, where the governing phenomenon is not that of incompressibility but rather that of a gradual but irreversible volume change, the medium may be approximated by the stress-strain curve of Fig. 4, which is a linear material exhibiting permanent strains at all stress levels.

It turns out that the materials characterized by Figs. 2a to 2c have been known for some time and their behavior under static loading has a considerable United States literature under the name of locking-media or materials of limited incompressibility [8-11]. The problem of stress-waves and shocks in these media have been studied by our group, and their application to ground

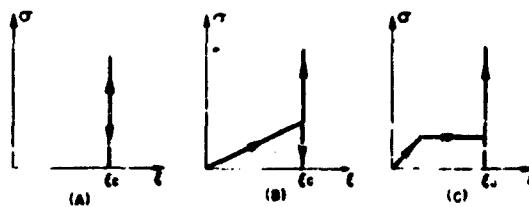
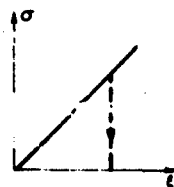


Fig. 2 - Idealized stress-strain curves



Fig. 3 - Idealized Curve - bilinear model

Fig. 4 - Stress-strain of a linear material exhibiting permanent strain at all stress levels



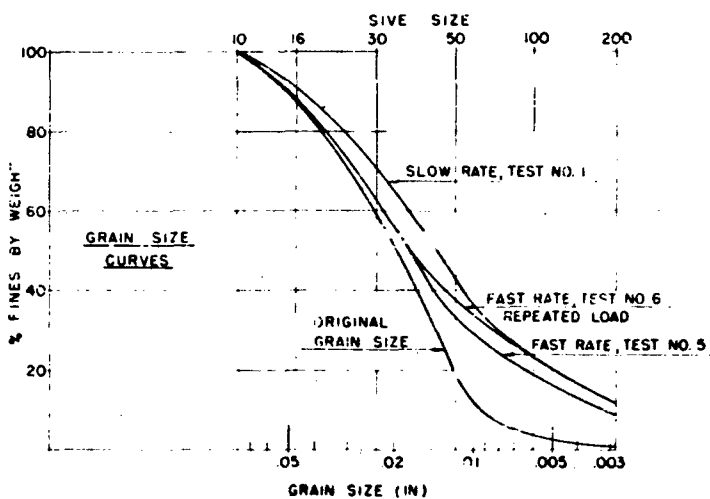


Fig. 5 - Grain size distribution before and after various test loadings.

shock phenomena has also been explored [13-21]. Further search of the literature shows a considerable work on these materials by USSR scientists which also seems to have been originated since 1952 and has been intensified in more recent years [22-29].

Comparison of our work and that of the USSR group shows a very great similarity in approach and results. Most of the USSR work is concentrated on spherical wave phenomena, but there is a single early attempt at formulating a two-dimensional theory [23]. Most of our work considers plane waves, but spherical waves have also been explored [18], which is similar to the work in Ref. 24. We note that both our work and that of the USSR group suffered for lack of experimental data. Ref. 23, however, describes an ingenious experiment with small-scale explosives for the exploration of spherical wave propagation. This experiment seems to verify the analytical results which have been obtained so far and is also useful to determine certain physical constants.

*These investigations have been sponsored by various organizations, including the Space Technology Laboratory and The MITRE Corporation, and currently the Air Force Special Weapons Center. Some of the work is based on unsponsored researches.

STATIC AND QUASI-DYNAMIC COMPRESSION TESTS

In order to obtain a basic verification of our assumption regarding the form of the stress-strain relation and the macroscopic mechanism of density changes, we have initiated high-pressure experiments with sand. Previous U. S. experiments were restricted to relatively small, pressure levels (40 psi), which seemed to indicate an initial elasto-plastic behavior and also showed some strain rate effects [30]. Stress wave propagation corresponding to this behavior also has been treated analytically [31].

Our experiments, performed at Columbia University, were carried to very high-pressure levels (16,000 psi) with consequent loss of detail at lower pressures. The procedures and results of these experiments will be published in the near future. A brief summary of preliminary results are given as follows:

The sand which was used is characterized by the standard grain size distribution curve shown on Fig. 5. Also shown in Fig. 5 is the distribution after single and repeated loadings. We note that initial loading produces a substantial comminution of grains and additional loading seems to have less effect on the larger grain sizes. Tests were carried out under constant compression and lateral friction in the container was eliminated to a

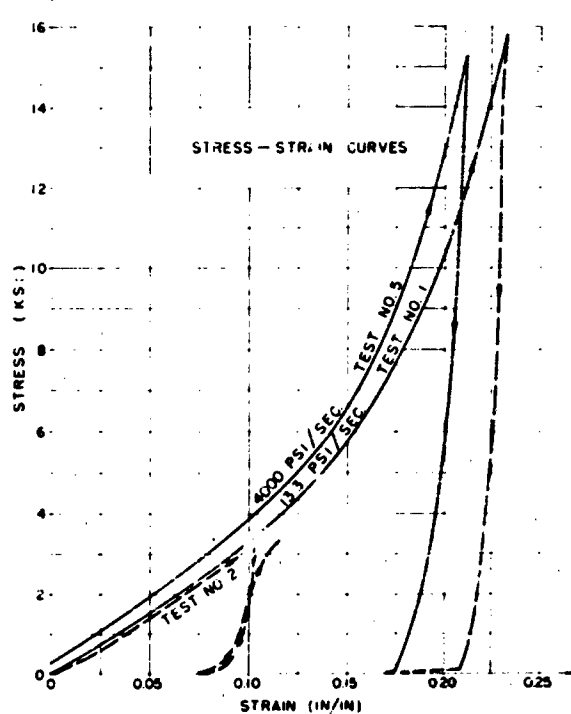


Fig. 6 Stress-strain curves for single loading under a slow and a rapidly applied load

degree that they do not produce measurable effects. The resulting stress-strain diagram for single and repeated loading under slowly applied loads (1130 psi per sec) and very rapid loading (4000 psi per sec) are shown in Figs. 6 and 7.

From these experiments we draw the following tentative conclusions:

1. Initial high intensity compression produces a stress-strain relation which shows generally upturning of the curve, similar to the one shown on Fig. 1.
2. This behavior indicates a gradual change in density, accompanied by comminution of grains.
3. Upon unloading, very large permanent strains are manifested, suggesting that this type of behavior may be approximated by a linear irreversible material characterized by the stress-strain diagrams shown in Fig. 4.

4. Strain rate and other dynamic effects within the ranges of the experiment are negligible.

5. Upon reloading, the material follows the original unloading curve which shows a slight recovery. Repeated loading diagrams seem to indicate that the principal mechanism may be that of the denser packing of grains.

6. The response to repeated loading suggests that it approximates that of an ideal locking medium as shown in Fig. 2.

ANALYTICAL WORK

The derivation of the equations governing the motion of the various media (Figs. 2, 3, and 4) have been published [4, 15] or are in the process of publication [17]. The following is a brief summary of this work.

The results which are given for plain wave propagation consider the case of a

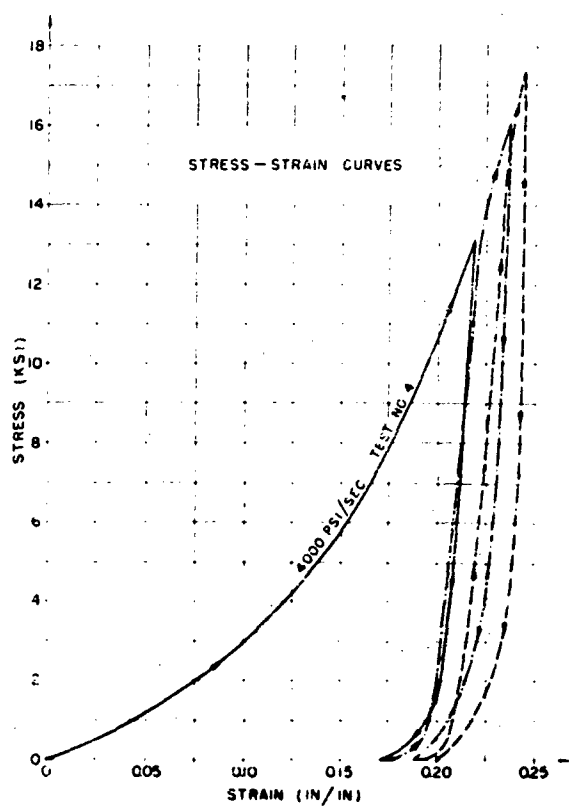


Fig. 7 - Stress-strain curve for repeated very rapid loading

semi-infinite medium of a compacted density of ρ , the surface of which is subjected to a suddenly applied (zero rise time) decaying pressure pulse $p(t)$, with an initial value $p(0) = p_0$. The impulse of the pressure at a time t is

$$I = \int_0^t p(t') dt'. \quad (1)$$

The wave front propagates in the vertical direction y and is located at a given time at depth z , propagating with the velocity i . The peak stress σ_i and peak particle velocity u_i occur at the front.

Linear Irreversible Medium (Fig. 4)

Upon application of the decaying pressure, the medium behind the compaction front acts

as a rigid mass, having a constant particle velocity u throughout. Conservation of momentum for the entire compacted mass and for any element thereof requires that

$$\frac{d}{dt} (\rho u) = p(t) \quad (2)$$

and

$$\frac{\partial \sigma}{\partial y} = -\rho \frac{\partial u^2}{\partial t^2} \quad (3)$$

which with the appropriate initial conditions provides the relevant free field parameters, as follows:

$$i = \left(\frac{E}{\rho}\right)^{1/2} = c_0 \text{ constant} \quad (4)$$

$$z = \left(\frac{E}{\rho}\right)^{1/2} t \quad (5)$$

$$\dot{u}_z = \frac{I(t)}{t} \frac{1}{\rho c_0} \quad (6)$$

$$\sigma_z = \frac{I(t)}{t} \quad (7)$$

We note that the front propagates at a constant velocity corresponding to the acoustic velocity c_0 of the medium. The peak stress at the front is the smallest "average pressure" of the impulse (i.e., the peak stress is equal to the intensity of a step pulse which contains the impulse of the applied pressure at any instant of time). Thus implies, that in case of rapidly decaying pressures a substantial attenuation of the peak pressure will be manifested. In the case of an exponential pressure pulse, with a relaxation time of τ_0 , the attenuation of the peak pressure at depth z at a time, when

$$\frac{p(t)}{p_0} \ll 1 \quad (8)$$

is given by

$$\frac{\sigma_z}{p_0} = \frac{c_0 t_0}{z} \quad (9)$$

and we note that the attenuation is inversely proportional to the depth.

Ideal Locking Medium (Fig. 2a)

The equation of motion of this medium is also given by Eq. (2); but, since the compacted medium can exist at a constant strain ϵ_c only, the following additional relationship exists:

$$\dot{u} = \epsilon_c \dot{z} \quad (10)$$

These equations yield

$$z^2 = -\frac{I^2}{2c_e} \int_0^t I dt \quad (11)$$

$$z^2 = -\frac{2}{c_e} \int_0^t I dt \quad (12)$$

$$z^2 = -\frac{I^2}{2} \int_0^t I dt \quad (13)$$

The long time attenuation of the peak front stress, is obtained as previously and is given by

$$\frac{\sigma_z}{p_0} \approx \frac{t_0}{\rho c_e z^2} \quad (14)$$

We note that the attenuation grows with the inverse square of the depth.

Bilinear Medium (Figs. 3 and 8)

This model recognizes the existence of an initial elastic behavior and some additional but much smaller residual elasticity after compression has occurred. If the second branch of the stress-strain curve is rotated, we obtain at one extreme a fully elastic medium and in the other extreme a locking medium. The range of possible responses (from elastic to locking) seems to imply that the general behavior, and especially the attenuation of peak pressure must be dependent on the physical constants of the medium. Detailed investigations, however, show that for each set of physical constants a depth can be defined beyond which the influence of these constants is negligible. This fact is crucial because it permits us to estimate the attenuation of the stresses with depth even when the magnitude of the physical characteristics of the material are given only approximately within a rather wide range.

The one-dimensional wave equations governing the behavior of the medium are

$$\frac{\partial \sigma^2}{\partial t^2} = c^2 \frac{\partial \sigma^2}{\partial z^2} \quad (15)$$

$$\frac{\partial u^2}{\partial t^2} = c^2 \frac{\partial u^2}{\partial z^2} \quad (16)$$

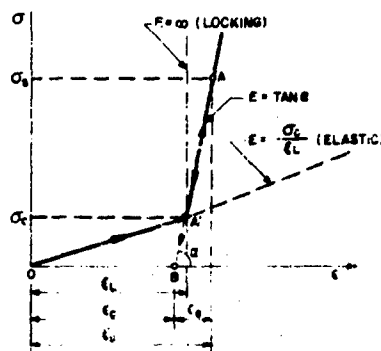


Fig. 8 - Bilinear stress-strain diagram

where c is the acoustic velocity associated with the second branch of the curve.

The shock velocity is

$$i = \sqrt{\frac{E}{\rho}} \quad (17)$$

where E is the secant modulus, given by

$$\bar{E} = \frac{\sigma_3}{c} \quad (18)$$

These quantities cannot be obtained in closed form but a simple numerical method is given in Ref. 17. The result of such computations is shown on Fig. 9, which also illustrates the independence of the attenuation beyond a given depth. This particular depth z_c is given by

$$z_c = \frac{c_0 t_0}{\sqrt{1 + \frac{\epsilon_c}{\epsilon_e} - \sqrt{\frac{\epsilon_c}{\epsilon_e}}}} \quad (19)$$

where ϵ_e is the elastic strain on the second branch of the curve measured from the strain ϵ_c . The physical interpretation of this depth (beyond which the attenuation of a bilinear medium is not significantly different from that

of a locking medium) is the location of the shock front at a time when the principal rarefaction wave from the surface catches up with the front. It is of interest to note that the USSR experimental work [28] in spherical wave propagation seems to confirm these analytical findings. These experiments show a very weak dependence of the velocity field on the properties of the medium.

Spherical Waves

To treat this case certain three-dimensional properties of a locking medium must be defined. The critical strain, or strain where locking occurs must be replaced by a critical value of the dilatation ξ so that

$$\xi = 1 - \frac{\rho_0}{\rho_1} \quad (20)$$

where ρ_0 and ρ_1 are the initial and compacted densities of the medium. Once this compaction has occurred, the medium becomes incompressible, and it satisfies a yield condition of the form

$$\sigma_x - \sigma_\theta = -c + \frac{1-k}{1+k} (\sigma_x + \sigma_\theta). \quad (21)$$

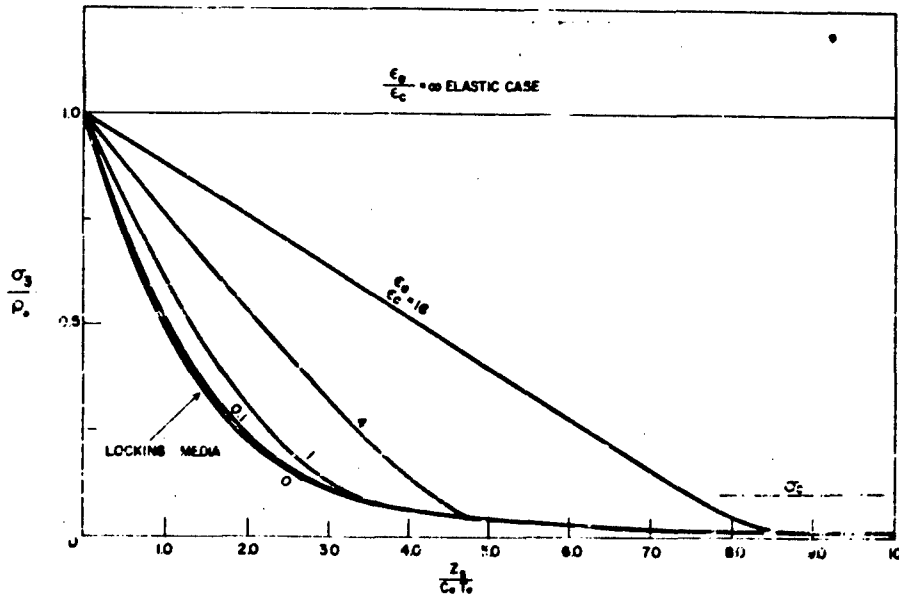


Fig. 9 - Results of computations for bilinear medium

This is derivable from Coulomb's law of failure and where σ_r and σ_θ are radial and tangential principal stresses, and c and k are constant characteristics of the medium. If cohesion is negligible, the expression simplifies to

$$\sigma_\theta = k\sigma_r \quad (22)$$

The spherical wave equation for this medium is given by

$$\frac{3\sigma_r}{r^2} + \frac{2(1-k)}{r} \sigma_r = -\rho_1 \ddot{w} \quad (23)$$

where \ddot{w} is the acceleration of a particle at a radial distance r . Closed form asymptotic short-time and long-time solutions of these equations are given in Ref. 16 for particular types of inputs. The stress at the wave front R is generally

$$\sigma_R = \rho_1 \cdot (1 - \gamma) R^2 \quad (24)$$

where the shock velocity R of the long time solution in case of an ideal gas explosion is of the form

$$R^2 = R_{\infty}^{-3\gamma} \quad (25)$$

where γ is a gas constant.

A second solution of interest is the case of an exploding point mass M with a kinetic energy of $1/2 M R_o^2$, which is given by

$$\dot{R} = \dot{R}_o \left[1 + \left(\frac{R}{R_o} \right)^3 \right]^{-\mu} \quad (26)$$

where R_o and μ are constants depending on the point mass and depending on the medium.

APPLICATION TO GROUNDSHOCK PHENOMENA

The analytical expressions which have been presented in the previous sections have been applied to various problems connected with groundshock phenomena:

1. Prediction of ground accelerations and displacements. In Ref. 13, a comparison has been made between predicted and measured

free field parameters obtained at Operation Plumbob. The results of this comparison indicate very good agreements with the accuracy of measurements.

2. The very high attenuation which is indicated by the analysis, suggests the use of dry, loose sand as a preferable site for deep underground shelters. The attenuation of peak stresses under ground zero of a very high yield burst is shown on Fig. 10, for two types of locking media.

We note that at a depth 500 to 1000 feet the stress in the medium decays to the order of 1000 psi; and we also observe (as predicted in the previous section) that this attenuation is nearly identical for materials where the critical strain at compaction is in the range 0.02 to 0.10. Further numerical computations indicate that the stresses due to reflection from an elastic rock layer (in which the shelter structure may be located) are also of a reasonable magnitude.

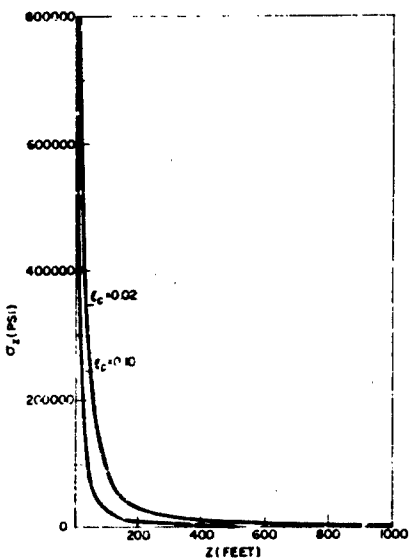


Fig. 10 - Attenuation of peak stresses under ground zero in cases of locking media and for very high yield burst

REFERENCES

- [1] Kumizi Pida, "Velocity of Elastic Waves in a Granular Substance," Bulletin of the Earthquake Research Institute, Tokyo Imperial University, Vol. 17, 1939, pp. 783-808.
- [2] Takehito Takhashi and Yasuo Sato, "On the Theory of Elastic Waves in Granular Substance," Bulletin of the Earthquake Research Institute, Tokyo Imperial University, Vol. 27, p. 11 and Vol. 38, p. 37.
- [3] H. Deresiewicz, "Stress-Strain Relations for a Simple Model of Granular Medium," Journal of Applied Mechanics, Paper No. 57-A-90.
- [4] C. W. Thurston and H. Deresiewicz, "Analysis of a Compression Test of a Model of a Granular Medium," ONR Project NR-064-388, Technical Report No. 27, Columbia University, Department of Civil Engineering.
- [5] Th. Von Karman and P. E. Dawez, "Propagation of Plastic Deformation in Solids," Proc. VI, Int. Congr. for Applied Mechanics, Paris, 1946.
- [6] M. P. White and L. Griffis, "The Propagation of Plasticity in Uniaxial Compression," Jour. Appl. Mech., Vol. 15, 1948, p. 256.
- [7] M. P. White and L. Griffis, "Permanent Strain in a Uniform Bar Due to Longitudinal Impact," Jour. Appl. Mech., Vol. 14, 1947, p. A337.
- [8] W. Prager, "On Ideal Locking Materials," Transactions of the Society of Rheology, Vol. I, 1957, pp. 169-175.
- [9] W. Prager, "Elastic Solids of Limited Incompressibility," Proceedings of the IX Int. Congress of Applied Mechanics, Brussels, 1957.
- [10] Aris Phillips, "A Theory of Ideal Locking Materials," Yale University, Feb. 1958, NR-064-415.
- [11] Aris Phillips and Asim Yildiz, "The Thick-Walled Howlow Sphere of an Elastic-Locking Material," Yale University, Dec. 1959, Nr 064-415.
- [12] Mario G. Salvadori and Paul Weidlinger, "Induced Ground Shock in Granular Media, Report No. 1," Report to the Space Technology Laboratory, Ballistic Missile Division, Mar. 1958.
- [13] Mario G. Salvadori and Paul Weidlinger, "Induced Ground Shock in Granular Media, Report No. 2" (U), Report to the Space Technology Laboratory, Ballistic Missile Division, Jul. 1958, CONFIDENTIAL.
- [14] M. G. Salvadori, R. Skalak, and P. Weidlinger, "Stress Waves in Dissipative Media," Transactions of the New York Academy of Sciences, Series II, Vol. 21, No. 5, Feb. 1959.
- [15] Mario G. Salvadori, Richard Skalak, and Paul Weidlinger, "Waves and Shocks in Locking and Dissipative Media," Journal of the Engineering Mechanics Division, ASCE, Apr. 1960.
- [16] Mario G. Salvadori, Richard Skalak, and Paul Weidlinger, "Spherical Waves in An Ideal Locking Media" (to be published).
- [17] Richard Skalak and Paul Weidlinger, "Attenuation of Stress Waves in Bi-Linear Materials" (to be published).
- [18] Paul Weidlinger, "On the Application of the Theory of Locking Media to Ground Shock Phenomena," The MITRE Corporation, 1960.
- [19] Paul Weidlinger, "Progress Report on Ground Shock at High Intensity Pressure Levels" (U), Consulting Engineer, Oct. 1959, The MITRE Corporation, SECRET.
- [20] "Vulnerability of Underground Installations" (Second Progress Report on Ground Shock Phenomena), The MITRE Corporation, Mar. 1960, SECRET.
- [21] Melvin Baron, Hans H. Belich, and Paul Weidlinger, "Theoretical Studies on Ground Shock Phenomena," The MITRE Corporation (to be published).
- [22] A. I. W. Ishlinskii and N. V. Sternanbo, "On the Dynamics of Ground Masses," DAN 1954, t. 95, No. 5.

- [23] A. I. W. Ishlinskii, "On the Plane Motion of Sand," Ukr. Mathematical Journal, 1954, t. 6, No. 4.
- [24] A. B. Kompaneets, "Shock Waves in a Plastic Compressible Medium," DAN, 1956, t. 109, No. 1.
- [25] E. E. Lovetskii, "Similarity Relations During An Explosion in a Plastic-Compacting Medium," I.A.N. 1958, No. 1, p. 120-122.
- [26] S. S. Grigorjan, "On the General Equations of the Dynamics of Solids," DAN, 1959, t. 124, No. 2.
- [27] N. V. Zvolinskii, "On the Emission of An Elastic Wave From a Spherical Explosion in the Ground," PMM, Vol. 24, No. 1, 1960, pp. 126-133.
- [28] A. N. Rojashov, V. N. Rodionov, and A. P. Sukhotin, "On An Explosion in an Inhomogeneous Compacting Medium," DAN, 1958.
- [29] E. I. Andrikian and V. P. Koryavov, "Shock Waves in a Variably Compacting Plastic Medium," DAN, 1959, Vol. 128, No. 2.
- [30] R. W. Whitman, "The Behavior of Soils Under Transient Loadings," Proc. of the Fourth Inter. Conf. on Soil Mechanics, and Foundation Engineering, Butterworths Scientific Publications, London, 1957.
- [31] R. W. Parkin, "Impact Wave Propagation in Columns of Sand," RM-2486, The RAND Corporation, Nov. 1959.

AN EXPERIMENT ON SOILS LOADED DYNAMICALLY

BY A SHOCK TUBE

Harold R. J. Walsh
AFSWC
Kirtland AFB, New Mexico

As a part of the program to develop improved methods for design of underground protective structures, the Air Force has been conducting a limited number of tests on soil samples using a shock tube as the dynamic loading device. The purpose of this paper is to describe the experimental techniques and procedures found appropriate for those tests, and also to describe the extent to which variations in properties of the soil samples were indicated by differences in the measurements made during the tests performed.

INTRODUCTION

Certain difficulties exist in any test intended to provide a measurement of the behavior of all soils under high dynamic loads. But, a test which demonstrated, even grossly, the differences in that behavior for soils of a wide range of properties might assist in the development both of better tests and of analysis methods, by providing a clearer view of the phenomenon. These tests were intended to investigate the experimental difficulties in the hope of making a clear view possible.

The difficulties arise largely from the fact that soil is a mass of particles, and so can to a considerable degree, both distribute applied forces, and deform, in three dimensions. As a result, soil can arch between the walls of rigid containers while undergoing the large strains of which it is capable. Also, it arches around and interacts with gages or structures buried in it, unless they have the same stiffness as the soil, both on every surface and in a volume sense; therefore, one would not expect a buried gage to read stress or strain directly. If the sample boundaries are given flexibility to prevent arching or friction, of course, the measurement of either stress or strain at a point on them is a problem even under static loads, as in the triaxial shear apparatus.

A further problem is that many soils, under the loads of interest, compact, or are deformed permanently. Therefore, they attenuate energy and cannot be expected to transmit a pulse unchanged. In combination with arching, interaction, and three-dimensional dispersion, this phenomenon makes it impossible either to predict the disturbance which will occur at a certain point; or to predict the response of a gage at that point, even if the disturbance were known; or from the observed output of a gage at any point to describe the disturbance felt by the soil. Thus, it would appear that no experiment could yield an analyzable reading, with a practical gage.

These experiments were designed to test certain assumptions concerning the difficulties described above which, if correct, would make possible tests with a more general application. The basic assumption was that a gage of given size and stiffness would always be affected by arching and interaction to about the same degree, whenever embedded in a soil sample of the same properties, or in different soil samples whose stiffness, in a bulk modulus sense, was approximately the same. Therefore, a method would exist to "calibrate" a gage for use in a soil sample of that stiffness provided the dynamic load were kept in the same range. Similarly, it was assumed that friction with

the container and arching between its walls would be reproduced in samples of the same properties, particularly in a relatively rigid container. Therefore, no attempt would be made to eliminate or to reduce the friction or the other boundary forces; instead, an attempt would be made to measure them, and from knowledge of the force-time history on all the boundaries, to describe the disturbance history at a particular point in the sample. In this way, the calibration for a gage at that point could be given real meaning.

The correlation of records of buried gage outputs with boundary forces would not be feasible, after a very short initial period, if the soil sample acted in a manner very similar to a linearly elastic body. The length of usable record, in that case, would depend on the sample size and wave velocities. After that time, the disturbance from the waves reflecting at the boundaries would so confuse the records at any point that it would not be possible to relate any later output to any boundary force. However, it was assumed that at least, the low-density soils would be loaded far beyond their elastic range, and the response would soon damp out, permitting, at least, correlation of integrated records on a total impulse basis; for this reason, a fairly long observation time was used.

It can be seen that the approach described, if the assumptions were correct, would permit study of the distribution of dynamic loads within the container of soil, and also within samples with different boundaries, by use of the calibrated gages. Also, even though it would not solve the arching and interaction about the gage used, it would permit use of those gages to study the phenomena near small structures in soil samples of any configuration. For either of these purposes, the soil samples would all have to be carefully prepared so as to be equal to those in which the gages had been calibrated.

APPARATUS AND PROCEDURE

The 6-ft shock tube has been shown in a series of previous experiments [1] to be capable of delivering an adequate and reproducible load to soil samples. In those tests, the piezoelectric gages embedded in the soil appeared to read forces in a systematic manner. Study of the apparatus and records did indicate, however, that there might well be disturbance of the soil container by the motions of the shock tube, upon which it was mounted.

It was decided, therefore, to manufacture a new container which would be mounted on supports independent of the shock tube motions and with a sufficient air gap to prevent contact. Also, the manner of mounting would permit instrumentation of the supports to read the container reactions. Eventually, the walls of the container could be instrumented with strain gages, if possible, in an attempt to measure the forces carried into them from the sample, by friction or arching. In this preliminary series of tests the reactions would be recorded separately as vertical and horizontal components, and the major overturning moment on the container. Piezoelectric gages would be buried in the samples, and others would monitor the air overpressure changes above the sample surface. The reaction records would be considered to be the response of the container supports to the gross sum of the forces exerted on the container by the soil sample. Together with the air monitor records, these would provide some measurement of the forces on all of the sample boundaries. In particular, to the extent that one could consider a plane wave to travel downward through the container, a comparison of the vertical forces on the sample to the output of buried gages, oriented vertically, would seem possible.

The shock tube that was used is 6 feet in internal diameter, and, at present, can be assembled to have a maximum length of 240 feet. The shock within it is produced by the explosion of prima-cord at one end; the energy released causes a wave of highly compressed air to travel down the length of the tube. The boundaries enclosing the traveling wave of air feel a very sudden rise in pressure, to some peak value, followed by a slower exponential decay. In these tests, the charge was adjusted to give chosen peak overpressures in a range from 2 to 50 psi. Normally, the rise time was much less than 1 msec, and the decay time was about 0.050 sec. Unfortunately, because of objections to noise in its present location, the shock tube had to be operated with both ends closed. As a result, the shock reflected back from the closed end, somewhat attenuated, reaching the test section 0.125 to 0.200 sec after initial shock arrival, depending on tube length. The second shock shows as a second, lesser peak on the records; such reflections, of course, continue until the energy has been dissipated.

In the test section of the shock tube, a circular access hole for mounting models was cut through the outer shell and the level testing

floor. A cylindrical shield was welded between the floor and shell, to prevent sticks from hitting the sides of the models. The container and its mounting system were designed to provide the largest sample which, when mounted in this hole, would be isolated from the tube motions by an air space between it and the shield. Also, all parts which would move with the soil sample were kept light in weight, to reduce the importance of inertia effects in the response. To permit the future use of strain gages on them, the walls of the container had to be rigid, but thin and not stiffened.

All of the above criteria resulted in the development of a cylindrical container with approximate internal dimensions of 23-1/4-inch depth and 17-1/4-inch diameter. The bottom, a circle, was cut from 1-1/2-inch-thick aluminum plate. The side walls were of 1/8-inch-thick aluminum sheet with all of the seams welded.

The container weighs 57 pounds and holds a soil sample, 3.14 cubic feet in volume with a 234-square-inch surface. Figure 1 shows the container arranged in the shock tube. Mounted on beams spanning the foundation of the shock tube, it has about 1/2-inch clearance from the shield.

Four rounded steel bars support the container and are instrumented with strain gages to record its reaction; they are bolted rigidly into the container bottom plate and their bottom ends are also bolted rigidly into a 1-1/4-inch aluminum base plate.

The base plate provided a rigid assembly for complete calibration outside the test location, and its instrumentation could be thoroughly checked, without the necessity of disturbing it in any way during installation. The supporting bars or legs consist of 7/8-inch-diameter, high-strength steel ground to close tolerances. The unsupported length of the legs was about 5-1/2 inches between the base plate and the container bottom. The leg height was adjusted in assembly to make the top surface of the container flush with the flat testing floor of the shock tube.

The two steel beams which bridge the foundation of the shock tube itself are each 6 inches deep and weigh 25 lbs per ft. Their ends are bolted to bearing plates which rest on the concrete floor of the building. Since these beams are 12 feet long, their bearings are outside the joints which separate the 10-feet-wide, shock-tube foundation from the

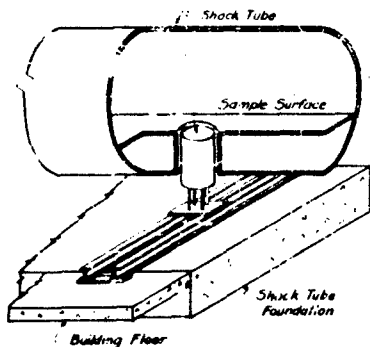


Fig. 1 - Arrangement of the container in the shock tube and the foundation

building floor. The container assembly is clamped to the bridge in the middle, on top of a 2-feet-square, 1/2-inch-thick steel plate which covers and is fastened to the top flanges of the two beams.

TESTS

The tests were recorded by photographing oscilloscope displays of gage outputs. Several combinations of recording cameras, amplifiers, and oscilloscopes were available and were used to give eventually a maximum total of 16 channels. The records, however, occurred in three different scales of time to amplitude because some channels used drum cameras and others used two sizes of normal cameras. It should be noted, therefore, that the task of obtaining a full set of records from a test, with each channel in correct calibration, remained a problem. The most important instrumentation items in the experiment were the gages buried in the soil sample—small piezoelectric gages—the same as those used by Durelli in earlier experiments [1]. These gages actually are cylindrical crystals mounted in a short metal tube about 3/8-inch wide and deep so that they read forces on the end surfaces, primarily. The gages had been calibrated previously by exposure to a known shock in air. All the gages were mounted on the center-line of the soil sample at varying depths below the surface, with their sensitive faces oriented to read forces in the vertical direction.

The legs, or bars, supporting the container, were instrumented with strain gages to read the reaction in both the vertical and horizontal directions. The strain gages which

read the axial force on each leg were assembled to eliminate the effects of moment or of temperature on that leg. The gages intended to read horizontal forces, were actually assembled to respond to bending moment on the leg only. These gages were calibrated with a known, static, horizontal force.

The air shock passing over the soil sample was recorded by additional piezoelectric gages mounted in the shock tube wall. Two gages were located, with their surface flush with the inside surface of the shock tube, immediately to the side of the soil sample.

Tests of two different soil types are discussed herein. One was a silty clay with a liquid limit of approximately 30; the other, Ottawa Sand, was between the 20-30 sieve sizes. With each, several densities and moisture contents were used.

Since the major purpose of the experiment required that the properties of each sample tested be thoroughly known and be uniform throughout the sample, care was taken in placing the samples in the container and in measuring their properties. To insure uniform moisture contents, the samples were carefully mixed before placing, and the moisture contents were measured. The samples were placed in layers of known weight and each layer was tamped with a specified number of blows by a hand-operated, dropped-weight tamper, specially built to suit the container dimensions and the soil types to be tested. The tamping blow was caused by a 5-pound weight dropped 12 inches, with the surface contacting the soil having an area of 12 square inches rather than the smaller base of standard tampers. For some samples, intended to have low density, no tamping was used. The elevation of the soil surface was measured, after placing each layer, to permit calculations from which the uniformity of the whole sample could be estimated. After a test, the sample was unloaded also in layers of measured thickness, and the weight and density of each layer taken.

In addition to the soil tests, some tests were run with specially cast concrete cylinders instead of the soil and container. The three cylinders were made of varied-density concrete for the intended purpose of providing a total weight on the supporting beams covering the major portion of the soil test range. The blocks provided a complete system which remained essentially linearly elastic. The purpose of these tests was to obtain information for developing a mathematical model for the soil by analysis of reaction records.

CONTAINER REACTIONS

Records of the strain-gage response to the axial force in the legs of the container on three separate tests are shown on Fig. 2. These records are grouped because certain test conditions were fairly comparable. In each test, the overpressure exerted by the shock in the tube was 20 psi, and the total weight of the sample and mounting assembly supported as a dead load on the isolating beams was nearly equal. In Test 1378, the container held 307 pounds of loose, dry Ottawa Sand; with the mounting plates and legs, the total weight was 564 pounds. In Test 1379, the container held 311 pounds of dry silty clay which had been compacted by 25 blows of a compacting hammer on each of its eight layers, and the comparable total weight was 568 pounds. Test 1461 was performed on one of the concrete cylinders which with its special plates and the legs gave a weight of 562 pounds for the comparable part of the responding system. Since the dynamic load and the mass in the system were the same, it was expected that differences between these reactions would be caused by differences in sample properties alone.

Figure 2(a) shows the recorded vertical reaction for a rear, or downstream, leg of the container in each test, and Fig. 2(b) shows similar records for the upstream legs. In each case, the record covers a length of time sufficient to include the arrival of a second air shock reflected back from the closed downstream end of the tube. Since both ends of the tube were closed, similar shocks of repeatedly reduced strength continued to pass the sample until the air shock had completely attenuated, but records were kept over the period of the first two arrivals only as shown.

A major difference, between Shot 1378 and the other two records which more nearly resemble each other, is obvious. The flatness of 1378, after about the first 50 msec, indicates that the large-amplitude response of the system has stopped, although it did not do so on the other two. Since the Ottawa Sand was placed as loosely as was practical, it was very weak in comparison to the tamped silt and even weaker when compared to the light-weight concrete. The difference appears to demonstrate that weak soils have good damping and energy-absorbing ability as they rapidly damp the large-amplitude motions of the system, whereas stronger materials continue to be subjected to large harmonic motions for some time. This damping ability was consistently demonstrated throughout the program,

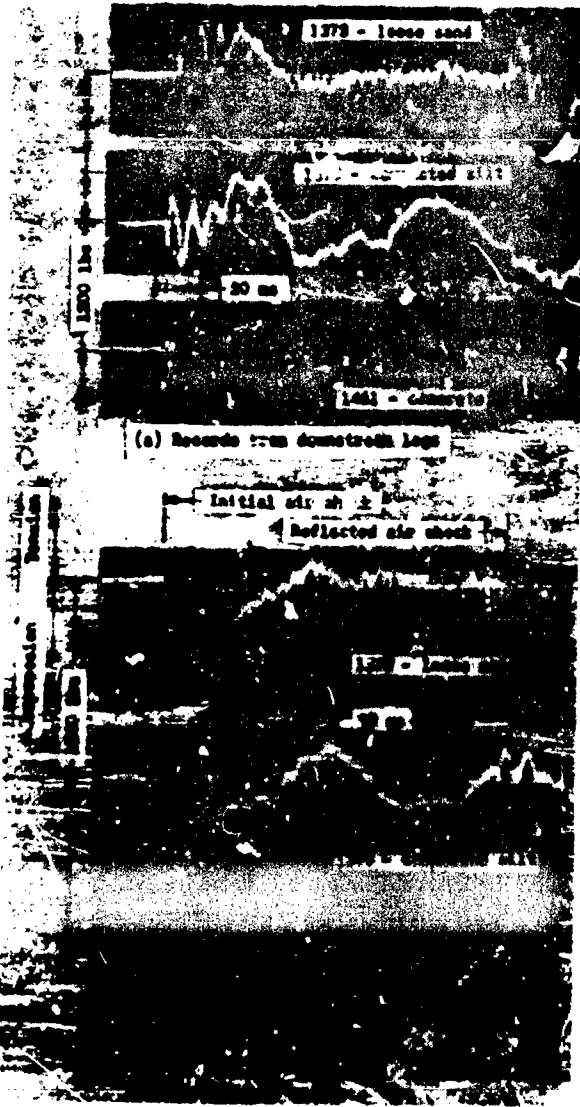


Fig. 2 - Vertical reaction: different materials, same weight

whenever the sample was weak in relation to the chosen overpressure.

Separate records of each leg were kept—as in the tests just described—for the purpose of checking instrumentation system failures in each leg. As a result, several modes of response of the system are combined in the records. One motion is a rocking of the entire container, similar to a cantilever bending at its base, in a vertical plane perpendicular to the front of the passing shock; in this motion, a forward leg will be in compression while the rear one is in tension. The rocking is apparent in two modes: a slow one with a period of about 75 msec which corresponds reasonably well with a motion in which everything is rigid except the two supporting beams bending vertically out of phase with each other; and a faster one, with a period of about 3 msec, in which the strains would be considered to be limited to the legs, the beams being assumed rigid. Another major mode would be described as a vertical bouncing of the entire container in which the supporting beams bend in phase again, with a period of about 75 msec. The periods quoted are those observed on records, rather than calculated values. Calculation of these values can, at best, indicate a range, depending upon the degree to which the ends of the beams are considered fixed and the values given do fall within the appropriate range.

It will be noted that during roughly the first 40 msec of these records, there appeared to be a moment tending to overturn the container upstream. That is, the upstream leg was in compression and the downstream leg was in tension. This will be discussed later.

The records (Fig. 2) cover only half the supports of the container. However, they do indicate the entire vertical reaction, since the records of symmetrical legs on any test usually have reproduced each other closely. The close similarity between the records for the corresponding legs indicates, among other things, that rocking of the container was negligible in the transverse direction, at least in comparison to the rocking in the direction of shock travel.

A high degree of reproducibility was achieved between separate tests in which the soils samples and shock loading were the same. Thus, Fig. 3 shows superimposed reaction records for Shots 1411 and 1421. For each of these tests, the container was filled with moist clayey silt compacted by 200 blows on each of six layers. In Shot 1411, the

moisture content was about 10 percent and the wet density was 105.2 lb per cu ft before the shot as against 9 percent and 104 lb per cu ft in Shot 1421. The overpressure was recorded as 19.4 psi on 1411 and 19.0 psi on 1421, but this difference appears to indicate the accuracy of this measurement rather than a real difference in the loading. The two sets of reaction records can be seen to correspond, even on a point-to-point comparison over most of their length, and have no significant difference.

The discussion (just presented) relates only to the vertical reaction or records of the axial force in the supporting legs. An attempt was also made to measure the horizontal reaction. This approach consisted of reading the sum of the moments on the top and bottom of each leg by strain gages, and interpreting this as a horizontal force. To obtain a calibration for this reading, the same values had been read with a static horizontal force exerted against the upstream side of the container.

The records achieved a reproducibility comparable to that of the vertical records, and they were useful for detecting disturbances of the container by motions of the recoiling tube. Usually the records indicated that no such disturbance existed, but in this case, the horizontal force on the soil surface, caused by the passing shock, cannot be determined from the records. These records indicate a horizontal impulse of the same order as the vertical but exerted on the soil in the direction opposite to that of shock travel. At first, this might seem so unreasonable that the assumptions upon which the calibration was based might be assumed wrong. Under the combined vertical and horizontal loads of the test, the deformation of the legs might be thought greatly different from that in the calibration. If the pattern of deformation is different, of course, then the sum of the moments could bear a different relation to the horizontal force. The reproducibility of the records, pertaining to tests with the same soil and load, is shown in the records of Shots 1421 and 1411 (Fig. 4). These two tests were conducted under similar conditions, and the vertical reactions of both tests are shown in Fig. 3. A comparison of the leg outputs shows reproducibility comparable to that of the axial force gages in the same tests.

It will be noticed, however, that the records indicate that the shock caused a horizontal force pulling the sample and its container upstream. This is in agreement with the direction of the overturning moment noted

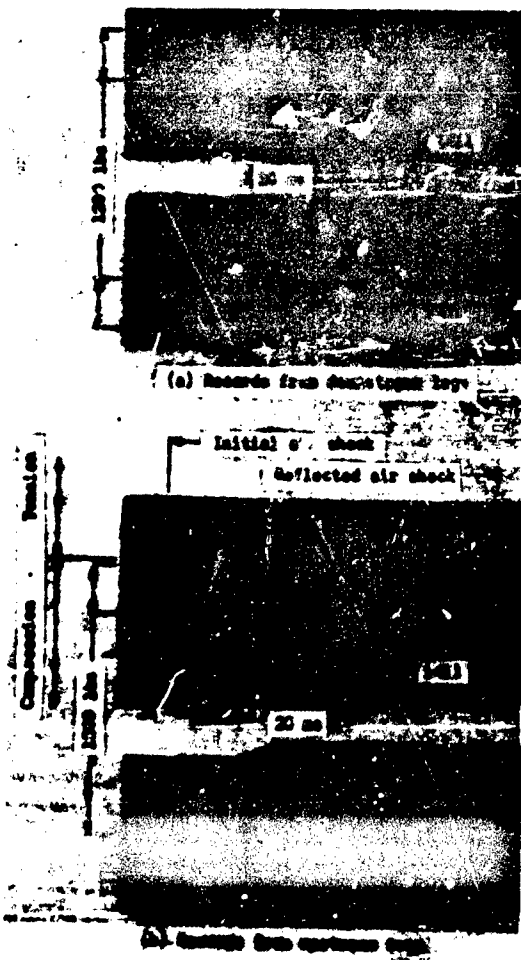


Fig. 3 - Vertical reaction: two samples
of th. same properties



Fig. 4 - Horizontal reaction: two samples
of the same properties

in the axial force records, presented earlier. Both of these observations would be consistent with a theory that the passing air shock builds up a pressure in the space between the container and the tube shield which is greater downstream of the sample than upstream. According to the knowledge of the manner in which air shocks reflect from surfaces opposing their direction of travel, such a difference seems to be quite possible, although no attempt to measure it was made. As further support, both the horizontal force and the moment seem to change little between tests on different soils at the same over pressure.

In the form so far presented, the reaction records could not be directly compared with the records of the buried gages or of the air-shock gages. Because they are response

records for such a complex system, they cannot be compared to the initial air shock loading at all on a point-by-point basis—only on a total impulse basis. A comparison with the records of the buried gages on a point-by-point basis would seem more valid, since dynamic forces exerted on any part of the container should cause a signal on the buried gages. However, it appeared that the vertically oriented buried gages showed effects related only to the total sum of the vertical leg reactions in the test performed. Therefore, the records of the separate legs need to be added vectorially, so as to eliminate the signals due to rocking and to be easily comparable, point by point, to the buried gage records. In addition, their sum was integrated to obtain total impulse.

Because of the harmonic nature of the record, this integration was carried to the quarter points of the major period of steady-state motion, after loading was completed, at which times the velocity of the masses concerned should be zero. Originally, some summations and integrations were done manually, and with a planimeter, as a rough check. Later, the wiring was changed to read the sum of one front and one rear leg on one channel, the other pair still being read separately as a check on instrumentation failures. To improve accuracy and also to reduce the drudgery, a computer program was used eventually to sum and integrate a number of these records. The integrated total impulse of the vertical reaction for a number of records, obtained from the computer program, was compared to the same quantity measured with a planimeter from the air-monitor record from that same shot. It demonstrated satisfactory agreement, especially considering that the air-shock record did not lend itself to precise measurement. On this basis, the reaction records must be considered to indicate the instantaneous value of the forces between the container and its support as well.

RECORDS OF BURIED GAGES

Figures 5 through 7 are records of the output from piezoelectric gages buried in soil samples. These records include the output of a piezoelectric air-pressure gage, mounted near the sample and a timing mark. The difference in appearance and in time scale from the reaction records is because the records were obtained by drum cameras. It will be noticed that the portions reproduced cover a shorter total time of observation and do not include the time of arrival of the reflected air shock.

The first records in Fig. 5(a) and (b), Shots 1297 and 1299, show the effects which can be caused by the manner in which the wires leading to the buried gages are arranged within the soil mass. In each case, dry silty-clay soil was placed and compacted to give roughly the same low density. Both were rather weak samples. The shock overpressure in each case was about 20 psi. The principal difference is that in Shot 1297, the gage leads were standard, shielded, plastic-covered, two-conductor cable, whereas in Shot 1299 the leads to each gage were two thin wires, insulated but not shielded. Within the soil mass the two wires were spread apart several inches, meeting only at the gage body and at their entrance through the container bottom.

On Shot 1299, the major outputs of the buried gages can be seen to occur during the period when the air-shock records indicate the sample surface is loaded. Also, the typical vertical leg forces for such weak soils (Fig. 2) show significant response only during the period when the buried gages show an output similar to the output in Shot 1299. The buried gages in Shot 1297, however, show significant outputs which cannot be compared to these boundary forces. No other method of wiring gages within the soil sample was found to give comparable results; therefore, thin spread leads were used on the piezoelectric gages during the rest of the test reported. Buried gage records (Fig. 5(c) and (d)) are for Ottawa Sand samples, compacted by about the same effort while at a 1.67-percent moisture content. The gage calibration (Fig. 5(c)) was approximately the same as Fig. 5(a) and Fig. 5(b) while Fig. 5(d) was at a much higher sensitivity. The Ottawa Sand records show the same lack of later outputs as Fig. 5(b), although, being soils of different properties, the shape of the output differs from Fig. 5(b).

An explanation can be given for the production of spurious signals from close-spaced wires leading to piezoelectric gages. These gages have a high impedance (that is, their output under load is a very small current and, in effect, they appear to the recording system somewhat similar to a condenser of high value). The wires leading to the gage, provided they are at all parallel, also act as a condenser, of a value similar to that of the gage. Pressure of the soil sample upon the length of the pair of wires buried within the soil, considering the large strains of the soil under dynamic load, can cause a change in spacing of the two wires, and so a change in capacitance between them. It appears that when the wires are within a single cable or twisted together, the change in capacitance can be large, as compared to their total capacitance, and can cause an alteration of the circuit characteristics, comparable to that produced by the gage output. When the wires are more widely spaced, their capacitance is much greater and the capacitance change, under the same wire movement, produces a negligible change in circuit value and so a negligible signal.

An additional reason for preferring the widely spaced thin leads is their lack of stiffness. Shielded cables, or even a twisted pair of the thin wires, have a significant longitudinal and bending stiffness as compared to the separate thin wires. The leads, buried in the soil, are laterally confined which causes their

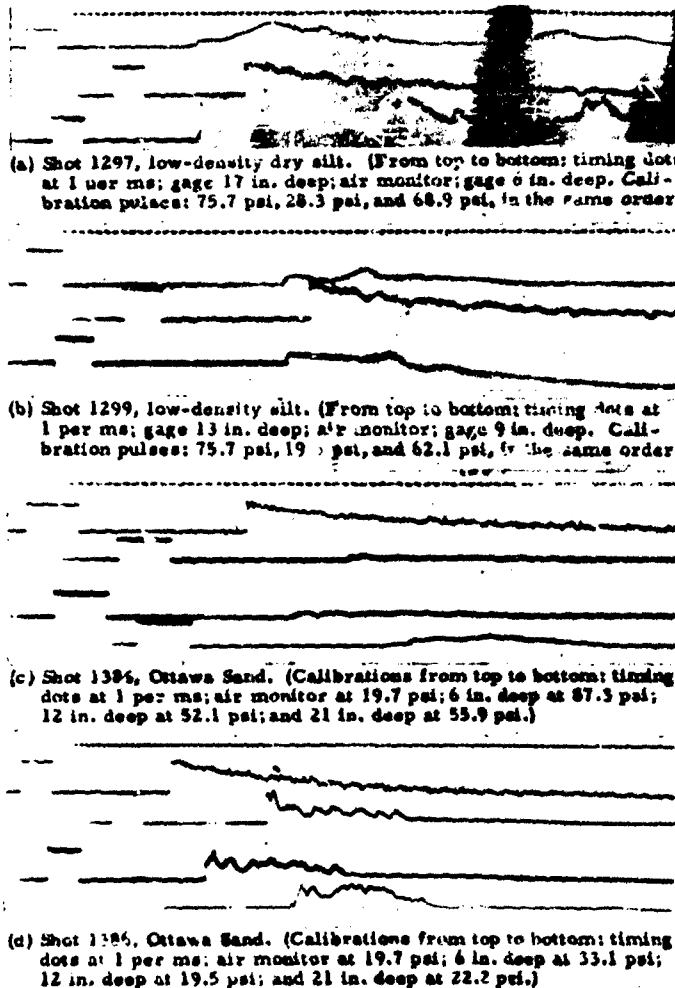
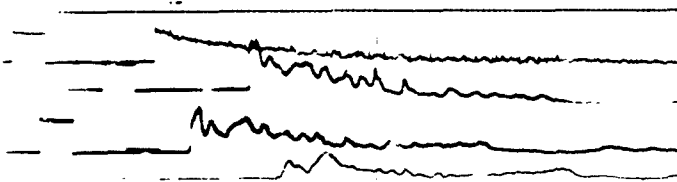
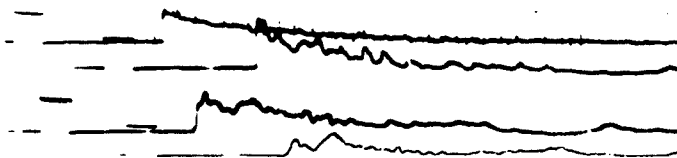


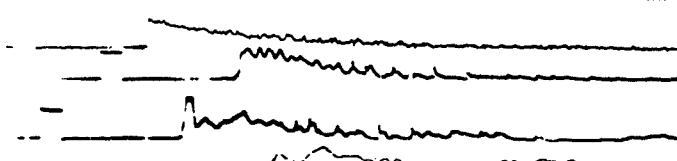
Fig. 5 - Buried gages in several samples.



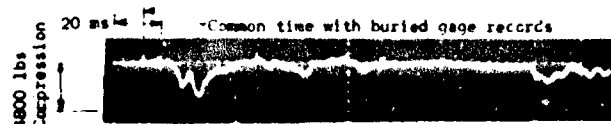
(a) shot 1392, dense silt, 5-percent moisture. (Calibration from top to bottom: timing mark at 1 per ms; air monitor at 19.8 psi; 6 in. deep at 20.3 psi; 12 in. deep at 20.4 psi; and 21 in. deep at 29.6 psi.)



(b) Shot 1393, dense silt, 5-percent moisture. (Gage calibrations were the same as for Shot 1392 but located 5-1/2 in. deep, 11 in. deep, and 21 in. deep.)

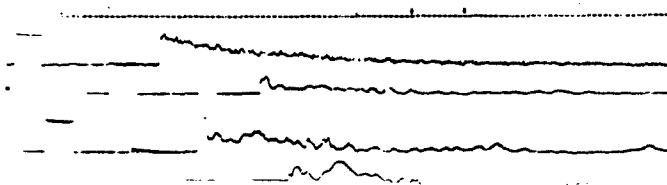


(c) Shot 1408, dense silt, dry. (Calibrations from top to bottom: timing mark at 1 ms; air monitor at 19.2 psi; 4-1/2 in. at 46.0 psi, 12 in. at 34.8 psi; and 21 in. at 37.2 psi.)

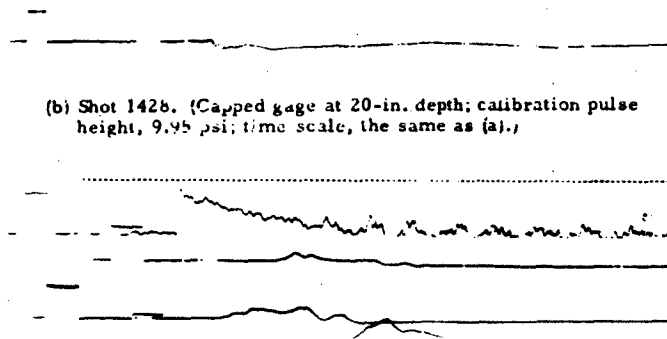


(d) Shot 1392. (Record of sum of vertical forces on an upstream and a downstream leg.)

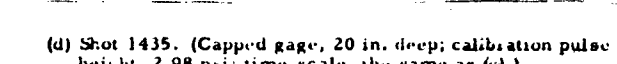
Fig. 6 - Buried gages in similar samples



(a) Shot 1428, dense silt, 15-percent moisture. (Calibrations from top to bottom: timing mark at 1 per ms; air monitor at 28.9 psi; 9 in. deep at 59.7 psi; 14 in. deep at 40.9 psi; and 20 in. deep at 40.9 psi.)



(b) Shot 1428. (Capped gage at 20-in. depth; calibration pulse height, 9.95 psi; time scale, the same as (a).)



(c) Shot 1435, loose dry Ottawa Sand. (Calibration from top to bottom: timing mark at 1 per ms, air monitor at 5.76 psi; 6 in. deep at 16.28 psi; 12 in. deep at 14.0 psi; and 20 in. deep at 15.5 psi.)

(d) Shot 1435. (Capped gage, 20 in. deep; calibration pulse height, 2.98 psi; time scale, the same as (c).)

Fig. 7 - Buried gages and capped, buried gages in different soils

stiffness to be greatly increased. Therefore, the leads tend to act as elastic supports, fixing the gage location relative to the point of anchorage of the leads. The ideal gage would be one that merely floats in the soil and possesses outputs related only to the stresses in the soil immediately surrounding it; no movement of the gage relative to the soil would be caused by support of the leads, either during first passage of the wave or during later efforts of the lead to elastically rebound. The use of separated thin wires, allowing a convenient amount of slack and therefore random bends, provides the nearest arrangement to a floating gage, and therefore an output caused more nearly only by the forces in the soil at the gage location.

The extent to which gage outputs are reproduced at like points, in like samples, is shown in Fig. 6(a) and (b). These records are from buried gages in samples, prepared with similar properties, as nearly as possible, and loaded by similar overpressures. In this case, the records have exceptional similarity; even minor differences are hard to find. Each of these samples, consisting of silty clay with a moisture content of about 5 percent, was compacted to nearly the maximum attainable density (200 lb/ft³ for each of the six layers). Also, Fig. 6(c) shows similar records for Shot 1408, a similarly compacted silty clay that differed only in that the clay was dry. The records for Shot 1408 are noticeably different, showing that only a small change in soil properties is enough to cause a change in the gage readings.

Figure 6(d) shows the electronic sum of the vertical reaction response for two legs (the same as test Fig. 6(a)). As these highly compacted samples are relatively strong, they provide less damping, as can be seen from the continuing peaks. Outputs from the buried gages on these shots will also be observed, after the air-shock has decayed. The time of these later buried gage outputs can be shown to compare reasonably well with that of the late response peaks, by measurement in accordance with the different time scales. Thus, it can be seen that these gages, when oriented to read vertical forces primarily, are affected by forces exerted on the soil at either its top or bottom boundary. This peak force, produced by the response of the supports, might be called a major reflection and demonstrates the use of the reaction measurements in interpreting the buried gage records. Even in such small containers, therefore, one cannot say that reflected waves will confuse the records to the point of making them unintelligible—

provided a system of measuring forces on boundaries is used. By this statement, of course, it is not meant that stress conditions within the sample are not changed, after a few milliseconds, by the fact that the boundaries are present, but only that these changes seem to be rational.

As had been noted in the earlier tests [1], the outputs of the buried gages alter systematically with depth in the soil. The alteration is most noticeable as an increase in rise time from the near shock, observed at the upper gages, to a finite value of nearly 1 ms at the lowest. As seen in the figures, this change was much greater, at the same depth, in samples of lesser compaction, or weaker soils.

Some comment is appropriate on the lack of smoothness of these records. It might be felt that the small variations are caused by the arrival of reflected waves from the boundaries. However, the first change is a reduction from the initial peak, whereas the arrival of a wave from a fixed bottom boundary would cause an increase. The major reflection, discussed earlier, indicates that the output of the buried gage will be positive whether a compressive force is exerted on either the top or bottom of the sample. Arrival times also are such, that this could not be a tensile wave reflected back from the soil surface. Neither does it coincide with the frequency of the fluctuations apparent in the air monitor record. Instead, these changes may be caused by momentary failures in the arching of the soil close to the gage. That is, the force being carried by this arch to the gage builds up until the arch fails, probably in shear; then, after small slippage, the arching is again effective, then again fails, and so on. However, acceptance of this theory requires one to accept that this failure—which might be expected to be rather random in a structure made of soil grains—happens in a very systematic way, because of the reproducibility evident in these details in Shots 1392 and 1393. Again, this reproducibility might support the belief that these are reflected waves, except that the gages were not at exactly the same location on the two tests.

PRESSURE IN VOIDS

In several tests, an attempt was made to observe pressures in the soil voids. The purpose was to determine the extent to which the air shock was propagated through the bonds, air or water, which occupy the pore space. Typical results are shown in the records of

Shots 1428 and 1435 in Fig. 7. For Shot 1428, an overpressure of 30 psi was imposed on a sample of silty clay which had been compacted by 200 blows on each layer at 15-percent moisture content. For Shot 1435, a sample of dry Ottawa Sand was placed at the loosest density practical and loaded by 5 psi.

In neither soil was a shock demonstrated on the capped gage; in fact, the pressure changed only a few psi at the most. The outputs shown are actually a combined result of several effects—the pressure changes in the voids, the movement of the gage leads, and the internal forces in the gage, created by its acceleration in moving with the soil around it, as well as perhaps others which are not understood. The combination of such effects may result in the apparent negative appearance of the output on these records. In any case, such a gage was used in several tests and always gave an output of about the magnitude shown, positive or negative, but very small, except in a test using crushed rock in which it went off scale at the same calibration.

This result is important to the design of underground structures. If the air shock had been found to penetrate the voids, then structures would have to be designed for the full surface overpressure because the soil overburden could not alter the force felt by the structure in any way. Also, the overpressure could not be considered a dynamic surcharge for determining the stability of footings, for example. Obviously, such a condition would make worthless these experiments, or any other experiment using an air-shock as a loading mechanism directly upon the soil surface. In an informal conversation, personnel of the United Kingdom's Atomic Weapons Research Establishment had reported such a result, but the air pressure over their sample had a rather long rise time.

The outputs of the usual uncapped buried gages on these tests also are shown on Fig. 7. In each test, the capped gage was located at the depth of the lowest uncapped gage, and it can be seen that the disturbance arrives at both gages at very nearly the same time. This also indicates that the air shock does not travel freely through the soil voids. The records from the normal uncapped gages are consistent with the earlier discussion.

STRAINS OF SAMPLE

No instrument for making a direct measurement of the pattern in which the sample

strained throughout the time of loading was used. However, certain information of an indirect nature was obtained, including the time of arrival of the disturbance at the successive buried gages, locations of the buried gages before and after tests, the pattern of compaction changes in the samples after testing, and high-speed motion pictures of the surfaces of a few samples during shock passage. When considered together, these present a qualitative history of the motions in samples, particularly those which compacted significantly.

Figure 8 shows the extent of compaction of two silt samples after testing. One of these samples, Shot 1393, was highly compacted initially, and therefore its surface was down only approximately 3/4 inch after a 20-psi loading, during which 3 pounds of soil were lost by erosive action. The pattern of density changes could not be detected in it by the methods used, as was the case with most soils of higher initial strength. The other sample, Shot 1402, however, was a very loose silt, screened into the container while at 15-percent moisture content. It was originally at a dry density of 53 lb per cu ft; after the 5-psi test in which it lost slightly more than 4 lb of soil, it had been compacted to an average dry density of 62.1 lb per cu ft with its surface down nearly 4 inches as shown in Fig. 8. Naturally, if the stronger soil of Shot 1393 had only been subjected to 5 psi, its permanent compaction would have been only about 1/8 inch, and many strong samples showed no measurable deflection under such low loadings. Also samples similar to Shot 1402 were depressed as much as 11 in. under a 20-psi load. In many tests, soils of such weakness were used to demonstrate the phenomena accompanying large compaction.

The buried-gage records obtained in these experiments appear to exhibit generally low velocities of wave travel. The time of arrival of the initial signal at each gage can be measured quite accurately from the common time of the calibration pulse, or from the later break in each record which also serves as a time mark on the reaction records. From the differences in arrival times and in depth, one can calculate a velocity for the travel of the first disturbance from the upper gage down to the next. Values so calculated appear to be quite low, at least in comparison to published seismic velocities for similar soils under the usual low-energy loading used for such measurements. Typical values, from the records shown in the figures, range from slightly less than 200 fps in Shots 1297 and 1299, to perhaps 750 fps in Shots 1392 and 1393. Even slower

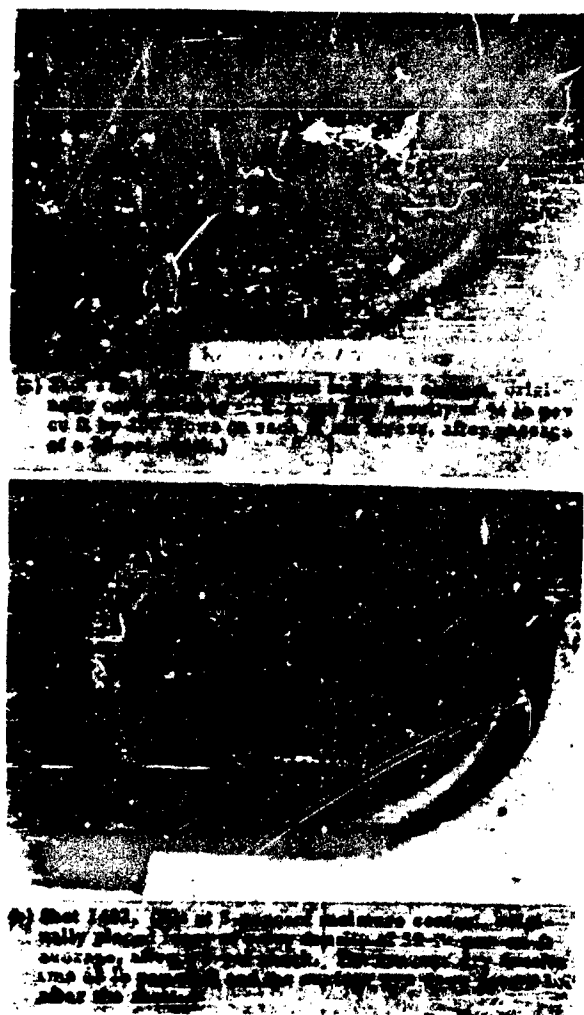


Fig. 8 - Soil samples after testing:
(a) Shot 1393 and (b) Shot 1402

velocities would be obtained by calculation of the time of the first peak on the successive gage outputs, of course, because of the increasing rise time. The formation of the first peak probably is related to the time required for development of arching in the soil near the gage; this process may require a different length of time from the rise time of the wave front itself. The measured velocities agree with theory in the sense that they are higher in stronger samples; however, they appear to be lower in a given sample, if the overpressure is increased. The least that might be inferred is that no value of wave velocity or of a modulus of elasticity, measured for a certain soil at a low stress level, can properly be used to predict its behavior at a higher stress except in a relative manner.

The velocities found from the buried-gage records were confirmed by similar calculations from the vertical reactions. The reaction records, after the first few tests, were marked by a time pulse common with the other channels. The records of axial force on the individual legs show a strong output almost simultaneous with the air shock arrival time. However, this early output appears to be caused by an overturning moment rocking the container and it nearly vanishes when the separate leg records are added. The starting time of significant response in the sum of the axial forces on the legs, usually coincides well with the travel time of the wave down through the soil as measured by buried gages on the same leg. This fact also indicates that the first impulse imposed on the surface of the soil sample travels through the soil to the container bottom, rather than being transferred by friction and arching into the walls which carry forces at much higher velocities.

Moving pictures of the sample surface were made to observe erosion of the sample surface by the shock passage, as well as the surface motion. As mentioned earlier, all samples lost some weight during the test. Losses ranged from less than 1 pound, to perhaps 10 pounds in extreme cases. In Shot 1451, a fairly good movie was obtained at a speed of approximately 3500 frames per second, lasting from before the initial shock arrival until after passage of the first reflected shock. The soil sample was the silt, at 15-percent moisture content, placed in the container loosely by being forced through a 1/8-inch mesh screen. Initially, then, it had a slightly lumpy structure and an average dry density of 52.5 lb per cu ft. After the test, it had lost about 1-1/4 pounds and had an average dry density of 64 lb per cu ft. caused by a

5-psi loading. It was very similar to Shot 1402 discussed earlier. No erosion or cracking of the soil surface appears to have occurred during the passage of the initial shock. Instead, the surface remained intact and started downward, and all areas seemed to move together. The motion was not at a constant velocity, but irregular, appearing to almost pause every few milliseconds. However, it did not appear to reverse. Approximately 0.050 sec after initial shock arrival, the surface was level and appeared to be about 2 inches down from its original position. The surface then appeared to explode, erupting up and out from the container to a height of perhaps 1 foot as a cloud of fine particles, not as a layer or as lumps; this apparently is caused by the rebound of the supports, inducing in the sample a compressive wave which, to reflect at the surface, requires a tension which the soil cannot support. Because the air shock has already passed, the cloud of soil is not swept away but hides the surface for nearly 100 msec. After that time, the cloud had settled and most of it apparently had landed in the container, leaving a surface which was level and at a depth of about 3 inches, but rough. At this time, the reflected air shock arrived and the downward motion of the surface resumed or continued, lasting from then until the end of the film. After the test, the soil surface was found to be about 4-15/16 inches below the original level.

Measurement of the locations of buried gages, during filling and emptying of the container, were quite consistent. In Test 1451, described earlier, two gages at 20-1/4 inches depth were found not to have moved at all. One at 12-3/8 inches was found at 12-11/16 inches and one at 8-3/8 inches was found at 11-3/4 inches. In general, all gages were usually found in their original orientation except occasionally the uppermost, which when very close to the surface was sometimes found tipped. In tests on all types of soils, however, the gage displacements agreed with a definite pattern of compaction, in which the upper part of the sample was greatly compacted, and the lower parts hardly at all.

The measurements of density changes in the sample showed a similar pattern. Unfortunately, those for Shot 1451 are unreliable; it appears that the lower layers may have been more densely compacted during filling. In a great number of other tests, however, in which the sample had initially been at a dependable uniform density it was found after the test that the density at the surface was slightly greater; that the density then increased with

depth down to a shallow depth, at which the densest layer was found; and that below that layer the density decreased with depth to a fairly uniform value only slightly above the pretest value. In soil such as that used in Shot 1431, the dry densities in percentage of the initial would be about 105 percent for the top 3-inch-layer, 110 percent for the next, 120 percent for the next, 110 percent for the next, and 105 percent for the lower half of the sample.

The density changes in Ottawa Sand followed the same pattern, except that the increase was not as great and the depth to the densest layer was less. Thus, Shot 1435 on dry Ottawa Sand—placed loose through a funnel held close to the surface at an average density of 98.9 lb per cu ft—was quite uniform. After a 5-psi test, the surface was down 3/4 inch; a gage at 8 inches, 1/2 inch, a gage at 12 inches, 3/8 inch, and the gages below that in their initial location. The densities, in percentage of the 98.9 lb per cu ft pretest density, were 107 percent in the top 3-inch layer, 103.5 percent in the next 3 inches, and about 102.5 percent for the remainder.

From the gage displacements and the pattern of compaction, one can visualize a history of strain in the sample which is consistent with the motion picture described earlier. During the first shock loading, the soil surface moved downward—largely because of compaction which was greatest near the surface. After passage of the first shock, in some samples only, this initial compaction was destroyed by a rebound of the entire container on its supports which caused a compressive wave to reflect in tension from the surface. After the material had fallen back into the container, the compaction was partly restored by passage of succeeding air shocks. In some samples, because of a different response of the supports, the initial compaction pattern may not be disturbed, of course. A planned relocation of the facility to have the end open, should eliminate the reflected shock; also, the mounting can probably be improved.

to eliminate the disturbing rebound. Under such conditions, a more accurate study of the strains and compaction pattern should be more rewarding because it can be related to a single shock passage.

CONCLUSION

Analyzing the test results, the behavior of the soil samples did not demonstrate those features usually prominent in bodies which had remained linearly elastic. In particular, the wave velocities seemed rather low, and the reflected waves from the boundaries were not observable.

Although the soils used in the experiments described were not typical of desirable construction materials or of those found at desirable sites, it is believed that the experiments demonstrated behavior which may occur in all soils under dynamic loads. In the case of the more desirable and stronger soils, however, the intensity of loading would need to be much increased for such behavior to be demonstrated—even by this experiment. In general, the test results indicated the production of great compaction in soil near a surface loaded with an impulse of appropriate rise time and intensity. At greater distances from the surface, the shape of the impulse changed and less compaction was produced. In addition, techniques for instrumentation and for soils handling were developed and described which will be useful in related experimental efforts.

ACKNOWLEDGEMENTS

The development of the testing program was greatly assisted by discussions between AFSWC personnel and personnel of Armour Research Foundation which operates the Shock Tube Laboratory under contract with AFSWC. The individuals who contributed significantly included: Mr. Wang, Mr. Sisson, and Mr. Mason, all of AFSWC; and Dr. Schiffman, Mr. Wiedermann, Mr. Gallagher, and Mr. Nagumo, all of Armour Research Foundation.

REFERENCE

- [1] A. J. Durelli and F. Riley, "Initial Investigation of Wave Propagation in Large Soil Models," AFSWC Trl-58-3 ASTIA-AD-212978, Dec. 1958

MOTIONS PRODUCED BY AN EXPLOSION ABOVE A NONHOMOGENEOUS ELASTIC MEDIUM*

C. M. Ablow, R. C. Alverson, F. Gair, and F. M. Sauer
Stanford Research Institute, Menlo Park, California

A finite difference numerical method of determining motions and stresses in an elastic half space due to a time dependent, axially symmetric surface loading is presented. The usual smearing of the compressional and distortional wave fronts in such methods is avoided by introducing a coordinate system following the front. In this characteristic system regions of influence may be traced before determining the actual motion. Numerical results are presented for cases in which the compressional wave speed varies linearly with depth, while the shear wave speed is constant. The method may also be applied to layered media where the elastic parameters are constant in each layer but differ from layer to layer.

INTRODUCTION

The stresses and displacements in an elastic earth of variable properties under blast loading are computed by a numerical method using characteristic coordinates. The principal advantage of this method of characteristics is that the location and magnitude of the leading edge of the disturbance are accurately determined. A second advantage is that the differential equations are reduced in dimension so that a numerical method of second order accuracy is readily constructed. The major disadvantage is the need for translating from physical to characteristic coordinates and back again.

It is assumed that the surface of the earth is plane and that the blast wave loading is circularly symmetric about a point on the surface. The portion of the earth under consideration is then referred to a system of cylindrical coordinates (r, θ, z) in which the z axis is normal to the surface through the point of symmetry and the plane $z = 0$ coincides with the earth's surface.

The earth is then assumed to be an elastic solid with a constant shear wave

velocity and compressional wave velocity increasing linearly with depth.

The equations of classical elasticity are to be integrated under prescribed normal and shearing stress on the plane $z = 0$. In the particular blast wave loading considered in this paper, the leading edge of the wave front on the surface of the earth moves with an initially supersersonic velocity which decreases linearly with time to subsonic velocity.

The equations of motion are written in characteristic coordinates and are replaced by difference equations in this coordinate system. The basic dependent variables of the problem are the first partial derivatives of potential functions from which the displacements may be computed directly. The numerical computation of these basic variables is carried out to a truncation error of second order.

Numerical differentiation of these computed data is then permissible to obtain the stresses in the interior correct to first order. The details of the method will concern with some

*This research is sponsored by the Research Directorate of the Air Force Special Weapons Center, Kirtland Air Force Base, New Mexico.

of the numerical results are presented in the following sections.

GOVERNING DIFFERENTIAL EQUATIONS

In cylindrical coordinates r , θ , and z , the equations of dynamic equilibrium become

$$\frac{\partial \sigma_r}{\partial r} + \frac{\partial \sigma_{rz}}{\partial z} + \frac{v_z - v_\theta}{r} = \frac{\partial^2 u}{\partial t^2} \quad (1)$$

and

$$\frac{\partial \sigma_{rz}}{\partial r} + \frac{\partial \sigma_z}{\partial z} + \frac{\sigma_{rz}}{r} = \rho \frac{\partial^2 v_z}{\partial t^2} \quad (2)$$

where σ_r , σ_θ , σ_z , and σ_{rz} are the usual radial, circumferential, axial, and shear stress components and u and v_z are the radial and axial displacement, and ρ is mass density.

Hooke's law gives

$$\sigma_r = \lambda \Delta + 2\mu \frac{\partial u}{\partial r} \quad (3)$$

$$\sigma_\theta = \lambda \Delta + 2\mu \frac{v_z}{r} \quad (4)$$

$$\sigma_z = \lambda \Delta + 2\mu \frac{\partial v_z}{\partial z} \quad (5)$$

$$\sigma_{rz} = \left(\frac{\partial u}{\partial z} + \frac{\partial v_z}{\partial r} \right) \quad (6)$$

where Δ is the dilation,

$$\Delta = \frac{\partial u}{\partial r} + \frac{v_z}{r} + \frac{\partial v_z}{\partial z} \quad (7)$$

and λ and μ are the Lame' parameters.

The solution of the above system of first order equations can be reduced to solving a pair of second order equations for two potential functions provided that ρ and μ are constant and λ is independent of time. The potential functions, ϕ_r and ϕ_θ , determine the displacements through

$$u = \phi_r + v_z \quad (8)$$

$$v_z = \phi_\theta + \partial_r \phi_r$$

where the literal subscripts denote partial differentiation.

Elimination of the stresses and displacements from the equilibrium equations gives

$$c_L^2 (\phi_r + \phi_{rr} + \phi_{zz}) = \phi_{tt} \quad (9)$$

and

$$c_s^2 (\phi_{rr} + \phi_{zz} - \partial_r^2 + \partial_{zz}^2) = \phi_{tt} \quad (10)$$

where

$$c_L^2 = (\lambda + 2\mu)/\rho$$

and

$$c_s^2 = \mu/\rho$$

c_L and c_s being the compressional and distortional wave speeds, respectively.

The potential equations, Eqs. (9) and (10), are replaced by difference equations below and solved numerically. The solution is best carried out in a coordinate system adapted to the equations and to the physical situation they represent.

As it stands, either potential equation contains second partial derivatives in every coordinate direction. It is possible, however, to introduce new independent variables such that the second derivative in one of the coordinate directions is missing. In this form, a solution with a jump in that second derivative is permitted without the added complication of special jump conditions. Thus, in particular, the correct discontinuity in stress and velocity at the initial wave front automatically results without smearing from a solution of the equations which uses that wave front as a coordinate surface.

Such a characteristic coordinate system for each potential equation is described later.

NONDIMENSIONAL COORDINATES

The particular variation of c_L , considered in this paper, is that when c_L varies linearly with depth beneath the surface of the earth.

In this instance, c_L may be written as

$$c_L = c_L(0) \left(1 + \frac{z}{l} \right) \quad (11)$$

where $c_L(0)$ is the value of c_L at $z = 0$ and l is a characteristic length.

The problem is then completely nondimensionalized by introducing the nondimensional quantities, as follows:

$$r' = \frac{r}{\ell}, \quad z' = \frac{z}{\ell}, \quad t' = \frac{c_L(0)}{\ell} t,$$

$$u' = \frac{u}{\ell} \quad \text{and} \quad w' = \frac{w}{\ell}$$
(12)

where ℓ is a characteristic length to be specified later.

In the remaining sections of this paper, the primes on these quantities have been omitted with the understanding that in the sequel nondimensional quantities are intended.

CHARACTERISTIC COORDINATES

A surface, $f(r, z, t) = 0$, which is a solution of the equation

$$c^2 (f_r^2 + f_z^2) = f_t^2 \quad (13)$$

is a characteristic surface for the potential equations, Eqs. (9) and (10), where c is the appropriate wave speed, c_L or c_S . Such a surface can be conveniently thought of as a wave front propagating through the medium with speed c . If the speed is independent of time, the family of surfaces,

$$f(r, z, t - t_1) = 0, \quad (14)$$

for various values of the time delay t_1 are also wave fronts. A more useful form of Eq. (14) is

$$t_1 = t - g(r, z). \quad (15)$$

If three distinct families of wave front surfaces are known, Eq. (15) determines the member of each family passing through a given point (r, z, t) by singling out the three values of t_1 . Conversely, if three values of t_1 are chosen from each family, the point (r, z, t) at which the corresponding surfaces intersect is determined. Thus three time delays, one for each family of wave fronts, can be used as coordinates. The surfaces, $t_1 = \text{constant}$, are characteristic coordinate planes each of which represents a wave front.

The compressional wave speed in nondimensional coordinates is

$$c_L = 1 + z. \quad (16)$$

A family of waves moving into the earth in the direction of positive z is represented in the form of Eq. (15) by

$$a = t - \ln(1+z). \quad (17)$$

The time delay, a , is seen to be the time when a particular wave of the family coincided with the surface of the earth, $z = 0$. Similarly a family of waves moving up from the interior of the earth toward $z = 0$ may be represented by

$$b = t + \ln(1+z). \quad (18)$$

The third family of wave front surfaces,

$$c = t - b(r, z), \quad (19)$$

is determined by requiring the $c = 0$ surface to be the wave front carrying the initial disturbance into the earth. That is,

$$f(r, z, t) = t - f(r, z) \quad (20)$$

is the solution of Eq. (13) passing through the leading edge of the load applied on the surface of the earth.

If the leading edge of the applied load is given in terms of a parameter τ by

$$r = R(\tau), \quad t = T(\tau) \quad \text{where } 0 \leq \tau \leq 1; \quad (21)$$

then $h(r, z)$ of Eq. (19) and hence c , is found by eliminating τ , p , and s from

$$h(r, z) = T(\tau) + s$$

$$s = \operatorname{arcsech}(-p) + \operatorname{arcsech}[-p(1+z)]$$

$$r = R(\tau) - \frac{1}{p} \left[\sqrt{1-p^2} + \sqrt{1-p^2(1+z)^2} \right] \quad (22)$$

$$p = \begin{cases} T'(\tau)/R'(\tau) & \text{on } 0 \leq \tau \leq 1 \\ -(1+\tau) T'(0)/R'(0) & \text{on } -1 \leq \tau \leq 0 \end{cases}$$

The sign (+) in the expressions for r and s are to be interpreted as negative for $s < \operatorname{arcsech}(-p)$ and positive otherwise. This change of analytic form is due to the refractive turning back of the wave front. The method of integrating the first order partial differential eqn. (13), subject to the boundary condition of Eq. (21) to obtain the solution, Eq. (22), is given in several standard texts, for example, R. Courant and D. Hilbert, *Methode der mathematischen Physik*, Vol. I, Ch. 2.

In a similar way, characteristic coordinates corresponding to the constant shear wave speed

$$C_s = k \quad (23)$$

are

$$\bar{a} = t + z/k \quad (24)$$

$$\bar{b} = t - z/k$$

and

$$\bar{c} = t + h(r, z)$$

where $h(r, z)$ is determined by eliminating τ , p and s from

$$\begin{aligned} \bar{h}(r, z) &= \bar{T}(\tau) + \bar{s} \\ z &= k\bar{s}\sqrt{1-k^2p^2} \\ r &= \bar{R}(\tau) = k^2ps \end{aligned} \quad (25)$$

$$p = \begin{cases} -\bar{\tau}'(-)\sqrt{\bar{R}'(-\tau)} & \text{on } 0 \leq \bar{\tau} \\ -(1+\bar{\tau})\bar{T}'(0)\sqrt{\bar{R}'(0)} & \text{on } -1 \leq \bar{\tau} < 0 \end{cases}$$

In these last equations, the leading edge of the disturbed region has been expressed in parametric form by

$$r = \bar{R}(-\tau), \quad z = \bar{h}(-\tau) \quad \text{on } 0 \leq \bar{\tau}. \quad (26)$$

The effect of the refraction of the compressional wave is to make it possible for the disturbed region of the earth's surface to outrun the applied load. Thus \bar{R} and \bar{T} are computed as the intersection of the initial compressional wave front, $c = 0$, with the earth's surface, $z = 0$.

As a result of putting both the $c = 0$ and $a = 0$ surfaces through the same r versus t curve on $z = 0$ and of making $c_x = c_y = 1$, c and a agree at every point of $z = 0$. Reference to Eqs. (18), (19), and (24) show that as $r \rightarrow 0$, $a \rightarrow a$ and $b \rightarrow b$. This identity of the two systems of coordinates on $z = 0$ is very convenient when the stress boundary conditions are satisfied in finite difference form.

The disturbed region of the earth at any time t lies between $r = 0$, $r = 0$, and the initial wave front surface $a = 0$. In characteristic coordinates the region lies between the planes $\bar{a} = \bar{b} = 2t$, $\bar{a} = \bar{b} = -t$, and $\bar{a} = \bar{c}$, the last corresponding to $r = 0$ where the plane wave surface, $a = \text{constant}$, meets the initial wave surface, $c = \text{constant}$.

The region disturbed in shear has the same characteristic plane boundaries

($a + b = 2t$, $b = \bar{t}$, $c = 0$, and $a = \bar{c}$) but corresponds to a smaller region of physical space.

The surfaces $a = 0$, $b = 0$, and $c = 0$, together with the disturbed region in physical space are shown in Fig. 1. The disturbed region in characteristic coordinates is shown in the left half of Fig. 1. The right hand portion of Fig. 2 indicates a typical mesh cube in characteristic coordinates. The partial differential equations are replaced by difference equations along the faces of the cube.

Under these changes of coordinates, the two potential equations can be written as

$$4A_b + D_1 A_c + D_2 B_c + (B - A) + D_3 C = 0 \quad (27)$$

and

$$4\bar{A}\bar{a} + D_4 \bar{A}\bar{c} + D_5 \bar{B}\bar{c} + D_6 \bar{C} + D_7 \bar{v} = 0 \quad (28)$$

where

$$A = c_{xx}, \quad a = c_{xz}, \quad \text{etc.}$$

and the coefficients in these equations are given by

$$D_1 = (1+z)c_z + 1, \quad D_2 = -2((1+z)c_z - 1).$$

$$D_3 = -(1+z)^2(c_{zz} + c_{xy} + c_{xz}),$$

$$D_4 = C_z c_z + 1, \quad D_5 = -2(C_z c_z - 1),$$

$$D_6 = -C_z^2(c_{zz} + c_{xy} + c_{xz}), \quad D_7 = \frac{C_z^2}{r^2}.$$

Equations (27) and (28) together with the equations

$$\begin{aligned} A_a &= B_a, & \bar{A}\bar{a} &= \bar{B}\bar{a} \\ A_c &= C_a, & \bar{A}\bar{c} &= \bar{C}\bar{a} \\ B_c &= C_a, & \bar{B}\bar{c} &= \bar{C}\bar{a} \end{aligned} \quad (29)$$

become the basic differential equations to be satisfied. The difference equations which represent the above differential equations together with the method of computation of the stresses and displacements from the dependent variables are given in the final report for Contract AF 29(601)-1948 (to be published) and are omitted herein.

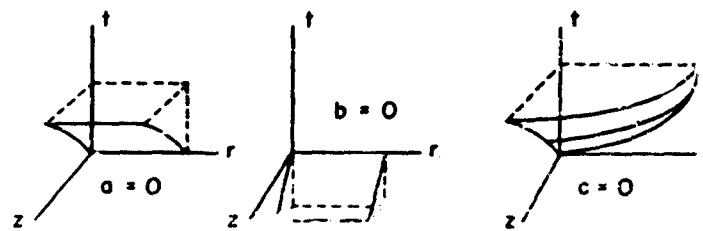


Fig. 1 - Wave surfaces and disturbed region in physical space

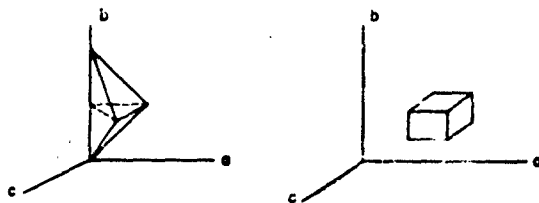


Fig. 2 - Disturbed region and typical finite difference lattice cube in characteristic coordinates

COMPUTED LEADING WAVE FRONTS

Numerical computation of the leading wave fronts, $c = 0$, have been carried out and the results are shown in Figs. 3 and 4. These curves have been computed for the case where the leading edge of the load on the surface, $z = 0$, moves according to the general rule,

$$R(\tau) = (K_1 + K_2)\tau - K_1 \frac{\tau^2}{2} \quad (30)$$

$$T(\tau) = K_2\tau$$

with $K_1 = K_2 = 3.5$, so that the elimination of τ gives

$$R = 2T - \frac{T^2}{7}. \quad (31)$$

The velocity of the leading edge of the load is given by

$$\frac{dR}{dT} = 2 - \frac{T}{3.5}. \quad (32)$$

These expressions show that the velocity of the leading edge is superseismic with initial nondimensional speed 2 and decreases so that it is locally seismic at $T = 3.5$. The position

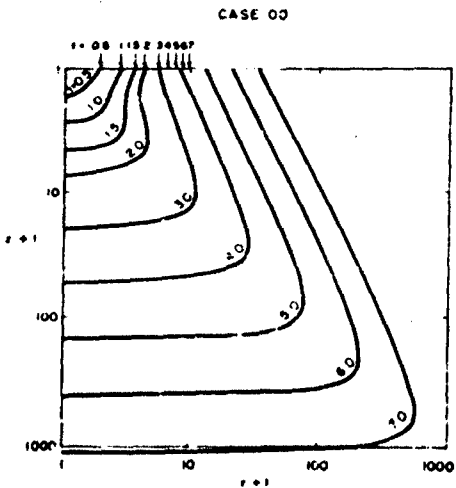


Fig. 3 - Position of the leading compressional wave

and magnitude of the leading edge of the load at various times T shown in Fig. 5. The load distribution in Fig. 5 was chosen to approximate the distribution which would occur in an actual bomb-blast above the surface of the earth.

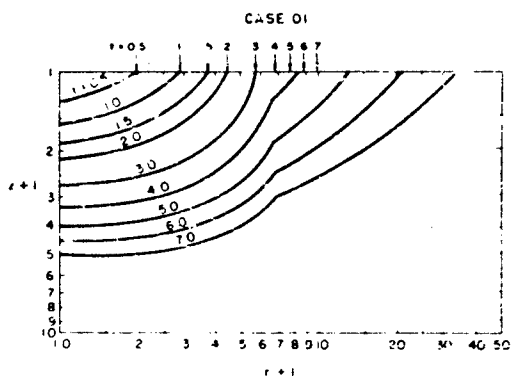


Fig. 4 - Position of the leading distortional wave

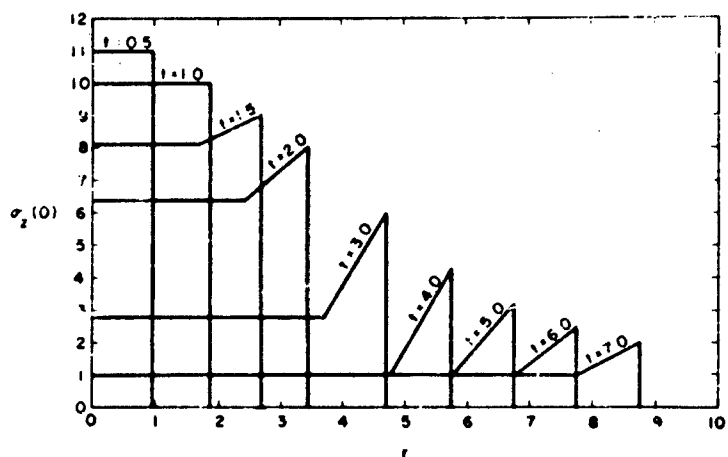


Fig. 5 - Time and space history of the loading on the surface of the earth

Figure 3 shows the shape of the compressional leading wave fronts in the planes, $t = \text{constant}$. The location of the leading edge of the load on the surface of the earth for various times is noted at the top of Fig. 3. It is seen that outrunning occurs at $t = 0$ for a value of r between 3 and 4. The exact calculated value of t for which this outrunning occurs is $t = 3.318$. In this case, outrunning occurs before the velocity of the leading edge becomes seismic. Complete refraction of the wave

front which is indicated by the point where the wave front is vertical, first occurs near $t = 1.5$.

The shape of the distortional wave front for several values of time is shown in Fig. 4. In this case no refraction occurs, since the speed of the shear waves is constant. The break in the slope of the curves—which appears for $t > 3$ —is due to the outrunning at the surface and thus first occurs for $t = 3.318$.

DISCUSSION

Mr. Mow (Allied Research Associates, Boston): Is there any particular reason that you chose the λ being varied with depth and μ constant? We know the shear wave also changes velocity as we go down.

Mr. Alverson: This is an approximation we made because the equations become more manageable when you have also a shear variable.

Mr. Mow: Because you can't decouple the equation between the shear wave and the dilatational wave?

Mr. Alverson: Yes. You don't have a distinct breaking up into two separate equations in that situation.

Mr. Weidlinger (Paul Weidlinger Consultants): In your computations did you notice any fronts which would indicate the presence of Rayleigh waves?

Mr. Alverson: So far we have not. What we have here is a sort of traveling source of Rayleigh waves. We have a leading edge of the load moving. We have not studied it in that detail yet.

Mr. Weidlinger: Don't you expect that something will blow up, for instance at some point where you will be matching Rayleigh wave velocities with the velocity of the advancing air blast?

Mr. Alverson: It could for the case we have but that would happen at a rather large value of time. We start with the air blast leading edge moving supersismically with velocity 2 where 1 would be the velocity of the medium. The velocity decreases linearly until it's seismic. In what we have, outrunning occurs even before the velocity of the leading edge of the load is seismic. We haven't really carried the calculation into the subsismic region yet.

Mr. Weidlinger: I am not sure if I interpreted the last two figures correctly. I noticed that the wave front is outrunning forward. Wouldn't that indicate that you are in the subseismic region?

Mr. Alverson: When refraction occurs, it occurs before the velocity of the leading edge of the load becomes seismic—but the velocity of the leading edge of the load which

is now outrunning is still fast with respect to any velocity you'd expect a Rayleigh wave to have, it's still superseismic.

Mr. Weidlinger: The discontinuity in Fig. 4, is this a Mach front?

Mr. Alverson: This first appears on the curve at the time when outrunning of a compressional wave occurs. That means the leading edge of the load is just at seismic velocity and the wave that has reflected and outruns is traveling so that the point moves at super-seismic velocity. The difference which means a little bit of a discontinuity in velocity reflects on the slope of $c = 0$ and will propagate throughout. It is pretty difficult to determine analytically what is its speed.

Dr. Brode (The RAND Corp.): Mr. Weidlinger, would you expect a different kind of reaction when the air blast is traveling at the same speed as your Rayleigh wave?

Mr. Weidlinger: Yes. I think Miles has shown..... that this solution blows up at various times. For instance, if the velocity of the air blast matches the Rayleigh wave velocity these isentropic solutions blow up and you get into special problems. The same thing occurs incidentally, when the p wave matches the velocity. It's a technical problem and I think it raises questions in numerical computations and in asymptotic approximations. It's not a real physical problem. Physically it just means the velocities have matched but it brings about all kinds of grief when you work with it.

Dr. Brode: And, in fact, with a numerical procedure such as this it might run right over it, since it's only an instantaneous and point type singularity.

(At this point some of the discussion was lost while the tape was being changed.)

Mr. Alverson: We recognize that it's important to run out a series of parameter variations and one of them will be to allow the wave speed to go through the Rayleigh wave speed. This we do by appropriate change of parameters in the elastic law. I don't think this will cause any trouble because my recollection of what Miles' conclusion was is that you won't have a singularity at the Rayleigh wave speed, provided you're going through the

Rayleigh wave speed with a finite acceleration or deceleration. We will see whatever happens when we have surface waves because the full solution is exact as far as the elastic equations go and the numerical methods are sufficiently refined to show us everything that happens. I also want to comment on the little cusp in Fig. 4. What it is really is the Von Schmidt wave—well, call it what you may—we recognize it.

Mr. Zajac (Bell Telephone Laboratories): Did you attempt to do a stability

analysis of the numerical scheme or convergence?

Mr. Alverson: The finite difference equations are so complex that a rigid stability analysis was almost precluded, but we are using a method of characteristics which we know converges. We know that it converges and we know that along characteristics a truncation error will be propagated but will not increase.

* * *

A DEVICE FOR DETERMINING DYNAMIC STRESS-STRAIN RELATIONSHIPS OF SOILS

Kenneth Kaplan, James V. Zaccor, and A. B. Willoughby
Broadview Research Corporation, Burlingame, California

A device for the rapid determination of stress and strain in small soil samples under dynamic loading conditions has been developed. Stress in the sample can be built up to a constant value in times as short as a few tenths of a millisecond through multiple reflections of the input stress pulse between the two ends of the sample and can be maintained at this level indefinitely.

INTRODUCTION

As part of a general program, sponsored by the Defense Atomic Support Agency to develop techniques and instrumentation for measuring stress and strain in soils under dynamic loading conditions, a test device has been developed at BRC in which stress and strain can be directly measured for very rapidly applied loads of "long" duration. This paper describes the device, discusses some of its more interesting design features, and presents some typical preliminary results acquired so far.

In this portion of the over-all study, attention has been restricted to the plane wave case, that is, to the determination of stress and strain in soils in which stress wave propagation takes place in only a single dimension. The desired specifications for the stress loading (Fig. 1) are:

1. The minimum rise time of the loading pulse should be between 0.2 and 1.0 msec.
2. The maximum loading should be as high as 500 psf.
3. The maximum loading duration should be between 50 and 300 msec.
4. The minimum time of fall should be on the order of 1 msec.

These specifications more or less reflect expected field conditions in that for the stress levels discussed, there should be few cases in

which the soil stress rise time is smaller than one msec., yet durations of a few hundred milliseconds are not inconceivable.

In trying to attain these specifications, it was found convenient to consider three relatively distinct problem areas: methods of containing the soil sample; methods of loading the soil sample; and methods of making the desired stress and strain measurements in the soil sample.

CONTAINMENT

The problems of containment arise from the first restriction, just mentioned, that we should consider plane waves alone. Ideally, plane wave studies call for uniform loading on a semi-infinite soil sample, one which extends indefinitely far normal to the direction of stress wave propagation; however, this is clearly not practical. The next best solution is to establish conditions at the boundaries of a sample of limited extent which resemble conditions within the semi-infinite sample. These boundary requirements are: The sample must be totally restrained laterally (that is, strain normal to the direction of stress wave propagation must be prevented), and the boundary must be essentially frictionless.

The approach we selected to satisfy these boundary conditions was to make the sample boundary a totally contained tube of fluid (with a very light membrane separating fluid and soil). With a relatively small fluid volume

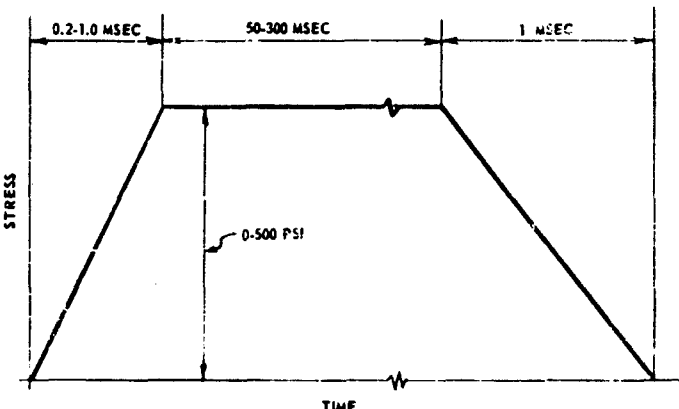


Fig. 1 - Characteristics of ideal (target) loading pulse

(the fluid being nearly incompressible), especially complete lateral restraint should be provided and the effects of boundary friction should be greatly lessened by the lubricating action of the fluid.

LOADING

The task of obtaining the load-time history on the desired soil sample presented some perplexing problems. For long-duration pulses, if the loading were to be applied through a single pulse unaffected by reflections, a very long sample (perhaps 100 feet long) could be necessary. It was concluded, however, that a single pulse would not really be required (that is, stress wave reflections could be permitted providing that the desired shape of the load-time history in the sample could be obtained). The technique of allowing stress wave reflections was termed the multiple-pulse technique.

The most serious problem, arising when stress wave reflections are permitted, is that nonuniform stress conditions can exist throughout the sample—in fact, local transient stresses can exceed a finally attained stress level; this can be seen in Fig. 2—which shows possible stress distributions for an elastic soil sample that has been subjected to an instantaneously applied uniform load.

The degree of nonuniformity of stress in the sample and the magnitude of overstressing are in large part dependent on the rate of sample loading and on the number of times the stress wave is allowed to traverse the sample

during the rise time of the loading: the greater the number of passages, the more uniform the loading and the smaller the transient overstressing. Since shortening the sample would allow more stress wave transits for any one value of pulse rise time, it seemed that the use of multiple-pulse technique reversed the sample length requirement, that is, a very long sample is required for single-pulse loading and a very short sample is required for multiple-pulse loading. The average stress-time pattern, in an idealized elastic sample for a loading pulse with a rise time equal to 10 passage times through the sample, compared to the ideal loading, is shown in Fig. 3.

MEASUREMENT

If simultaneous measurements of stress and associated strain in a soil sample are to be made, single-pulse loading techniques require that strain and perhaps stress measurements be made within a sample in such a manner that the sensors do not disturb stress wave propagations and that they respond to the stresses and strains that would exist in their absence. Such stringent requirements need no longer be met when multiple-pulse loading is used. Strain measurements can be made over the entire sample. Stress in the sample must be uniform for such measurements to have any meaning; however, approximately uniform stress will be obtained throughout the sample in satisfying the requirement that large transient overstressing be prevented.

To avoid problems of stress concentration or stress relief in the vicinity of a stress

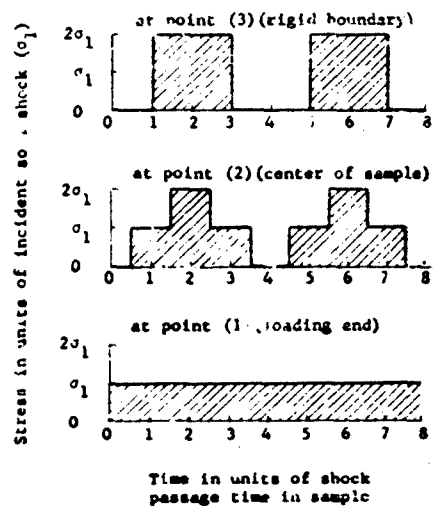
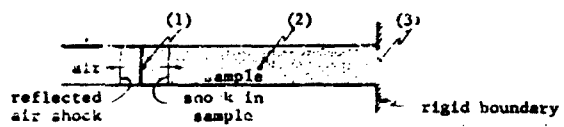


Fig. 2 - Stress versus time at various points within a soil shock tube

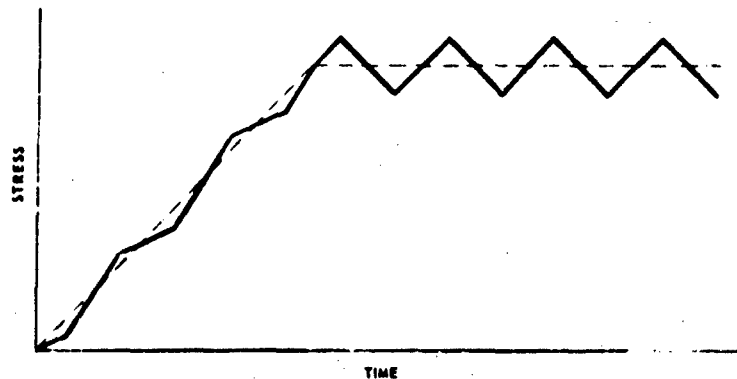


Fig. 3 - Average stress in an elastic sample for a loading pulse with a rise time equal to 10 passage times through the sample. (Note. The ideal loading pulse is shown as a dashed line.)

gage (due to differential motion of the gage, with respect to the remainder of the boundary), we chose to have the fixed end boundary consist of a stress sensor of uniform characteristics—in particular, a wafer of piezoelectric ceramic.

Measurement of strain is made by monitoring the displacement of the opposite end of the sample. A variety of small displacement sensors are available (linear variable differential transformers, capacitance change detectors, and even an optical system). For reasons of cost and flexibility, one which detected small changes of capacitance was chosen for these tests.

TESTER DESIGN

A schematic diagram of the tester, developed in accordance with these requirements, is shown on Fig. 4. The input loading is supplied by a modified shock tube, consisting of a large compression chamber that is separated from a small expansion chamber (the sample holder itself) by a frangible diaphragm. By suitably adjusting the volumes of the two chambers, the final pressure level in the system can be made approximately the same as the initial reflected shock overpressure. Baffling inserted into the compression chamber (not shown in Fig. 4) serves to smooth the transition between the initial air shock loading and the final loading, minimizing any loading-pulse oscillations caused by internal reflection of shock and rarefaction waves.

The loading pulse is further smoothed and the desired finite, but very rapid, rise time of the loading pulse is achieved by causing the air shock to pass through a constriction in the expansion chamber prior to loading the sample (generally the constriction takes the form of a perforated metal plate).

The air shock loading is actually applied to the sample through a very lightweight buffer whose displacement is monitored to give the strain in the sample. The walls of the buffer form one plate of a cylindrical condenser, the capacitance of which changes when the buffer is displaced. (The sensitivity of the displacement system is such that a 0.001-inch movement of the buffer causes a 1.3-inch displacement of a spot on an oscilloscope.) Note the fluid layer surrounding the sample and the piezoelectric ceramic wafer at the reflecting end.

It is intended to use the shock tube type of loading for pressures up to about 100 psi, and a Boynton laboratory model 500-psi loader for still higher pressures.

The assembled tester is shown in Fig. 5 and the various components of the tester are shown in Fig. 6.

TESTS

The initial work with the soil tester was devoted to a separate evaluation of various components of the tester. Figures 7, 8, and 9 show the types of air pressure loadings obtained from the shock tube loader by suitably modifying the compression chamber. It is evident that these loadings are good approximations to the desired loadings.

The wafer stress gage was tested under dynamic conditions using an air shock and found to operate satisfactorily. The linearity and sensitivity of the strain gage were found to be satisfactory by static tests and the changes in stray capacitance under dynamic loading were found to be small.

Some tests were also made to evaluate the fluid layer concept. In these tests, in place of the full-disk soil-stress gage, the base of the tester was fitted with two sensors, having 1/16-inch-diameter sensitive areas, one in the center of the base, and one near the edge. "Samples" of modeling clay were used, in one case, in direct contact with a steel boundary (inserted in place of the fluid layer). In another case, the sample was enclosed in a membrane and surrounded by a fluid layer consisting of a layer of grease between the membrane and the steel wall. The results from two such tests are shown in Fig. 10. In both cases, the center and edge gage traces resembled each other; but where the sample was in direct contact with a steel boundary, the stress recorded by the edge gage was only 88 percent of that recorded by the center gage, whereas for the fluid boundary, the two gages read the same.

In additional tests of this same general type with rigid boundaries, the edge gage readings varied from 50 to 90 percent of the center gage readings, and in some cases had different rise characteristics. For the fluid boundary, however, no differences were observed. Figure 11 shows the results so far obtained with simulated soils and shows the

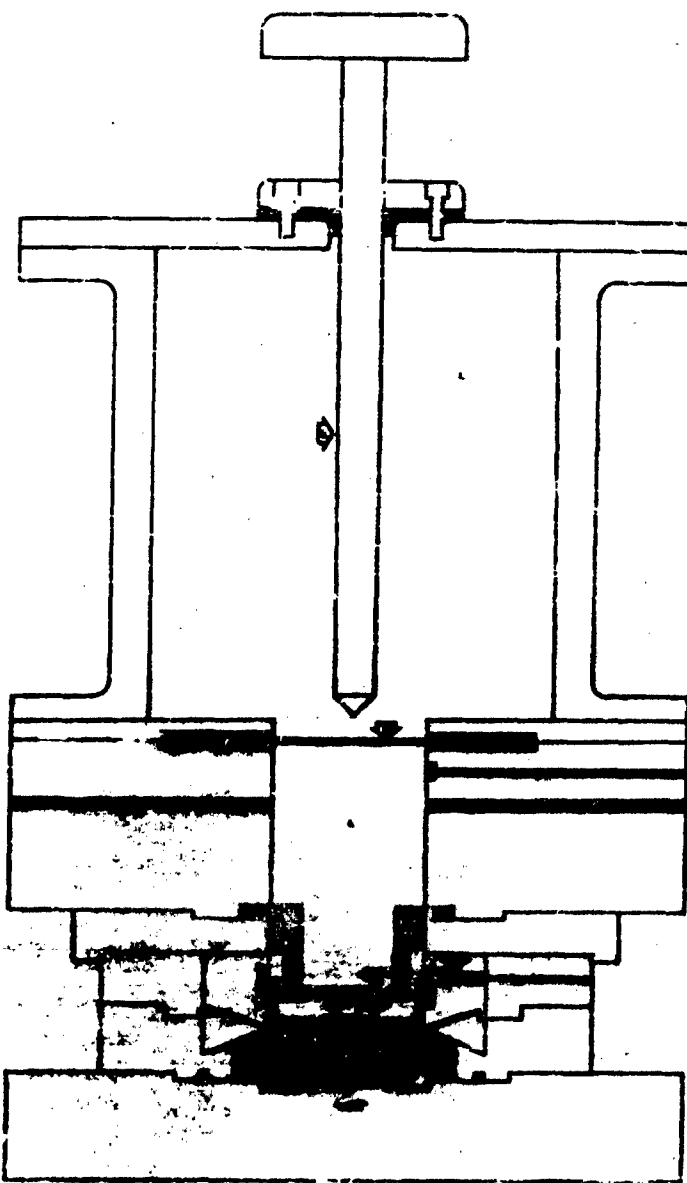


Fig. 4 - Schematic diagram of the soil tester, showing components as follows: (1) compression chamber, (2) plunger, (3) frangible diaphragm, (4) expansion chamber, (5) screen, (6) air-pressure gage, (7) base plate, (8) soil sample, (9) fluid boundary, (10) wafer soil-stress gage, (11) rubber membrane, (12) displacement sensor plate

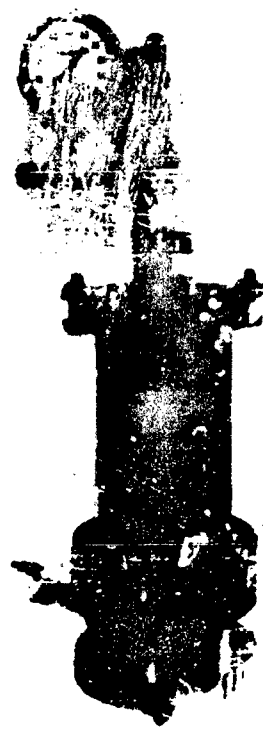


Fig. 5 - The soil tester
(assembled)



Fig. 6 - Soil tester components (left to right): the wafer stress gage on the tester base; the lightweight buffer; the displacement and air-pressure gage housing; the screen and screen holder

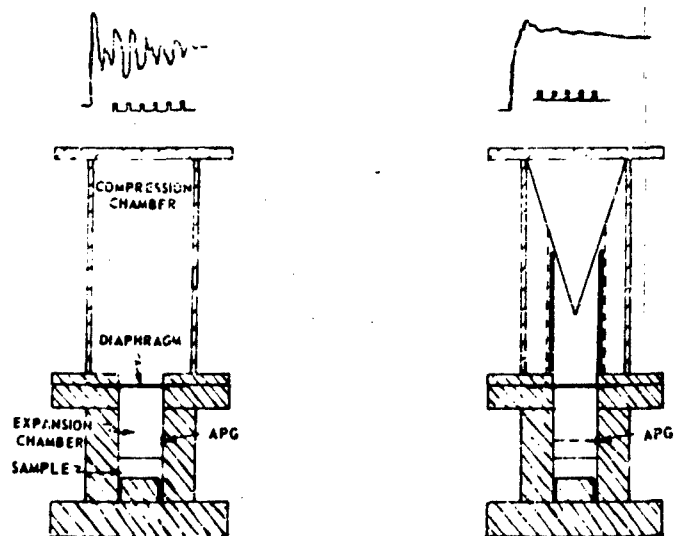


Fig. 7 - Air-pressure gage (APG), pressure-time records from unmodified (left) and modified (right) tester, with an initial compression chamber pressure of 76.9 psi. (Note: Timing traces are 1-kc-per-sec square wave. Modifications consist of a wooden cone, a pipe nipple, and a cylindrical screen, all within the compression chamber, and a screen, immediately above the APG.)

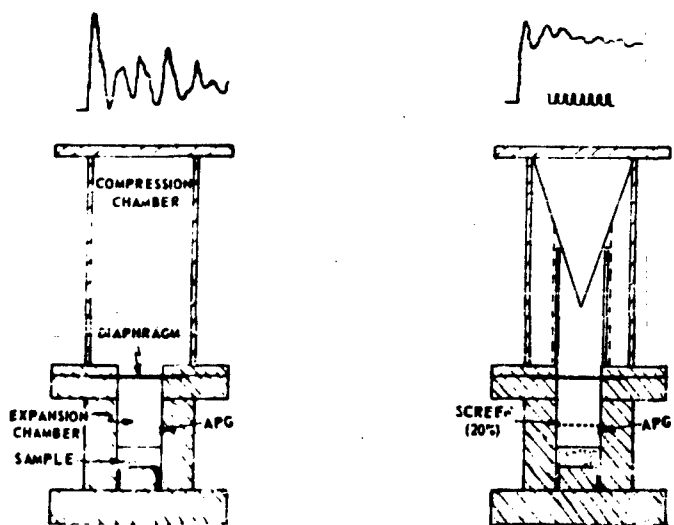


Fig. 8 - Air-pressure gage (APG), pressure-time records from unmodified (left) and modified (right) tester, with an initial compression chamber pressure of 24.2 psi. (Note: The timing trace is a 1-kc-per-sec square wave. Modifications are shown in Fig. 7. See also Fig. 9.)

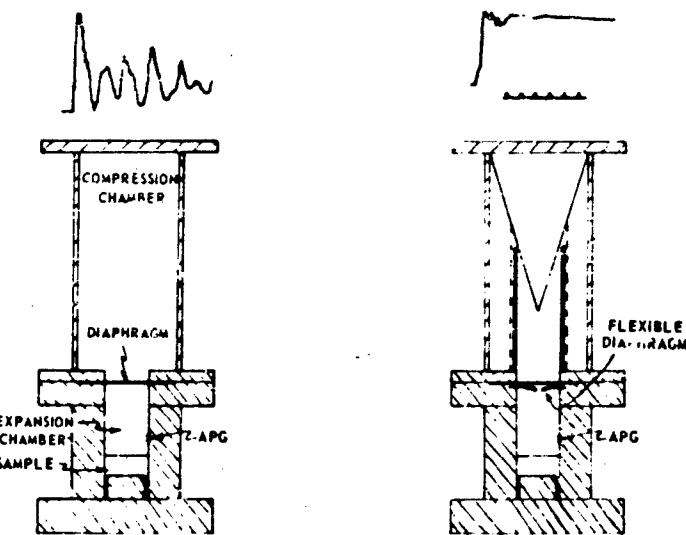


Fig. 9 - Air-pressure gage (APG), pressure-time records from unmodified (left) and modified (right) tester, with an initial compression chamber pressure of 24.2 psi. (Note: The timing trace is a 1-kc-per-sec square wave. Compression chamber modifications are as in Figs. 7 and 8, i.e. the screen immediately above the APG has been replaced with a flexible diaphragm—immediately below the frangible diaphragm.)

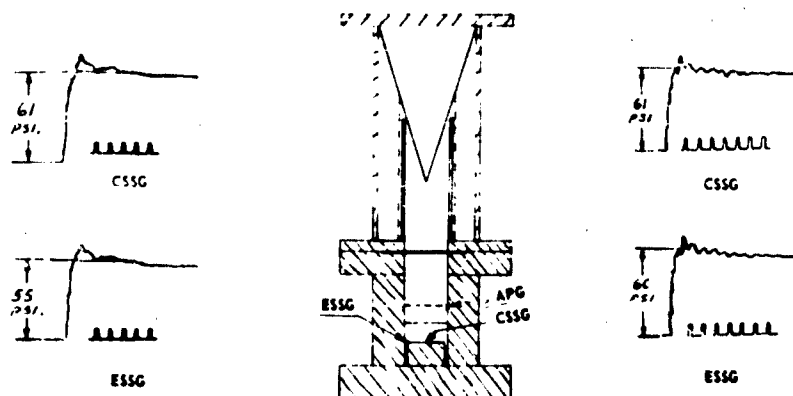


Fig. 10 - Comparison of center soil-stress gage (CSSG) and edge soil-stress gage (ESSG) readings of stress versus time for (left) a sample in direct contact with a steel boundary and (right) a sample separated from the boundary by a rubber membrane and grease layer. (Note: The timing traces are 1-kc-per-sec square waves.)

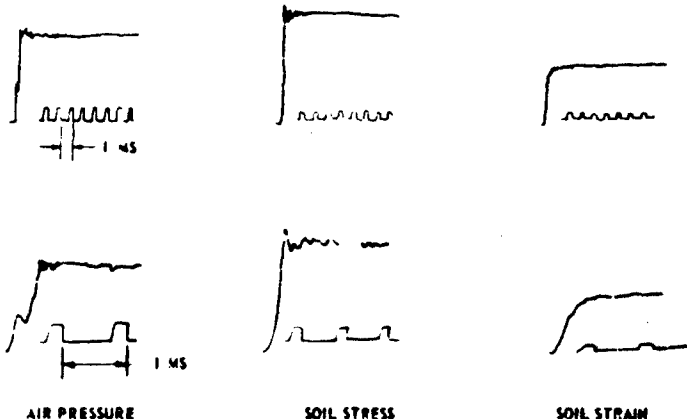


Fig. 11 - Traces from a single test, with a modeling clay "sample." (Note: The soil-stress records in the center are from the full-disk stress gage. The soil-strain records on the right are of the output of the displacement sensing system.)

type of records that Broadview researchers can expect to analyze.

The tester is now developed virtually to the point at which testing of real soils can

begin. All components and concepts have been tested—still with simulated soils—with all components operating satisfactorily.

DISCUSSION

Mr. Clough (Lockheed, Burbank): Do I infer that there is little or no attenuation of these reflected waves during the time of interest of the experiment?

Mr. Kaplan: In the case of an elastic sample, there would be no attenuation since there is no attenuating mechanism.

Mr. Clough: How realistic is this in the case of soil samples?

Mr. Kaplan: For real soils there would be attenuation. You would expect the oscillations to damp out, as in fact they did.

Mr. Clough: Then I am puzzled by the summary which said, "The stress pulse can be maintained at this level indefinitely."

Mr. Kaplan: The compression chamber is pumped up to, say 77 psi, and the frangible diaphragm is ruptured. The pressure stays there, in the chamber. You can keep it up as long as the seals last. The recording system

might have a little difficulty in staying with it, but the load on the sample can be maintained indefinitely.

Dr. Brude (The RAND Corp., Chairman): It is not a matter of dissipation?

Mr. Kaplan: No, it's a static situation.

Mr. Hammer (Shannon & Wilson): What were the primary results you hoped to get by testing actual soil samples with this device?

Mr. Kaplan: The relationship between stress and strain in particular materials under dynamic loading conditions. The knowledge of this relationship serves, I think, for many purposes as an equation of state. Dynamic stress-strain relations should differ from the static.

Mr. Hammer: Then you are after the constraint of values of different loading times?

Mr. Kaplan: Right.

Mr. Weidlinger (Paul Weidlinger Consultants): You inserted a screen in your device to produce a rise time in your pulse. Why wouldn't you prefer a clean shock?

Mr. Kaplan: A clean shock bounces off the opposite end of the sample and increases the stress. It is necessary, therefore, to slow the loading so that only a portion of the shock reflects from the opposite end at any one time. In this way, many reflections of different portions of the pulse allow the actual stress within the sample to build up over a period of time. You have to make the soil sample small enough so that many transients are permitted before the stress attains its final level. If the sample is too long, the stress transient will increase above the final stress.

Mr. Weidlinger: Is there any problem of lateral reflections from the side of your sample? You might have dispersive effects—lateral propagation?

Mr. Kaplan: We have just equipped the tester with a port for making lateral pressure measurements in the fluid boundary.

Mr. Miklowitz (National Engineering Science Co.): On this point, the closer you get to the lubricated interface the more assurance you have that there will not be any dispersion for the plane wave case. This is just a slice cut of the plane wave case for the two-dimensional model. In other words, you would not expect mode conversion?

Mr. Kaplan: Yes, ideally you should.

Mr. Chilton (Stanford Research Institute): I am particularly interested in your strain gage and I wondered if you can say a little about its speed and frequency response? I noticed in Fig. 11 that you got an attenuated wave. I was wondering whether that was due to the sample or due to the strain gage.

Mr. Kaplan: No. The strain gage has a natural frequency of 30 kc. The recording system is quite rapid, much faster than is needed for rise times of greater than 0.2 msec. The rounding was not due to the recording anyhow.

A Voice: I did not understand why you had the compression chamber a greater diameter than the expansion chamber. It may have caused some of the difficulties that were in your records.

Mr. Kaplan: You are probably right that some of the difficulties are caused by this. Our first thoughts were that the volume of the compression chamber should be very large compared to the volume of the expansion chamber. If this were so, then the final pressure would, essentially, be the initial pressure; however, there were much greater reflections than we had anticipated—shocks bouncing off, and rarefactions forming at the shoulders. We have used compression chambers the same size as the expansion chamber for different purposes. We still see, of course, the reflections back and forth through the combined expansion and compression chamber, but not quite to the degree that we have now. The present baffling in the compression chamber has materially decreased its size, so our first concept isn't holding. What is needed is some mechanism for smoothing out the reflections whether from small or large compression chambers.

A Voice: I was not too concerned about the reflections from the back. You can always make your compression chamber much shorter than your expansion chamber.

Mr. Kaplan: But you will still see the reflections for long duration loadings. You may not be worried about the reflections from the back of the compression chamber because your interest does not extend for that length of time. But we want to go on long enough for the rarefaction from the back of the compression to impinge on our measuring scheme. So there must be some way of smoothing that out.

A Voice: You can get a free region in a shock tube—several milliseconds during which you will be free completely of any reflections from any place else in the tube.

Mr. Kaplan: Yes, but for 10 msec you'd need about a 5-feet-long chamber. We are shooting for hundreds of milliseconds. It then becomes extremely difficult.

IMPACT WAVE PROPAGATION IN COLUMNS OF SAND*

Blaine R. Parkin
The Sand Corporation

SUMMARY

A phenomenological theory is developed in order to study the propagation of unidimensional compression waves in columns of sand. The medium of the theory is treated as an elastic-plastic continuum. It is assumed that each element of the substance exhibits a strain-rate effect such that, at a given strain, the plastic strain rate is proportional to the difference between the compressive stress on the particle and that stress which would act on the element under static conditions. Published

experimental results on the propagation of stress waves in sand are used as a basis of comparison between experiment and theory. The present theory gives satisfactory agreement with experiments on two dry sands. In addition, the theory is used to investigate the response of drum-type pressure gages to impact loading and problems connected with the derivation of "dynamic" stress-strain curves from experimental stress histories at fixed points in a sand. Conditions derived from the theory which might permit the proper scaling of laboratory results are discussed in this paper.

*This paper—on the Supplementary List for the 29th Symposium—is being published by the American Society of Civil Engineers in the Journal of the Soil Mechanics and Foundations Division, April 1961.

EQUATIONS OF STATE STUDIES FOR SOIL*

Michael A. Chastey¹
Armour Research Foundation
Chicago, Illinois

The pressure-volume variations of several different solids, from atmospheric pressure to millions of atmospheres, are concisely presented to illustrate the possibilities of compression of solids under pressures which are possible from nuclear explosions. Rankine-Hugoniot equation of state curves are developed for silica glass and an aggregate of the silica glass and air, i.e., a dry "sand" of silica glass globules, from the isothermal equation of state of the silica glass. The "waste heat concept" is derived from fundamental thermodynamic principles. This paper shows that the thermal energy corresponding to the entropy change in a shocked porous or solid material is partially "wasted" in raising the temperature of the material and a small fraction of it is utilized as hydrodynamic energy. Laboratory static experiments for obtaining equations of state data for soils, up to pressures of millions of atmospheres and down to the elastic pressure range, are described.

INTRODUCTION

The Rankine-Hugoniot equation of state for a soil provides information essential for predicting shock wave propagation in the soil. For hard rocks, Rankine-Hugoniot data from as high as hundreds of thousands of atmospheres is necessary in order to predict the shock wave propagation from a nuclear underground explosion. Conversely, the seismic pulse at some distance from an underground explosion is premised on the equation of state of the soil at the low pressures in the transition region.

The extremely high pressures generated by nuclear explosions challenge the imagination beyond normal intuition. High pressure-density data obtained by diverse means for a number of solids and for air, are presented in this paper to illustrate the effects of high pressures.

The Rankine-Hugoniot and isentropic equations of state are derived below for solid silica glass from its empirical isothermal equation of state based on static

experiments. A Rankine-Hugoniot curve is constructed for an aggregate of the silica glass globules and air (i.e., dry "sand" of silica glass), using the Rankine-Hugoniot equation of state curve of the solid. The term "aggregate" is used for this simple combination of air and solid because it is desired to establish a generic term which will apply to many combinations of air, water and solids to be studied. "Aggregate" as used in this sense is defined as confluent solids with fluids filling the intergranular spaces.

The relation between the thermal energy, the entropy change and the "waste heat" is explained. It is shown that the "waste heat," which is the energy loss that attenuates the shock, is less than the thermal energy due to the entropy change from isentropic to shocked conditions.

The temperature of the silica glass and the equilibrium temperature of the aggregate are found and the transition region of the aggregate, wherein the strong shock changes to a seismic pulse, is analyzed. Silica glass was chosen for this study because silica is a

*This paper was not presented at the Symposium.

major constituent of most soils and fortuitously there is high pressure density data available for it. Dynamic experiments for determining Rankine-Hugoniot relationships in porous media are described.

COMPRESSIBILITY OF SOLIDS

Underground nuclear explosions compress soils to millions of atmospheres and instantaneously reduce them to small fractions of their initial volumes. The precise determination of the pressure-density relationship in the soils at these extreme pressures is yet to be accomplished. In the attempt to provide answers to the questions raised by nuclear explosions, it is necessary to make the best possible use of all information on extreme pressures that is available.

Experimental data on shock waves generated by explosions with peak pressures of hundreds of kilobars (1 bar = 0.97 atm) are available for aluminum, copper, zinc, and other metals [1]. One type of experiment measures the free surface velocity and another is of the impedance-matching type. Certain innovations must, however, be introduced to such experiments to make them useful for investigating the pressure-density relations in porous materials and aggregates.

Recently silicon dioxide glass was subjected to static pressure ranging up to 200,000 atmospheres [2]. Below 50,000 atmospheres, Bridgman provides pressure-volume data on silica glass in increments of pressure that are useful in computations [3]. These experimental results are used in the investigation of the behavior of the aggregate of silicon dioxide globules, initially in a normal atmosphere of air, which are then subjected to strong shocks.

The Fermi-Thomas method of quantum mechanics has been applied to materials such as iron to explore the pressure-density relations at extremely high pressures [4,5]. These results provide an insight into the behavior of materials at pressures which are beyond the normal realm of intuition.

Representative examples of data obtained from some of the above pressure-density determinations are shown in Fig. 1 in order to provide in a concise form an illustrative reference of the pressure-density behavior of solids.

The curves for iron and for atomic numbers 18 and 54 are shown in Fig. 1 merely to illustrate the possible compressibilities of

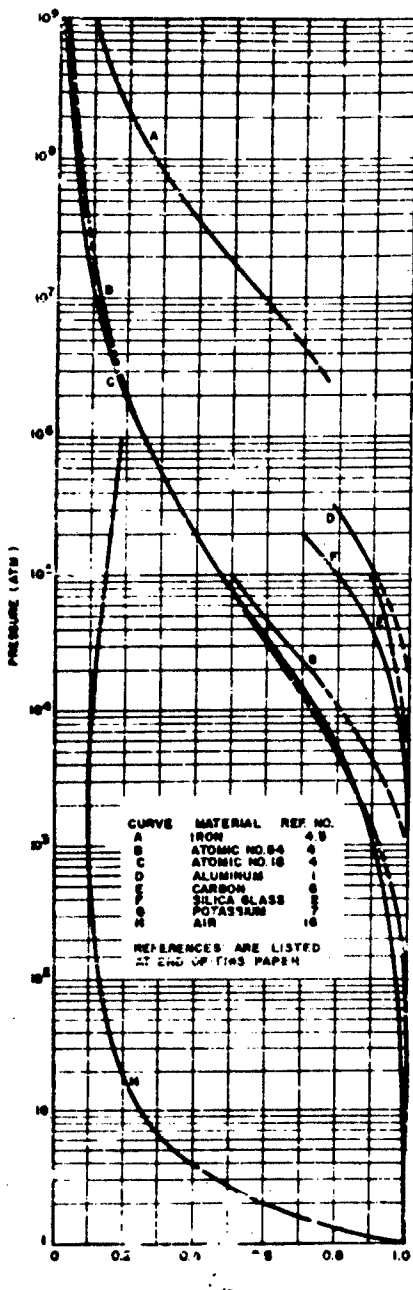


Fig. 1 - Pressure-density of various solids and air

solids at extremely high pressures. The curves for carbon and potassium are used to compare the trends of static compressibility experiments and quantum theoretical calculations respectively [6,7]. The curve for silica glass is based on the static compressibility experiments. The method of arriving at this curve and its use for developing equations of state for silica glass and an equation of state curve for an aggregate of silica glass globules are presented in this paper.

SOILS AND SILICA GLASS

The type of soil is as important with regard to the transmission of pressures from nuclear explosions as it is for pressures from chemical explosions [8]. In field experiments, the instrumentation and its application affect the "scatter" in the data. For the purpose of making a quantitative estimate of the actual equation of state of soils and to develop the method of obtaining a Rankine-Hugoniot equation of state from static pressure-density data, a dry silica glass aggregate is used. Silica is a major constituent found in many soils; for instance, the tuffs at the site of the first underground nuclear explosion, Rainier, consisted primarily of glass with phenocrysts of quartz and orthoclase [9].

The pressure-density variation of silica glass is given in the literature in increments of pressure c. 100 bars to 50,000 bars as a result of static experiments [3]. Above 50 kilobars, the pressure-density relation may be approximated from experiments on the compression of silica glass beyond the elastic limit, up to 200 kilobars [2].

Despite the irreversibility of compression for some isothermal compressions, the use of "reversible" pressure-density data in the present paper is feasible because glass will return to its original density when annealed [2,10]. It is shown later that shocked silica attains annealing temperatures. The irreversible compressibility of silica glass was found by measurements of the change in density of the glass after the pressure upon it was relieved. The percentage change in density of the silica glass is shown in Table 1 for various pressures. That the silica glass retained considerable elasticity even after "irreversible" compression is shown by the fact that the rapid reduction of pressure often resulted in the "blowout" of the specimen from the retaining ring.

TABLE 1
Dependence of Percentage Residual Density Change on Pressure

Pressure (kilobars)	Percentage Change in Density
00	
20	0.1
40	0.2
60	0.8
80	2.3
100	4.2
150	8.7
200	13.2

The pressure-volume variation for the silica glass above 40 kilobars is premised on the assumption that the volume of the glass will decrease beyond that at 40 kilobars by at least its correspondence to the percentage change in density as shown in Table 1. The pressure-volume relationship based on that premise is shown in Fig. 2. Some overrun of the volumetric change is possible.

EQUATION OF STATE

Solid

A curve representing the Rankine-Hugoniot equation of state is found by appropriately relating the shock wave factors to the isentropic equation of state. It is shown that because of the small differences between the isentropic and isothermal compressibilities of the solid, the isothermal equation of state closely approximates the isentropic equation of state.

The experimental isothermal compression curve shown in Fig. 2 serves as a reference for determining the constants in an isothermal equation of state which will take into account the overrun of the volumetric change not shown by the experiments.

The isothermal equation of state is expressed in the following form [11]:

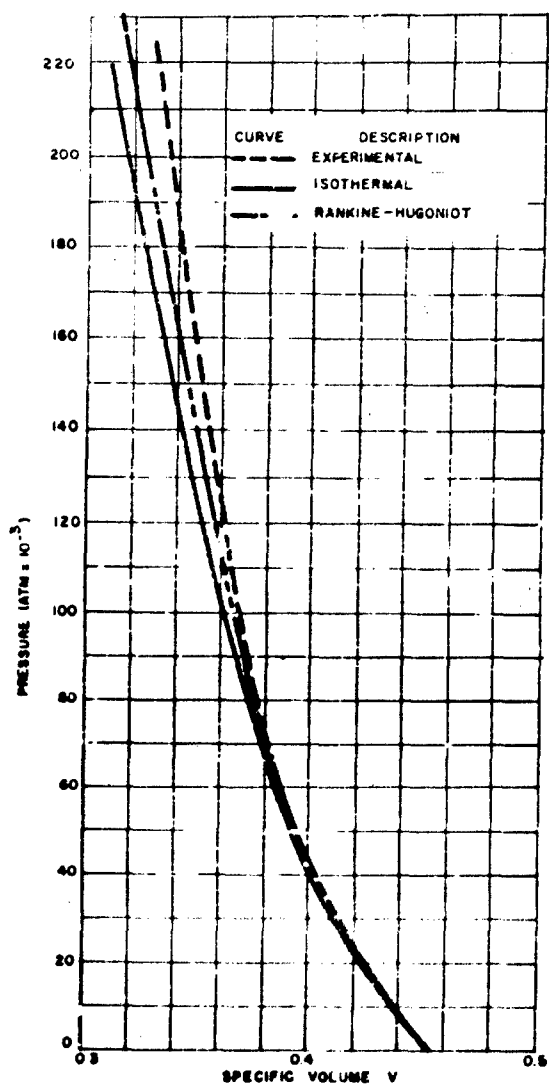


Fig. 2 - P-V of silica glass

$$P - P_0 = A \left(\frac{V_0 - V}{V_0} \right) + B \left(\frac{V_0 - V}{V_0} \right)^2 \quad (1)$$

where

$$A = \frac{1}{b} \left(1 + \frac{2ac}{b^2} \right) \quad \text{and} \quad B = \frac{c}{b^3} \quad (2)$$

The parameters a , b , and c are functions of temperature and correspond to the coefficients of thermal expansion, isothermal compressibility, and the change of compressibility with pressure respectively. They are found at ambient pressure on the basis of physical arguments from measured data.

The variations of parameters a , b , and c with temperature and pressure over the entire range of conditions to which the silica glass is exposed are not known. The coefficients A and B are approximated by fitting to the experimental curve. The values for A and B are 12,000 and 1,850,000, respectively. These numbers are of the order of magnitude of those found for A and B by substitution of the appropriate measured values of the parameters a , b , and c into Eq. (2). The empirical equation of state found by substituting the values of the coefficients into Eq. (1) is shown as the solid curve on Fig. 2.

The isentropic equation of state is required to find the "Rankine-Hugoniot" relationships in the solid. It is shown below that the isothermal and isentropic equations of state for a solid are practically the same.

The relationship between the isothermal and isentropic compressibilities is derived from the two TDS equations of classical thermodynamics, the result is

$$\frac{k_T}{k_S} = \frac{C_p}{C_v} = , \quad (3)$$

where k_T and k_S are the isothermal and isentropic compressibilities respectively and C_p and C_v are the heat capacities at constant pressure and constant volume respectively.

The specific heat at constant pressure is a slowly varying parameter in solids and for these purposes can be taken as constant. The value of the specific heat at constant volume is approximated by use of the Nernst-Lindemann Equation:

$$c_p - c_v = A C_p^2 T \quad (4)$$

where

$$A = -\frac{c}{k_T C_p}$$

v = specific volume, $\frac{\text{cm}^3}{\text{mole}}$

α = volume expansivity, $\frac{1}{\text{deg}}$

and the other factors are as previously defined.

Upon substitution of appropriate values into Eqs. (3) and (4), it is found that the isothermal compressibility is about 5 percent greater than the isentropic compressibility. The curve of the isentropic equation of state then lies somewhat to the right of the isothermal curve in Fig. 2. Because this displacement of the isentropic curve would be only slight and because the degree of experimental accuracy, together with the validity of the assumption made with regard to the irreversible compressibility, may be just of this order of magnitude, the plotted isothermal curve is taken to represent the isentropic curve also.

From the thermodynamic conservation of energy the change in internal energy caused by a shock of peak pressure P is

$$E_i - E_0 = \Delta E_i = \frac{P_f + P_0}{2} (V_0 - V) \quad (5)$$

where E_0 , P_0 , V_0 are the ambient internal energy, pressure and specific volume respectively of the material. V is the specific volume at the shock front. The energy change required to attain the same final volume V by an isentropic compression can be found from

$$E_i - E_0 = \Delta E_s = \int_V^{V_f} p_s dV \quad (6)$$

where E_s is the internal energy at constant entropy.

The difference between the shock and isentropic internal energies at constant volume is the thermal energy caused by the shock, i.e.,

$$\Delta E_i - \Delta E_s = \frac{P_f + P_0}{2} (V_0 - V) - \int_V^{V_f} p_s dV. \quad (7)$$

For any process at constant volume, the change in energy may be written as $\Delta E = C_v \Delta T$. Writing $dT = (\partial T / \partial P)_v dP$, the thermal energy is

$$\Delta E_1 - \Delta E_2 = \int_{P_1}^{P_2} C_v \left(\frac{\partial T}{\partial P} \right)_v dP. \quad (8)$$

Because C_v and $(\partial T / \partial P)_v$ are slowly varying, they are taken as essentially constant. By combination of Eqs. (7) and (8), there is obtained Eq. (9).

$$P_f - P_s = \frac{\frac{P_f + P_o}{2} (V_o - V) - \int_{V_o}^V p_s dV}{C_v \left(\frac{\partial T}{\partial P} \right)_v}. \quad (9)$$

With some algebraic manipulation, and without further approximations, Eq. (9) is readily transformed into the following explicit solution for $P_f - P_s$, given in terms of P_s rather than P_f and V_o as in Eq. (9):

$$P_f - P_s = \frac{\frac{(P_s + P_o)}{2} (V_o - V) - \int_{V_o}^V p_s dV}{C_v \left(\frac{\partial T}{\partial P} \right)_v - \left(\frac{V_o - V}{2} \right)}. \quad (10)$$

The relationship between the shock peak pressure and volume, which is readily found from Eq. (10) becomes

$$P_f = \frac{\frac{(P_s + P_o)}{2} (V_o - V) - \int_{V_o}^V p_s dV}{C_v \left(\frac{\partial T}{\partial P} \right)_v - \frac{V_o - V}{2}} + P_s. \quad (11)$$

The "Rankine-Hugoniot" equation of state as determined from Eq. (11) is shown in Fig. 2. An adiabatic expansion from any point on the Rankine-Hugoniot curve would end to the right of P_o , V_o . This increment of volume would be very small however because of the small effect of temperature on the expansion of the silica. The adiabatic expansion curve is nearly coincident with the Rankine-Hugoniot.

The Rankine-Hugoniot equation of state may be expressed in a form similar to Eq. (1). However, a third term, a cubic to take into account additional changes in thermal expansion and compressibility incurred by the shock process, may be required to obtain a closer fit to the Rankine-Hugoniot curve than is possible with Eq. (1).

The Rankine-Hugoniot curve may also be fitted with Eq. (12) [12]

$$P - P_o = \frac{C \left[\left(\frac{V_o^n}{V} \right)^n - 1 \right]}{4 - \frac{V_o}{V}} \quad (12)$$

where

$$C = \frac{3 C_s^2 \rho_o}{n}$$

C_s = sonic velocity

ρ_o = ambient density.

The important fact to observe is that the constants in either an equation of the form of Eq. (1) or Eq. (12) must be determined by curve fitting of a predetermined Rankine-Hugoniot at present. On the basis of experience with several solids, the constants in the equations may be estimated to provide roughly approximate equations of state of similar solids.

Waste Heat and Thermal Energy

A mathematical expression for the Rankine-Hugoniot equation of state, though convenient to have, is not essential for the prediction of the shock-wave propagation in a solid; a curve showing the pressure-volume relations from the shock compression is sufficient. The data required for integrating the blast wave to obtain the pressure-distance relation for the shock front are readily obtained from the graph of the Rankine-Hugoniot curve [12].

The explosive energy is dissipated in the shock wave propagation as "waste heat." Waste heat is the residual energy per unit mass remaining in the shocked material after the material has expanded adiabatically to its initial pressure. The waste heat is obtained from the graph of the Rankine-Hugoniot curve. It is illustrated as follows:

The energies per unit mass that generated by a shock wave are:

Total energy behind the shock front:

$$E_t = P(V_o - V) \quad (13)$$

Kinetic energy:

$$E_k = \frac{(P - P_o)}{2} (V_o - V) \quad (14)$$

Internal energy:

$$E_i - E_o = \frac{(P + P_o)}{2} (V_o - V) \quad (5)$$

The energies are identified graphically on Fig. 3. The total energy is the rectangle with the altitude P and base $(V_o - V)$. The kinetic energy is the upper right triangle. It follows that the internal energy added to the material by the shock is the trapezoid beneath the line between P and P_o .

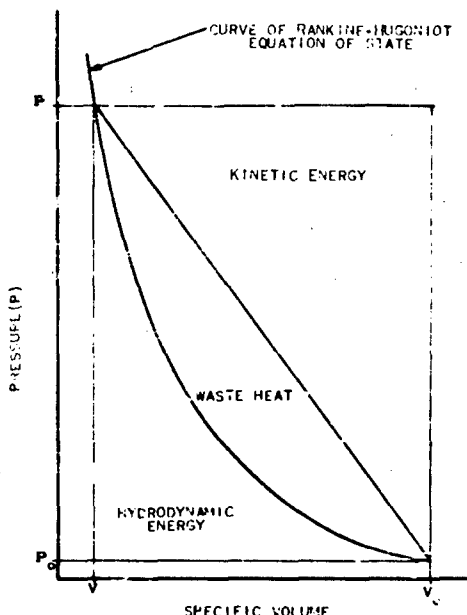


Fig. 3 - Energy relations on the graph of the equation of state

For practical purposes, solids expand adiabatically along the Rankine-Hugoniot curve to the original pressure P_o and volume V_o . The area under the expansion curve is available energy. The difference between the total internal energy and available energy must be the waste heat, which is the lens-shaped area between the diagonal and the Rankine-Hugoniot curve.

The difference in internal energies, Eq. (7), generated by a shock, and an isentropic compression is the thermal energy caused by the shock. This thermal energy is

proportional to the entropy change that occurs during the shocking process. Because the material expands along the Rankine-Hugoniot rather than along the isentrope, it can be seen in Fig. 2 that the waste heat is less than the thermal energy change from the isentropic to the shock process. It follows that the increased entropy goes partially into waste heat, and the remainder into the hydrodynamic energy. The hydrodynamic energy added by the change of entropy corresponds to the graphical area bounded by the Rankine-Hugoniot, the isentrope, and the ordinate of the compressed volume.

Porous Media—Aggregate

A porous specimen of a solid, or as defined above, an aggregate, involves a greater increase in entropy than the solid alone. Because of the greater entropy change of the shocked aggregate, a higher pressure is required to compress the aggregate than the solid alone to a given volume; also, a greater waste heat is obtained in the aggregate. An empirical equation of state based on that of the solid can be derived for the aggregate.

The Rankine-Hugoniot curve derived for a dry aggregate of silica glass and air is shown in Fig. 4. The aggregate is of spherical silica glass grains ranging in size between 20 and 30 sieve. The density is the maximum that could be packed by vibration: 1.53 gms/cm³ or 69-percent silica - 31-percent air. The crushing pressure of the aggregate is assumed to be approximately one kilobar. Because of the pressure scale of the graph the transition region appears as the base of pressure-volume curve. The waste heat corresponding to a pressure of 100 kilobars is shown as the cross-hatched area.

Figure 5 illustrates the Rankine-Hugoniots for the aggregate and the solid silica-glass taken from Fig. 2. The scale of the ordinate is enlarged below one kilobar in order to better show the transition region. It is readily apparent that the waste heat for the aggregate is considerably greater than for the silica glass. The greater waste heat of porous media accounts for the greater shock attenuation in them.

TEMPERATURE RISE

The temperature of a solid caused by an isentropic compression is found from the

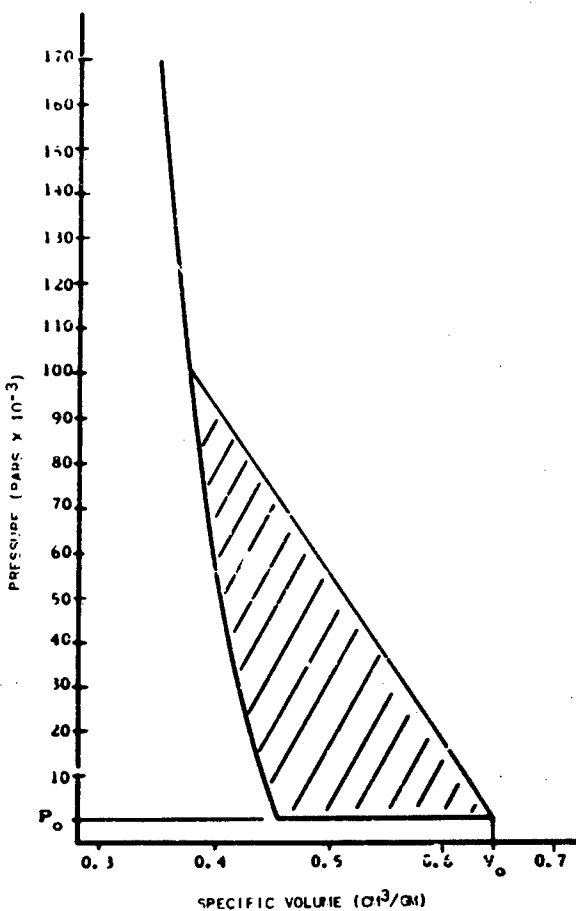


Fig. 4 - Rankine-Hugoniot curve and waste heat area - aggregate

following equation, derived from the first T ds equation of thermodynamics [13]

$$T_s = T_o e^{\beta B_t / C_v} (V_o - V) \quad (15)$$

where

T_s = isentropic temperature

T_o = ambient temperature

β = volume expansivity

B_t = isothermal bulk modulus.

The other quantities are as defined previously.

The equilibrium temperature T_e of the aggregate is found from the following heat balance equation.

$$T_e - T_o = \frac{Q_a + Q_s}{(m_a + m_s) C_p} \quad (16)$$

where Q_a is the heat in the air and Q_s the heat in the solid. The specific heat C_p is practically the same for both the air and the solid at and below the equilibrium temperature [14]. The mass of the solid is m_s ; that of air m_a . The waste heat is designated by $Q(P)$.

$$Q_a + Q_s = Q(P) \quad (17)$$

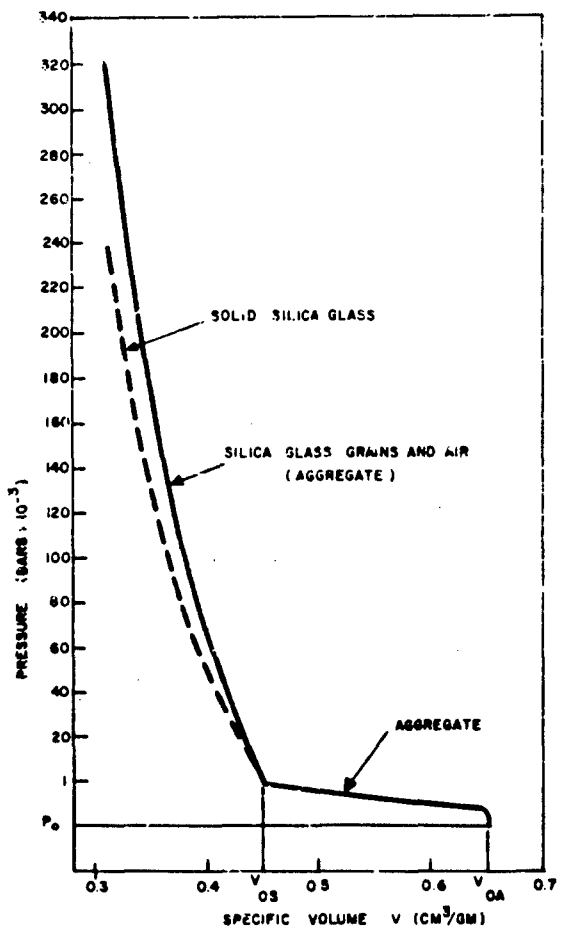


Fig. 5 - Rankine-Hugoniot equation
of state - solid and aggregate

The waste heat is found by graphical integration of the Rankine-Hugoniot as indicated on Fig. 4.

The temperatures found by Eqs. (15) and (16) are graphed on the pressure-temperature curves in Fig. 6.

TRANSITION REGION

The transition region in which the shock changes to a weak shock which propagates as an elastic wave is not especially distinct for a

malleable isotropic solid with negligible air content. In such a material the shock weakens from a strong shock with decreasing deformation of the solid until at lower pressures it gradually changes into a sonic wave.

In a porous solid or aggregate with an appreciable air content, the shock propagation changes considerably in the transition from a strong shock to an "elastic" wave. At peak shock pressures which are greater than the crushing strength of the aggregate, the shock propagation is designated as hydrodynamic. Near the upper limit of the crushing strength

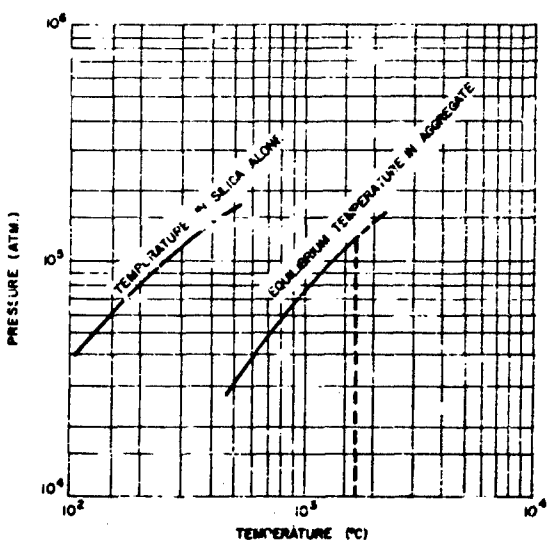


Fig. 6 - Temperature at the shock front

there is a transition in the shock from hydrodynamic behavior to that of propagation such that for each shock peak pressure there is an invariant reduced volume. Further decay of the peak overpressure by attenuation of energy by thermal and work losses causes another transition wherein the material changes to plastic behavior. Continued energy losses reduce the shock to a seismic pulse. Figure 7 illustrates the transitions. The upper crushing limit is designated by P_{cu} ; the lower P_{cl} . The vertical lines show that the crushed aggregate remains at essentially the volume to which it is reduced by P_{cl} .

Some rocks with few pore spaces, such as sandstone, may have PV curves in the transition region such as shown by the "step" in Fig. 7. This type of material has a narrow crushing pressure range, if any range at all, at which it crushes down to during the hydrodynamic phase, but below which it compresses elasto-viscously and finally elastically.

For a porous medium, such as the aggregate, the small fraction of bomb energy (less than 3 percent) that remains in the shock wave by the time P_{cu} is reached is largely dissipated in crushing the solid fraction. The shock overpressure decreases because of the crushing work losses and divergence.

For the dense rock, there is a relatively small decrease from shock energy at P_{cu} . The pressure decay in a dense rock is $P \sim 1/R^3$ whereas in the aggregate it is $P \sim 1/R^6$. The result is a strong seismic pulse at pressures somewhat below the crushing limit of the rock.

EXPERIMENTATION—LABORATORY AND FIELD

Laboratory-scale experiments utilizing high explosives to generate strong shocks in metals have been in use for several years [15], however, special provisions are required to apply one of those methods to soils. Because of the low-tensile strength and brittleness of dense rocks and the porosity, looseness, and melting upon rarefying of aggregates, the free-surface or splitting-off method is not suitable, but the impedance or deceleration method is applicable to those materials.

A schematic arrangement for the impedance method is shown in FIG. 8. As shown, with the aluminum base plate the method is for pressures in the hundreds of kilobars range. For lower pressures, especially below the complete-crushing pressures, a material

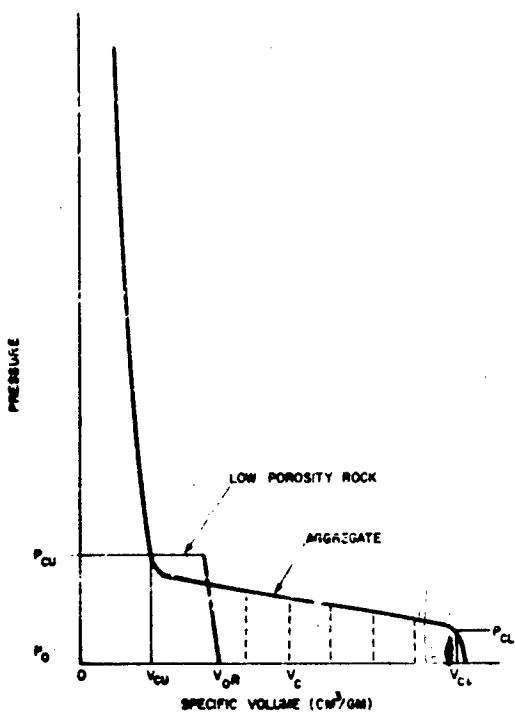


Fig. 7 - Transition regions

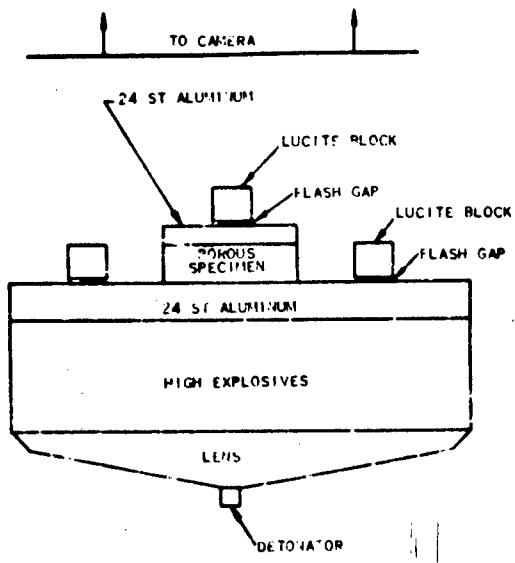


Fig. 8 - Schematic arrangement
for the impedance method

must be found for the base plates which behaves hydrodynamically, yet will not melt upon rarefying.

Aluminum is used in the base plates because its equation of state and pressure-material velocity curves are well determined [1,15]. There must be similar data for any other material that is used for base plates in this experiment.

Although a porous specimen is designated in Fig. 8, this arrangement is equally applicable to dense rocks. The upper base plate is used to contain the specimen and permit a means of determining the velocities at the upper interface. It is mandatory that the thickness of the base plates and the specimen be so chosen that a rarefaction wave will not propagate from the lower surface of the bottom base plate and interfere with the proper measurement of the shock velocity at the top surface of the upper plate.

With the equation of state of the base plate known, it is necessary only to measure the times, distances of travel and the shock wave velocities at the top surfaces of both base plates to acquire sufficient data to determine the pressure-density relations in the specimen.

When $[(\rho_0 U)_{\text{base plate}}] > [(\rho_0 U)_{\text{specimen}}]$, a rarefaction will propagate backward to the lower base plate. A shock is transmitted from the shocked specimen into the upper base plate. With $[(\rho_0 U)_{\text{specimen}}] < [(\rho_0 U)_{\text{base plate}}]$, a shock is reflected from the upper base plate.

In Fig. 9, Curve 1 is a set of pressure-material velocity states for aluminum. Curve 2 is a complete set of pressure-material velocity states for reflected rarefactions and shocks specified by Point I from free-surface velocity measurements. In Fig. 8, the part of Curve 2 below Point I corresponds to the lower base plate and a porous specimen; the part of Curve 2 above that point corresponds to the lower base plate and a dense rock. Shock pressure-density relations for the specimens is determined by using the base plate equation of state data, measured shock velocities and the conservation equations for momentum and mass, Eqs. (18) and (19), respectively.

$$P = P_0 + \rho_0 U u \quad (18)$$

$$\frac{\rho_0}{\rho} = \frac{U - u}{U} \quad (19)$$

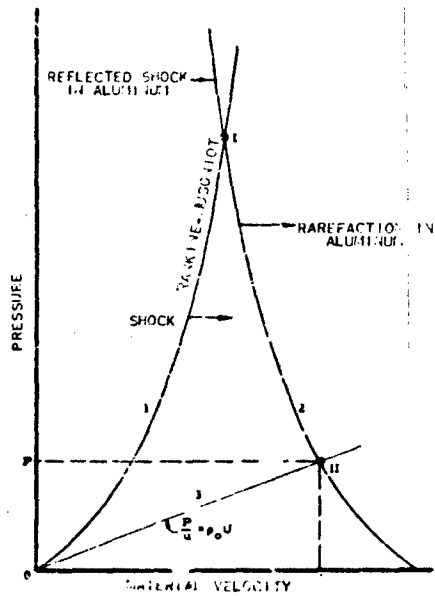


Fig. 9 - Typical graphical solution on 24 ST aluminum pressure vs material velocity curves

Another experimental method for the transition region is that of a ram impacting upon a specimen to measure the crushing characteristics of the specimen. In this method the impulse of the ram and corresponding volumetric change of the specimen are observed. From these data approximate dynamic pressure-density data are determined for the specimen.

An experimental arrangement to measure the material and shock velocities of the specimen and the impulse of the ram should incorporate high-speed cameras and instrumentation similar to that associated with the upper plate of the impedance method (Fig. 8).

Future field tests with nuclear explosions should include instrumentation to study the transition region. Instrumentation, such as accelerometers and pressure gages, should be placed before, in, and after the predicted transition region to acquire

SUMMARY

Equations of state can be approximated from static isothermal compressibility data

for solids and aggregates. More accurate equations of state may be obtained from the experimental methods which are described above. To be complete, equations of state must include the transition region. Quantitative solutions of the transition region depend on experimental data. The transition region is of particular interest with regard to soil motion at a distance from the source of the explosion.

It has been shown that the "waste heat concept" is more than just a graphical coincidence; that it is, in fact derivable from

thermodynamic principles. This concept is the basis of the blast wave integration, a powerful tool in shock wave propagation analyses.

The temperature rise of the solid, though relatively low, does get up to annealing intensity. The temperature of the aggregate is well into the annealing range. The temperature may be useful in demolitions explosions near underground petroleum storage tanks because ignition of the fuel provides additional explosive energy.

REFERENCES

- [1] J. M. Walsh and R. H. Christian, "Equation of State of Metals from Shock Wave Measurements," Physical Review, Vol. 97, No. 6, Mar. 1955.
- [2] V. D. Gogarty, "The Irreversible Compressibility of Silica Glass," Report No. IV, College of Engineering, University of Utah, 1958, (Armed Services Technical Information Agency No. AD 162 491).
- [3] P. W. Bridgman, "The High-Pressure Behavior of Miscellaneous Minerals," American Journal of Science, Vol. 237, p. 7, 1933.
- [4] H. Jense, "Das Druck - Dichte - Diagramm der Elemente bei höheren Drücken am Temperaturnullpunkt," Zeit. F. Physik, 111:373-385, 1938.
- [5] R. W. Goranson, "Physical Effects of Extreme Pressures," Scientific Monthly, Vol. LI, pp. 524-535, Dec. 1950.
- [6] P. W. Bridgman, "The Compression of Twenty-one Halogen Compounds and Eleven Other Simple Substances to 100,000 kg/cm²," Proceedings American Academy, Vol. 76, pp. 1-7, 1945.
- [7] P. W. Bridgman, "The Physics of High Pressure," London: G. Bell and Sons, Ltd, 1952.
- [8] C. W. Lampson, "Effects of Underground Explosions," Final Report, National Defense Research Committee of the Office of Scientific Research and Office of Scientific Research and Development, NDRC Report No. A-479, OSRD Report No. 6645, 1946.
- [9] University of California Radiation Laboratory, "The Underground Nuclear Detonation of Sept. 19, 1957, Rainier, Operation Plumbbob," UCRL 512-, UNCLASSIFIED.
- [10] R. B. Sosman, "The Properties of Silica," New York: The Chemical Catalog Co., Inc., 1927.
- [11] M. A. Chaszyk, Armour Research Foundation, "Studies of Surface and Underground Nuclear Explosions," Project 4195, Phase Report IV, June 1960, UNCLASSIFIED.
- [12] M. A. Chaszyk, and F. B. Porzel, Armour Research Foundation, "Study of Blast Effects in Soil," Project No. D119, Final Report, pp. 10-11, Aug. 1958, UNCLASSIFIED.
- [13] M. A. Chaszyk, Armour Research Foundation, "Studies of Surface and Underground Nuclear Explosions," Project 4195, Phase Report V, Nov. 1960, UNCLASSIFIED.
- [14] J. O. Hirschfelder, and C. F. Curtiss, University of Wisconsin Naval Research Laboratory, "Thermodynamic Properties of Air II," NORD 9938, Table VIa, Dec. 1948.
- [15] F. Seitz, and D. Turnbull, "Solid State Physics, Vol. C, Advances in Research and Applications," p. 15, Academic Press, Inc., New York, 1958.
- [16] L. V. Al'tshuler, et al., "Dynamic Compressibility and Equation of State of Iron Under High Pressure," J. Exptl. Theor. Physics (USSR), 34, 874-885, Apr. 1958.

COMMENTS OF THE CHAIRMAN - SESSION B

(FREE-FIELD PHENOMENA)

H. L. Brode
The RAND Corporation

Having failed to exercise a chairman's privilege to comment at the end of the session, I do not intend to abuse the practice here with a lengthy critique of the papers presented. I should like, rather, to comment on some general trends characterized by the work reported in this session on free-field phenomena, and then to reach beyond the speakers to urge the attendees toward more impressive accomplishments in this research. Because of my further involvement in the program as a co-author of the first paper, I will leave it to the observer to evaluate for himself the merits of each paper (a not too difficult task for those who stayed awake). Let me, instead, make two incontrovertible (if trite) statements which may suffice to epitomize the papers not only of this session but of all the protective construction sessions: (1) It is clear that a great deal of effort is going into the various aspects of protective construction research. (2) It is also obvious that there are plenty of problems left.

Although the level of effort is impressive, and no one could justifiably claim that the subject lacked sponsorship, and although there may exist more government contracts concerned with ground-shock effects than have been written for any other nuclear weapon effect, there is evidence that the effort has not been as fruitful as hoped. I do not resubscribe each year to the tenet that we don't know anything about the subject (and so must have a huge program initiated immediately), but I do recognize a number of burning questions, three, four, and even five years old, that apparently have a good fuel supply, because they are still burning.

Some of us are still waiting to be told what the important differences in dynamic response of hard rock and soil are. We are still waiting for some measure of the applicability of elasticity theory to the response of

natural media. We are still wondering about the stress field directly below a cratering explosion, and elsewhere at great depth. We are still at odds about the significance of plasticity and strain-rate effects at intense stress levels. We are still concerned about the influence of phase changes and of other more subtle solid state changes on shock wave propagation in solids. We are still unable to predict with useful definitiveness the size and depth of craters from multimegaton explosions in any medium except water-washed coral sand. I have heard it proposed that hard rock over soft rock was the best configuration above a deep installation—that soft rock over hard was good, that layered media of any sort was helpful, that homogeneous material to great depth was safest—all advocated, some supported, none proven. How directly is the current work aimed at answering such questions?

The unlikelihood of full-scale experimental explosions in dry soil or rock media will force us to depend for many years on the laboratory experiments and the theoretical developments typified by the papers of this session. But I can foresee two immediate dangers involved in this indirect approach. Without occasional checks on lab work and on theory through tests in full scale, a variety of plausible but divergent concepts can arise and can persist unresolved in an atmosphere of rivalries born of commitments and convictions which in turn are often generated more from large investments in established methodology and apparatus rather than from genuine diversity and utility of approach.

A second danger lies in the tendency toward emphasizing the problems which can be most easily investigated—with less and less concern for their relevance to a nuclear explosion in a natural environment. Both theory and lab-work lean in this direction, as the months since the last atomic test series

become years and we pound our Ottawa sands and flex our elastic media with increasing confidence. The central problems may thus remain inviolate, safely preserved for future programs, as so often is the case with "classical" fields—a process of ossification within the dignity of scientific manner.

To improve the understanding and the validity of prediction of free-field phenomena most expeditiously, both those working in this subject area and those with responsibility for the funding and direction of this research need periodically to evaluate each individual effort in the light of some well-defined goals and to encourage those projects which bear most directly on the immediate design requirements. At the same time, we must all allow (as we surely already do) that such concentration on criteria for practical protective design must not preclude or seriously postpone the more fundamental development of knowledge along canonical lines in associated fields such as soil mechanics, rheology, ground shock, and seismology. However, in my opinion, this latter requirement is generally overstressed, since none of the useful programs (existing or proposed) to improve prediction of ground-shock phenomena from nuclear explosions appears to be specific enough to interfere with or be incompatible with any of the more general research.

An outstanding deficiency of the program, then, lies in the apparent lack of strong overall supervision of the applications-oriented part of the work. Coordination between various theoretical efforts and between theory and experiment does not seem to be effective. As exemplified by the presentations at this meeting, where there was little or no effort reported in comparisons of either methods or results, it would appear that individuals or groups are working in comparative isolation, interrupted only by an occasional symposium.

If this sounds like a condemnation of the efforts of such agencies as the sponsor of this symposium or of the Defense Atomic Support Agency, whose responsibilities include coordination or supervision, or both, of much of this effort, it is not. Most of the direct applied effort is generated and sponsored by a military

"using" service (or by DASA in response to an expressed requirement from some service branch), and as such is directed toward some immediate requirement and aimed to satisfy some clearly justifiable need for design criteria associated with an existing or developing weapon system. In spite of the short range and urgent nature of these aims, such contracting agencies manage to encourage a fairly broad and basic program of research, this without concerted coordination between agencies and with no strong guidance or monetary sponsorship beyond the purview of their designated missions.

Control or supervision of research is always a sensitive subject, loaded with philosophical and ethical implications as well as questions about ultimate efficiency; and I do not suggest that the "general and basic" research be subjected to any control other than that of the interest and time requirements on the individual researchers or groups involved. I do wish to plead for the establishment of more forceful and pragmatic direction of that effort aimed at establishing better design criteria for hardened installations, and primarily using defense department or service funds. Much of the work in this category is both large scale (and expensive) and of long duration, and we can ill afford to shrug it off as a necessary expense in the research surrounding new weapons systems—if, indeed, it cannot contribute directly and decisively to their design.

Specifically, then, I would urge that either more and broader authority and support be given to the existing Defense Atomic Support Agency or, if that role is unalterable, that some advisory group be established to periodically review and recommend—to occasionally get out and help our underground trolley back on the track.

Where the broad and basic efforts may never suffer from overdiversification and the inefficiency of leisurely searching for research, the critical decisions in design criteria for our weapon systems may well be quite urgent and our shelter programs may be seriously lagging. The consequences of this applied effort may be lifesaving or catastrophic, and the day of their testing may be closer than most of us care to consider.

Section 2

INTERACTION OF SOILS WITH STRUCTURES

CHAIRMAN'S INTRODUCTORY REMARKS - SESSION D

G. A. Young
Air Force Special Weapons Center

As an introduction to this morning's session, I would like to take a few minutes, for the benefit of the uninitiated, to define our overall problem, and then take a few additional minutes to indicate the specific area of the overall problem with which we shall be concerned this morning.

The primary function of a protective structure is to provide an environment in which weapons and equipment, and in many cases personnel, can survive the effects of nuclear weapons. Survival in this case indicates that these respective items shall be able to perform their assigned functions during, or shortly after, being subjected to an enemy nuclear attack. Please note that the sessions of the 29th Symposium dealing with protective structures are concerned with only one aspect of nuclear weapons effects, i.e., with the phenomena of shock and its associated effects upon protective structures and upon the contents of protective structures. This, then, is our overall problem.

Today we are greatly concerned with high levels of protection. That is, we desire to provide structures which are capable of protecting their contents from the "close-in" effects of nuclear weapons. Protective structures are being placed underground in nearly all cases. Hence, we are confronted with a complex problem of design, and I might add without exaggeration, we are also confronted with a complex problem of research. The design problem requires a knowledge of the overall soil motion resulting from air blast and other forms of energy released by the detonation of a nuclear device. This area of the overall problem, the free-field ground

motions, was the subject of discussion in Session B, yesterday afternoon.

In order to properly design our protective structures, and to shock isolate the contents of such structures, we require a knowledge of the pressures and motions transmitted from the ground to the structure, and of the motions transmitted through the structure to the shock isolation systems or to unisolated equipment. These problems, the design of the structure and of shock isolating equipment are the subjects of Session F this afternoon and Session H tomorrow. The problem of obtaining the pressures and motions transmitted to the structure for use in design represents the area for our discussion this morning. We refer to this area as the soil-structure interaction problem. We should recognize that the word "soil" is probably not the best descriptive word in this case, since we are concerned with the interaction of underground structures with a wide variety of soil and rock media.

In making an analytical approach to the soil-structure interaction problem, we are currently inclined to rely heavily upon approaches which assume the earth's media to be ideally elastic. There are two reasons for this approach. First, in some cases, such as in rock or deep underground in soils, the behavior of the earth media may be nearly elastic if the magnitude of the pressure waves under consideration are not excessive. However, I am sure that each one present who has carefully studied the properties, and the behavior of rock during construction of nations, will feel comfortable if we refer to rock as a homogeneous, isotropic, elastic material. The second reason for utilizing

an elastic approach is perhaps of greater concern. To assume the earth media to be anything other than elastic in an interaction study, complicates the problem to the extent that based upon our present accomplishments, we have no analytical solutions. Thus, our designs in the immediate future must utilize the results of solutions based upon elastic assumptions as well as a liberal dose of intuition and good judgement on the part of the designer, particularly when the earth media under consideration is decidedly nonelastic in behavior. However, this requirement for the use of intuition and good judgement on the part of the designer, is not a new requirement for experienced engineers.

* * *

We are extremely fortunate this morning to have a collection of papers which treats with both the real and nonideal aspects of our problem. We have, for example, two excellent papers by Dr. Baron and Mr. Wiedermann which consider the elastic properties of earth media. We also have papers by Drs. Sisson and Grine which contribute greatly to our discussion by introducing the non-elastic properties of soil and some of the energy absorption characteristics of rock. In addition, we have some of the very practical aspects of the problem presented in a paper by Tom Morrison.

PRESENT ROLE OF SOIL DYNAMICS IN THE DESIGN OF UNDERGROUND PROTECTIVE STRUCTURES

G. N. Sisson

AFSWC

Kirtland AFB, New Mexico

Some aspects of the store of knowledge available to the designer of underground protective structures are surveyed. Particular attention is directed to the role of soil mechanics and to the confidence which a designer may place in current theories and empirical methods.

INTRODUCTION

Modern military requirements demand large underground structures to resist high overpressures resulting from nuclear blasts. This demand places a challenging burden upon firms engaged to design one of these structures. Not only is the structure expected to retain its integrity over periods measured in years, but for at least one brief spectacular interval which may last only one second, it must survive the violent motions resulting from the blast. Therefore, the designer asks:

1. What normal or conventional problems must be considered in the design of the structure?

2. How does the earth medium behave when subjected to the shock effects of a nuclear weapon?

3. What forces and motions does a structure, buried in an earth medium, experience when the earth medium is subjected to the shock effects of a nuclear weapon?

Before the designer is finished, he will ask many more very important questions. Since the primary purpose of the structure is to protect the contents, he will ask how the contents respond to the motions of the structure. He will also study all the problems associated with quickly "buttoning" up the installation when an attack comes, and of operating during the buttoned-up period. However, the following discussion deals only with the three questions above.

STATIC DESIGN PROBLEMS

In considering the first question, the design problems associated with static or conventional loads, it is appropriate to look briefly at current design procedures. The construction industry is of gigantic proportions and in our nation alone, involves the annual expenditures of some 50 billion dollars of private and public funds. Since all of us contribute to these expenditures one might logically ask, "What assurance do designers have, prior to the expenditure of 5 million dollars per mile on a public highway, 10 million dollars for a single large structure; or 300 million dollars for a large dam, that the structure being designed will not collapse and result in loss of lives and investment?" Indeed he has no complete assurance as witnessed by occasional highly publicized failures. This has been mankind's experience for many generations. The leaning tower of Pisa stands today only through a property which we might call grace rather than the foresight of its designers. The wide-spread damage now occurring in Mexico City is occurring for reasons which we can now explain, but the effects were not predicted prior to the initiation of subsidence in this area. However, in the past 30 years and more particularly in the past 10 years, knowledge of the behavior of soils under superimposed loads has become much less subject to opinion and whim, and much more amenable to rational treatment. This has resulted largely from the scientific application of well known laws of mechanics to the behavior of soils. Although soil mechanics is still regarded by many as an art

rather than a science, Dr. Karl Terzaghi combined past classical treatments of the behavior of materials with many empirical crutches to enable us to approach a design problem today with a very high degree of confidence in the successful performance of a structure after it is built.

It must be noted here that when the designer of protective construction asks his first question, "What are the conventional problems in the design of an underground structure?", he does not have a great deal of experience on which to rely for the particular kinds of structures involved. However, he has a great many facts at his disposal. If, for example, he is interested in the design of a large structure, buried so that its top surface is near the original ground surface, he is interested in the horizontal and vertical components of force which the soil or rock impart to the structure and how the structure reacts to these forces. He already has considerable experience in estimating vertical stresses in the soil under the foundations of structures. For example, a large structure may transfer all its weight and loads to isolated points of support which are the column foundations. For settlement estimates the problem reduces to one of determining stresses and strains within a semi-infinite solid which is subjected to concentrated loads acting normal to its free surface. Toward the end of the nineteenth century J. Boussinesq considered the problem—given a point force normal to the free surface of a homogeneous, isotropic, elastic body of semi-infinite extent, what stresses are produced in the interior of this mass, and what change of position do various points within this mass suffer, as a result of the induced stresses. In 1885 Boussinesq published a solution to this idealized problem, and as a result, a procedure is available for estimating desired stresses and strains at any interior point of a soil mass. Thus, theoretically the designer has only to determine the total force acting in each column of the structures, and assume the column forces to be acting at points normal to the surface of the earth medium. The design problem then becomes simply one of assigning column loads to the structure which will insure that the stresses in the medium remain within the elastic limit of the material and that deformations are held within allowable limits. Unfortunately, this approach taxes theory beyond its capacity to supply useful information. Of all the vital bits of information yielded by the Boussinesq equations, the hard facts of experience teach that only the determination of vertical stress (and this tempered with judgment) is a trustworthy

quantity which may be applied to soil in nature which is a nonelastic semi-infinite medium, and which is also nonhomogeneous and nonisotropic.

A judicious use of theories formulated by such men as Boussinesq, Coulomb, and Rankine, combined with experience, intelligent sampling, testing, and interpretation of tests on soils on which structures are placed, constitute the practice of the top design firms in our present-day construction industry. Thus, although many challenging questions arise, the designer has confidence in answering his first question.

BEHAVIOR OF EARTH MEDIUM

The second question facing the designer, "How does the earth medium behave under the blast load?" is more difficult. An encouraging first step would be to have a theoretical solution for the dynamic Boussinesq problem, from which stresses, strains, and particle motions could be readily determined [1]. However, instead of the Boussinesq point force on the surface of an ideal body, it is necessary to consider a surface nuclear blast load which initially acts with great intensity on a relatively small area and then expands in the form of a ring over the surrounding terrain. This load travels over a nonideal body with a variable velocity and intensity, and induces compressional and shear body waves, and surface waves, into the earth. In the vicinity of the burst, an important aspect of the blast load is the system of forces directly induced by the cratering process.

Here again, the classical work of such men as Love, Lamb, Rayleigh, and others furnished the basis for formulating intelligent questions regarding the special conditions relevant to the blast design of structures buried beneath the surface of the earth. The classical theories have been of inestimable value to geophysicists, particularly seismologists, in discovering the structure of the earth, and in many prospecting applications. They have also been of great help to the construction industry in the field of earthquake design of structures. It is probable that the classicals were not even interested in the rather restricted problem of an expanding ring load on the surface of an ideal body, but whatever the reason, the fact remains that we do not have a readily useable dynamic solution to even the Boussinesq point force problem.

Several research efforts are currently being devoted to this end. As a matter of fact, work in progress is expected to yield theoretical solutions not only to the three-dimensional problem involving ideal elastic media, but layering and some form of damping will be introduced; this is at least a step closer to a medium which behaves somewhat more like real soils. Research is also underway on problems in one and two dimensions which involve plastic and locking media under dynamic loads. In the meantime, designers are being furnished empirical prediction methods based on full-scale nuclear field test data in order that current design and construction may be based on the most advanced state of knowledge available [2].

It is in order, at this time, to examine realistically some of the implications resulting from the departure of soils in nature from ideal media. On Fig. 1 are plotted the static stress-strain curves for several relatively ideal construction materials (steel, aluminum, and concrete), and on this same plot is included a region in which soils behave under static load. The stresses and strains shown are all within practical ranges for the mechanical behavior of materials. They are plotted on the same scale to indicate the relative differences between soil and other structural materials. It is true that steel, aluminum, and concrete behave somewhat differently

under dynamic rather than static loads, but soil may exhibit large differences in both moduli and strength under dynamic loads. These differences are shown on a later plot.

Most soils in nature exist at dry densities lying between 50 and 135 pounds per cubic foot. Over widespread areas these densities commonly are confined between narrower limits of perhaps 80 to 115 pounds per cubic foot. Many investigators who are engaged in theoretically predicting the behavior of soil, but have had no previous experience with soil mechanics, are startled to find that even for extremely dense soils only 80 percent of a unit volume is mineral material. Theoretically, at least, there is a 20 percent potential for volume change. At the other extreme, for a 50 pounds per cubic foot soil, only 30 percent of a unit volume is mineral material which implies a limiting value of 70 percent volume change. Perhaps an extreme example of low density soils is associated with the case of Mexico City, previously mentioned. It was found that certain portions of the 200-foot thick clay stratum underlying the City actually contain 92-percent void space. A 200-foot thick stratum of such soil, if it were to be compressed to a new volume containing even as much as 50 percent voids, would nevertheless suffer a surface settlement of approximately 170 feet. Fortunately much of the soil is denser than that noted, and settlements of

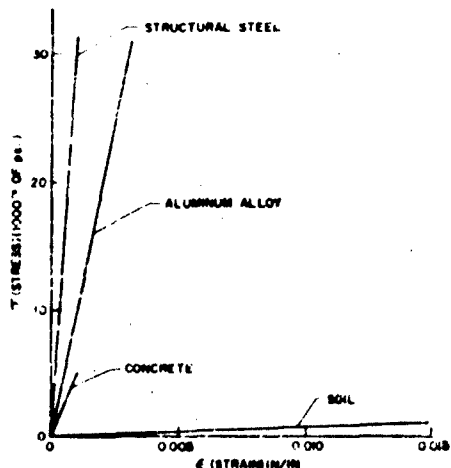


Fig. 1 - Stress-strain characteristics for various materials

this order are not anticipated. It is also true that no simple relationships exist between the amount of voids and the compressibility of a soil, but it is of interest to compare the void quantities for commonly encountered soils with, say, limestone, which often contains less than 1 percent voids.

The important point to be made is that much of our protective construction will be placed in soils which commonly contain 30- to 40-percent void space. These soils are characterized by a very low stiffness (in comparison to concrete, aluminum, and steel) which may become even lower for some range of higher stresses; depending on the kind of constraints to which they are subjected. It is not implied that they are bad construction materials—on the contrary, they may prove to be the very best media in which to place certain blast resistant structures because the damping provided by the soil, the energy attenuation characteristics related to its nonlinear behavior, etc., the economics involved in its use make it highly desirable for many purposes. In predicting behavior, however, attempts to idealize such behavior must proceed with care and caution.

Figure 2(a) represents a static stress-strain curve for a confined soil sample while Fig. 2(b) represents the same material tested under unconfined conditions, both statically and dynamically. While Fig. 2(a) is an actual stress-strain curve for a particular clay with lateral strain prevented, Fig. 2(b) is intended only to represent the kind of behavior characteristic of a comparable sample under unconfined conditions [3,4,5,6]. The attempt here is to illustrate that confinement implies large differences in strength and stiffness characteristics of soils. Even for unconfined conditions (Fig. 2(b)), there are also significant strength and stiffness differences for conditions of static and dynamic loading. Since relatively little work has been done on static and dynamic testing of soils under various conditions of confinement, these curves can be evaluated only in a qualitative way. Important features to note and which deserve additional study are the changing moduli at various stress levels, the hysteresis loops under both confined and unconfined conditions, and a feature not apparent from these plots; namely, the strain-time relations during both the loading and unloading portions of the curves. Static tests on confined soil samples commonly exhibit strain recovery persisting over long times after the load is removed. Dynamic strain data from full-scale field tests suggest

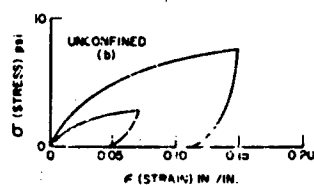
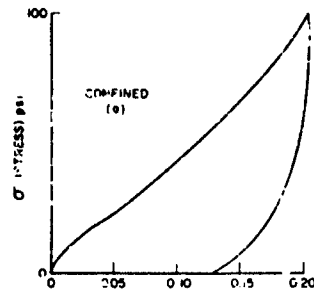


Fig. 2 - Confined and unconfined stress-strain relationships for soil

that the strain recovery or "rebound" phase also continues for a considerable time after the load has passed. There is an implication that during the time of significant response, the material behaves as a nonlinear viscoelastic material or perhaps even as a plastic solid.

Figure 2(a) also offers a possible explanation for the relatively high seismic velocities which have been measured in the field and from which the "elastic" moduli for soils have been derived. Whether or not the initial steep slope noted in this curve is characteristic of most soils, or even for some soils under dynamic load, has not been fully determined. However, laboratory tests using "sonic" methods wherein extremely low stresses are produced have shown that the moduli determined using classical wave propagation theory range orders of magnitude higher than those determined at some specified high-stress level [7]. It is reasonable to postulate that soil behavior, under the extremely low-stress levels associated with seismic measurements, is essentially elastic; whereas the behavior at high-stress levels is distinctly different phenomenon. Seismologists utilize the relationship

$$v = \sqrt{\frac{E(1-\nu)}{\rho(1-2\nu)(1+\nu)}}$$

v = Compressional Wave Velocity

E = Young's Modulus

ρ = Mass of Medium

ν = Poisson's Ratio

for the compression wave velocity in a three-dimensional ideal medium. It is apparent that the compression wave velocity may vary widely if "E" fluctuates widely during the response of soils to dynamic loads. Full-scale field test data also suggest that the energy absorption process at high-stress levels is accompanied by an attenuation of stress, strain, and particle motion [8]. Soil tests in the Air Force six-foot shock tube and analytical work on the behavior of "bi-linear locking" media (i.e., those media in which strains occur largely through progressive compaction of the material, further indicate that the near-surface behavior of the soil plays a prominent part in the total response of the earth to blast loads [9,10]. These phenomena are of direct and immediate interest to the designer who must estimate the free-field behavior of a potential construction site which may be subjected to a nuclear blast load. There is widespread belief that current prediction methods are adequate but conservative. Investigations based on more realistic material behavior promises not only more economical underground construction but may well reveal advantages which current conservative methods do not recognize.

LOADING AND RESPONSE

Having utilized empirical and theoretical guidance the better to determine the anticipated behavior of the earth, the designer is now ready for the third question regarding loading and response of underground structures. In considering this problem, it is well to recognize that when dynamic loads begin to

come into play, the structure, having a stiffness different from that of the surrounding soil, incrementally acquires an effective mass different from its own and thus alters the forces acting on it [11]. Because of its changed effective mass, it then responds in a different fashion. The changing effective mass is associated with arching effect in the soil. In its simplest form arching may be best visualized by considering the static forces indicated in Fig. 3. The force acting on plane x in Fig. 3(b) is simply the weight of the material above. Figure 3(a) is the same section but a rectangular unlined opening has been excavated with its roof at plane x . The roof of the unlined opening will not necessarily collapse in spite of the fact that no material exists in this region to carry its portion of the load. (Whether a small portion of the roof falls out or not is not important to this argument.) Since the total load remains constant above plane x , it follows that the stress must "flow" around the opening and the intensity of the stress must be altered. Since all principal stresses are thus altered and each face of the opening is acted upon by a different set of forces, the arching action will occur on every face in a different manner. If a structure which is very stiff, relative to the soil, is placed in the opening, arching will also occur but in such manner as to concentrate load onto the structure rather than to permit it to flow around the structure. The manner in which this arching effect occurs for dynamic loads on underground structures is a matter of prime interest since the design will be vitally affected by the manner in which the structure is loaded.

Even if it is assumed that the structure remains elastic throughout the dynamic disturbance and maintains a relatively constant stiffness, the preceding soil stress-strain curves illustrate that the stiffness of the soil may vary appreciably. When the interaction between a buried structure and the medium is better understood, it is hoped that the arching phenomenon may be used to provide even greater assurance of survival during attack.

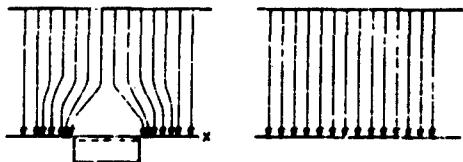


Figure 3

CONCLUSION

The preceding discussion has indicated that the designer is at least on somewhat familiar ground in considering problems involving static loads on underground protective structures. For dynamic loads, he is currently utilizing every bit of theoretical and empirical knowledge available, although much remains to be done in the field of nonlinear behavior. For the soil-structure interaction problem, there is as yet, little in the way of a rational approach. Instead, there is a great dependence upon outstanding engineers and scientists who have in the past demonstrated ability to exercise intuitive judgment in regions where knowledge is limited. An active research program is methodically adding

building blocks to the answers to designers' questions. There is great hope and confidence that a wise marriage of science and engineering, tempered with experience, will continue to furnish guides to intelligent and economic design of underground blast resistant structures. Even though hardened construction is only a small portion of the national construction program, it is presently being funded at an impressive annual rate. It deserves serious attention since it is an important part of our defense posture.

The overall effectiveness and economy with which design and construction are carried out depends in a large measure upon the success of a research program to furnish knowledge of the phenomena involved.

REFERENCES

- [1] Cui, Lili and Fugelso, "Theoretical Study of Ground Motion Produced by Nuclear Blasts," AFSWC TR 60-8.
- [2] Fred M. Sauer, "Ground Motion Produced by Aboveground Nuclear Explosions (U)," AFSWC TR 59-71, 1959 (Secret).
- [3] MIT, 1954, "The Behavior of Soils under Dynamic Loadings," (Final Report on Laboratory Studies).
- [4] MIT, 1959, "First Interim Report on Dynamic Soil Tests," (The Response of Soils to Dynamic Loads).
- [5] B. Jakobson (1957), "Some Fundamental Properties of Sand," Proc. of the Fourth International Conference on Soil Mechanics and Foundation Engineering.
- [6] Liu Chi-in (1958), "A New Apparatus for the Determination of the Coefficient of Lateral Earth Pressure at Rest," Scientia Sinica, Vol. VII, No. 5.
- [7] T. B. Goode, R. W. Cunny, et al, Operation Plumbbob, "Soil Survey and Back Fill Control in Frenchman Flat (U)," ITR 1427, Nov. 1957.
- [8] W. R. Perret, Operation Plumbbob, "Ground Motion Studies at High Incident Overpressures," WT-1405, June 1960.
- [9] H. R. J. Walsh, "An Experiment on Soils Loaded Dynamically by a Shock Tube," 1960, AFSWC (SWRS).
- [10] R. Skalak, "Attenuation of Stress Waves in Bi-linear Materials," AFSWC TN 60-30.
- [11] N. M. Newmark, and W. Hall, "Preliminary Design Methods for Underground Protective Structures (U)," AFSWC TR 60-5, 1959 (Secret).

DISCUSSION

Mr. Weissman (Ammann & Whitney):
When you were referring to the stress-strain curves for the soil, you mentioned that for design purposes the present methods were conservative. Were you referring to a method that was based on the seismic velocity?

Mr. Sison: When I discussed the dynamic characteristics of the stress-strain curves, I was not talking about something that has really been pumped into design today. We are using seismic velocities to estimate behaviors of materials in the field. I'm not quite sure what

you're asking. We're not using for these underground protective structures design methods which are directly analogous to the design of a structure under static loads.

Mr. Weissman: I'm aware that we are using the seismic velocity as a means of determining a modulus in the design procedures. You pointed out on the stress-strain curves that the modulus associated with the seismic velocity is much higher than the actual modulus that would probably occur under the pressures that we design for. I thought you implied that these procedures, using the seismic velocity, were conservative. I didn't quite understand that.

Mr. Sisson: Well, let me say this. I represent a research organization and I like to discuss the question from the standpoint of what I consider a fair question. It's my opinion that it's highly likely in nature that a soil, subjected to sufficiently low stress, will behave linearly elastically and therefore you can

determine its elastic constants using classical wave propagation theory. However, when you subject this soil mass to a pressure of 100, 200, 300 psi, I'm not at all convinced this is the case. I think in the meantime if you must design, you must use something which you can say is no or at least which has some basis in theory or fact, rather than someone's opinion such as my own. I'm not enthusiastic about the use of seismic velocities for determining elastic constants for soils.

Mr. Weissman: I was wondering why you mentioned that it was conservative.

Mr. Sisson: I don't know what conservative means. If you're primarily concerned with displacements and if you're using a seismic velocity which indicates a very high stiffness, then this is not conservative. I think this is a design problem and I think you'll have to agree on what you're concerned with.

Mr. Weissman: Thank you.

A CONCEPT FOR SOIL-STRUCTURE INTERACTION DUE TO GROUND SHOCK WAVES

A. H. Wiedermann
Armour Research Foundation, Chicago

This paper presents a theory or concept which can be used to estimate the forces acting on a buried structure when the structure is subjected to a ground shock wave. This work was intended to be applicable primarily for soils which are elastic, at least in an approximate manner.

INTRODUCTION

A discussion of the free-field variables is given together with an idealization of the stress wave forms of interest. The basis of the soil-structure interaction concept lies in the assumption of the nature of the forces acting on the buried structure. The force acting on the structure is assumed to be composed of two parts. One, the wave force, is due to the sudden motion of the surrounding media and the subsequent state of stress in the ground shock wave. The other, the arching force, is due to the local deformation or displacement of the structure relative to the surrounding media. The motion of the structure is governed by the usual equation of motion; however, in this treatment the forcing term has been split into two uncoupled terms. The wave force term is a function of time and the arching force term is a function of the relative displacement between the structure surface and its corresponding soil position.

The response of the buried structures is given for a range of ground shock wave parameters, structure configurations and structure parameters, and includes some analysis of shock isolation systems.

The results presented in this paper represent some work¹ recently completed at Armour Research Foundation under the sponsorship of the Structures Division of the Air Force Special Weapons Center.

LIST OF SYMBOLS

<u>Dimensional Symbol</u>		<u>Dimensionless Symbol</u>
	Amplitude of Oscillation	A
c ₀	Seismic Velocity	
C _a	Arching Coefficient	
D	Diameter of Structure	
E	Modulus of Elasticity of Soil	

¹AFSWC-TR-60-3, Appendix B, Contract I.O. AF33(616)-1169.

<u>Dimensional Symbol</u>		<u>Dimensionless Symbol</u>
E_b	Modulus of Elasticity of Buffer	ϵ
F_a	Arching Force	
F_b	Force on Back Face of Structure	β_b
F_f	Force on Front Face of Structure	β_f
F_{ba}	Arching Force on Back Face of Structure	β_{ba}
F_{bw}	Wave Force on Back Face of Structure	β_{bw}
F_{fa}	Arching Force on Front Face of Structure	β_{fa}
F_{fw}	Wave Force on Front Face of Structure	β_{fw}
K	Flexibility Parameter	λ
t	Buffer Thickness	L
L	Length of Structure	τ
L'	Compressed Length of Structure	
M_0	Mass of the Structure	β^2, μ^2
t	Time	T
t_d, t_e	Critical Times of Free-Field Waves	
u	Particle Velocity of Soil	U_s
	Velocity of Structure	U_s, Y
	Velocity of Structure at $T = \tau$	U°
x, x'	Displacement of Soil	X, X'
y, y'	Displacement of the Structure	Y
	Displacement of the Structure at $T = \tau$	Y°
z, z'	Relative Displacement	Z, Z'
	Stress Relief Parameter	a
ϵ_{xx}, ϵ	Strain in Soil	
	Buffer Parameter	v
ρ	Density of Soil	
ρ_0	Ambient Density of Soil	
σ	Stress in Soil	
σ_0	A Constant	
$\sigma_{xx}, \sigma_{yy}, \sigma_{zz}$	Stress	

FREE-FIELD VARIABLES

The free-field variables are necessary inputs for the study of the interaction of ground shocks with buried structures. It is the purpose of this section to delineate these variables and to elaborate, somewhat, on the assumptions which must be made to make the problem tractable.

In general, interest lies in ground shock disturbances whose stress levels are in the range of hundreds of pounds per square inch. The range of earth media of interest is essentially unlimited; thus, at the level of stress of interest, we are dealing with media which behave physically in vastly different ways; that is, the behavior of the various media can be described as elastic, plastic, fluid, elastic-plastic, visco-elastic, etc. Any attempt to formulate a simple description of the behavior of the free-field variables must be tempered by the physical behavior of the media of interest. In general, this specific report will deal with a medium which is essentially elastic in its gross behavior.

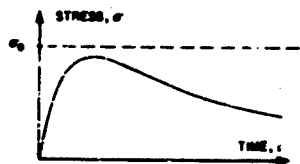


Fig. 1 - Illustration of general stress-time variation

The type of ground shock of interest in this work was restricted to plane waves which do not attenuate significantly in distances of the order of the size of structure of interest. Also, no boundary effects of the medium are considered (i.e., the medium is infinite in extent). The disturbances considered have fronts which are discontinuous (step pulse) or have finite rises; the stress fields behind the front are either uniform or decaying with time. Figure 1 illustrates the general stress-time variations and the following equation is an idealization of this variation.

$$\sigma = \sigma_0 (1 - e^{-t/t_d}) e^{-t/t_s} \quad 0 \leq t \leq \infty \quad (1)$$

where σ is stress, t is time, and σ_0 , t_d , and t_s are constants. The results discussed in this paper are limited to the step pulse case where the stress is constant ($\sigma = \sigma_0$). The propagation velocity of the disturbance, c_s , is assumed to be constant and a function only of the media.

Since the disturbance is plane and in an infinite medium, only one nonzero component of strain exists in the free field, $\epsilon_{xx} = \epsilon$ (where ϵ is the direction of propagation of the disturbance). The stress components are related to the strain component, but this relationship is unknown for the general case. For an elastic medium the most important stress is the normal stress in the direction of the propagation of the disturbance (σ_{xx}) to σ_{yy} (i.e., σ_{yy} and σ_{zz}). For the purposes of the following analysis the normal stress $\sigma_{xx} = \sigma$ will be the only stress considered.

Across a discontinuous front or quasi-stationary nondiscontinuous front, the following equations are valid.

$$\text{Continuity of Mass: } \rho_0 c_0 = \rho(c_0 - u) \quad (2)$$

$$\text{Continuity of Momentum: } \sigma = \rho_0 c_0 u \quad (3)$$

where:

ρ_0 = ambient density of the earth media

ρ = density of the media at the stress level σ

c_0 = sound velocity

u = particle velocity of the media at the stress level σ .

It should be pointed out that the disturbance is advancing into a medium which is at rest and at a zero level of stress. Thus, the stress due to gravity (overburden) is neglected when compared to the σ_{xx} .

Equation (3) yields a relationship for u , directly,

$$u = \frac{\sigma}{\rho_0 c_0} . \quad (4)$$

By using the equations for the propagation of a disturbance in an elastic medium,

$$c_0^2 = \frac{E}{\rho_0} , \quad (5)$$

we obtain

$$u = \frac{\sigma c_0}{E} , \quad (6)$$

where E is the modulus of elasticity for the medium. In any event, the particle velocity is proportional to the stress where the constant of proportionality is a function of the properties of the medium. The velocity-time variation cannot be derived; therefore, it is assumed that the instantaneous particle velocity is related to the instantaneous stress by Eq. (4) or Eq. (6). The ambient density of the medium, ρ_0 , and the sound velocity, c_0 , are readily obtainable and should be known to a reasonable degree of accuracy.

NATURE OF THE FORCES ACTING ON A BURIED STRUCTURE

The purpose of this section is to present and discuss the types of forces which are assumed to act on a buried structure when this structure is struck by ground shock. The state of the art is quite meager at the present time, and a considerable amount of work, both experimental and theoretical, must be done before the interaction phenomenon will be satisfactorily understood.

For the purpose of this paper, the geometry of the buried structure is taken as a cylinder of diameter D and length L . Sections other than a circular section can also be treated in a similar manner with minor modifications. The direction of propagation of the plane disturbance is in the axial direction such that the interaction first occurs on the end of the cylinder.

Whatever forces are applied to the buried structure are applied to the three surfaces (front, back, and side) of the structure. These surfaces will form the basis for categorizing the forces in the following treatment.

For the purposes of making estimates of the response of a buried structure when subjected to ground shock, the following types of forces are assumed to act on the structure:

1. Wave Forces
2. Arching Forces
3. Shear Forces.

These forces, which are explained in detail in the following paragraphs, do not have a firm basis. However, it was thought at this time, that the problem could best be approached by making assumptions as to the nature of the forces involved rather than making assumptions about any other physical parameters. In addition to the above forces there may exist normal compressive forces on the sides of the structure. These normal forces are symmetrically distributed and do not give rise to any net response in the direction of wave propagation. The effects of these forces are neglected in this work.

Wave Forces

It is well known that, when an acoustic wave reflects normally from an infinitely rigid boundary of infinite extent, the intensity of the disturbance is increased by a factor of two. If the

boundary is another media of identical physical properties, the disturbance will be transmitted without any reflection and the intensity of the disturbance at this fictitious boundary will be equal in magnitude to the intensity of the original disturbance. If the acoustic impedance of the boundary media lies somewhere between the above two cases, the intensity of the reflected disturbance (at the boundary) will vary by a factor of one to two.

For the purposes of this paper, it is assumed that the rigidity of the front face of the structure will be considerably greater than that of the surrounding media so that the reflection factor will be equal to two.

We are dealing here with structures of finite size, such that any local wave reflections will be relieved in a period of time which is a function of the properties of the media and the size of the structure. To a first approximation, this time will be proportional to the size, in this case the diameter, D , and inversely proportional to the propagation velocity, c_0 .

When any forces are applied to the structure, the structure will begin to move as a whole or to deflect locally. This motion will not, in general, correspond to the motion of the surrounding media. That is, there will be a relative displacement of the structure and, in the neighborhood of the structure, the displacement of the media will be distorted from the displacement which would have occurred if the structure had not been present. In attempting to separate the forces which act on a single face of the structure, we are assuming that the stresses in the media which give rise to these forces are also separable.

By separating the forces acting on the structure, it is possible to determine the magnitude of the wave force on the front face of the structure after local reflections have been relieved. The term "wave force" here refers to those forces which are due to the sudden motion of the surrounding media and the subsequent state of stress in the ground shock wave as differentiated from those forces arising from the local deformation or displacement of the structure relative to the surrounding media. Thus, the magnitude of the wave force on the front face of the structure after the local reflections have been relieved is equal to that force which would exist if the structure-soil interface were displaced so that the surrounding medium was not disturbed by the presence of the structure. The magnitude of the wave forces will then be equal to the product of the front face area and the instantaneous stress (σ_{xx}) in the soil due to the ground shock wave.

For the case of a step pulse disturbance, the wave force on the front face, F_{fw} , has an initial value of $2\sigma_0\pi D^2/4$ and then decays down to a value equal to $\sigma_0\pi D^2/4$. To formulate the problem analytically, it is necessary to make some specific assumptions as to the relief time of the reflected wave. We, therefore, assume that the relief time will be characterized by a time equal to $aD/2c_0$ where a is a constant which should be of the order of one. We will use a value of $a = 2$ for numerical purposes. Thus, the wave force on front face corresponding to the step disturbance can be written as

$$F_{fw} = \sigma_0\pi D^2/4 \left[1 + e^{-t(2c_0/aD)} \right] \quad (7)$$

where $t = 0$ when the disturbance reaches the front of the structure. It should be emphasized here that the wave force is only a function of time; that is, the response of the structure itself does not affect this force.

A wave type of force also exists on the rear face of the structure. This force will not come into effect until the disturbance reaches the back face, that is, until $t = L/c_0$. The time required for the disturbance to propagate the slight additional distance that the rear face of the structure has moved during this period has been neglected. When the disturbance wave reaches the rear of the structure, it will propagate around the back corner and begin to increase the wave force, F_{bw} , from zero to a value corresponding to the free-field value of the disturbance. The build up time is similar in character to the relief time; hence, the same assumptions and constants which were used in developing the wave force on the front face of the structure will be used. The wave force on the back face can then be written as

$$F_{bw} = \sigma_0\pi D^2/4 \left\{ 1 - e^{-t(2c_0/aD-L/c_0)} \right\} \quad (8)$$

The wave force is illustrated in Fig. 2.

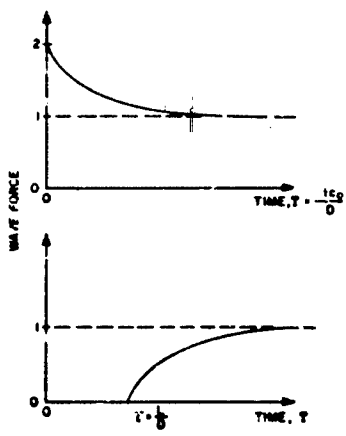


Fig. 2 - Wave forces on front and rear faces of structure

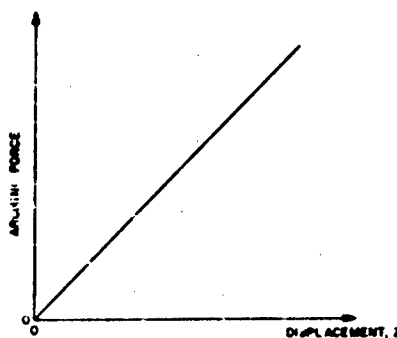


Fig. 3 - Arching forces

Arching Forces

Those forces acting on the front and rear faces of the structure which arise from the relative displacement (or deformation) between the structure and the surrounding medium are called the arching forces. This term is perhaps not the best term; however, it is used here for the lack of a more descriptive one.

Consider the static force which exists on the end of a rigid cylinder when the cylinder is forced axially into an earth medium. The deflection of the cylinder face from the position of zero force is given by x and the frictional forces on the side of the cylinder are neglected. Then this force, called the arching force, F_a , is approximated by the simple equation

$$F_a = \frac{\pi D^2}{4} C_a x \quad (9)$$

where C_a is a constant. This type of relationship does not take into consideration the many other factors which exist such as loading rates, hysteresis effects, ambient stress level, etc. For the elastic case, the arching coefficient, C_a , is known for the cylinder² to be:

$$C_a = \frac{\pi E}{2D} \quad (10)$$

The arching force is illustrated in Fig. 3. Figure 4 illustrates some experimental results³ with compacted Ottawa sand and demonstrates that Eq. (9) yields reasonable estimates for this soil.

It is possible for the arching force to become negative; that is, it is only necessary to require that the total force acting on the front or back face of the structure be zero or greater. Since the total force acting on the front or back face of the structure is equal to the sum of the arching and waveforms, the arching force can become negative to the extent that the wave force is positive.

In defining the arching force as we have done, we are actually assuming that the end of the cylinder does not deflect locally, or if it does, that the relative displacement must be large compared to any local deflections.

It is now necessary to write the more specialized equations for the arching forces acting on the front and back faces respectively. Let x be the absolute displacement of the soil particle at the position of the front face when the structure is not present. Let y be the absolute displacement of the front face of the structure. Then

$$z = x - y \quad (11)$$

²Love, A. F. H., "The Stress Produced in a Semi-Infinite Solid by Pressure on Part of the Boundary," Transaction Royal Society (London), Series A, pp. 377-402, 1926.
³Wia TM 210-1, July 1944.

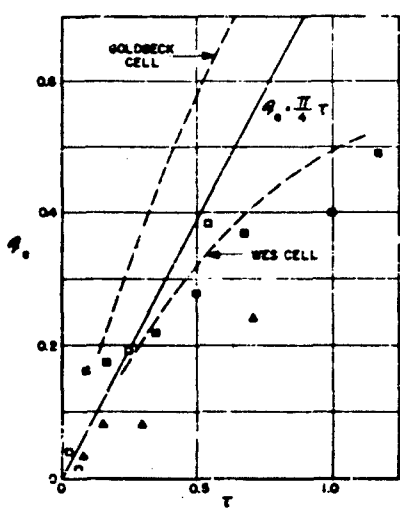


Fig. 4 - Some experimental arching force curves obtained with compacted Ottawa sand

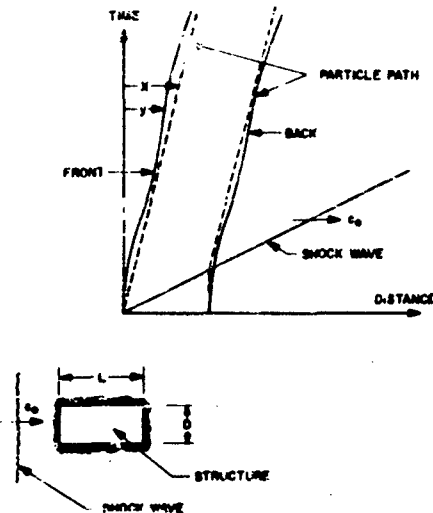


Fig. 5 - Shock wave and structure motions

is the relative displacement. If x' , y' , and z' are the corresponding variables for the back face of the structure, then for the back face

$$F_{ba} = \frac{\pi D^2}{4} \cdot \frac{\pi E}{2D} \cdot y' \quad 0 \leq t \leq L/c_0 \quad (12)$$

and

$$F_{ba} = \frac{\pi D^2}{4} \cdot \frac{\pi E}{2D} \cdot (y' - x') \quad L/c_0 \leq t. \quad (13)$$

It should be noted that $x' = 0$ during the time interval $0 \leq t \leq L/c_0$.

Shearing Force

A shear force between the side of the structure and the surrounding medium will exist. This force will resist any relative motion between the soil and the structure. For the purpose of this work it has been assumed that the shearing force can be made vanishingly small by properly treating the side surfaces of the structure and hence the shear force has been omitted from the subsequent analysis. This force is of secondary importance in its influence on the arching phenomenon but does influence to some degree the response of buried structures.

RESPONSE OF BURIED STRUCTURES

The previous sections have delineated the free-field variables and the subsequent forces which are assumed to act on the buried structure. The response of the buried structure will be treated in this section for the special cases of a rigid structure buried in an elastic medium.

The term "rigid structure" is used here to designate the treatment of the response of the structure as a single degree of freedom system. Thus, the absolute deflection of the structure as

a whole (and the absolute deflection of both the front and back surfaces) can be characterized by a single variable, y .

The equation of motion of the rigid structure buried in the earth media can be written in differential form as

$$M_0 \ddot{y} = F_{fw} + F_{fa} - F_{be} - F_{bs} \quad (14)$$

where M_0 is the mass of the structure and \ddot{y} is the acceleration of the structure.

For the purposes of illustration the solution for the step-pulse uniform field will be treated in some detail. Figure 5 presents a wave diagram which illustrates the motion of the structure.

It will be convenient at this time to introduce a set of dimensionless variables and to obtain the solution in terms of these new variables.

Let:

$$Y = \frac{yL}{D\sigma_0}, \quad X = \frac{xL}{D\sigma_0}, \quad Z = \frac{zL}{D\sigma_0}$$

$$T = C_0 t/D, \quad \tau = L/D,$$

$$\mu^2 = \frac{M_0}{D^3 \rho}, \quad \beta^2 = \frac{\pi^2}{4\mu^2},$$

and

$$S_{fw} = \frac{F_{fw}}{\frac{\pi D^2}{4} \sigma_0}, \text{ etc.}$$

It follows directly that

$$Z = X - Y, \quad X = \pi T$$

$$\dot{Y} = \dot{y} \left[\frac{\pi E}{\sigma_0 C_0} \right], \quad \ddot{Y} = \ddot{y} \left[\frac{\pi ED}{\sigma_0 C_0^2} \right]$$

$$S_{fw} = 1 + e^{-T}, \quad S_{fa} = 1/2 Z$$

$$S_{be} = 1/2 Y, \quad 0 \leq T \leq \tau$$

$$S_{bs} = 1/2 (\pi \tau - Z), \quad S_{bs} = 1 - e^{-(T-\tau)}, \quad \tau < T.$$

Equations (14) can now be rewritten in terms of the dimensionless variables:

$$Y + \beta^2 Y = \beta^2 (1 + e^{-T}) + \frac{\pi}{2} \beta^2 T, \quad 0 \leq T \leq \tau \quad (15)$$

and

$$\ddot{Y} + \beta^2 Y = \beta^2 (1 + e^{-T}) e^{-T} - \frac{\pi}{2} \beta^2 \tau + \beta^2 \pi T, \quad \tau \leq T. \quad (16)$$

The solution to Eq. (15) for the initial conditions $Y(0) = \dot{Y}(0) = 0$ is

$$Y = 1 + \frac{\pi}{2} T + \frac{e^{-T}}{1 + \frac{1}{\beta^2}} - \left[1 + \frac{1}{1 + \frac{1}{\beta^2}} \right] \cos(\beta T) + \frac{1}{\beta} \left[\frac{1}{1 + \frac{1}{\beta^2}} - \frac{\pi}{2} \right] \sin(\beta T), \quad 0 \leq T \leq \tau. \quad (17)$$

Also

$$U = \dot{Y} = \frac{\pi}{2} - \frac{e^{-T}}{1 + \frac{1}{\beta^2}} + \beta \left[1 + \frac{1}{1 + \frac{1}{\beta^2}} \right] \sin(\beta T) + \left[\frac{1}{1 + \frac{1}{\beta^2}} - \frac{\pi}{2} \right] \cos(\beta T), \quad 0 \leq T \leq \tau. \quad (16)$$

We define

$$\begin{aligned} Y^* &= \dots \\ U^* &= U(\tau) \end{aligned} \quad (19)$$

hence,

$$Y^* = 1 + \frac{\pi}{2} + \frac{e^{-\tau}}{1 + \frac{1}{\beta^2}} + \beta \left[1 + \frac{1}{1 + \frac{1}{\beta^2}} \right] \cos(\beta\tau) + \left[\frac{1}{1 + \frac{1}{\beta^2}} - \frac{\pi}{2} \right] \sin(\beta\tau), \quad (20)$$

and

$$U^* = \frac{\pi}{2} - \frac{e^{-\tau}}{1 + \frac{1}{\beta^2}} + \beta \left[1 + \frac{1}{1 + \frac{1}{\beta^2}} \right] \sin(\beta\tau) + \left[\frac{1}{1 + \frac{1}{\beta^2}} - \frac{\pi}{2} \right] \cos(\beta\tau). \quad (21)$$

The solution of Eq. (16) is

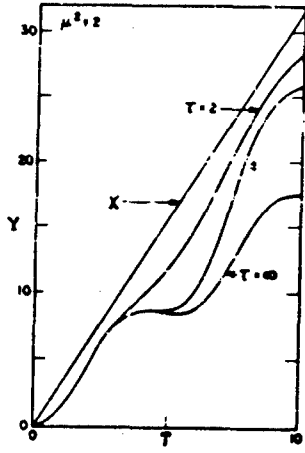
$$\begin{aligned} Y &= \left\{ \frac{1}{\beta} \left[\pi - \frac{1 + e^{-\tau}}{1 + \frac{1}{\beta^2}} - U^* \right] \sin(\beta\tau) - \left[\frac{\pi\tau}{2} + \frac{1 + e^{-\tau}}{1 + \frac{1}{\beta^2}} - Y^* \right] \cos(\beta\tau) \right\} \cos(\beta T) \\ &\quad + \left\{ - \left[\frac{\pi\tau}{2} + \frac{1 + e^{-\tau}}{1 + \frac{1}{\beta^2}} - Y^* \right] \sin(\beta\tau) - \frac{1}{\beta} \right. \\ &\quad \left. \cdot \left[\pi - \frac{1 + e^{-\tau}}{1 + \frac{1}{\beta^2}} - U^* \right] \cos(\beta\tau) \right\} \sin(\beta T) - \frac{\pi}{2} \tau + \pi T + \frac{(1 + e^{-\tau})e^{-\tau}}{\left[1 + \frac{1}{\beta^2} \right]}, \end{aligned} \quad \tau \leq T. \quad (22)$$

Figure 6 illustrates various results for a specific case.

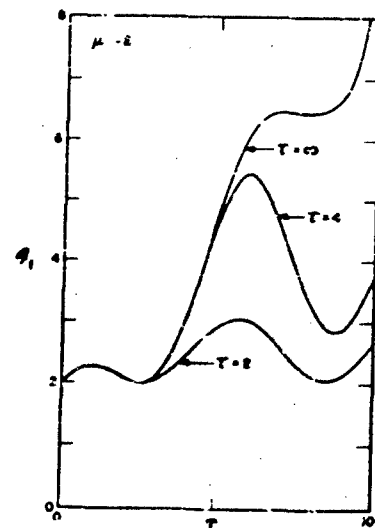
The displacements given by Eq. (17) exhibit an oscillatory nature, superimposed upon a mean velocity of one-half the free-field velocity. The exponential term, due to the wave forces, decays quite rapidly and in general does not have any appreciable effect on the results except during the very early portion of the interaction.

The effect of the mass parameters on the structure velocity appears primarily in the period of oscillation; the larger the mass, the greater the period. The variation of the net force ($\beta_f - \beta_b$) is also oscillatory in nature and is, of course, affected by the mass parameter in the same manner as is the velocity. The normalized peak acceleration decreases approximately linearly with increasing structure mass. The arching forces acting on the front and on the back faces of the structure and the total force on the front of the structure increases quite rapidly with time. The reason for this is that the relative displacement increases with time since the mean velocity of the structure is only one-half of the soil velocity.

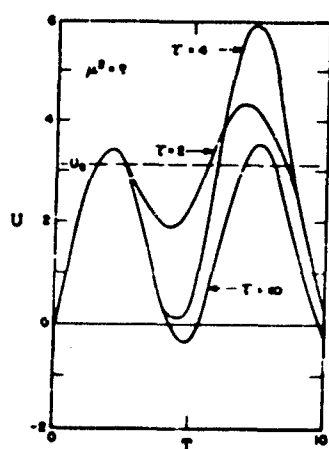
Since the value of the relief time parameter α was selected intuitively, a comparison was made of the total force acting on the front face of the structure for the selected value of α (= 2), for $\alpha = 4$ and for the limiting case of $\alpha = 0$. The results do not show a great deviation between the



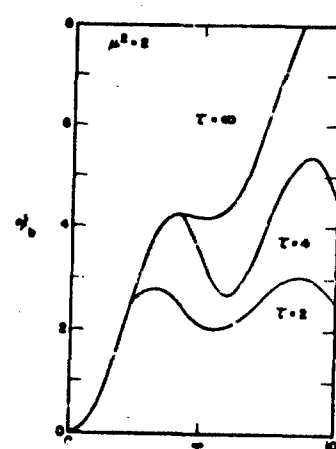
(a) - Displacement
of structure (Y)



(c) - Force on front of structure (F_f)



(b) - Structural velocity (U)



(d) - Force on back
of structure (F_b)

Fig. 6 - Structural response results for a specific case

three cases. It should be pointed out, however, that the limiting case, inherently, possesses a reflection coefficient of unity as opposed to the factor two which is being used. The above variation in α represents a variation of ± 100 percent in the impulse (for $\lambda = 2$) due to the reflection and relief of the shock wave; that is, the impulse due to the force in excess of $\sigma_0 D^2/4$.

The mean value of the total force on both the front and back faces of the structure is equal to $1 + (\pi/4)\tau$; the term $(\pi/4)\tau$ is due to the relative displacement of the structure face and the soil particles and the term "unity" is due to the free-field stress. The length parameter, τ , is also influential in another manner. Since there is no damping factor involved in the above equation, it is expected that oscillations, if set up, will persist.

The magnitude of these oscillations will be a function of the structural parameters, ν^2 and τ . The amplitude, A , of the oscillation of the displacement about the mean is given by

$$A = \sqrt{\left[\frac{\pi\tau}{2} + \frac{1 + e^{-\tau}}{1 - \frac{1}{\nu^2}} Y^* \right]^2 + \frac{1}{\nu^2} \left[\pi - \frac{1 + e^{-\tau}}{1 - \frac{1}{\nu^2}} - U^* \right]^2} \quad (23)$$

A number of other free field and structural parameters were examined and the results are discussed in Reference 1.

A brief discussion of the effect of structural flexibility and a shock isolation system will be summarized here.

The isolation system consists of surrounding the buried structure with an elastic buffer. The material should have a modulus of elasticity which is smaller than the modulus of the earth medium which surrounds the structure.

For this isolation system, the arching force is modified in that smaller forces are required for a given relative deflection. A layer of material, characterized by an elastic modulus, E_b , and a thickness, t , is placed at both ends of the structure. In general, $t \ll D$, so that the edge effects are not predominant.

The arching force becomes

$$S_a = \frac{Z}{2} \left[\frac{1}{1 + \frac{\pi t}{2 E}} \right] = \nu \frac{Z}{2} \quad (24)$$

where

$$\nu = t/D$$

$$\epsilon = E_b/E \leq 1.$$

Figure 7 illustrates the effect of this parameter.

The mean value of the total force on both the front and back faces of the structure is equal to $1 + \nu(\pi/4)\tau$.

In treating the flexible structure, it should be pointed out that it is desirable to use a single variable to determine the position of the structure. In this analysis, the coordinate, y , is used to specify the absolute displacement of the center (the mass center) of the structure. It will be further assumed that the structure will be shortened uniformly and proportional to the force applied to the structure; that is,

$$L' = L - K(F_f + F_b) \quad (25)$$

where L' is the length of the structure corresponding to the compressive load ($F_f + F_b$) and K is a flexibility parameter of the structure. It is possible to use a more equitable form for Eq. (25),

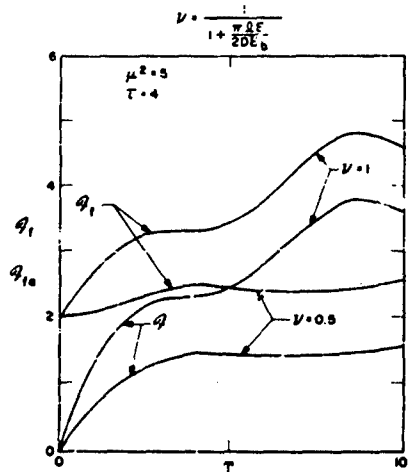


Fig. 7 - Effect of including an isolation system

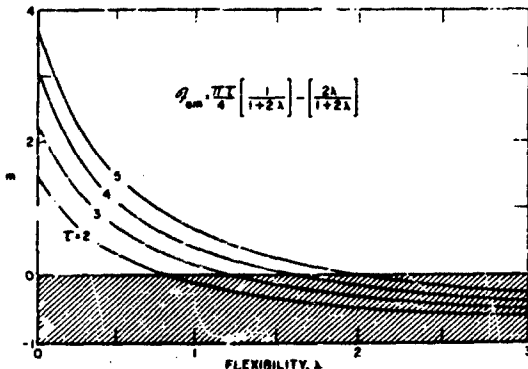


Fig. 8 - Mean arching force for system with isolation

such as one which allows the two halves of the structure to be compressed to different lengths. The change in length being proportional to the load acting on the respective half would complicate the analysis considerably and may not improve the results appreciably. It is thought that the use of Eq. (25) will yield a good first order solution.

The resulting equation of motion is independent of the flexibility parameter. Therefore, the motion of the mass center, $y(t)$ is identical to that presented previously in this paper; however, the arching forces acting on the structure are reduced and may even be negative up to the value of the wave force. The mean force acting on each face of the flexible structure for the step pulse case is:

$$1 + \frac{\pi T}{4} \left[\frac{1}{1 + 2\lambda} \right] - \frac{2\lambda}{(1 + 2\lambda)}$$

where

$$\lambda = \frac{\pi D^2}{4} \cdot \frac{\pi E}{2D} \cdot \frac{K}{2}$$

where the term unity is due to the free-field stress and last two terms are due to the relative displacement between the soil and structure. Figure 8 illustrates the mean arching force.

THE EFFECTS OF NUCLEAR EXPLOSIONS ON DEEP UNDERGROUND CYLINDRICAL TUNNELS IN ELASTIC MEDIA

M. L. Baron
Paul Weidinger Consultants
New York City

Stress-time history, velocity, acceleration and displacements produced at and near a tunnel boundary by waves from a 20 MT surface burst are given at various pressure contours. Stresses are shown for both P and S waves. General influence coefficients are presented to allow wider application.

INTRODUCTION

Nuclear explosions on the surface of an elastic half-space produce a complex stress pattern in the medium. In the most general case, the circularly-symmetric surface pressures from the explosion, which expand radially outward from Ground Zero in space and decay in time, produce a stress pattern at points in the medium in which the two principal stresses change in magnitude and direction with time. The diffraction of the stress field by a cavity containing a hardened underground installation must be considered in order to obtain the following information:

1. Stresses produced by the dynamic loading of the cavity with a view towards determining the strength of the cavity as a whole. In addition, the velocities, displacements, and accelerations of points on and near the cavity boundaries are required for the determination and evaluation of shock effects and for the establishment of failure criteria for the cavity and its contents.
2. Shock spectra for (a) total accelerations imparted to the contents of the cavity, and (b) the relative displacements of the contents of the cavity (relative to the cavity boundaries) when the cavity is enveloped by the stress waves produced by the explosion. The cavity contents may be shock mounted and the shock spectra are required for optimizing the design of the installation.

The solution to the general problem of the diffraction of the rather complicated stress field by the cavity in an elastic medium can be constructed for cases of interest by the superposition of the results obtained from some basic, less complicated, problems, which will be described in this paper. Specifically, the diffraction of the stress field produced by P (dilatational) and S (shear) waves respectively with plane wave fronts are considered. In both cases, general solutions are obtained for a step pressure in time, and these solutions can then be used as influence coefficients to give the results for waves with arbitrarily time varying pressures by means of Duhamel integrals.

The solutions of the diffraction problems for the P and S waves respectively can be used to construct solutions for the general case in which the incoming stress history has a more complicated character. Moreover, they are of direct use and importance in the supraseismic range ($V > c_p$) in which the loading on a cavity has been shown to consist of P and S waves with plane fronts carrying pressure components which decay in time [1,2]. For this range, the solutions represent an approximate answer to the actual physical problem and can be used directly.

The general diffraction problem for P and S waves with plane fronts has been completely solved for a cylindrical cavity in an elastic medium and the theoretical work has been

reported in [3,4]. Results have been obtained with the assumption that the cavity containing the installation is unlined. Practically speaking, the problem of the cavity lining—structured or anti-spalling—is quite important in the design of these installations and must be studied. A method of attack in which the results obtained for unlined cavities are used as influence coefficients in integral equations for the corresponding solutions to cavities with linings has been presented in [5]. Computations have been started on some problems of this type.

The next section of this paper gives the results for stresses, velocities and displacements produced at the boundary of a cylindrical cavity in an elastic medium as it is enveloped by plane P and S waves. Curves are presented for the case in which pressure inputs in the waves are step functions in time, as well as for waves with particular decaying pressures produced by a hypothetical 20 MT surface burst.

The final section of the paper presents shock spectra curves for the total acceleration and relative displacement of installations which are shock mounted in the cavity. Heretofore, the shock spectra used in this type of design were computed from free field input pressures, and the effects of the diffraction of the waves by the cavity were neglected. The shock spectra which are presented here include the diffraction effects and they are consequently more appropriate; they will now supersede the free field spectra and should be of use in obtaining more accurate design data for the shock mounting of the cavity contents.

The following recurring symbols are used in this paper:

c_p Velocity of pressure (P) waves in a linear elastic solid.

c_s Velocity of shear (S) waves in a linear elastic solid.

$U(t)$ Unit step function $\begin{cases} = 1 & t \geq 0 \\ = 0 & t < 0. \end{cases}$

STRESSES, VELOCITIES AND DISPLACEMENTS PRODUCED IN AN ELASTIC MEDIUM BY THE DIFFRACTION OF PLANE "P" AND "S" WAVES BY A CYLINDRICAL CAVITY

An infinitely long cylindrical cavity in an infinite elastic homogeneous and isotropic medium is acted on by a plane shock wave whose wave front is parallel to the axis of the cavity. The shock wave propagates through the medium with a constant velocity c_p (P wave) and envelopes the cavity (Fig. 1). For generality, it is assumed that the direct stress components carried by the wave are $\sigma U(t)$ and $\tau U(t)$, which are respectively parallel and perpendicular to the direction of wave propagation. The solution of this problem for the pressure inputs $U(t)$, ($\epsilon = 0$) or $\epsilon U(t)$ only, may be used to construct the solutions to problems in which the free field has a more general nature.

For the supraseismic range in which a component of the input may be considered as

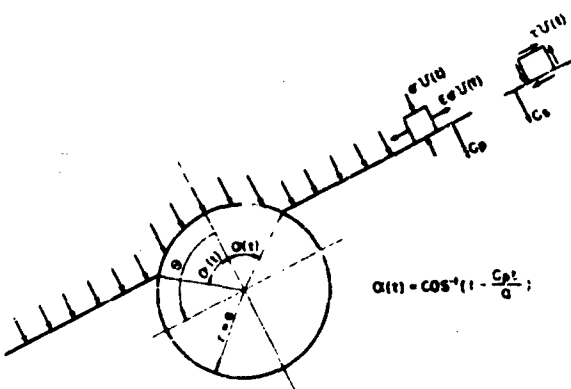


Fig. 1 - Plane shock wave enveloping cavity

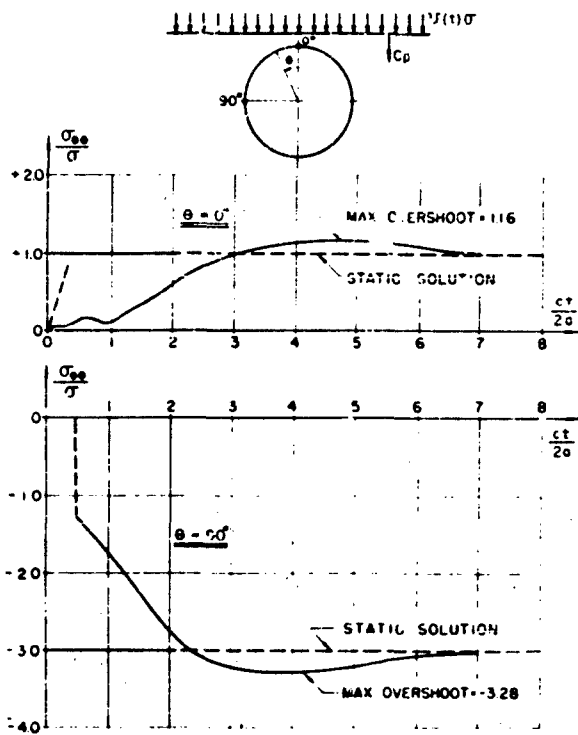


Fig. 2 - Incoming step pressure $\sigma U(\epsilon)$, $\epsilon = 0$

a plane wave, [1,2], the value of ϵ for a plane wave front must be taken as $\epsilon = -1/3$.*

The complete plane strain solution to the diffraction problem has been presented in [3] for the stresses and in [1], Appendix D for the velocities and displacements which are produced in the medium by the incoming shock wave. The present paper presents some computed results for both incoming P (pressure) and S (shear) waves.

The true physical problem under consideration requires a semi-infinite medium with a roughly plane boundary at $z = 0$. In the range of practical interest, it may be shown, [6], that this plane boundary has no significant effect for tunnels where the depth "D" is greater than 4 to 5 times the radius of the cavity, "a", since for such installations, the

major effects such as maximum hoop stresses occur at the cavity boundary at times which are considerably shorter than the arrival time of the relief wave from the plane surface at $z = 0$.

Figures 2-10 show the hoop stresses $\sigma_{\theta\theta}$ produced at points on the cavity boundary by the P and S waves which envelop the cavity. The stresses are presented at two points on the cavity boundary: $\theta = 0^\circ$, the point at which the shock front first hits the tunnel; and $\theta = 90^\circ$, the point at which the maximum stress concentration is expected. Figure 2 shows the hoop stress at the cavity boundary which is produced by an incoming plane shock wave with a step pressure distribution in time. The results obtained for long times must approach the well known static solution for a cylindrical hole in a uniaxial pressure field, i.e., a stress concentration at $\theta = 90^\circ$ of 3 (compression) while the stress at $\theta = 0^\circ$ is a tension equal in magnitude to unity. The stress amplifications due to the dynamic loading are 3.28 to 3 at $\theta = 90^\circ$ and 1.16 to 1.10 at $\theta = 0^\circ$. It is also of

*All computations given in this paper are based on a material in which the Lame constants λ and μ are equal; this corresponds to a Poisson's ratio of $\nu = 1/4$.

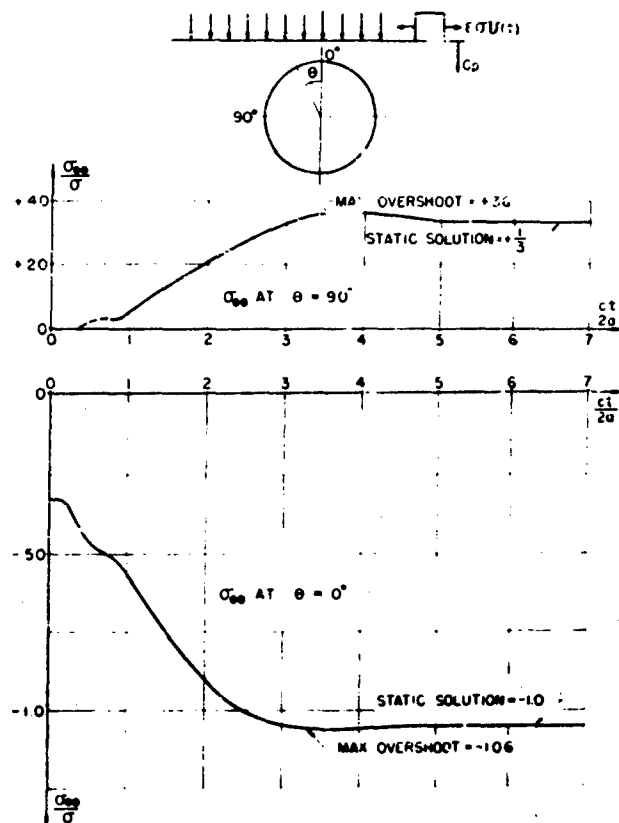


Fig. 3 - Incoming step wave $\epsilon \sigma U(t)$, $\epsilon = -1/3$

interest to note that for a step pressure input, the maximum stresses are produced at about 4-5 transit times of the shock wave across the cavity.

Figure 3 shows the corresponding results for a plane shock wave with a step pressure $\epsilon U(t)$ in the direction perpendicular to the propagation direction of the wave.

The results of Figs. 2 and 3 may be used to construct, by suitable integrations, solutions for cases in which the free-field pressure is of a more general nature.

Figure 4 shows the stress $\sigma_{θθ}$ at $θ = 0^\circ$ and $θ = 90^\circ$ for a step shock wave with a plane front progressing through the medium with a velocity c_1 [the standard "P" wave of linear elasticity theory]. The requirement of a plane wave front necessitates, in addition to the

direct stress component $\epsilon U(t)$ in the direction of wave propagation, a transverse pressure component with $\epsilon = -1/3$, i.e., $-1/3 U(t)$. The stress amplifications due to the dynamic loading are 2.92 to 2.67 at $θ = 90^\circ$ (compression) and 0.11 to 0.00 at $θ = 0^\circ$ (tension). These results may be used directly in the super-seismic range in which the shock waves, which envelop a cavity, are essentially plane waves.

The hoop stress $\sigma_{θθ}$, produced by a shock wave with a unit step pressure distribution in time may be used as an influence function to determine the corresponding stress produced by a wave with a time varying pressure, $P(t)$, by the Duhamel integral^{*} (Eq. 5),

*For a discussion on the range of pressure distributions $P(t)$ for which this procedure can meaningfully be applied, the reader is referred to Ref. [1], Pg. 99 and 102 ff.

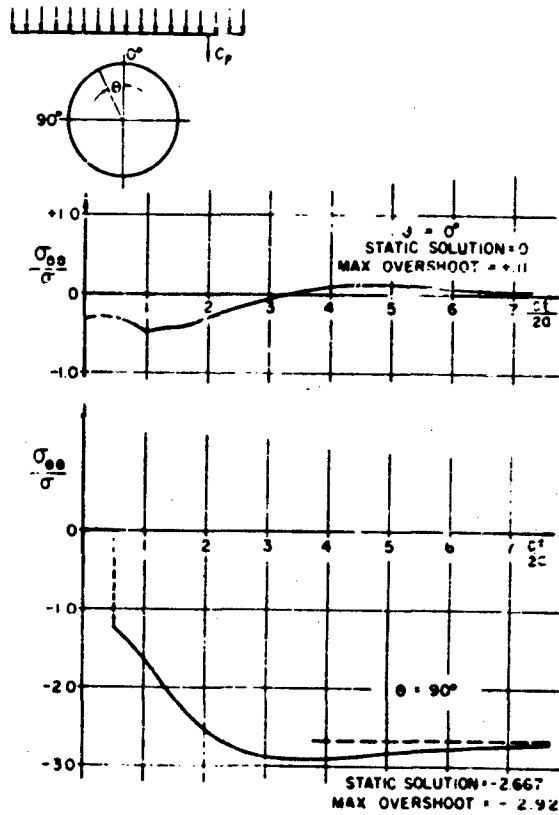


Fig. 4 - Incoming step pressure $\sigma U(\epsilon)$, $\epsilon = -1/3$

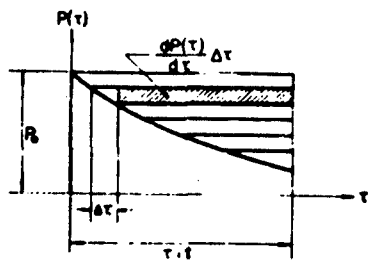


Fig. 5 - Duhamel integral

$$\sigma_{θθ} = P_0 \sigma_{θθ,0} + \int_0^t \frac{dP(\tau)}{d\tau} \sigma_{θθ,0}(t-\tau) d\tau \quad (1)$$

To illustrate the above procedure, Figs. 6 and 7 present the hoop stresses produced by plane

P waves with decaying pressure time histories. The pressure histories in the waves were taken as those produced on the surface of the medium by a 30 MT surface burst at the 6500 psi and the 2000 psi pressure contours respectively. These pressure-time curves have been given by Brode [7]. The cavity was assumed to have a radius, $a = 17.3$ feet, in an elastic medium in which $c_p = 17,300$ ft/sec. and $c_s = 10,000$ ft/sec.

It is of interest to note that the amplification of the compressive stress at $\theta = 0^\circ$ over the peak pressure P_0 in the incoming wave was 2.25 for the 2000 psi loading and 1.89 for the 6500 psi loading, as compared with 1.92 for a step pressure loading. Since the pressure-time decay for the 2000 psi wave was considerably slower than that for the 6500 psi wave, the hoop stresses are closer to those produced by a step wave for this case.

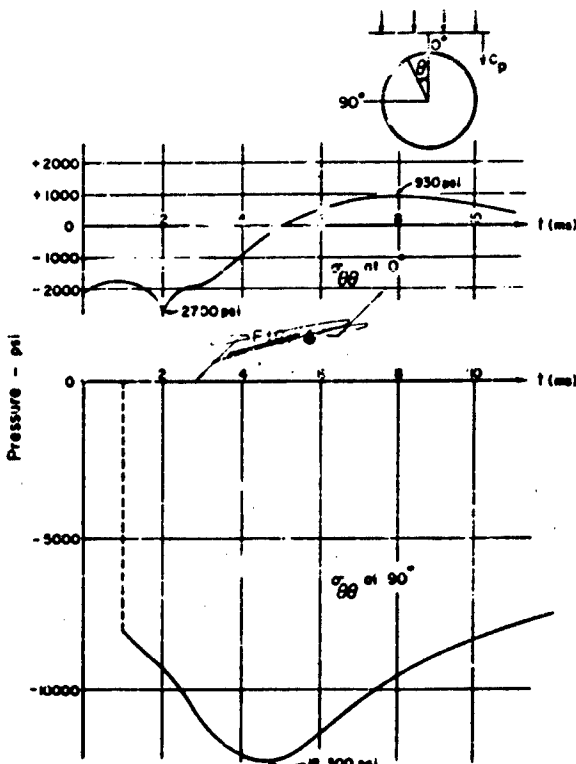


Fig. 6 - Decaying loading, $P_0 = 6500$ psi, $\epsilon = -1/3$,
 $d = 35$ feet, $c_p = 17,300$ ft/sec

Figure 8 shows the hoop stress* $\sigma_{\theta\theta}$ at $\theta = 0^\circ$ and $\phi = 45^\circ$ for a plane step shear wave with a plane front and a constant velocity c_s (the standard S wave of linear elasticity theory). At long times, the stress approaches the static solution for a cylindrical hole in a bi-axial pressure field that produces the shear stress distribution which the wave carries, i.e., a stress amplification at $\theta = 45^\circ$ of 4 (compression). The amplification of the stress by the dynamic loading is 4.37 to 4 at $\theta = 45^\circ$ and occurs at about 2.5 transit times of the S wave across the cavity.

In the superseismic range (the velocity of the air shock V on the surface is greater than c_p), the pressure waves which propagate

through the medium are standard P and S waves with plane fronts. Huth and Cole have shown that these waves can be considered to have the same pressure-time history as the surface pressure, and amplitude factors which are defined by the Mach numbers, V/c_s and $V c_p$. [See Appendix A, Ref. [1], Fig. 2]. If the cavity is located at a sufficient depth so that surface wave effects are negligible,* one can obtain a realistic picture of the stress build up at the cavity boundary by superimposing the incoming P and S waves with their proper amplitude factors and time delays due to

*The Huth-Cole solution for wave progressing across the surface of a semi-infinite elastic half space does not include Rayleigh surface wave effects. For a discussion of the effect of Rayleigh waves on free-field stresses produced in the elastic medium by surface explosions, the reader is referred to Sec. (6) and Appendix E of Reference [1].

*The theoretical derivations for the diffraction of S waves by the cylindrical cavity are given in Appendix C, Ref. [1].

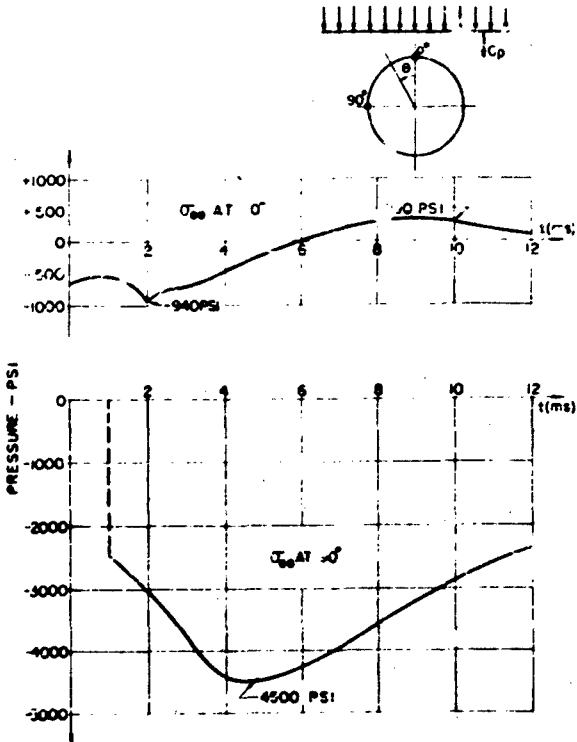


Fig. 7 - Decaying loading, $P = 2000$ psi, $\epsilon = -1/3$,
 $d = 35$ feet, $c_p = 17,300$ ft/sec

different angles of inclination and velocities of propagation. An example of this superposition is shown in Figs. 9 and 10 for a cavity of radius $a = 17.5$ feet, located at a depth of 500 feet at the 6500 psi surface pressure contour for a 20 MT surface burst. The P and S waves which travel through the medium and envelop the cavity are shown in Fig. 9. Due to the difference in propagation velocities of the two waves, the delay time between the arrival of the P and S waves is considerably in excess of 5 transit times. Consequently, for the particular case, the peak hoop stress is produced by the P wave alone at $\theta = 90^\circ$ and at early times before the arrival of the S wave at the cavity. It should be noted, however, that a considerable impulse is imparted to the cavity by the S wave at a later time and hence, any shock spectra for installations which are mounted on the cavity must include the effects of both the P and S waves on the cavity.

The theoretical development of the expressions for the displacement and velocity components u , v , w and \dot{v} which are produced at points in the elastic medium is given in Appendix D of Ref. [1]. Numerical results are presented for these quantities at points in the cavity boundary. As in the case of the stresses, the velocities and displacements produced by a step shock wave may be used as influence functions to determine the corresponding quantities produced by a wave with a time varying pressure $P(t)$ by Duhamel integrals similar to Eq. (1). In turn, these results can be used as input functions for the determination of the acceleration \ddot{w} and displacement shock spectra which are given in Sec. (3) of this paper. Figures 11 and 12 show the radial and tangential velocities v_r and v_θ respectively, which are produced by a plane step pressure wave (P_0 rise) at various points on the cavity boundary.

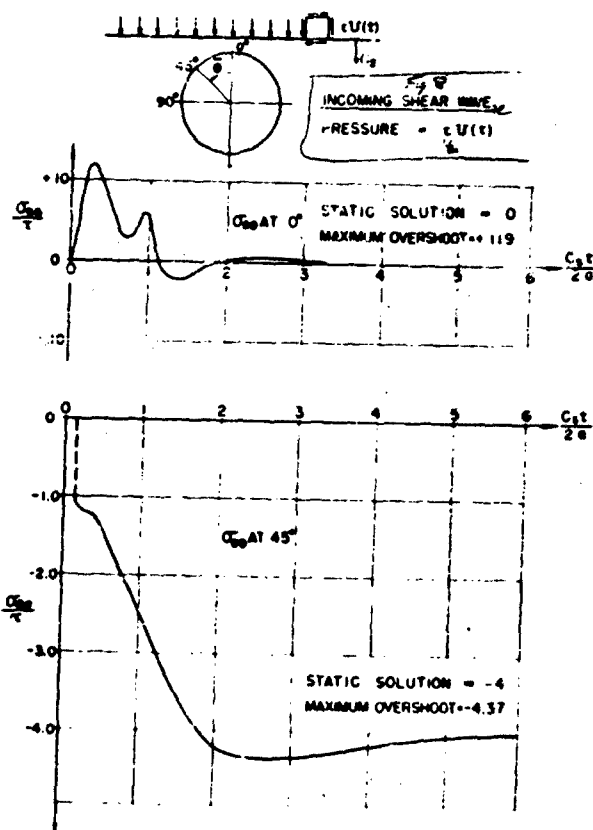


Fig. 8 - Incoming shear wave, pressure = $\tau U(t)$

The mean (rigid body) translational motion of the cavity boundary, in which the cavity retains its cylindrical shape and translates in the direction of the shock wave propagation, is extracted from the total motion of the cavity in Appendix D, Ref. [1]. Figure 13 shows the mean (rigid body) displacement, velocity and acceleration of the cavity boundary, under the step pressure shock wave

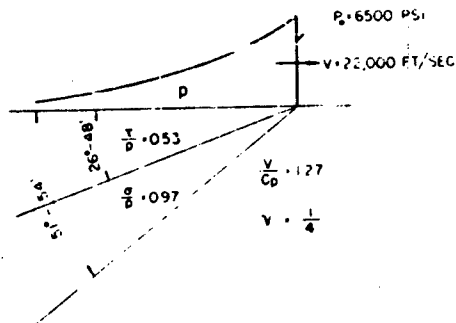


Fig. 9 - P and S waves

loading. The Duhamel technique can again be applied to obtain these results for incoming shock waves with time varying pressures.

SHOCK SPECTRA FOR INSTALLATIONS IN CYLINDRICAL CAVITIES IN ELASTIC MEDIA

The motion of points on the boundary of a cavity, subjected to shock waves, impart accelerations to installations which are located within the tunnel and are attached to these points. In many cases, these installations will be quite shock sensitive, and consequently they may require special mountings to absorb the shock effects produced by the pressure waves.

In order to optimize the designs of the shock mounted equipment, shock spectra for (1) the peak relative displacement of the installation, with respect to the motion of the points on the cavity boundary to which it is attached and (2) the peak absolute acceleration which is imparted to the shock mounted installation, are required. The latter spectra give the acceleration design requirements for a

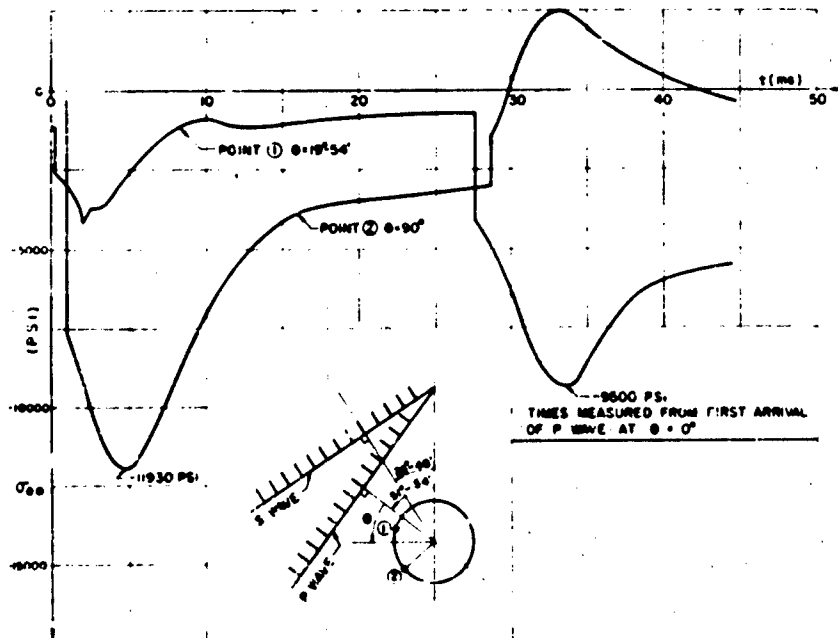


Fig. 10 - Hoop stress, $\sigma_{\theta\theta}$. $P = 6500 \text{ psi}$, $a = 17.5 \text{ feet}$,
depth = 500 feet, $c_p = 17,300 \text{ ft/sec}$.

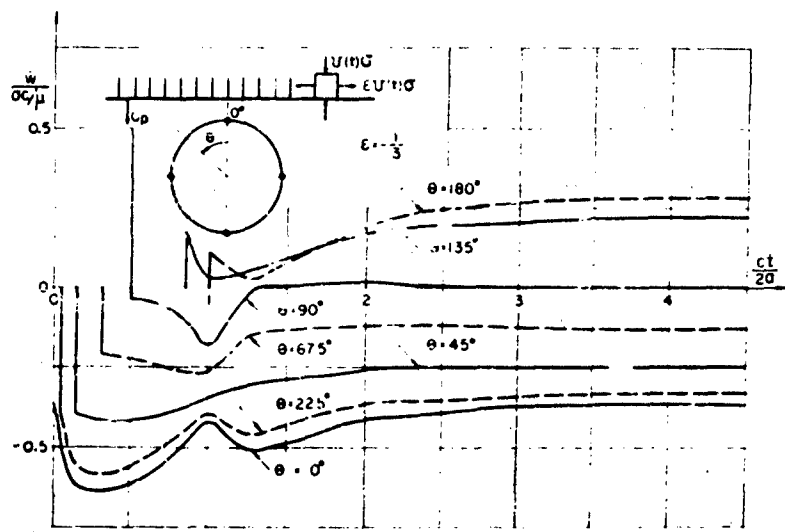


Fig. 11 - Radial velocity $\dot{w}(\theta, t)$

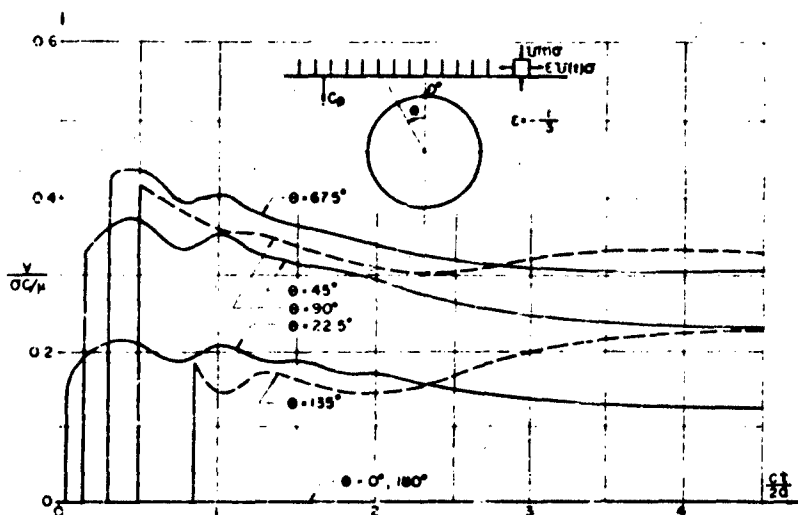


Fig. 12 - Tangential velocity $\dot{v}(\theta, t)$

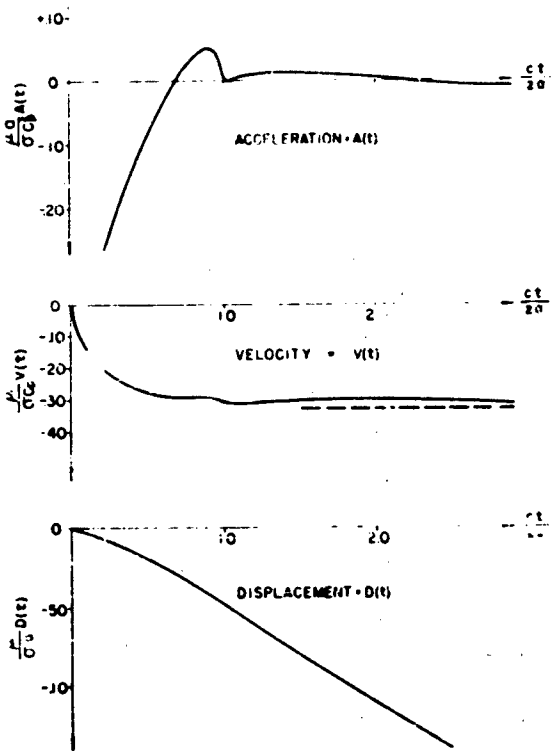


Fig. 13 - Mean (rigid body) motion of a cavity. Shock loading = P wave with unit step pressure and $\epsilon = -1/3$.

given shock mounted installation; the former give the clearance requirements for the mounting of the installation in the cavity.

The theoretical formulations for the determination of these shock spectra for waves which carry decaying pressures as given by Brode [8] are presented in Appendix E of Ref. [1]. This analytical treatment includes the diffraction effects produced by the diffraction of the shock wave by the cavity. Heretofore, shock spectra used in the design of underground installations were computed from the free field input pressures only and the diffraction effects were neglected. Consequently, the shock spectra presented in this paper are more accurate and should supersede the free field spectra, particularly for installations in which the shock mounted equipment has high-frequency components.

For illustrative purposes, shock spectra for cavities acted on by incoming P waves* with Brode pressure inputs from a 20 MT surface burst are presented in this section. As a comparison, the free field acceleration spectrum is also shown in each case.

It should be noted that the shock spectra which are presented here as illustrative examples, are based on an input of a sharp fronted pressure wave with a zero rise time.

*For practical applications for cavities located at a given point relative to Group Zero in the elastic media, the input displacement for the determination of the shock spectra must be evaluated from the complete pressure loading on the cavity, e.g., in the super seismic range, by the combined effect produced by the loading P wave and the trailing S wave.

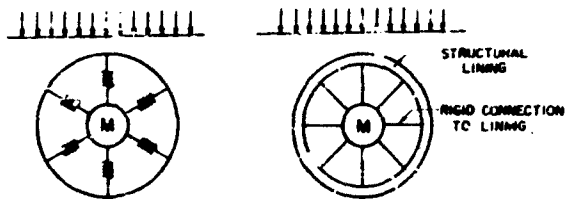


Fig. 14 - Idealized mathematical model used in constructing shock spectra

For the case of a pressure wave with a finite rise time, the intensity of the high-frequency portions of the shock spectra would be substantially decreased.

Figure 14 shows the idealized mathematical model used in the construction of the shock spectra. The problem is idealized by considering a linear oscillator consisting of a concentrated mass M on a linear spring of constant K . The oscillator is attached to a support which is subjected to a motion equal in magnitude to the displacement of the point or points on the cavity boundary at which the mass is attached. Letting the displacement of the support and of the mass, both related to a fixed datum, be $\bar{U}(t)$ and $Y(t)$, respectively; the relative motion of the mass M with respect to the support is $Y(t) - \bar{U}(t)$. The equation of motion of the oscillator is

$$Y + \omega^2 [Y - \bar{U}] = 0 \quad (2)$$

where

$$\omega^2 = \frac{K}{M} \quad (3)$$

For initial rest conditions, the solution of Eq. (2) is given by the integral

$$Y(t) = \int_0^t \omega \bar{U}(\tau) \sin \omega(t-\tau) d\tau \quad (4)$$

For a given value of ω , the peak acceleration of the mass M , $\omega^2(Y - \bar{U})_{\text{maximum}}$, and the peak relative displacement, $Y - \bar{U}_{\text{maximum}}$, are evaluated and the peak absolute acceleration spectra and peak relative displacement spectra are constructed.

Figure 15 shows the acceleration and relative displacement spectra for masses which are mounted in the cavity so that they react to the average motion of the cavity, i.e., a rigid body translation of the cavity in the direction of the shock wave propagation. An example of such a mounting would be where the mass is connected as rigidly as possible to a stiff structural lining. It is noted that the peak accelerations are considerably smaller than those given by the free-field shock spectrum.

Figures 16 and 17 give the corresponding shock spectra for masses which are mounted by a linear spring to the cavity boundary at the points $\theta = 0^\circ$ and $\theta = 180^\circ$. In both cases, the spectra allowing for diffraction differs considerably from the free field spectra. The peak accelerations for a point $\theta = 0^\circ$ are considerably increased by the diffraction. However, the opposite situation prevails at $\theta = 180^\circ$, in which the shock accelerations including diffraction effects are lower than the free-field values.

In each case, a pressure wave (P wave), carrying a Brode input pressure from a 20 MT surface burst ($P_0 = 6500$ psi) was considered.

It is obvious that the most favorable conditions for shock effects will be encountered if the equipment can be shock mounted so that it will react to the average (rigid body) motion of the cavity as a whole, rather than to the motions of individual points on the cavity boundary. However, such mountings may be very difficult to obtain practically. Moreover, one should note that most points on the cavity boundary will undergo both radial and tangential displacements and shock spectra for both directions will be required.

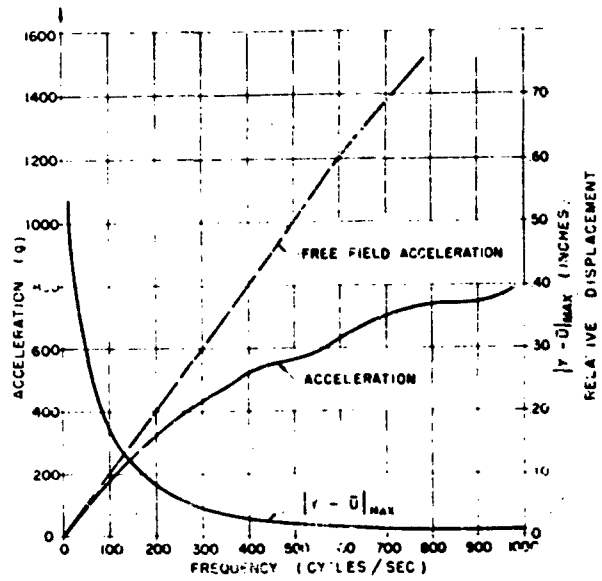


Fig. 15 - Shock spectra for rigid body motion;
 $P_0 = 6500$ psi, $c_p = 17,300$ ft/sec, $a = 17.5$ feet

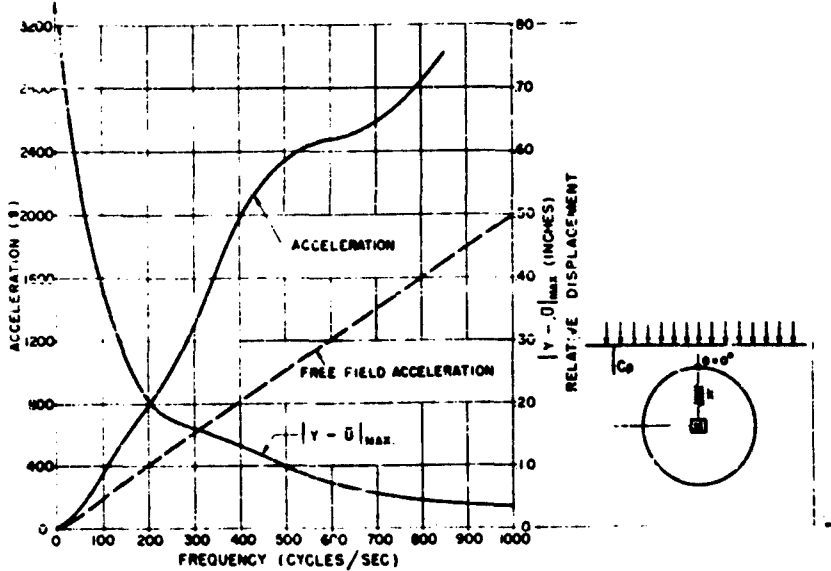


Fig. 16 - Shock spectra for motion at the boundary point $v = 0$;
 $P_0 = 6500$ psi, $c_p = 17,300$ ft/sec, $a = 17.5$ feet

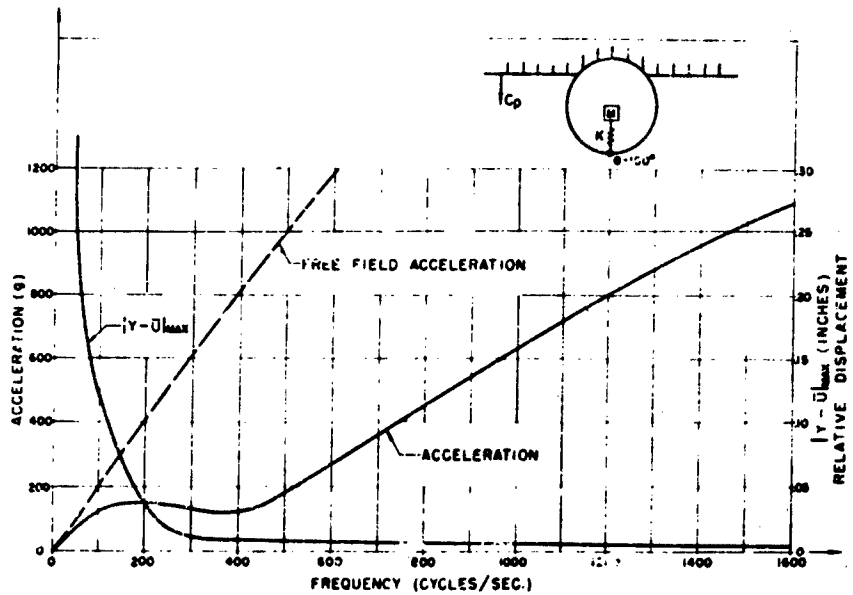


Fig. 17 - Shock spectra for motion at the boundary point $\theta = 180^\circ$; $P_0 = 6500 \text{ psi}$, $c_p = 17,300 \text{ ft/sec.}$, $a = 17.5 \text{ ft/sec.}$

REFERENCES

- [1] Baron, M. L., Bleich, H. H. and Weidlinger, P.: "Theoretical Studies on Ground Shock Phenomena," The MITRE Corporation, Lexington, Mass., Oct. 1960.
- [2] Cole, J. D. and Huth, J. H.: "Elastic Stresses Produced in a Half-Plane by Steadily Moving Loads," RAND Report P-884, Jan. 1956. Also J. Appl. Mech., Vol. 25, Dec. 1958.
- [3] Baron, M. L. and Matthews, A. T.: "Diffraction of a Pressure Wave by a Cylindrical Cavity in an Elastic Medium," RAND Report P-2109, Nov. 1960.
- [4] Baron, M. L. and Parnes, R.: "Displacements and Velocities Produced by the Diffraction of a Pressure Wave by a Cylindrical Cavity in an Elastic Medium," Forthcoming paper. See also, Reference [1], Appendix D.
- [5] See Reference [1], Section 11, "Diffraction of Pressure Waves by a Cylindrical Elastically Lined Cavity in an Elastic Medium."
- [6] "Survivability of Air Defense Systems for the MITRE Corporation, October 1959 - Ground Shock Report," Paul Weidlinger, Consulting Engineer - Guy B. Panero, Engineers, (SECRET), Oct. 1959.
- [7] Brode, H.: "Space Plots of Pressure, Density and Particile Velocity for the Blast Wave from a Point Source in Air," RAND Report, RM-1913-AEC, June 1957.
- [8] Brode, H.: "The Effect of Nuclear Bomb Blast Due to the Loss of Energy by Thermal Radiation," RAND Report RM-2076, Dec. 1957.

A SIMPLIFIED THEORY OF THE INTERACTION OF SHELL STRUCTURES WITH SOIL

Thomas G. Morrison
American Machine and Foundry Company
Niles, Illinois

This paper approaches the problem of structure-soil interaction by simplifying the basic problem to its essential elements in order to minimize the mathematics and bring out the essential physical relationships involved.

INTRODUCTION

The majority of underground structures for hardened installations being constructed and proposed for future construction are shells. These include arches, domes, cylinders, conical shells and toroids. There exists a considerable volume of literature on the design of shells to resist blast waves above ground. However, the field of dynamically loaded underground shell structures is still in its infancy. It is not surprising that the work that has been accomplished has shown that the dynamic behavior of underground shells differs markedly from the behavior of similar above ground structures.

It is the purpose of this paper to consider the general behavior of the shell structure in the underground condition rather than to go into a detailed mathematical analysis. It is the intention to take an overall look at the problem, considering only the major physical effects and utilizing gross simplifications where possible, so that the picture presented will be simple physically and unobscured by mathematical details. Thus the results obtained will be far short of a final solution to the problem but will have the virtues of simplicity and intuitive reasonableness. The results bound the problem and direct attention to areas deserving more rigorous study.

DAMPING AND RESISTANCE TO MOTION

When a shell is immersed in soil there are two major physical effects which influence

the response of the structure to dynamic loading. These are the damping effect of the soil and the resistance to motion offered by the soil. We normally think of damping as a conversion of mechanical energy into heat. However, if a vibrating system is considered to be a system within which a cyclic interchange of energy between the potential and kinetic states takes place, a more generalized concept of damping is any mechanism which removes a portion of the cyclic energy from the vibrating system during the course of a period of vibration.

If a structure is set into vibration in a vacuum it will exhibit a spectrum of discrete natural frequencies. If this structure had no damping the vibrations, once set into motion, would continue indefinitely. In air the vibration of even this theoretically perfect structure would slowly decay because a slight amount of energy would be removed by radiation through the air during each cycle of vibration. Now, if the same structure was to be immersed in soil, regardless of the assumed properties of the soil (elastic, elastoplastic, or other), free vibrations would be damped out at a much greater rate because a larger portion of the total cyclic energy would be radiated during each cycle. The single property that must be postulated to insure this effect is that the soil be capable of transmitting energy waves, regardless of the mechanism of transmission.

The accurate general solution of this problem is quite complex even for an assumed ideal elastic soil. At least two types of waves, the compression waves and the shear waves,

must be considered. These travel at different velocities and are induced by different components of the same motion. But the mathematical problem can be greatly simplified if the hypothetical soil within which the structure is immersed is assumed to have identical velocities of propagation of shear and compression waves. Of course, we are not likely to find real soil having this remarkable property. However, we can determine something of the nature of the general phenomena by assuming such a material. It turns out that the net response is rather insensitive to differences between the propagation velocities of shear and compression waves and that acceptable accuracy can be obtained by using a weighted average of the two wave velocities. A method for computing the weighted average is given in the Appendix. Its value is generally over 90 percent of the compressional wave velocity.

With this simplification of equal seismic velocities for shear and compression waves, the equation of free vibration of each normal mode becomes identical with the equation of free vibration of a mass-spring-dashpot system. Solution of this simple equation results in the following formula for δ , the ratio of actual damping to critical damping for a soil immersed shell structure:

$$\delta = \frac{\nu c}{2 w \bar{w}} \quad (1)$$

where ν = soil density in lb/ft^3

c = weighted seismic velocity in ft/sec

\bar{w} = shell unit weight in lb/ft^2 and

w = undamped shell circular frequency in radian/sec.

An important result of the application of Eq. (1) is that, for shell geometry with which we are ordinarily concerned, it turns out that the first several modes of reasonably proportioned structures are over-critically damped. That is, when immersed in soil the modes will not ring, but will respond to an imposed deformation with so-called dead-beat motion. The phenomenon can be observed very easily. Take a small bell, ring it and plunge it into a pan of water. The vibrations are damped out instantly.

Were it not for the direct restraining effect of the soil the circular frequency to be used in Eq. (1) would be just the circular frequency of vibration as ordinarily computed for the structure vibrating in air or more strictly in a vacuum. However, the soil does

have resistance and, therefore, the circular frequency of the structure vibrating in soil is increased over the value that it has vibrating in air. Making the simplest approximation that one can, we assume that the resisting force is linearly proportional to this displacement. Then the relation between the circular frequency in soil and the circular frequency in air is found to be

$$\omega^2 = \omega_0^2 + \frac{K}{w} \quad (2)$$

where

$$K = \frac{\nu c_1^2}{\pi(1+\nu)} \quad (3)$$

ω_0 = undamped shell circular frequency in vacuum (rad/sec)

K = soil resistance factor (lb/ft^3)

ν = gravity constant (ft/sec^2)

c_1 = soil compression wave seismic velocity (ft/sec)

ν = Poisson's ratio of the soil

λ = a characteristic length of the structure (ft).

The proportionality factor, K , depends on the structure size and configuration as well as on the soil properties. In fact it is probable that a sophisticated analysis would show that it is not a constant over the surface of a given structure. However, since even the simplified equation (Eq. (2)) involves Poisson's ratio, a tenuous constant for soil, it is doubtful that the value of K can ever be more than an estimate. For cylinders the characteristic length, λ , is the cylindrical radius; for spheres it is half the spherical radius.

DYNAMIC LOADING AND RESPONSE

The dynamic loading of an underground shell structure differs significantly in at least one respect from the conditions discussed previously. The energy of motion does not begin within the structure and then become radiated through the soil by the motion of the structure. Rather it is the ground shock waves proceeding through the soil which impinge on the structure. We will consider the effect of this difference. Figure 1 illustrates three successive instants during the history of the engulfment of a cylinder by a ground shock wave which, for convenience,

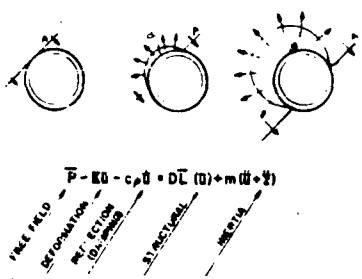


Fig. 1 - Reflection of wave from shell

is assumed to have an abrupt rise at Point "A" the pressure would be the wave front pressure, at Point "B", however, the pressure would differ from that at "A". Depending on the characteristics of the structure and the soil in which it is immersed, the pressure at Point "B" might be either lower or higher than at "A". Actually, the pressure at "B" can be considered to be composed of three components when viewed from the outside looking in and of two components when viewed from the inside looking out. The three components are: (1) the incident wave or free-field pressure, (2) the pressure introduced by deformation of the soil by the structure which we might term the "deformation pressure," and (3) the pressure resulting from the wave reflection.

In elastic materials this third pressure is proportional to the velocity of the Point "B" on the surface of the structure with respect to the free-field particle velocity. The two components of pressure whose sum is equal to the sum of the three components just enumerated are: (a) the pressure due to the deformation of the structure; for a statically loaded structure this would be the entire interface pressure, and (b) the pressure due to the inertia of the structure, the so-called inertia force.

The vector equation of motion of the structure, in generalized form, making use of the simplifications previously introduced, is shown in Fig. 1. Each term in the equation can be identified with its physical counterpart. The terms are not ordered in the usual way but grouped as just discussed. For a statically loaded structure all terms, except the first one on the left and the first one on the right side of the equal sign would be equal to zero. This, in fact, defines the generalized linear vector operator \bar{L} . Note that in the equation, the absolute free-field displacement

of soil particles is represented by u and the relative displacement of structure with respect to free-field soil particles is represented by \dot{u} .

Figure 2 shows the vector equation with the terms regrouped. Also it shows the correspondence between the terms and the terms in the equation of motion of a simple mass-spring-dashpot system. It should be noted that the grouping for the vector equation is equal to the algebraic sum of the free-field pressure P , the deformation pressure K_0 , and the free-field acceleration of the structure, $m\ddot{u}$. Now if we assume that the damping factor, c , of the second equation is sufficiently large that the system is over-critically damped, then the response of the mass-spring-dashpot system appears as shown on the accompanying graph. Whether or not the response, x , overshoots the static displacement depends on the rate of decay of the initial portion of the static displacement. In any event, for a monotonic static displacement the response asymptotically approaches the static displacement after a certain time interval. If the static displacement has a significant rise time then the response almost invariably lies below the static displacement.

Each normal mode of the structure can be represented as a mass-spring-dashpot system, though admittedly for a real structure it might be a considerable task to determine accurately the shape of the normal modes and the history of the various waves of energy propagating through the soil. However, the over-critically damped modes, which include the important modes for most realistic structures, tend to approach asymptotically not the static displacement corresponding to the free-field pressure but to the difference between the static displacements corresponding to free-field pressure and the deformation pressure, the term $m\ddot{u}$ having practically vanished

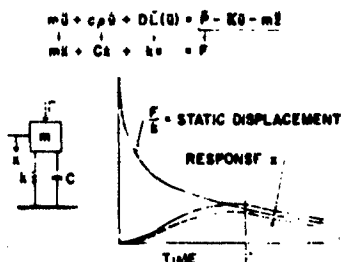


Fig. 2 - Analogy between buried structure and mass-spring-dashpot equations

shortly after structure engulfment by the ground pressure wave. The computations necessary to evaluate these factors with any degree of accuracy are quite tedious. However, certain physical arguments obviate the necessity for carrying out these computations and at the same time bring out certain important design consideration. It should be noted that the response of the mass-spring-dashpot system shown (Fig. 2) is essentially quasi-static after some time t^* , that is, the response obtained from an accurate dynamic solution is practically the same as would have been obtained had the instantaneous load F been applied as a static load and dynamic effects neglected. The time t^* , it is true, occurs shortly after peak response. However, the decrease in displacement from peak displacement to that at time t^* is very small. Thus we can conclude for each normal mode of the shell structure that by the time that peak displacement and peak stress are developed, the stresses and displacements will be very nearly those developed by a quasi-static process.

Membrane Structures

Consider now a restricted class of structures — the so-called membrane structures. These are shells having walls sufficiently thin that the pressures resisted by bending are negligible in comparison with the pressures exerted by tensions and compressions of the middle surface of the shell. If such a structure is immersed in soil or other media which develops pressure to resist deformation of the structure, and if a nonuniform static loading is applied to the structure through the soil, the structure will tend to deform in such a way that the interface pressure between soil and structure is uniform. The degree of uniformity actually achieved depends on the characteristics of both soil and structure. For developable shells such as cones and cylinders the degree of uniformity is very nearly perfect, limited only by the departure of the real shell from the ideal membrane shell and the changes of radius of curvature resulting from deformation. On the other hand, for nondevelopable structures, such as domes and toroids, there is a limit to the amount of deformation that the shell can undergo without rupture. If the soil is so stiff that the full deformation pressure can be mobilized at a fraction of the tolerable shell deformation, then these shells also will achieve a state of nearly uniform interface pressure. On the other hand, if the soil is very soft so that large deformations are necessary in order to mobilize the full

deformation pressure then, if the shell has been adequately proportioned, it will achieve an equilibrium configuration in which the interface pressure is nonuniform and the shell is not overstressed. In either event, the terminal configuration of the shell can be determined by static analysis.

One further point is worthy of note. If the shell has a widely spaced spectrum of natural frequencies then the most severely excited modes are generally those of the lower frequencies. Thus, if the first few modes are over-critically damped, by the time the lowest frequency and most severely excited mode has reached its maximum response the other modes will have already reached the state of quasi-static response with their corresponding forcing functions. Therefore, if for a particular structure it can be established that the significant modes are over-critically damped, then for design purposes it is necessary only to determine the frequency of the fundamental mode and the time required for it to reach maximum response. The various components of pressure, horizontal and vertical, existing in the free-field at that particular instant of time can be determined and applied to the structure as static pressure. The static response can be determined by conventional techniques. The resulting design will closely approximate the results of a true dynamic analysis of the structure. It is probable that errors introduced by the use of such an analysis would be of smaller order than those inherent in the variability of structure, soil and blast wave parameters, though further study would be necessary definitely to establish this conjecture.

DEPTH OF BURIAL

One problem remains — how deep must we bury the structure in order that the cover be adequate to enable the structure to respond as assumed in the foregoing analysis? Again, a mathematical determination of the depth of cover is an extremely complex process. However, a simple graphical method can be used to estimate the depth of cover with acceptable accuracy.

Figure 3 shows a cylindrical arch shell. The criterion adopted for sufficient cover is this — using the principles of geometric optics the cover shall be sufficient deep that no more than 10 percent of the energy reflected by the surface of the shell and subsequently re-reflected by the ground surface shall impinge upon the shell. To meet this criterion

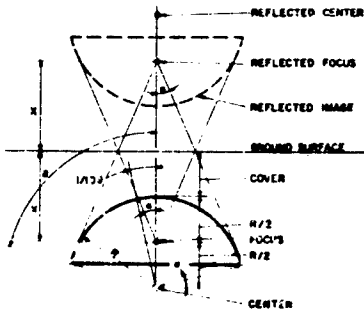


Fig. 3 - Graphical determination of cover

the cover required for a semicircular arch turns out to be slightly less than one-half of the span. This, of course, is actually quite arbitrary in that the 10-percent figure adopted is arbitrary. Comparison of the results of more elaborate studies should ultimately yield a reasonable value for the percentage to be used and thereby provide in conjunction with the graphical method a simple way to determine the required cover.

For a dome structure in which the reflected waves expand spherically the ratio of cover to span required turns out to be considerably less than for the arch. For instance, for a 90° central angle dome the cover over the crown works out to be about 3/16 of the span according to this criterion; for a hemisphere less than 10 percent of the span. It is interesting to see the results of these simple theories when applied to an extreme example.

Figure 4 shows a large dome shell having an interior framed structure providing a total of 165,000 square feet of useable floor space. The dome is designed for the 10,000 psi surface overpressure region. In order to achieve such a large structure we have to assume the

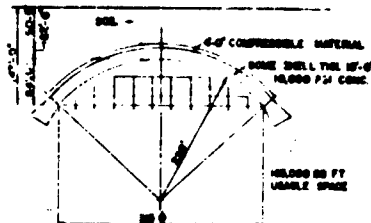


Fig. 4 - 10,000 psi dome

availability of high strength concrete. In this case 10,000 psi concrete was used. The circular frequency of vibration of a structure of the geometry shown in air is about 54 radians per second. In 3000-foot per second seismic velocity soil the damping factor computes to be about 1.1. Actual design was carried out for a damping factor of 1. You will note that a 4-foot layer of soft material has been placed $\frac{1}{2}$ way in the earth cover and the dome shell. The purpose of this layer is to decrease the restraint of the cover on the dome shell, thereby reducing the K factor to a small value and avoiding increase in the circular frequency of the very heavy shell and consequent reduction of the damping factor. Expanded light-weight aggregate might be an appropriate material for this fill.

Figure 5 shows the ground pressure wave assumed. This approximates the unattenuated ground pressure wave from a very large bomb. The response of the structure assuming unity damping factor also is shown. The equalization of vertical and horizontal ground pressure has been neglected. Even so the necessary static design pressure for the shell turns out to be only 1665 pounds per square inch.

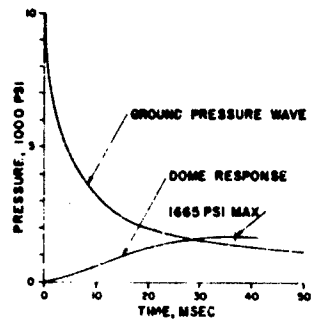


Fig. 5 - Assumed ground pressure wave

CONCLUSION

In conclusion we state that the theories presented in this paper involve a number of simplifications and approximations. Therefore, they can hardly be considered validly established design theories. However, they do indicate that if sufficient research effort is carried out in the directions outlined it should be possible to construct very large structures in the very high over-pressure regions.

APPENDIX

DAMPING OF A STRUCTURE IMMERSED IN A VELOCITY SENSITIVE MEDIUM

Consider a linear, elastic, statically loaded shell structure. The result of loading can be represented by

$$D\bar{L}(\bar{u}) = \bar{p} \quad (1)$$

where

D is a scalar constant

\bar{u} is the vector displacement of a point on the shell

\bar{p} is the vector pressure at a point on the shell

$\bar{L}(\bar{u})$ is a linear vector operator, a function of \bar{u} and its spacial coordinates

The equations of free vibration of the above system in vacuum are then (damping neglected)

$$D\bar{L}(\bar{u}) + m\ddot{\bar{u}} = 0 \quad (2)$$

$$\bar{B}_n(\bar{u}) = 0 \quad (n = 1, 2, \dots) \quad (3)$$

where

m is the unit mass of the shell, a function of the spacial coordinates

$\bar{B}_n(\bar{u})$ are the boundary conditions.

Equations (2) and (3) can always be solved in the form

$$\bar{u} = \sum_{i=1}^{\infty} A_i \bar{\varphi}_i \sin(-\omega_i t - \theta_i) \quad (4)$$

where

A_i are arbitrary constants

θ_i are arbitrary phase angles.

$\bar{\varphi}_i$ are a set of orthogonal vector functions of the spacial variables only satisfying the boundary conditions and the orthogonality relation

$$\int_A \bar{i}_i \cdot \bar{\varphi}_j dA = 0 \dots \text{if } i \neq j \\ = N_i \dots \text{if } i = j \quad (5)$$

The area integral is taken over the entire surface of the shell. A rather long development shows that the functions $\bar{\varphi}_i$ always exist.¹

The N_i are constants, termed the norms, of the orthogonal system.

The circular frequencies ω_i satisfy the relations

$$D\bar{L}(\bar{\varphi}_i) = -\omega_i^2 \bar{\varphi}_i. \quad (6)$$

If the structure is subjected to a dynamic load \bar{p} then the equations of motion become

$$D\bar{L}(\bar{u}) + m\ddot{\bar{u}} = \bar{p} \quad (7)$$

$$\bar{B}_n(\bar{u}) = 0,$$

and have a solution in the form

$$\bar{u} = \sum_{i=1}^{\infty} T_i(t) \bar{\varphi}_i, \quad (8)$$

where $T_i(t)$ are the solutions of equations of the form

$$\ddot{T}_i + \omega_i^2 T_i = \tau_i. \quad (9)$$

The functions τ_i are given by

$$\tau_i = \frac{1}{N_i} \int_A \bar{p} \cdot \bar{\varphi}_i dA. \quad (10)$$

Consider, now, the free vibrations of the same structure immersed in a velocity sensitive medium. (The medium is assumed to offer resistance to velocity only, not to displacement. Water is typical.) The equation is

$$D\bar{L}(\bar{u}) + c_1 \rho \bar{n} \bar{u} \cdot \bar{n} + c_2 \bar{i} \bar{u} \cdot \bar{i} + m\ddot{\bar{u}} = 0 \quad (11)$$

where \bar{n} is the unit vector normal to the shell and \bar{i} is the unit vector tangent to the shell and lying in the plane defined by \bar{n} and \bar{u} .

c_1 is the compressional seismic velocity

c_2 is the shear seismic velocity

ρ is the unit mass of the medium.

¹See, for instance, Air Force Special Weapons Center Technical Report TR-59-2 "Protective Construction," T. G. Morrison, Part III Unci.

The boundary conditions might or might not be the same as those of Eq. (3).

The solution of Eq. (11) is extremely complex. A much more tractable equation can be obtained by assuming the seismic velocities to be equal (an unlikely condition for real materials).

Thus set

$$c_1 = c_2 = c. \quad (12)$$

Then Eq. (11) becomes

$$D\ddot{u} + c\rho\dot{u} + m\ddot{u} = 0. \quad (13)$$

Assume the solution of Eq. (13) to be of the form

$$\ddot{u} = \sum_{i=1}^{\infty} \ddot{u}_i = \sum_{i=1}^{\infty} T_i \ddot{\phi}_i. \quad (14)$$

Then, substituting Eq. (6) into Eq. (13) and writing the equation for \ddot{u}_i

$$T_i \omega_i^2 \ddot{\phi}_i + c\rho \dot{T}_i \ddot{\phi}_i + m \ddot{T}_i \ddot{\phi}_i = 0. \quad (15)$$

This simplifies to

$$\ddot{T}_i + \frac{c\rho}{m} \dot{T}_i + \omega_i^2 T_i = 0. \quad (16)$$

Equation (16) is of the same form as the equation of a damped mass-spring system having the damping constant $c\rho/m$.

If δ is defined to be the ratio of actual damping to critical damping, then

$$2\delta\omega_i = \frac{c\rho}{m} \quad (17)$$

and

$$\delta = \frac{c\rho}{2m\omega_i}. \quad (18)$$

Thus for a structure having a spectrum of modal frequencies $\omega_1, \omega_2, \dots$ all modes for which

$$\omega_i < \frac{c\rho}{2m} \quad (19)$$

are over-critically damped.

FREQUENCY AND DAMPING OF A STRUCTURE IMMersed IN A VELOCITY AND DISPLACEMENT SENSITIVE MEDIUM

Consider, now, the free vibration of the shell immersed in a medium that is velocity sensitive and also offers resistance to displacement. Denote the displacement resistance constant by K . Then Eq. (13) becomes

$$D\ddot{u} + Ku + c\rho\dot{u} + m\ddot{u} = 0. \quad (20)$$

Again taking the solution to be in the form of Eq. (14)

$$T_i \omega_i^2 \ddot{\phi}_i + KT_i \ddot{\phi}_i + c\rho \dot{T}_i \ddot{\phi}_i + m \ddot{T}_i \ddot{\phi}_i = 0. \quad (21)$$

This simplifies to

$$\ddot{T}_i + \frac{c\rho}{m} \dot{T}_i + \left(\omega_i^2 + \frac{K}{m} \right) T_i = 0. \quad (22)$$

Denote

$$\Omega_i^2 = \omega_i^2 + \frac{K}{m} \quad (23)$$

$$\Omega_i^2 = \omega_i^2 + \frac{Kg}{w}$$

where

Ω_i is the undamped circular frequency in soil

g is the gravity constant

w is the unit weight of the shell.

Then the damping factor is given by

$$\delta = \frac{\gamma c}{2w\Omega_i} \quad (24)$$

where γ is the unit weight of the soil.

When writing the equation of forced vibration of the shell immersed in a velocity and displacement sensitive medium account must be taken of the free-field motion imparted to the soil by the forcing function, i.e., the free-field ground pressure wave, β . This component of motion is denoted \bar{u} . Denoting by \ddot{u} the relative motion between a point on the structure and the free-field the equation of forced vibration is

$$D\bar{L}(\bar{u}) + K\bar{u} + c\rho\dot{\bar{u}} + m(\bar{u} + \bar{I}) = \bar{p}. \quad (25)$$

If the motion is assumed to be quasi-static the time derivative terms vanish and the interface pressure, $D\bar{L}(\bar{u})$, becomes

$$D\bar{L}(\bar{u}) = \bar{p} - K\bar{u}. \quad (26)$$

Thus a developable membrane structure which deforms so as to achieve uniform surface pressure reaches equilibrium with the average value of pressure around the structure, the component $K\bar{u}$ taking the form necessary to eliminate the nonuniform component of free-field pressure.

DETERMINATION OF WEIGHTED AVERAGE SEISMIC VELOCITY

The value of c can be estimated by setting the energy radiated by the second term of Eq. (13) equal to that radiated by the second and third terms of Eq. (11).

Denote the energy U . Then

$$\begin{aligned} U &= c\rho\dot{u} - \dot{u} = c_1\rho(\bar{n}\dot{u} \cdot \bar{n}) + (\bar{n}\dot{u} \cdot \bar{n}) \\ &\quad + c_2\rho(\bar{l}\dot{u} \cdot \bar{l}) + (\bar{l}\dot{u} \cdot \bar{l}). \end{aligned} \quad (27)$$

Denote

$$\dot{u}^2 = \dot{u} \cdot \dot{u}. \quad (28)$$

Then

$$\begin{aligned} \frac{\dot{u} \cdot \bar{n}}{\dot{u}} &= \cos \psi \\ \frac{\dot{u} \cdot \bar{l}}{\dot{u}} &= \sin \psi \end{aligned} \quad (29)$$

where ψ is the angle made by the velocity vector \dot{u} with the normal to the surface of the shell. In general it is a function of position and time but its modal components are functions of position only.

For the i th mode the energy equation then becomes

$$\dot{u}_i = c\rho\dot{u}_i^2 = (c_1\rho \cos^2 \psi_i + c_2\rho \sin^2 \psi_i)\dot{u}_i^2. \quad (30)$$

The terms $\cos \psi_i \dot{u}_i$ and $\sin \psi_i \dot{u}_i$ represent, physically, the normal component and tangential component of the velocity.

Integrating over the surface of the structure

$$c = c_1 \frac{1}{A} \int_A \cos^2 \psi_i dA = c_2 \frac{1}{A} \int_A \sin^2 \psi_i dA. \quad (31)$$

The integrals in Eq. (31) represent mean square values.

Denote

$$\frac{1}{A} \int_A \cos^2 \psi_i dA = \overline{\cos^2 \psi_i} \quad (32)$$

$$\frac{1}{A} \int_A \sin^2 \psi_i dA = \overline{\sin^2 \psi_i}. \quad (33)$$

Then

$$c = c_1 \overline{\cos^2 \psi_i} + c_2 \overline{\sin^2 \psi_i} \quad (34)$$

$$c = (c_1 - c_2) \overline{\cos^2 \psi_i} + c_2. \quad (35)$$

The value of Eq. (34) lies in that, even if the modal geometry is known only approximately, the mean values $\overline{\cos^2 \psi_i}$ and $\overline{\sin^2 \psi_i}$ can be estimated quite accurately.

As an example consider a cylindrical shell. A point on its surface is defined by the coordinates θ and Z . For simplicity consider only those modes which are independent of Z . Further for simplicity consider the inextensible middle surface theory to apply.

Then the normal components of the modes are

$$n_i = a_i \cos i\theta \quad (36)$$

and the tangential components are

$$l_i = b_i \sin i\theta. \quad (37)$$

By the inextensible theory

$$\frac{\partial l_i}{\partial \theta} = n_i. \quad (38)$$

Thus

$$b_i = \frac{n_i}{i} \quad (39)$$

and

$$\tan \psi_i = \frac{l_i}{n_i} = \frac{b_i}{a_i} = \frac{i}{a_i}. \quad (40)$$

$$\cos \psi_i = \frac{1}{\sqrt{i^2 + a_i^2}}. \quad (41)$$

Integration yields

$$\cos^2 c_1 = \frac{1}{1+\nu} \quad (42)$$

Then

$$\frac{c}{c_1} = \left(1 - \frac{c_2}{c_1}\right) \frac{1}{1+\nu} + \frac{c_2}{c_1} \quad (43)$$

Values of c/c_1 are given in the following table:

c_2/c_1	2	3	4	5	6
1	1.000	1.000	1.000	1.000	1.000
$\frac{5}{6}$	0.944	0.958	0.967	0.972	0.976
$\frac{2}{3}$	0.889	0.917	0.934	0.945	0.953
$\frac{1}{2}$	0.835	0.875	0.900	0.917	0.931

ESTIMATION OF SOIL RESISTANCE FACTOR K

By the methods of the theory of elasticity it can be shown¹ that the variation of the radial stress in an infinite elastic medium containing a circular cylindrical hole containing uniform pressure P is

$$\sigma_r = P \frac{R^2}{r^2} \quad (44)$$

where R is the radius of the hole and r is the radial distance to the point at which the radial stress, σ_r , obtains.

The radial displacement u_r is given by

$$u_r = \frac{(1+\nu)PR^2}{E} \quad (45)$$

where E is the Young's modulus of the medium and ν is Poisson's ratio.

At the surface of the hole

$$\begin{aligned} \sigma_{rs} &= P \\ u_{rs} &= \frac{(1+\nu)PR}{E} \end{aligned} \quad (46)$$

¹Timoshenko, Theory of Elasticity, First Edition, McGraw-Hill, Chapter 3.

The soil resistance factor is defined to satisfy the equation:

$$K u_{rs} = P \quad (47)$$

Thus

$$K = \frac{P}{(1+\nu) R} \quad (48)$$

or since

$$c_1^2 = \frac{Eg}{\gamma} \quad (49)$$

where c_1 is the compression wave velocity

g is the gravitational constant and

γ is the soil unit weight

$$K = \frac{c_1^2}{(1+\nu) g R} \quad (50)$$

The factor K can be represented in general

$$K = \frac{c_1^2 \gamma}{(1+\nu) g \lambda} \quad (51)$$

where λ is a length characteristic of the structure.

For a spherical shell

$$\lambda = \frac{R}{2} \quad (52)$$

where R is the spherical radius of the shell.

Determination of λ for more complex geometry is a tedious process and of questionable value because of the indeterminateness of Poisson's ratio for soils. However, noting that for a cylinder

$$\frac{\lambda S}{V} = 2.0 \quad (53)$$

where V is the volume

S is the surface area

and for a sphere

$$\frac{\lambda S}{V} = 1.5 \quad (54)$$

It is suggested that for more complex shells λ be taken as

$$\lambda = 1.75 \frac{V}{S} \quad (55)$$

DISCUSSION

Mr. Stallybrass (Stanford Research Institute): I am wondering about your assumption of equal wave velocities on your postulate of an elastic medium. If I remember rightly, the two Lame's constants, λ and μ , for an elastic material have to be positive. If you assume that the dilatational and shear wave velocities are equal, this is equivalent to $\lambda = \mu$, which makes λ negative.

Mr. Morrison: You are quite correct. That assumption was made, perhaps I didn't emphasize it strongly enough, for one purpose only - mathematical simplicity. The details leading to the assumption are given in the appendix. It turns out, however, that as far as the total energy capacity of the shell is concerned that, if we had a and b seismic velocities - compressional and shear - an average value can be used purely for mathematical purposes - no physical reason. The resulting seismic velocity, the artificial one, will be on the order of somewhere between 90 and 95 percent of the compressional seismic velocity. It just doesn't make any difference in the design of the structure.

Mr. Mow (Allied Research Associates): Did you say you used a membrane analysis for the shell?

Mr. Morrison: I did, and you will notice that the thicknesses are very high.

Mr. Mow: How do you account for the sudden jump in loading? In the membrane theory when your loading has a sudden jump then your solution will encounter some difficulties because there are bound to be local bendings.

Mr. Morrison: This has been looked into in very considerable detail. I refer you to the Air Force Special Weapons Center Report AFSWC TR 59-2; it consists of three volumes. The various factors were investigated and it does turn out that you can use the membrane theory for the dynamically loaded structure without being in gross error - 90-95 percent perhaps. This may not be true for structures with a radius to thickness ratio somewhat higher, say 15 or 20 or greater than the 11 that was shown in that last structure.

DYNAMIC STRENGTH OF ROCKS

D. R. Grine
Stanford Research Institute
Menlo Park

Production of new surface area by fracturing of rock behind an explosive-initiated high-amplitude wave is probably an important mechanism for energy absorption in the region near an explosion in rock. In this paper, fracturing of rock by high-amplitude pulses and the effects of such fracturing on pulse propagation are considered.

INTRODUCTION

The ability to compute the stress field in the wave produced by a specified blast in contact with a specified rock would be useful in design of protective underground construction and in studies of production of seismic waves by underground explosions. In such computations [1], it is normally assumed that the medium possesses a dynamic confined shear strength. When shear stress in the computed field exceeds this strength, the rock behaves plastically or hydrodynamically and the wave shape and amplitude change more rapidly than they would in the elastic case. A change in the assumed dynamic strength of the rock will therefore change the calculated shape and amplitude of the wave in the rock. This paper concerns experimental methods of determination of dynamic strength of rocks.

Any attempt to compare a "dynamic" strength with a "static" one is qualitative unless the complete stress-time histories of the dynamic event and static test are given. In general, strength or yield point is a continuous function of the stress tensor and its time derivatives. "Dynamic" will be arbitrarily used in this paper to refer to events lasting less than one second. However, strength of a substance might vary as much between loads lasting one microsecond and one second as between one lasting one second and a static test lasting a week.

A high amplitude wave in rock produces strain rates of from 10^3 to 10^6 per second. Duration of load ranges from a few microseconds in small tests to several tenths of a

second in large nuclear shots. Experiments with waves in metals [2] have shown that, in general, yield points are sensitive to rates of strain. In brittle materials such as rocks, the dynamic compressive strengths may be similarly sensitive to strain rate or duration of loading and therefore differ for small explosive tests from either the strengths on nuclear shots or the results of static tests.

Another difficulty in determination of dynamic strengths of rocks arises from the fact that stress distributions in large amplitude waves normally are not the same as those in static tests. All waves of practical interest in rocks are in diverging geometries, e.g., spherical or cylindrical. Any diverging elastic pulse affects an element of the medium in which it propagates in a qualitatively similar way [3]. Initially, an element undergoes radial compression with zero tangential strain. Tangential stress is compressive and has the amplitude needed to maintain this condition of uniaxial strain. This initial effect is the same as that of a plane wave. Then, as shells of material surrounding the blast move outward, tangential stress drops to zero while radial stress is still high. During this drop of tangential stress, the difference between radial and tangential stress (i.e., shear stress) remains high. At the time when tangential stress is zero, a condition of uniaxial stress exists. Finally large tangential tensions, commonly called hoop stresses, are developed while radial stress gradually falls to zero.

Response of rocks during the suddenly applied initial radial compression near the blast will be by close-spaced microfracturing

at the wave front when confined dynamic strength is exceeded. Outside the region in which initial compression is sufficient to produce microfracturing, the rock will still fail in shear some distance behind the wave front as the confining tangential stress falls while shear stress remains high. Since the confining tangential stress is removed gradually, the cracks would be widely spaced. Formation of one crack has time to relieve the stresses tending to fracture nearby rock. Outside the region of coarse shear failure, hoop stresses produce widely spaced radial cracks. Finally the wave passes outward as an elastic wave which does not damage the rock, at least until it interacts with a free surface.

Experiments on small samples of rock lead to the qualitative picture of interaction of a stress wave with rock given above. A description of these experiments and interpretation of their results form the body of this paper.

DAMAGE BY WAVE OF UNIAXIAL STRESS

Explosive-initiated high-amplitude pulses in cylinders of rock were studied to determine the pulse amplitude needed to damage the cylinders [4]. The cylinders were surrounded by air or loose sand with much lower acoustical impedance than that of the rock. Radial stress at the cylindrical surface of each sample was, therefore, near zero. Axial stress of the lowest amplitude wave which damages the surface of a rock cylinder will be compared with axial stress attained in an unconfined static test before failure of the same rock type. We attempted to produce uniaxial stress in the static test by capping the ends of test cylinders with sulfur. Test cylinders were all cut to a length equal to their diameters for the static tests.

Three cylinders of the greywacke rock used in most of the explosive experiments

were recovered. Damage to all three cylinders was similar to that shown in Fig. 1. About 45 millimeters of the end nearer the explosive is missing and another 45 millimeters left as a conical shape. Neglecting the failure along a quartz vein, the rock was apparently undamaged by the compressive wave beyond a hundred millimeters from the charge. The cylinder was divided into 10-spalled fragments by the tension wave reflected from the free end. These tension fractures are approximately perpendicular to the cylinder axis.

To calculate the axial stress σ_{zz} in a wave at a point in a rock cylinder, we use the equation for the conservation of momentum across the front of a wave moving with velocity, v , into an undisturbed medium of density ρ_0

$$\sigma_{zz} = \rho_0 U v. \quad (1)$$

v is the particle velocity associated with the wave. The density of the rock was computed by dividing the measured weight of a sample by its volume.

A schematic diagram of the experiment used for determining particle velocity at a point in a rock cylinder is given in Fig. 2. The damaged cylinder of Fig. 1 was recovered from such an experiment. The explosive cylinder on each shot was 45 millimeters long and the same diameter as the rock cylinder. The greywacke cylinders were 30 millimeters in diameter and took 50 grams of C-3 explosive. Forty-two millimeter diameter limestone cores were shot with 98 grams of C-3. Data from one greywacke shot using a hundred millimeter length of core are plotted in Fig. 3. The initial velocity of the top of the rock core was 99 meters per second. Particle velocity of the wave at a distance of a hundred millimeters from the explosive charge is 49.5 meters per second. The approximation that velocity of a free surface is twice the particle

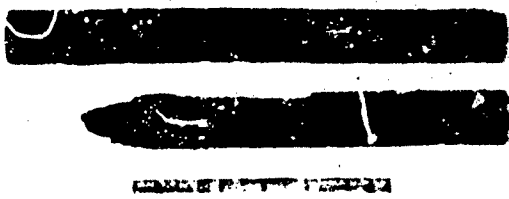


Fig. 1 - Damage to greywacke cylinder

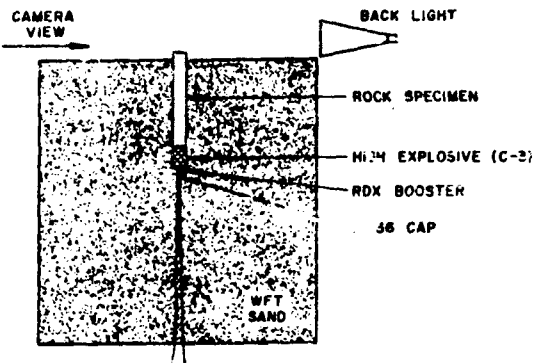


Fig. 2 - Particle velocity experiment

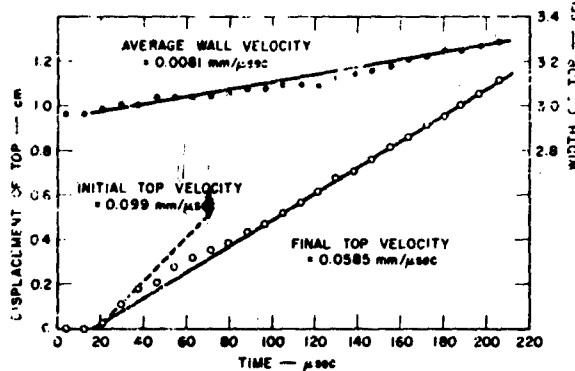


Fig. 3 - Displacement-time data from particle velocity experiment

velocity of an incident wave is discussed by Rice et al [5]. It is a good approximation for the wave amplitudes observed in the greywacke cores but is very likely the largest source of error in the final computed stress levels in the limestone cores. Particle velocities were obtained for four different lengths of greywacke and three different lengths of limestone.

The propagation velocity of a large amplitude wave is not necessarily the same as that of a small elastic wave. Wave velocities were determined in two ways. The first method used took advantage of the radial movement plotted as "average wall velocity" in Fig. 3. Rock cores were shot under water so that this wave-induced lateral motion would produce waves in the water which could be photographed. Figure 4 shows two frames of the underwater

shot on greywacke. The wave velocity in the greywacke agreed closely with the previously measured velocity of small amplitude waves. The wave velocity in the porous limestone varied over the length of the core and averaged about half the velocity of small amplitude waves.

Another determination of wave velocity in the greywacke was made by photographing a striped core with a smear camera. A still photograph of the experiment and a print of the smear camera film are shown in Fig. 5. The smear photograph was taken through a slit aligned along the core axis as shown. The image, a series of white dots, was smeared along the film by a rotating mirror producing the parallel white lines shown at the left of the smear camera record. As the wave in the core

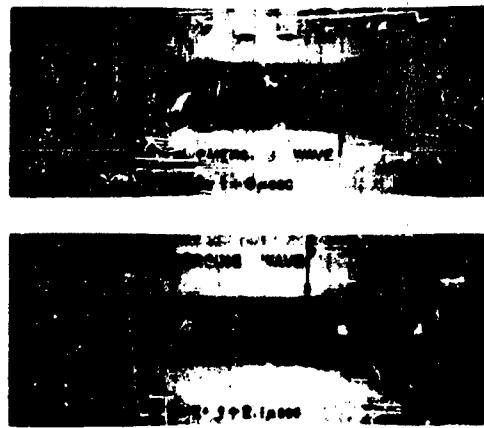


Fig. 4 - Wave velocity experiment—
underwater shot

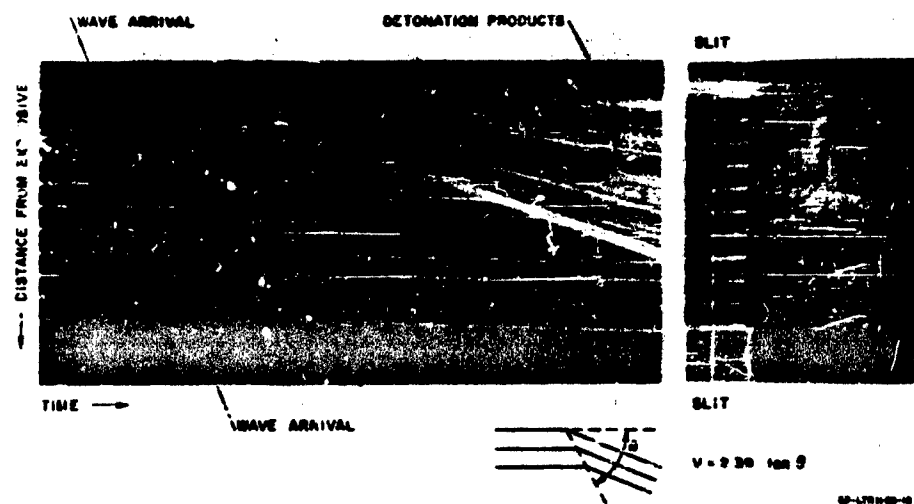


Fig. 5 - Wave velocity experiment—striped cylinder

passed each stripe, the stripe moved and the line representing it on the smear camera record bent. The bends thus determine the wave arrival. The slope of each line on the smear camera record gives a value of the axial component of particle velocity of the cylindrical surface at the corresponding point on the rock. Wave velocity in the greywacke was higher than that for small waves for the first 30 millimeters of the core but equalled small amplitude wave velocity along the rest of the core.

We had planned to use the particle velocities obtained from the slope of the lines on the smear record of Fig. 5 in computing axial stress along our rock cores. In Fig. 6, these outside axial components of particle velocity are plotted together with values obtained from observation of the motion of the axes of cores of different lengths. Agreement is poor up to a distance of 100 millimeters from the explosive. Values of particle velocity observed on the core axes were used in computing the stress levels plotted in Fig. 7.

The nonporous greywacke was not damaged by a compressive pulse with an axial stress 6.7 times the static compressive strength of the rock. The porous limestone

was crushed by a pulse with an axial stress less than twice the static strength of the rock. Maximum stress level in the limestone decreased much more rapidly than in the greywacke.

WAVES OF UNIAXIAL STRAIN*

A large amplitude plane wave is unstable over some stress range in any substance having a finite rigidity modulus and capable of withstanding only some limited stress difference. The argument for instability is given on pages 10 and 11 of [Ref. 5]. The one-dimensional compression curve shown schematically in Fig. 8 represents the locus of pressure-specific volume points attainable by passage of the double wave system. The precursor wave of amplitude, P_1 , is the largest elastic plane wave which can propagate in the substance without exceeding the dynamic stress difference, γ , which the medium can withstand. It propagates with the

*This work was done for the Lawrence Radiation Laboratory, Livermore, California, under the auspices of the Atomic Energy Commission.

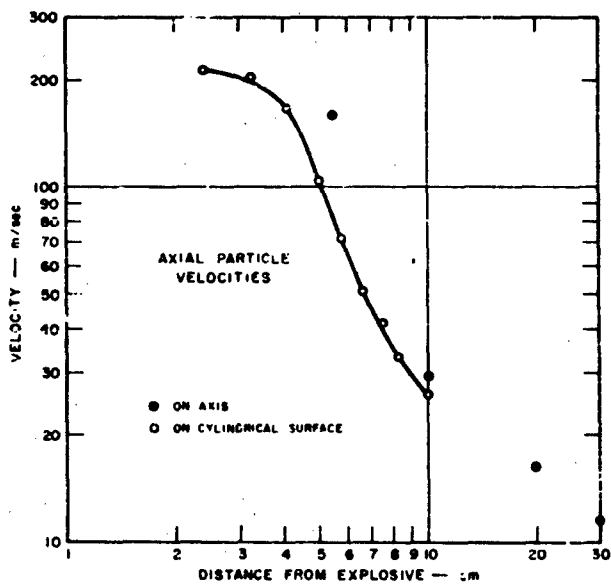


Fig. 6 - Particle velocity at surface and center of rock cylinder

Fig. 7 - Axial stress in greywacke and limestone and static strength of greywacke

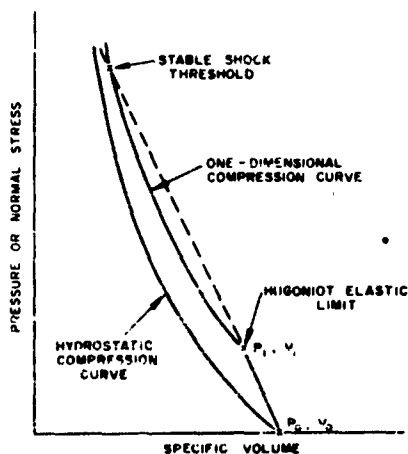
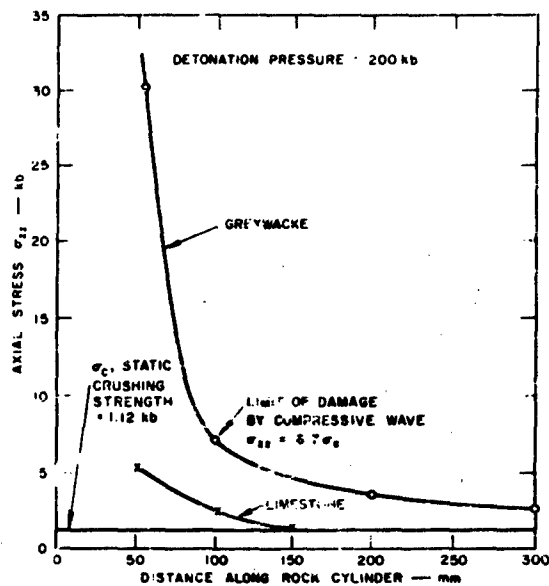
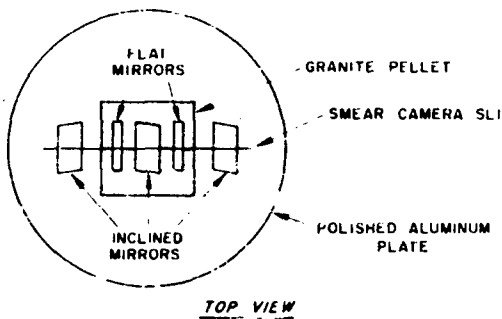
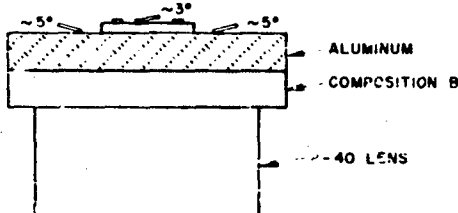


Fig. 8 - One dimensional compression



TOP VIEW



SIDE VIEW

Fig. 9 - Precursor wave experiment

velocity of a small plane longitudinal wave. The dynamic yield point of the medium may be written

$$\gamma = \left[1 - \frac{1}{\frac{\sigma}{\sigma_0} - 1} \right] P_1 \quad (2)$$

γ is the Poisson ratio of the medium.

P_1 can be computed from Eq. (1); it is the same as γ_{ss} of that equation. Figure 9 is a diagram of an experiment used to determine wave velocity and free-surface velocity in a pellet of granite from the Nevada Test Site of the Atomic Energy Commission. The moving intersection of the free surface under each tilted mirror with the mirror is photographed with a smear camera. The velocity of the free surface is then calculated from the smear camera record by the formula

$$v = k (\tan a) (\tan b)$$

where k is a constant determined by the image magnification and film writing speed, a is the angle of inclination of the mirror, and b is the angle between the time axis and smear trace

on the record. A still picture and smear record of one shot are shown in Fig. 10. The time AB is the time taken for the precursor wave to traverse the granite pellet. Wave velocity is taken as the pellet thickness divided by the time AB . Particle velocity is very nearly half the free-surface velocity. The stress, P_1 , normal to the wave front of the precursor wave in the granite was 36.5 kilobars. Poisson's ratio of the granite is 0.272. Using Eq. (2), the stress difference at which yield occurred can be calculated as 22.8 kilobars. This figure agrees very well with average stress differences observed in granites by Griggs et al [6] for granites constrained by a 5-kilobar hydrostatic pressure. The strain rate in the wave experiment was about 10^5 per second, the strain was 3.6 percent.

The amplitude of precursor waves in rock can probably be predicted from static compressive tests on jacketed specimens under hydrostatic constraint. The constraint could be servo controlled to give uniaxial strain. We wished to predict precursor waves in rocks without elaborate equipment. We therefore used the results of Brace [7] who found that the stress difference withstood by rocks

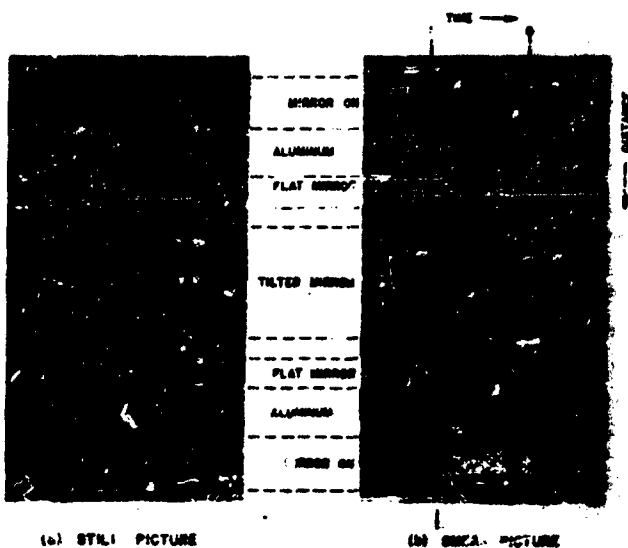


Fig. 10 - Record of precursor wave experiment

under constraint was nearly equal to one third of the Vickers hardness of the rocks. Vickers hardnesses of many minerals are listed by Mott [3]. They were used with Eq. (2) to predict the amplitude of the precursor waves in salt and in quartz. The predicted amplitudes of 1.8 kb for salt and 60 kb for quartz agree well with the observed values of 1.4 kb for salt [9] and 65 kb for quartz. The quartz precursor was measured by G. R. Fowles of Poulter Laboratories using the inclined mirror technique which he developed. The more elaborate testing of samples under hydrostatic constraint must be used on rocks which are coarsely crystalline because an indentation test gives scattered results.

Our determination of dynamic strength by observation of precursor waves has been done on rocks with low porosity. The presence of pore spaces would remove the

constraint imposed by uniaxial strain in a plane wave. Small rock particles would be free to move tangentially into pore spaces. We expect dynamic strength to be much lowered by small percentages of pore space in a rock. The nonlinear effects which lead to wave attenuation should be important at comparatively low stresses. The rapid attenuation and crushing observed in limestone cylinders with about one percent pore space supports these predictions. We hope to do experiments on precursor waves in porous rocks in the future.

ACKNOWLEDGEMENT

The experimental work described in this paper was financed by the United States Atomic Energy Commission under contract AT(04-3)115 and under project agreement No. 26-U.C.L.R.L. subcontract No. 122.

REFERENCES

- [1] John H. Nuckolls, "A Computer Calculation of Rainier," Proceedings of the Second Plowshare Symposium, UCRL-5676, May 15, 1959.
- [2] A. H. Cottrell, "Deformation of Solids at High Rates of Strain," Proceedings of Conference on Properties of Materials at High Rates of Strain, Published by the Institution of Mechanical Engineers, 1 Birdcage Walk, Westminster, London SW1, 1957.
- [3] H. L. Selberg, "Transient Compression Waves from Spherical and Cylindrical Cavities," *Arkiv för Fysik*, 5, No. 7, pp. 97-108, 1952.
- [4] D. R. Grine, "Finite Amplitude Stress Waves in Rocks," Poulter Laboratories TR-012-59, 1959.
- [5] M. H. Rice, R. G. McQueen, and J. M. Walsh, "Compression of Solids by Strong Shock Waves," *Solid State Physics*, 6, Academic Press, 1958.
- [6] D. T. Griggs, F. J. Turner, and H. C. Heard, "Deformation of Rocks at 500°C to 800°C," *G. S. A. Memoir* 79, 1960.
- [7] W. F. Brace, "Behavior of Rock Salt, Limestone, and Anhydrite During Indentation," *J. Geophys. Res.*, 65, No. 6, pp. 1773-1788, June, 1960.
- [8] B. W. Mott, "Micro-Indentation Hardness Testing," Butterworths, London, 1958.
- [9] John H. Nuckolls, "Theory of Underground Explosions," UCLRL Memorandum UOPD 60-3, April 27, 1960.

SOIL DISPLACEMENT INDUCED BY AIR BLAST*

W. H. R. Ferret
Sandia Corporation, Albuquerque, New Mexico

The paper describes part of an experiment designed to study transient ground displacement caused by an air burst, nuclear explosion.

INTRODUCTION

Response of soils to static loads has long been of concern to designers of foundations for large structures and of earth dams. A vast fund of knowledge and an understanding of the reaction of soils to such loads has been developed in the field of soil mechanics. But the response of soils or rocks to high dynamic loads, and most particularly to transient loads of the type associated with air blast from large explosions, is neither well understood nor has it been very comprehensively explored until recently.

This paper describes briefly part of an experiment performed at the AEC's Nevada Test Site during June, 1957, under the Priscilla Shot of Operation Plumbbob [1]. This experiment was designed to study transient displacement of the ground caused by the blast wave generated by a nuclear explosion equivalent to 40 kilotons of TNT. The explosive charge was suspended from a captive balloon 700 feet above a dry playa lake bed called Frenchman Flat.

THE SOIL ENVIRONMENT

The soil environment of this experiment is best described as a 200-foot-thick mass of weakly cemented sandy soil of remarkable uniformity. No appreciable change of material was found in the sample and instrument borings at depths shallower than 201 feet at which depth gravel was encountered. Analysis of numerous undisturbed samples taken from borings in the test area showed that 80 to 90 percent of the material passed a 200-mesh

screen and dry densities varied through a range from 75 to 95 pounds per cubic foot. A typical profile of density and seismic velocity for the environment is shown in Fig. 1. The high velocity region near 20-foot depth is a result of locally increased cementation rather than a difference in material or compaction.

INSTRUMENTATION AND RECORDS

The experiment plan included four stations at ranges between 650 feet and 1350 feet from ground zero on a blast line extending westward. Relative positions of the instrument stations and burst point are shown schematically in Fig. 2.

Instruments were installed at each station to measure relative displacements between the ground surface and five gage anchors at various depths to 200 feet. Figure 3 shows some of the details of a station. The surface slab accommodated transducer elements of relative displacement gages and air blast gages. Accelerometers were installed in the slab and in most displacement gage anchors, but their performance is not relevant to the purpose of this paper.

A relative displacement gage, shown exploded in Fig. 4, consisted of a piano wire stretched under continuous tension between a buried anchor and a spring-loaded drum in the transducer unit. An auxiliary helical spring, protected in a rigid tube, ensured sufficient loading to keep the wire taut. A flexible metal tube surrounded each piano wire to permit free movement of the wire

*This paper was not presented at the Symposium.

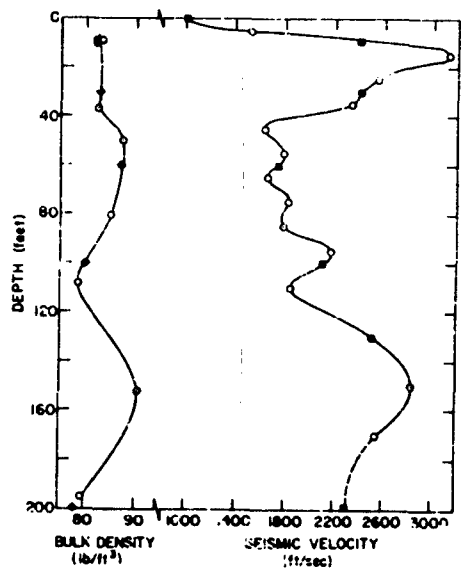


Fig. 1 - Soil density and seismic velocity profile for Frenchman Flat

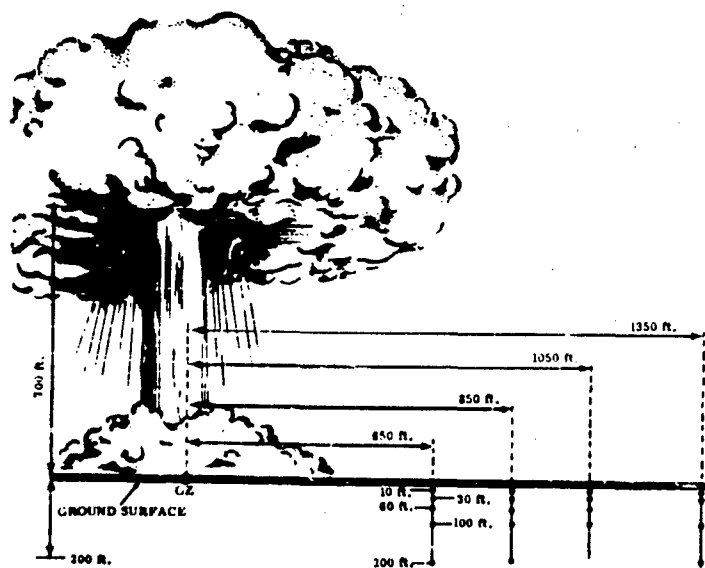


Fig. 2 - Schematic view of instrumentation line

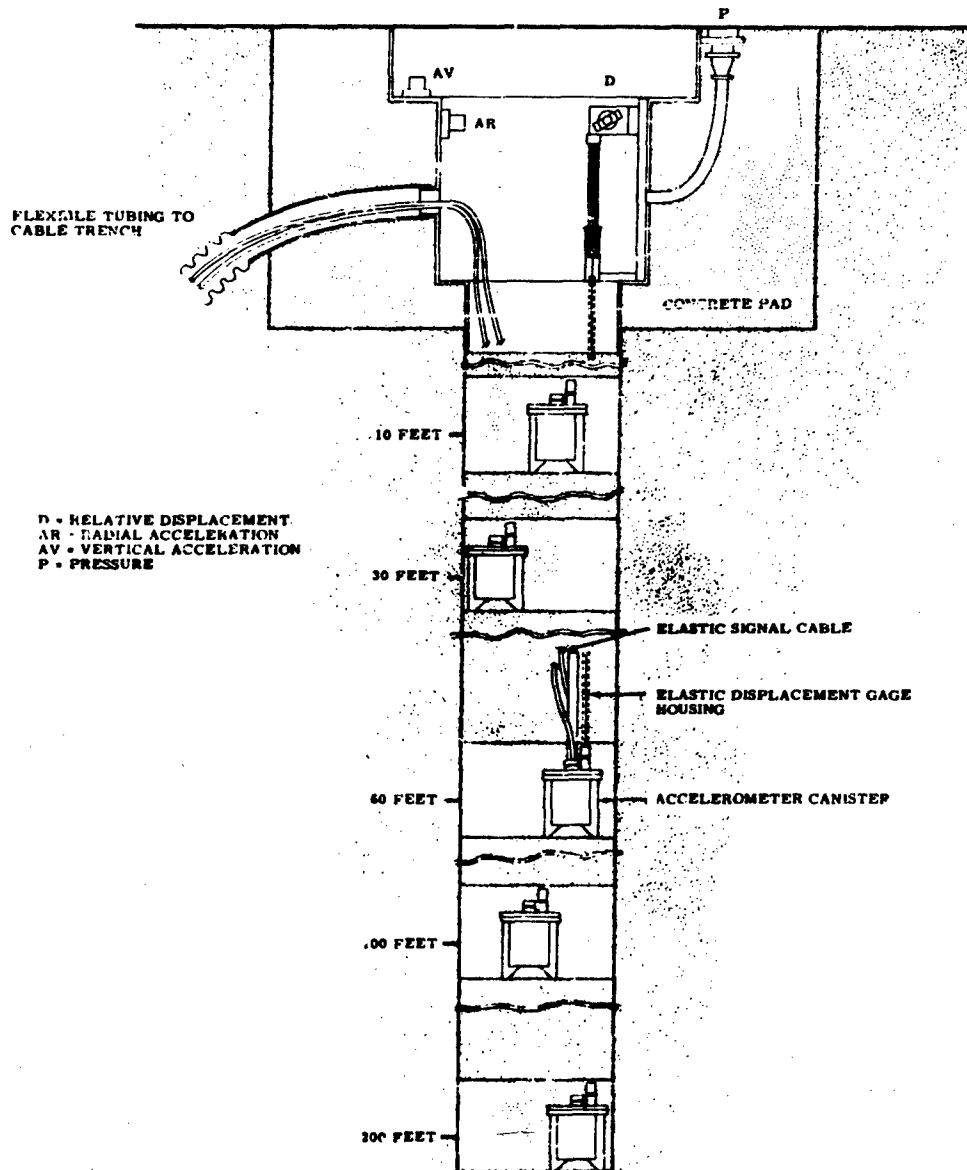


Fig. 3 - Schematic elevation of typical instrument station

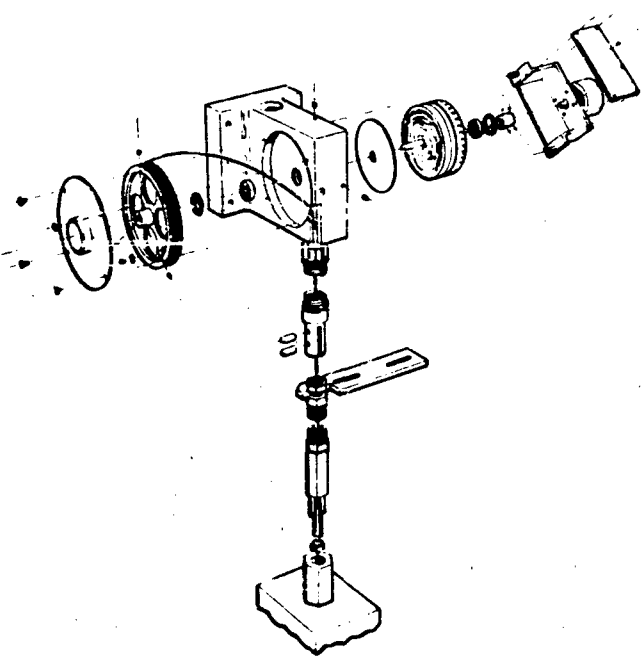


Fig. 4 - Relative displacement gage, exploded view

within the tightly compacted sand backfill. Relative movement of the anchor and slab rotated the drum and drove a spiral potentiometer which gave a varying resistive signal directly proportional to the motion.

Gage anchors were placed in the boring, bonded to the adjacent soil by quick-setting concrete, and dry sand backfill was compacted above the anchor to the elevation of the next anchor. All five transducer elements for the displacement gages were attached to each surface slab which contained an air pressure gage to provide a precise record of air blast-overpressure history at the station. All gages were connected through appropriate cables to a 3-kc carrier-amplifier system, the rectified output of which was converted to an FM signal and recorded on magnetic tape.

Incident overpressure records from the four stations are presented in Fig. 5. Peak values were 270, 187, 120, and 59 psi at 650, 850, 1050, and 1350 feet from ground zero, respectively, and positive-phase durations ranges from 210 to 440 milliseconds. Relative displacements for the station at the 650-foot range are shown as a function of time in Fig. 6. Records from other stations followed

a similar pattern. Initial compression is followed by an expansion and a final residual compression. The long-span gage record includes one of the minor data analysis problems; the expansion peak of the 200-foot-span gage was clipped. Similar clipping occurred on several other records. Evidently, as the surface slab rebounded after its initial downward motion, the base of the rigid protective tube moved up against the bottom of the helical spring, and further relative motion signal could not be generated until the slab started to move downward again. Fortunately, the rigid tubes for three other gages at this station were long enough to make the springs completely free throughout the motion. Since all gages were attached to the same slab, it is reasonable to correct the peaks of the 4D-200 and 4D-100 curves by superimposing corresponding parts of the unrestrained records.

Peak compressive displacement values are plotted in Fig. 7 as a function of gage span. As would be expected, displacements are greater for greater overpressure loading and for greater gage spans. But in all cases relative differences between data from gages of 100-inch and 200-inch span are either

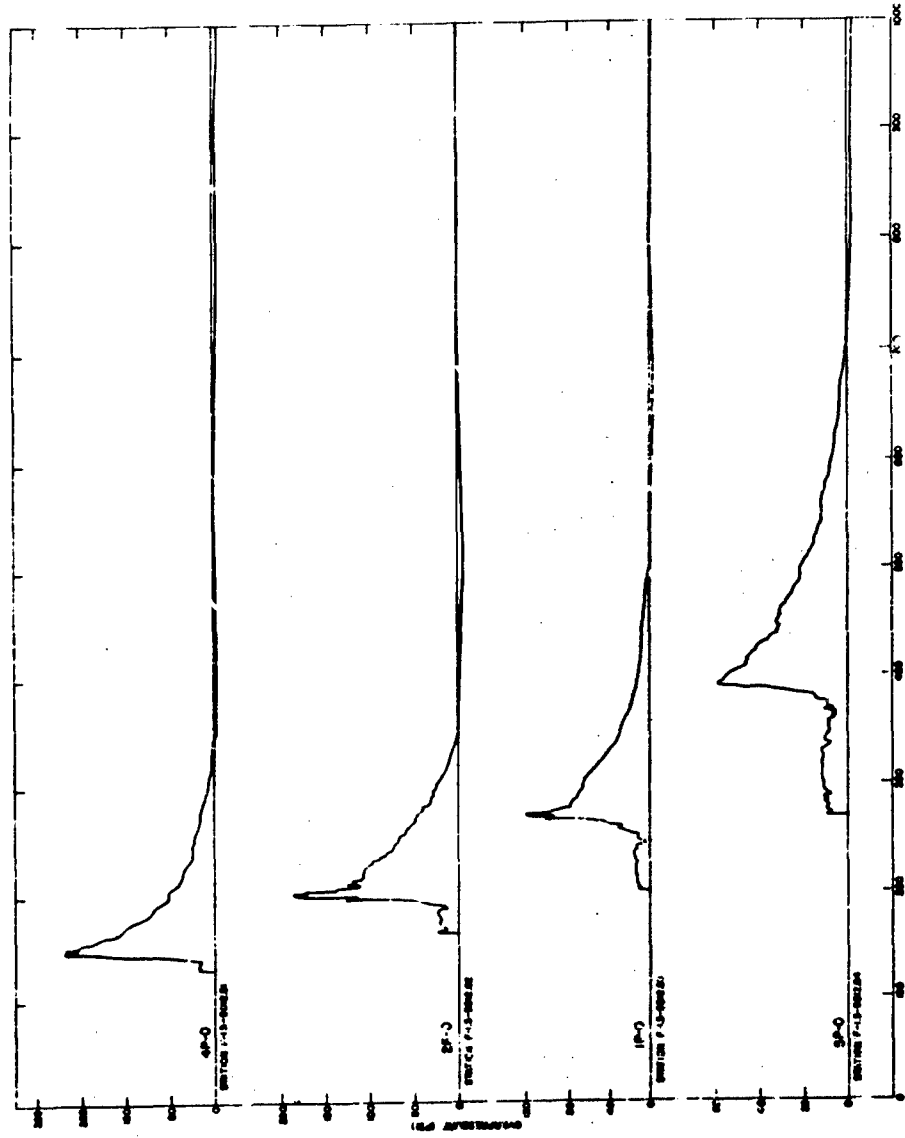


Fig. 5 - Overpressure incident on ground surface at instrumented stations

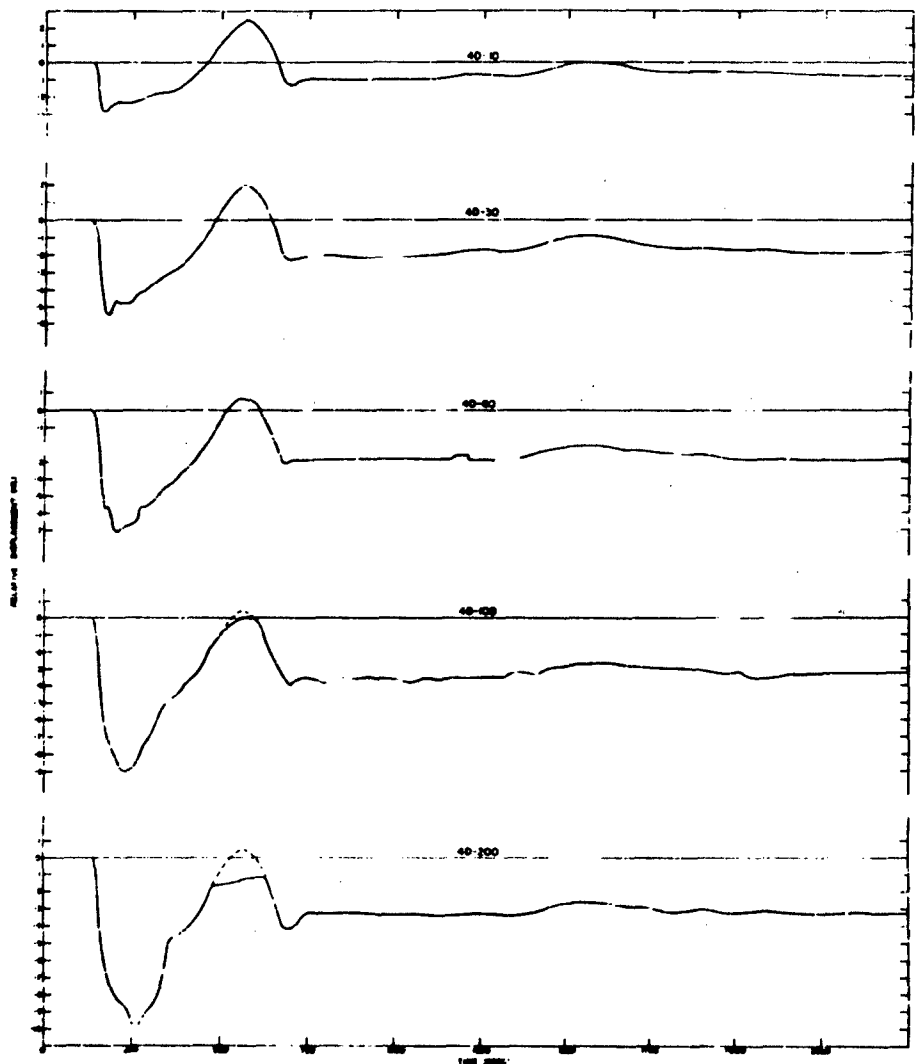


Fig. 6 - Relative displacements at 650 feet radial range

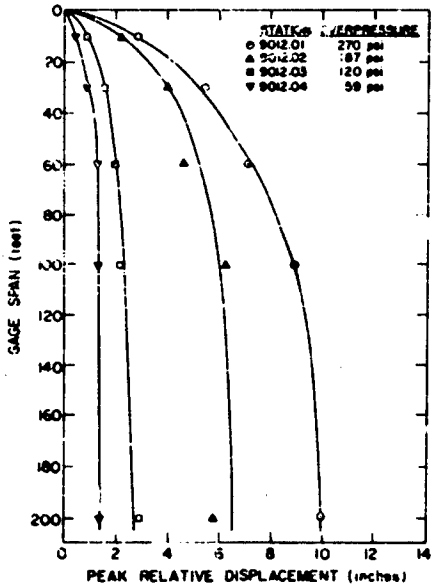


Fig. 7 - Peak relative displacement versus gage span

negligible or at least small enough to imply that anchors of the 200-foot gages did not move appreciably. Remember, the ground surface was loaded, and loading pressures are so high that the upper portions of the porous, weakly cemented soil must have acted inelastically. It then becomes reasonable to assume that displacement of the anchors 200 feet deep was negligible, and the 200-foot span record represents absolute or real downward motion of the surface slab.

DISCUSSION OF THE RESULTS

From this premise it is a simple step to find absolute displacement of the anchors of each shorter span gage by subtracting recorded relative displacements from data at corresponding times for the longest span gage. Absolute displacements derived in this manner are presented in Fig. 8. These curves are not quite as smooth as the recorded ones, particularly for displacement at the 100-foot depth, since we are dealing here with the small differences between nearly similar quantities, and precision necessarily suffers.

What can these records tell us about motion of the ground under load? First, we

plot contours of peak-downward displacement on a vertical cross section along the instrument line as shown in Fig. 9. The scales are distorted for emphasis, but it is apparent that equal dynamic displacements occur on flat bowl-like surfaces centered at ground zero, and that downward displacements decrease at a slower rate as depth increases.

This raises the question of primary interest to designers of underground structures: How do the displacements decrease with depth? Figure 10 is a plot of logarithms of peak downward displacement versus depth for each instrumented station. Data for each station defines a straight line within precision of the experiment, and slopes of the lines are identical. This information may be described in the form

$$\delta = \delta_0 e^{-0.017D}$$

where δ is maximum displacement induced at depth D in Frenchman Flat soil by airblast loading which produced a surface displacement of δ_0 . Note that Frenchman Flat soil must be specified, because the coefficients δ_0 and 0.017 are both strongly dependent on soil characteristics, although δ_0 is also dependent on the incident overpressure as indicated by the values shown on each curve.

Obviously, the next requirement is to derive a relationship between the incident overpressure function and δ_0 . Several theoretical approaches made to this problem, assuming purely elastic response of the soil, have met with qualified success. Results include an exponential term of the form found in the Priscilla experiment, but theoretical coefficients of D to the exponent have been smaller than 0.017 by factors as great as 6.

A part, if not all, of the difference between theoretical results and data from this study must stem from the fact that porous granular materials such as soil, respond inelastically in varying degrees to loads, and the extent to which departure from elastic reaction affects response becomes rapidly greater as peak loads and duration of loading increases. We do not now know precisely how soil response varies under dynamic loads, so it is difficult to develop a mathematical model suitable for describing the data from our experiment. Soil mechanics laboratories are beginning to study dynamic response of soils, and within a year or two we should be better able to develop a reasonable mathematical model.

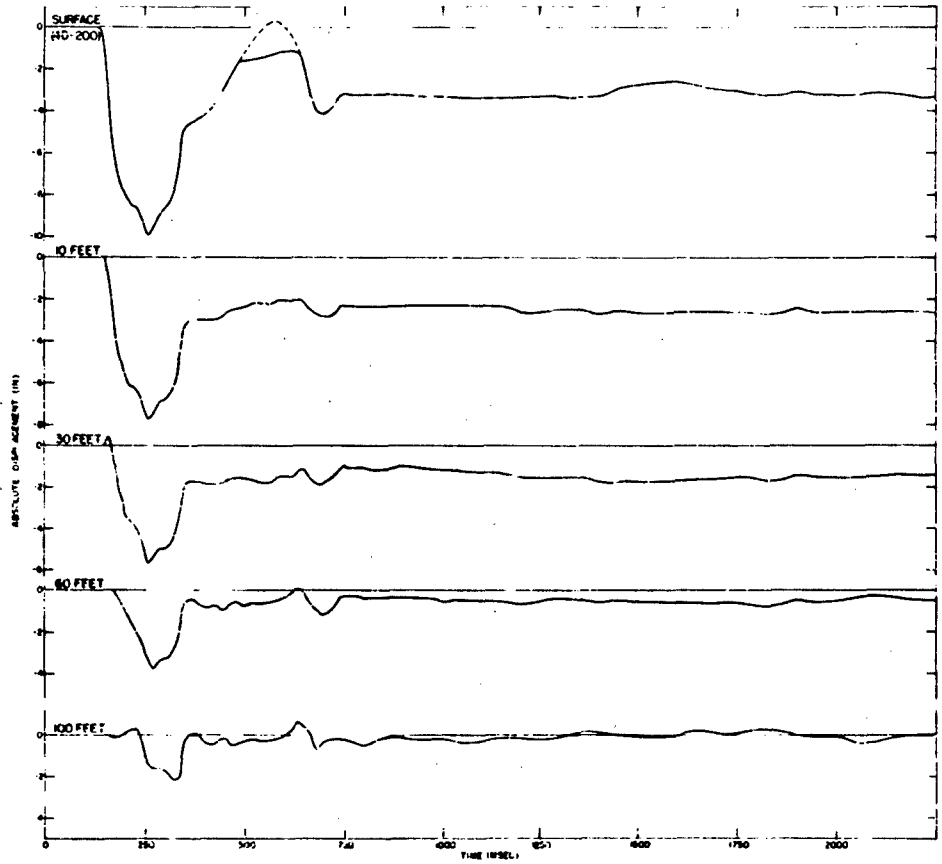


Fig. 8 - Absolute displacements at 650 feet radial range

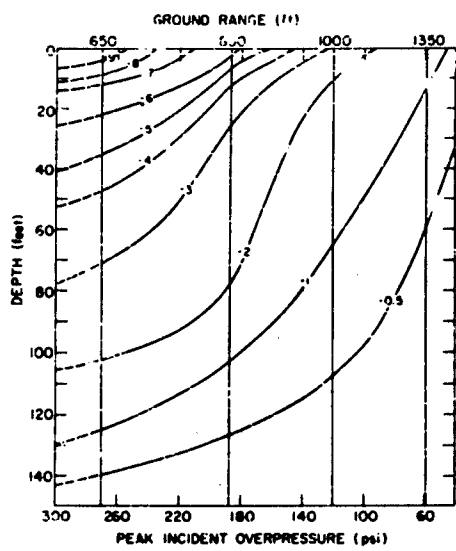


Fig. 9 - Peak displacement contours on vertical cross section along instrument line

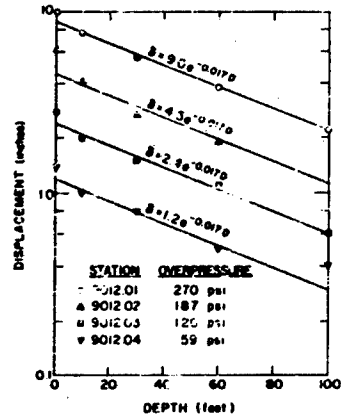
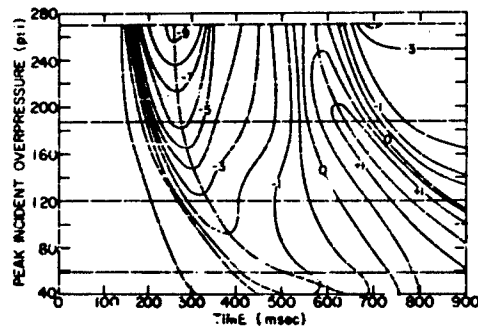


Fig. 10 - Peak displacement versus depth

Fig. 11 - Displacement contours for incident pressures versus time; surface



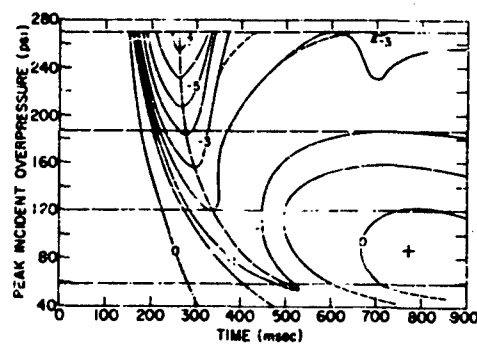


Fig. 12 - Displacement contours for incident pressure versus time; 10 feet deep

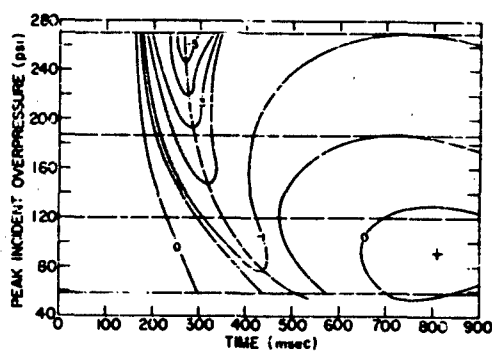


Fig. 13 - Displacement contours for incident pressure versus time; 30 feet deep

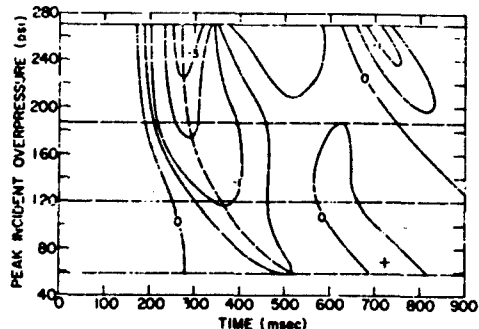


Fig. 14 - Displacement contours for incident pressure versus time; 60 feet deep

Fig. 15 - Displacement versus depth at 650 feet range at specific instants

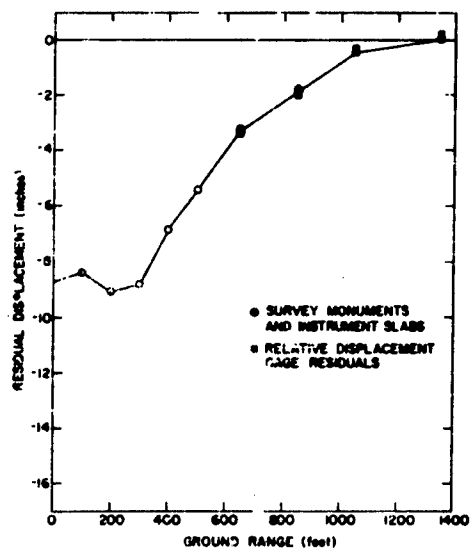
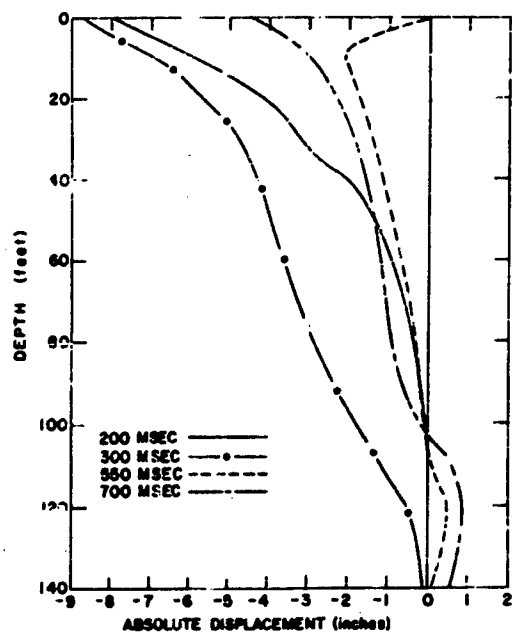


Fig. 16 - Permanent and residual displacements versus range

The next four illustrations, Figs. 11, 12, 13, and 14, present the Priscilla displacement data in a form particularly useful to theoretical studies. Deflection contours are developed at each of several depths as a function of incident overpressure and time; an analogous set of maps of deflection contours as functions of depth and time have been published in the final report of this project [1]. Some idea of the displacement history as a function of depth may be derived from curves plotted in Fig. 15 for one station at several specific times.

Finally, Fig. 16 gives some confirmation of gage performance and reliability. It shows permanent displacements measured by first order surveys of a series of monuments and the four instrument slabs before and about six days after Priscilla was detonated, together with residual displacements of the slabs derived from gage records. Data from the two sources agree within 0.2 inch, considerably better than the expected precision of the dynamic displacement measurements.

REFERENCE

- [1] William R. Perret, Ground Motion Studies at High Incident Overpressure, Operation

Plumbbob, Project 1.5, WT-1405, HQ/FC,
DASA, Albuquerque, New Mexico, June 1960.

Section 3

STRUCTURAL DESIGN

THE EARTHQUAKE GROUND SHOCK PROBLEM AND ITS RELATION TO THE EXPLOSIVE-GENERATED GROUND SHOCK PROBLEM

George W. Housner
California Institute of Technology

The earthquake ground shock problem is sufficiently similar to the explosive-generated ground shock problem that the techniques and instruments developed to solve the earthquake problem, such as shock spectra, reed gages, and accelerometers, have been applied to the explosive-generated ground shock problem. However, there are certain significant differences, such as in the character of the spectra, in the degree of ground coupling, in the relative scale of phenomena, and in the influence of soil properties, which make the earthquake problem the simpler of the two. It appears that certain difficulties encountered in the earthquake problem which retarded progress may also be encountered in the explosive-generated ground shock problem.

INTRODUCTION

The problem of designing structures to resist earthquake ground motions is similar to the problem of designing against explosive-generated ground shock, so that an exposition of the methods used for the earthquake problem may throw light upon approaches that can be used for the explosive-generated ground shock problem. The features of the earthquake problem are better known and in certain ways are simpler than for the explosive-generated ground shock problem. As a consequence, the earthquake problem is more easily explained and more readily understood. This paper will discuss the earthquake problem, calling attention to the similarities with the explosive-generated ground shock problem and also pointing out those places where there are significant differences between the two problems.

Although sporadic studies of the earthquake engineering problem were made as far back as 1850, serious and continuing work did not get underway until the earthquake that destroyed Tokyo, Japan in 1923. Following this catastrophe, groups were formed in Japan and in the United States to collect and study data on destructive earthquakes. These steps were only the beginning and subsequently the work gradually built up over the years, receiving an added impetus from each successive destructive earthquake. It appears that the major reason for the delay in getting the work started and then built up was a general misapprehension as to the role played by seismologists. There was a belief that since many seismologists were studying earthquakes, and since numerous seismographic stations were recording ground motions in many parts of the world, it was only necessary to wait for them

to provide the data needed to solve the engineering problems of earthquakes. It was only gradually realized that the interests of the seismologists were so far removed from those of the engineer that hardly any of their studies, or their seismographic recordings, had direct bearing on the earthquake engineering problem. It was only when this state of affairs was generally recognized that the engineering work really got underway. This fact is stressed here since it is a situation that might well obtain in the explosive-generated ground shock problem, namely that the persons studying the explosive-generated ground shock problem and measuring the ground motions may have interests different from the engineering problems of ground shock and hence their studies and their measurements may not be really pertinent to the engineering problems. This may be summed up by saying that if it is desired to solve the engineering ground shock problem, it is essential that the proper engineering studies and engineering measurements be made.

SEISMIC INSTRUMENTS FOR EARTHQUAKE ENGINEERING

In 1926 in Japan [1], there was constructed an instrument for recording the earthquake-induced vibrations of a set of thirteen cantilevers covering a range of natural frequencies of vibration. This was the forerunner of the reed-gage now commonly used to measure explosive-generated ground motion and similar excitations. After the nature of strong earthquake ground motion was better understood, it was realized that a much simpler instrument could give the required information. One hundred of these simpler instruments, which consist essentially of a single reed of proper period and damping [2], have been installed in California.

In the early 1930's the U. S. Coast and Geodetic Survey strong motion accelerometer was developed [3]. This was the first instrument of its type to be designed specifically to record engineering data. These instruments, which are still in use, had a heavily damped pendulum with a natural period of approximately 1/18th of a second which gives an accurate time-history of earthquake ground acceleration. The instrument is designed so that its natural frequency is greater than any of the natural frequencies of structures pertinent to earthquake resistant design. The natural frequency of the instrument also exceeds that of any of the significant frequency components of the ground motion. The

frequency range over which there are significant components in the ground motion is pretty much the same as the range of pertinent frequencies of vibration of structures, and in this sense the ground motion is well suited to the problem. This means that the details on the accelerogram are directly pertinent to the structures under consideration.

The explosive-generated ground motion is not, in general, well suited to the engineering problem in that it may contain strong components having frequencies far removed from the pertinent frequencies of the structures under consideration. In this case, the instrument used to record the motion may give a record whose details are not pertinent to the structural problem. It appears that the decisions as to proper instrument characteristics, what to measure and where to measure it, etc., are more critical in the case of the explosive-generated ground shock problem than in the corresponding earthquake problem. This means that it is important that the persons making these decisions have a good understanding of the engineering problems for which the measurements are to be made.

EARTHQUAKE GROUND MOTION

A typical strong-motion earthquake accelerogram, recorded approximately 30 miles from the center of a Magnitude 7.7 shock, is shown in Fig. 1 (Taft, California, July 21, 1952). It will be noted that the number of zeros (crossings of the axis) are approximately 10 per sec, the maximum accelerations are of the order of one quarter of the acceleration of gravity, and the duration of the strong motion is of the order of 20 seconds. Figure 2 shows the integrated ground velocity and ground displacement.

The Magnitude, M , of an earthquake is defined in terms of instrumental measurements [4], physically M is related to the energy released by the earthquake in the form of seismic waves by the approximate expression [4]

$$\log_{10} E = 9.4 + 2.14 M - 0.05 M^2 \quad (1)$$

where E is the energy in ergs. No earthquakes having Magnitudes greater than 8.6 have been recorded. A Magnitude 7 earthquake releases approximately 10^{15} ergs of energy in the form of stress waves. This would be released by shear-type slipping over a fault plane of the order of 100 miles in length and 25 miles in vertical dimension, so

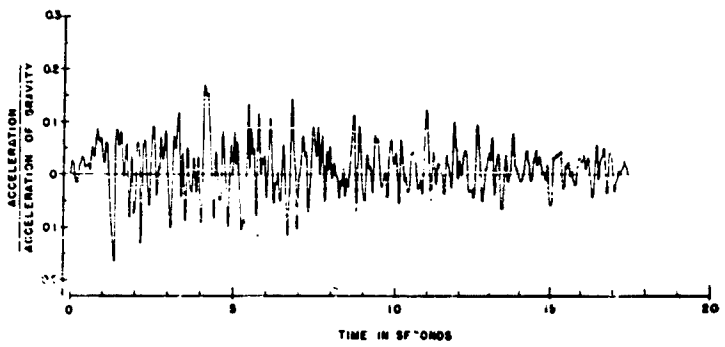


Fig. 1 - Recorded ground acceleration at Taft, California during the earthquake of 21 July 1952; S69E component of motion. The instrument was located approximately 30 miles from the center of the shock.

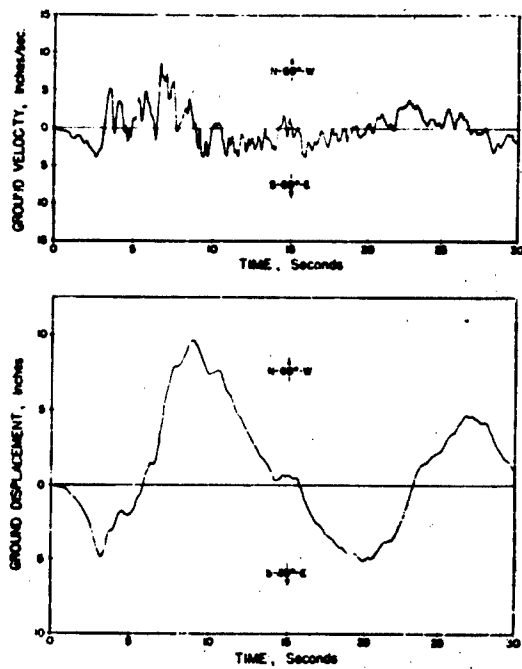


Fig. 2 - Integrated ground velocity and ground displacement for the S69E component of ground motion at Taft, California, 21 July 1952

that the energy release is far from being a point source. A Magnitude 3.5 earthquake can be treated as a point source of energy release and the strongest ground motion in the epicentral region for $M = 3.5$ is just on the threshold of being felt. The usual California earthquake originates at a depth between 6 to 15 miles beneath the ground surface. Figure 3 shows the ground acceleration measured at a distance of approximately 10 miles from the center of a 5.3 Magnitude shock [2, 5] which may be compared with the really strong motion of Fig. 1.

For comparison with earthquake-induced ground motion, Fig. 4 shows the ground acceleration recorded approximately 1000 ft from the detonation of approximately 200 tons of buried high explosive (Nitromon) used in a quarry blast [6].

It was recognized in the 1940's that the recorded ground accelerations of strong-motion

earthquakes had the properties of random functions [7] and that the significant average properties of the ground motion should be determined. For engineering purposes, the most informative property of the ground motion is the so-called response spectrum [6, 9, 10]. This quantity is defined as

$$S_v = (A^2 + B^2)^{1/2} \quad (2)$$

where

$$A = \int_0^t \tilde{x} e^{-\frac{2\pi}{T} \zeta(t-\tau)} \cos \left(\frac{2\pi}{T} \tau \right) d\tau$$

$$B = \int_0^t \tilde{x} e^{-\frac{2\pi}{T} \zeta(t-\tau)} \sin \left(\frac{2\pi}{T} \tau \right) d\tau$$

where S_v is evaluated at the time t that gives the maximum value attained by $(A^2 + B^2)^{1/2}$

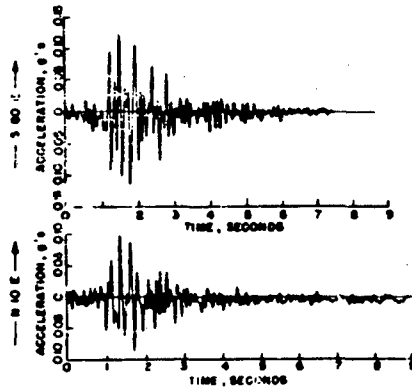
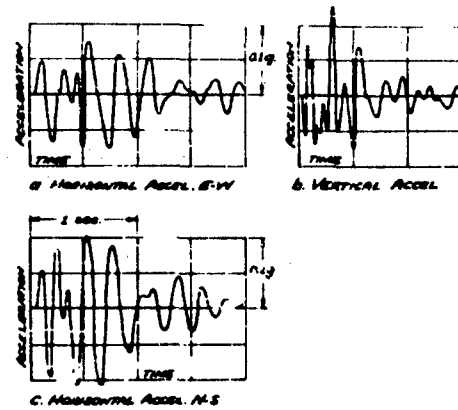


Fig. 3 - Ground acceleration recorded in Golden Gate Park during the 5.3 Magnitude earthquake of 22 March 1957 in San Francisco

Fig. 4 - Ground accelerations recorded 1000 feet from a buried explosion of approximately 200 tons



during the ground acceleration \ddot{x} . In these expressions, T is the period of vibration and ζ is the fraction of critical damping, so that S_v is a function of T and ζ . S_v has the dimensions of a velocity.

It is seen that S_v is, in a sense, a generalization of the Fourier spectrum [11]. If, in Eq. (2), ζ is set equal to zero and the evaluation is made at time t corresponding to carrying the integration over the complete range of \dot{x} , then S_v corresponds to the Fourier spectrum of \dot{x} . There is a practical advantage in using the response spectrum rather than the Fourier spectrum. This arises from the fact that structures always have damping and hence the response spectrum is directly indicative of maximum response of the structures. Also, the accelerograms of strong earthquake motion always show two phases, the strong phase (direct reception) followed by a long tail (reverberations). It is known that the tail has no significant effect upon the maximum stresses produced in damped structures, and if the tail is arbitrarily cut off of the record, the corresponding damped response spectra curves will be little if at all affected. However, the undamped response spectrum and the Fourier spectrum would both be significantly affected by the exclusion of the tail. It is customary, when computing the response spectra, to cut off the tail of the record. In this case, it is found that the Fourier spectrum has essentially the same shape as the undamped response spectrum but with ordinates approximately 5 to 10 percent smaller than the undamped response spectrum.

Response spectra have been computed for a large number of earthquake ground motions [8]. A typical set of spectrum curves is shown in Fig. 5. Ground motions recorded in the general epicentral regions of large Magnitude earthquakes are found to have similarly shaped spectrum curves and the shapes of the average spectrum curves are shown in Figs. 6 and 7 to an arbitrary scale [12].

It is also found that the spectra of ground motions recorded close to the centers of small Magnitude (short duration) earthquakes are relatively stronger in the short period end. The spectra of ground motions recorded at larger distances from the epicentral region show a relative attenuation in the short period end. This is illustrated in Fig. 8 where the spectrum curves of three such earthquake motions are shown [12].

Ground accelerations produced by air blast have been measured during bomb tests and the response spectra have been computed. Because of the wide range of frequency components in the air-blast induced ground motion it is customary to plot the spectra with frequency as abscissa instead of period as is done in the case of earthquake spectra.

Only a relatively small number of spectra have been computed for air-blast induced ground shock so that the average shapes, and the trends with yields, distances, etc., are not so well established as in the case of earthquakes. Moreover, the interest in the explosive-induced ground shock is not only in the spectra at the ground surface, but also at various depths beneath the surface. It is desirable to establish the typical shapes of these spectra for the conditions under which they are to be applied.

RESPONSE OF STRUCTURES TO EARTHQUAKE GROUND MOTION

Figure 9 indicates a structure resting on the ground and subjected to recorded earthquake ground acceleration \ddot{x} . The way Fig. 9 is drawn implies that two special conditions are satisfied by earthquake problems. First, there is the implication that all parts of the structure that are in contact with the ground are pulled back and forth with the same ground motion, or in other words, the shortest wavelengths in the seismic motion are sufficiently long compared to the dimensions of the structure so that there is no significant tendency to produce differential displacements of the parts of the structure that are in contact with the ground. In the case of explosive-generated ground shock, however, the wavelengths of some of the strong components of ground motion may be appreciably shorter than the dimensions of the structure. The structure will then interfere with the transient deformation of the surrounding soil, and in this way the motion of the surrounding ground, as well as the consequent motion imparted to the structure, is modified by the presence of the structure itself. This makes the explosive-generated ground shock problem more difficult to analyze than is the earthquake problem.

Even if all the wavelengths of the ground motion are long compared to the dimensions of the structure, there may be mutual influence between the ground motion and the building motion. Under the proper conditions, such as soft ground, massive structure, etc., the inertia

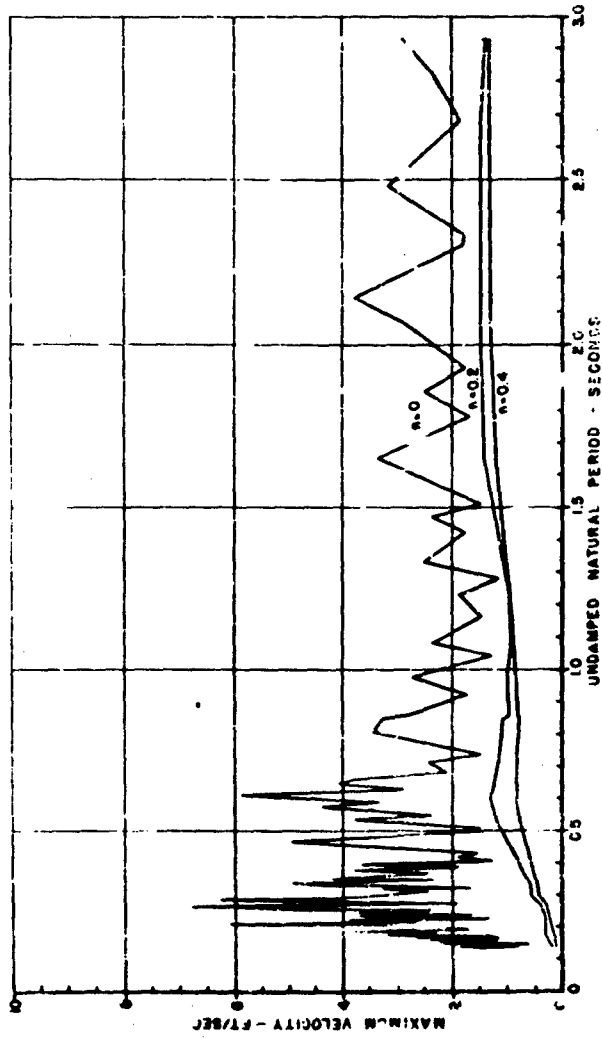


Fig. 5 - Velocity spectrum for ground acceleration recorded at Olympia, Washington during the earthquake of 13 April 1949. Component S30W.

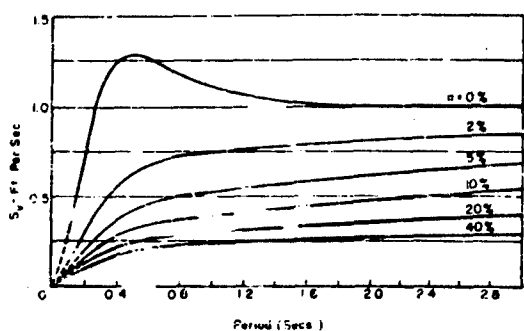


Fig. 6 - Average velocity spectrum curves for ground motion recorded in the epicentral regions of large earthquakes

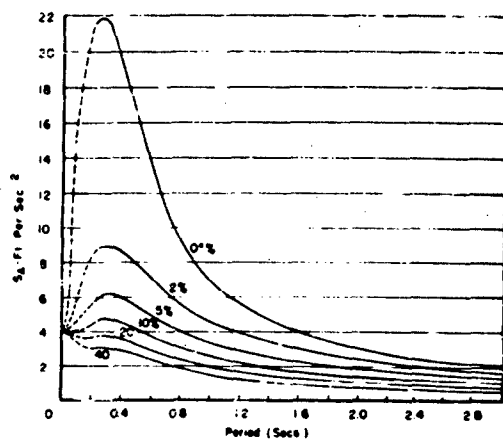
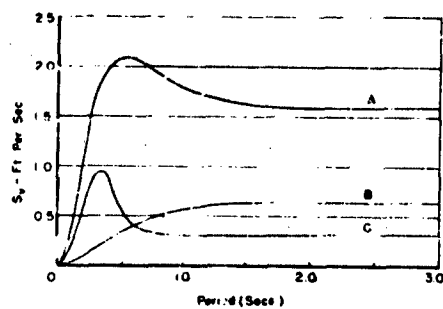


Fig. 7 - Average acceleration spectrum curves for ground motion recorded in the epicentral regions of large earthquakes

Fig. 8 - Undamped velocity spectra of strong earthquake ground motions. Curve A corresponds to ground motion recorded approximately 30 miles from the center of a Magnitude 7.7 shock. Curve B corresponds to the ground motion recorded approximately 70 miles from the center of the same shock. Curve C corresponds to ground motion recorded approximately 10 miles from the center of a Magnitude 5.3 shock.



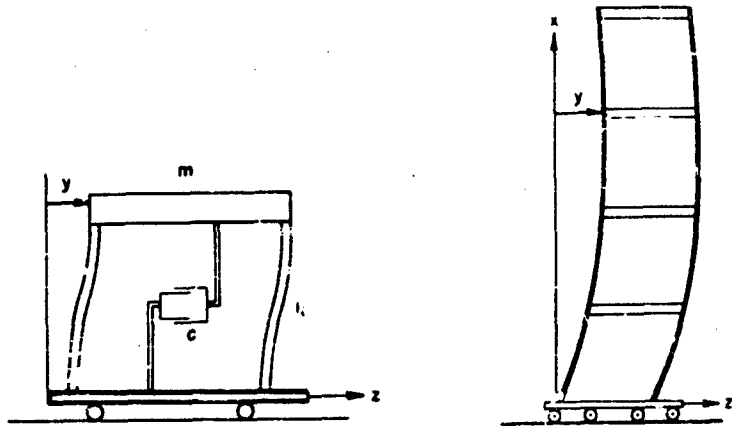


Fig. 9 - Single and multiple degree of freedom structures

of the moving building can impart deformations to the ground. Although this type of ground coupling, and the type described in the preceding paragraph, have been observed during earthquakes, significant effects are observed only under very special conditions and ordinarily ground coupling can be neglected in the earthquake problem [2,5,13,14].

If the structure of Fig. 9 has a period T , and fraction of critical damping ζ , the motion produced by the ground acceleration \ddot{z} can be written

$$y = \frac{T}{2\pi} S \sin\left(\frac{2\pi t}{T} - \alpha\right) \quad (3)$$

$$\dot{y} = -S \cos\left(\frac{2\pi t}{T} - \beta\right) \quad (4)$$

$$(\ddot{y} + \ddot{z}) = \frac{2\pi}{T} S \sin\left(\frac{2\pi t}{T} - \gamma\right) \quad (5)$$

where, in the notation of Eq. (2):

$$S = (A^2 + B^2)^{1/2}$$

and α , β , γ are phase factors involving A and B . The foregoing equations make use of the approximation $(1 + \zeta^2)^{-1/2} \approx 1$. Equation (4) can also be written in the more commonly encountered form:

$$\dot{y} = - \int_0^t \ddot{z} e^{-\frac{2\pi}{T}(t-\tau)} \sin \frac{2\pi}{T}(t-\tau) d\tau \quad (6)$$

This represents an oscillatory motion which at its extreme values coincides with the envelope S of Eq. (4). It is found that for earthquake ground motion the maximum value of \dot{y} given by Eq. (6) differs only slightly from the maximum value of S in Eq. (4). In this case, Eq. (6) can be used to calculate the spectrum S_v .

As can be seen from Eqs. (3), (4) and (5), the maximum relative displacement, relative velocity, and absolute acceleration are given by

$$y_{\max} = \frac{T}{2\pi} S_v \quad (7)$$

$$\dot{y}_{\max} = S_v \quad (8)$$

$$(\ddot{y} + \ddot{z})_{\max} = \frac{2\pi}{T} S_v \quad (9)$$

The velocity response spectrum S_v thus gives directly the maximum relative velocity, \dot{y}_{\max} , which also determines the maximum displacement and acceleration. The displacement spectrum S_d and the acceleration spectrum S_a are defined by:

$$S_d = \frac{T}{2\pi} S_v$$

$$S_a = \frac{2\pi}{T} S_v$$

Figure 7 shows the average acceleration spectrum corresponding to the velocity spectrum shown in Fig. 6.

It is seen that the value of S_v is a measure of the maximum effect of the ground motion upon structures. The spectrum intensity of the ground motion is defined to be [15]:

$$(SI)_0 = \int_{0.1}^{2.5} S_v dt. \quad (10)$$

The range of periods 0.1 to 2.5 seconds covers the range of commonly encountered building periods in California. The spectrum intensity is a function of the damping, ζ , and strong ground motions recorded in the United States have had values of $(SI)_0$ ranging from 4.5 to 9 ft per sec and the same motions had values of $SI_{0.2}$ ranging from 1.9 to 2.7 ft per sec. It may be noted that the spectrum shown in Fig. 6 has $(SI)_0 = 1$ ft per sec.

If the structure has more than one degree of freedom, such as a multi-story building vibrating in the $y-z$ plane, the lateral displacement y is given by:

$$y = - \sum_i B_i \phi_i \frac{T_i}{2\pi} \int_0^t e^{-\frac{2\pi}{T_i} \zeta_i (t-\tau)} \sin \frac{2\pi}{T_i} (t-\tau) d\tau \quad (11)$$

where ϕ_i is the shape of i -th mode of vibration, T_i is the period of the i -th mode, and

$$B_i = \frac{\int \phi_i dm}{\int \phi_i^2 dm}$$

with integrals being taken over the mass of the structure. By analogy with Eqs. (4) and (8), the foregoing Eq. (11) can be written:

$$y = - \sum_i B_i \phi_i \left\{ \frac{T_i}{2\pi} S_i \sin \left(\frac{2\pi}{T_i} t - \alpha_i \right) \right\}. \quad (12)$$

An upper bound for the maximum response may be written

$$y_{max} < \sum_i B_i |\phi_i| \frac{T_i}{2\pi} S_{v_i}. \quad (13)$$

Similar expressions can be written for the maximum velocity, the maximum acceleration, the maximum shear force, etc. Those cases where the oscillations of structures during earthquakes have been recorded show that the spectrum approach gives good results [7,16]. Investigations have been made

of the amounts by which the right side of Eq. (13) exceeds the left side [17].

It is seen that a knowledge of the response spectrum S_v permits very informative calculations to be made as to the maximum responses of structures. For practical purposes it is, of course, necessary that the pertinent characteristics of the expected S_v be predictable.

THE EFFECT OF GROUND PROPERTIES AND GROUND COUPLING

In the case of earthquake ground motions it is still a moot question as to the precise influences of local geological conditions, and similar questions arise concerning the effects of the local geology on explosive-generated ground motion. Actually, the effects are probably much greater for the explosive-generated ground shock than for the earthquake ground motions. For example, earthquakes always originate in the same geological stratum, the earth's crust, and the seismic waves travel through the crust into the region of local geology where the structure is located. In the case of the explosive-generated ground shock, however, the significant seismic waves will usually originate in the same geological formation that contains the structure and hence the effect of ground properties can be expected to be magnified. Again, the energy source of a large earthquake is a large area of fault over which slipping occurs. The dimensions of this area are large compared to characteristic dimensions of local geological strata, and hence the influence of local geology can be expected to be less pronounced than in the case where the dimensions of the energy source are of the same order as the characteristic dimensions of the local geology, as may be the case for explosive-generated ground shock. Also, in the case of earthquakes the significant wave lengths in the ground motion tend to be long compared to the characteristic dimensions of local geology which is usually not the case for explosive-generated ground shock.

The effect of ground coupling can be expected to be important in the case of explosive-generated ground shock. In this case the dimensions of the structure may be large compared to the wavelengths of significant ground motion, and the rigidity of the structure may be large compared to the rigidity of the surrounding soil. The effect of these conditions is that the structure will inhibit the natural deformation of the soil, and because of this, the structure will be subjected to

certain forces. Also, because of this the motion imparted to the structure will be different from the motion the ground would have had in the absence of the structure. Further studies of the general character and influence of ground coupling are needed to clarify the situation.

Another difference between the earthquake problem and the explosive-generated ground shock problem is that in the case of the earthquake the stresses produced in the soil by the seismic waves are not very large. It is, in general, only in the vicinity of the hypocenter of the earthquake that the stresses are sufficiently large to produce failure and straining beyond the elastic range. In the case of the explosive-generated ground shock, however, the structure may be at a location where the seismic waves produce stresses in the ground that are far beyond the limit for elastic stresses. In this case, the effect upon the structure may depend strongly upon the nonlinear properties of the soil.

THE RULES FOR THE DESIGN OF STRUCTURES

Both in the case of earthquakes and of explosive-generated ground shock it is quite impossible to predict the ground motion that the structure will actually experience in the future. It is thus also impossible to predict the stresses that will be induced in a structure by some future ground motion. It is important to realize that expected ground motions and expected stresses can be discussed only in terms of probabilities. Because of this, the design of a structure can be judged only from the following two points of view: first, what is the probability that the structure will be overstressed; that is, then it

have an adequate factor of safety? and second, are the strengths of the various parts consistent; that is, are factors of safety of the parts the same?

The first of the above questions can be answered only on the basis of a quite arbitrary decision for it is not possible to estimate the maximum ground shock to which the structure may be subjected, nor is it possible to evaluate accurately the probabilities of occurrence. To achieve uniform factors of safety is highly desirable, particularly to avoid points of weakness. Design specifications are aimed at achieving this uniformity of strength but because of the complexities and indeterminacies in the ground-shock problem, it is not at present possible to write an airtight design specification that will cover all aspects of the problem with equal validity. In fact, the problem is so complex that it will, probably, never be possible to compose such design specifications. The designer must keep in mind that the specifications are not completely correct and in deciding how to apply the design specifications, he should be guided by the intent to achieve uniform factors of safety.

Design specifications often embody idealized spectra that are based on free-field measurements in a particular type of soil. These specifications will not describe accurately the ground motion to be expected in soil having different properties or having other local geological differences; neither will they describe accurately the motion to be expected if a structure is built in the soil and there is significant coupling. This requires that considerable judgment should be used in the application of the specifications, and the difficulties encountered in applying the specifications should serve as an indication of the proper measurements to be made in future tests.

REFERENCES

- [1] K. Suyehiro, "Engineering Seismology, Notes on American Lectures," Proc. Amer. Soc. Civ. Eng., 58, May 1932.
- [2] D. E. Hudson and G. W. Housner, "Analysis of Strong-Motion Accelerometer Data from the San Francisco Earthquake of March 22, 1957," Bull. Seism. Soc. Amer., 47, 1957.
- [3] Special Publication No. 201, Earthquake Investigations in California, U. S. Government Printing Office, Washington, D. C., 1936.
- [4] B. Gutenberg and C. F. Richter, "Earthquake Magnitude, Intensity, Energy," Bull. Seism. Soc. Amer., 46, 1956.
- [5] Special Report 57, San Francisco Earthquakes of March 1957, California Division of Mines, 1959.
- [6] D. E. Hudson and G. W. Housner, "Structural Vibrations Produced by Ground

- Motion," Trans. Amer. Soc. Civ. Eng., 122, 1957.
- [7] G. W. Housner, "Characteristics of Strong-Motion Earthquakes," Bull. Seism. Soc. Amer., 37, 1947.
- [8] M. A. Biot, "Analytical and Experimental Methods in Engineering Seismology," Trans. Amer. Soc. Civ. Eng., 108, 1943.
- [9] G. W. Housner, R. R. Martel, and J. L. Alford, "Spectrum Analysis of Strong-Motion Earthquakes," Bull. Seism. Soc. Amer., 43, 1953.
- [10] D. E. Hudson, "Response Spectrum Techniques in Engineering Seismology," Proc. 1956 World Confer. Earthquake Eng., Earthquake Engineering Research Institute, San Francisco, 1956.
- [11] K. Kawasumi, "Notes on the Theory of Vibration Analyzer," Bull. Earthquake Research Institute of Japan, March 1956.
- [12] G. W. Housner, "Behavior of Structures During Earthquakes," Proc. Amer. Soc. Civ. Eng., EM4, October 1959.
- [13] G. W. Housner, "Interaction of Building and Ground," Bull. Seism. Soc. Amer., 47, 1957.
- [14] R. G. Merritt and G. W. Housner, "Effect of Foundation Compliance on Earthquake Stresses in Tall Buildings," Bull. Seism. Soc. Amer., 44, 1954.
- [15] G. W. Housner, "Spectrum Intensities of Strong-Motion Earthquakes," Proc. Symposium on Earthquake and Blast Effects on Structures, Earthquake Engineering Research Institute, San Francisco, 1952.
- [16] G. W. Housner, "The Behavior of Structures in Earthquakes — Modern Designing with Steel," Kaiser Steel Corp., 3, No. 2, May 1957.
- [17] R. L. Jennings and N. M. Newmark, "Elastic Response of Multi-Story Shear Beam Type Structures Subjected to Strong Ground Motion," Proc. 2nd World Confer. on Earthquake Eng., Tokyo, 1960.

DISCUSSION

Mr. Stern (General Electric Co.): I wonder if you would comment on how you calibrate the instruments that are used. The reason I ask this is that a while back we were concerned with building a reference platform for calibrating inertial devices. I got into the business of measuring microseisms; I believe these are very fine earth tremors. Apparently no one has a satisfactory method for calibrating real fine earth tremors which might be equivalent to calibrating real accurate inertial equipment. Do you have any information on this or have you done any work along these lines?

Dr. Housner: No, I can't answer that question. You are now asking about ground motions that are outside of the scope of the engineering problem. In our case the instruments we are interested in are the accelerometers and those do not need to be calibrated as accurately as I think the instruments you are concerned with must be.

Mr. Burns (AMF, Greenwich): I noticed you had acceleration response spectra there that seemed to increase in magnitude with increased damping. Did I read it right?

Dr. Housner: Yes.

Mr. Burns: Would you consider this typical of all ground disturbances, including nuclear weapons, or would you consider this peculiar to earthquake environments?

Dr. Housner: The effect is more pronounced in the case of the strong motion earthquake because of the long duration. On a very short disturbance the effect of the damping is very small.

Mr. Burns: In effect you are suggesting that there is a fair amount of resonance and the damping depresses this in the earthquake application.

Dr. Housner: Yes, in a sense, if it has a long duration, if we're talking about 15 or 20 seconds which is a big earthquake.

Mr. Burns: Do you have any reason to suspect that this is not typical of a nuclear weapon?

Dr. Housner: All I would say is the corresponding spectra made from explosive generated ground shock have different shapes. For one thing, the high frequency end is much exaggerated in those cases and the duration of the ground motion doesn't by any means come out to 15 or 20 seconds for the explosive generated ground shock.

Mr. Bendat (Ramo-Wooldridge): I would like to ask a question about further statistical analysis of the data. Your use of the word spectrum was quite limited and displayed only velocity information as a function of period. In other connotations, and particularly the analysis of random phenomena, the word spectrum usually has the interpretation, let us say, of the mean square acceleration per cps as a function of frequency. And besides this common idea of power spectral density function, there is also the requirement for making statistical analyses of amplitude probability densities and distributions for the acceleration data. I wonder if you could comment on both of these additional requirements for further statistical information.

Dr. Housner: I can say this; the spectra shown are the so-called response spectra. They are not the Fourier-type spectrum. Studies have been made in the case of earthquakes that show that the earthquake ground motion can be considered to be a random function which is a sample from a population of random functions. If you compute on the basis that the random function is gaussian and white you can duplicate almost all of the

properties of the earthquake. So that part of the statistical theory has been worked out quite in detail.

Mr. Blaite (Lockheed): When I was working on Navy ship shock we used the earthquake spectrum and called it a shock spectrum. We ran into a difficulty which was that the shock spectrum taken at the foundation of a heavy piece of equipment showed a pronounced dip at the anti-resonance of that equipment, something which is usually called the natural frequency of the equipment. You associated a peak with the resonance of a building and I was wondering whether we have things backwards or whether the same sort of thing occurs in earthquake spectra?

Dr. Housner: The same thing does not occur in earthquake spectra. The peaks we observe are the influence of the force exerted by the building on the foundation on the ground. Now in your case it sounds to me as if you had a situation in which some of the energy was being pumped into some mass and, as a consequence, the point at which you were measuring did not vibrate as much as it would have otherwise.

Mr. Blaite: Yes. A crude analogy is that it acts like a vibration damper. It's not a good analogy but a crude one.

Dr. Housner: That is not observed in the case of earthquake. Largely, I think, because of the random nature of the excitation and its long duration.

MODEL EXPERIMENTS PERTAINING TO THE DESIGN OF UNDERGROUND OPENINGS SUBJECTED TO INTENSE GROUND SHOCKS

John S. Rinehart
Mining Research Laboratory
Colorado School of Mines

In these experiments explosives were detonated above openings precast in five brittle rock-like modeling materials. The shapes of the openings and the depths from a free face were varied. This paper describes the results of some two hundred tests which provide an excellent insight into the nature of failures.

INTRODUCTION

Model experiments pertaining to the design of underground openings subjected to intense ground shock have been initiated and preliminary observations made. Most underground openings, in practice, are designed by using statically determined rock properties and liberal safety factors. In an opening specifically designed to withstand dynamic loads it is the dynamic properties of the material and the rapidly changing dynamic stress situation that must be taken into consideration. These experiments were begun with the thought that they would eventually provide certain guide lines for the design of underground openings having somewhat increased resistance to failure when subjected to intense transient dynamic loads.

In these experiments an explosive was detonated above an opening precast in several brittle rock-like modeling materials, plaster of Paris, paraffin-salt mixture, and so forth. The explosive charge, 9 grams of composition C3, and the over-all size of the models were kept constant. The shape of the opening and the depth to the opening from a free face were varied. Five modeling materials having different physical properties and three general shapes of openings were used. To simulate an infinite medium as would be found underground, the model was confined during the experiment.

Two hundred tests were run. Fifty were used to determine the correct size of explosive charge and the proper size model. The remaining one hundred and fifty were used in the actual experiment on fracture patterns.

MODELING MATERIALS AND PHYSICAL PROPERTIES

Five simulated rocks were made up and used with these basic constituents: Ideal Portland cement, Type 1; Red Top, No. 1, moulding plaster; Tex-Wax; vermiculite No. 1; salt; water. Table 1 gives the actual compositions of the five different mixtures.

Six physical properties of the model materials were tested: hardness, compressive strength, tensile strength, shearing strength, modulus of rupture, and the velocity of sound. For each physical property three small specimens were prepared and tested; the test specimens were cubes 1 inch by 1 inch, and parallelopipeds 2 inches by 1 inch by 1 inch and 6 inches by 1.5 inches by 3 inches. Results are listed in Tables 2 and 3.

To test the compressive strength and hardness, the specimens were first allowed to dry for two weeks. Hardness of the specimens was determined before compression with a Shore sclerometer. The specimens were then placed between two pieces of

TABLE 1
Composition of Model Materials

Model Material	Composition (Percent by Weight)					
	Plaster of Paris	Portland Cement	Tex Wax	Vermiculite	Salt	Water
Plaster of Paris	63	—	—	—	—	37
Plaster of Paris-Cement (5-1 ratio)	53	10	—	—	—	37
Plaster of Paris-Cement (5-3 ratio)	39	24	—	—	—	37
Vermiculite-Cement	—	13	—	53	—	34
Paraffin-Salt	—	—	—	—	83	—

TABLE 2
Physical Properties of Modeling Materials

Material	Hardness	Physical Properties					
		Compressive Strength (lb/in ²)		Tensile Strength (lb/in ²)		Shear Strength (lb/in ²)	
		Avg.	Avg.	Avg.	Avg.	Avg.	Avg.
Plaster of Paris	4	1460 1485 1502 1580	— 299 270 215	296 498 548 504	641 712 612	224 266 246 248	234 236 235 234
Plaster of Paris-Cement (5-1 ratio)	5	1910 1960 1866 1730	— 396 426 466	415 712 585	430 612	222 245 235 237	234 236 235 234
Plaster of Paris-Cement (5-3 ratio)	6	1490 1450 1433 1390	— 240 263	274 575 552 557	525 575 552 557	146 154 137 140	146 154 137 140
Vermiculite-Cement (4-1 ratio)	0	316 356 319 286	— 10	10 10	10 10	— 10	— 10
Paraffin-Salt (1-5 ratio)	0	306 295 322 364	— 10	141 92 119 125	146 154 137 140	— 10	— 10

TABLE 3
Velocity of Longitudinal Sound Wave

Model Material	Velocity of Sound (ft/sec)
Plaster of Paris	7579 - 9088
Plaster of Paris-Cement (5-1 ratio)	8530 - 9877
Plaster of Paris-Cement (5-3 ratio)	8300 - 8497
Vermiculite-Cement	not measured
Paraffin-Salt	7447 - 8497

cardboard and loaded to failure in a testing machine; the rate of loading was uniform.

As the specimens had a height-width ratio which was greater than one to one, the results were converted to the equivalent 1:1 ratio by the following equation:

$$C_c = \frac{C_p}{0.778 + 0.222 \frac{D}{h}}$$

where C_c is the compressive strength of an equivalent cubical specimen; C_p , the compressive strength of the specimen having a height greater than the diameter or lateral dimension; D , the diameter or lateral dimension; and h , the height.

The specimens were prepared for tensile strength determinations by gluing circular steel plates onto the ends of the specimens with "plastic steel." The plates had a threaded female joint sunk in the center, the male end of a universal joint being screwed into this plate, and this in turn was connected to the testing machine by means of a bar. They were then pulled to failure.

In the case of the vermiculite-cement and the paraffin-salt no ultimate failure load could be obtained because the specimens failed in the testing machine before a load could be applied.

Shearing strength was determined by placing the specimen in a shearing device which consisted of two cutting edges, the load being transmitted by means of a plate and ball bearing. The shearing strength was calculated by dividing the load by twice the cross-sectional area as the specimens failed in double shear.

The method of testing for the modulus of rupture was to lay the specimen on two knife edge 4 inches apart, and load them in the middle by means of a third knife edge, until failure. The modulus of rupture, MR , was calculated from the equation:

$$MR = \frac{3/2 PL}{bd^2}$$

where P is the load in pounds; L , the distance between knife edges in inches; b , breadth of the specimen in inches; and d , its depth in inches.

The velocity of sound through the material was measured by placing a barium titanate crystal on each end of a prepared specimen. An electrical pulse was produced by a pulse generator and converted to a mechanical pulse by one of the crystals, the transmitted pulse then being picked up at the far end of the specimen by the other crystal. The time it took the pulse to travel along the specimen was measured by means of an oscilloscope. Knowing the length of the specimen and time of travel of the pulse, the velocity of sound was readily determined (see Table 3).

THE EXPERIMENTS

Selection of Size of Model and Explosive Charge

An 8-inch cube was selected as the best size for the model, three factors being taken into consideration: (1) ease of handling, (2) economy of material, and (3) ease of obtaining results. Early models, 8 inches by 8 inches by 4 inches were found to be too small for desired results, while 12-inch cube models proved to be too large for easy preparation and handling.

Openings simulating tunnels were formed by casting the model material around a wood block and removing the block after the material had set. Tunnels of circular, saw-toothed, and rectangular cross section each having dimensions of the order of an inch or so were made in this way. The stratagem was to try to make the opening of such size and to so place it with respect to the explosive charge that various qualities of failure would manifest themselves.

Determination of the size of the explosive was a major problem. Blasting caps alone did not produce the desired effects and charges of Composition C3, proving more successful,

were used. Cylindrical charges of 1/4, 3/8, 1/2, 5/8, and 3/4 inch diameter and lengths of 2-1/2 times the diameter were tested, the charges being initiated with an Engineers Special No. 10 electric blasting cap. The 1/2-inch diameter charge, 9 grams in weight and 2-1/2 inches long, gave best results. In most cases the charge was placed on end in the center of the block directly above the center of the tunnel and detonated from the top. In a few cases it was placed eccentrically.

The sizes, shapes, and locations of the many model tunnels can best be appreciated by examining the numerous drawings in the Appendix. Three general shapes of openings were used: circular, rectangular including square, and saw-toothed, each opening running the full length of the block and having uniform cross section. The circular openings were 1-3/16 inches and 1-5/8 inches in diameter and were placed 2 inches, 2-1/2 inches, and 3 inches below the surface. One group of openings ranging from 1 inch to 3 inches in width had saw-tooth shaped roofs with one, two, and three notches.

Preparation of the Models

Cardboard boxes of the proper size were used for the molds, with the wood block tunnel molds placed at the desired distance from the bottom of the box and held in place by screws. The box was confined by steel plates to prevent bulging of sides.

In paraffin-salt models the paraffin was brought to a temperature considerably higher than its melting temperature, after which the salt was stirred into the melt. The salt and paraffin were thoroughly mixed and after being molded the mixture was allowed to cool for 24 hours at room temperature. The paraffin-salt models required no additional treatment.

The other four types of blocks were prepared by mixing the materials with the required amount of water and then pouring the mixture through a No. 4 sieve into the box.

The plaster of Paris and plaster of Paris-cement models were dried in an oven for 48 hours at a temperature of 55°C and left there an additional 24 hours after the oven had been turned off. A different method was employed to cure the cement-vermiculite models. After removal from the paper molds and removal of the tunnel mold they were placed under water for five days after which they were treated

as the plaster of Paris and plaster of Paris-cement models above.

Firing Tests

Prior to firing the explosive, all models were inspected to see that the surface to which the explosive would be affixed was perfectly smooth. The open ends of the tunnel were taped shut and the model was placed in a hole of depth equal to model height. Dirt was tamped around the model to simulate an infinite medium and the explosive was placed on the model with the detonator in place.

After firing the charge, the model was recovered. In some cases the model was so badly fractured that it was of no use and was disposed of immediately.

Preparation for Post-Mortem Examination

After blasting, the model was sectioned through the crater perpendicular to the axis of the tunnel. The cut face was cleaned and lithium-grease applied to bring out the minute fractures clearly. A fluorescent paint and black light method did not prove satisfactory although it did show the compressed and crushed zone around the crater quite clearly.

After measurements of the crater and the fractured areas were completed, drawings, sheets 1 through 15 of which are reproduced in the Appendix, were made and arranged six or nine to a sheet. These drawings are cross-sectional views, showing individual fracture patterns. The depression at the top of center of each sketch is a cross-sectional view of the crater produced by the explosive, the dashed line being the original surface of the block. The fine lines define the fractures and the heavy lines the shape and location of the original opening. Where a part of the opening is blown clean away, the original opening is shown dashed.

DISCUSSION OF RESULTS

When an explosive charge is detonated in intimate contact with a massive body, such as one of the models described here, a high-intensity transient stress wave moves out spherically from the source of the explosion leaving damaged material in its wake. The pattern of damage generated is usually complex with the origins of certain fractures being

obscure and others being reasonably well understood. It is usually not possible to specify a priori which of the many possible fracture patterns will predominate.

The attempt to choose the models large enough to eliminate the boundary effects was substantially successful, the models in general acting as bodies of semi-infinite extent *c. cont* in the area surrounding the underground opening.

View temporally the damage falls into three categories: (1) that occurring concomitantly with passage of the initial wave; (2) that which waits until the stress wave has been influenced by one or more boundaries; and (3) that which takes place much more leisurely, arising from the diverse residual velocities imparted to different regions of the mass as a consequence of passage and interference of stress waves. Crushing, cratering, shearing, and radial fracturing fall into the first category; spalling or scabbing of the tunnel roof and walls into the second; and caving into the third.

All five materials reacted, qualitatively, about the same except for the paraffin-salt mixture which, being more pliable than the others, underwent considerable plastic distortion in situations where the other, more brittle, materials did not.

Cratering

When the explosive detonates, rock in the immediate neighborhood of the explosion fractures and is blown out, leaving a permanent crater shown in cross section in each of the drawings. Since in these tests only one size of charge was used, there was not opportunity to observe effect of size of explosive on size and shape of craters. Approximate typical crater dimensions are given in Table 4. Crater diameters range from 2 inches for the hard plaster of Paris to about 4 inches for the soft vermiculite, it being expected that somewhat larger craters would be made in the weaker materials, vermiculite-cement and paraffin-salt; the crater depths were about one-half to one-third crater diameters. The quantitative correlation between any one physical property and the crater dimensions is not especially high.

Crushed Zone

Immediately below the crater, in those cases where the tunnel did not completely

TABLE 4
Approximate Typical Crater Dimensions

Model Material	Crater Dimensions	
	Diameter (in.)	Depth (in.)
Vermiculite-Cement	3.7	1.8
Paraffin-Salt	quite variable 2.5 - 3.7	1.1
Plaster of Paris	2.8	0.9
Plaster of Paris-Cement (5-1 ratio)	2.0	0.8
Plaster of Paris-Cement (5-3 ratio)	2.0	0.7

collapse, there is a quasi-hemispherical zone of heavily compacted or crushed material. In this region, the affected plaster of Paris is less pervious to liquids, its extent being clearly delineated by soaking in a liquid dye. The region extends in plaster of Paris down about 1 inch below the bottom of the crater, being thickest at the center and tapering off toward the edge.

Shearing

In several instances (listed in Table 5), the force of the explosion was sufficiently intense to shear the model material clean through, plugging the tunnel. The weaker materials, as was to be expected, sheared most readily. Compare the three vermiculite-cement specimens 61, 62, and 63, Sheet 6, and the three paraffin-salt specimens 21, 49, and 52, Sheet 3 with similar plaster of Paris specimens 17, 27, and 30, Sheet 9. A photograph of the plugged opening of the paraffin-salt specimen number 52 is reproduced in Fig. 1.

The three plaster of Paris specimens 43, 44, and 51 show clearly the effect of size of opening, the 3-inch-wide tunnel having sheared, while the 1-inch and 2-inch tunnels did not. It is significant that the resistance to shear, proportional to the area to be sheared, is the same in each of the three cases, but that the total force available to produce the shear is greatest for the 3-inch tunnel. All three similar tunnels, specimens 61, 62, and 63 sheared in the vermiculite-cement mixture, a material with about one-fifth of the shear strength

TABLE 5
Cases in Which Plugging
Due to Shear Occurred

Sheet	Specimen	Material
1	113	Paraffin-Salt
2	122, 128	Paraffin-Salt
3	49, 52	Paraffin-Salt
4	134, 131, 132	Vermiculite-Cement
5	137, 141 144	Vermiculite-Cement
6	61, 62, 63 64, 65, 66, 69	Vermiculite-Cement
12	31	Plaster of Paris- Cement (5-1 ratio)

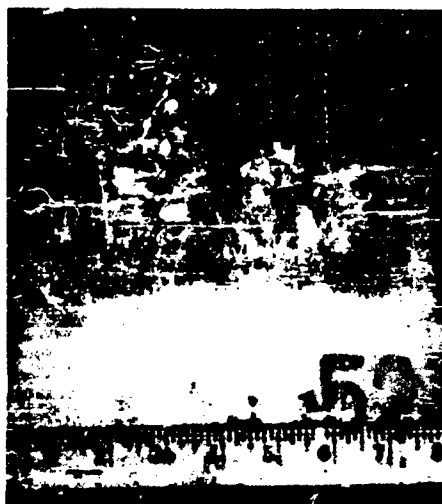


Fig. 1 - Shearing. The plugged opening of a paraffin-salt specimen No. 52.

of plaster of Paris. Only two of the tunnels, the 2 inch and 3 inch, specimens 49 and 52, Sheet 3, of the paraffin-salt models sheared. This material had about one-fifth the shear strength of plaster of Paris. Generally the probability of shear occurring is greater with square and rectangular openings than with

circular or saw-toothed. Shearing, of course, becomes less likely to occur the deeper the opening is buried. Many of the specimens illustrate this point but drawings on Sheet 6 are especially germane.

Permanent Deformation

The paraffin-salt material was the most pliable of the materials used for the models and showed a marked tendency to deform permanently, a circular tunnel opening 1-3/16 inches in diameter, buried 3 inches, assuming a more or less elliptical shape (specimen 120, Sheet 1, shown also in Fig. 2).



Fig. 2 - Permanent deformation. A circular tunnel opening 1-3/16 inches in diameter and buried 3 inches, has assumed a more or less elliptical shape. Material, paraffin-salt.

Radial Fractures

In some of the specimens (see particularly numbers 18 and 26, Sheet 9), several fractures extend out radially from the crater area. There are five such fractures in specimen 18, spaced about 30 degrees apart. It is likely that these radial fractures develop as the spherically expanding shock wave moves outward, the fractures being a direct consequence of the hoop stresses which are indigenous to the front of such a diverging wave.

Spalling

The roofs of many of the tunnels spalled. An example is shown in the photograph reproduced as Fig. 3, plaster of Paris specimen 26, containing a 2-inch-wide tunnel. Spalling can arise when a sharp-fronted transient compression wave reflects from a free face, generating a tension wave, which in interfering with the remainder of the compression wave establishes a high concentration of net tensile stress. Occasionally when the intensity of stress in the incident wave is quite high, several spalls may be formed.



Fig. 3 - Spalling. An example in a plaster of Paris specimen, No. 26, containing a 2-inch-wide tunnel.

Single spalls are clearly evident in specimens 21 and 22, Sheet 3; numbers 17, 18, 26, 28, 29, and 30, Sheet 9; numbers 43, 40, 44, 41, 32, and 42, Sheet 12; and numbers 46 and 47, Sheet 15. Multiple spalling is evident in numbers 50 and 53, Sheet 3; and numbers 35, 37 and 38, Sheet 15.

The stress in the wave lessens as it moves through the material due to both divergence and attenuation so that at some point the stress is no longer sufficient to produce a spall. Note from the drawings of Sheet 3 that spalling occurs in the tunnels buried 2-1/2 inches, but not in those buried 3 inches.

The thickness of the spall is an indication of the sharpness of decay of the wave behind its abruptly rising front, a thin spall indicating very rapid decay and a thick spall, relatively slow decay. Usually, a wave lengthens and its peak stress decreases as it travels through a material, thus giving rise to thicker and thicker spalls. This effect, for some unexplainable reason is not discernible in the

specimens, except perhaps for specimens 17 and 18, Sheet 9.

The shape and size of the opening determines the manner in which the wave is reflected. There will be almost no coherent reflection from a circular opening so that spalling will not in general occur. The correctness of this supposition is borne out by inspection of Sheets 1, 4, 7, 10, and 13, no spalls being present in any of the specimens. The wave-interference pattern about the saw-toothed shape openings must be exceedingly complex and the complicated nature of the fracture patterns around these openings attests to this fact (see Sheets 2, 5, 8, 11, and 14). The situation is relatively simple in the case of the rectangular openings since the roof is plane, the only complication being the influence of the corners formed by intersection of the walls with the roof. It is unfortunate that no flat plates, openings of infinite width, have been tested; for it would be interesting and instructive to compare spalling within these plates with spalling above the rectangular openings tested here. Such tests are contemplated for the future. It appears from an examination of the fracture patterns that the walls do influence significantly the spall pattern. Specimens 22, 50, and 53, Sheet 3, spalled paraffin-salt models, having tunnels 1 inch, 2 inches, and 3 inches wide, respectively, and buried 2-1/2 inches, illustrate these effects splendidly. Substantially similar effects can be seen in plaster of Paris-cement specimens 47, 38, and 35, Sheet 15. Two spalls of approximately equal thicknesses, were produced in the 3-inch wide and 2-inch wide tunnels, the spalls being somewhat thinner in the 2-inch tunnel. Only one spall developed in the 1-inch-wide tunnel, edge effects evidently preventing the second spall from forming. The second spall forms as a result of reflection of the wave from the freshly created surface of the first spall. For the 1-inch-wide tunnel the surface of the first spall is so narrow that not enough of the wave is reflected to give a second spall. The thickness of the spall is nearly constant across the span, thinning out near the corners. This is to be expected from the nature of the wave pattern.

Generally, the spall patterns are in accordance with prediction.

Fractures Around Openings

In several cases fractures developed which ran outward from the tunnel walls.

Such fractures, usually running out either horizontally or vertically, were particularly prevalent around the circular openings (see Sheets 7, 10, and 13), although there are several running from the corners of the rectangular openings. The origin of these fractures is not fully understood. It seems probable that they are caused by tensile stresses developing during gross deformation of the opening. Consider a circular opening subjected to a strong compressive transient shock. It will, during compression, first transform itself into an ellipse with its major axis parallel to the wave front during which time tensile forces perhaps strong enough to sunder the material develop along this axis. On release of load the material will expand, overshooting its original shape to form an elliptical opening oriented perpendicular to the first, the horizontal fractures forming at this time. Somewhat similar stresses will develop around rectangular openings.

Cave Ins

When a material spalls, considerable momentum can be trapped in the spall, enabling the spall to break itself away from the parent mass, often with violence. At other times the momentum is insufficient to dislodge material, the spall remaining *in situ*, bounded by a fracture. Spalls were dislodged in specimens 21 and 22, Sheet 3; numbers 17, 27, and 30, Sheet 9; and number 40, Sheet 12; and remained in place in numerous other instances, particularly the specimens shown on Sheet 15.

Specimens 46, 47, 37, and 35, Sheet 15, exhibit another interesting fracture, a central break in the spall. This must come about in the following way: because the incident wave is most intense at a point directly below the point of application of the explosive charge, the central part of the spall begins to move with a higher velocity than the edges. In addition the edges are constrained and must be sheared from the parent mass if the spall is to pull loose. The spall thus acts as a beam, fixed at both ends, bending and breaking in the middle.

The most complex fracture patterns of all occurred with the saw-toothed shape openings; these patterns are very difficult to analyze. In general, the openings caved in badly (see Fig. 4), undoubtedly the combined result of spalling, corner fracturing (each saw-tooth being a good corner reflector), and for other

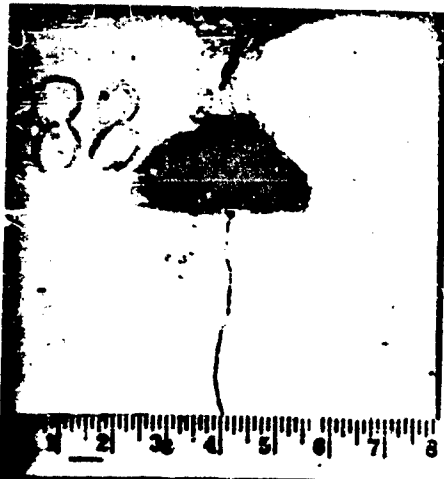


Fig. 4 - Cave ins. An example in a saw-tooth opening which had 3 notches. Material, plaster-cement (5-1). Specimen No. 88, Sheet 11.

reasons. The net effect (see Sheet 11 in particular), was to produce an arched structure above the area where the saw-teeth formerly existed. Further analysis of the fracture pattern is needed.

CONCLUSIONS

This series of tests has provided an excellent insight into the nature of the failures around underground openings subjected to intense impulsive loads. The nine specimens of Sheet 3 form an almost complete panorama of the several qualities of failure: radial fractures, single spall formation, multiple spalling, plugging by shear, no fracturing at all.

The tests carried on in this experiment were entirely preliminary with the intention of covering as broad a field as possible in the allotted time. It would be very desirable to run further tests with several models of the same material, tunnel shape, and depth with a view to gathering quantitative data on spall thickness, crater depth, crater area, and relating this data to such variables as depth of opening, area of opening, physical properties of the material, and shape of opening.

APPENDIX

Drawings of the Results of the Model Experiments

For the post-mortem examination, the models were sectioned and, after measurements of the crater and fractured areas had been completed, drawings were made and

arranged six or nine to a sheet. Sheets 1 through 15 are reproduced here. For ease of reference, two lists, A and B, are also given to assist in the location of specimens.

LIST A
List Showing on Which Sheet Specimen Numbers are Located

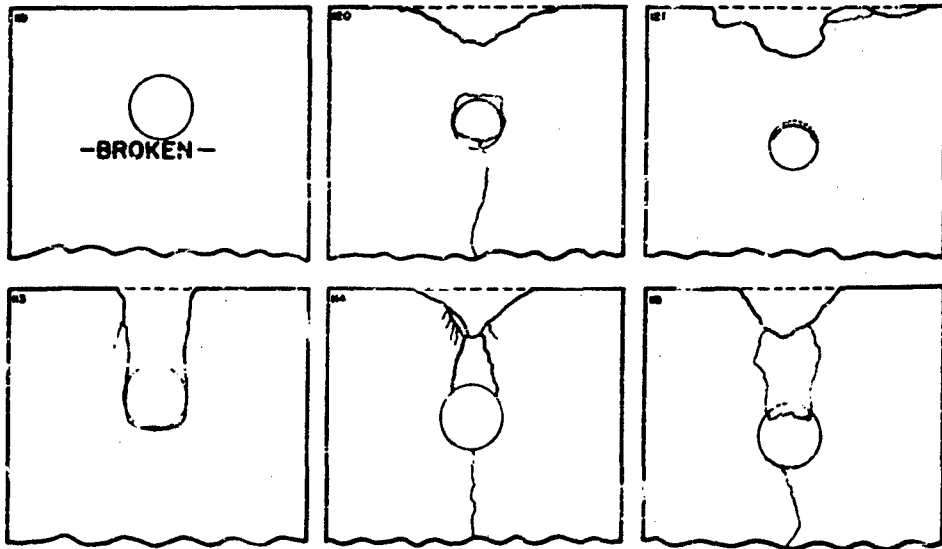
<u>Sheet</u>	<u>Specimen Number</u>
1	113, 114, 115, 119, 120, 121
2	122, 123, 124, 125, 126, 127, 128, 129, 130
3	12, 22, 23, 49, 50, 51, 52, 53, 54
4	13, 132, 133, 134, 135, 136
5	137, 138, 139, 140, 141, 142, 143, 144, 145
6	61, 62, 63, 64, 65, 66, 67, 68, 69
7	55, 56, 57, 58, 59, 60
8	74, 75, 76, 77, 78, 79, 80, 81, 82
9	17, 18, 19, 25, 26, 27, 28, 29, 30
10	92, 93, 94, 95, 96, 97
11	83, 84, 85, 86, 87, 88, 89, 90, 91
12	31, 32, 33, 40, 41, 42, 44, 45
13	71, 72, 73, 110, 111, 112
14	98, 99, 100, 101, 102, 103, 104, 105, 106
15	34, 35, 36, 37, 38, 39, 46, 47, 48

LIST B
List Showing Specimen Numbers and the Sheets on Which They are Located

Specimen No.	Sheet No.								
17	9	43	12	69	6	95	10	121	1
18	9	44	12	70	-	96	10	122	2
19	9	45	12	71	13	97	10	123	2
20	-	46	15	72	13	98	14	124	2
21	3	47	15	73	13	99	14	125	2
22	3	48	15	74	8	100	14	126	2
23	3	49	3	75	8	101	14	127	2
24	-	50	3	76	8	102	14	128	2
25	9	51	3	77	8	103	14	129	2
26	9	52	3	78	8	104	14	130	2
27	9	53	3	79	8	105	14	131	4
28	9	54	3	80	8	106	14	132	4
29	9	55	7	81	8	107	-	133	4
30	9	56	7	82	8	108	-	134	4
31	12	57	7	83	11	109	-	135	4
32	12	58	7	84	11	110	13	136	4
33	12	59	7	85	11	111	13	137	5
34	15	60	7	86	11	112	13	138	5
35	15	61	6	87	11	113	1	139	5
36	15	62	6	88	11	114	1	140	5
37	15	63	6	89	11	115	1	141	5
38	15	64	6	90	11	116	-	142	5
39	15	65	6	91	11	117	-	143	5
40	12	66	6	92	10	118	-	144	5
41	12	67	6	93	10	119	1	145	5
42	12	68	6	94	10	120	1		

PARAFFIN-SALT (1:5) MODELS

SCALE:
0' 1' 2' 3'



Sheet 1

PARAFFIN-SALT (1:5) MODELS

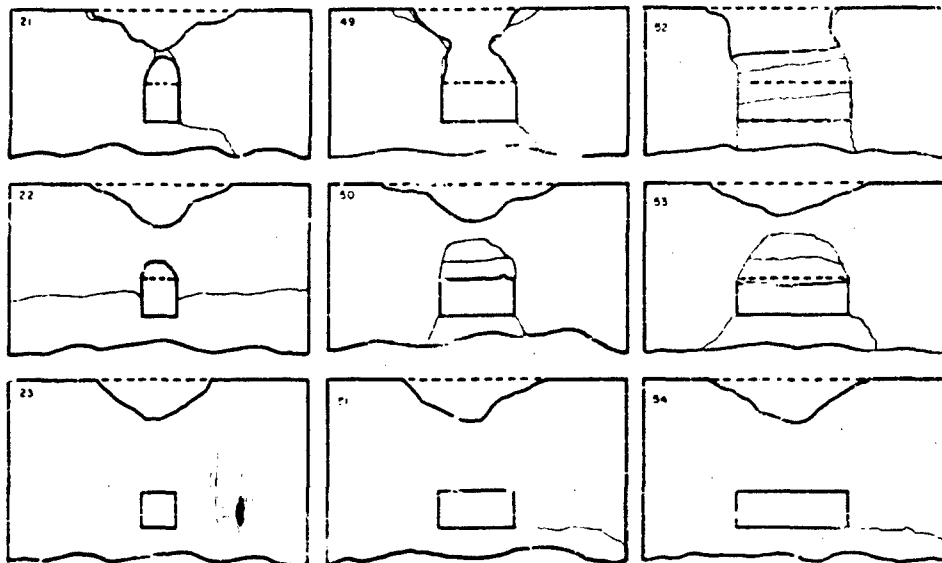
SCALE:
0' 1' 2' 3'



Sheet 2

PARAFFIN-SALT (15) MODEL

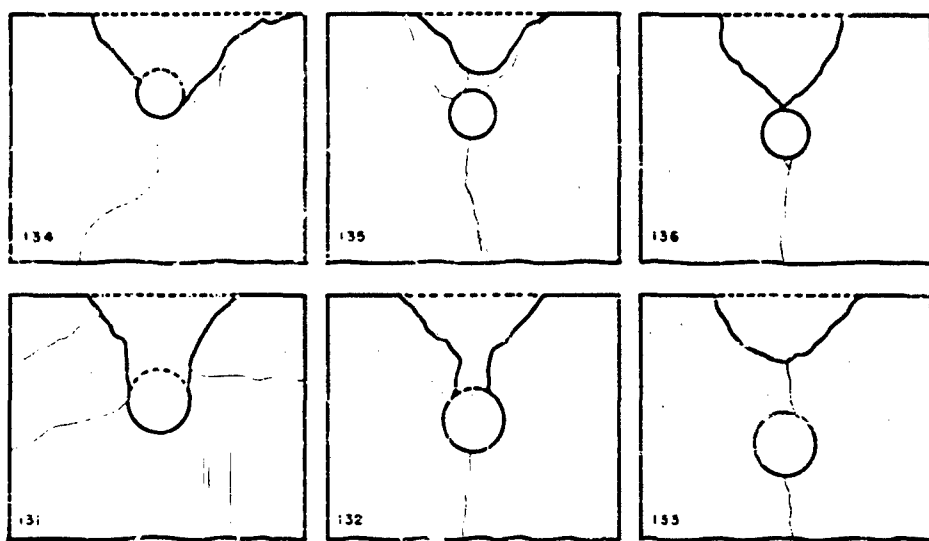
SCALE
0' 1' 2' 3'



Sheet 3

VERMICULITE-CEMENT (4:1) MODELS

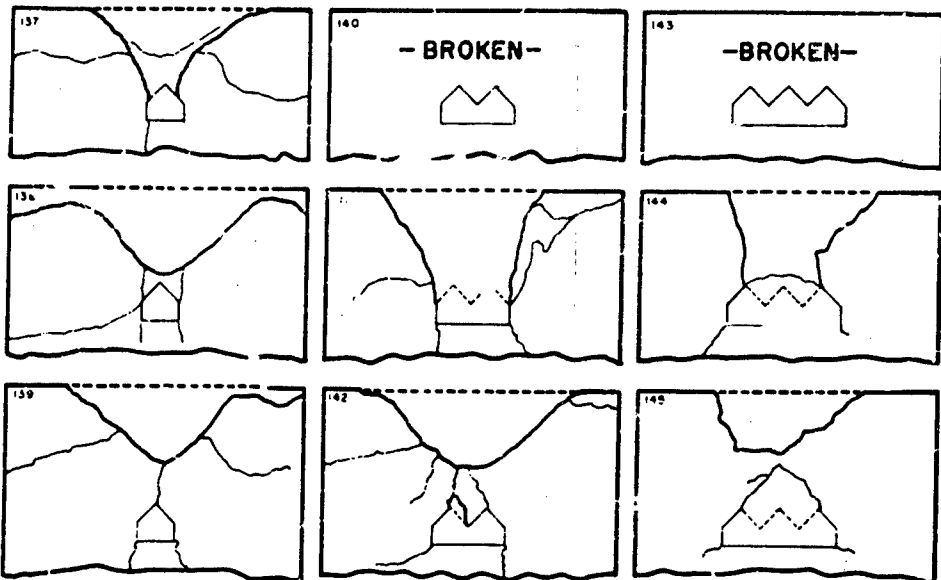
SCALE
0' 1' 2' 3'



Sheet 4

VERMICULITE-CEMENT (4:1) MODELS

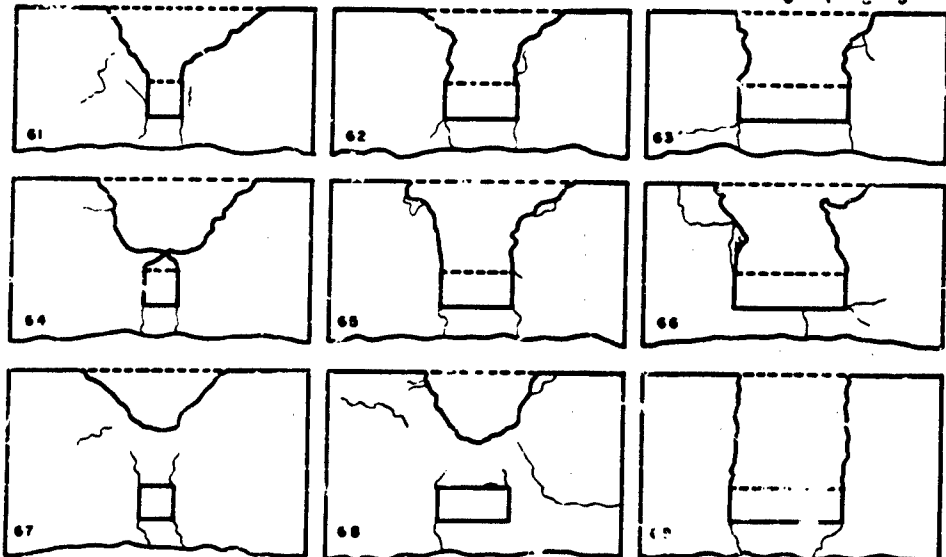
SCALE:
0' 1' 2' 3'



Sheet 5

VERMICULITE-CEMENT (4:1) MODELS

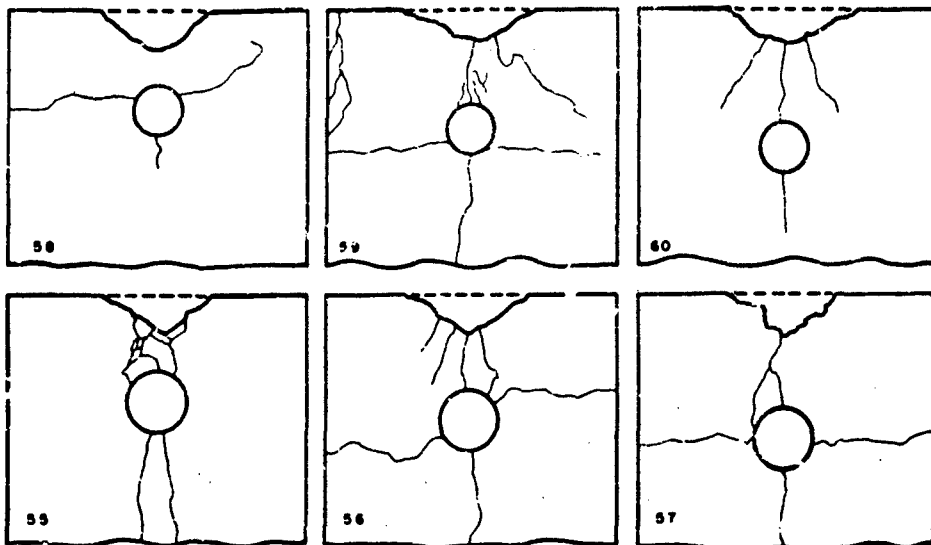
SCALE:
0' 1' 2' 3'



Sheet 6

PLASTER OF PARIS MODELS

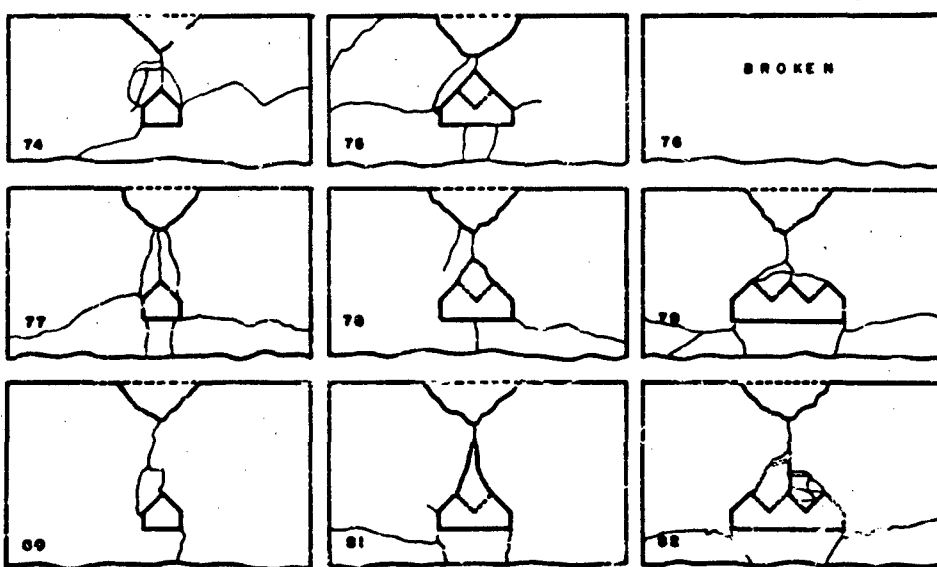
SCALE:
0 1 2 3



Sheet 7

PLASTER OF PARIS MODELS

SCALE:
0 1 2 3

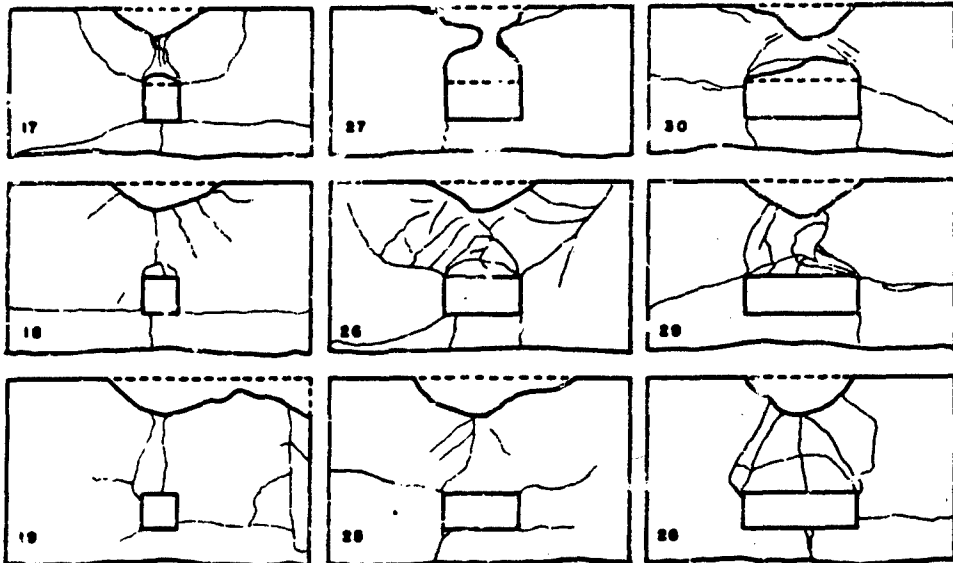


Sheet 8

182

PLASTER OF PARIS MODELS

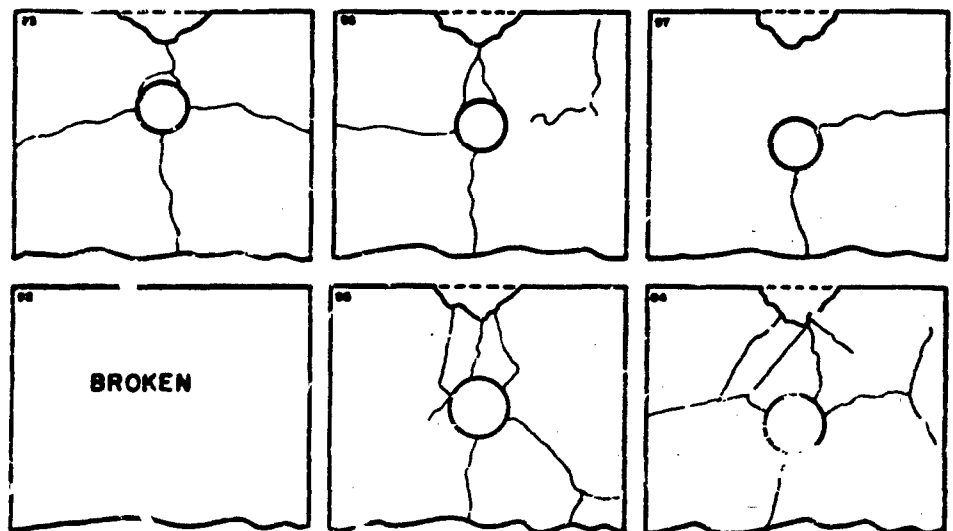
SCALE:
0 1 2 3



Sheet 9

PLASTER-CEMENT (5:1) MODELS

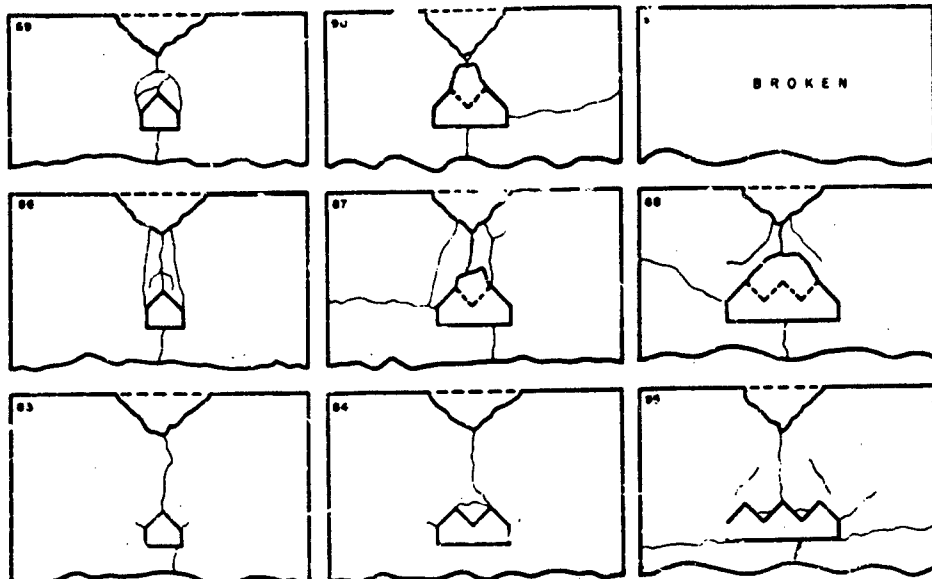
SCALE:
0 1 2 3



Sheet 10

PLASTER-CEMENT (5:1) MODELS

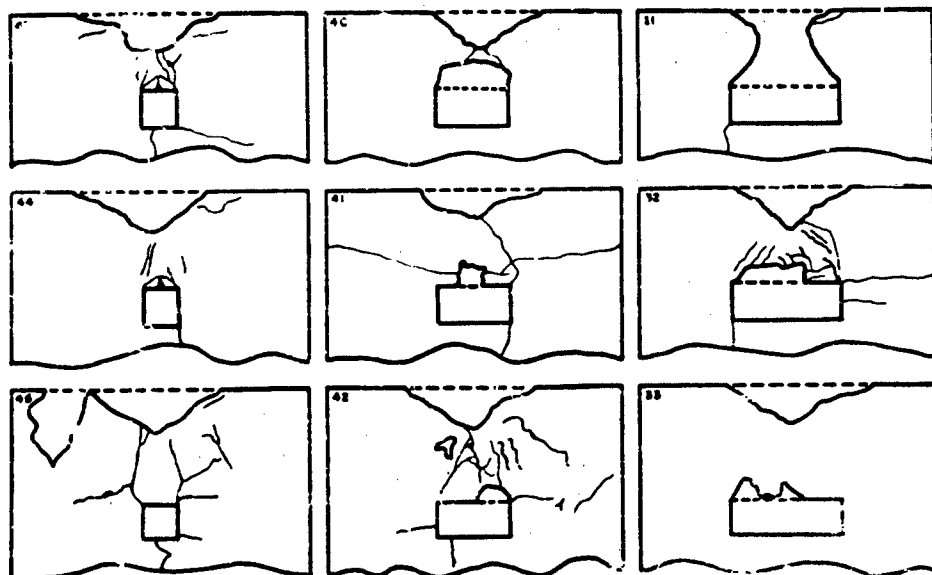
SCALE
0' 1' 2' 3'



Sheet 11

PLASTER-CEMENT (5:1) MODELS

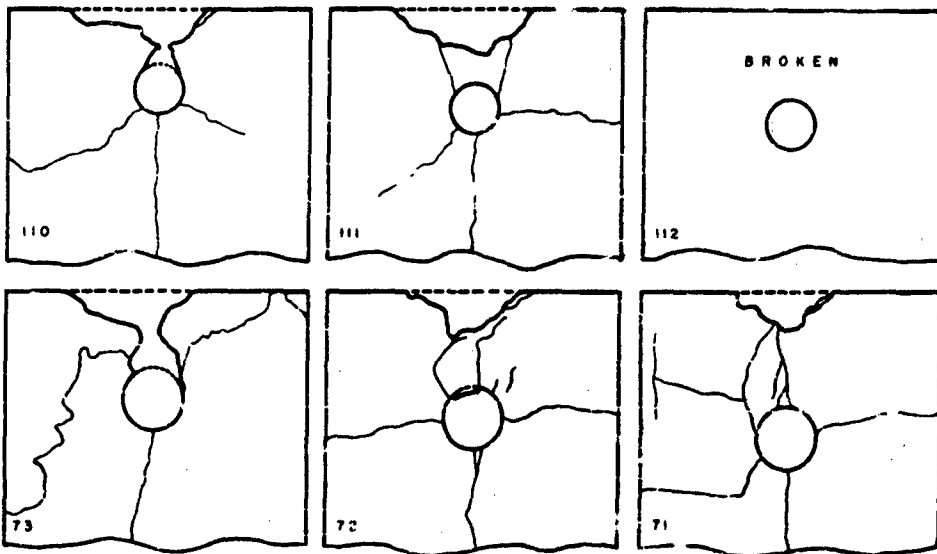
SCALE
0' 1' 2' 3'



Sheet 12

PLASTER-CEMENT (5-3) MODELS

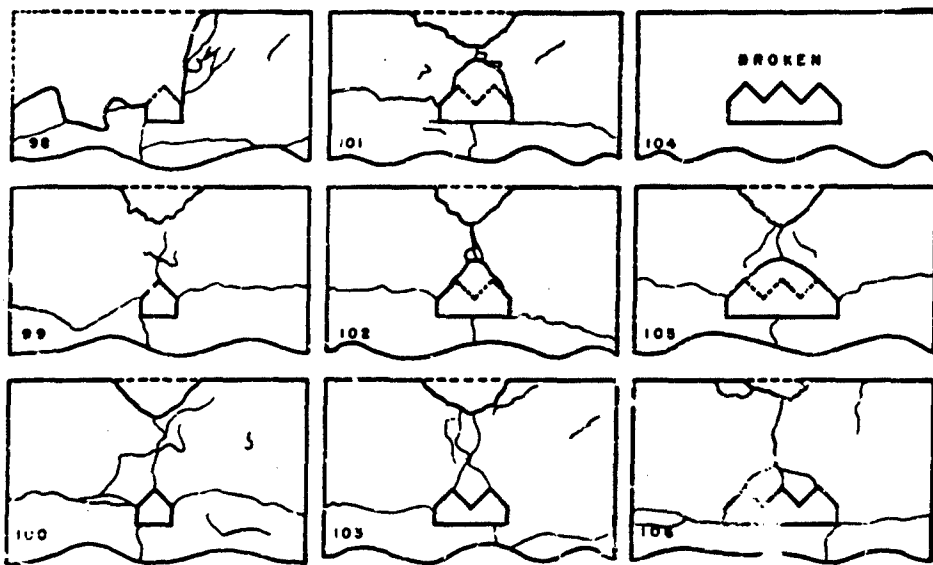
SCALE:
0' 1' 2' 3'



Sheet 13

PLASTER-CEMENT (5-3) MODELS

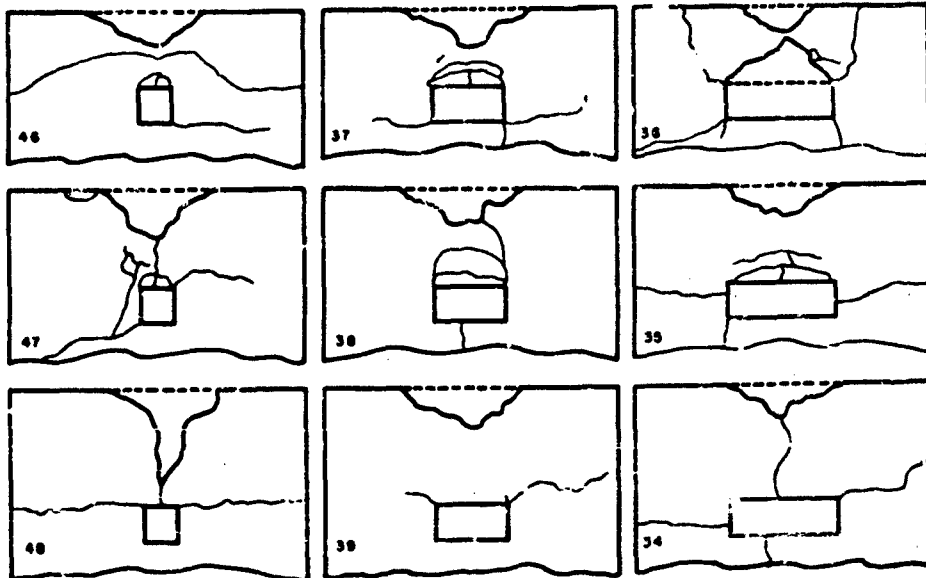
SCALE:
0' 1' 2' 3'



Sheet 14

PLASTER-CEMENT (5:3) MODELS

SCALE
0' 1' 2' 3'



Sheet 15

DISCUSSION

Mr. Chaszyka, Armour Research Foundation: You described a pressure wave as triangular and you said that in Rainier it was something like that except the front was sloped. Would you care to define that more precisely?

Dr. Rinehart: I don't happen to have it with me, but the Rainier Shot is well documented and you will find it, I think, in some of the UCRL reports.

Mr. Chaszyka: Would you say it was more like a trapezoid approaching a square wave?

Dr. Rinehart: No. I would say that it was like a triangle with a sloping front. As I remember it, it was almost a right triangle with the hypotenuse lying along the axis.

Mr. Chaszyka: It was not an infinitely sharp rise time?

Dr. Rinehart: No.

Mr. Chaszyka: Well, I believe it's more like a trapezoid approaching a square wave with a slow drop off. It has a slow rise time. It's not an infinitely steep rise time as you would have in a gas, but the fall off in pressure is not quite as rapid as you would indicate with a triangle.

Dr. Newmark, Chairman, Univ. of Illinois: This would not cause spalls to occur quite as readily as you were inferring.

Dr. Rinehart: If one takes the Rainier blast and figures out where it's spalled, what occurred, the rock in which it occurred and the blast that was set off, you will find the spall should be about 225 feet thick. This is roughly what it should be and there were layers which apparently separated. They were about that thick. Whether this is spalling or not I don't know.

Mr. Chaszyka: Well, the reason those layers separated is because they dropped down. The soil was loose enough, it was

crushed out to about that radius and it fell down. But as far as the radial spalling is concerned that went out to about 400 feet. The damage as found in the tunnel was to about 400 feet, where the rails were actually displaced.

Dr. Rinehart: I think the primary point I want to make here is that when waves have an opportunity to reflect they can impart destructive motions to various things. I think this is the main point.

Mr. Chaszeyka: Your point is well taken. I was just questioning the type of wave.

Dr. Rinehart: In most structures in which you will be finding yourselves, the material is not strong; it may well be soil which has no tensile strength at all. It may be heavily faulted and fractured ground, etc., so that in general you will not have to fracture the material. The material will already be fractured. All you do is to throw it off and I think this is the most important point I was to make. There is a mechanism whereby you can throw this material off with a lot of velocity and if there is nothing to impede its motion it will keep going.

Mr. Saffian, Picatinny Arsenal: Maybe I missed this point, but in setting up this model experiment, I assume the idea was to be in a position to predict what would happen in a large-scale operation of some sort. In setting this up, especially with explosive charges of this size, has any consideration been given or will it be given to the shape, the geometry of the charge, and the possible deviation of this charge from the axis of the cavity in the rock?

Dr. Rinehart: Yes, Consideration has been given to the shape of the charge but our decision was simply that we took a nice cylindrical charge. Now if one took a charge of a different size you would find the effect to be somewhat different in magnitude, but I think not in principle. Now as to putting charges off center and that sort of thing, this is certainly the direction in which model studies should be extended. These were very preliminary and exploratory studies and there are a whole host of other model studies which I think would yield extremely fruitful information.

(At this point some of the discussion was lost while changing tapes.)

Dr. Miklowitz, NESCO: I'd like to ask Dr. Rinehart whether or not he has considered taking some motion pictures of this fracture phenomenon around the hole? It seems to me you have an excellent chance here to say something about the wave action about the hole. For instance, in one case that you showed which had a vertical crack above the hole and a vertical crack below the hole, at 180° opposite the initial one, assuming the earlier picture showed the first crack and the later picture showed the second one, you would conclude, of course, that the second crack occurred later; it seems to me that the unloading waves, very typical of the kind of thing you talk about in scabbing, could be creating the second crack. In other words, unloading waves from the upper crack propagate around circumferentially, superimpose at the lower end, and cause enough tension to create the second crack. I think there's a little support in this from the fact that you also showed one which had again a secondary process of a similar nature with two horizontal cracks.

Dr. Rinehart: Yes. I'm very curious as to where these came from and I think about the only way to get at it is to do just exactly what you suggest—to take pictures. And, fortunately, these occur in exactly the same way in holes in lucite specimens which are treated this way. So that one could, I'm sure, take pictures of these without very much trouble. I think it's probably a two-stage process, a squeezing this way and an expansion this way. I think this is probably what happens.

Mr. Stern, General Electric Co.: Let me suggest, if you want to take pictures you can use photostress. I know it has been used experimentally on window panes to show the stress distribution as a bullet goes through a pane to get some sort of a picture of what happens when a bullet penetrates a steel plate. If you have this on a concrete model and you were to take color high-speed pictures you'd actually see the stress pattern running through it. In fact, with lucite, if you had polaroid light you can do this.

Dr. Mains, General Electric Co.: One additional comment about the photostress. You don't have to have a lucite model because what you use is a back reflection technique.

Dr. Rinehart: Yes, as a matter of fact we have in our own laboratory now a reflective photostress meter. I have a student who is working on this very present, but he's not very far along yet.

DESIGN BELOW GROUND ARCH AND DOME TYPE STRUCTURES EXPOSED TO NUCLEAR BLAST*

E. B. Laing and E. Cohen
Ammann and Whitney, New York City

Some of the problems encountered in the design of hardened shallow-buried and earth-mounded arch and dome type structures are discussed. Design equations for determining idealized loadings, frequencies, response values, and stresses are proposed. Effects of change of arch curvature, nonrigid subgrade, arching, and compatibility of edge displacements are discussed.

BLAST LOADS

Geometry

Figure 1 illustrates the assumed geometry of an ideal air induced ground shock at a typical arch type structure. This ground shock may be either superseismic or outrunning depending on the pressure level and seismic conditions [1,2].

Buried Arches

A complete analysis of an underground structure involves the diffraction of the shock wave around the reinforced cavity and the response of the structure shell as an elasto-plastic liner. Such a solution considering all the important parameters, which is applicable to design, is not yet available. In the interim a simplified reasonably safe approach is needed. In this paper it has been assumed that the diffraction effects in the soil around the structure may be neglected. This is consistent with most of the peak pressure data recorded on buried test structures [3-8]. The distribution of the applied blast pressure on a buried arch during the transverse transit of the shock front is shown in Fig. 2, in which the applied loads consist of nonuniform radial and tangential forces. For design purposes this loading is replaced with a combination of idealized modal loads. Figure 3 shows the typical pressure-time curves for each of the modal loadings considered, i.e., compression, deflection, and bending-compression. Figure 4 illustrates the shape and magnitude of these loads. For the compression mode the vertical reaction at the springing line is taken equal to the average surface pressure applied over half the span and is based on the assumption that the full radial and tangential forces are transmitted through the arch. The extent of the bending-compression mode loads have been chosen to make the vertical reactions in this mode zero. These recommendations include an allowance for redistribution of the applied loads as a result of the mobilization of passive pressure but do not include arching effects (which may be negative or positive), or the effects due to vertical acceleration of the supports. P_w and P_l , in these figures represent the average blast pressures on the windward and leeward surfaces of the arch, respectively, and are estimated by passing the inclined ground-shock front across the arch and computing the pressures on a hydrostatic basis. It is further assumed that the depth attenuation factor (k , shown in Fig. 1) is unity, i.e., there is no attenuation of pressure with depth for

*This paper is based in large measure on studies made by Ammann and Whitney for the Office of the Chief of Engineers, Department of the Army, under Contract DA-49-129-ENG-464.

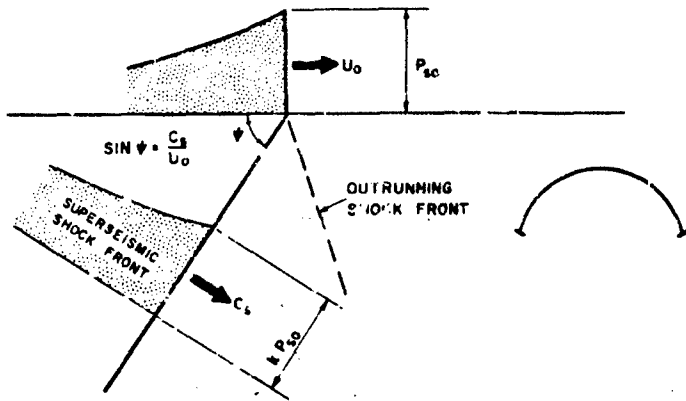


Fig. 1 - Assumed geometry of ideal air-induced ground shock

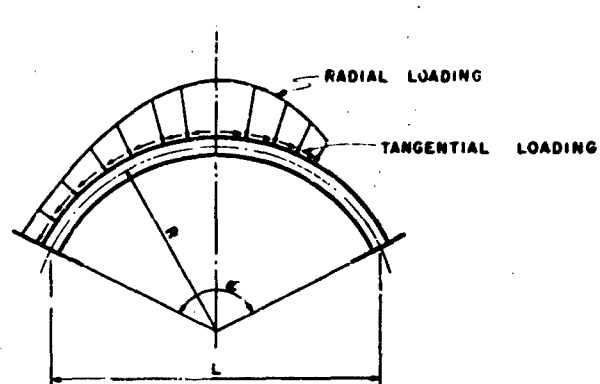
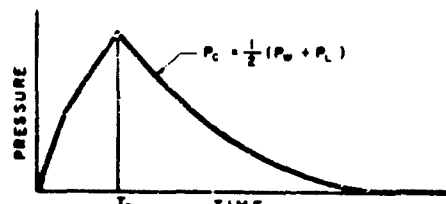


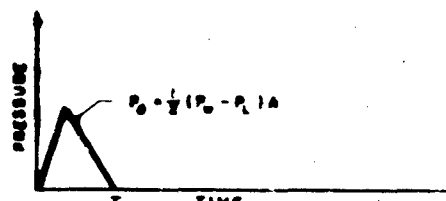
Fig. 2 - Distribution of blast pressures on buried arch during transverse travel of shock front

shallow-buried structures. This in combination with a zero rise time assumption, is admittedly a somewhat conservative approach and may be modified when and if these factors become better established. The magnitude of the peak modal pressures shown in Fig. 4 are obtained using the following assumptions:

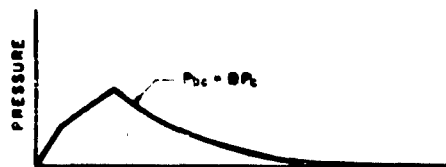
- (1) A semicircular arch with an average depth of cover equal to one-half the radius is considered as fully buried and will be subjected to full compression mode only. Fully buried implies that sufficient passive pressure can be mobilized to prevent excessive flexural motion [9,10].
- (2) A semicircular arch with the crown level with the earth's surface will be subjected to full compression mode plus full deflection mode. The modal loads for semicircular arches with intermediate depth of burial are obtained by interpolation based on the average depth of cover. These recommendations defining complete burial for semicircular arches are in accordance with Ref. 11.
- (3) A 30-degree (interior angle) arch is considered fully buried if it has an average depth of cover equal to its radius and will be subjected to a full compression mode plus a full bending



(a) COMPRESSION MODE



(b) DEFLECTION MODE



(c) BENDING COMPRESSION MODE

Fig. 3 - Time variation of modal loadings
for buried arches

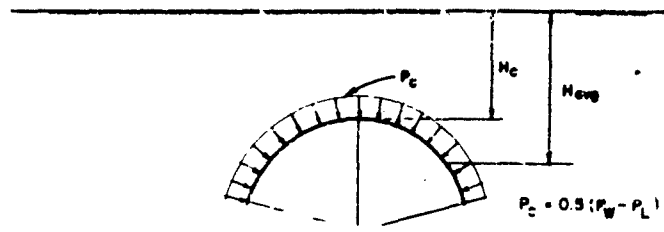
compression mode. The bending compression mode in this case has a peak pressure equal to 15 percent of the peak compression mode pressure.

(4) A 60-degree arch with the crown level with the earth's surface will be subjected to the full values of all three modes. For intermediate burial, modal loads are again determined by interpolation. The bending compression mode recommendations given for this case will result in bending moments comparable in magnitude to those obtained if the compression mode pressures were applied vertically rather than radially.

(5) For arches having interior angles between the 60 and 180 degree limits, a double interpolation is used to obtain the modal loads.

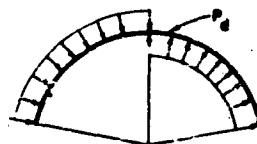
Buried Domes

The blast pressures on buried domes are taken similar to those on buried arches. Densive pressure will be mobilized essentially only for the antisymmetric loading, and to a lesser extent than for arches, thus resulting in less pressure redistribution than obtained with the more flexible arch type structures. Since most of the loading in domes is carried by membrane action, the inclusion of a bending compression type load is unimportant, and therefore only the compression and deflection modes are considered. These idealized loadings for the dome are obtained in a similar manner as for the arches.



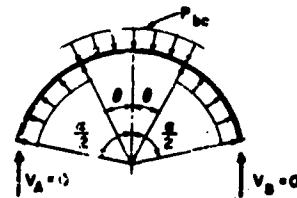
$$\text{MAX. } H_c = R \left[\frac{1}{4} - \frac{3\epsilon}{4\pi} + \frac{1}{2} \cos \frac{\epsilon}{2} + \frac{\epsilon}{4 \sin \frac{\epsilon}{2}} \right]$$

(a) COMPRESSION MODE



$$P_d = 0.5 (P_w - P_L) \left[\frac{H_c}{R \left(\frac{3\epsilon}{4\pi} - \frac{1}{2} \cos \frac{\epsilon}{2} - \frac{\epsilon}{4 \sin \frac{\epsilon}{2}} - \frac{1}{4} \right)} + 1 \right]$$

(b) DEFLECTION MODE



$$P_{bc} = 225 \left(1 - \frac{\epsilon}{\pi} \right) P_c$$

(c) BENDING COMPRESSION MODE

Fig. 4 - Idealized modal loadings for buried arches

Blast Pressures on Mounded Surfaces

Figure 5 shows the geometry of a typical earth mounded arch type structure. The determination of the design loadings on a structure of this type has the same uncertainties as for the buried type plus the problem of determining the time variation of the pressure on the mounded surface. The method currently employed in the Corps of Engineers design manual (Ref. 12-EM-413) for obtaining the pressures on the earth mound consists of two parts, (1) the determination of the reflected pressures on the windward slope and (2) the determination of the drag pressures over the entire mound. These are combined as described in Ref. 12 (EM 413). The reflections on the windward slope can be estimated with reasonable accuracy using the available reflection coefficients for inclined surfaces. The effects of this reflection on the horizontal and leeward slopes, however, is not well defined and may justify some additional study. The drag pressures are obtained in the manual by use of an "equivalent circle concept" in which the mounded surface is replaced with a circular arc for which empirical drag coefficients are recommended. These coefficients, however, are based upon steady-state flow around a complete cylinder and may be significantly different for a segment of a cylinder set directly on a ground plane.

A second approach, "transonic wedge," to determining the enveloped phase drag pressures has been made recently [13] utilizing a combination of theoretical and empirical results for steady-state transonic flow over double wedges. The general features of the flow depend on the Mach number of the given conditions behind the original shock wave. When all parts of a flow have a Mach number less than one, the flow is called subsonic. If the Mach number is everywhere greater than one, the flow is called supersonic. If the Mach number is less than one in some places and greater than one in other parts of the same flow, it is called transonic. Most initial flows and geometries currently being used in the design of earth mounded structures fall in the transonic range for which both experiments and theory are relatively scarce and complex.

In the subsonic case the usual concept of pressure coefficients, C_p , to be multiplied by the dynamic pressure, $1/2 \rho V^2$, are applicable. Coefficients given for incompressible flow may be used with less than 1-percent error for Mach numbers, M , from zero to 0.1. This covers the range intended for most wind load coefficients. From Mach numbers 0.1 to 0.5 the incompressible pressure coefficients may be used if first multiplied by

$$\frac{1}{\sqrt{1 - M^2}}.$$

(Prandtl-Glauert rule, see Ref. 14.) For large Mach numbers, more elaborate methods must be used.

In the supersonic case the flow pattern is illustrated in Fig. 6(a). On hitting the corner at A, the flow forms a shock wave which turns the oncoming flow abruptly, so it is parallel to AB. This

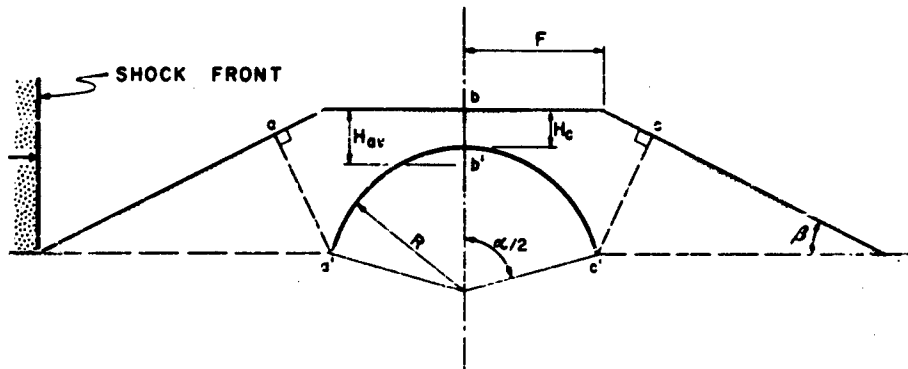
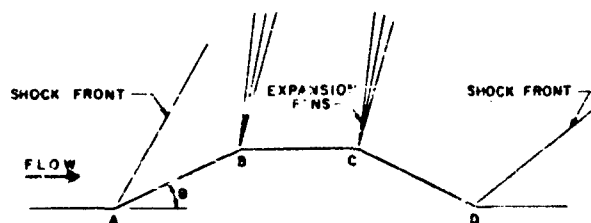
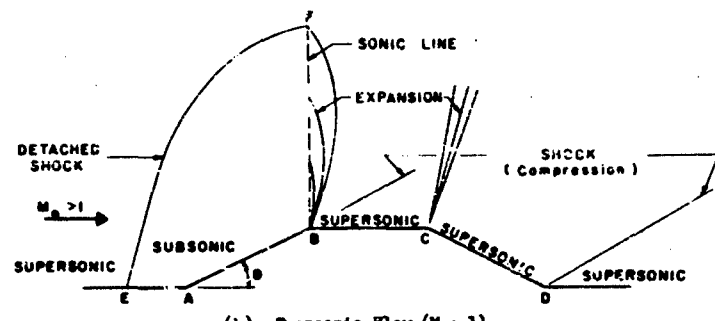


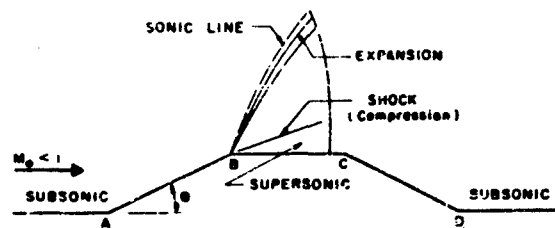
Fig. 5 - Geometry of typical earth mounded arch type structure



(a) Supersonic Flow



(b) Transonic Flow ($M_0 > 1$)



(c) Transonic Flow ($M_0 < 1$)

Fig. 6 - Steady-state flow over wedges

causes a pressure rise. At B, the flow goes thru a Prandtl-Meyer expansion fan which again turns the flow, this time with a pressure reduction. At C there is another expansion fan and then a compression shock wave at D returning the flow to its original direction. The changes of pressure at each shock and expansion can be conveniently figured. The pressure is relatively uniform on each of the faces AB, BC and CD, being of course greatest on AB. The shock at A is called an attached shock wave because it starts right at A. As the Mach number decreases toward one, there will be a certain Mach number (Fig. 7) at which the attached shock will no longer be possible for the given angle θ . Below this Mach number the shock wave is detached as shown in Fig. 6(b) and the flow will be in the transonic range.

In the transonic flow shown in Fig. 6(c), the flow is supersonic throughout except for the embedded subsonic region EFBAE. The initial flow is assumed supersonic, i.e., $M_\infty > 1$ [15]. As the initial Mach number decreases to 1, the detached shock forms further ahead of point A. When the Mach number falls below 1, the typical situation in the transonic range is as shown in Fig. 6(c) with one supersonic region embedded in the subsonic flow. The conditions shown apply to Mach numbers not too close to one. As the Mach number increases and approaches one, the supersonic region grows, finally covering the mound from B to D. In this condition there would be a shock wave starting from D as in Fig. 6(b).

The flows shown in Figs. 6(b) and 6(c) have certain features of interest in common. In both cases the pressure at A is equal to the stagnation pressure of the subsonic flow upstream of A. At B the local Mach number is always unity at the start of the expansion fan. These facts have been established experimentally and theoretically [16].

Further, it has been shown that the pressure distribution on the face AD is the same for a wide range of transonic flows, for a given angle θ , when the pressure is expressed in terms of the stagnation pressure rather than a pressure coefficient [17]. These facts are the basis for the following methods used in computing the pressure distribution for the transonic cases at hand.

In the case where the initial flow is supersonic the first computation is to find the stagnation pressure in the subsonic region. This may be conveniently done using Figs. 8 and 9. This stagnation pressure at point A (Fig. 6(b)), is obtained by first determining the supersonic downstream pressure corresponding to the free-stream Mach number, $M_c = M_1$, from Fig. 8 (using $\gamma = 1.4$), then using Fig. 9 to determine the pressure at A. For points between A and B, there is theory, and experiments are available, giving the ratio of the pressure at any point x (Fig. 10) to the stagnation pressure which occurs at A. For an angle of 26.6 degrees (2:1 slope) these ratios are summarized in Table 1.

It will be noted that the experiments and theory in most of the references deal with wedges as shown in Fig. 11. The structures considered herein are effectively one-half of the wedges tested.

The test results and theory available are concerned primarily with the face AB which is the most heavily loaded region and the data given in Table 1 is applicable. Unfortunately, equally precise data is not available for the faces BC and CD. On the basis of examination of test results and of the underlying theory the following procedure is tentatively suggested.

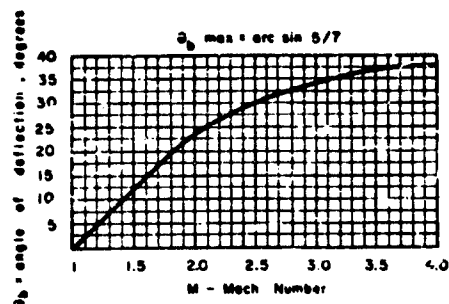


Fig. 7 - Maximum deflection angle for which the shock wave will remain attached [18]

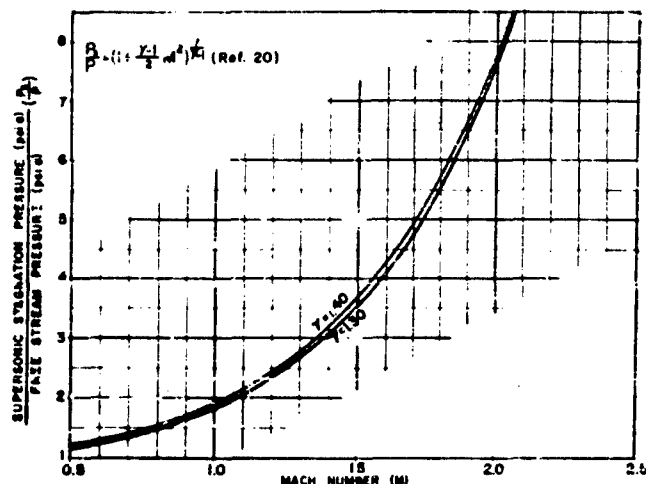


Fig. 8 - Ratio of supersonic stagnation pressure to free stream pressure vs. Mach number

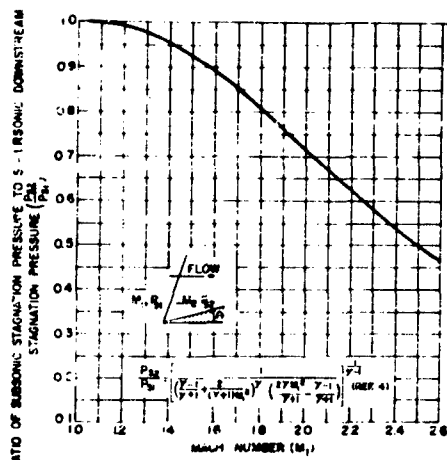


Fig. 9 - Stagnation pressure ratio across a normal plane shock (psia)

sure may be obtained by determining the Mach number, M_2 , on the SC side of the corner corresponding to the deflection angle θ from Fig. 12 and then entering Fig. 8 with this value to obtain the pressure, P . Depending on the length of the top surface (SC) of the corner, the flow may or may not be returned to the pressure of the original supersonic flow upstream of C before the corner C is reached. In the absence of sufficient data a linear distribution of pressure between B and this point is assumed.

The pressure on the downstream side of C may be estimated by assuming a Prandtl-Meyer expansion fan starting from the free-stream Mach number. Along the face CD, it is suggested that

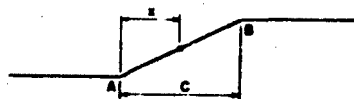


Fig. 10 - Definition of x and c



Fig. 11 - Typical wedge profile

The pressure at B, on the BC side of the corner may be computed by assuming there is a Prandtl-Meyer expansion fan starting from Mach number one on the downstream side of the corner as the net effect on an overexpansion and compensating compression at the corner. This pres-

TABLE 1
Pressure at x, p
Pressure at A, p_A for $\theta = 26.6^\circ$ [18]

$\frac{x}{c}$ (Fig. 10)	$\frac{p}{p_A}$
0	1
0.1	0.875
0.2	0.840
0.3	0.822
0.4	0.793
0.5	0.772
0.6	0.743
0.7	0.723
0.8	0.687
0.9	0.655
1.0	0.521

the pressure be assumed uniform. The pressure on CD may be obtained from Fig. 12 and 13 as follows:

(1) enter Fig. 12 with free-stream Mach number to obtain the Prandtl-Meyer angle, γ (angle through which a supersonic stream is turned to expand from $M = 1$ to $M > 1$), (2) add γ to the deflection angle (26.6° for our case) to obtain the Mach number on CD using Fig. 12, (3) using this Mach number enter Fig. 13 to obtain the ratio P_{CD}/P_{∞} where P_{∞} is the static pressure on face CD and P_{∞} is the total pressure downstream of C. Since there are only isentropic processes between A and D, P_A is the same as at A, therefore, compute P_D from the ratio P/P_A .

In the case where the initial flow is subsonic, the pressure at A is the stagnation pressure and is obtained from Fig. 8 by entering the figure with the free-stream Mach number to obtain the pressure ratio. The coefficients given in Table 1 apply for the region AP, using the stagnation pressure for the angle $\theta = 26.6^\circ$.

The pressure on the downstream side of A is computed assuming an expansion fan from Mach number one and may be obtained from Figs. 8 and 12 for $\phi = 26.6^\circ$ as for the superconic initial flow case.

The downstream pressure at C is estimated according to there being a separation of the subsonic flow at the corner and with the help of experimental data [19]. Simple inviscid theory would indicate that the flow expands to zero pressure at the corner and thereafter resumes free-stream velocity. However, since for these Mach numbers of approach to an edge of such a large angle as that at C, the flow separates, viscous effects cannot be ignored [19]. The pertinent data in Ref. 19 (page 28 for station 12, 16) applies to a 30° flap deflection at an angle of attack of the flap of 9° . It would be desirable to have data for a leading edge flap deflection of 26.6° at an angle of attack of the flap of 0° but the above data is the closest we have seen at this time. The pressure coefficient, $P = (p - p_\infty)/q$ indicated by the above test data is between -0.6 and -0.7, where p = the static pressure (psia), p_∞ = free-stream pressure (psia) and q = the dynamic pressure. From another standpoint, if we can apply data from a wedge to represent flow on a half wedge following a straight section, as we did on the forward face AB, then we can apply data from a sharp edged plate at an angle of attack of 26.6° , with about the same validity. The data on pages 18 and 19 (zero flap deflection) of Ref. 19 shows that the flow is separated and P is constant over the entire chord for $\alpha > 15^\circ$, so it surely is also for $\alpha = 26.6^\circ$. The value of P is about -0.6, and this is used in this case.

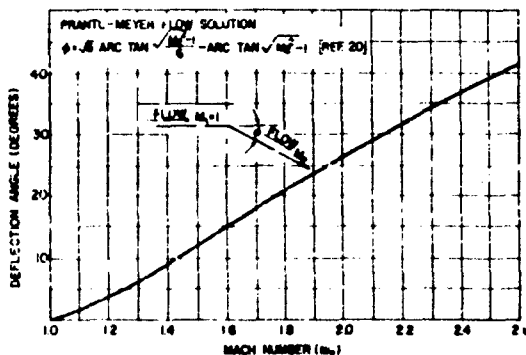


Fig. 12 - Deflection angle required to expand to a given Mach number

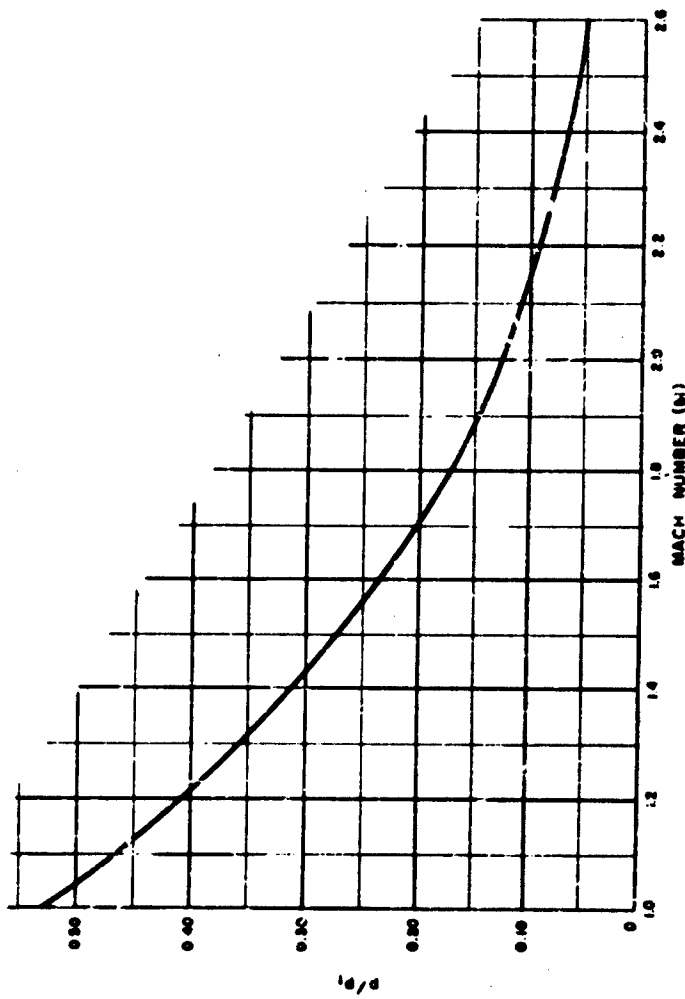
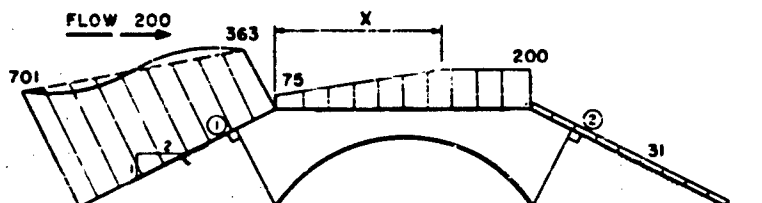


Fig. 13 - Ratio of static pressure, p_1 to total pressure, p_t vs. Mach number, M [15]

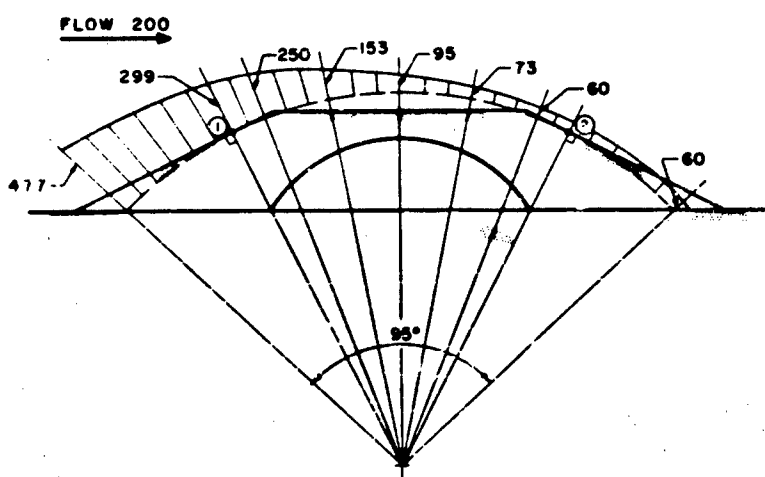
Figures 14 and 15 show a comparison of the total pressures obtained using the "transonic wedge" and "equivalent circle" procedures for steady-state flows of 200 and 25 psig and ideal dynamic, q , pressures. The comparison of these methods, and the obvious shortcomings of both, indicate that it would be worthwhile to obtain additional shock tube and wind tunnel test data on wedges, arcs, and spherical segments (including data on dust laden flows) in order to better establish the drag effects on mounded surfaces.

Earth Mounted Arches

Since the wedge approach has not been developed further, the equivalent circle procedure has been retained for the present in Ref. 12 (EM 413) to estimate the pressures on mounded surfaces. The modal loadings are similar in shape to those of the buried arches. The average pressures on the arch surface are obtained by computing the average windward and leeward pressures on the equivalent circle within the angle obtained by passing the radii through the arch springing lines and using these values to compute the compression and deflection mode loadings. The bending compression mode is computed as a function of the average arch central angle similar to the below ground arches. The main differences between the loads on mounded arches as compared to buried

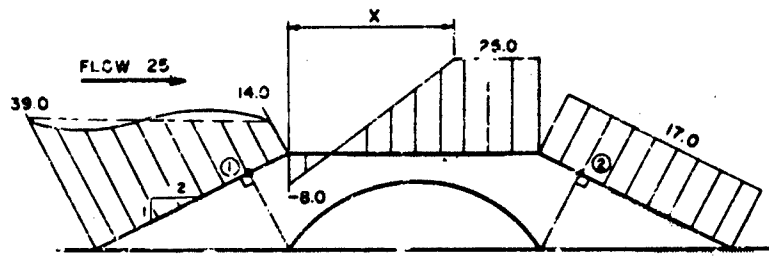


WEDGE METHOD

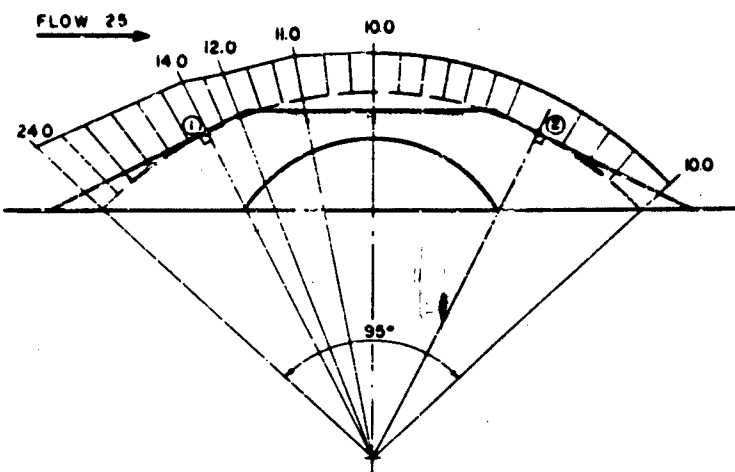


EQUIVALENT CIRCLE METHOD

Fig. 14 - Comparison of wedge method with equivalent circle method (pressure = 200 psig)



WEDGE METHOD



EQUIVALENT CIRCLE METHOD

Fig. 15 - Comparison of wedge method with equivalent circle method (pressure = 25 psig)

arches (aside from the reflection effects) is (1) the deflection mode loading for the mounded arch, due to the dynamic pressures, may last several times longer than in the case of the buried structure and (2) the available passive pressure for the mounded case may be considerably less than for the buried case. The deflection mode pressures are used without reduction if the arch crown is at the surface level or if the top corner of the slope is located directly above the springing line (or closer to the arch centerline). If the average cover of the arch meets the full burial requirements described for the below ground arches and if the top of the slope is located far enough away from the springing line to prevent transmission of the reflected and drag pressures on the windward and leeward slopes (assuming pressures transmitted normal to slope) to the arch structure, the deflection mode may be neglected. For intermediate cases the deflection mode reduction may be estimated by double interpolation.

Earth Mounted Domes

The equivalent circle procedure has been retained tentatively in the Corps of Engineers manual (Ref. 13 - EM 413) to obtain pressures on mounded surfaces over domes. The modal loadings are

, similar to mounded arch structures with the exception that the bending compression mode is omitted.

RESPONSE OF ARCHES AND DOMES

The dynamic response of arches and domes depend upon the natural period of the member, the load shape and the extent of deformation permitted.

Natural Period

The proposed equations for the natural period of earth covered arches and domes for the various modal loads discussed in this paper are as follows:

ARCHES

Compression Mode

Hinged Ends:

$$T_{nd} = \frac{2\pi L^2}{C_1} \sqrt{\frac{M}{EI}}$$

$$C_1 = 4 \sin^2 \frac{\alpha}{2} \sqrt{0.82 \left(\frac{R}{K} \right)^2 + \left(\frac{\pi^2}{\alpha^2} - 1 \right)^2}$$

Fixed End:

$$T_{nd} = \frac{2\pi L^2}{C_2} \sqrt{\frac{M}{EI}}$$

$$C_2 = 4 \sin^2 \frac{\alpha}{2} \sqrt{\frac{2}{3} \left(\frac{R}{K} \right)^2 + \frac{1}{3} \left(\frac{4\pi^2}{\alpha^2} - 1 \right)^2}$$

ARCHES

Deflection Mode

Two Hinged:

$$T_{nd} = \frac{2\pi L^2}{C_3} \sqrt{\frac{M}{EI_A}}$$

Fixed End:

$$T_{nd} = \frac{2\pi L^2}{C_4} \sqrt{\frac{M}{EI_A}}$$

Where C_3 and C_4 are obtained from Ref. 12 (EM 420).

ARCHES

Bending Compression Mode

Two Hinged:

$$T_{nbc} = \frac{0.8\pi L^2}{C_3} \sqrt{\frac{M}{EI_A}}$$

Fixed End:

$$T_{nbc} = \frac{0.8\pi L^2}{C_4} \sqrt{\frac{M}{EI_A}}$$

DOMES COMPRESSION AND DEFLECTION MODES

$$T_{nc} \approx T_{nd} \approx \sqrt{R} \sqrt{\frac{M}{2EI}}$$

The mass in these expressions represents the mass of arch or dome plus the mass of the average earth cover per unit of arch or dome surface area. The upper limit of the average earth cover used for obtaining the earth mass is taken equal to the span of the structure. The gross moment of inertia is used in the arch compression mode equations whereas the average of the gross and the cracked is used for computing the arch flexural modes. The periods for two hinged arches are between 1 and 2-1/2 times that of the fixed end arches in the compression mode and between 1-1/2 to 2 times that of the fixed end arches in the flexural modes.

Load Shape

The time variation of the modal loads may, in most instances, be approximated by triangular loads with or without a rise time. Conservative estimates of the rise time can be obtained by assuming that the rise time at the surface, if any, does not increase with depth. Then, for large inclinations (with the horizontal surface) of the ground shock, the rise time can be estimated by dividing the arch or dome rise by the soil seismic velocity. A similar situation exists for the deflection mode, however, as the ground shock inclination falls below one-fourth of the interior angle the deflection mode pressures begin to decrease rapidly. Although many uncertainties are involved in estimating both the natural period and the load rise times, it is expected that the recommended rise times will provide conservative results in those cases where the rise time may have appreciable effect on the response.

Allowable Deformations

After the natural periods and idealized loadings are established, the structure can be designed for the desired degree of protection. Allowing plastic deformation will usually result in a substantial reduction in required strength and material and it is proposed that this be considered for all modal loadings. The ultimate uniform compressive strain in reinforced concrete is normally taken at about 0.0035 and increases several fold if the reinforcement is bound [26]. The resistance function used for determining the compression mode response is usually based upon an initial tangent modulus which peaks at a theoretical elastic strain of 0.0010 (for a compressive strength of 3000 psi), less than one-third of the ultimate cylinder strain. Using this approach the allowable strain in the compression mode could probably be taken up to at least twice the "elastic" value. This still leaves some allowance for possible subsequent loadings plus additional compressive strains (such as compression hinges) normally not provided for. Also, since the probability of several repeated loadings of the same magnitude is quite remote [27] this approach appears to be reasonable. The ratio of allowable plastic deformation to peak elastic deformation in the deflection and bending compression modes should be limited to three unless a check of the actual numerical value indicates that further deformation would not result in significant deflection amplification and excessive strains at the compression hinges. If such amplification occurs it may be necessary to investigate the arch-soil interaction in more detail [28] to obtain a reasonable approximation of the load capacity. Charts for determining the elastic or plastic response values for various load shapes (with or without rise times) are found in Refs. 13, 29 and 30.

Other Factors Influencing Response

The response to the various modal loadings discussed will be influenced to some degree by many other factors such as the presence of a nonrigid base and rotation of the foundation at the

springing line. In most cases these effects will result in a reduced primary structural response. Several other secondary factors, however, such as curvature changes and horizontal spreading of the springing line may result in increased stresses or strains or both, and should be given consideration in design. Soil arching is influenced by the deformational characteristics and motion of the structure in addition to the excavation and backfilling procedures used and may increase or decrease the arch loading. A load reduction due to arching should not be applied without first giving all factors thorough consideration.

ARCH AND DOME MODAL LOAD STRESS EQUATIONS

Arches

Equations for the moments, shears and thrusts for two hinged and fixed ended arches are given in this section for the blast nodal loadings discussed. The effect of arch change of curvature due to the axial strains has not been included in the basic equations as this effect can be computed separately assuming that the loads remain radial after axial shortening. Figure 16 gives an indication of the magnitudes of the elastic bending stresses and strains in a fixed ended arch caused by this curvature change under the compression mode loading. Figure 17 shows the reduction of axial load capacity caused by this bending, computed by conventional ultimate strength theory. Since the flexural strains are not sufficiently large to cause failure, the stress increases and load-capacity reductions can be omitted in the design if there is no objection to plastic compression hinge formation. Similar stress increases will occur in two hinged arches, but to a lesser extent. It should be noted that in flat arches the change in curvature in the compression mode may also create a significant change of radius resulting in an increase of thrust. This thrust increase, for a 60-degree arch (fixed or two hinged) for example, is approximately 10 percent for a 0.0010 strain and 20 percent for a 0.0020 strain. Both the strain and thrust increases will be amplified if there is a spreading of the springing line and should be checked accordingly for any particular design. Another aspect that may sometimes require checking is the numerical magnitude of the flexural mode deflections to insure that the deflections are not so large as to create large secondary effects. As an example, if we consider a 180-degree fixed ended arch having a radius of 20 feet and a thickness of 12 inches we obtain a peak radial elastic deflection mode displacement of about 1/4 inch per psi of resistance. A plastic to elastic deformation ratio much greater than 3 may be unrealistic in such a case. It should be noted, however, that if the ratio is relatively large, the passive pressure mobilized on the leeward side will increase considerably due to the blast surcharge and the computed deflections in this mode will be conservative. For preliminary design

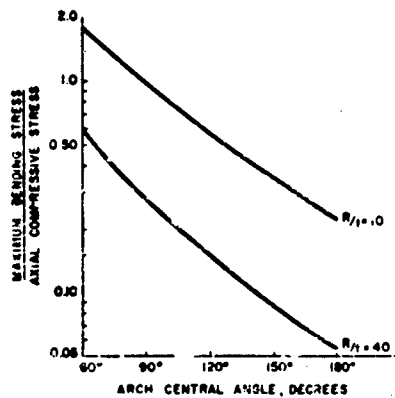


Fig. 16 - Ratio of maximum elastic bending stress due to curvature change to elastic axial compressive stress for fixed ended arch under compression mode loading assuming rigid supports

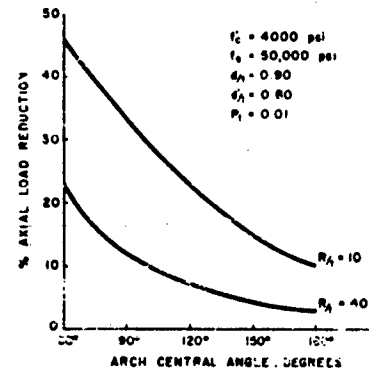


Fig. 17 - Reduction in apparent ultimate axial load capacity at critical section due to change in curvature under compression mode loading

the arch dead load (earth plus concrete) may be assumed as a uniform radial load in combination with the proposed blast loads. The magnitude of the dead load flexural stresses may then be checked using the relations given in Appendix A and the design modified if necessary.

Two Hinged Arch Modal Load Relations

See Figs. 4 and 18 for notation.

Deflection Mode Load

$$V_A = V_B = \frac{P_d R \left(1 - \cos \frac{\alpha}{2}\right)}{\tan \frac{\alpha}{2}} \quad (1)$$

$$H_A = H_B = P_d R \left(1 - \cos \frac{\alpha}{2}\right) \quad (2)$$

$$M_A = M_B = 0. \quad (3)$$

At any point defined by the angle ϕ the moment, thrust, and shear relationships are as follows:

$$M_z = V_A \left[R \left(\sin \frac{\alpha}{2} - \sin \frac{\alpha}{2} - z \right) \right] + H_A \left[R \left(\cos \left(\frac{\alpha}{2} - \phi \right) - \cos \frac{\alpha}{2} \right) \right] = 2P_d R \sin^2 \frac{\alpha}{2} \quad (4)$$

$$N_x = V_A \sin \left(\frac{\alpha}{2} - z \right) + H_A \cos \left(\frac{\alpha}{2} - z \right) = P_d R \cos \phi \quad (5)$$

$$S_x = V_A \cos \left(\frac{\alpha}{2} - z \right) + H_A \sin \left(\frac{\alpha}{2} - z \right) = P_d R \sin \phi. \quad (6)$$

Compression Mode Load

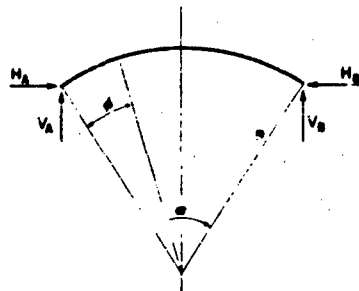
$$V_A = V_B = P_c R \sin \frac{\alpha}{2} \quad (7)$$

$$H_A = H_B = P_c R \cos \frac{\alpha}{2} \quad (8)$$

$$N_\phi = P_c R \quad (9)$$

$$M_A = M_B = 0; \quad S_\phi = 0. \quad (10)$$

Fig. 18 - Notation for two hinged arch under blast loading



Bending-Compression Mode Load

$$V_A = V_B = 0; \quad M_A = M_B = 0 \quad (11)$$

$$H_A = H_B = H'_A - P_{bc} R \cos \frac{\alpha}{2} \quad (12)$$

where

$$H'_A = 2P_{bc} R \frac{(C_1 + C_2 + C_3 + C_4)}{C_3}$$

$$C_1 = \sin \frac{\alpha}{2} \sin^2 \theta - \frac{\theta \sin \alpha \sin \theta}{2}$$

$$C_2 = \theta \cos \frac{\alpha}{2} - \sin \theta + \cos \theta \left(\frac{\theta}{2} + \frac{\sin 2\theta}{4} \right)$$

$$C_3 = - \frac{\sin 2\theta \cos \frac{\alpha}{2}}{2}$$

$$C_4 = - \sin \theta \left\{ \frac{(\frac{\alpha}{2} - \theta)}{2} \sin \alpha + \frac{3 \cos \frac{\alpha}{2}}{4} - \cos \left(\frac{\alpha}{2} - \theta \right) + \frac{\cos 2\theta}{4} \right\}$$

$$C_5 = \frac{3}{4} - \frac{3 \sin \alpha}{4} + \frac{\alpha \cos^2 \frac{\alpha}{2}}{2}$$

$$\sin \phi = \frac{1}{2} \sin \frac{\alpha}{2}$$

for $\theta \leq \phi \leq \alpha/2$

$$M_\phi = 2P_{bc} R^2 \sin \theta \left[\sin \frac{\alpha}{2} - \sin \theta \right] - H'_A R \left[\cos \phi - \cos \frac{\alpha}{2} \right] \quad (13)$$

$$N_\phi = 2P_{bc} R \sin \theta \sin \phi + H'_A \cos \phi - P_{bc} R \quad (14)$$

$$S_\phi = 2P_{bc} R \sin \theta \cos \phi - H'_A \sin \phi \quad (15)$$

for $0 \leq \phi \leq \theta$

$$M_\phi = 2P_{bc} R^2 \left(\sin \theta \sin \frac{\alpha}{2} - 1 + \cos \phi \cos \theta \right) - H'_A R \left(\cos \phi - \cos \frac{\alpha}{2} \right) \quad (16)$$

$$N_\phi = 2P_{bc} R (1 - \cos \phi \cos \theta) + H'_A \cos \phi - P_{bc} R \quad (17)$$

$$S_\phi = 2P_{bc} R \sin \phi \cos \theta - H'_A \sin \phi. \quad (18)$$

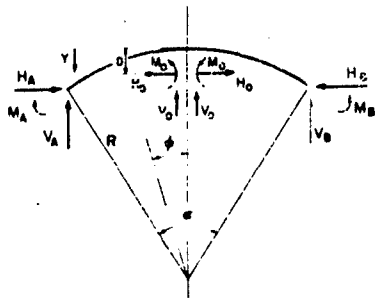
Fixed End Arch Modal Load Relations

See Figs. 4 and 19 for notation.

Deflection Mode Load

$$H_A = H_B = 2P_d R \sin^2 \frac{\alpha}{4} \quad (19)$$

Fig. 19 - Notation for fixed end arch under blast loading



$$V_A = V_B = P_d R \sin \frac{\theta}{2} = S_c \quad (20)$$

where

$$S_c = \frac{P_d R \left(\cos \frac{\theta}{2} + 4 \cos \frac{\theta}{2} + 3 \right)}{1 - \sin \frac{\theta}{2}} = f_o \quad (21)$$

$$M_A = M_B = 2P_d R^2 \sin^2 \frac{\theta}{2} = S_c R \sin \frac{\theta}{2}.$$

At any point defined by the angle ϕ :

$$M_\phi = S_c R \sin \phi = 2P_d R^2 \sin^2 \frac{\phi}{2} \quad (22)$$

$$S_\phi = S_c \cos \phi = P_d R \sin \phi \quad (23)$$

$$N_\phi = S_c \sin \phi = P_d R \cos \phi. \quad (24)$$

Compression Mode Load

$$V_A = V_B = P_c R \sin \frac{\theta}{2} \quad (25)$$

$$H_A = H_B = P_c R \cos \frac{\theta}{2} \quad (26)$$

$$N_\phi = P_c R \quad (27)$$

$$M_A = M_B = 0; \quad S_\phi = 0. \quad (28)$$

Bending Compression Mode Loading

$$M_A = M_B = M_c = H_o R \left(\cos \frac{\theta}{2} - \frac{2 \sin \frac{\theta}{2}}{\alpha} \right) = 4P_{bc} R^2 \sin \frac{\theta}{2} \left(\frac{3 - \alpha}{2} \right) \quad (29)$$

$$H_A = H_B = H_o + P_{bc} R \left(2 \cos \theta - \sin \frac{\theta}{2} \right) \quad (30)$$

$$V_A = V_B = 0 \quad (31)$$

where

$$M_o = 2P_{bc} R^2 \left[\frac{1}{2} - \sin \frac{\alpha}{2} \left(\frac{1 + \cos \frac{\theta}{2} - 2 \cos \alpha}{1 - 2 \cos \alpha} + \frac{1}{2} \right) \right]$$

$$H_o = P_{bc} R \left(1 + \frac{4(C_6 - C_7)}{C_8} \right), \quad V_o = 0$$

$$C_6 = \frac{\sin^2 \left(\frac{\alpha}{2} \right)}{2x} - \frac{3 \sin^3 \left(\frac{\alpha}{2} \right)}{32} + \sin^2 \left(\frac{\alpha}{2} \right) \left[\frac{1}{4} + \frac{\sin \alpha}{4} - \frac{\alpha}{2} - \frac{\sin 2\alpha}{4} \right]$$

$$C_7 = \frac{2 \sin \frac{\alpha}{2}}{x} \sin \frac{\alpha}{2} \cos \left(\frac{\alpha}{2} - \frac{\theta}{2} \right)$$

$$C_8 = \sin \frac{\alpha}{2} \left(\frac{1}{2} - \frac{2\theta}{x} - \frac{\sin \frac{\alpha}{2}}{x} \right) + \frac{\alpha}{4} - \frac{\theta}{2} + \frac{\sin \alpha}{4} - \frac{\sin 2\alpha}{4}$$

for $0 < \varphi < \alpha$

$$M_x = M_o - H_o(d - y) - 4P_{bc} R^2 \sin^2 \frac{\varphi}{2} \quad (32)$$

$$N_\varphi = H_o \cos \varphi + 4P_{bc} R \sin^2 \frac{\varphi}{2} - P_{bc} R \quad (33)$$

$$S_\varphi = 2P_{bc} R \sin \varphi - H_o \sin \varphi \quad (34)$$

for $\alpha < \varphi < \pi/2$

$$M_x = M_o - H_o(d - y) - 4P_{bc} R^2 \sin^2 \frac{\theta}{2} \quad (35)$$

$$N_\varphi = H_o \cos \varphi + 4P_{bc} R \sin \frac{\theta}{2} \sin \left(\varphi - \frac{\theta}{2} \right) - P_{bc} R \quad (36)$$

$$S_\varphi = 4P_{bc} R \sin \frac{\theta}{2} \cos \left(\varphi - \frac{\theta}{2} \right) - H_o \sin \varphi \quad (37)$$

where

$$d = \frac{R \left(1 - 2 \sin \frac{\alpha}{2} \right)}{a}; \quad y = R (1 - \cos \varphi).$$

Domes

Equations for the dome stresses produced by the two blast modal loadings discussed are presented in this section including the equations for the edge moments for each of the modal loads. The membrane stresses for the asymmetrical load can be computed by using a Fourier series or a harmonic mode procedure to approximate a uniform or nonuniform antisymmetrical loading. The edge moments for this loading are approximated by computing the peak edge displacement for the membrane solution and using this displacement in the moment displacement equations for a uniform radial compression load which are available. These moments are adjusted to provide close agreement with the more exact (but much more tedious) method used by Havrilla [32] by derived scaling factors. Deflection mode flexural stresses are higher than those computed for the compression mode flexural stresses per psi of loading, however, the rate of decay of the moment away from the edge for the asymmetric case is similar to the uniform load variation [32].

Both the moment and thrust effect penetrate deeper into the dome as the interior angle is reduced. The edge stresses due to flexure in a fixed ended dome can be of the same order of magnitude as the membrane stresses, therefore, if complete fixity is to be retained, provision should be made for these stresses. If there is no objection to plastic compression hinge formations these edge effects may be disregarded. If there is also a substantial spreading of the supports the strains should be checked to determine whether they are sufficiently large to cause a local failure from which a general failure could develop.

Fixed End Dome Modal Load Relations

See Fig. 20 for notation.

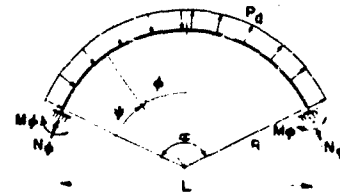
Compression Mode Load

$$N_a = \frac{C \cot \left(\frac{\lambda}{2} - \nu \right) \sin \left(\lambda\psi + \frac{\pi}{2} \right)}{2} + \frac{P_c R}{2} \quad (38)$$

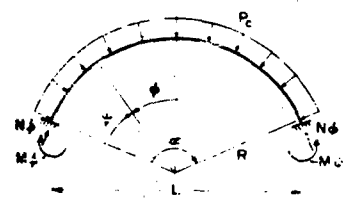
$$N_{a\theta} = \frac{-C [2 \cos \left(\lambda\psi + \frac{\pi}{2} \right) - (K_1 + K_2) \sin \left(\lambda\psi + \frac{\pi}{2} \right)]}{4} + \frac{P_c R}{2} \quad (39)$$

$$M_\phi = \frac{-CR}{4\lambda^2} \left[K_1 \cos \left(\lambda\psi + \frac{\pi}{2} \right) + \sin \left(\lambda\psi + \frac{\pi}{2} \right) \right] \quad (40)$$

$$M_r = \frac{-CR}{8\lambda^2} \left\{ [(1 + \nu^2)(K_1 + K_2) - 2K_2] \cos \left(\lambda\psi + \frac{\pi}{2} \right) + 2\nu^2 \sin \left(\lambda\psi + \frac{\pi}{2} \right) \right\} \quad (41)$$



(a) DEFLECTION MODE



(b) COMPRESSION MODE

$$C = \frac{P_e R (1 - \lambda) \sqrt{\sin \frac{\pi}{2} e^{i\phi}}}{K_3 \sqrt{\sin \left(\frac{\pi}{2} - \lambda \right)}}$$

$$\lambda = \frac{\pi}{2} - \beta$$

$$A = 3e^2 \cdot (\frac{1}{2})^2 \left(\frac{u}{v} \right)^2$$

$$K_1 = 1 + \frac{1 + 2}{2} \cot \left(\frac{\pi}{2} - \beta \right)$$

$$K_2 = 1 + \frac{1 + 2}{2} \cot \left(\frac{\pi}{2} - \beta \right)$$

$$K_3 = 1 + \left(\frac{1 + 2}{2} \right) \cot \frac{\pi}{2}$$

If boundary effects are neglected the above equations simplify to:

$$N_x = N_y = \frac{P_e R}{2} \quad (42)$$

$$u_x = u_y = 0 \quad (43)$$

Detection Mode Load

$$M_{2e} = (M_{2re} + M_{2he}) \cos \theta \quad (44)$$

where:

$$\bar{M}_{2re} = -\frac{\lambda^2 R}{36 \sin^2 \beta} \left\{ -6 + 16 \cos \beta + 18 \cos^2 \beta + 8 \cos^3 \beta + 2 \sin^2 \beta \cos^2 \beta + \sin^4 \beta \cos^2 \beta \right\}$$

$$\bar{M}_{2he} = e^{i\phi} \left\{ \bar{M}_{2he} (\cos \beta_e + \sin \beta_e) + \frac{R}{v} \bar{s}_e \sin \beta_e \right\}$$

$$\bar{u}_{2re} = K \left(a_1 \bar{v}_e \sin \frac{\pi}{2} - a_4 \bar{v}_e \right)$$

$$\bar{s}_e = K \left(a_3 \bar{v}_e - a_1 \bar{v}_e \sin \frac{\pi}{2} \right) \sin \frac{\pi}{2}$$

$$K = \frac{1}{a_1 a_4 - a_2 a_3}$$

$$\lambda = 1.316 \sqrt{\frac{R}{v}}$$

$$C = 1 + \frac{1}{2} \cot \frac{\pi}{2}$$

$$a_1 = \frac{4\lambda^3}{CE \cdot R}$$

$$a_2 = a_3 = \frac{2e^2 \sin \frac{\pi}{2}}{CEt}$$

$$a_4 = \left(c + \frac{1}{c} \right) \frac{3 \sin^2 \left(\frac{\pi}{2} \right)}{Et}$$

$$A = - \frac{PA}{3Et} \left(1 + \sin \frac{\pi}{2} \right) \frac{1}{\sqrt{3 + \cos \frac{\pi}{2} + \cos^3 \left(\frac{\pi}{2} \right)}}$$

$$T_e = \frac{AR^2}{3Et \sin^2 \left(\frac{\pi}{2} \right)} \left[2 \cos \frac{\pi}{2} + 3 \sin^2 \left(\frac{\pi}{2} \right) - 2 \cos^4 \left(\frac{\pi}{2} \right) \right]$$

$$C_1 = \left[-3(1-X_e)X_e^{5/2}(2-X_e)^{-5/2} \right] \left[-X_e^2(2-X_e)^2 \log(2-X_e) - (1-X_e)^4 - X_e^3 + 4X_e^2 - 4X_e - C_3 X_e (2-X_e)^2 \right]$$

$$\bar{V} = \frac{RA \sin \frac{\pi}{2}}{2Et} (C_1 + C_2)$$

$$C_2 = X_e^{3/2} (2-X_e)^{-3/2} \left[4X_e(1-X_e)(2-X_e) \log(2-X_e) - 4(1-X_e)^3 - X_e^3 - X_e^2 + 8X_e - 4 - 4C_3 X_e (1-X_e)(2-X_e) \right]$$

$$C_3 = -\frac{\log(2-X_e)}{(2-X_e)} = \frac{1-X_e}{X_e} + \frac{4-X_e}{X_e(2-X_e)^2}$$

$$X_e = 1 - \cos \frac{\pi}{2}$$

$$\pi = \frac{\pi}{2} - \varphi$$

$$N_g = (\bar{N}_{gm} + \bar{N}_{gb}) \cos \varphi \quad (45)$$

where

$$\bar{N}_{gm} = -\frac{RA \cos \frac{\pi}{2}}{3 \sin^3 \frac{\pi}{2}} (2 - 3 \cos \varphi + \cos^3 \varphi)$$

$$\bar{N}_{gb} = +2e^{1/2} \left[\left(\bar{S}_e + \frac{1}{R} \bar{V}_{she} \right) \cos \varphi + \frac{1}{R} \bar{M}_{she} \sin \varphi \right]$$

$$N_g = (\bar{N}_{gm} + \bar{N}_{gb}) \cos \varphi$$

(46)

where

$$\bar{N}_{gm} = -\frac{RA}{3 \sin^3 \varphi} (2 \cos \varphi - 3 \sin^2 \varphi - 2 \cos^4 \varphi)$$

$$\bar{N}_{gb} = 2e^{1/2} \left\{ \left[\bar{S}_e + \frac{1}{R} \bar{M}_{she} - \frac{1}{R \sin \varphi} \bar{M}_{she} \right] \cos \varphi \right.$$

$$\left. + \left[-\frac{1}{2 \sin^2 \varphi} \bar{S}_e + \frac{1}{R} \bar{V}_{she} + \frac{1}{R \sin \varphi} \bar{M}_{she} \right] \sin \varphi \right\}$$

$$N_{\phi\theta} = (\bar{N}_{\phi\theta m} + \bar{N}_{\phi\theta b}) \sin \theta \quad (47)$$

where

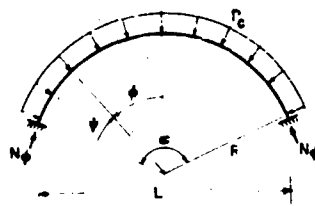
$$\begin{aligned}\bar{N}_{\phi\theta m} &= \bar{N}_{\phi\theta m} \\ \bar{N}_{\phi\theta b} &= e^{-\lambda\psi} \left\{ \left(\bar{S}_e + \frac{1}{R} \bar{M}_{\phi\theta e} \cot \varphi \right) \cos \lambda\psi \right. \\ &\quad \left. - \left(\bar{S}_e + \frac{2}{R} \bar{M}_{\phi\theta e} - \frac{\bar{S}_e \cot \varphi}{\lambda} - \frac{\bar{M}_{\phi\theta e}}{R} \right) \sin \lambda\psi \right\} \\ M_\theta &= (\bar{M}_{\theta m} + \bar{M}_{\theta b}) \cos \theta \end{aligned} \quad (48)$$

where

$$\begin{aligned}\bar{M}_{\theta m} &= -\frac{t^2}{12R \sin^2 \varphi} \bar{N}_{\theta m} \\ \bar{M}_{\theta b} &= \frac{\sqrt{3}te^{-\lambda\psi}}{6R} \left\{ \left[-\frac{1}{\sin^2 \varphi} \left(\frac{R\bar{S}_e}{\lambda} + \bar{M}_{\phi\theta e} \right) \right. \right. \\ &\quad \left. \left. + \lambda \cot \varphi \left(\frac{R\bar{S}_e}{\lambda} + 2\bar{M}_{\phi\theta e} \right) \right] \cos \lambda\psi + \left[\frac{\bar{M}_{\phi\theta e}}{\sin^2 \varphi} + \lambda \cot \varphi \left(\frac{R\bar{S}_e}{\lambda} \right) \right] \sin \lambda\psi \right\}. \end{aligned}$$

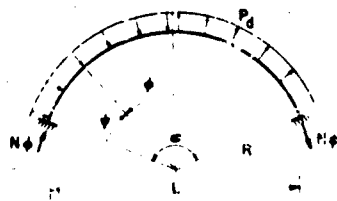
Simply Supported Dome Modal Load Relations

See Fig. 21 for notation.



(a) DEFLECTION MODE

Fig. 21 - Blast load and notation for simply supported domes - M_θ = ring moment, M_ϕ = meridional moment, N_θ = ring axial thrust, N_ϕ = meridional axial thrust, and $N_{\phi\theta}$ = shear in plane of shell



(b) COMPRESSION MODE

Compression Mode Load

See Fig. 21(b) for notation.

$$N_\phi = \frac{-C \cot\left(\frac{\alpha}{2} - \psi\right) \sin(\lambda\psi + \gamma)}{2\lambda} - \frac{P_c R}{2} \quad (49)$$

$$N_\theta = -\frac{C}{4} \left[2 \cos(\lambda\psi + \gamma) - K_1 - K_2 \right] \sin(\lambda\psi + \gamma) - \frac{P_c R}{2} \quad (50)$$

$$v_\phi = \frac{-CR}{4\lambda^2} \left[K_1 \cos(\lambda\psi + \gamma) + \sin(\lambda\psi + \gamma) \right] \quad (51)$$

$$M_\theta = \frac{-CR}{8\lambda^2 L} \left\{ \left[(1 + \nu^2) (K_1 + K_2) - 2K_2 \right] \cos(\lambda\psi + \gamma) + 2\nu^2 \sin(\lambda\psi + \gamma) \right\}. \quad (52)$$

If boundary effects are neglected Eq's. (36) and (37) may be used where

$$C \approx \frac{P_c R (1 - \nu) e^{-\lambda\psi} \sqrt{\sin \frac{\alpha}{2}}}{\left(K_4 + \frac{1}{K_3} \right) \sin \frac{\alpha}{2} \sqrt{\sin \left(\frac{\alpha}{2} - \psi \right)}}$$

$$\approx \frac{\alpha}{2} - \psi$$

$$\lambda^4 \approx 3(1 - \nu^2) \left(\frac{R}{L} \right)^2$$

$$K_1 \approx 1 - \frac{1 - 2\nu}{2\lambda} \cot \left(\frac{\alpha}{2} - \psi \right)$$

$$K_2 \approx 1 - \frac{1 + 2\nu}{2\lambda} \cot \left(\frac{\alpha}{2} - \psi \right)$$

$$K_3 \approx 1 - \frac{1 - 2\nu}{2\lambda} \cot \frac{\alpha}{2}$$

$$K_4 \approx 1 - \frac{1 + 2\nu}{2\lambda} \cot \frac{\alpha}{2}$$

$$\cot \gamma \approx -\frac{1}{K_3}$$

Deflection Mode Load

$$M_\phi = (M_{\phi a} + M_{\phi b}) \cos \theta \quad (53)$$

where

$M_{\phi a}$ is same as for dome with fixed supports

$$M_{\phi b} = \frac{R}{L} S_\phi e^{-\lambda\psi} \sin(\lambda\psi)$$

$$S_\phi = \frac{P_d (\alpha - \sin \alpha)}{\pi \left[\frac{2}{3} - \cos \frac{\alpha}{2} + \frac{\cos^3 \frac{\alpha}{2}}{3} \right]}$$

$$\lambda = 1.316 \sqrt{\frac{R}{t}}$$

$$c = \pi - 1 + \frac{\cot \frac{\psi}{2}}{2\lambda}$$

$$\bar{S}_e = \frac{-Et \sin \frac{\psi}{2}}{\left(\epsilon + \frac{1}{\epsilon}\right) \lambda R \sin^2 \frac{\psi}{2}}$$

$$\psi = \frac{1}{2} - \frac{\phi}{\lambda}$$

$$\bar{N}_e = \frac{RA}{3Et \sin^3 \frac{\psi}{2}} \left(2 \cdot \cos \frac{\psi}{2} + 3 \sin^2 \frac{\psi}{2} + 2 \cdot \cos^4 \frac{\psi}{2} \right)$$

$$N_e = (\bar{N}_{\theta m} + \bar{N}_{\theta b}) \cos \psi \quad (54)$$

where

$$\bar{N}_{\theta m} = \frac{-RA \cos \frac{\psi}{2}}{3 \sin^2 \psi} (2 + 3 \cos \psi + \cos^3 \psi)$$

$$\bar{N}_{\theta b} = 2 \cdot \bar{S}_e e^{-\lambda \psi} \cos (\lambda \psi)$$

$$N_{\theta} = (\bar{N}_{\theta m} + \bar{N}_{\theta b}) \cos \psi \quad (55)$$

where

$$\bar{N}_{\theta m} = \frac{RA}{3 \sin^3 \psi} (2 \cos \psi + 3 \sin^2 \psi + 2 \cos^4 \psi)$$

$$\bar{N}_{\theta b} = 2 \cdot e^{-\lambda \psi} \left(\cos \lambda \psi - \frac{\sin \lambda \psi}{\lambda^2 \sin \psi} \right) \bar{S}_e$$

$$N_{\theta} = (\bar{N}_{\theta m} + \bar{N}_{\theta b}) \sin \psi \quad (56)$$

where

$$\bar{N}_{\phi m} = \bar{N}_{\phi b}$$

$$\bar{N}_{\phi b} = \bar{S}_e e^{-\lambda \psi} \left[\cos \lambda \psi - \left(1 - \frac{\cot \frac{\psi}{2}}{\lambda} \right) \sin \lambda \psi \right]$$

$$N_{\phi} = (\bar{N}_{\phi m} + \bar{N}_{\phi b}) \cos \theta \quad (57)$$

where

$$\bar{N}_{\phi m} = - \frac{t^2}{12 R \sin^2 \phi} N_{\theta}$$

$$\bar{N}_{\phi b} = - \frac{\sqrt{3} t e^{-\lambda \psi}}{6} \left\{ \left(\frac{-1}{\lambda \sin^2 \phi} + \cot \phi \right) \cos \lambda \psi + \cot \phi \sin \lambda \psi \right\} \bar{S}_e$$

SHELL ACTION IN ARCHES

End walls or intermediate diaphragms, or both, can modify the arch response, strength, and stresses under the deflection mode loading by providing a longitudinal transfer of part of this

loading to the walls or diaphragms. Some estimate of the relative shell versus arch action can be obtained using folded plate analogy or by analyzing each half of the arch separately as a shell satisfying common boundary conditions at the crown. The diagonal tension stresses caused by the longitudinal spanning should be estimated to determine whether enough reinforcement is provided to insure against local failure which could cause a reduction of the arch capacity and progress to general failure.

REFERENCES

1. E. Cohen and S. Weissman, "Underground Shock Environment Data Application to the Design of Underground Structures," Proceedings of the 23th Symposium on Shock, Vibration, and Associated Environments, Bulletin No. 28, Part III, Office of the Secretary of Defense, Research and Engineering, Washington, D. C., September 1960.
2. E. Cohen and S. Weissman, "Nuclear Weapon Ground Shock Effects in Relation to Hardened Design," Symposium on Scientific Research in Protective Construction, Ernst-Mach Institut, Freiburg i. Br., Eckerstrasse 4, West Germany, September 1960.
3. F. F. Sauer et al., "Ground Motion Induced by Nuclear Explosions, A Study of Fundamental Problems," (prepared for Air Force Special Weapons Center under Contract AFSWC-TN-58-23) (Confidential), November 1958.
4. E. Cohen and N. Dobbs, Operation PLUMBOB, WT-1453, "Test of French Underground Personnel Shelters," 1961.
5. E. Cohen and A. Bottenhofer, Operation PLUMBOB, WT-1454, "Test of German Underground Personnel Shelters," 1961.
6. L. J. Vortman, Operation TEAPOT, WT-1218, "Evaluation of Various Types of Personnel Shelters Exposed to an Atomic Explosion," May 1958.
7. E. Cohen and E. Laing, Operation PLUMBOB, WT-1449, "Response of Dual-Purpose Reinforced Concrete Mass Shelter" (Confidential), 1961.
8. W. Flathau, R. Breckenridge, and C. Wienie, Operation PLUMBOB, WT-1420, "Blast Loading and Response of Underground Concrete-Arch Structures" (Confidential), 5 June 1959.
9. J. E. Smith, "Tests of Concrete Deadman Anchorages in Sand," ASTM Technical Publication #206. "Large Retaining Wall Tests," Engineering News Record, 1934.
10. J. E. Smith, "Passive Resistance of Earth Anchors in Sand, Part 2," U. S. Naval Civil Engineering Laboratory, Port Hueneme, Calif., 8 March 1963.
11. J. L. Merritt and N. M. Newmark, "Design of Underground Structures to Resist Nuclear Blast," University of Illinois (prepared for Office of the Chief of Engineers, U. S. Army under Contract DA-49-129-ENG-312), April 1958.
12. "Design of Structures to Resist the Effects of Atomic Weapons," EM-1110-345-411 through EM-1110-345-421, Manual - Corps of Engineers, U. S. Army.
13. "Engineering Study of Atomic Blast Resistant Design for Several Different Building Types," Ammann & Whitney (prepared for the Office of the Chief of Engineers, U. S. Army under Contract DA 49-129-ENG-317), February 1959.
14. H. W. Liepmann and A. E. Puckett, "Introduction to Aerodynamics of a Compressible Fluid," Wiley & Sons, 1947.

15. W. G. Vicenti and C. B. Wagoner, "Transonic Flow Past a Wedge Profile with Detached Bow Wave," Report 1095, National Advisory Committee for Aeronautics, 1952.
16. A. E. Bryson, "An Experimental Investigation of Transonic Flow Past Two-Dimensional Wedge and Circular-Arc Sections Using a Mach-Zehnder Interferometer," Report 1094, National Advisory Committee for Aeronautics, 1952.
17. W. Griffith, "Shock Tube Studies of Transonic Flow over Wedge Profiles," Journal of the Aeronautical Sciences, Vol. 19, No. 4, pp. 245-257, April 1952.
18. E. R. C. Miles, "Supersonic Aerodynamics," McGraw-Hill, 1950.
19. J. W. Cleary and J. A. Mellanthin, "Wing Tunnel Tests of a 0.16 Scale Model of the X-3 Airplane at High Subsonic Speeds - Wing and Fuselage Pressure Distribution," NACA RM A50D07, 22 June 1950.
20. C. L. Dailey and F. C. Wood, "Computation Curves for Compressible Fluid Problems," Wiley & Sons, 1949.
21. H. W. Liepmann and A. E. Bryson, "Transonic Flow Past Wedge Sections," Journal of the Aeronautical Sciences, Vol. 17, No. 12, pp. 745-755, Dec. 1950.
22. Ames Research Staff, "Equations, Tables, and Charts for Compressible Flow," NACA Report 113, 1953.
23. J. R. Spreiter, "Theoretical and Experimental Analysis of Transonic Flow Fields," NACA - University Conference on Aerodynamics, Construction and Propulsion, Vol. II - Aerodynamics, 20-22 October 1954.
24. Anon, "Transient Drag and Its Effect on Structures," Final Report, Project MR 1013, American Machine and Foundry Company (Confidential), 25 February 1955.
25. J. R. Spreiter and A. Y. Alksne, "Thin Airfoil Theory Based on Approximate Solution of the Transonic Flow Equation," NACA, TN 3970, May 1957.
26. A. L. L. Baker, "Further Research in Reinforced Concrete and Its Application to Ultimate Load Design," Paper 5894, British Institution of Civil Engineers, August 1953; A. L. L. Baker, "The Ultimate Load Theory Applied to the Design of Reinforced and Prestressed Concrete Frames," Concrete Publications Limited, London, 1956.
27. P. Weidlinger, "On the Analysis of a Salvo" (Prepared for RAND Corporation).
28. "Analysis and Design of Flexible Underground Structures," Volumes 1 and 2, Newmark, Briscoe, and Merritt (prepared for U. S. Army Waterways Experiment Station Corps of Engineers, Vicksburg, Mississippi under Contract DA-22-079-ENG-225) (Confidential), May 1960.
29. "Preliminary Design Methods for Underground Protective Structures," Newmark & Hall (prepared for Air Force Special Weapons Center under Contract AF 29 (601)-1171), December 1959.
30. "Development of Procedures for Rapid Computation of Dynamic Structural Response," Brooks, M. sh and Newmark (prepared for Headquarters, USAF under Contract AF 33(600)-24994) (Confidential), 1 July 1954 and June 1955.
31. A. Havers, "Non Symmetrical Deformation of Spherical Shells," Engr.-Arch. Vol. 6, p. 292, 1935.
32. S. Timoshenko, "Theory of Plates and Shells," Second Edition, 1959, McGraw-Hill, Chapter 16, 1959.

APPENDIX

Arch and Dome Dead Load and Earth Load Equations

This Appendix contains the arch relations for fixed and two hinged arches subjected to dead loads, earth loads, and temperature change. The relations given include rib shortening.

TWO HINGED ARCH RELATIONS

See Fig. A1 for arch notation.

Arch Dead Weight

$$V_A = V_B = \text{wt } R \frac{\alpha}{2} \quad (A1)$$

$$H_A = H_B = \frac{\text{wt } R^3 (C_9 - C_{10})}{C_{11}} \quad (A2)$$

where

$$C_9 = \frac{\alpha}{2} \left(-\frac{5 \cos \alpha}{4} + 1 - \frac{\alpha \sin \alpha}{4} \right) + \frac{9 \sin \alpha}{8}$$

$$C_{10} = \frac{t^2}{96 R^2} (\sin \alpha - \alpha \cos \alpha)$$

$$C_{11} = \frac{R^2}{4} \left[\alpha (2 + \cos \alpha) - 3 \sin \alpha \right] + \frac{t^2}{48} (\alpha + \sin \alpha)$$

w = unit weight of concrete.

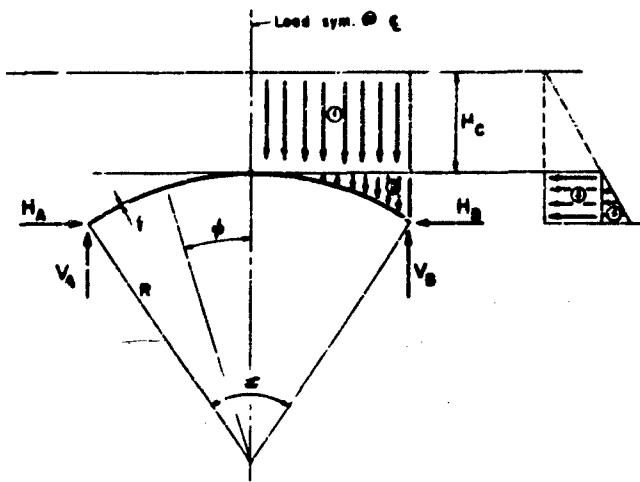


Fig. A1 - Notation for two hinged arches under dead loads

Vertical Earth Load for Portion of Earth Above Crown

Load 1 in Fig. A1.

$$V_A = V_B = \gamma H_c R \sin \frac{\alpha}{2} \quad (A3)$$

$$H_A - H_B = \frac{H_c R \left(C_{12} + C_{13} \right)}{\sqrt{1 - \frac{C_{15}}{C_{14}}}} \quad (A4)$$

where

$$C_{12} = \frac{4}{3} \sin^3 \frac{\alpha}{2} + \cos \frac{\alpha}{2} \left[\frac{1}{2} - \alpha \sin^2 \frac{\alpha}{2} - \frac{\sin \alpha}{2} \right]$$

$$C_{13} = \frac{t^2}{6R^2} \left(\frac{1}{2} \cos^2 \frac{\alpha}{2} - \frac{3}{4} - \frac{\sin \alpha}{4} \right)$$

$$C_{14} = \alpha \cos^2 \frac{\alpha}{2} + \frac{\alpha}{2} - \frac{3 \sin \alpha}{2}$$

$$C_{15} = \frac{t^2}{12R^2} \left(\frac{1}{2} + \frac{\sin \alpha}{2} \right)$$

γ = unit weight of earth.

Vertical Earth Load for Earth Surface at Crown

Load 2 in Fig. A1.

$$V_A = V_B = \gamma R^2 \left(\sin \frac{\alpha}{2} - \sin \alpha - \frac{\alpha}{4} \right) \quad (A5)$$

$$H_A = H_B = \gamma R^4 \left(\frac{-C_{16} + C_{17} + C_{18} + C_{19}}{C_{11}} \right) \quad (A6)$$

where

$$C_{16} = \frac{\sin \alpha}{96} \left(8 \sin^2 \frac{\alpha}{2} + 2 + 12 \cos \frac{\alpha}{2} + \cos \alpha \right)$$

$$C_{17} = \frac{\alpha}{4} \left[\frac{\sin \alpha}{4} \left(\frac{\sin \alpha}{3} + \alpha \right) - \sin^2 \frac{\alpha}{2} + \frac{\cos \frac{\alpha}{2}}{2} \left(\cos \frac{\alpha}{2} - 12 \right) + \frac{5 \cos^2 \frac{\alpha}{2}}{3} + \frac{9}{24} \right]$$

$$C_{18} = \frac{\sin \frac{\alpha}{2}}{2} \left[\frac{1}{2} - \frac{\cos \alpha}{2} - \frac{5 \cos \frac{\alpha}{2}}{3} - \frac{\sin^2 \frac{\alpha}{2}}{3} - \frac{\sin^2 \frac{\alpha}{2} \cos \frac{\alpha}{2}}{9} \right]$$

$$C_{19} = \frac{t^2}{12R^2} \left[\frac{\sin \alpha}{16} \left(1 - \frac{\cos \alpha}{2} \right) - \frac{\alpha}{16} \left(\cos \alpha - \frac{1}{2} \right) - \frac{\sin^3 \frac{\alpha}{2}}{3} \right]$$

$$C_{11} = \frac{R^2}{4} \left[\alpha (2 + \cos \alpha) - 3 \sin \alpha \right] + \frac{t^2}{48} (\alpha + \sin \alpha)$$

Horizontal Earth Load for Portion of Earth Above Crown

Load 3 in Fig. A1.

$$V_A = V_B = 0 \quad (A7)$$

$$H_A = H_B = \gamma K H_c R^3 \left(\frac{C_{20} + C_{21}}{C_{11}} \right) \quad (A8)$$

where

$$C_{20} = \sin \frac{\alpha}{2} \left(\frac{11}{12} \sin^2 \frac{\alpha}{2} - \frac{1}{4} - \frac{\alpha \sin \alpha}{8} \right) + \frac{5\alpha \cos \frac{\alpha}{2}}{8}$$

$$C_{21} = \frac{t^2}{12R^2} \left[\frac{\alpha \cos \frac{\alpha}{2}}{4} - \sin \frac{\alpha}{2} \left(\frac{1}{2} + \frac{\sin^2 \frac{\alpha}{2}}{6} \right) \right]$$

$$C_{11} = \frac{R^2}{4} \left[\alpha (2 + \cos \alpha) - 3 \sin \alpha \right] + \frac{t^2}{48} (\alpha + \sin \alpha)$$

$$K = \frac{1 - \sin \phi}{1 + \sin \phi},$$

and ϕ is angle of friction of earth.

Horizontal Earth Load, Earth Surface at Crown

Load 4 in Fig. A1.

$$V_A = V_B = 0 \quad (A9)$$

$$H_A = H_B = \gamma K R^4 \left(\frac{C_{22} + C_{23} + C_{24}}{C_{11}} \right) \quad (A10)$$

where

$$C_{22} = \frac{\sin \alpha}{2} \left(\frac{19}{32} - \frac{7 \sin^2 \frac{\alpha}{2}}{12} - \frac{3 \cos \frac{\alpha}{2}}{4} \right) - \frac{\sin \frac{\alpha}{2}}{2} \left(1 - \frac{\sin^2 \frac{\alpha}{2}}{3} \right)$$

$$C_{23} = \alpha \left(-\frac{\cos^4 \frac{\alpha}{2}}{6} + \frac{\cos^3 \frac{\alpha}{2}}{4} - \frac{\cos^2 \frac{\alpha}{2}}{8} + \frac{5 \cos \frac{\alpha}{2}}{8} + \frac{1}{32} \right)$$

$$C_{24} = \frac{t^2}{12R^2} \left[\frac{z}{4} \left(\cos \frac{\alpha}{2} - \cos^2 \frac{\alpha}{2} + \frac{3}{8} \right) - \frac{\sin \frac{\alpha}{2}}{2} \left(\frac{3}{8} + \frac{\cos^3 \frac{\alpha}{2}}{2} + \frac{3 \sin^2 \frac{\alpha}{2}}{4} \right) \right]$$

$$C_{11} = \frac{R^2}{4} \left[\alpha (2 + \cos \alpha) - 3 \sin \alpha \right] + \frac{t^2}{48} (\alpha + \sin \alpha)$$

$$K = \frac{1 - \sin \phi}{1 + \sin \phi},$$

ϕ is angle of friction of earth.

Temperature Change

$$V_A = V_B = 0 \quad (A11)$$

$$H_A = H_B = \frac{Et^3 b \Delta T \sin \frac{\alpha}{2}}{3R^2 [a(2 + \cos \alpha) - 3 \sin \alpha] + \frac{t^2}{12}(a + \sin \alpha)} \quad (A12)$$

where ΔT = change in temperature

α = coefficient of thermal expansion.

FIXED END ARCH RELATIONS

See Fig. A2 for a γ notation.

Arch Dead Weight

$$H_A = H_B = 0 \quad (A13)$$

$$V_A = V_B = \frac{\alpha}{4} \left(R_o^2 - R_i^2 \right) \quad (A14)$$

$$M_A = M_B = M_0 + H_0 K \left(\frac{2 \sin \frac{\alpha}{2}}{2} - \cos \frac{\beta}{2} \right) - V_{AR} \left(\sin \frac{\alpha}{2} - \frac{4 \sin^2 \frac{\alpha}{2}}{n} \right). \quad (A15)$$

where

$$H_0 \in \mathbb{R}^3 \frac{(C_{28} - C_{29} - C_{30})}{C_{11}}$$

$$E_{28} = \frac{a}{4} \left(1 - \cos \frac{a}{2} \right)^2 = \left(\frac{3}{2} - \frac{t^2}{12R^2} \right) \left(\frac{3a}{4} - 2 \sin \frac{a}{2} + \frac{\sin a}{4} \right)$$

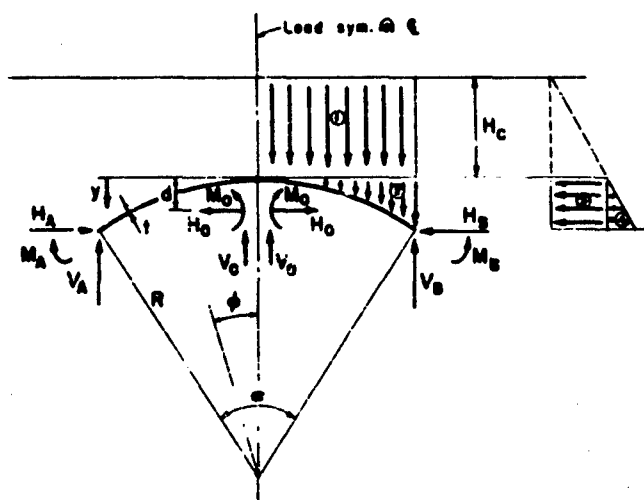


Fig. A2 - Notation for fixed end arch under blast loading

$$C_{29} = \left(1 - \frac{t}{a} - \frac{\sin \frac{a}{2}}{a} \right) \left[\sin \frac{a}{2} - \frac{a}{2} \cos \frac{a}{2} - \left(1 + \frac{t^2}{12R^2} \right) \left(\frac{a}{2} - \sin \frac{a}{2} \right) \right]$$

$$C_{30} = \frac{t^2}{96} (\sin a - a \cos a)$$

$$C_{31} = \frac{12R^2 + t^2}{48} (a + \sin a) = 2R^2 \left(\frac{\sin^2 \frac{a}{2}}{a} \right)$$

$$M_0 = \frac{2wt R^2}{a} \left[\sin \frac{a}{2} - \frac{a}{2} \cos \frac{a}{2} - \left(1 + \frac{t^2}{12R^2} \right) \left(\frac{a}{2} - \sin \frac{a}{2} \right) \right]$$

w = unit weight of concrete.

Vertical Earth Load, Portion of Earth Above Crown

Load 1 in Fig. A2.

$$V_A = V_B = \gamma H_c R \sin \frac{a}{2} \quad (A16)$$

$$H_A = H_B = \gamma H_c R^3 \left(\frac{C_{32} - C_{33}}{C_{34} - C_{35}} \right) \quad (A17)$$

$$M_A = M_B = \gamma H_c R^2 \left(\frac{1}{4} - \frac{\sin^2 \frac{a}{2}}{2} - \frac{\sin a}{4a} \right) + H_A R \left(\frac{2 \sin \frac{a}{2}}{a} - \cos \frac{a}{2} \right) \quad (A18)$$

where

$$C_{32} = \frac{1}{4} \left(-2 \sin^2 \frac{a}{2} \cos \frac{a}{2} + \sin \frac{a}{2} \right) - \frac{\sin^3 \frac{a}{2}}{6}$$

$$C_{33} = \frac{t^2}{36R^2} \sin^3 \frac{a}{2}$$

$$C_{34} = \frac{12R^2 + t^2}{48} (a + \sin a)$$

$$C_{35} = \frac{2R^2}{a} \sin^2 \frac{a}{2}$$

w = unit weight of earth.

Vertical Earth Load, Earth Surface at Crown

Load 2 in Fig. A2.

$$V_A = V_B = \gamma R^2 \left(\sin \frac{a}{2} - \frac{\sin a}{4} - \frac{a}{4} \right) \quad (A19)$$

$$H_A = H_B = H_o \quad (A20)$$

$$M_A = M_B = M_D + M + H_o R \left(\frac{2 \sin \frac{a}{2}}{a} - \cos \frac{a}{2} \right) \quad (A21)$$

where

$$M = \frac{\gamma R^3}{12} \left(6 \sin^2 \frac{\alpha}{2} - 2 \sin^2 \frac{\alpha}{2} \cos \frac{\alpha}{2} - 3x \sin \frac{\alpha}{2} + 4 - 4 \cos \frac{\alpha}{2} \right)$$

$$M_o = \frac{\gamma R^3}{12} \left[a \left(7 + 6 \cos \frac{\alpha}{2} \right) - 2 \sin \frac{\alpha}{2} \left(10 + \frac{2 \sin^2 \frac{\alpha}{2}}{3} \right) - 3 \sin \alpha \right]$$

$$H_o = \frac{\gamma R^4}{6} \left(\frac{C_{36} + C_{37} + C_{38}}{C_{39}} \right)$$

$$C_{36} = \frac{\sin \frac{\alpha}{2}}{a} \left[\frac{\alpha}{2} \left(7 + 6 \cos \frac{\alpha}{2} \right) + \sin \frac{\alpha}{2} \left(\frac{2 \cos^2 \frac{\alpha}{2}}{3} - \frac{32}{3} - 3 \cos \frac{\alpha}{2} \right) \right]$$

$$C_{37} = \frac{\alpha}{2} \left(3 \cos^2 \frac{\alpha}{2} - 3 \right) + \sin \frac{\alpha}{2} \left[5 - 3 \cos \frac{\alpha}{2} - 3 \cos^2 \frac{\alpha}{2} + \cos^3 \frac{\alpha}{2} \right]$$

$$C_{38} = \left(6 - \frac{t^2}{2R^2} \right) \left[\frac{\alpha}{2} \left(\cos^2 \frac{\alpha}{2} - \frac{3}{16} \right) + \sin \frac{\alpha}{2} \left(\frac{1}{3} - \frac{3 \cos \frac{\alpha}{2}}{16} - \frac{\cos^2 \frac{\alpha}{2}}{3} + \frac{\cos^3 \frac{\alpha}{2}}{8} \right) \right]$$

$$C_{39} = \frac{12 R^2 + t^2}{48} (\alpha + \sin \alpha) + \frac{2R^2 \sin^2 \frac{\alpha}{2}}{a}$$

Horizontal Earth Load, Portion of Earth Above Crown

Load 3 in Fig. A2.

$$V_A = V_B = 0 \quad (A22)$$

$$H_A = H_B = -H_o + \gamma K H_c R \left(1 - \cos \frac{\alpha}{2} \right) \quad (A23)$$

$$M_A = M_B = M_o + H_o R \left(\frac{2 \sin \frac{\alpha}{2}}{a} - \cos \frac{\alpha}{2} \right) - \frac{\gamma K H_c R^2}{2} \left(1 - \cos \frac{\alpha}{2} \right)^2 \quad (A24)$$

where

$$H_o = \frac{\gamma K H_c R^2}{a} \left[\frac{1}{4} (3x + \sin \alpha) - 2 \sin \frac{\alpha}{2} \right]$$

$$H_o = \gamma K H_c R^3 \left(\frac{C_{40} + \frac{t^2 C_{41}}{6R^2}}{C_{42}} \right)$$

$$C_{40} = \frac{\alpha}{2} + \frac{\sin \alpha}{2} \left(1 + \frac{\sin \frac{\alpha}{2}}{2} \right) - \frac{\sin \frac{\alpha}{2}}{3} \left(\cos \frac{\alpha}{2} + 1 + \frac{12 \sin \frac{\alpha}{2}}{a} \right)$$

$$C_{41} = \frac{1}{4} (\alpha + \sin \alpha) - \frac{\sin \frac{\alpha}{2}}{6} (\cos \alpha + 5)$$

$$C_{42} = \frac{12 R^2 + t^2}{24} (\alpha + \sin \alpha) + \frac{4R^2 \sin^2 \frac{\alpha}{2}}{a}$$

$$K = \frac{1 - \sin \phi}{1 + \sin \phi}$$

ϕ = angle of friction of earth.

Horizontal Earth Load, Earth Surface at Crown

Load 4 in Fig. A2.

$$V_A = V_B = 0 \quad (A25)$$

$$M_A = M_B = M_o + H_o R \left(\frac{2 \sin \frac{\alpha}{2}}{\omega} - \cos \frac{\alpha}{2} \right) - \frac{\omega' R^2}{6} \left(1 - \cos \frac{\alpha}{2} \right)^2 \quad (A26)$$

$$H_A = H_B = - H_o + \frac{\omega' R \left(1 - \cos \frac{\alpha}{2} \right)}{2} \quad (A27)$$

where

$$M_o = \frac{\omega' R^2}{3 \left(1 - \cos \frac{\alpha}{2} \right)} \left[\frac{5\alpha}{4} - \frac{\sin \frac{\alpha}{2}}{3} \left(11 + \cos^2 \frac{\alpha}{2} \right) + \frac{3 \sin \alpha}{4} \right]$$

$$H_o = \frac{\omega' R}{24 \left(1 - \cos \frac{\alpha}{2} \right)} \left[\frac{R^2 (C_{43} - C_{44}) + \omega'^2 C_{45}}{C_{46}} \right]$$

$$\omega' = \gamma K R \left(1 - \cos \frac{\alpha}{2} \right)$$

$$C_{43} = \frac{35\alpha}{4} - \frac{\sin \frac{\alpha}{2}}{3} \left(16 \cos^2 \frac{\alpha}{2} + 80 - 3 \cos^3 \frac{\alpha}{2} \right) + \left(\frac{27 \sin \alpha}{4} \right)$$

$$C_{44} = 4 \left(1 - \frac{2 \sin \frac{\alpha}{2}}{\alpha} \right) \left[\frac{5\alpha}{4} + \frac{3 \sin \alpha}{4} - \frac{\sin \frac{\alpha}{2}}{3} \left(11 + \cos^2 \frac{\alpha}{2} \right) \right]$$

$$C_{45} = \frac{7}{16} (\alpha + \sin \alpha) - \sin \frac{\alpha}{2} \left(\frac{2 \cos^2 \frac{\alpha}{2}}{3} + \frac{4}{3} - \frac{\cos^3 \frac{\alpha}{2}}{4} \right)$$

$$C_{46} = \frac{12 R^2 + \omega'^2}{4 R} (\alpha + \sin \alpha) - \frac{2 R^2 \sin^2 \frac{\alpha}{2}}{\alpha}$$

Temperature Change

$$H_A = H_B = H_o \quad (A28)$$

$$V_A = V_B = 0 \quad (A29)$$

$$M_A = M_B = H_t R \left(\frac{2 \sin \frac{\alpha}{2}}{\omega} - \cos \frac{\alpha}{2} \right) \quad (A30)$$

where

$$H_0 = \frac{4Et^3 \Delta T \sin \frac{\alpha}{2}}{(12R^2 + t^2)(1 + \sin \alpha) - \frac{96R^2 \sin^2 \frac{\alpha}{2}}{t}}$$

ΔT = temperature change

α = coefficient of thermal expansion.

FIXED END DOME RELATIONS FOR DEAD LOAD

See Fig. 20 for nomenclature.

$$N_d = \frac{-wR}{1 + \cos \gamma} - \cot\left(\frac{\alpha}{2} - \gamma\right) \sqrt{\frac{Ce^{i\lambda\psi}}{\sin\left(\frac{\alpha}{2} - \gamma\right)}} \sin(\lambda\psi + \gamma) \quad (A31)$$

$$N_r = wR \left(\frac{1}{1 + \cos \gamma} - \cos \gamma \right) + \frac{C\lambda e^{i\lambda\psi}}{2\sqrt{\sin\left(\frac{\alpha}{2} - \gamma\right)}} [2 \cos(\lambda\psi + \gamma) - (K_1 + K_2) \sin(\lambda\psi + \gamma)] \quad (A32)$$

$$M_d = \frac{RCe^{i\lambda\psi}}{2\sqrt{\sin\left(\frac{\alpha}{2} - \gamma\right)}} [K_1 \cos(\lambda\psi + \gamma) + \sin(\lambda\psi + \gamma)] \quad (A33)$$

$$M_r = \frac{RCe^{i\lambda\psi}}{4\sqrt{\sin\left(\frac{\alpha}{2} - \gamma\right)}} \left\{ [(1 + \nu^2)(K_1 + K_2) - 2K_2] \cos(\lambda\psi + \gamma) - 2\nu^2 \sin(\lambda\psi + \gamma) \right\} \quad (A34)$$

where

$$C = \frac{wRK'}{K_3 \sin \gamma} \sqrt{\sin \frac{\alpha}{2}}$$

$$K' = \left[\frac{1 + \nu}{1 + \cos \frac{\alpha}{2}} - \cos \frac{\alpha}{2} + \frac{(2 + \nu) \sin \frac{\alpha}{2}}{2\lambda} \right]$$

$$\cot \gamma = \frac{-K_3(2 + \nu) \sin \frac{\alpha}{2}}{2K' \lambda}, \quad \mu = \frac{\gamma}{2} - \frac{\alpha}{2}$$

$$\lambda^4 = 3(1 - \nu^2) \left(\frac{R}{t} \right)^2$$

$$K_1 = 1 - \frac{1 + 2\nu}{2\lambda} \cot\left(\frac{\alpha}{2} - \psi\right)$$

$$K_2 = 1 - \frac{1 + 2\nu}{2\lambda} \cot\left(\frac{\alpha}{2} - \psi\right)$$

$$K_3 = 1 - \frac{1 + 2\nu}{2\lambda} \cot \frac{\alpha}{2}$$

SIMPLY SUPPORTED DOMP EQUATIONS FOR DEAD LOAD

See Fig. 21 for notation.

$$N_A = \frac{-wR}{1 + \cos \varphi} - \cot\left(\frac{\pi}{2} - \nu\right) \frac{Ce^{-\lambda\psi}}{\sqrt{\sin\left(\frac{\pi}{2} - \nu\right)}} \sin(\lambda\psi + \gamma) \quad (A34)$$

$$N_C = wR \left(\frac{1}{1 + \cos \varphi} - \cos \varphi \right) + \frac{-\frac{wR}{2} e^{-\lambda\psi}}{\sqrt{\sin\left(\frac{\pi}{2} - \nu\right)}} [2 \cos(\lambda\psi + \gamma) - (K_1 + K_2) \sin(\lambda\psi + \gamma)] \quad (A35)$$

$$M_B = \frac{RCe^{-\lambda\psi}}{2\sqrt{\sin\left(\frac{\pi}{2} - \nu\right)}} [K_1 \cos(\lambda\psi + \gamma) + \sin(\lambda\psi + \gamma)] \quad (A36)$$

$$M_D = \frac{RCe^{-\lambda\psi}}{4\sqrt{\sin\left(\frac{\pi}{2} - \nu\right)}} \left\{ [(1 + \nu^2)(K_1 + K_2) - 2K_2] \cos(\lambda\psi + \gamma) + 2\nu^2 \sin(\lambda\psi + \gamma) \right\} \quad (A37)$$

where

$$C = \frac{wRK' \sqrt{\sin \frac{\pi}{2}}}{\lambda \left(K_4 + \frac{1}{K_3} \right) \sin \gamma}$$

$$\cot \gamma = \frac{1}{K_3}$$

$$K' = \left[\frac{1 + \nu}{1 + \cos \frac{\alpha}{2}} - \cos \frac{\alpha}{2} \right]$$

$$\nu = \frac{\pi}{2} - \omega$$

$$\lambda^4 = 3(1 + \nu^2) \left(\frac{R}{t} \right)^2$$

$$K_1 = 1 + \frac{1 + 2\nu}{2\lambda} \cot\left(\frac{\pi}{2} - \nu\right)$$

$$K_2 = 1 + \frac{1 + 2\nu}{2\lambda} \cot\left(\frac{\pi}{2} - \nu\right)$$

$$K_3 = 1 + \frac{1 + 2\nu}{2\lambda} \cot \frac{\pi}{2}$$

$$K_4 = 1 + \frac{1 + 2\nu}{2\lambda} \cot \frac{\pi}{2}$$

ANTENNAS FOR HARD RADIO COMMUNICATION SYSTEMS— A PRELIMINARY STUDY

S. P. Morgan and E. E. Zajac
Bell Telephone Laboratories, New Jersey

The study considered in particular the problem of designing radio antennas to survive at the 500-psi point under multiple attacks by nuclear weapons in the megaton range. The study was based upon fundamental physical principles rather than "hardening" of existing designs.

INTRODUCTION AND SUMMARY

This paper reports a feasibility study for very hard radio communication systems. The situation envisioned is that of a buried control center or military headquarters which is expected to survive multiple near misses by nuclear weapons in the megaton range.

One would like a communication connection consisting of a single radio antenna on top of a buried control center, the antenna being just as hard as the center itself. Such an antenna would present a point target, and would require the enemy to knock out the center itself in order to destroy the antenna. A radio communication system of this sort could serve as a substitute for, or at least as a supplement to, a hard communication system using buried cable. In this paper we shall concentrate on the structural problems encountered in designing such a system. We shall only mention in passing some of the interesting electrical questions that are involved.

We have considered a couple of situations which seem to blanket a range of possible objectives. First we have considered an omnidirectional system with a range of about 25 miles and a small communications capacity of one or a few voice channels. For the hardness level we have more or less arbitrarily adopted 500 psi since at much higher overpressure levels one is inside the plastic zone surrounding the bomb crater. As a second type of objective, we have considered a very hard radio relay system, again at an overpressure of 500 psi. In this case we have

envisioned point-to-point, large capacity communication links of many voice channels or several TV channels.

NATURE OF THE ENVIRONMENT

Figure 1 shows a sketch of the crater for an 8-MT surface burst obtained from data given in an unclassified handbook [1]. In addition, Ref. 1 gives the following values at the 500-psi point for this location:

Range from ground zero:	3850 feet
Static overpressure:	500 psi
Dynamic overpressure:	1000 psi
Duration of positive phase:	1.3 seconds
Velocity of air shock wave:	4000 mph
Wind velocity behind wave front:	3300 mph
Peak reflected overpressure:	3500 psi.

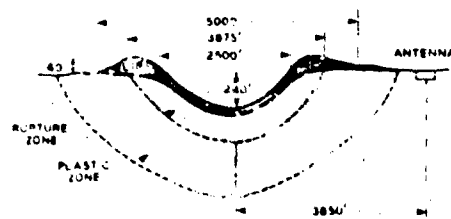


Fig. 1 - Sketch of crater for 8-MT burst

The data on ground shock that are available [2] give us only very crude estimates of what to expect. For example, it seems reasonable to expect surface accelerations at the 500-psi point for an 8-MT burst to be at least 100g, and possibly much more, with displacements of the order of a foot or more, and velocities something like 30 ft/sec.

It was assumed that the effects of thermal and nuclear radiation on the mechanical strength of the antenna structure would be negligible, although it is expected that a small amount of material per shot would be lost by ablation. The important thermal and nuclear effects on dielectric materials would have to be studied further in any actual antenna design.

ANTENNA TYPES

The types of antennas fall into one of two broad classes, flexible (or disposable) structures, and inflexible structures. Examples of the first class would be: (1) A vertical rod mounted on a heavy, helical spring. The rod ducks down during the blast and then returns to its operating position. (2) A conducting wire held upright by a captive balloon. After the blast a dispenser sends up another balloon to replace the one that has blown away. All such schemes, however, require some mechanism with moving parts which can withstand the enormous shocks and pressures of the 500-psi environment; and it appears that it would be easier to prove the feasibility of rugged, completely stationary structures.

The best solution for an omnidirectional radiator appears to be a flush-mounted annular slot, shown schematically in cross section in Fig. 2. All conductors are made of steel, and the feed structure is filled with a refractory dielectric (fused silica, fused alumina, fused mullite, fused stabilized zirconia, and recrystallized glass are possibilities). Radial steel bolts may be placed across the large coaxial for impedance-matching purposes and also to add mechanical strength. The center plug of the antenna may be made of reinforced concrete. At 30 Mc, the diameter of the proposed antenna would be about 16 feet; and its depth would be about 4 feet.

The best type of microwave antenna for the point-to-point system appears to be an array of steel slotted waveguides, filled with a refractory dielectric. The electrical studies indicate that a reasonable operating frequency for this array would be 1000 Mc and that it should be about 25 feet above ground.

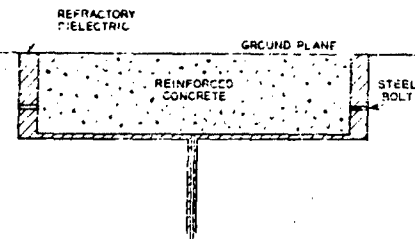


Fig. 2 - Annular slot radiator

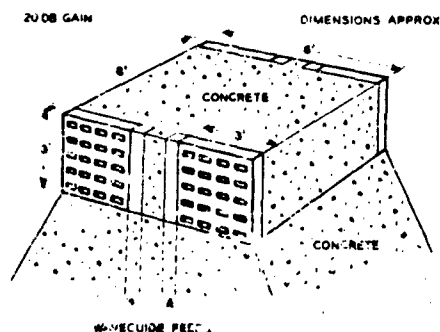
MECHANICAL DESIGN

Omnidirectional, Flush-Mounted Antenna

We have assumed a center plug (Fig. 2) of reinforced concrete, surrounded by a thin skin of steel. The 500-psi air-induced ground shock has been assumed to double upon reflection, sending a 1000-psi stress wave into the plug. We design against shattering of the concrete by a three-dimensional system of reinforcing rods. (This system is discussed later in the case of the microwave tower.) With a sufficiently strong dielectric, only a thin skin of steel is required as the outer conductor. If such a dielectric is unavailable, electrically invisible bolts made of a fiberglass-reinforced epoxy resin can be used to transmit the load from the outer skin to the inner plug.

Microwave Tower

Roughly speaking the problems of designing a 25-foot microwave antenna (Fig. 3) are



FOUR SLOTTED ARRAYS AT TOP OF 25-FOOT CONCRETE TOWER
WAVEGUIDE FEET
Fig. 3 - 1000-Mc broadside slotted waveguide array

four types: (1) stresses due to the 500-psi enveloping pressure, (2) anchorage of the structure to keep it from blowing away, (3) stress waves generated by the impact of the 3500-psi reflected pressure, and (4) stresses due to the drag loads.

The buckling problem dictates thick-walled structures. For example, the standard formula [3] for a steel cylinder yields a thickness-to-radius ratio of 3/25 to prevent static buckling under the total static plus drag pressure to 1500 psi.

Similarly the high drag forces preclude the use of a frame structure. For example, pin-ended members made of 100,000-psi yield strength steel would require a length-to-diameter ratio of 6 to 1 for the drag loads at hand. With such stubby members, a structure would be very difficult and expensive to fabricate.

We are thus led to a structure made of solid or very thick-walled rather than thin-walled members, and one which is made of one or a few stubby members rather than a great many stubby members. Two designs look promising. One is a truncated, thick-walled steel cone filled with concrete. The concrete provides a solid inner core that helps keep the thick-walled steel outer cylinder from buckling. Lacking an analysis of the dynamic buckling strength, we arbitrarily take a thickness-to-radius ratio of 1/10 for the outer steel shell. Because of the concrete core and the short time of loading, it is felt that this thickness will be adequate.

An alternative structure is a tower made of a single material with a tensile strength of over 3500 psi. For the purposes of this study, we have considered reinforced concrete. The amount of reinforcing steel is very nearly the same as that contained in the thick steel-walled design (18 percent to 19 percent by volume). Thus the weights of the two structures are roughly equal, and the subsequent discussion will apply to both.

To support the proposed antenna, the tower is required to have an 8-foot square section (Fig. 3), at a height of 25 feet. We take the half opening angle of the tower as 25 degrees (Fig. 4) as a compromise between various electrical and mechanical factors.

Anchorage Problem

Horizontal Displacement. Consider first that the tower is sitting on the surface of the

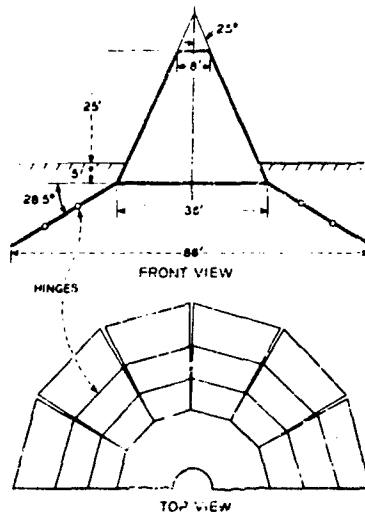


FIG. 4 - Sketch of microwave tower

ground. If we assume a coefficient of friction of 0.3 between the ground and the tower, we find that the wind forces translate the tower horizontally at a considerable $9g$ while the total vertical force acting on the tower is capable of accelerating it downward at $40g$ (Appendix). On the other hand, the data of Ref. 2 indicate that the ground acceleration may be more than $100g$. Hence we may have a situation where the air shock pushes the ground out from under the tower while simultaneously striking the tower with an enormous horizontal force.

To overcome this problem, one could tie the tower into deep piles, or else deepen the foundation so that not only the tower but a very large volume of earth must be moved in order to translate the tower horizontally. Both of these alternatives may be feasible. However, both lead to a very speculative dynamic soil mechanics calculation. We therefore use another scheme which is amenable to simple calculations. This is to attach to the tower a buried "friction brake" or "root" structure (Fig. 4). The brake extends all around the tower to a considerable distance from it; thus a blast wave advancing from any direction first clamps down on the brake and moves it as the friction force. When the wave strikes the above-ground portion of the tower, the tower has already been secured against horizontal motion (Appendix).

We envision the brake to be made of pivoted link sections of grillages (Fig. 4). These act like wide flexible strings that can transmit only forces in their planes and cannot transmit shear forces and bending moments. The grillages ride along with the ground motion, and the ground transmits force to the grillage only by virtue of its relative motion tangent to the grillage.

Overturning. In order for the tower not to rotate, the sum of the moments of all forces about the tower's center of gravity must be zero. We design to this condition by inclining the grillage. We assume that the inclination angle is approximately constant during the ground motion, that the forces from the grillage acting on the tower are directed along the grillage, and that the reaction forces from the ground in contact with the structure are negligible. Under these assumptions, the inclination angle of the grillage necessary to give no moment about the center of gravity of the structure is approximately 28 degrees (Appendix).

Vertical Motion. The downward force on the tower is limited, being essentially a coefficient of friction times the projected area of the grillage times the overpressure. Detailed calculations are given in the appendix; the result is a 33g acceleration of the tower from the downward grillage force alone. However, the average value of the stresses resulting from this acceleration is low, being an average of 450 psi over the bottom cross section for the reinforced concrete tower, and 2360 psi for the steel-walled tower. These stresses are further reduced by the 500-psi overpressure pushing down on the tower.

In the extreme case, the 33g force of the grillage will combine with the 40g downward force of the overpressure to give a net 73g downward acceleration. As we remarked, this still may be less than the downward acceleration of the ground; that is, there may be a tendency to uproot the tower from the ground. To prevent this, we have placed the bottom of the tower (Fig. 4) 5 feet below the ground.

Compressive stresses caused by the upward ground motion do not appear to be a problem. For example, a 200g upward acceleration contributes an average compressive stress at the bottom cross section of only $(200/33) \times 450 = 2730$ psi in the case of the reinforced concrete and 14,300 psi in the case of the steel-wall tower.

Internal Stresses Due to the Reflected Overpressure

In the case of a reinforced concrete structure the 3500-psi peak reflected overpressure is a problem. For one thing, it is of very short duration (5 milliseconds for a 25-foot high tower), and one cannot compute the resulting stresses from an equivalent static load approach. For another thing, recent tests indicate that when reinforced concrete fails dynamically the bond between the concrete and the reinforcing rods is broken [4]. It is felt that the impact-generated stress waves travel faster in the steel rods than they do in the concrete and thus break the bond. However, it is not clear to what extent this diminishes the strength of reinforced concrete, and failing more knowledge, we shall assume that reinforced concrete can be used.

In the case of a steel-walled tower, the high reflected overpressure can be expected to be substantially reduced upon passage through the thick steel outer cylinder into the concrete core. However, even if the concrete core fractures, no harm will be done since the core merely prevents buckling.

The high reflected pressure leads to spalling. This effect is illustrated by the impact on a rod (Fig. 5) of a pressure pulse

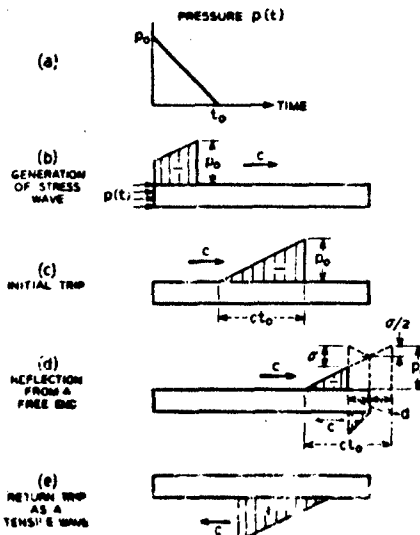


Fig. 5 - Elementary theory of spalling

which initiates a compressive stress wave. Upon reflection as a tension wave, the pulse may cause a rod that has a low tensile strength to fail. An elementary theory of spalling due to Rinehart is included in the appendix. For concrete with a tensile strength of 100 psi and a stress wave velocity of 10,000 ft per sec, it indicates that a 3500-psi, 5-millisecond pulse will produce 35 spalls, each 0.72 feet thick.

The 3500-psi peak reflected pressure acts over only a small portion of the front of the tower and tapers off to the ambient 500-psi pressure at the sides. Also, the stress wave generated by the peak pressure disperses in three dimensions in the solid, thus reducing its strength. On the other hand, reflections off the base and sides and subsequent recombination may lead to local stress concentrations that exceed the peak reflected pressure of 3500 psi.

The rod model indicates that a rough-and-ready design is to reinforce so as to give the tower a tensile strength of 3500 psi in any direction. We assume here that the isotropic strength requirement may be achieved by a pattern of rods spaced uniformly along three mutually orthogonal directions, with the ratio of steel area to the total area in each of the three orthogonal planes made equal to $\frac{3500}{c_y}$ (c_y is the yield strength of the steel in psi). For a pull is exerted in the direction of one of the systems of rods, a stress of 3500 psi is required to cause failure. A pull in an arbitrary direction such as normal to the plane ABC (Fig. 6), will be resisted by the rods in the three mutually perpendicular directions

(x, y, z in Fig. 6). The resistive force in each rod will increase until the rod is at its yield strength. Finally, when all the rods are at their yield strengths and the stress on the three orthogonal planes is 3500 psi, a state of hydrostatic tension will exist. Thus, the stress on the plane ABC in this case will also be the yield stress of 3500 psi.

The amount of steel required by this scheme is high. For example, for a 60,000-psi steel, 18 percent of the total volume is steel. Further, we wish to caution that we have assumed that the shear and bond strength of the concrete will be sufficient to transfer the load from any plane to the rods, and from rod to rod. In any serious consideration of a reinforced concrete design, these assumptions and the assumption that the dynamic strength of reinforced concrete is not overly diminished by the stripping phenomenon would have to be checked by experiments.

Internal Stresses Due to the Static and Dynamic Overpressures

To determine the stresses due to the static and dynamic overpressures, we resort to the usual structural dynamics assumption, namely: For loadings of long duration compared to the fundamental period of the structure, the peak dynamic stress is less than twice the corresponding peak static stress. Hence to compute the effect of the 3300-mpg wind, we assume that the wind pressure is proportional to the square of the normal component of the wind velocity, which is in turn assumed to be constant in direction and magnitude. We then compute the stresses resulting from this pressure applied statically and take twice the resulting stress to be the dynamic stress. We assume that the enveloping overpressure results in a hydrostatic state of stress of 500 psi which is superposed on the stresses resulting from the wind loading.

The calculations, based on beam theory, are given in the appendix. We find the resulting maximum tensile stress to be 1800 psi in the case of the reinforced concrete tower, and 8000 psi in the case of the steel-walled tower. Thus, in neither case are the stress levels excessive.

CONCLUSIONS

The upshot of the present study is that it appears feasible to get any amount of radio communication up to bandwidths of many

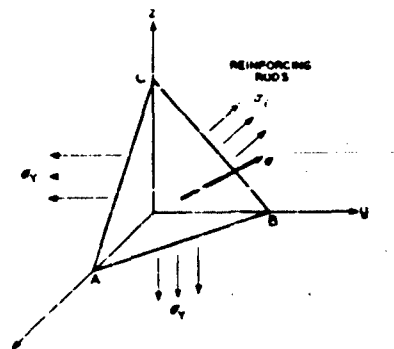


Fig. 6 - Stress on an arbitrary plane in triaxially reinforced concrete

megacycles in a 500-psi system — if one is willing to pay for it. As is already clear, however, there are many unanswered questions, which fall into three general categories.

(1) We need further information on the strength of reinforced concrete under shock loading and under multidimensional reinforcing in order to complete the design of the tower.

(2) More extensive analytical analyses to discover cheaper designs are in order. For example, by a more careful analysis, one probably can design a thick-walled reinforced concrete hollow tower that contains considerably less steel than our steel-walled or solid reinforced concrete tower.

(3) Data are required on the strength of various refractory dielectrics under mechanical and thermal shock, and also on the effects of neutron irradiation of such dielectrics.

ACKNOWLEDGMENTS

It is a pleasure to thank R. C. Prim for promoting the present work, and F. T. Geyling for numerous stimulating discussions. K. Bullington supplied radio-propagation data, J. C. Williams consulted on questions regarding dielectrics, and J. M. Hardesty and R. A. Shunk provided information on structural and mechanical problems.

REFERENCES

1. S. Glasstone, editor, The Effects of Nuclear Weapons, Government Printing Office, 1957.
2. W. Perrett, Ground Motion Studies at High Incident Overpressure, Joint DASA-AEC Report WT 1405 (to be issued shortly).
3. S. P. Timoshenko, "Theory of Elastic Stability," McGraw-Hill, New York, p. 450, 1956.
4. G. L. Neidhardt, et al., Field Test of Reinforced Concrete Dome Shelters and Prototype Door, Project 30.1, Interior Tech. Report 1448, Amer. Mach. and Foundry Co., 20 December 1957.

APPENDIX Design of Tower

HORIZONTAL AND VERTICAL FORCES AND ACCELERATIONS

Horizontal Force

We assume that the normal pressure is $\frac{1}{2} \rho V_N^2$, where V_N is the velocity component normal to the surface. Further, we assume that the worst situation occurs when the blast wave approaches horizontally. Then if V is the magnitude of the particle velocity in the blast wave, we have from Fig. 7

$$V_H = V \cos \phi \cos \theta,$$

and hence

$$P_D = \frac{1}{2} \rho V^2 = P_D \cos^2 \phi \cos^2 \theta,$$

where $P_D = \rho V^2 / 2$ is the dynamic pressure. Let F_H be the total horizontal load; then

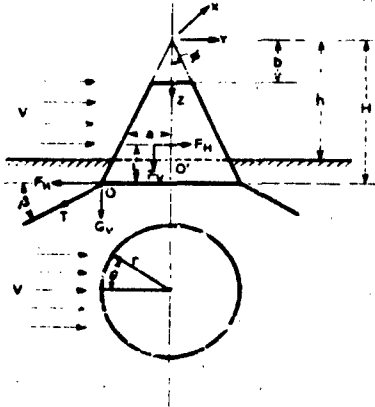


Fig. 7 - Wind forces on the tower

$$F_H = \int_b^h \int_{-\pi/2}^{\pi/2} \left(p \frac{dz}{\cos \phi} d\phi \right) \cos \phi \cos \theta$$

where

$$a = z \tan \phi,$$

giving

$$F_H = \frac{2}{3} p_D (h^2 - b^2) \sin \phi \cos \phi.$$

Vertical Force

The vertical wind load due to a horizontal wind against the tower of Fig. 7 is given by

$$Q_W = \int_b^h \int_{-\pi/2}^{\pi/2} \left(p_a \frac{dz}{\cos \theta} d\theta \right) \sin \phi \\ = \frac{\pi}{4} p_D (h^2 - b^2) \sin^2 \phi.$$

Let Q_A be the vertical load due to static overpressure p_S ; then

$$Q_A = p_S \pi h^2 \tan^2 \phi,$$

and the total vertical load F_V is

$$F_V = Q_W + Q_A = p_D \frac{\pi}{4} (h^2 - b^2) \\ \sin^2 \phi + p_S \pi h^2 \tan^2 \phi.$$

Vertical Acceleration

Neglect b^2 and b^3 compared to h^2 and h^3 . Then the vertical acceleration due to static and dynamic overpressures is

$$a_V = \frac{F_V}{W} \approx \frac{p_D}{W} \left(\frac{h}{R} \right)^2 \left(\frac{3}{4} \cos^2 \phi + 3 \frac{p_S}{p_D} \right) = 40g.$$

Horizontal Acceleration on a Surface with Friction

Let f be the coefficient of friction. Then

$$a_H = \frac{F_H - f F_V}{W} = \frac{p_D}{W} \left(\frac{h}{R} \right)^2 \\ \left[\left(\frac{2}{\pi} \frac{\cos^2 \phi}{\sin \phi} - \frac{3f}{4} \cos^2 \phi \right) + \frac{3fp_S}{p_D} \right].$$

For $f = 0.3$, $p_S = 500$ psi, and $p_D = 1000$ psi, we find

$$a_H = 9g.$$

GRILLAGE ANGLE

Let F_H and F_V be the resultant horizontal and vertical wind loads due to a horizontal wind. The grillage must resist with a horizontal load F_H in order to prevent sliding. Therefore there is a couple $F_H l$ acting on the tower (Fig. 7). To find this, sum the moments of the horizontal wind forces about 0 in Fig. 7:

$$F_H l = \int_b^h \int_{-\pi/2}^{\pi/2} \left[\left(\frac{pa}{\cos \theta} dz \right) \cos \phi \cos \theta \right] (l - z) \\ = \frac{4}{3} p_D \sin \phi \cos \phi \left[h \left(\frac{h^2 - b^2}{2} \right) - \left(\frac{h^3 - b^3}{3} \right) \right].$$

Further, the moment of the vertical wind forces about the center of gravity is

$$M_{VG} = \int_b^h \int_{-\pi/2}^{\pi/2} \left[\left(\frac{pa}{\cos \theta} dz \right) \sin \phi \right] a \cos \theta \\ = - p_D \sin \phi \cos \phi \tan^2 \phi \frac{(h^3 - b^3)}{3}.$$

Assume that at the points of attack a to the tower the grillage is free to move tangentially, that is, that force is transmitted only in a radial direction. The pull on each pie section of the grillage is therefore radial. Since the pie sections are of equal area, the force, say T per unit length, at which slippage relative to the ground begins will be equal in magnitude for each section. For horizontal equilibrium we have

$$F_H = \int_{-\pi/2}^{\pi/2} T \cos \beta \cos \theta r d\theta = 2Tr \cos \beta,$$

where β is the grillage angle; or

$$T = \frac{F_H}{2r \cos \beta}.$$

The vertical component of the grillage unit force is $T \sin \beta$. The resultant moment M_{VG} of the vertical components of the grillage forces about the center of gravity is

$$M_{VG} = - \int_{-r/2}^{r/2} T \sin \varphi r^2 \cos \beta \, dr$$

$$= -\frac{4}{3} p_D \sin \varphi \cos \varphi \frac{(h^2 - b^2)}{2} H \tan^2 \beta.$$

The total moment about the center of gravity is

$$M = F_H \ell + M_{VW} + M_{VG}.$$

With our previous assumption that b^2 and b^3 may be neglected compared to h^2 and h^3 , we obtain

$$M = \frac{2}{3} p_D h^2 H \sin \beta \cos \beta$$

$$\left[1 - \tan^2 \beta - \frac{2}{3} \frac{h}{H} \sec^2 \beta \right].$$

Setting the bracketed term to zero to find β at which the moment about the center of gravity is zero, we get

$$\tan^2 \beta = 1 - \frac{2}{3} \frac{h}{H} \sec^2 \beta.$$

For $\beta = 25$ degrees, $h/H = 33.6/38.6$, and $\beta = 28.5$ degrees.

DESIGN OF THE GRILLAGE STRUCTURE

Outer Radius

We assume that a hydrostatic pressure field of $p_S = 500 \text{ psi}$ exists in the soil and that the coefficient of friction between the soil and the grillage is f . The resistive friction force per unit area of the grillage is $2fp_S$ and the force per unit length T is given by (Fig. 8)

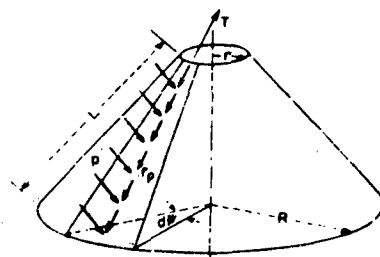


Fig. 8 - Forces in the grillage

$$Tr \, d\beta = 2fp_S(R^2 - r^2) \frac{d\beta}{2},$$

$$Tr = fp_S(R^2 - r^2).$$

From the previous section we have that

$$Tr = \frac{F_H}{2 \cos \beta},$$

and hence

$$R^2 - r^2 = \frac{F_H}{2fp_S \cos \beta}.$$

We take $f = 0.2$. Then for

$$\beta = 28.5 \text{ degrees},$$

$$r = 18 \text{ feet},$$

and the value of F_H used previously, we get

$$R = 43 \text{ feet}.$$

Size of Members in the Grillage

Consider the inner radius r of the grillage (Fig. 8). The required cross-sectional area A of the radial members of the grillage for one foot of circumference is given by

$$A = \frac{T}{\sigma_y}.$$

Here T is force per unit length of circumference at the inner radius and σ_y is the yield strength of the steel. For $\sigma_y = 10^5 \text{ psi}$ we find

$$A = 12.3 \frac{\text{in.}^2 \text{ of steel}}{\text{ft of circumference}},$$

So, for example, we may take rectangular cross sections of $2\text{-}1/8$ inches \times 6 inches spaced on one-foot centers.

VERTICAL ACCELERATION OF TOWER DUE TO GRILLAGE FORCES

The net downward grillage force is

$$G_y = \pi r T \sin \beta$$

$$= \frac{\pi}{2} \frac{2}{3} p_D (h^2 - r^2) \cos \beta \cos \varphi.$$

This gives a vertical acceleration of

$$a_y = \frac{G_y}{W} \approx \frac{p_D}{\rho H} \left(\frac{h}{H} \right)^2 \frac{\cos^3 \varphi}{\sin \varphi} = 33g.$$

ELEMENTARY THEORY OF SPALLING*

Assume that a triangular pulse of maximum pressure p_0 and duration t_0 is applied at one end of a rod (Fig. 5). It is easily shown from elementary rod theory that after the pulse is applied, but before it is reflected from the other end, stresses travel down the rod at a constant velocity c , distributed linearly over a distance $c t_0$, as shown in Fig. 5(c). Reflection from a free end is shown in Fig. 5(d), where the reflected wave has traveled a distance d back up the rod. The stresses may be obtained by "folding" a distance d of the original pulse shown in Fig. 5(a) and subtracting the "folded" portion from the pulse. The result yields a tensile stress returning to the impacted end. By simple geometry, we have

$$\frac{c^2}{4} = \frac{p_0}{ct_0}$$

or

$$d = \frac{ct_0}{2p_0}$$

Then d equals the tensile strength of the rod, a spall flies off. This creates another free end, and leaves a triangular compressive pulse in which the ratio p_0/ct_0 is the same as in the original pulse. If the peak compressive stress in the new pulse exceeds the tensile strength σ_0 of the rod another spall will form, and so on. Since the peak compressive strength is diminished by σ_0 upon the formation of each spall, the total number of spalls will be the integer part of p_0/σ_0 .

*J. S. Rinchart, "Spalling and Large Blasts," Proceedings of the Second Protective Construction Symposium, RAND Corp., Santa Monica, Calif., pp. 111-130, 1959.

INTERNAL STRESSES DUE TO DYNAMIC AND STATIC OVERPRESSURES

We assume the tower is a tapered beam, and compute the bending moment M_B about the point O' of Fig. 7. This has been done earlier in the appendix giving

$$\begin{aligned} M_B &= \bar{F}_H \cdot z \cdot M_{Ww} \\ &\approx \frac{2}{3} p_0 h^2 H \sin \beta \cos \psi \\ &\quad \left[1 - \frac{1}{2} \frac{h}{H} \left(\frac{4}{3} + \tan^2 \beta \right) \right] \end{aligned}$$

or

$$M_B = 49.6 \times 10^7 \text{ lb-ft.}$$

From elementary strength of materials theory the bending stress is

$$\sigma = \frac{M_B}{Z}$$

where Z is the section modulus. For the reinforced concrete tower $Z = 3000 \text{ ft}^3$, while for the steel-walled tower $Z = 810 \text{ ft}^3$. Hence

$$\sigma = 1150 \text{ psi (reinforced concrete).}$$

$$\sigma = 4250 \text{ psi (steel-walled).}$$

We multiply by 2 to account for dynamic effects and superpose the hydrostatic compressive stress of 500 psi. This gives

$$\sigma_{\max} = 1800 \text{ psi (reinforced concrete).}$$

$$\sigma_{\max} = 8000 \text{ psi (steel-walled).}$$

REVIEW OF BLAST CLOSURE SYSTEMS*

Marvin Hassman and Edward Cohen
Aimmann & Whitney, New York City

Results are presented of studies made on existing self-acting blast actuated and remote actuated blast closure systems and analyses of available test data. Recommendations are made concerning the various structural and mechanical design parameters. Existing designs are reviewed critically. Limitations of protection afforded by remote actuated designs are presented. It is concluded that maximum system reliability is obtained through the use of self-acting blast actuated valves which are not dependent upon external sensors and are suitable for multibursts. New valve concepts are developed and discussed, with designs presented which have inherent advantages over existing valves, for high-volumetric flow capacities and for combustion-type equipment. The delay path concept is described.

An appropriate method is developed for shock flow into plenums prior to valve closure. An orifice method of analysis is developed for flow into a chamber past a valve which is closing. These methods are checked against existing test data and proven to be conservative in all cases. Plenum chambers are sized to limit pressure build-up to 2 psi using the approximate method, for all existing valves studied. Recommendations are made for improvement in valve design and installation.

INTRODUCTION

General

Protection of the interior of structures from the air blast overpressure effects of nuclear blasts may be accomplished by using either remote actuated valves with flash, pressure, thermal or gamma radiation, or other sensors or by using self-acting blast actuated valves. Where large volumes of air must be handled during normal operation, positive closures are needed which under normal operating conditions do not unduly obstruct the air passage. These restrictions would increase pressure losses in the system, thereby increasing the ventilation power requirements. Two of the additional factors that must be considered before the selection of a given type, remote or self-actuated, are described below.

Reaction or Closing Time

Remote actuated valves are dependent upon external sensing devices. This eliminates certain problems but creates others. One of these considerations is arrival time. It can be seen from Fig. 1 that a closure time of about 200 msec is acceptable for a hardness of 300 psi for a 1-megaton burst but not for smaller weapons. Thus, an overall design criteria based on a 20-megaton weapon or greater may be conservative for structural design, shock mounting, etc., and still be inadequate for closure design, since the arrival time for a given pressure level for smaller weapons is much shorter than for larger weapons.

An idealized pressure-time curve of a nuclear detonation is given in Fig. 2 illustrating an ideal zero rise time, the decay of

*This paper is based in large measure on studies and reports prepared by Aimmann and Whitney, Consulting Engineers, for the RAND Corp., Contract No. 59-117; Mosler Safe Co., Hamilton, Ohio, under contract with the Office of Chief of Engineers, U.S. Army, Contract No. DA-49-129-Eng-434; and the U.S. Air Force Ballistic Missile Division (ARDC), Inglewood, California, AFMID Contract No. AF04 (647)-276 Suppl. 1.

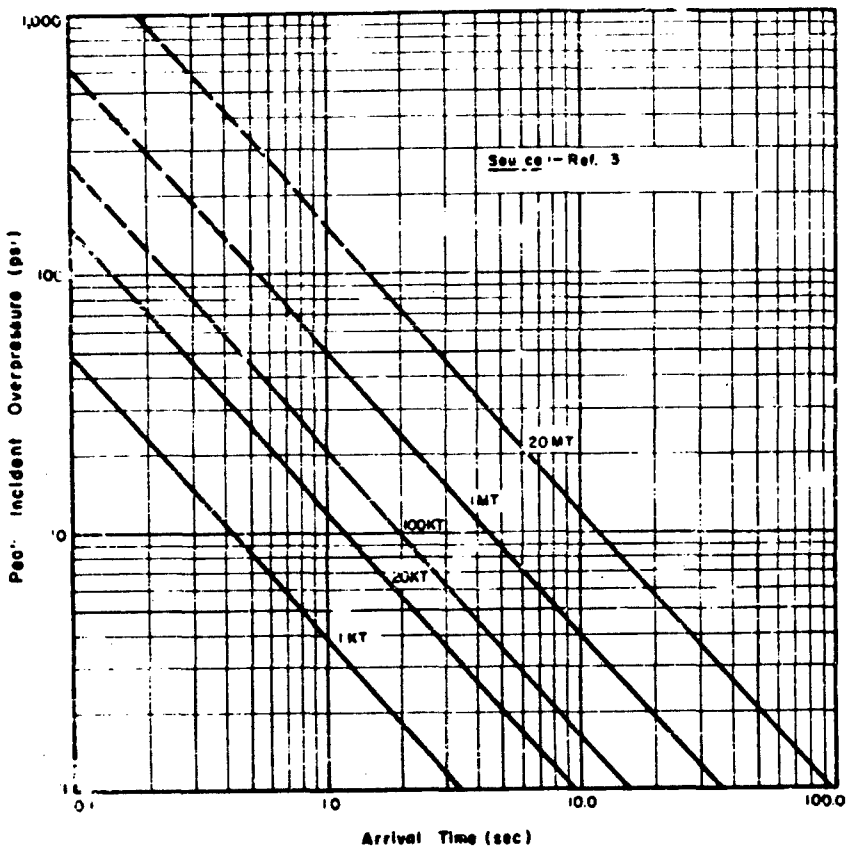


Fig. 1 - Blast wave arrival time (surface detonation)

positive pressure to zero and the negative phase which follows. It is seen that the positive phase duration is short compared to the negative phase. However, the negative phase pressures are small, the maximum pressure in this phase being 3.1 psig [2]. Duration of positive phase vs. peak incident overpressure for various weapon sizes is shown in Fig. 3, and duration of negative phase in Fig. 4.

A pressure sensing device cannot be placed too distant from a structure or a nuclear detonation between it and the structure will reach the protected area before the signal to close is received at the valve. Peak incident pressure vs. distance for air bursts and for ground bursts with different size weapons is depicted by Fig. 5. Using a pressure sensor situated a short distance

away from a structure, for a 1-KT burst at the 300-psig level, the device would be about 200 feet from ground zero. The arrival time is very short, less than 100 msec, as seen from Fig. 1 and closure time of the valve plus electrical delay time must be comparable to protect the structure. For small weapons, the delay time between sensor and valve would be approaching or greater than the arrival time as shown in Fig. 1 and the pressure sensor in the above example would not protect the structure. There is no point in using pressure sensors if the closing time is too long. For instance, at 200 psig with a 1-MT weapon, the arrival time is about 300 msec. At this pressure level the arrival time for a 20-KT weapon is less than 100 msec. Therefore, remote valves for which closing time is 100 msec would be satisfactory for

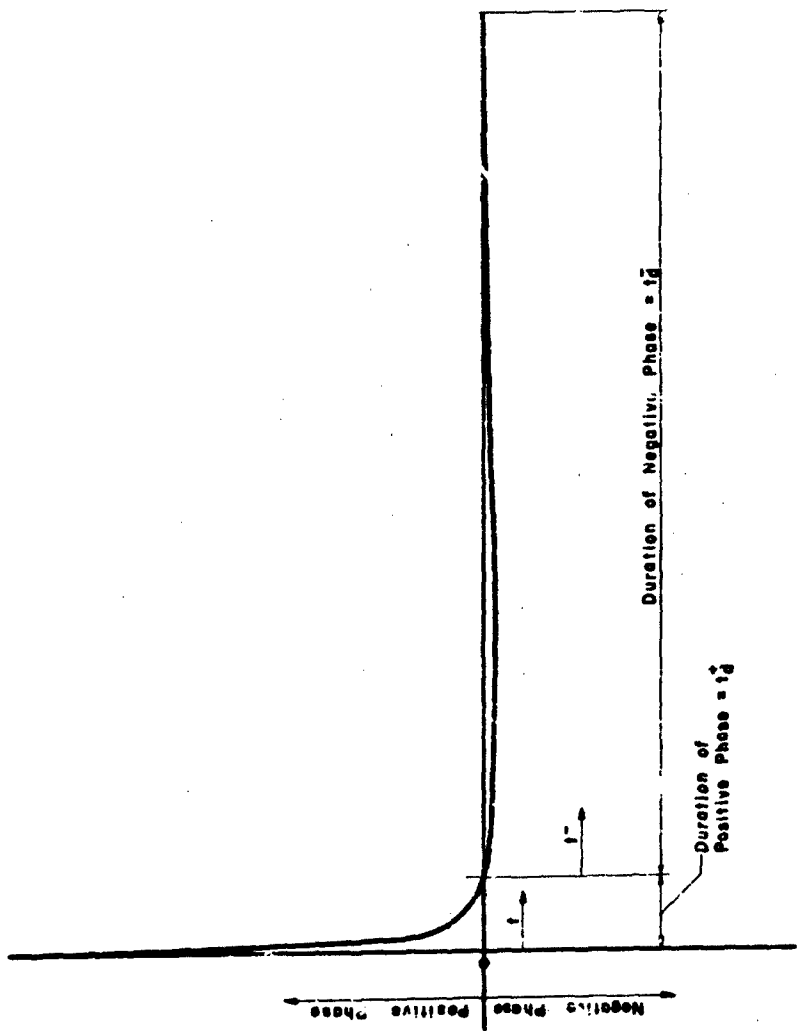


Fig. 2 - Idealized pressure-time curve

NOTE: CURVES INDICATED BY - - - - - WERE DERIVED FROM DATA
IN "NUMERICAL SOLUTIONS OF SPHERICAL BLAST VALVES" BY
H.L. BROWN.
SOLID LINE CURVES ARE REFERRED AS INDICATED AT THE RIGHT.

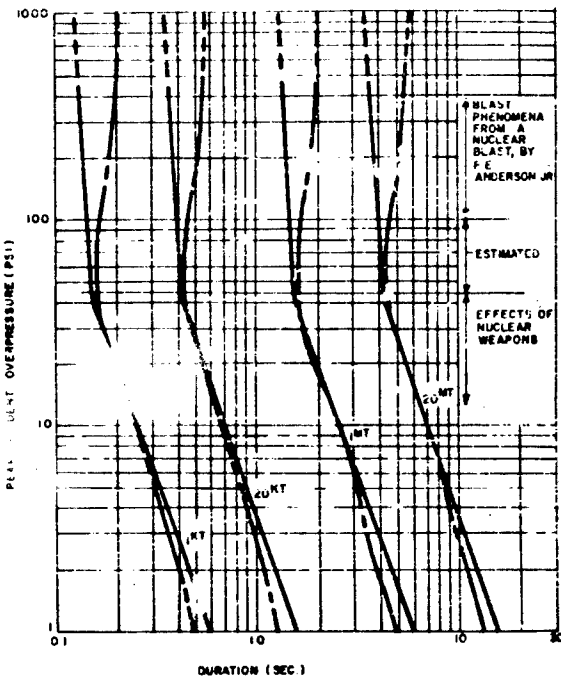


Fig. 3 - Duration of positive phase for ground burst

the megaton weapon, but unsatisfactory for the kiloton weapon.

Pressure sensors, spaced radially around an area to be protected, would receive the blast simultaneously with the structure for an overhead burst and consequently offer no protection unless a long tunnel or shaft intervenes between the entrance and the blast valves. A sufficiently long path must be provided also for pressure sensors placed at ventilation inlets before the valve to assure closure before blast wave arrival at the valve.

Remote actuated valves present problems of protection against multibursts and 'button up' time for combustion-type equipment installed within the structure. In addition to problems of hardenability and suitability for multiburst operation, it is often necessary for sensors to initiate reopening of the valves as soon as dangerous pressures have subsided. Again, allowable 'button up' time, dependent upon dissipation of heat loads and fresh air

requirements for the particular installation, must be considered before final design. Time delay caused by electrical and mechanical control equipment would add to this problem, if 'button up' time is critical.

Self-acting blast actuated valves overcome some of the disadvantages described previously and present other factors to be considered. Since the valves are closed by pressure, they are not dependent upon sensing devices for operation. They can be automatically reopened after passage of the positive phase, or latched closed during the negative phase if this is required. Blast actuated valves are suitable for multibursts, and will keep 'button up' time to a minimum if not latched. Of course, since blast actuated valves are closed by the blast, there is an inherent leakage problem to be considered due to the finite closing time. (This may be overcome by adding a delay path to the air intake.) Although this is in the order of milliseconds for most valves, sufficient flow to cause

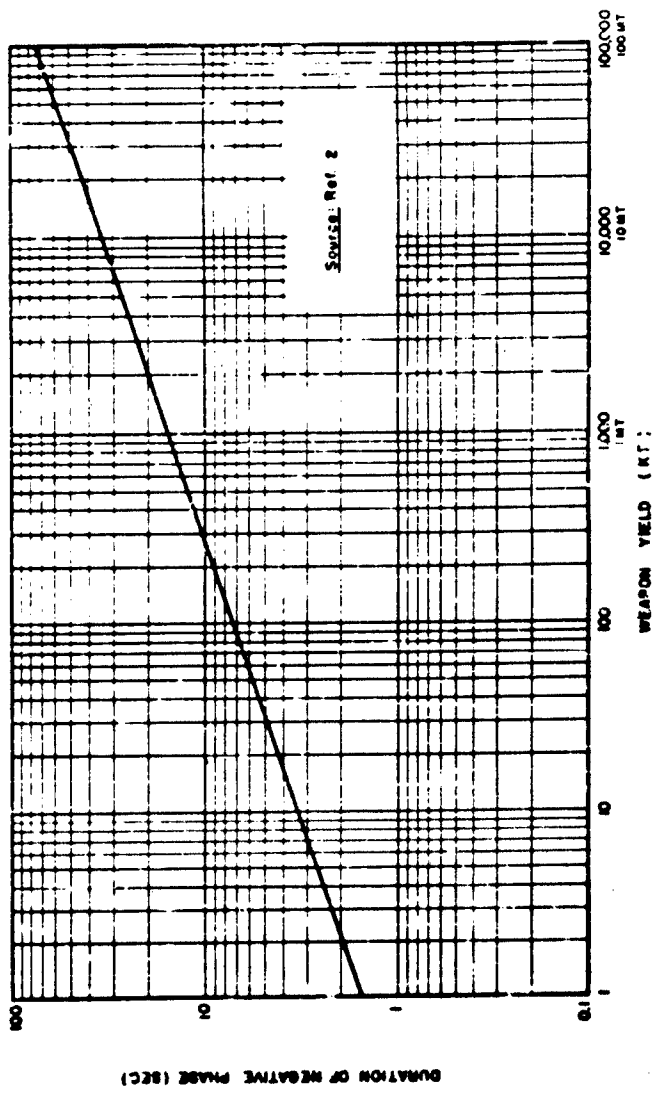


Fig. 4 - Duration of negative phase for ground burst

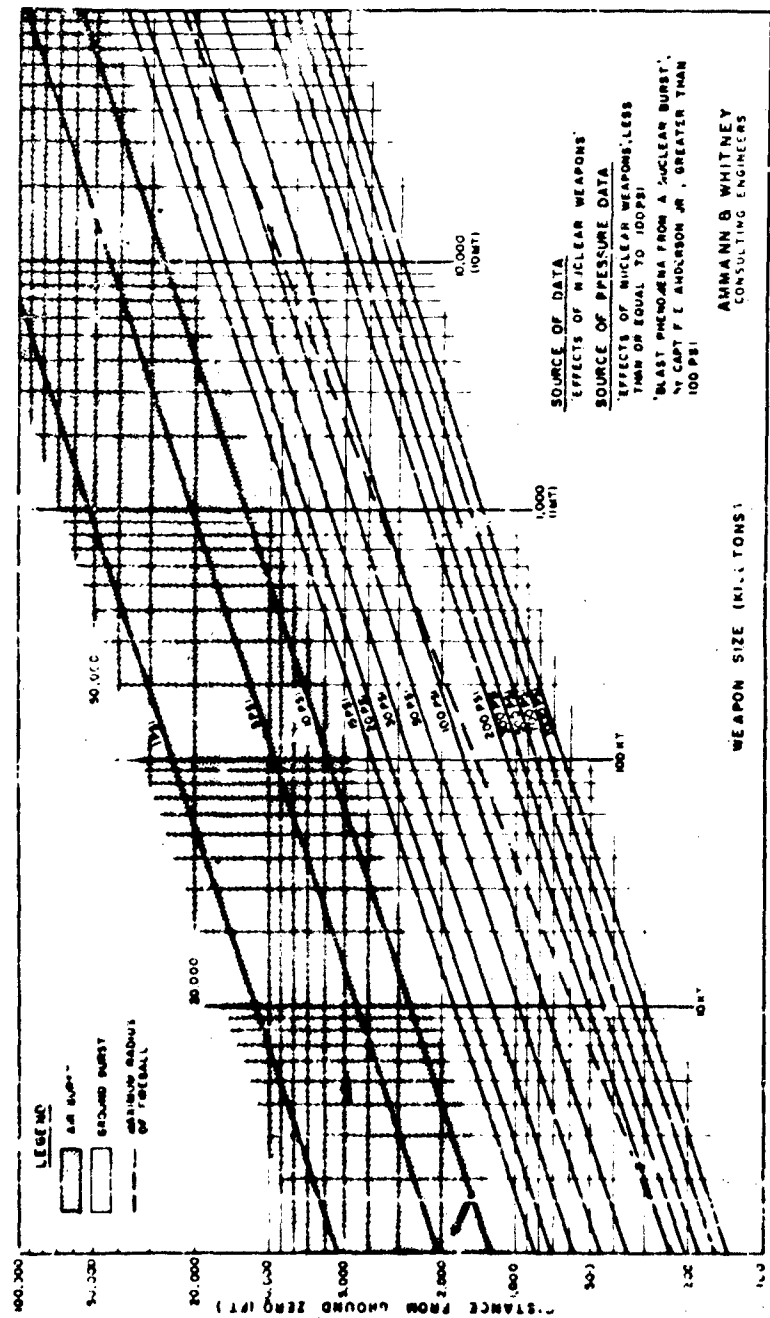


Fig. 5 - Peak incident pressure vs. distance

damage may pass the port openings for certain valve designs. Latching during the negative phase is necessary only if peak negative pressures cannot be tolerated within the equipment. Peak negative pressure vs. distance from ground zero for various size surface bursts is given in Fig. 6. Peak negative pressure that can be produced is approximately 3.1 psig. Effectiveness of closing at both high and low pressure ranges must therefore be checked for blast actuated valves. The ideal characteristics of a self-acting blast actuated closure device are as follows:

1. Instantaneous closure or no leakage during closure.
2. No rebound.
3. No leakage after closing.
4. Equal efficiency for all incident overpressures.
5. Complete operational reliability.
6. Complete structural reliability.
7. Minimum of moving parts.
8. Multiple shot capability.
9. Double action where necessary (negative phase latching).
10. Minimum volume and easy installation.
11. Long life, easy maintenance, and easy replacement.
12. Suitability for large range of normal flow with low head loss.
13. Low cost.

Although instantaneous closure is not physically possible, the actual closing time can be reduced sufficiently to obtain complete protection. This may be done by use of a time delay path in conjunction with a valve as described later in the section on Proposed New Designs, by increasing the activating overpressure force to moving mass ratio, decreasing the length of travel, permitting no deceleration during closure, and other methods. For a given valve the leakage pressure may be controlled by proper selection of plenum size. Rebound may be controlled by

dash-pot energy dissipation after closing. Leakage after closing may be eliminated by overclosure and sealing.

Air Volume and Heat

Load considerations

Outside air requirements for a facility powerhouse would consist of combustion air for the prime movers, and ventilation air for carrying heat away from mechanical and electrical equipment and for personnel requirements. Similarly, exhaust from the powerhouse would consist of exhaust gases from combustion equipment, such as diesel engines, and ventilation exhaust. If operation of the diesel-engine generators must be maintained during a nuclear attack, a critical heat problem may exist within the facility. This is dependent upon the net volume of the facility, heat load input from the prime movers and length of time for complete "button up." In many installations this problem may be eliminated by cutting off the fuel supply simultaneously with valve closure. If a powerhouse is considered to be completely "buttoned up" during a nuclear blast by using remote actuated blast valves and operation must be continuous, the diesel engine combustion air would be taken from within the powerhouse. Also, the diesel-engine exhaust gases and other heat sources would have to be discharged to the interior of the powerhouse shelter. The heat loads from the diesel engine and other sources all tend to increase the temperature and pressure of the confined air in the powerhouse. Therefore, temperature and pressure limitations of equipment within the "buttoned up" structure must be evaluated to ascertain reliability of operation during attack.

From the graphs presented it is seen that remote actuated valves with an activator sensitive to thermal or gamma radiation at the 2-psig incident pressure range from a 20-megaton weapon, would close 50 seconds before arrival of pressure and remain closed approximately 12 seconds during the positive phase for a "button up" time of 62 seconds, minimum. The "button up" time is increased by about 45 seconds if the negative phase duration is added, and total "button up" time would be 107 seconds in this case. Blast actuated valves, by eliminating the arrival time portion of "button up," remain closed only during the 12 second positive phase of the wave, if not latched open for negative phase protection.

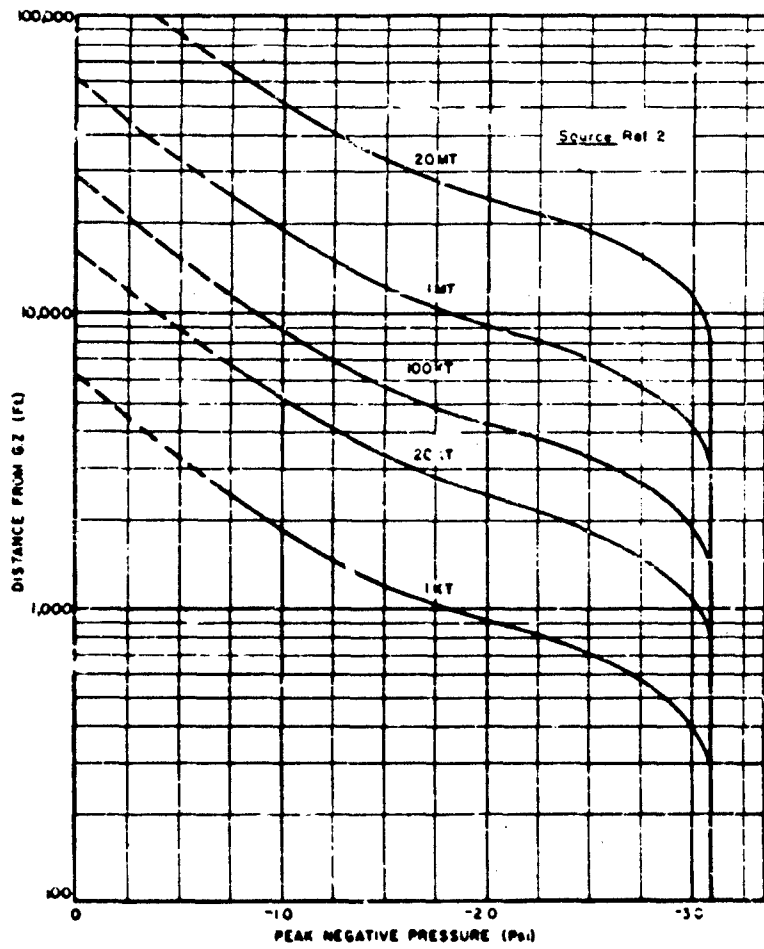


Fig. 6 - Peak negative pressure vs. distance

DESCRIPTION OF EXISTING BLAST VALVES STUDIED

General

Various blast valves have been developed during the past ten years. These closures are of two types, self-acting blast actuated and remote actuated.

For present self-acting blast actuated valve designs, closing time under blast conditions and the size of orifice will determine the volume of the expansion or plenum chamber behind the valve which is necessary to limit the pressure rise to any specified maximum value. The closing time for a poppet valve depends on the area and shape of the disk, the magnitude and distribution of pressures acting on the disk, the mass of moving parts, disk travel distance, and restraining or friction forces. Changes made with the objective of decreasing closing time may adversely affect the strength of the valve or resistance to normal air flow. A short closing time must be obtained by making the valve disk mass and disk travel as small as possible consistent with the low-pressure drop required under normal ventilating conditions. In addition to providing protection against the positive phase pressures, the valves should be latched or double-acting for protection against negative phase pressures where the installation is subject to damage from this effect. Although field tests of blast valves are described below, the reader is warned that caution should be used in the interpreting the effectiveness of valves from test results unless exterior pressure-time curves are available. The relationship between the interior and exterior peak pressures obtained from field tests on these valves may be misleading where the blast wave was nonideal. In tests where this was the case, the valve may have closed long before arrival of the peak pressure and at a pressure which was only a fraction of the peak.

E4 (M1) Valve

In 1950, at the U. S. Army Chemical Warfare Laboratories, development work in connection with the instrumentation of a CBR shelter for the Corps of Engineers at "Operation Greenhouse" [14] was initiated to develop a device which could protect the filter from blast effects. The device was designated the E1 valve (later M1) as shown in Fig. 7. At the normal air-flow rate of 300 cfm a light plate sustained by a spring permitted the air flow

to pass around the plate and through the perforations in the bed-plate. Under pressure, the flat plate seats on the bed-plate, sealing off the system to further flow. The E4 is equipped with flanges for interconnection with standard pipe (6-inch blast side, 5-inch protected side). This valve was successfully tested at "Operation Greenhouse" and was one of the earliest developments in this field. Following "Operation Greenhouse," work on antiblast closure devices was discontinued by the Chemical Warfare Laboratory. Soon after, the Office of the Chief of Engineers initiated a development program to assess the relative merit of other types of pressure reducing mechanisms such as rock grilles, mufflers, baffles, pipe tee, etc. These projected blast dampening mechanisms were partially evaluated on the shock tube at Aberdeen Proving Ground and field tested at the Nevada Proving Ground in "Operation Upshot Knothole." It was concluded that a quick closing closure valve would provide the best blast protection for a ventilation system. The data associated with the E4 valve is shown in Table 1. Late in 1954, the Chemical Corps was requested to equip two prototype Civil Defense Shelters in "Operation Teapot" [18]. The subsequent development work prepared one shelter as a nonmechanically ventilated and a second as a mechanically ventilated type. These shelters were evaluated at Nevada Proving Ground in early 1955. In the nonmechanically ventilated shelter protected by two E4 valves, which was subjected to a peak overpressure of 47 psi, pressure gauges both ahead of the filter system and in the shelter proper showed zero pressure readings. The E4 valves performed well in the mechanically ventilated shelter, which was subjected to a higher peak overpressure, in preventing damage to the blower motor, filter, elbow and air register, and the anti-back draft valves. The peak incident pressure in this case was 92 psi. Pressure rise in the shelter was again negligible. The valve disks in both of the shots as shown in Fig. 8, accelerated under precursors of approximately 20 to 25 psi and were in the closed position before arrival of the respective peak overpressures.

F19R1 Valve

In 1958, development of the E19 valve [8] was initiated by the Chemical Corps on the request of the Bureau of Yards and Docks, the objective being an antiblast valve having a rated flow of 600 cfm for use with pressurized types of CBR shelters. This valve is shown in Figs. 9(a) and 9(b). Additional design

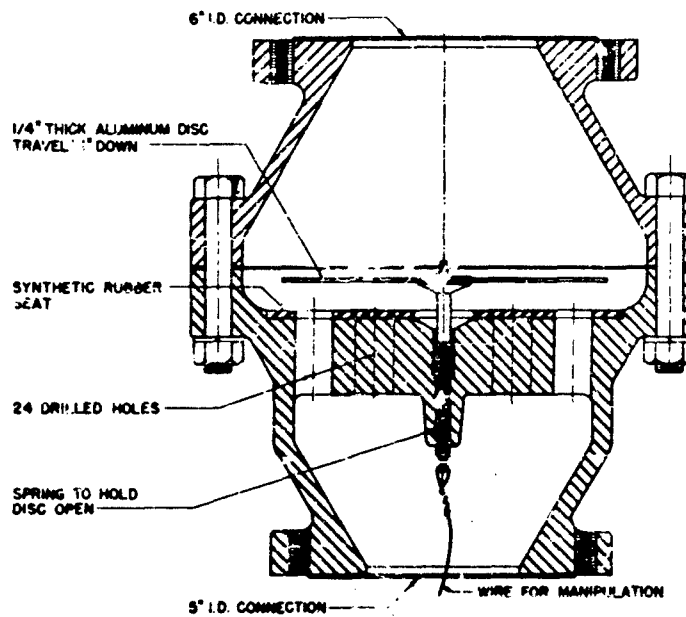


Fig. 7 - E4 valve

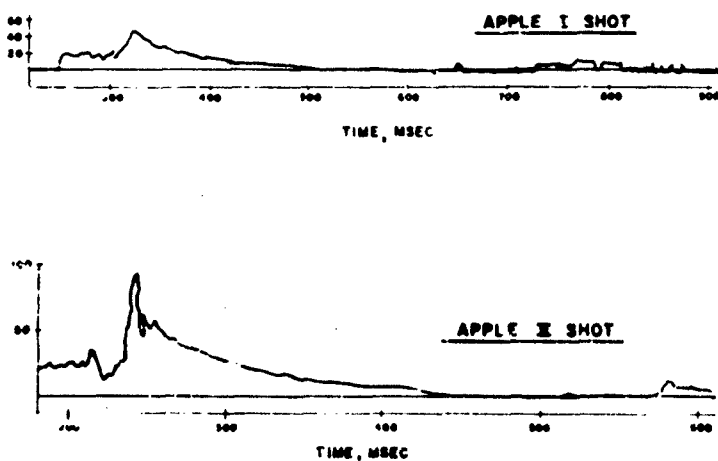


Fig. 8 - Pressure vs. time records in Operation Teapot for ground baffle
(gage i.o. P-1050-16)

TABLE 1
Blast Valve E4 (New M1)

(a) Design Criteria and Physical Data

Nominal Size:	6 inches	Max Side-On Blast Pressure:	100 psi
Valve Body:	(a) Overall Dimensions 16-1/4 inch x 16-1/4 inch x 17-1/16 inches	Rated Air Flow:	300 cfm
	(b) Weight - 330 pounds	Pressure Drop at Rated Flow:	1 inch w.g.
	(c) Material - Cast Steel	Inlet Area:	29.9 square inches
Disk:	(a) Diameter 10-5/8 inches (b) Travel - 1 inch (c) Material - Aluminum	Open Area Through Valve:	26.8 square inches
Weight of Moving Parts:	1 pound	Ratio Valve/Connection:	0.90
Seat Gasket Material:	Synthetic Rubber	Seat Opening:	18 holes, 1-1/4 inch diameter 6 holes, 1 inch diameter
		Protected Side-Duct Area:	20 square inches

(b) Field Tests. Summary of Recorded Data

Test*	Incident Pressure (psig)	Mounting Position	Protected Chamber (cu ft)	Max Pressure in Chamber (psig)
Greenhouse	530 (Av) 52.0 (Av) 14.25 (Av)	Vertical Vertical Vertical	5 5 5	12.6 8.48 2.45
Upsilon-Knothole	20.3 (Max)	Vertical	87	0.3
Teapot	47 (Max) 92 (Max)	Vertical Vertical	1900 (2 valves) 2000 (4 valves)	Negligible Negligible

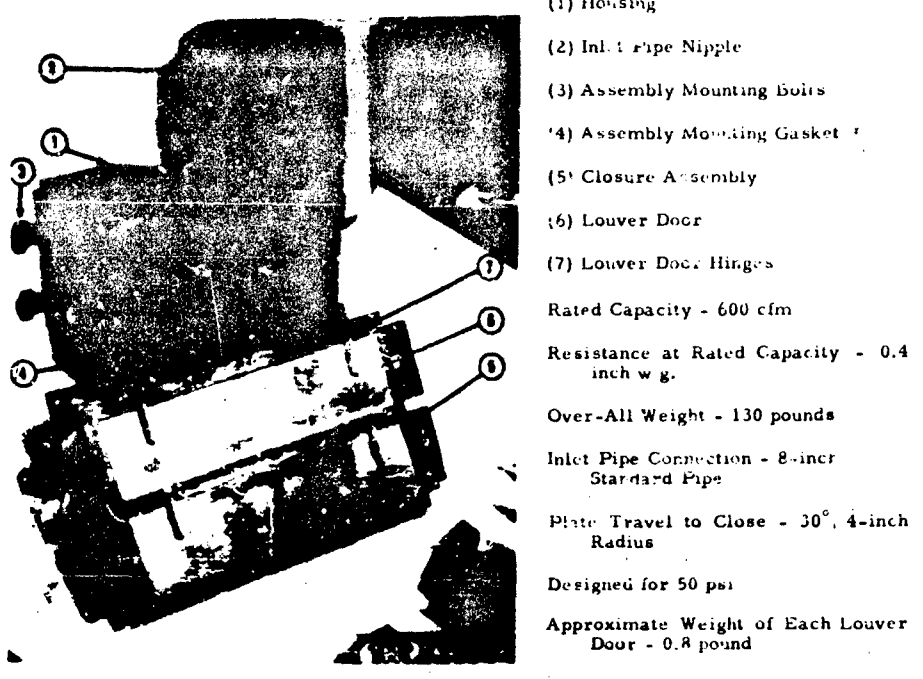
*Date and Location of Tests -
(1) 1951 Operation Greenhouse - Eniwetok
(2) 1953 Operation Upsilon-Knothole - Nevada
(3) 1955 Operation Teapot - Nevada

requirements of the Bureau of Yards and Docks were as follows:

1. Mode of Actuation - Blast actuated
2. Method of Reopening Following the Blast - Manual
3. Design Overpressure - 50 psi

4. Rated Flow of 600 cfm - Less than one (1) inch w.g.

Shock tube tests were conducted on the E19 by BRL at Aberdeen Proving Ground, and a single prototype was evaluated under field conditions in "Operation Plumbbob." The data associated with the E19 valve is shown in Table 2.



(a)

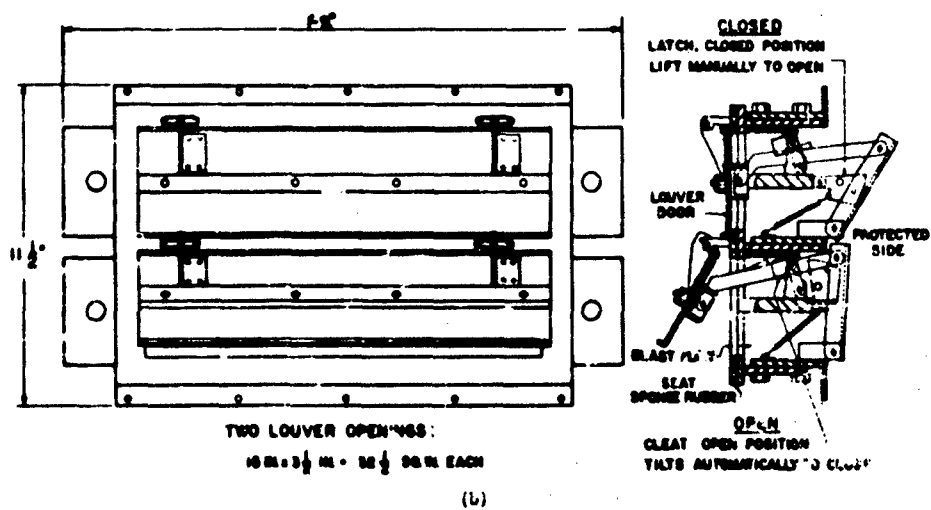


Fig. 9 - E19K1 valve

TABLE 2
Blast Valve E19R1
(E19 Valve, Predecessor to E19R1, with 30-Degree Door Opening)

(a) Design Criteria and Physical Data

Nominal Size:	8 inches	Seat Gasket Material:	Neoprene Sponge Rubber
Valve W/Housing:	(a) Overall Dimensions 21-1/4 inch x 18-5/8 inch x 17-3/4 inch (b) Weight - 130 pounds (c) Material - Steel	Max Side-On Blast Pressure:	50 psi
Louver Doors:	(a) Size - 2, 4 inch x 15-1/2 inch doors at 30 degrees (b) Travel - 2 inches plus (c) Material - Aluminum	Rated Air Flow:	600 cfm
		Pressure Drop at Rated Flow:	0.4 inch w.g.
Weight of Moving Parts:	(a) Size - 2, 4 inch x 15-1/2 inch doors at 30 degrees (b) Travel - 2 inches plus (c) Material - Aluminum	Inlet Area:	50.8 square inches
		Open Area Through Valve:	45.3 square inches
		Ratio Valve/Connection:	0.9
	1 pound per door approx.	Seat Opening:	90.6 inches
		Protected Side Duct Area:	unrestricted

(b) Field Test, Summary of Test Data Reported

Test	Peak Incident Pressure (psig)	Mounting Position	Protected Chamber (cu ft)	Closure Time (msec)	Max Pressure in Chamber (psi)
Plumbbob	64	Horizontal; 5 feet below grade; fed by 8-inch steel pipe and tee inlet	194	-	0.32

*Date and location of test - June 1957, Priscilla Shot (Operation Plumbbob), Nevada Proving Grounds.

OCDM Valves

The valves shown in Fig. 10 were designed and constructed by Arthur D. Little, Inc., under contract with Office of Defense and Civilian Mobilization and fabricated in 12-, 16-, and 24-inch nominal sizes. Data for these valves are given in Tables 3, 4, 5, and 6.

Adaptation of the OCDM valve for remote operation has been made by attaching a remote-operated pneumatic cylinder for

closing the valve prior to arrival of the blast. Closing may be accomplished by using a photoelectric relay exposed to the fireball or other sensing device for triggering an air cylinder. The air cylinder is designed to hold the valve closed against a negative pressure of 5 psi. One 16-inch OCDM valve was supplied for testing with a remote closing cylinder and a photoelectric sensor in Operation Plumbbob, and was horizontally mounted on the test cell wall at the 7.9-psig range attached to a pipe expansion chamber which was not vented

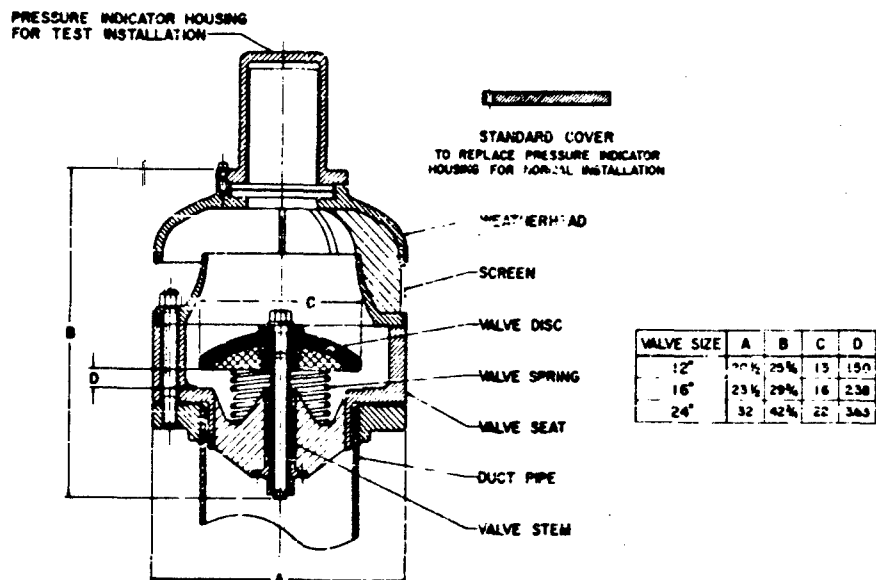


Fig. 10 - OCDM valve assembly

TABLE 3
Particulars of OCDM Valves

Nominal Size (inch)	Rated Air Flow (cfm)	Maximum Pressure Drop (in water)	Maximum Side-On Blast Pressure (psi)
12	600	1	100
16	1200	1	50
24	2500	1	50

to the cell interior. This valve started to close about 90 msec after the detonation and was fully closed in 140 msec. The pressure wave reached this valve approximately 180 msec after the valve had closed. Since the valve was successfully closed before blast arrival, there was no pressure rise in the chamber protected by this valve.

OCE Valve

The OCE blast actuated valve shown in Fig. 11 is essentially the same as the OCE remote actuated poppet, but without the remote devices and compression spring release for closing under emergency conditions.

Valve travel and basic valve parameters are identical. It is rated by the designers for 5000-cfm capacity with approximately 1-inch w.g. pressure drop, and may be used for intake or exhaust service. Although the valve has not been field tested it was briefly subjected to shock tube tests at the BRL Shock Tube Facility. Additional valve data are presented in Table 7.

The OCE remote actuated poppet shown in Fig. 12, was developed by the Corps of Engineers at approximately the same time as the blast actuated version and has been included in numerous installations. The valve is closed by the seating of a 16-inch diameter disk traveling through a distance of 4 inches.

TABLE 4
OCDM 12-Inch Blast Valve

(a) Design Criteria and Physical Data

Nominal Size:	12 inches	Max Side-On Blast Pressure:	100 psi
Valve Body:	(a) Diameter - 20.5 inches (b) Weight - 600 pounds (c) Material - Ductile Iron	Rated Air Flow:	600 cfm
Disk:	(a) Diameter - 13 inches (b) Travel - 1.5 inches (c) Material - Aluminum	Max Pressure Drop at Rated Flow (Test):	0.66 inch w.g.
Weight of Moving Parts:	23 pounds	Inlet Area:	55 square inches
Seat Material:	Ductile Iron	Open Area Through Valve:	65 square inches
		Ratio Valve/Connection:	1.18
		Diameter of Seat Opening:	10.5 inches
		Protected Side Duct Area:	113 square inches

(b) Field Test, Summary of Reported Data (Operation Plumbbob)*

Station No.	Peak Incident Pressure (psig)	Mounting Position	Protected Chamber (cu ft)	Closing Time (msec)	Peak Pressure in Chamber (psig)
FF 8097.04	8	Vertical	274	23	2.7

*Date 1957. Location - Nevada Proving Grounds.

TABLE 5
OCDM 16-Inch Blast Valve

(a) Design Criteria and Physical Data

Nominal Size:	16 inches	Max Side-On Blast Pressure:	50 psi
Valve Body:	(a) Diameter - 23.5 inches (b) Weight - 760 pounds (c) Material - Ductile Iron	Rated Air Flow:	1200 cfm
Disk:	(a) Diameter - 16 inches (b) Travel - 2.38 inches (c) Material - Aluminum	Max Pressure Drop at Rated Flow (Test):	0.9 inch w.g.
Weight of Moving Parts:	31 pounds	Inlet Area:	114 square inches
Seat Material:	Ductile Iron	Open Area Through Valve:	125 square inches
		Ratio Valve/Connection:	1.07
		Diameter of Seat Opening:	13.8 inches
		Protected Side Duct Area:	182 square inches

TABLE 5—CONTINUED

(b) Field Test, Summary of Reported Data (Operation Plumbbob)*

Station No.	Peak Incident Pressure (psig)	Mounting Position	Protected Chamber (cu ft)	Closing Time (msec)	Peak Pressure in Chamber (psig)
FF 8007.02	63	Vertical	274	31	4.6
FF 8007.05	8	Vertical	274	35	4.4

*Date - 1957. Location - Nevada Proving Grounds.

TABLE 6
OCDM 24-Inch Blast Valve

(a) Design Criteria and Physical Data

Nominal Size:	24 inches	Max Side-On Blast Pressure:	50 psi
Valve Body:	(a) Diameter - 32 inches (b) Weight - 1620 pounds (c) Material - Ductile Iron	Rated Air Flow:	2500 cfm
Disk:	(a) Diameter - 32 inches (b) Travel - 3.63 inches (c) Material - Aluminum	Max Pressure Drop at Rated Flow (Test):	1.13 inches w.g.
Weight of Moving Parts	91 pounds	Inlet Area:	228 square inches
Seat Material:	Ductile Iron	Open Area Through Valve	264 square inches
		Ratio Valve/Connection:	1.16
		Diameter of Seat Opening:	20 inches
		Protected Side Duct Area:	424 square inches

(b) Field Test, Summary of Reported Data (Operation Plumbbob)*

Station No.	Peak Incident Pressure (psig)	Mounting Position	Protected Chamber (cu ft)	Closing Time (msec)	Peak Pressure in Chamber (psig)
FF 8007.03	63	Vertical	274	58	16.9
FF 8007.06	8	Vertical	274	53	2.0

*Date - 1957. Location - Nevada Proving Grounds.

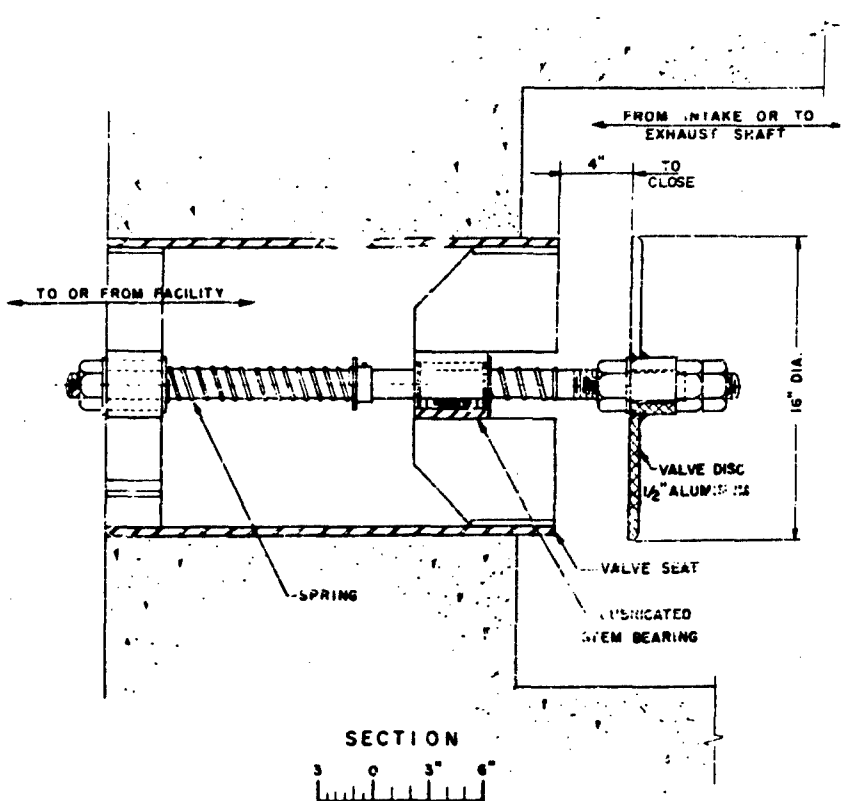


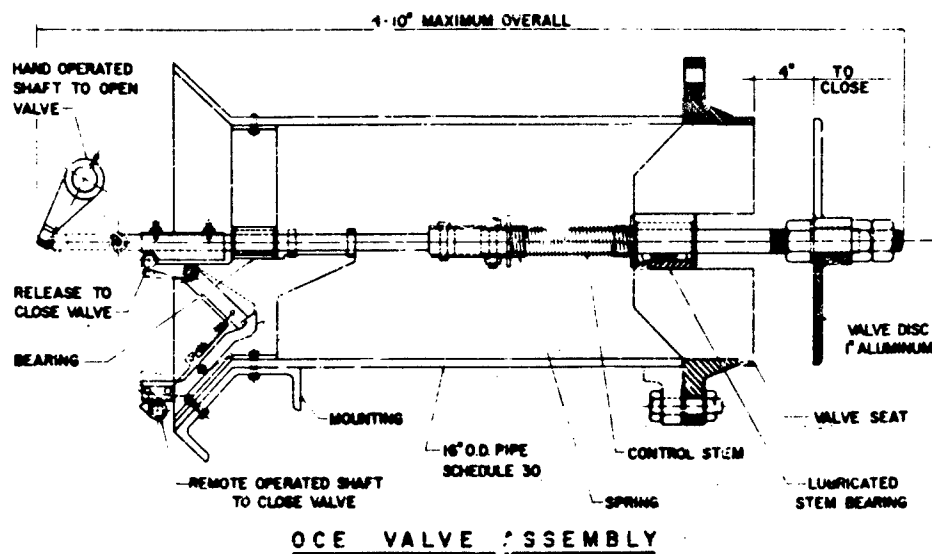
Fig. 11 - OCE blast actuated valve

TABLE 7
OCE Blast Actuated Valve

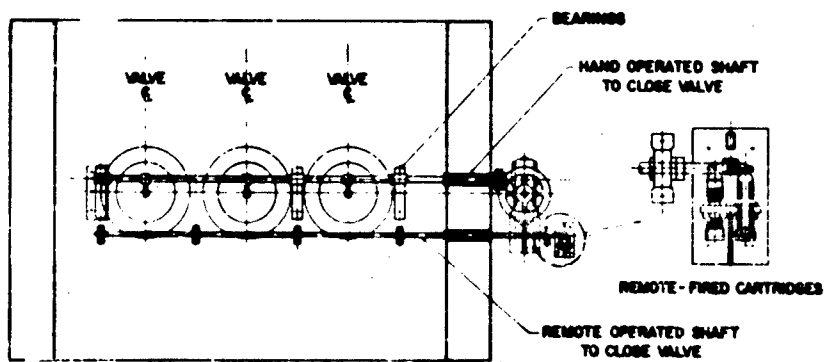
(a) Design Criteria and Physical Data

Nominal Size:	16 inches	Max Side-On Blast Pressure:	-
Valve Body:	(a) Diameter - 16-inch nominal (b) Weight - - (c) Material - Steel	Rated Air Flow:	5000 cfm
Disk:	(a) Diameter - 16 inches (b) Travel - 4 inches (c) Material - Aluminum	Max Pressure Drop at Rated Flow (Stated):	1 inch w.g.
Weight of Moving Parts:	32 pounds	Inlet Area:	191.6 square inches
Seat Material:	Steel	Open Area Through Valve:	147.5 square inches
		Ratio Valve/Connection:	0.77
		Diameter of Seat Opening:	13.5 inches
		Protected Sid Duct Area:	182 square inches

(b) Field Test: None.



(a)



OCE VALVE INSTALLATION

(b)

Fig. 12 - OCE remote actuated valve

Several valves in battery may be used to protect large interior volumes, as shown in Fig. 12(b). Triggering of the valves to initiate closing is accomplished by explosive capsules fired from a remote nuclear attack detection control station. The impulse of the charge provides sufficient torque to rotate the cam-shaft, thereby tripping the locking mechanism which maintains the valves in their open positions. This action simultaneously releases the compression of the closure springs, seating the valve disks. A test performed by the manufacturer determined closing time of the remote actuated valve to be 20 msec. Hand operation may be accomplished through reduction gear for opening and closing.

Bureau of Yards and Docks - AMF Valve

As a result of a feasibility study conducted for the Bureau of Yards and Docks [9], the American Machine and Foundry Co. has developed a remote actuated closure device, Fig. 13, triggered by the flash of the nuclear detonation. Valves are rated from 2200 to 30,000 cfm, with these sizes varying from 1 foot to 4 feet in diameter. Upon being triggered, the electronic circuitry fires an explosive charge. This, in turn, actuates a pneumatic cylinder which affects closing by pulling the head tight against a gasketed seat for sealing against positive and negative phases of the blast. Valve closure times are given as 500 msec, with opening times in the order of 3 to 5 milliseconds. There is an automatic cycling device which is designed to permit three cycles of the closure system in the event of a multi-weapon attack. The closures were designed specifically for installation in unmanned shelters.

Office of Chief of Engineers - Mosler Safe Co. Valve

The blast valve shown in Fig. 14, which was developed for the Office of Chief of Engineers, U.S. Army, under Contract No. DA 49-129-Eng.-434, is a self-acting blast actuated design, closed by the blast. It consists essentially of two sets of 1/2-inch diameter stainless steel cylinders 11-3/4 inches long, one set being movable and the other set stationary. Under impulse of a shock wave, the movable cylinders close against resistances of light springs and effect a seal when they mesh with the stationary set. Sections may be added or removed to alter the rated air-flow capacity of the valve. The closure for which static air-flow tests yielded 550 cfm at 1-inch water,

was shock tube tested at the BRL Shock Tube Facility in 1959 [12,13]. Additional data for this valve are given in Table 8.

Järn and Plåt Valve

The principal design characteristics of the Swedish blast valve design are illustrated in Fig. 15. These valves are presently manufactured by Järn and Plåt in Sweden in 4-inch, 8-inch, and 14-inch sizes. The design side-on pressure rating is 280 psi. Rated air flows are 150, 600, and 1750 cfm, respectively, at 1 inch w.g. Fig. 15(a) shows a longitudinal section of the valve fixed in a reinforced concrete wall. Fig. 15(b) shows a cross section of the enlarged portion of the valve with the conical valve disk removed. Normal ventilation air flow can pass the valve in either direction, but the valve must be placed in such a way that the blast wave enters through a special inflow channel to directionalize blast impingement against the disk. The valve disk is mounted on a stationary shaft and is kept in the desired open position for ventilation purposes by means of two helical springs mounted around the shaft on either side of the disk. In passing the inflow channel, the incident blast wave is directed towards the center of the valve disk and this effect is strengthened by the concave shape of the disk. Under action of a blast wave the light-weight disk will accelerate towards the strong grained seat which has closely spaced bars. During the negative phase of the blast the conical valve disk is sucked outwards and reseated against the outer oblique wall of the enlarged channel as shown in Fig. 15(a). When the blast effect has ceased, the valve disk is returned to its initial position by the spring forces.

WS-107 A-2 Technical Facilities Remote Actuated Valve

In Fig. 16 is shown another type of remote actuated valve that has been developed for large flow capacities, the valve with dimensions as shown being capable of handling 35,000 cfm. The valve is closed upon release of the spring-tensioned stops upon signal from the sensor, the action of which relieves compression of the contained spring to seat the valve behind the secondary stops. It is reopened pneumatically after passage of dangerous overpressures.

D. Evaluation of Results

Available experimental (field or shock tube) data on the valves discussed in this paper

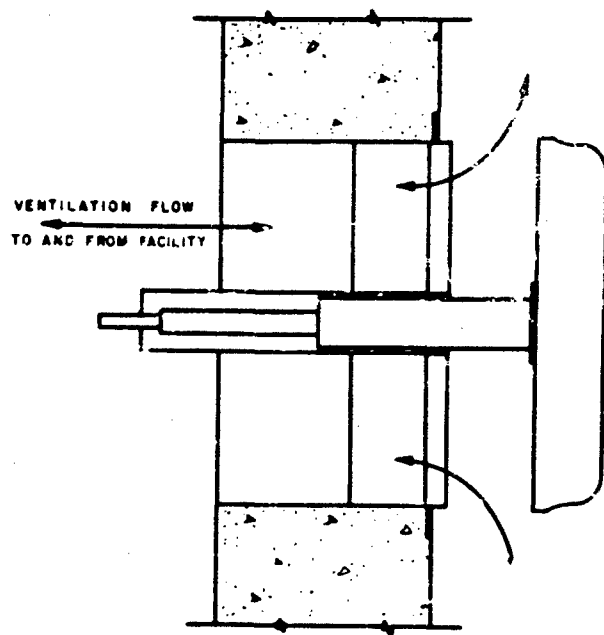


Fig. 13 - AMF protective blast closure device (remote actuated)

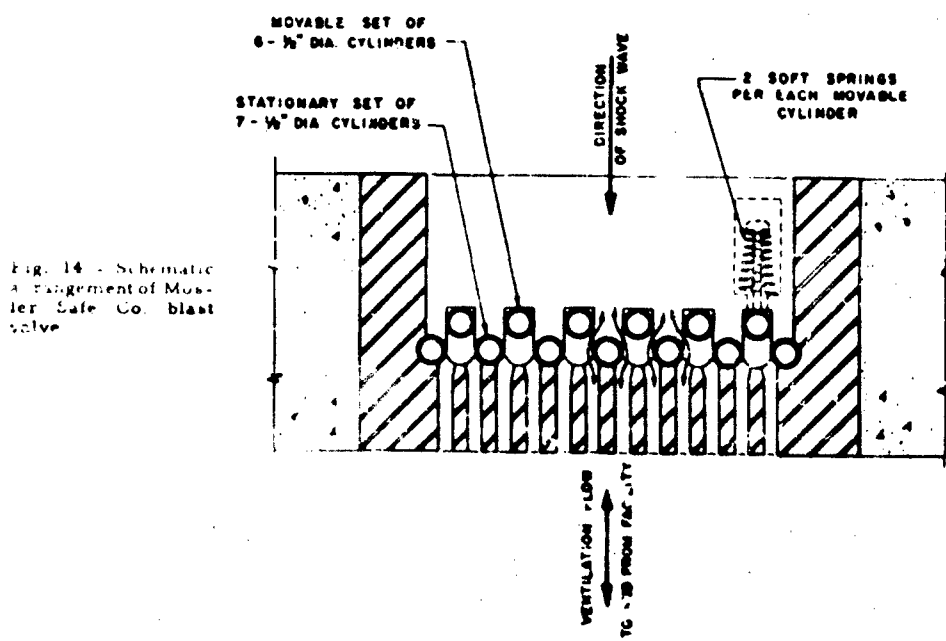


Fig. 14 - Schematic arrangement of Mueller Safe Co. blast valve

TABLE 8
Mosler Safe Co. Design ' Valve

(a) Design Criteria and Physical Data

Nominal Size	-	Weight of Moving Parts:	1/2 pound per cylinder, approximately
Valve Body:	(a) Overall Diameter - -	Design Side-On Blast Pressure:	100 psi
	(b) Weight - -	Rated Air Flow:	550 cfm
	(c) Material - Steel	Pressure Drop at Rated Flow (Test):	1 inch w.g.
Moving Cylinders:	(a) Size - 1/2 inch diameter nominal x 11-3/4 inches long (b) Number - 6 (c) Travel - 1/2 inch (d) Material - Stainless Steel	Inlet Area:	22.4 square inches
		Open Area Through Valve:	22.5 square inches
		Ratio Valves/Connection:	1.01

(b) Field Test. None.

were investigated. While these data were quite limited in most cases in quantity and/or scope, they provided the source of information or basis for development of the design method developed from the study. Although nuclear field test results over a range of pressures were lacking in most cases, good correlation was obtained with data available. Some of the valves have never been field tested but have been subjected to a limited shock tube evaluation. While the results of the shock tube tests indicate certain trends in valve behavior, the short durations obtained in experimentation were often insufficient to complete closure. Temperature effects and wave-shape peculiarities of a nuclear blast would tend to limit use of the shock tube results as proof tests. Often the intent of the shock tube or field evaluation was for purpose other than a subjective test of the valve itself, and therefore variables were introduced or data omitted which prevents rigorous analysis of valve behavior.

The Plumbbob test of the OCDM valves [16] provides the bulk of usable valve test data available for a reasonably comprehensive analysis. Included in these data were the tabulated pressure-time records for various outside blast line, hood, and chamber gages, and the recorded time-displacement gage records of valve stem movement. It was then possible to reconstruct the complete valve

history for the records available, although gages at several stations which would have been useful to the analysis had failed or indicated only peak pressures. Using an orifice analysis developed by the study, the measured pressure build-ups in the chambers were checked quite accurately.

Valve disk displacement gage readings were plotted vs. time for the duration of the valve closing cycle. The velocity and acceleration of the valve disk vs. time, as portrayed by the displacement curves, were not indicative of uniform motion and would be represented by complex equations, at best. Therefore, the velocity and acceleration diagrams were constructed by a method of graphical differentiation. Interpretation of the curves may be undertaken by considering an increase in slope of the tangent to the displacement-time diagram as representing an increase in velocity and, conversely, a decrease in slope as representing a velocity decrement. Constant velocity is indicated by a straight line on the displacement curve inclined to the axis of abscissas, and this will be considered to be the case between given data points. On the velocity-time diagram, no motion would be represented by a "straight" line parallel to the axis of abscissas. For constant acceleration or constant retardation the displacement-time curve is a parabola, the velocity-time curve is a straight line inclined away from

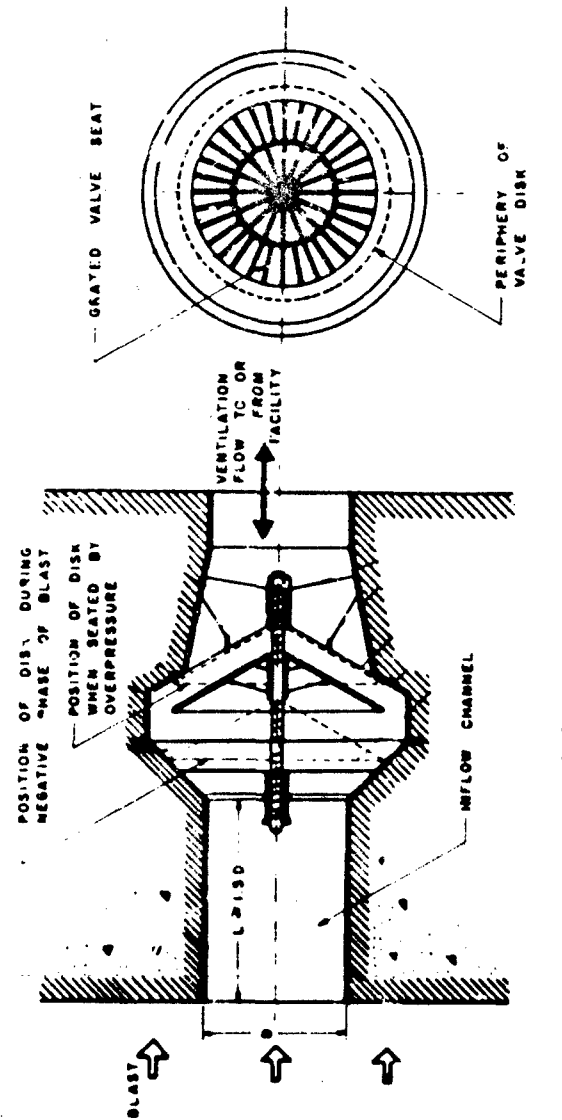


Fig. 15 - Swedish blast valve (Jär. and Väg)

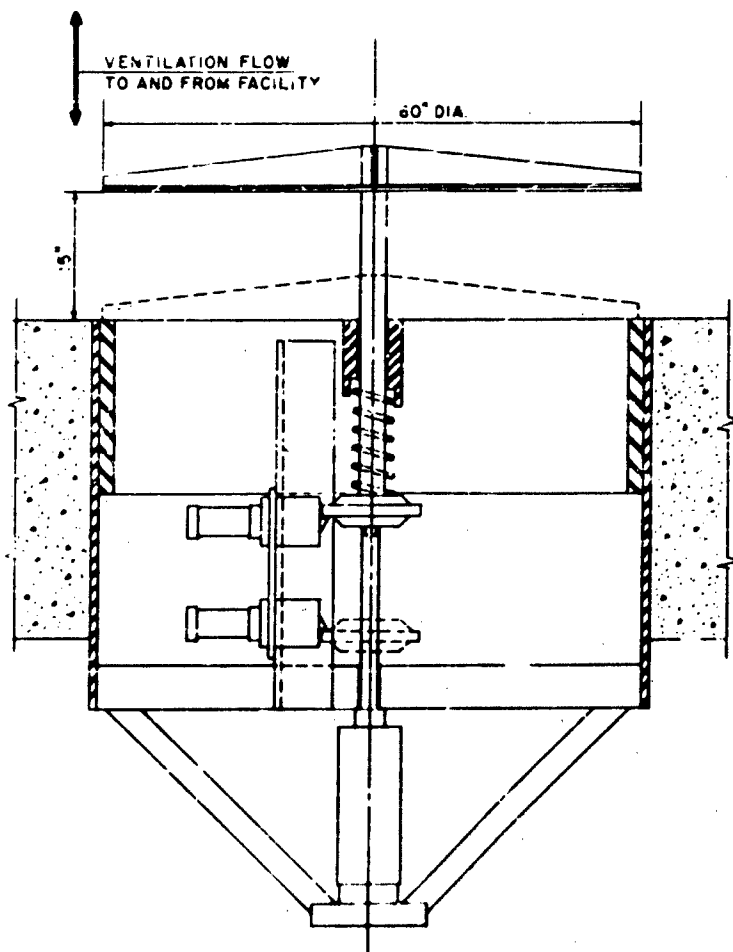


Fig. 16 - Large capacity spring-closing valve (35,000 cfm)

or toward the abscissa depending upon whether the velocity increases or decreases, and the acceleration-time diagram is a straight line parallel to the abscissa.

The displacement-time curves (Figs. 17 and 18), are for the 24-inch OCDM valve situated at the 63-psig overpressure range. Figure 19 is the recorded blast line pressure curve for this overpressure range. The valve was closed in the first phase due to a precursor with an incident pressure of approximately 12 psig which preceded arrival of the 63-psi peak overpressure. It is seen from Fig. 17 that the valve was closed 60 msec after arrival of the blast. However, several milliseconds thereafter, the outside overpressure curve dipped practically down to zero and leakage past the valve which had pressurized the chamber downstream to approximately 12 psig, caused the valve to reopen about half way. After the valve had traveled part of this distance the dip in the precursor ended and the valve decelerated to a stop. Then the outside overpressure rose nearly instantaneously to the 63-psi level, reclosing the valve at 108 msec (Fig. 18). As a result of the reopening and secondary

closing, final measured chamber pressure reached 16.9 psig. Calculated velocity vs. time diagrams are shown in Figs. 20 and 21 and acceleration vs. time diagrams in Figs. 22 and 23. Valve acceleration in the final interval rose to nearly 18,000 ft per sec² in the second phase diagram (Fig. 23). In this instance, the valve disk which had been in motion, accelerated in excess of that possible as a 2.5% of the apparent pressure differential. (The peak reflected pressure measured in the hood was 122 psig.) The maximum calculated velocity, the magnitude of which was approximately 50 ft per sec, was attained during the second phase (Fig. 21). The orifice analysis, upon application, yielded 16.0-psig maximum pressure build-up in the chamber, using a step-by-step procedure for the entire cycle of operation. This is in good agreement with 16.9-psig pressure actually recorded (peak pressure only obtained).

The 16-inch OCDM valve installed vertically at the 63-psig range was placed in a chamber next to the 24-inch valve. This valve actually closed in 29.5 msec (Fig. 24), and pressure in the chamber rose 1.45 psig at the

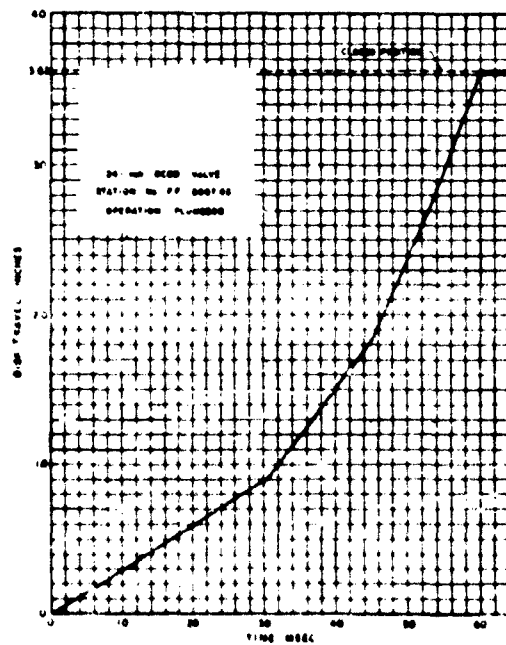


Fig. 17 - Displacement-time diagram (first phase)

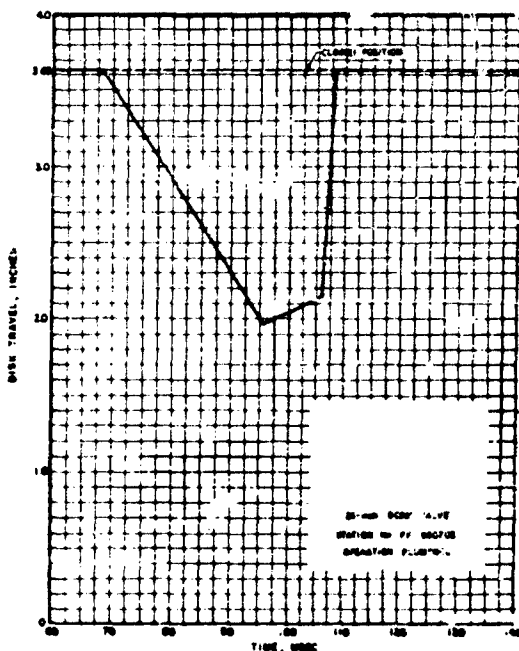


Fig. 18 - Displacement-time diagram (second phase)

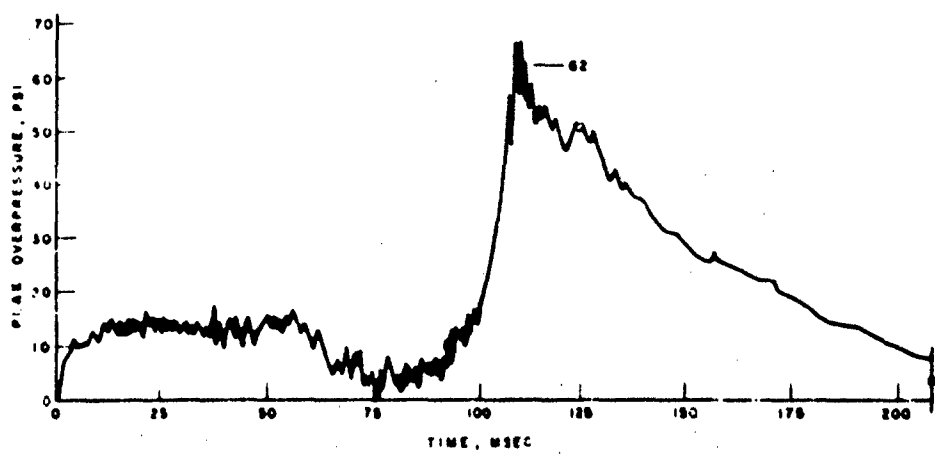


Fig. 19 - Main blast line overpressure curve, station No. 9041.00 - Gage No. 959, Shot Priscilla

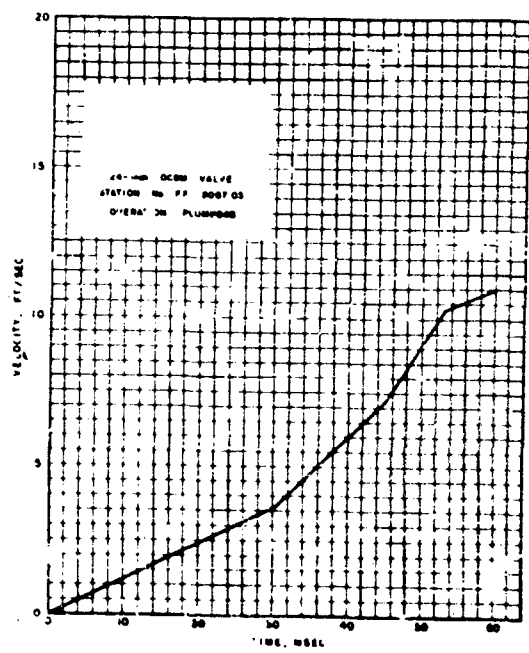


Fig. 20 - Velocity-time diagram
(first phase)

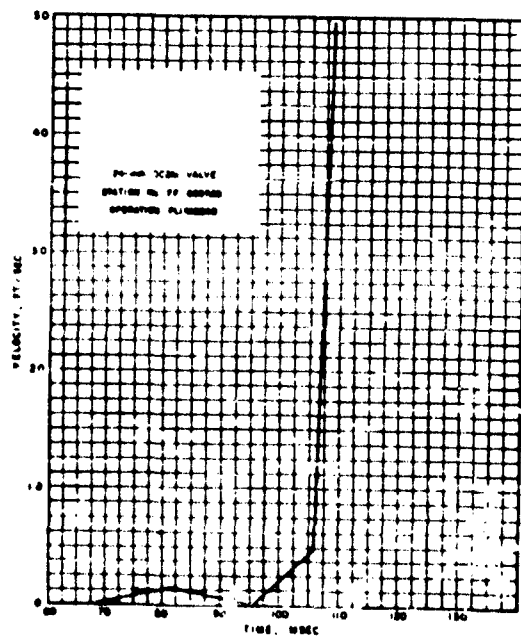


Fig. 21 - Velocity-time diagram
(second phase)

Fig. 22 - Acceleration-time diagram
(first phase)

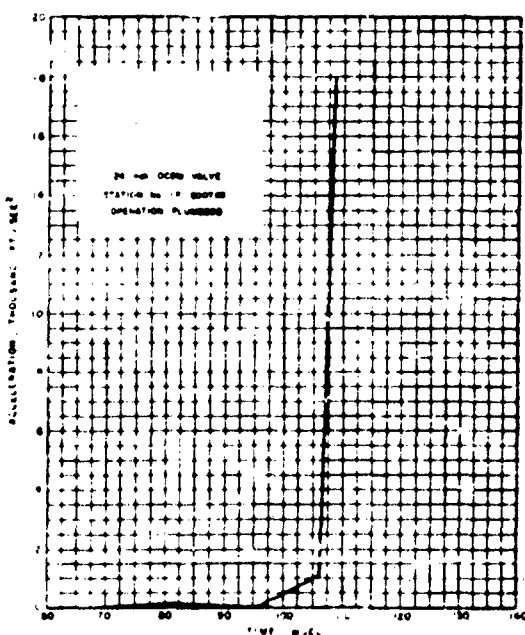
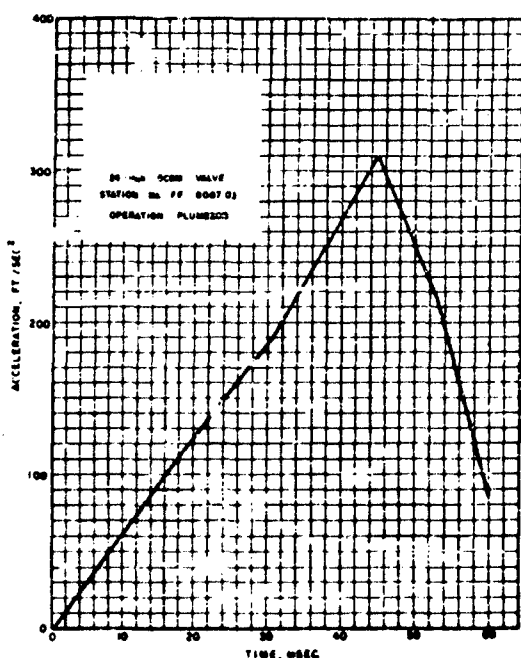


Fig. 23 - Acceleration-time diagram
(second phase)

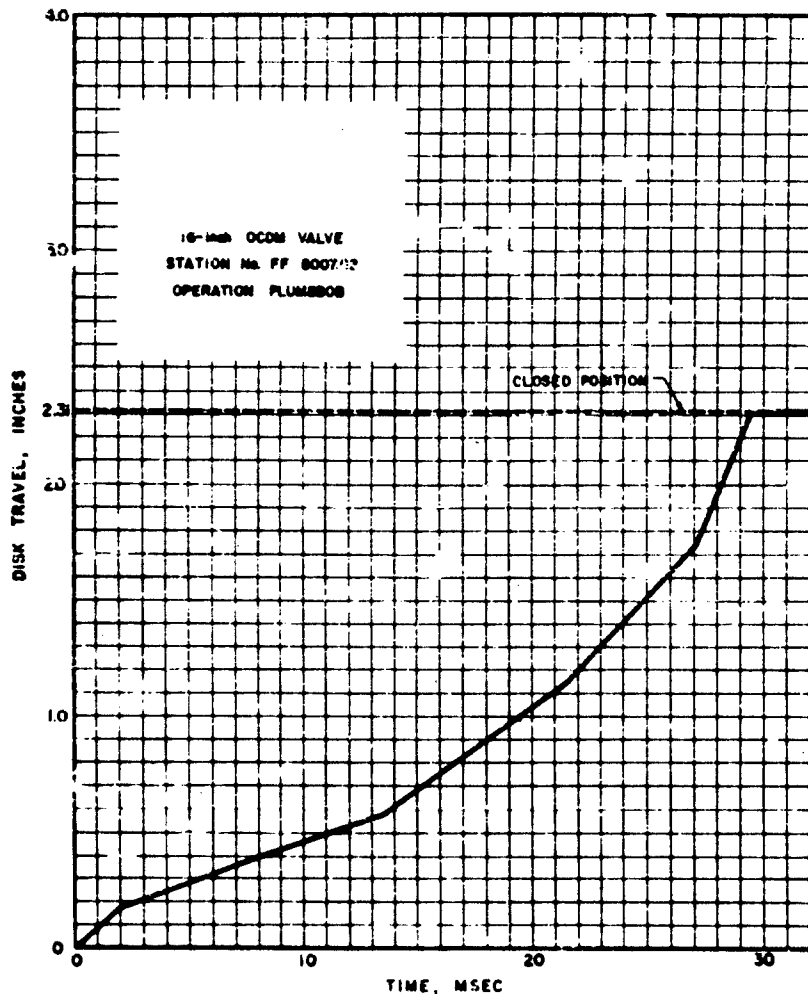


Fig. 24 - Displacement-time diagram

end of this interval (data from pressure-time chamber gage record). The velocity-time diagram for the valve closing is shown by Fig. 25. If the valve had continued its initial acceleration after the first two msec, as depicted in Fig. 26, closure would have been effected in one-half the actual time, or less. Calculated pressure increase for the above interval was 1.38 psig. However, the pressure-time chamber record indicates that pressure continued to increase after the valve had closed and actually reached a maximum value of 4.71 psig, 243 msec after the initial overpressure

in the chamber. This valve or the installation was, therefore, defective in sealing the chamber which was not isolated from the blast after closure in 29.5 msec.

The same OCDM valves used at Plumbbob were removed and relocated for the Hardtack [17] tests. It was then discovered that a machining difficulty during manufacture of this valve had prevented the disk from sealing. This would account for the chamber being pressurized during the first 243 msec of the positive phase and for the maximum pressure recorded.

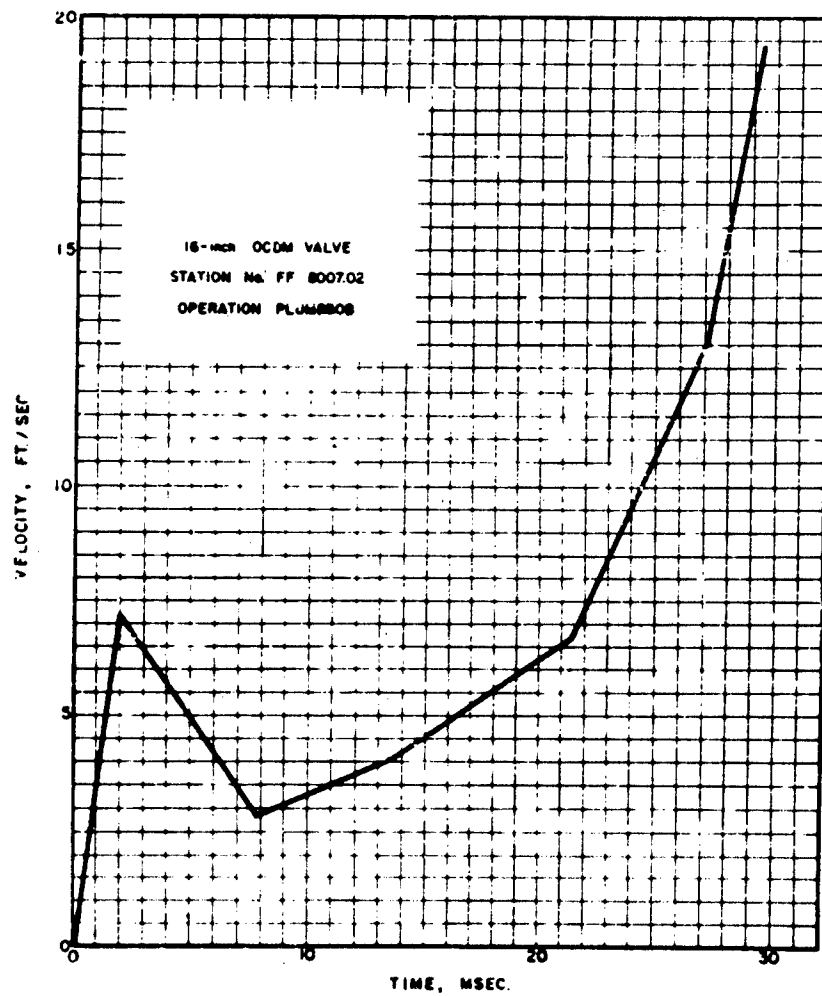


Fig. 25 - Velocity-time diagram

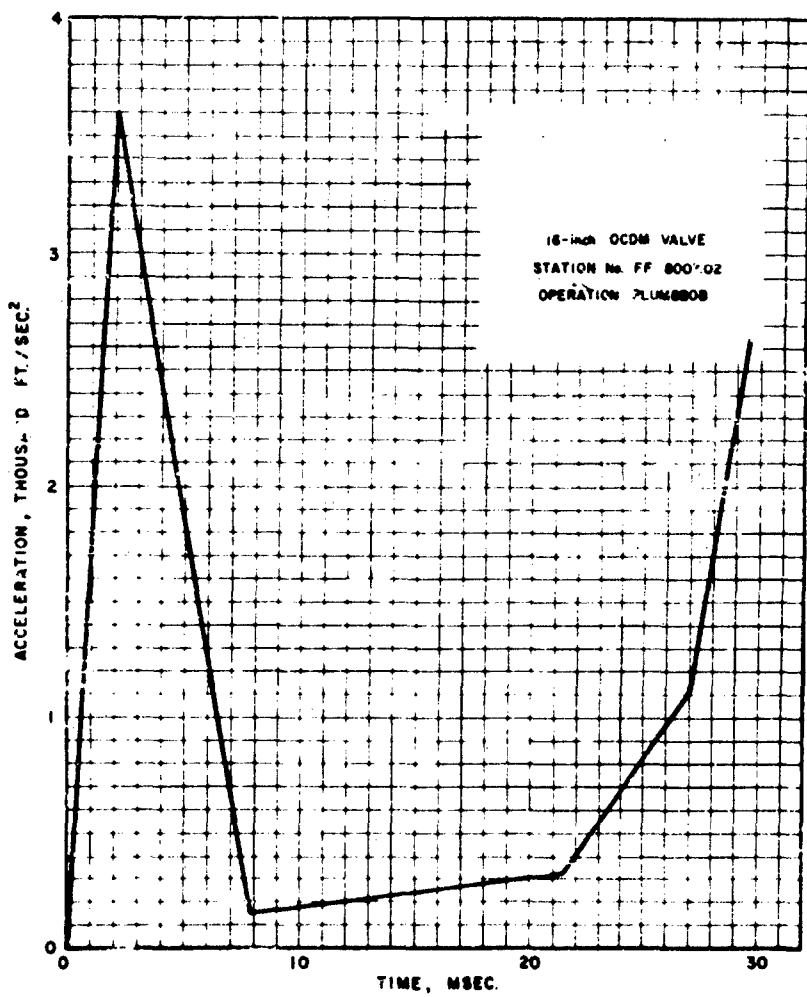


Fig. 26 - Acceleration-time diagram

The E4 antiblast closure was initially field tested in 1951 at Operation Greenhouse [14]. Valves were installed below ground at various pressure ranges, each protecting a 5-cubic foot chamber. The air inlet was a standard 300-pound 6-inch pipe tee with the two open ends parallel to the ground. The vertical connection was attached by a standard pipe nipple and flange to the inlet of the anti-blast closure. A standard 6-inch pipe nipple and flange were bolted to the underside of the surge tank cover immediately beneath the closure unit. There were holes in the wall of this nipple to permit air flow to the chamber. Only peak outside overpressure and peak pressure inside the chamber were recorded for the valve stations. Valve closing times and pressure-time data at the stations were not recorded. Recorded field data are given in Table 9 together with our calculated closing time.

Overpressures considered in the duct impinging on the valve disk were 50 percent of the average recorded peak line pressure value (see discussion below for "Upshot-Knothole Test"). The above results indicate that the E4 valve was closed by effective pressures of magnitude equal to reflected pressure. Stations 6102 and 6103 were checked using the orifice analysis for inflow to the chamber, and satisfactory agreement was obtained using 50 percent of the average line pressure value. At Station 6101, located within the fireball, overpressure varied considerably (from 340 to 720 psi) along the two measured lines of pressure instrumentation, between which the

closure was placed. At this high-overpressure range, the pressure-time history at the valve is essential for an analysis to determine closing time and inflow to the chamber. In view of the wide variation between the two blast line readings, the use of average blast line pressure may be seriously in error. Consequently, closing time and inflow were not computed for the valve at station 6101. The E4 valve was then field tested in 1953 at Operation Upshot-Knothole. One closure was installed below a 6-inch tee inlet and protected a Chemical Corps Filter and an 84-cubic foot chamber. Recorded test data are shown in Table 10.

Duct pressure readings were measured at a location after the valve and filter. However, since a peak overpressure of 10.4 psi was recorded in the duct of the 6-inch tee (no valve or filter) feeding into a chamber of similar size, adjacent to the installation under discussion, this pressure was taken as impinging on the E4 valve disk. Due to the short lengths of duct involved, in the order of a few feet only between the valve disk and duct gage, no increase in upstream pressure due to attenuation could be considered. Valve closing was again determined to result from actuation by pressure in the order of magnitude of reflected pressure, and good agreement was obtained for pressure inflow using the orifice analysis. A 30-man shelter was protected by the E4 antiblast closure units in Operation Teapot [18]. However, malfunction of pressure instrumentation made records obtained not usable for analysis of valve performance.

TABLE 9
Operation Greenhouse, Tests of E4 Antiblast Closure

Station	Average Measured Peak Blast Line Overpressure (psi)	Peak Pressure Measured Protected Side of Closure (psi)	Calculated Time Closure was Open (msec)
6101	530	12.6	(see text)
6102	52.5	8.48	1.67
6103	14.25	2.45	1.73

TABLE 10
Operation Upshot-Knothole, Test of E4 Antiblast Closure

Peak Line Overpressure (psi)	Peak Overpressure Measured in Adjacent 6-inch tee inlet (no valve) (psi)	Peak Pressure Measured in Chamber (psi)	Calculated Closing Time (msec)
20.3	10.4	0.3	1.75

The E19 antiblast louver-type closure was field tested in 1957 at Operation Plumbob. It was installed in a horizontal cylinder whose overall length was 8 feet, 7 inches and diameter was 5 feet. Attached to the horizontal cylinder, at right angles and in a vertical position, was a second cylinder whose length was 6.5 feet and diameter, 3 feet. The upright cylinder contained a ladder and a hinged steel cover plate on the top to permit personnel access. The E19 closure was mounted within the horizontal cylinder and connected to an 8-inch standard steel pipe which extended vertically through 5 feet of dirt fill, through a 1.5-foot thick concrete pad at the ground surface, and above ground for a distance of about 2 feet. A standard 8-inch welding tee was installed on the upper end of the pipe. The calculated free volume of the test installation was approximately 194 cubic feet. Pressure measurements obtained in this test and calculated results are given in Table 11.

TABLE 11
Operation Plumbob,
Test of E19 Antiblast Closure

Peak Overpressure at Test Installation (psi)	Peak Pressure in Test Chamber (psi)	Calc. Closing Time (msec)
64	0.32	2.7

Since there existed a 12-psig precursor preceding the arrival of peak overpressure at the station, this pressure existed at the above-ground pipe tee. A peak overpressure of 6 psi was considered in the duct impinging on the valve during its operation consistent with G-shot-Knothole results discussed previously. Valve closing was under approximately 15-psig pressure (reflected pressure for 6-psig incident) and calculated pressure build-up in the chamber was found to be in agreement with measurements at the test site.

The OCE elast actuated valve has not been evaluated by field tests but was briefly subjected to a shock tube test in 1954, the purpose of which was to determine the closure time versus pressure. However, the peak pressure of the shock wave which passed the valve before complete closure was considerably below anticipated incident shock pressures and the durations of positive phase were only about 3 msec, except for pressures so low that the valve did not close.

Shock tube tests at 5, 15, and 30 psi were performed in 1959 [12] on the Mosler Safe Co. valve design. A first series of tests produced some deformation in the 1/2-inch diameter cylinders, which caused the rods to bind in the closed position. After some additional testing, the valve was modified so that the rods would move freely back and forth from the open to the closed position. In the next phase of testing, the E-18 Particulate Filter was attached to the back end of the plenum and protected by the valve. Post-shot inspection of the filters showed them to be undamaged. Valve uncertainties encountered in the tests and desirability of additional data not obtained did not warrant detailed flow analysis of these test results.

Blast Pressure Leakage

Blast pressure leakage into the protected chamber past a valve which is closing, is dependent directly upon the mass of moving parts, initial open area, and travel to close. Initial open area and travel, of course, are functions of the volumetric capacity of the valve and pressure drop requirements consistent with the design. The mass of moving parts will vary with valve design, size, and pressure rating. The mass will, in turn, relate accelerations and terminal velocity attainable, with resultant impact energies. The three basic valve parameters described above, when lumped together for a particular valve closure system, will combine to give a closing time under an overpressure. This will then directly determine the chamber volumetric capacity necessary to limit pressure build-up to say 2 psi, or less, which is again dependent upon the hardness of the structure and the level of protection desired. The total accelerating force acting on the valves tested was found to be less than that calculated using the differential between measured external pressure and average pressure within the chamber. This may be accounted for by local disturbances in the pressure pattern due to the protective hoods and method of installation, and pressure build-up in the passage behind the disk which is greater than chamber pressure. For valves with the same effective projected area, those with light masses will be accelerated more rapidly, permitting a lower pressure build-up beyond the seal during the travel and are therefore, not seriously hindered from closing. In addition, valve impact energies, which must be absorbed by the body structure or an energy dissipating device, are directly dependent upon mass of moving parts, indicating an obvious advantage to be

accrued in minimizing the latter. The reduction in accelerating force from that indicated by the apparent pressures requires additional study.

In sizing plenum chambers to limit pressures to 2 psig for the various valves studied, valve malfunction or failure to close were not considered, since for long duration weapons with durations in seconds, full outside overpressure can then be anticipated within. Valve closing is influenced by factors which at present cannot easily be predicted for most installations, and which are variable and dependent upon type of installation and characteristics of the particular nuclear detonation. For the purpose of these calculations, each of the valves were considered installed in a duct or tunnel such that blast flow would be directed normal to the moving part or parts. Under these conditions valve closing was conservatively calculated considering overpressure actuation. The analysis also considers valve installation such that there is no restriction downstream of the valve. This will be discussed subsequently when the one valve violating this condition is discussed. It is also necessary that immediately downstream of the valve a chamber exist whose area ratio is considerably above that of the valve outlet, preferably greater than 4:1, so as to diffuse the flow as quickly as possible. A chamber which has the prescribed necessary volume but has little change in area would act like a shock tube or tunnel and the inflow pressure would experience little attenuation in the lengths involved. It is advisable to make the area ratio as large as consistent with good design, so long as the depth of chamber is not made too shallow. In general a cubic design would be a good rule of thumb. All plenum chambers were calculated to limit pressures to 2 psig using the method of shock wave flow through intakes developed in the study, and were found to be conservative for all field test data described previously. However, additional verification is highly desirable.

In general, the closing of a poppet valve depends on the restriction downstream of the valve and upon how rapidly the disk can be accelerated by the stream velocity. The E4 valve, which has been field tested successfully, possesses several desirable characteristics in its present design, such as light-weight disk, short travel, large bearing area for disk impact and rubber-cushioned seat. Plenum chambers for the E4 valve have been sized using a minimum closing time of 1.5 msec, although calculated times are less for the higher pressure ranges. Figure 27 indicates

plenum chamber sizes for various valves. Figure 27(a) illustrates the volume of plenum chamber in cubic feet required to limit internal pressure to 2 psi versus peak overpressure for the E4 valve under these criteria. Plenum sizes for the E19R1 valve are given in Fig. 27(b). Since the E19R1 is rated at 50-psi maximum overpressure, plenums are calculated only for pressures up to this value. The plenums shown in Figs. 27(c), 27(d), and 27(e), for the OCDM valves, are plotted up to 100 psi despite the fact that the 16-inch and 24-inch sizes are now rated at 50 psi. These valves are presently undergoing redesign for purposes of lightening the valve moving parts and decreasing closing times, and the accompanying alterations may increase valve ratings. Plenum sizes for the Mosler Valve at various peak outside overpressures are given in Fig. 27(f). This valve is the most recent addition to the field of the ones analyzed and has been modified since first being shock tube evaluated.

The OCE blast actuated valve is the only valve studied in which there is an appreciable restriction downstream or in which the orifice is smaller than the inlet (see Table 12). In other words, the flow area around the moving disk is not the governing restriction. During blast conditions this downstream restriction would remain as the critical orifice until about 30 percent of the travel and may result in a cushioning action which would seriously impair the valve's closing. Since, as our investigations with blast actuated valves have shown, a displacement-time pattern is established wherein the valve travels approximately 1/4 of the total distance in 1/2 the time and the remaining 3/4 of the distance in the same time, anything which would delay the start of closing might cause an unacceptable pressure build-up in the interior of the facility. The valve's closing cannot be predicted in accordance with the procedures used for the other valves. With initially subsonic flow entering the valve, the restriction would produce nozzle effects tending to decrease downstream pressure and increase velocity, thereby increasing inflow to the chamber. With supersonic flow past the valve, the restriction would decrease downstream velocity and increase downstream pressure, thereby increasing closing time of the valve. If, however, the disk open height was reduced from 4 inches to 2-3/4 inches, then the valve's closing pattern could be estimated. It is estimated that this would reduce the volumetric capacity to approximately 2250 cfm (calculated) at 1 inch of water pressure drop. It was on the basis of this reduced open height, that the plenum chambers shown in Fig. 28 were calculated.

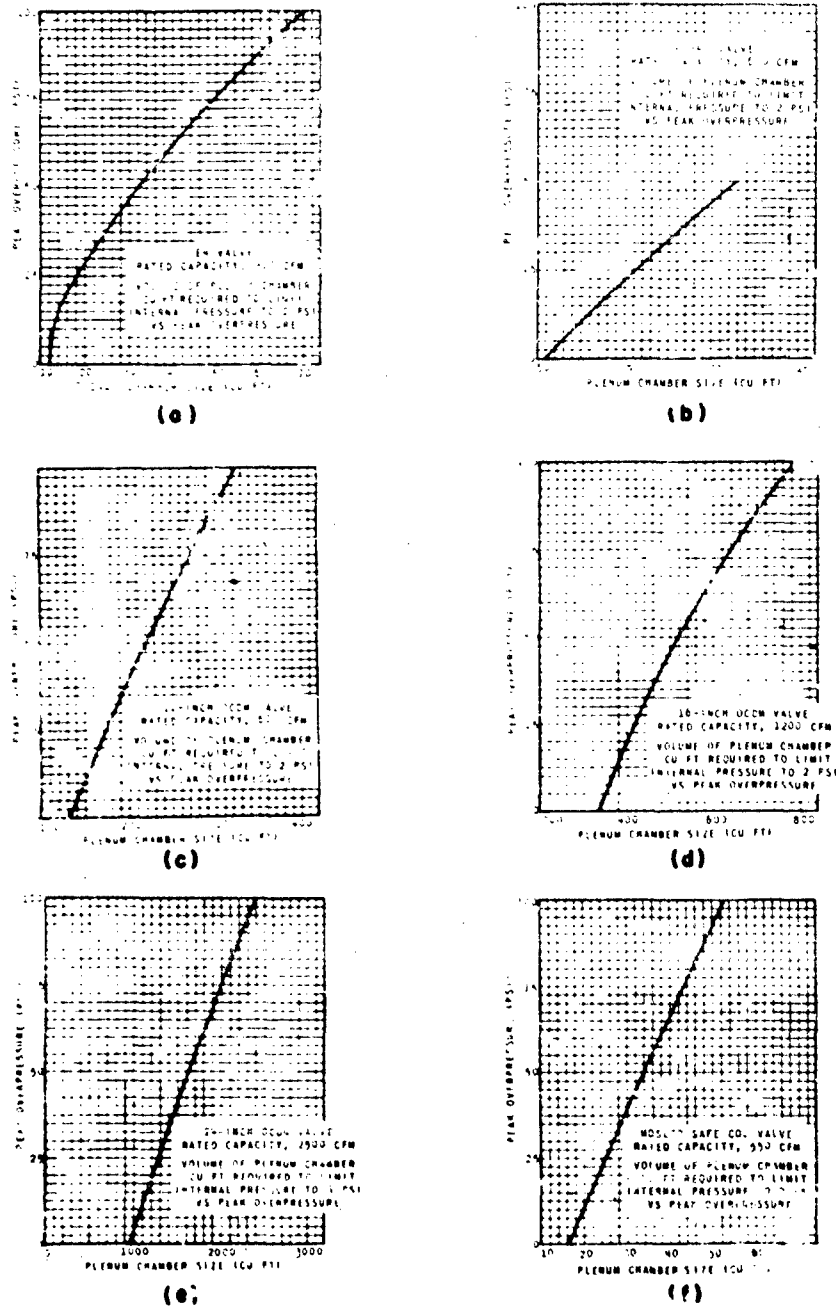


Fig. 27 - Valve plenum chamber sizes

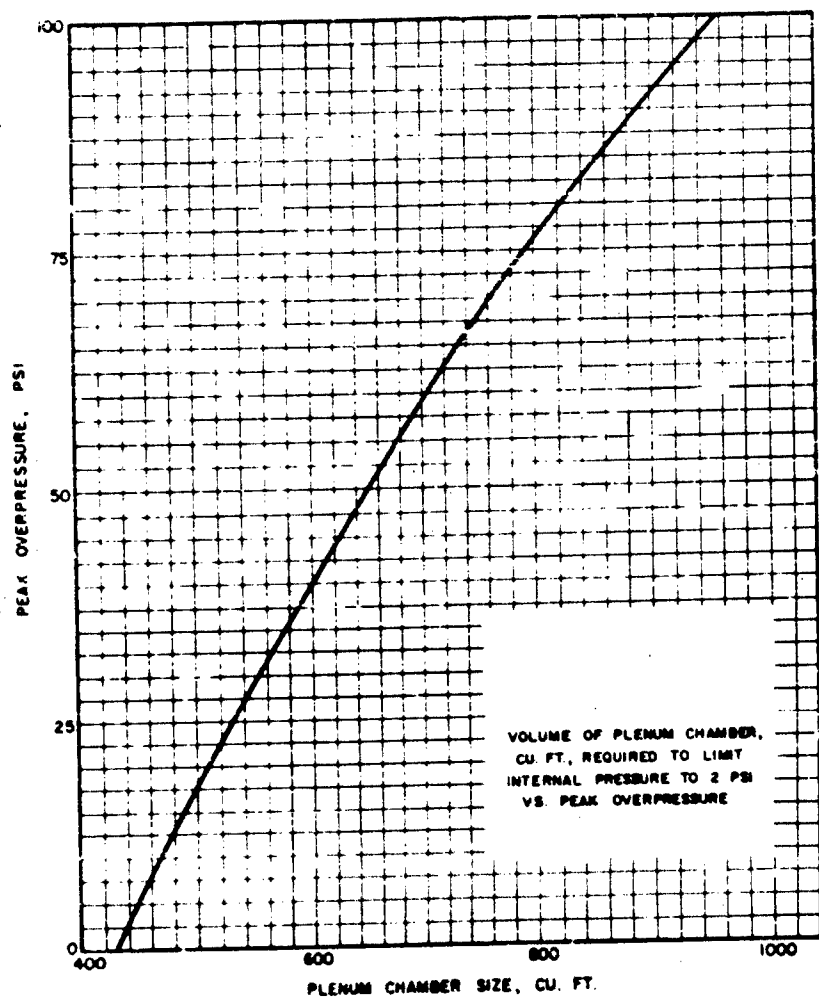


Fig. 28 - OCE valve (modified) capacity, 2250 cfm—calculated capacity, 2250 cfm at 1-inch of water.

TABLE 12
Valve Flow Areas

Valve	Valve Open Area (sq in)	Valve Port Area (sq in)	Major or Governing Restriction	Valve Port Area/Valve Open Area
E4	29.85	26.80	Valve Port	0.90
E19R1	50.64	45.31	Valve Port	0.90
OCE	191.64	147.53	Valve Port	0.77
OCDM 12 Inch	55.5	64.69	Valve Opening	1.18
OCDM 16 Inch	114.2	122.11	Valve Opening	1.07
OCDM 24 Inch	228.07	264.24	Valve Opening	1.16
Mosler	22.36	22.5	Valve Opening	1.01

PROPOSED NEW DESIGNS

Existing self-acting blast actuated poppet valve designs do not lend themselves readily to redesign for the purpose of increasing rated flow capacity to the 10,000 to 20,000 cfm range. It would be necessary to use many valves in parallel for the volumetric requirements in installations requiring large air flows.

New designs have been proposed for a large range of capacities at low-pressure drops, and are believed suitable for successful operation over a wide-pressure range. The valves are actuated by exterior overpressure and are not dependent upon external sensors or remote devices. However, they may also be combined with remote sensors for double assurance. One valve of this type is the Cohen - Ammann and Whitney guillotine poppet valve (AFISMD Contract No. AF04 (647) - 276 Suppl. 1) shown in Fig. 29. The valve possesses a favorable ratio of over-all weight of moving parts to activating pressure since the moving parts consist essentially of only a top disk with skirt (2). Travel and/or diameter of the valve, which forms the peripheral air intake or exhaust, (3), can be varied to give an optimum combination of closing time, sealing, and overtravel requirements for energy dissipation by shock absorption devices and inertia forces for a given capacity. It is maintained in the open position by soft springs (4), so that under normal ventilation flow pressure, air intake and/or exhaust from the chamber or facility (5), may be accomplished. The interior pressures resisting closure in the guillotine poppet valve are

negligible since the area exposed to such blast pressure leakage is only that of the cross-sectional area created by the moving sleeve thickness. Therefore, this resisting force is insignificant, unlike the situation with true poppet valves. This is a desirable feature of this design especially at low overpressure, since back pressure caused by leakage will not delay closing.

The only stresses in the dome head are those due to the acceleration of the skirt. When the head is closed by blast actuation, these forces are low since the skirt is light weight, facilitating design of the head as a light element. Since for the large air-flow capacities feasible with this design the weight of moving parts is relatively small, closing times of the guillotine poppet valve are also favorable. Under excessive outside pressure resulting from a nuclear detonation, or other causes entering the intake and/or exhaust, the valve moving part (top disk with skirt) is accelerated to its seat against the resistance of the soft springs. Air trapped below the valve moving part is vented to low-pressure areas in the protected structure, if necessary, to prevent any cushioning effect which would delay closure of the valve. Soft springs return the valve moving part (top disk with skirt) to the normally open position after the positive phase of the blast or load. At the conclusion of the negative phase in those installations where negative pressures are critical and latching is required, shock absorbing or cushioning devices (6), which will come into action after closure, are provided to operate efficiently over a complete range of loads and automatically compensate for the

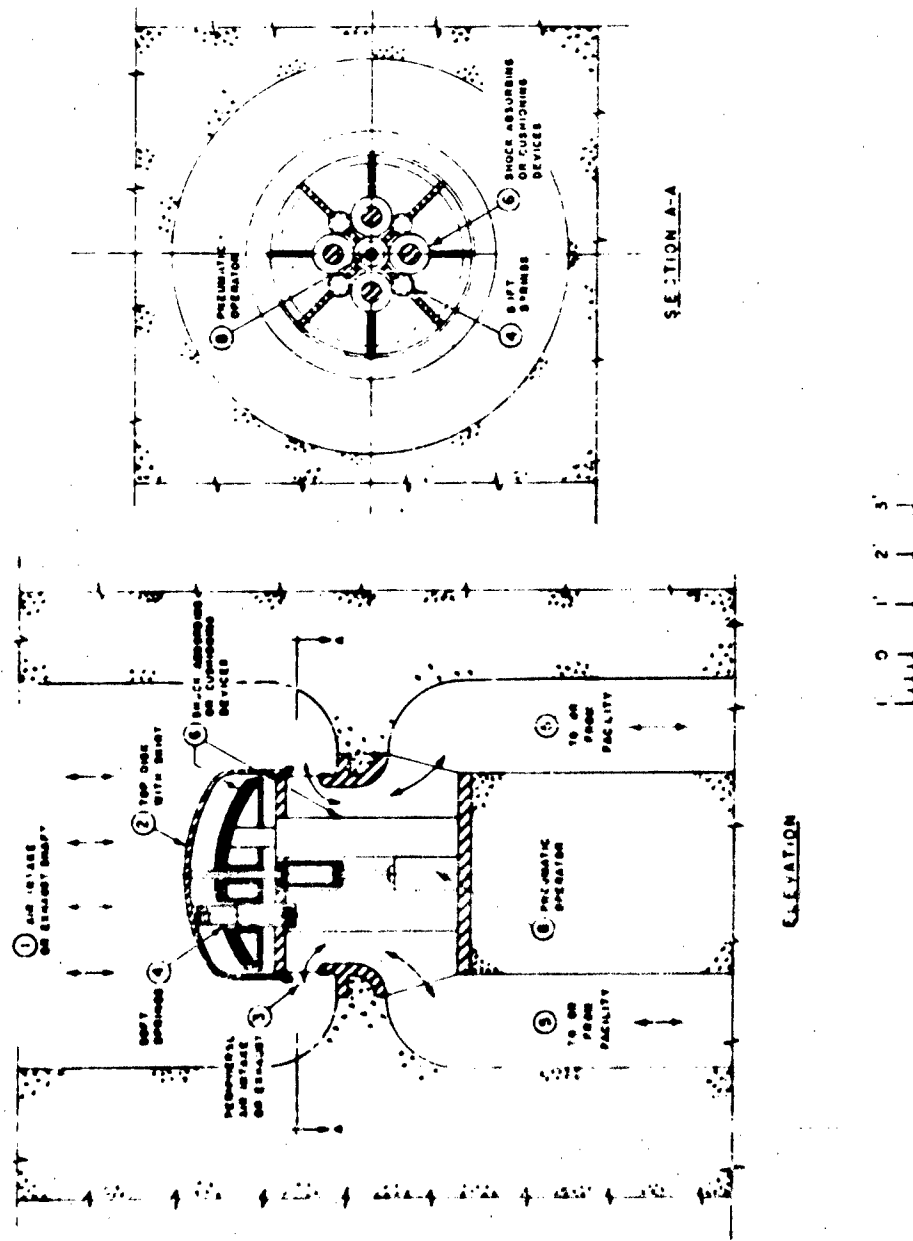


Fig. 20 - Guillotine poppet valve.

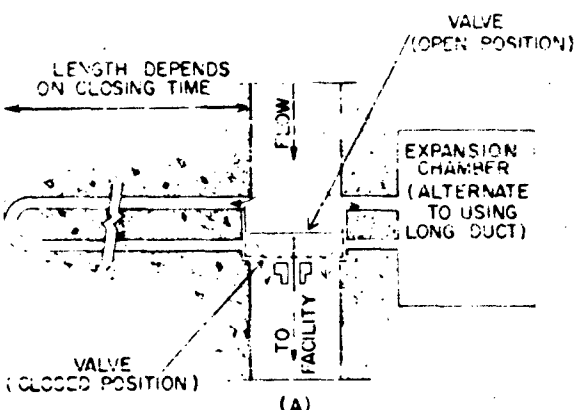
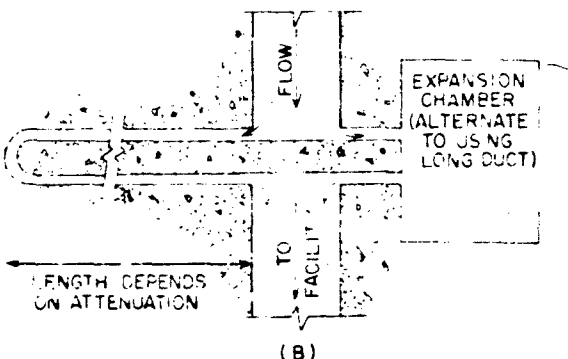


Fig. 30 - Time-delay path or expansion plenum, used with or without self-acting blast actuating valve

different impact speeds. Spring-cushioned stops prevent any upward motion of the valve moving part relative to the main structure beyond the open position (ambient pressure).

A pneumatic operator (8) with a four-way valve will allow remote override actuation of the guillotine poppet valve from a control center and/or local remote operation of the equipment if required. Switches, tripped by the valve moving part, will indicate full open and full closed position. Valve operation can be combined with a remote sensor, for double assurance, to increase reliability under blast conditions. The valve can be mounted in a horizontal as well as a vertical position and structural supports provided to accommodate the equipment.

A time-delay path as proposed by Cohen [1] may be used in conjunction with most valve types as shown diagrammatically in Fig. 30, and will enable the valve to be partially or completely closed before dangerous overpressures arrive at the inlet to the interior facility. The length of delay path depends upon the speed of closing of the valve after activation for a remote actuated valve, or after arrival of the shock wave at the exterior surface of a self-acting blast actuated valve, and the allowable interior pressure. If the path is sufficiently long, the facility will be completely isolated from the effects of the blast. Outside overpressure entering the inlet will also be attenuated directly as a function of the length and diameter of the duct. With this arrangement, normal ventilation flow will enter the

facility through the blast valve after traveling the time delay path. An exhaust duct will operate in reverse fashion. The delay path may be combined with closures of many configurations such as guillotine, plug, etc., to provide positive closure.

An adequately sized expansion plenum chamber used in lieu of the delay path will provide attenuation of the outside overpressure during the time the valve is closing, and will limit transmission of any pressures not tolerable within the facility before complete closure of the valved air intake and/or exhaust.

The guillotine poppet valve with delay path (7) is shown in Fig. 31.

CONCLUSIONS AND RECOMMENDATIONS

An optimum combination of self-acting blast actuated valve parameters is necessary for protection against the effects of high yield, long-duration weapons with sharp pressure rise times. For example, an excessive travel with a moderately heavy disk would create large dynamic loads upon impact and the valve body or structure would be required to absorb this energy. If the structure cannot sustain this impact then failure of disk and/or body will occur. An alternative to this would be to provide overclosure on the valve travel and energy absorption devices which would cushion the impact loads of the moving masses. Local disturbances affecting initial movement and causing high pressure leakage in this first interval when the valve is wide open, could be extremely detrimental to the interior of the facility. This may be overcome by the use of a time delay path which will enable partial or complete closure before dangerous overpressures arrive at the valved inlet. Effective closing of a poppet valve by blast depends upon removing any restriction or pressure build-up downstream of the valve opening.

The use of many valves in parallel, for installations with large air requirements, decreases over-all system reliability by increasing the number of independent elements maintenance, etc. The proposed guillotine poppet valve designs are advantageous when compared to existing poppet designs in that closing is not retarded by pressurization on the downstream side of the valve caused by blast leakage during a nuclear blast. Valve behavior under blast conditions can, therefore, be predicted with greater confidence. The guillotine poppet designs allow for increased

capacities over existing valves through optimum sizing of diameter and/or travel with little penalty. A time delay path for diverting blast flow may be included in the installation to isolate completely the facility from blast. The length of this delay path is dependent on the extent to which absolute isolation is required.

Plenum chambers were conservatively sized as sufficient to limit pressure build-up to 2 psi within. Plenum sizes are directly dependent upon how fast the valve moving element can be accelerated to the closed position, and are smallest for valves with light weight of moving parts. For a large volumetric capacity, requiring installation of several existing self-acting blast actuated valves in parallel, the required total plenum size for an interior limiting pressure of 2 psig, would be the sum of individual plenum sizes. In lieu of the above, installation of a larger capacity guillotine valve is expected to result in a smaller total plenum. In combination with a time-delay path, the plenum size required with a guillotine installation may be drastically reduced.

For high yield weapons without precursors, it is recommended that valve moving parts be designed structurally for loadings and accelerations corresponding to reflected pressure due to peak overpressure in the approaching shock wave and considered to be acting during the entire closing time. Where the inlet shaft or tunnel has a favorable orientation with respect to the shock wave or when a precursor is predicted, the design peak overpressure may be reduced [26,27]. Valves should be installed, if possible and practical, so as to minimize the effective overpressure in the duct and to direct blast flow normal to the valve moving part or disk. Valves should possess a moving element as light in weight as structurally feasible in order to reduce closing times, pressure build-up downstream of the disk while closing, and inertia loading. Valve seats protected by resilient materials are advantageous for damping the elastic impact of disk against seat and reducing energies transmitted to the seat and structural supports. The materials used should be checked for their thermal characteristics.

During maintenance periods means should be provided to take a blast valve requiring service off the line and to fit a spare in operation simultaneously. To better accomplish this, a device should be provided to blank off the opening ahead of the valve to be serviced. All valves should be operated and maintained

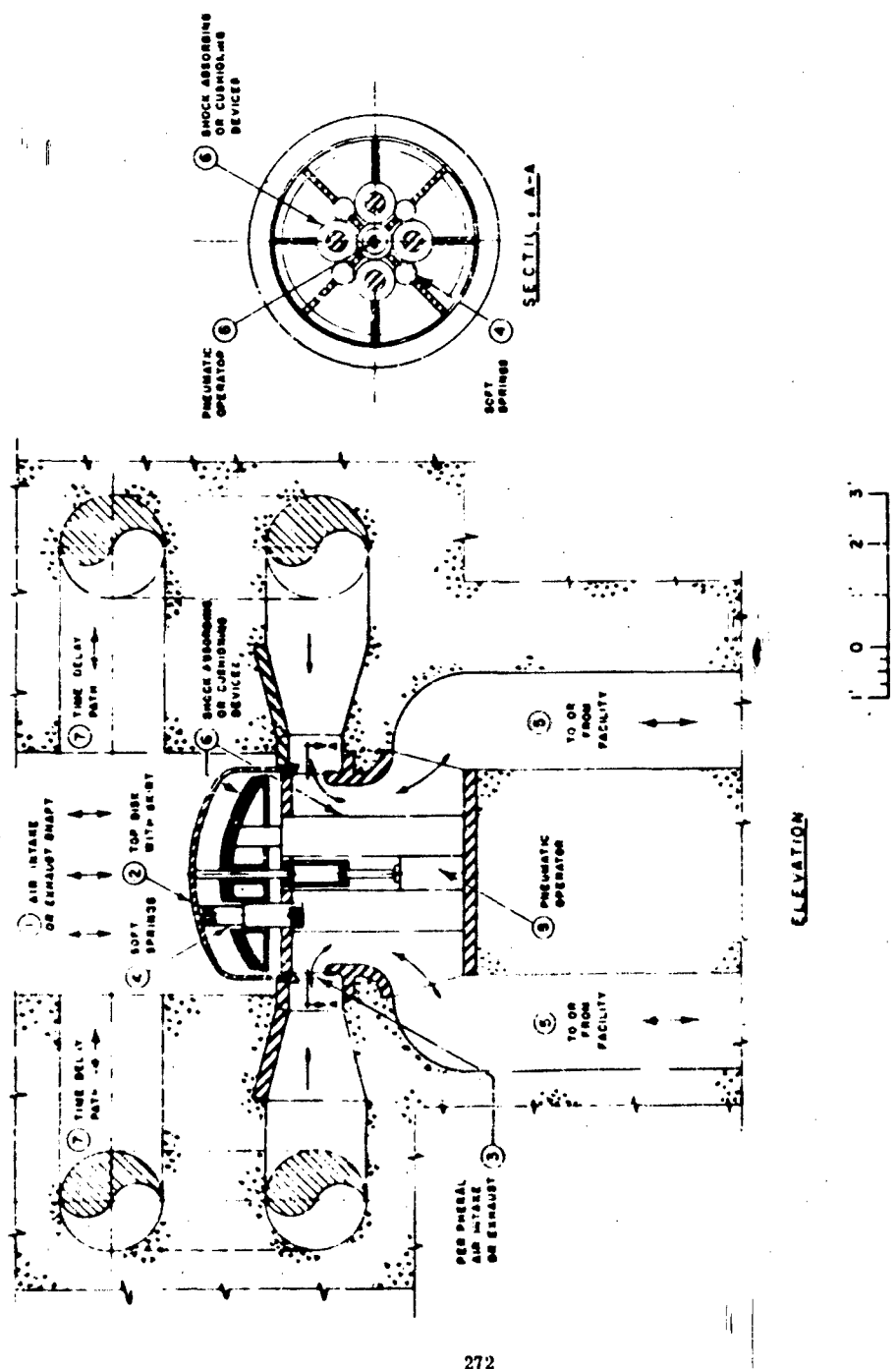


Fig. 31 - Guillotine poppet valve with time-delay path

on a periodic schedule to assure maximum reliability.

Remote actuated valves depend for their operation on sensing devices, electrical relays, etc., with the possibility of malfunction of one or more of the system components. By including blast wave arrival time in the "buttoning up" period, these may present a problem for combustion equipment within the protected structure. Additional problems are sensitivity of the sensors for multiburst operation and degree of hardening of the sensors. Remotely actuated valves which are pneumatically or hydraulically operated, are dependent upon

equipment for maintenance of pressure if they are to function when needed. If "fail safe" features are incorporated in the design, the valve may close upon power failure, thereby "buttoning up" the facility for a period of time which might be extremely detrimental, since for some facilities times in the order of a few minutes are not tolerable. In addition to reliability of system operation, the sensors actuating remote valves must be satisfactorily hardened and made suitable for multiburst operation. Therefore, it appears that at the present time maximum system reliability is obtained through the use of self-acting blast actuated valves.

BIBLIOGRAPHY

- [1] Edward Cohen, Ammann and Whitney, "Blast Vulnerability of Deep Underground Facilities As Affected by Access and Ventilation Openings," Second Protective Construction Symposium on Deep Underground Construction, sponsored by the RAND Corporation, March 1959.
- [2] Harold L. Brode, "Numerical Solution of Spherical Blast Waves," *Journal of Applied Physics*, Vol. 26, No. 6, June 1955.
- [3] "Effects of Atomic Weapons," Published by the United States Atomic Energy Commission, June 1957.
- [4] F. E. Anderson, Jr., "Blast Phenomena From a Nuclear Blast," *Proceedings of the American Society of Civil Engineers*, November 1958.
- [5] R. Dennis and C. E. Billings, "Blast Effects on an Air-Cleaning System," Operation Plumbbob Interim Report ITR-1475, November 1957.
- [6] "Protection of Structures from Chemical, Biological, and Radiological CBR Contamination," U. S. Army Chemical Corps Report ENCR No. 30, June 1959.
- [7] "Collective Protection Against Chemical, Biological, and Radiological Warfare Agents; Design Criteria," U. S. Corps of Engineers, Office of the Chief of Engineers.
- [8] "The Development of the Closure," Protective Shelter, Antiblast, 600 cfm, E19R1, CWL Technical Memo No. 32-26.
- [9] "Investigations Concerning Feasibility of Various Designs for a Blast Closure Device," American Machine and Foundry Co., on Contract No. ND-13330 for Bureau of Yards and Docks.
- [10] "Test of French Underground Personnel Shelters," Preliminary Report Operation Plumbbob, Project 30.6. Submitted by Ammann and Whitney, Consulting Engineers, September 1958.
- [11] "Test of German Underground Personnel Shelters," Preliminary Report Operation Plumbbob, Project 30.7. Submitted by Ammann and Whitney, Consulting Engineers, September 1958.
- [12] "Shock Tube Test of Mosler Safe Company Blast Valve," Explosion Kinetics Branch, BRL Information Memorandum No. 20, May 1959.
- [13] "Shock Tube Test of Mosler Safe Company Blast Valve, Phase II," Explosion Kinetics Branch, BRL Information Memorandum No. 25, August 1959.
- [14] Frank G. Ort and Merton D. Mears, "Scientific Director's Report of Atomic Weapon Tests at Eniwetok, 1951, Annex 6.10 Operation Greenhouse. Evaluation of Collective - Protector Equipment," U. S. Army Chemical Center, March 1952.
- [15] J. J. Meszaros, H. S. Barden, and J. D. Day, "Instrumentation of Structures for Air-Blast and Ground-Shock Effects," Operation Plumbbob, Project 3.7, ITR-1434, Ballistic Research Laboratories, December 1957.

- [16] F. C. Allen, A. M. Hatch, D. E. Keyt, and D. P. Rohrer, "Test and Evaluation of Antiblast Valves for Protective Ventilating Systems," Operation Plumbbob, Project 31.5, ITR-1460, Office of Civil and Defense Mobilization, January 1959.
- [17] James E. Roembke, "Retest and Evaluation of Antiblast Valves," Operation Hardtack, Project 70.3, ITR-1717, Office of Civil and Defense Mobilization, March 1959.
- [18] "Evaluation of Various Types of Personnel Shelters Exposed to an Atomic Explosion," Operation Teapot Projects 34.1 and 34.3, Report WT-1218, May 1956.
- [19] A. H. Shapiro, "The Dynamics and Thermodynamics of Compressible Fluid Flow," Ronald Press (1953).
- [20] H. W. Liepmann and A. Roshko, "Elements of Gasdynamics," John Wiley (1957).
- [21] L. L. Monroe, "Investigation of the Transmission of a Shock Wave Through an Orifice," California Institute of Technology Hypersonic Research Memorandum No. 46, September 1958.
- [22] I. I. Glass, "Shock Tubes Part I: Theory and Performance of Simply Shock Tubes,"
- Institute of Aerophysics, University of Toronto, May 1958.
- [23] H. L. Broe, "Shock Wave Attenuation in Tunnels," RAND Corporation, Proceedings of the Second Protective Construction Symposium (Deep Underground Construction) March 1959.
- [24] J. D. Day, "Attenuation of Shock Waves in the BRL 24-Inch Shock Tube," BRL Report AFSWP No. 814, August 1955.
- [25] "Laboratory Tests of Anti-Blast Valves for the Federal Civil Defense Administration," Hydraulic Laboratory Report No. R-HYD-7, February 1959.
- [26] "First Information Summary of Blast Patterns in Tunnels and Channels," Ballistic Research Laboratories, Aberdeen, Maryland, March 1960.
- [27] R. O. Clark and W. J. Taylor, "Shock Pressures in Tunnels Oriented Face-On and Side-On to a Long Duration Blast Wave," Proceedings of the 28th Symposium on Shock, Vibration, and Associated Environments, Bulletin No. 28, Part III, Office of the Secretary of Defense, Research and Engineering, Washington, D.C., September 1960.

FOUNDATIONS FOR PROTECTIVE STRUCTURES*

K. E. McKee
Armour Research Foundation
Chicago, Illinois

The behavior of foundations subjected to dynamic loads is of major interest to the designers of protective structures. This paper presents the results of research both analytical and experimental, which considers the behavior of footings under dynamic loads with particular attention to the applications for protective structures.

The purpose of this research is: "...to investigate the problems associated with the design and analysis of foundations for protective structures subjected to dynamic loads from nuclear blast." The more basic problem posed for the purpose of the research has been to explain the behavior of foundations on arbitrary soil subjected to an arbitrary time-dependent force. It is further specified that the foundations do not fail which restricts consideration to soil failures. The experiments, both static and dynamic, which were conducted as part of this program will be described and related to the theoretical studies. These experimental results combined with the analytical work will be combined to provide a paper defining the limits of current knowledge and making recommendations for design procedures.

NOMENCLATURE

- B = vertical force
- c = cohesion
- C = center of failure
- D = depth of burial
- e = eccentricity
- P = vertical force
- q = pressure on surface
- r = radius of failure surface
- τ = shear stress
- x, y = distances
- x, y = coordinates
- ϕ = angle of internal friction
- n = normal stress
- v = gross weight per unit volume

INTRODUCTION

The behavior of foundations subjected to dynamic loads is of major interest to the designers of protective structures. During the last few years protective construction has forsaken the research offices and test sites for the design offices and construction sites. Foundations for protective structures had received relatively little attention during the research phases and, hence, represented a technical area where much additional investigation was required. During the past three years considerable research on foundations for protective structures has been conducted resulting in improvements, in understanding, and, hence, in design knowledge. The purpose of this paper is to describe some of the research which has been done, to recommend design procedures, and to point out limitations.

Specifically this paper will be based on research, both analytical and experimental, conducted at the Armour Research Foundation under contracts sponsored by the Air Force

*This paper was not presented at the Symposium.

Special Weapons Center, Air Research and Development Command, Kirtland Air Force Base, New Mexico starting early in 1950. The basic problem posed for this research has been to explain the behavior of foundations on arbitrary soils subjected to arbitrary time-dependent forces. It has been specified that the foundation, itself, will not fail (this represents a design problem, but no fundamental difficulty). As for any type of design the assumptions regarding load distribution should be conservative from the point of view of the foundation and hence consideration is limited to soil failure.

"Foundations" is a general term used here to refer to any method of transmitting loads from a structure into the earth, including such diversified systems as pile foundations, piers, spread footings, caissons, mats, raft foundations, retaining walls, etc. The assumption has been made that the many existing types of foundations can be divided broadly into (1) foundations or spread footings. Methods are being developed to handle these two types of foundations with the understanding that this knowledge should provide a suitable general approach for any type of foundation.

The requirements governing the design of foundations for protective construction are two fold. First the structure certainly must be designed for normal conditions. In the case of the foundation this means that they should be designed to support the dead loads plus normal live loads for long times, and that the possibility of consolidation below the structure must be considered. Of more direct interest here is the second type of requirement relating to the blast loading transmitted through the structure. The durations are sufficiently short so that consolidation under these blast loads can be neglected. One must however be interested in the displacement (which will also be referred to as settlement) under dynamic loads. Depending on the over-all structural design concepts, one may wish to limit settlements under single or multiple applications of blast forces. On the other hand it may be advantageous to design for large settlements when the foundations are subjected to blast loads. This decision is up to the designer and must depend on the specific requirements in each instance. As far as foundation behavior is concerned this means that methods should be developed for predicting and designing for either large or small settlements, or both.

For the purposes of this paper the following soil parameters were selected for use in both static and dynamic investigations (1):

cohesion, c ; (2) angle of shearing resistance, ϕ ; and (3) gross weight per unit volume, γ . The values of these parameters for an actual soil in the vicinity of a foundation subjected to either static or dynamic loads may depend on many factors, including such items as grain-size distribution, permeability, strain rate, shape of stress-strain curve, lateral pressure, etc. The assumption, which could prove to be extremely optimistic, is that other research studies will provide methods of relating the selected parameters to the various factors which can influence them. It is further assumed that, in general, this internal shear resistance follows Coulomb's law; namely

$$s = c + \gamma \tan \phi$$

where s = shear resistance and γ = normal stress on plane of shear.

In organizing this paper the attempt has been to describe briefly the research which has been conducted. Based on this, recommendations with regard to design procedures are presented. Particular attention will be given to the limitations which must accompany these recommendations.

ANALYTIC RESEARCH

The analytical work has been based on two premises: first, that a crude theory is better than none and second, that experimental research should be conducted to verify or disprove the analytical work. These premises have resulted in consideration of many theoretical approaches, rejection of some, modification of others, and—it is hoped—an ever-improved analytic understanding of foundation behavior. The analytical approaches have been based, in general, upon extensions of theoretical approaches for static loads to the problem of dynamic loading.

Research into soil failure has followed two related but quite distinct approaches. The first of these, which is that normally used in soil mechanics, postulates the existence of slip surfaces of certain simplified forms. This approach reduces the problem to determining the most dangerous of the slip surfaces having this form. This soil mechanics approach, which has little theoretical basis, gives in many instances satisfactory answers, and therefore is often used. The second approach, which normally is associated with the theory of plasticity, attempts to develop rigorous theoretical methods of treating critical equilibrium. The plasticity approach although

theoretically sound, is limited by the assumptions which must be made and the complexity of the mathematics involved in obtaining a solution. Hence, the plasticity approach can thus far be used to solve only limited problems. Both of these approaches have been extended in attempting to predict the behavior of footings subjected to dynamic loads.

Most of our initial work was limited to the soil mechanics type of failure, i.e., selecting a form for the surface of failure and selecting the parameters defining that form which failed under the least load, first using the form introduced by Andersen for one-sided failure [1] and then introducing the concepts of dynamic forces [2] and surface overpressure [3]. This approach was also extended to eccentric loads [4]. For all of the above the one-sided failure patterns were used because they were simple, because the resulting free body was capable of finite motion, and because they are representative of at least a portion of actual failures. Figure 1 shows the one-sided failure pattern including overpressure and eccentricity.

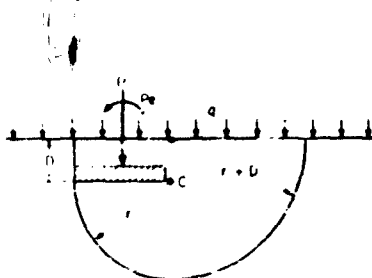


Fig. 1 - One-sided failure

Any consideration of two-sided failure using the soil mechanics approach must be limited to incipient motions—or must assume crushable soil. Figures 2 and 3 show two assumed failure surfaces which were considered. The first assumption (Fig. 2) is based on Prandtl's plasticity solution [5] while the second (Fig. 3) is based on Hill's [6] plasticity solution.

The plasticity solutions for static loads are characterized by Prandtl's and Hill's solution mentioned above. An extensive literature exists relating to theoretical approaches to such problems. A general method of approach to such problems is contained in a book by V. V. Sokolovski [7]. Extensions of this approach to the dynamic problem have recently

been initiated by P. G. Hodge [8] and A. J. M. Spencer [9]. Actual application of these approaches are limited by the complexity of the numerical solutions and the simplifications in the assumption. This method of approach appears to offer the only long-range hope of understanding the actual behavior under dynamic loads—for current application, however, it is of little value.

All of the above has related to critical equilibrium considerations. The other possibility must not be forgotten, i.e., unacceptable settlement prior to reaching critical equilibrium. There is much work still to be done here in relating theory to experiments. The theoretical approach developed as part of our research [10] gave results differing from those observed in the laboratory. Both the theory and experiments must remain doubtful until further research is available to clarify this situation.

EXPERIMENTAL RESEARCH

The experimental investigations have considered the behavior of two- and three-dimensional footings on cohesive or cohesionless soil with static or dynamic loads applied to the footings. These experiments were conducted to verify theoretical studies and to provide the basis for further analytical research. Sufficient controls were established to assure the maximum possible reproducibility—standard and special tests were conducted to establish soil properties, several identical tests were conducted to check reproducibility, etc.

Figures 4 and 5 show the experimental setup for two- and three-dimensional static tests respectively. Figures 6 and 7 are similar photographs with the dynamic load apparatus in place. The details of the experimental approach and its results will not be included here. Interested readers are referred to reports on the project [11,12]. The attempt will be made herein to outline the work which was done.

A series of three-dimensional static tests (62) were conducted on dense, dry Ottawa sand. Figure 6 shows a sketch, and Fig. 9 a photograph, of an example of the surface failure pattern. Figure 10 is a plot of three load-deflection curves for 4-in. \times square footings. Dynamic loading experiments were conducted in the same soil using dropped weights (53 tests) and a pneumatic-hydraulic dynamic loading device (47 tests) shown in Fig. 7. Force-time and displacement-time records

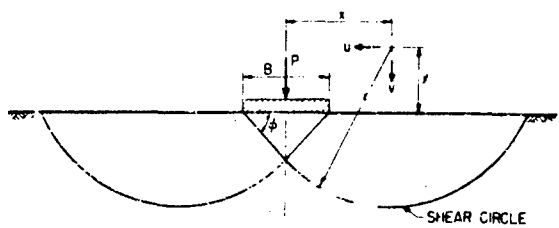


Fig. 2 - Simplified two-sided failure based on
Prandtl's solution

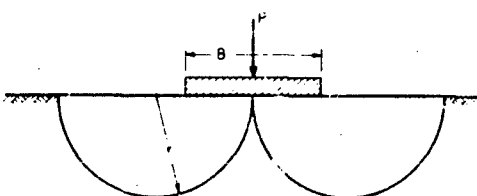


Fig. 3 - Simplified two-sided failure based on
Hill's solution

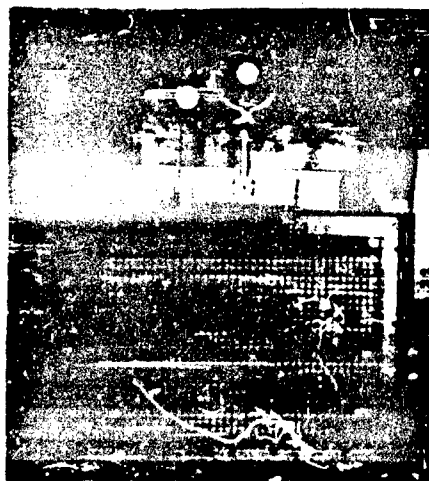


Fig. 4 - Static setup on glass box

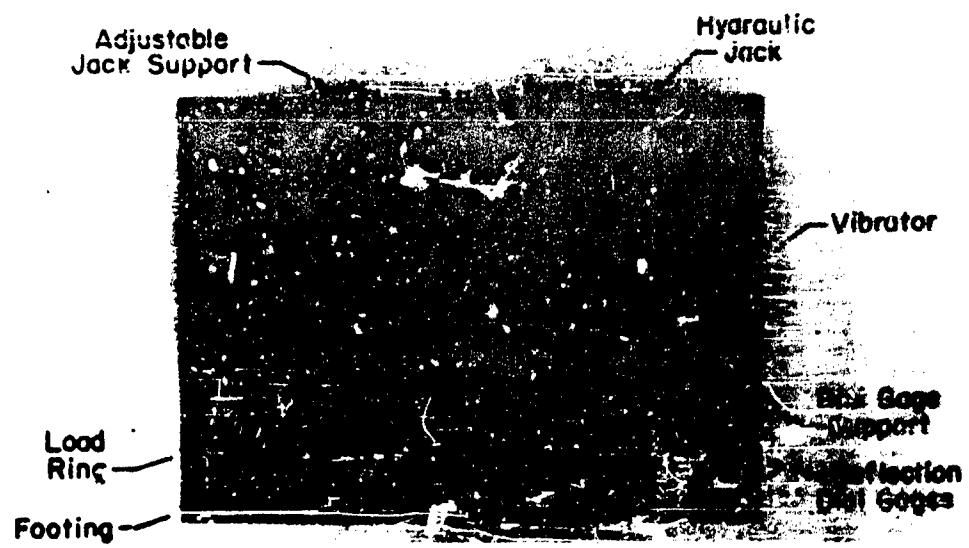


Fig. 5 - Static three-dimensional setup

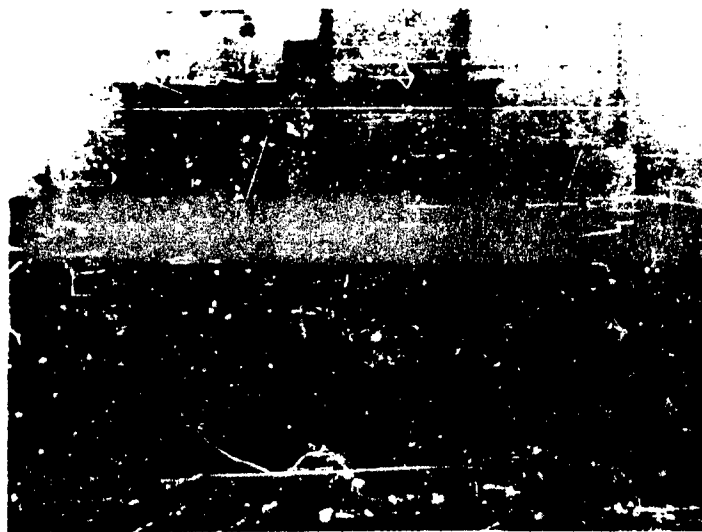


Fig. 6 - Dynamic apparatus on glass box

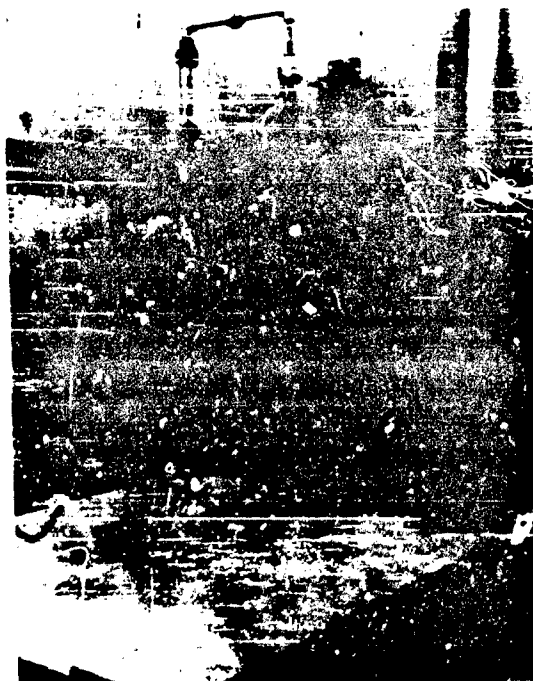


Fig. 7 - Dynamic three-dimensional setup

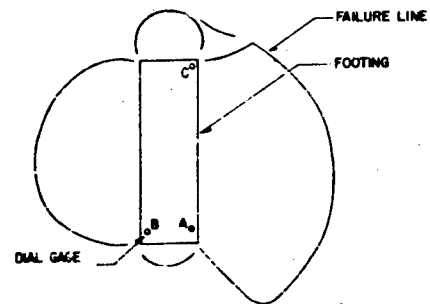


Fig. 8 - Sketch of failure surface for
3-inch x 9-inch footing



Fig. 9 - Photograph of failure surface for
3-inch x 9-inch footing

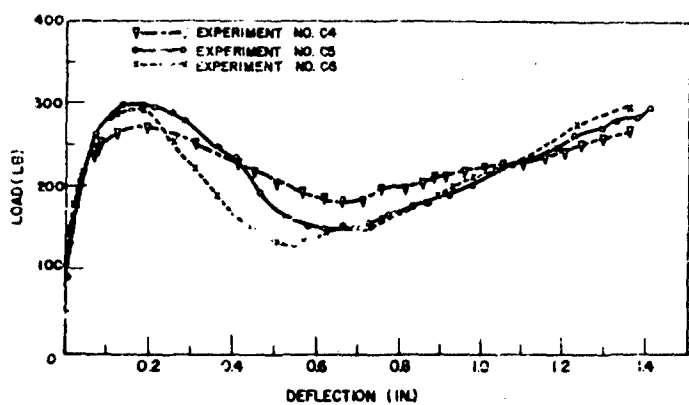


Fig. 10 - Load-displacement measurements for 4-inch-square footings



Fig. 11 - Records for 4-inch x 4-inch footing



Fig. 12 - Surface after drop test



Fig. 13 - Surface after dynamic load

for the footings subjected to dynamic loads were obtained. Figure 11 shows a record for a dynamically loaded footing; the top trace being the force and the bottom the displacement. Figures 12 and 13 show a footing failed by a dropped weight and by the dynamic loading machine, respectively.

Two-dimensional footings in the glass box have been tested under static and dynamic loads using both cohesionless and cohesive soils. Although some meaningful quantitative measurements were obtained, it was felt that the main purpose of the two-dimensional tests were the visual observations, still photography, and Fastex movies obtained during these experiments. Figures 14 and 15 show one-sided and symmetrical failures, respectively, for a statically loaded footing on dense, dry Ottawa sand. Figures 16 and 17 show a sequence of photographs taken from Fastex film for a footing on the same soil. Both static and dynamic tests have also been conducted on loose Ottawa sand and cohesive material.

INTERPRETATION OF RESULTS

The static experiments in part are directly comparable to the accepted theories [13]. The first maximum on the load-deflection curves of Fig. 10 represents the bearing capacity—the quantity predicted by the theories. Using the soil properties determined by triaxial tests, it was possible to correlate theory and experiment for the static experiments. However, the first maximum of the load-displacement curve represents, as can be seen

from Fig. 10, only part of the story. The subsequent decrease and still later increase in load with increased deflection is of considerable importance in understanding footing behavior. Large deflections have not previously been of interest and hence theoretical and/or experimental studies have considered only the behavior up to the first maximum. Static experiments associated with ARF's investigations have provided some information, but a complete understanding must depend on a theoretical approach and will undoubtedly require additional experimental studies.

The dynamic tests were of primary interest for the research considered herein. The initial dynamic tests made use of a dropped weight. Figure 18 shows that the settlement versus the drop height is linear for each footing size when the dropped weight remains constant. Because of the limitations on the instruments used, attempts to record the force-time history for the dropped weight were not successful. It was possible to correlate these tests with the static tests by means of an energy approach [14]. The measured behavior can be explained by assuming that the dropped weight, the footing, and a mass of soil move as a single body after contact.

Subsequent dynamic experiments were conducted using the pneumatically driven dynamic loading device discussed earlier. For these tests both force-time and displacement-time curves were obtained. These experiments are currently being concluded and the parallel analytical studies are only partially



Fig. 14 - Static experiment, 2-inch footing, buried
2 inches, after failure



Fig. 15 - Static experiment, 2-inch footing, after failure



Fig. 16 - Dynamic test of footing on dense Ottawa sand

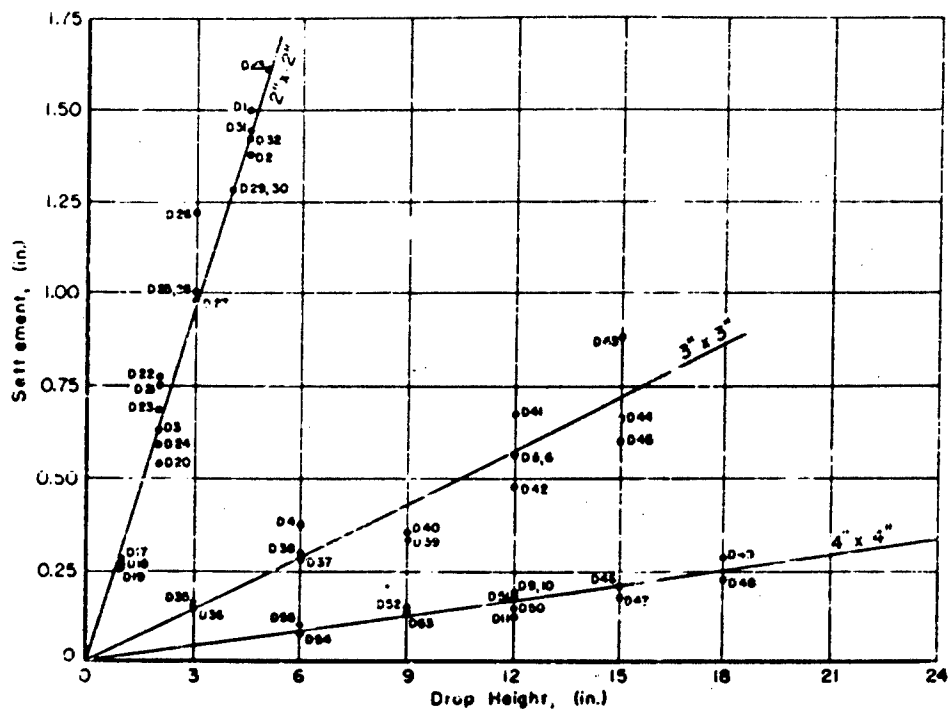


Fig. 16 - Drop height vs. settlement for square footings (drop weight = 11.2 pounds)

completed. Using dynamic equations for footings developed earlier [14,15], it is possible to numerically determine the resistance-displacement curve of the footing for each applied force time. This approach is based on the assumption that the resistance is dependent only on the displacement. Figure 19 shows the resistance-displacement curve for 4 inch x 4 inch footings on dense sand subjected to four similar dynamic loads. The scatter of points for any particular footing is a function of the measurements and numerical solutions—a single curve appears to fit all of these points relatively successfully. The average static-resistance curve for the same size footing (Fig. 10) is also shown in Fig. 19. The dynamic resistance displacement is lower than the static resistance-displacement curve. This is contrary to what is encountered for many other materials, e.g., steel, timber, etc. At least intuitively one could explain such behavior in a manner similar to "st-reak" and sliding friction.

DESIGN RECOMMENDATIONS

The research reported here has provided much data regarding the behavior of footings subjected to dynamic loads. It has been demonstrated that the bearing capacity of the footings tested in the laboratory under static loads behave in accordance with theory. The behavior under static loads at increased deflection has been measured but as yet is not amenable to analytical explanation. In this respect the next that can be claimed at present is a qualitative understanding of this behavior.

In the case of dynamic loads on footings the research has in many respects been primarily negative. Differences were observed in the failure modes associated with identical displacements under static and dynamic loads. For the same footing and soil conditions the dynamic resistance-displacement curves can be of different shape and magnitude than the static curves (Fig. 19). Of particular interest

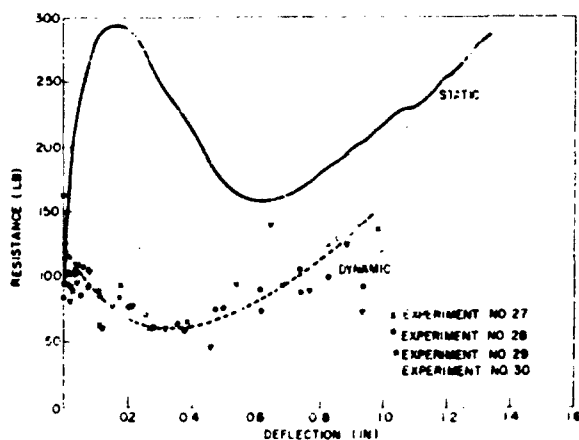


Fig. 19 - Resistance-displacement curves

in this respect is the fact that the dynamic resistance can be less than the static resistance. Such other forms of resistance as may exist, e.g., those dependent on velocity, would tend only to reduce the dynamic resistance even more. The test data did confirm theoretical studies indicating that the inertial effects are negligible for most surface footings. It should be emphasized that interpretation of the dynamic experiments are only partially completed and that the soils considered above are limited to dry, dense Ottawa sand.

Recognizing all of these limitations, it is still necessary to provide a current method for use by footing designers. For this design it is suggested that no increase or decrease in the resistance be introduced to account for the dynamic characteristics of the applied force. It is recommended that the normal static properties for the soil be used with the appropriate shear failure in the soil under the footings.

Air pressure acting on the surface in the vicinity of the footings may significantly influence the behavior of the footing. It is recommended that the peak overpressure be treated as a static overburden and introduced as a modification into normal bearing capacity formulas. Three conditions for this overpressure-induced overburden must be considered: (1) if there is none (e.g., interior footings), and hence the normal bearing capacity solutions apply; (2) that the overpressure acts on the entire surface surrounding the footing (e.g., a footing for an antenna), and hence a modification

must be added to the normal bearing capacity solutions; and (3) that the overpressure acts on one side of the footing (e.g., an exterior footing), and hence a modification must be introduced for both the magnitude and eccentricity of the additional overburden (generally this will mean a one-sided failure away from the overpressure).

Once the overpressure is included in one of the above ways, the ultimate capacity of the footing can be computed by normal means. It should be noted that the locations of the failure surfaces will depend on the overpressure as well as on the nature of the forces applied to the footing. For essentially downward forces, including those which are inclined and eccentrically applied, this represents a straightforward modification of the procedures used in static design. The extent of complexity involved in introducing these modifications will vary depending on the specific situation. For inclined and eccentric loads, the solutions are complex even for normal conditions and, hence, will be complex here. On the other hand, for vertical forces and overpressure on the entire surface, the modification is trivial; e.g., Terzaghi's formula [16] can be modified by including the overpressure as an additional overburden.

It is felt that the behavior of piles under dynamic loads is better understood than the behavior of spread footings under dynamic loads. This is not to say that the behavior of piles under dynamic loads is completely understood—even a cursory survey of the current literature would quickly demonstrate

that it is not. However, at least a qualitative understanding of the behavior is available.

One primary requirement in a dynamic analysis is knowledge of the resistance displacement provided by the foundation. For pile foundations, it appears reasonable to neglect settlement-type displacements, since settlement would be expected to be essentially elastic and to be due primarily to shortening of the piles themselves. Resistance can rise along the length of the piles and at the point. An interaction between resistances from these two sources prevents simple addition of the resulting resistances. Since the pile changes length under load, it is reasonable to assume that the full resistance along its length must be developed before the point can transmit forces. Furthermore, based on observations of piles driven into clay, it is assumed that the cohesion along the length of the pile disappears with initial movement. This means that the initial resistance offered by a pile equals the friction and cohesion along its length. Before any resistance can be offered by the point, the cohesion disappears, resulting in a maximum resistance equal to the point bearing resistance and the friction along the length of the pile.

The peak resistance, therefore, is either the combination of cohesion and friction along the pile or the combination of the friction along the pile and the point bearing capacity. If motion of the foundation is to take place, the peak force applied to the pile must equal or exceed the peak resistance. The resistance associated with subsequent displacement would be the friction along the pile added to the point resistance. The same assumptions are used for a pile group, taking the base of the entire group for the point resistance and the outside area of the pile group in calculating the cohesion and friction. Both individual pile failure and group pile failure should be considered,

with the mode of failure requiring the lowest load being selected.

CONCLUSIONS

The recommendation of the previous section represents perhaps the simplest approach that could be suggested. This simplicity should not be allowed to deceive the reader—the problem of foundation analysis and design is far from being solved. The research discussed in this paper has, it is hoped, given some indication of the possible pitfalls. It is the author's opinion that only improved theoretical understanding, supplemented and guided by experimental studies, can offer hope for satisfactory solutions.

In applying even the simplified design procedures of the previous section, care should be taken to insure correct applications of static solutions for foundation failure. Many structural engineers lack familiarity with soil mechanics and too often incorrect methods are used or correct solutions are applied to the wrong problem. As an example of this consider footing designs based on a specified bearing pressure—this approach has no basis in theory since bearing capacity depends on footing size and depth in addition to soil properties. Similarly many tabulated or plotted solutions are suitable only under conditions which may not be clearly stated.

ACKNOWLEDGMENTS

Credit is given to Air Research and Development Command for sponsoring the original research and for permitting publication of this paper. Particular credit is given to Mr. C. Wiehle and Mr. H. Mason of AFSC for their criticisms and suggestions which substantially aided the research.

REFERENCES

- [1] P. Anderson, Substructure Analysis and Design, The Ronald Press Co., New York, p. 81, 1956.
- [2] Armour Research Foundation, Design and Analysis of Foundations for Protective Structures, Phase Report III, Interim Technical Report, January 1959.
- [3] K. E. McKee, Design and Analysis of Foundations for Protective Structures, Final Report, AFSC-TR-59-56, October 1959.
- [4] K. E. McKee, Design and Analysis of Foundations for Protective Structures, Interim Technical Report, Armour

- Research Foundation, Chicago, Illinois,
Appendix C, September 1960.
- [5] L. Prandtl, "Über die Harte plastischer
Körper," Göttinger Nachr., Math.-Phys.
Kl., pp. 44-85, 1920.
 - [6] R. Hill, "The Plastic Yielding of Notched
Bars Under Tension," Q. J. Mech. Appl.
Math., 2, pp. 40-52, 1949.
 - [7] V. V. Sokołowski, Statics of Soil Media,
Butterworths Scientific Pub., London,
1960.
 - [8] P. G. Hodge, "The Method of Character-
istics Applied to Plane Plastic Strain with
Inertial Effects," Design and Analysis of
Foundations for Protective Structures,
Interim Report, Armour Research Foun-
dation, Chicago, Illinois, Appendix B,
September 1960
 - [9] A. J. M. Spencer, "The Dynamic Plane
Deformation of an Ideal Plastic-Rigid
Solid," Jour. of Mechanics and Physics
of Solids, London, to be published.
 - [10] E. T. Selig, "Response of Foundations to
Dynamic Loads," Design and Analysis of
Foundations for Protective Structures,
AFSWC-TR-59-56, October 1959.
 - [11] K. E. McKee, Op. Cit., October 1959.
 - [12] K. E. McKee, Op. Cit., September 1960.
 - [13] K. Terzaghi and R. B. Peck, Soil Mechan-
ics in Engineering Practice, John Wiley
and Sons, Inc., New York, p. 171, 1948.
 - [14] K. E. McKee, Op. Cit., Appendix B, Octo-
ber 1959.
 - [15] K. E. McKee, Op. Cit., September 1960.
 - [16] K. Terzaghi and R. B. Peck, Op. Cit.
- * * *

PROTECTIVE CONSTRUCTION BY PROVEN COMPONENTS*

Captain Ralph H. Sievers, Jr., U.S. Army
United States Army Engineer Research and Development Laboratories

The United States Army Engineer Research and Development Laboratories, in conjunction with the Engineer School, have developed a flexible system for protective construction design and employment. The principal basis of the system is the use of structures and structural components which have had their resistance to blast effects proven by various nuclear tests. The components, of basic construction materials in prefabricated shapes, are generally such that they can be assembled into a full structure by relatively unskilled labor under competent direction. This system of design has been set forth to fulfill a need for flexible and proven designs without full-scale tests on each protective structure.

INTRODUCTION

The system sets forth families of structures and structural components which are designed to permit the engineer in the field to adapt to the requirements established for a protective structure, those components which most adequately suit his construction force, material and time available, and the functional criteria placed upon the structure. The structures and structural components are, in general, independent of each other and range in complexity from nestable corrugated pipe to arched reinforced concrete construction. The structural categories of components used are: the basic structure, endwalls, entrance configurations, blast-resistant doors and frames, and floors. The system provides illustrations of each choice within each category and links these choices in the order in which their usage should be considered. This ranking for selection purposes has been established from analysis of test results and from design and construction considerations.

THE DESIGN SYSTEM

The basic guide to protective structure design is presented as Table 1, Protective Structures and Structural Components. The system presents designs for earth berms

which permit semi-buried structures to be protected to a degree that they will react as though they were fully buried and consequently permit such structures to be designed from Table 1. The empirical results of Nevada and Rainier nuclear tests, and of high explosive and nondestructive vibration test programs, have been used as the principal design criteria for the structural elements. The system presents designs for each of the structures and structural components that essentially permit their selection without consideration for the choices available in the other categories. For example optimum endwall design, that which is man supported, may be employed with a basic structure of circular reinforced concrete, corrugated steel, or other design. Each of the basic structures and structural components presented is illustrated in the system by specific designs which in general allow dimensions to be varied and, thereby, the construction of various size structures. Theory which has been developed from the various test programs or from dynamic and ultimate strength tests has been used to extrapolate or otherwise derive designs or dimensions for which no test results upon an identical element were available.

A brief development of the test, theory, and empirical background of one type of one structural component is presented as an

*This paper was not presented at the Symposium.

TABLE I
Protective Structures and Structural Components

Basic Structure Type, Length Immaterial	Endwalls	Entrance Configuration	Blast-Resistant Doors and Frames	Floors
1. Corrugated steel, circular	1. Deadman supported	Vertical tube to horizontal passage	1. Designed personnel hatch 2. Designed walk-through door	1. Sand or earth 2. Sectional wood floor
2. Corrugated steel arch	2. Structure (and deadman) supported	2. Rectangular shaft to horizontal passage	3. Hatch for rectangular shaft	3. Pierced steel plank
3. Circular reinforced concrete	3 Reinforced concrete buried	3 Horizontal circular	4. Massive "drawbridge" door	4. Concrete
4. Reinforced concrete arch	4. Reinforced concrete exposed	4. Horizontal rectangu- lar	Alternatives Dependent on Availability from Supply Channels	
5. Rectangular rein- forced concrete	5. Earth at angle of repose (alternative for limited applica- tion)	5. Entrance through exposed endwall	5. Rock steel hatch	
6. Rectangular struc- tural steel	6. Pipe filled with sand (emergency exit for limited application)	6. Pipe filled with sand (emergency exit for limited application)	6. Stock steel door	

*Components in each column are listed in the order in which their usage should be considered.

example of the procedures employed: the design of corrugated steel circular and arched basic structures and entrance sections. Structures of arched corrugated steel construction have failed under nuclear blast pressures in the compressive mode, indicative of fully buried conditions. Compressive mode failure has been evidenced in these structures by bearing failure of bolts joining plates in longitudinal seams. Static load tests of 1000 lb bolted joints for different thicknesses of plate and spacing of bolts were used to relate the ultimate strengths of the corrugated steel sections for various gage plate. The tangential stress in true arch action due to uniform loading at the ground surface varies linearly with the radius of the curved section. A spectrum of design for such structures, circular and arch, can thus be developed. The computed static ultimate strength and the peak overpressure at ground surface were used for design, justification being the positive nuclear test results. The apparent effects of attenuation of overpressure with depth, a long response time of a buried structure when the surrounding soil responds with the structure, and the increased yield stresses in steel under dynamic loading may have combined to increase the actual resistance of buried structures well beyond that previously determined by theory. The results of this design study was a readily used graph for corrugated steel structure selection (Fig. 1). A limitation is put on the use of the graph to structures of finite root radius or less, due to the lack of tests on structures of greater radius and because the vulnerability to flexural action of such a structure increases as the square of the radius while the vulnerability to compressive failure only increases directly as the radius of the structure.

Utilities and emergency equipment to be employed with a protective structure designed under this system are similarly presented as components to the field engineer. As with the structural components, selection has been based, where necessary, on positive results of nuclear and high explosive tests. The emergency equipment and supplies are present standard military supply items. The use of these items for design is dependent on the intended structure employment and is adaptable to the combination of structural components which may have been selected. The testing and development of the Chemical Corps, Signal Corps, and the Corps of Engineers have been utilized to insure adequacy and effectiveness of the components and consequently of the completed protective structure. In addition to the table for selection of

utilities and closures based on structure utilization (Table 2), the system presents the basic engineering and dimensional data that the field engineer would require to adequately design a structure to fulfill the requirements placed upon it. Such data is presented as the B.T.U. output of the generator cooling systems, the physical dimensions of the military standard generators and their fuel and oil consumption, the human engineering factors of required air supply volume, critical temperature and humidity requirements, food and water supply criteria, the dimensions of standard rations, and the various means of effectively incorporating the utility requirements into the basic structure.

ILLUSTRATIVE EXAMPLE

An illustration of some of the structural and utility components and the intended usage of the system of design by components is provided by a sample design problem such as may be faced by the field engineer. For this example a continuous occupancy working station has been selected. Typical requirements of such a structure might be as follows:

- (1) Serve continuously as command post and communications center,
- (2) Provide approximately 1000 square feet of floor space,
- (3) Be capable of providing for the long-duration occupancy of up to two weeks for sixteen personnel,
- (4) Provide protection in the side-on overpressure range of 50 psi.

It is assumed that the design is not restricted by limitations of material availability.

The initial step of the field engineer is to go to the table for selection of utilities and closures based on structure utilization (Table 2), where the various utilities and the recommended entrance configuration are presented. The recommended entrance configuration is a vertical pipe with two blast closures and an emergency filled pipe. To fulfill the utility requirements separate closures for a latrine and for the generator, exhaust fan, and fuel storage will be built. The air intake unit may be placed below floor level within the basic structure as it is available with electric motor drive. Various storage bins will be provided below the basic structure floor to fulfill food, water, and other requirements.

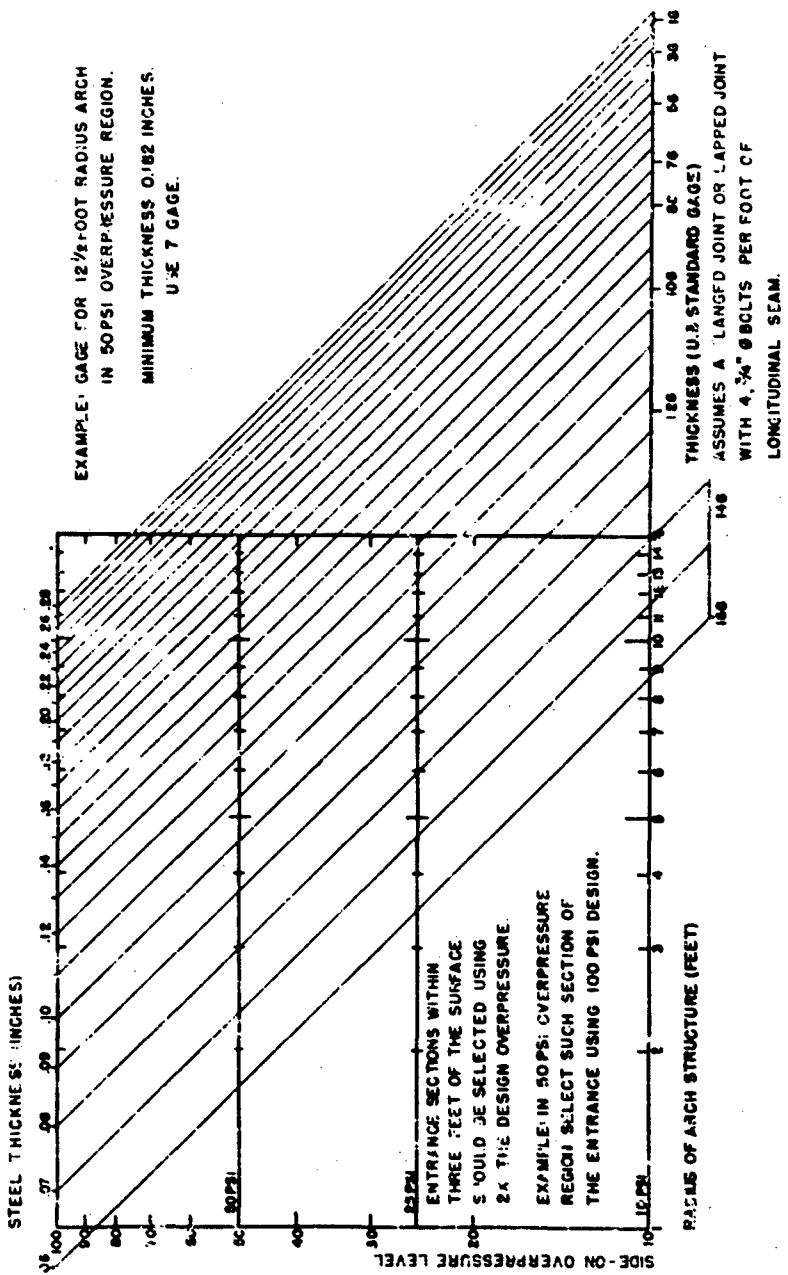


Fig. 1 - Corrugated steel gage selection for circular and arch sections

TABLE 2
Selection of Utilities Based on Structural Utilization

Intended Structure Employment	Recommended Entrances*	Revolving needed Electric Power and Lighting	Air Treatment	Water Supply	Sanitary Utilities	Emergency Equipment
1. Storage	Vertical shaft (if possible, horizontal and small diameter vertical pipe with closure).	Battery lighting (and, if available, central power source)	None	Conventional water supply, if any, minimum storage	Conventional units and outlet, or none	Gasket seal for massive entrance
2. Emergency personnel, short duration	Vertical type	Battery-powered lighting	None, volume selected from table	5-gallon cans storage	None, or bucket type, drainage to separate pit	Radiation detection equipment
3. Emergency personnel, ionization; duration	Vertical pipe	Battery lights and an engine-driven generator	Electric motor or engine-driven filter and exhaust fan	5-gallon cans storage	Bucket-type latrine latrine to separate pit	Radiation detection, food supplies
4. Personnel sleeping quarters and shelter	Vertical pipe; and emergency filled pipe	Battery lights (if available a central power source) and an engine-driven generator	Electric motor filter and exhaust heater	Conventional water supply and 5-gallon cans storage	Conventional units and outlet, bucket-type latrine with separate pit for emergency	Radiation detection, food, communications equipment
5. - Severe icy, personnel working and living station, long duration	Vertical pipe and emergency filled pipe	Engine-driven generator; if available, central power source; and emergency battery power for lights and signal equipment	Electric motor filter and exhaust (heat ex)	(Emergency water system) 5-gallon cans storage	(Use of emergency water system) drainage to separate pit, bucket-type latrine	Radiation detection, food, decon. equipment, communication, gas tanks
6. Continuous occupancy vertical air station	Vertical pipe with two blast closures and emergency filled pipe	Engine-driven generator, central power source, and emergency battery power for lights and signal equipment	Electric motor ventilation (if required) anti-backdraft valves (water, air conditioning)	Conventional water supply (emergency water system) 5-gallon cans storage	Conventional units and outlet, bucket-type latrine with separate pit	Radiation detection, food, decon. equipment, radiation monitoring, clothing, gas tanks
7. Radiological contamination shelter, no action	Vertical pipe with gastight partitions and emergency filled pipe	Engine-driven generator, lighting and emergency battery	Electric motor filter, exhaust, anti-backdraft valves in partitions	(Emergency water system) over-head or plenum shower feed, 5-gallon cans storage	Drainage to large separate pit, bucket-type latrine, showers	Radiation detection, food, decon. equipment, radiation monitoring, clothing, gas tanks

*An air lock consisting of two personnel blast closures, each designed for fullblast overpressure, is recommended for every personnel shelter.

†Emergency equipment of all underground structures: wrecking and entrenching equipment.

The next step is the actual design of the basic structure with its structural components. Reference to Table 1 provides the framework for this design. As the circular corrugated steel section is too small to provide the floor area to satisfy the space requirements, corrugated steel arch is selected for the basic structure. The actual radius and gage selected is dependent on the stock available and the graph (Fig. 1) requirements. For this example, utilize 12-1/2-foot radius corrugated steel. From Fig. 1, 12-1/2-foot radius and 50-psi overpressure require a steel thickness of seven gage. Alcoves for the latrine and generator and the entrance configuration tunnels may be made of the circular corrugated steel. The thicknesses of these components shown on the various illustrating figures were selected using Fig. 1. The type of endwall employed is partially dependent upon the dimensions of the structure. The basic structure of 12-1/2-foot radius will employ a deadman-supported type endwall to prevent longitudinal loads upon the basic structure. As the longitudinal loads imposed by an endwall are not as severe on the smaller structures, these structures may employ structure-supported endwalls. As can be seen from Fig. 3, the generator alcove, an endwall with earth at angle of repose, is sometimes most convenient and it can fulfill specific requirements for entry of utilities into the structure. The main entrance configuration employs an airlock to prevent structural damage should a closure be open at the time of blast arrival. The emergency exit is to be a pipe filled with sand, or relatively small diameter, to keep to a minimum the amount of sand which must be removed to employ the exit. A small diameter will also keep the emergency exit flexible and

allow it to be made of a thin gage steel. The blast resistant closures to be employed are to be fabricated from flat steel stock. The nature of this design can be seen in the entrance illustration (Fig. 3). Due to the below floor placement of the filter unit and storage bins, a sectional wood floor is selected for the basic structure. The entrance configurations and generator alcove need only use an earth floor. For sanitation, the latrine alcove should have a concrete floor.

The final assembly of the various components is illustrated in Fig. 4, the floor plan of the continuous occupancy working station. Details of portions of the structure illustrating construction or utilities placement are shown in Figs. 2 through 5. The structure is not set forth as a prototype and it is doubtful that an identical structure will ever be built. This structure and similar structures that can be designed from the tables of utility and structure components do, however, take advantage of ten years of nuclear tests and continuing nondestructive and high explosive test programs.

CONCLUSION

The basis of protective construction by proven components is flexibility and positive test results. Proof tests have not been conducted of prototype structures which would suit every requirement of military or civil construction. Sufficient test results are available, however, on various components, structural shapes, and construction methods, that satisfactory design tools can be made available to the field engineer to meet his construction needs.

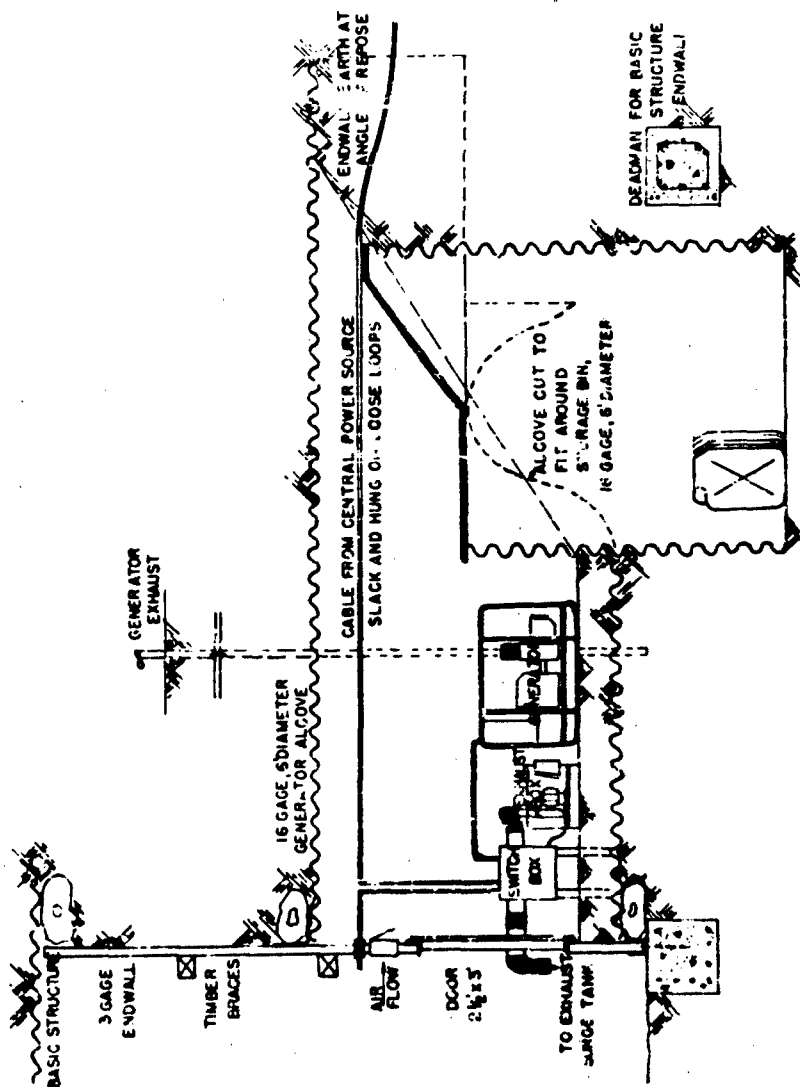


Fig. 2 - Generator alcove

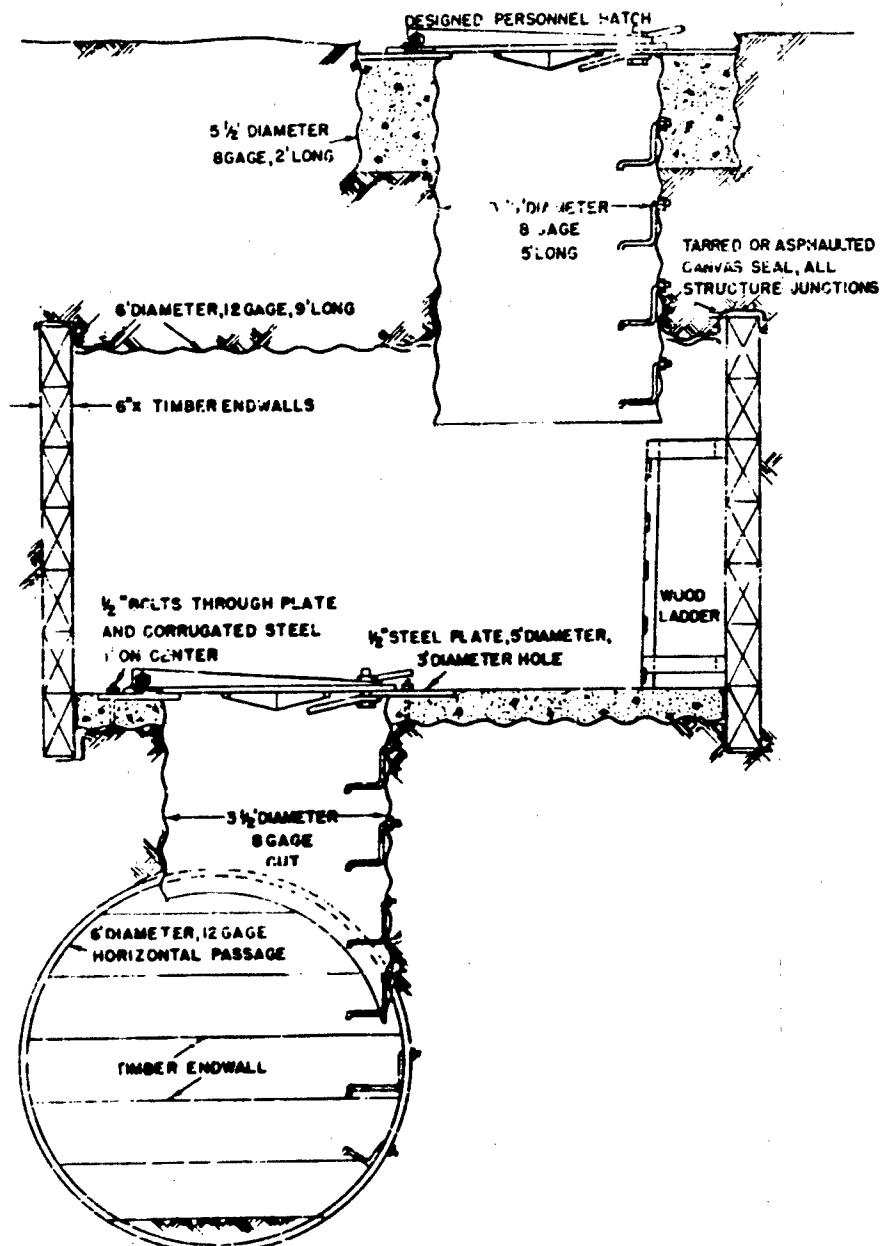


Fig. 3 - Entrance configuration

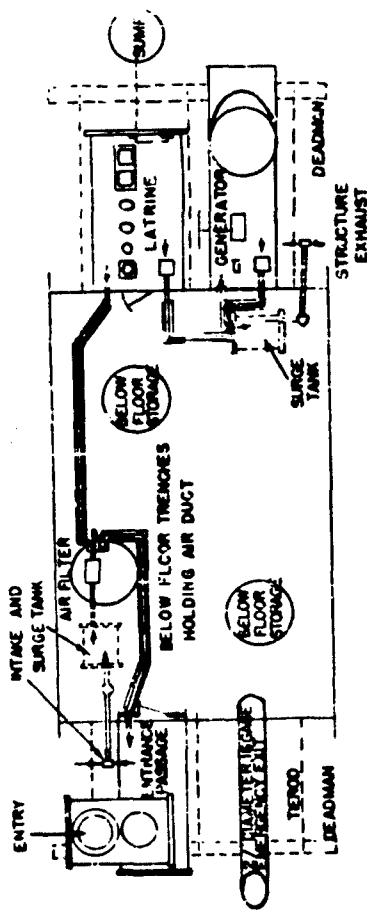


FIG. 4 - Continuous occupancy work station, floor plan

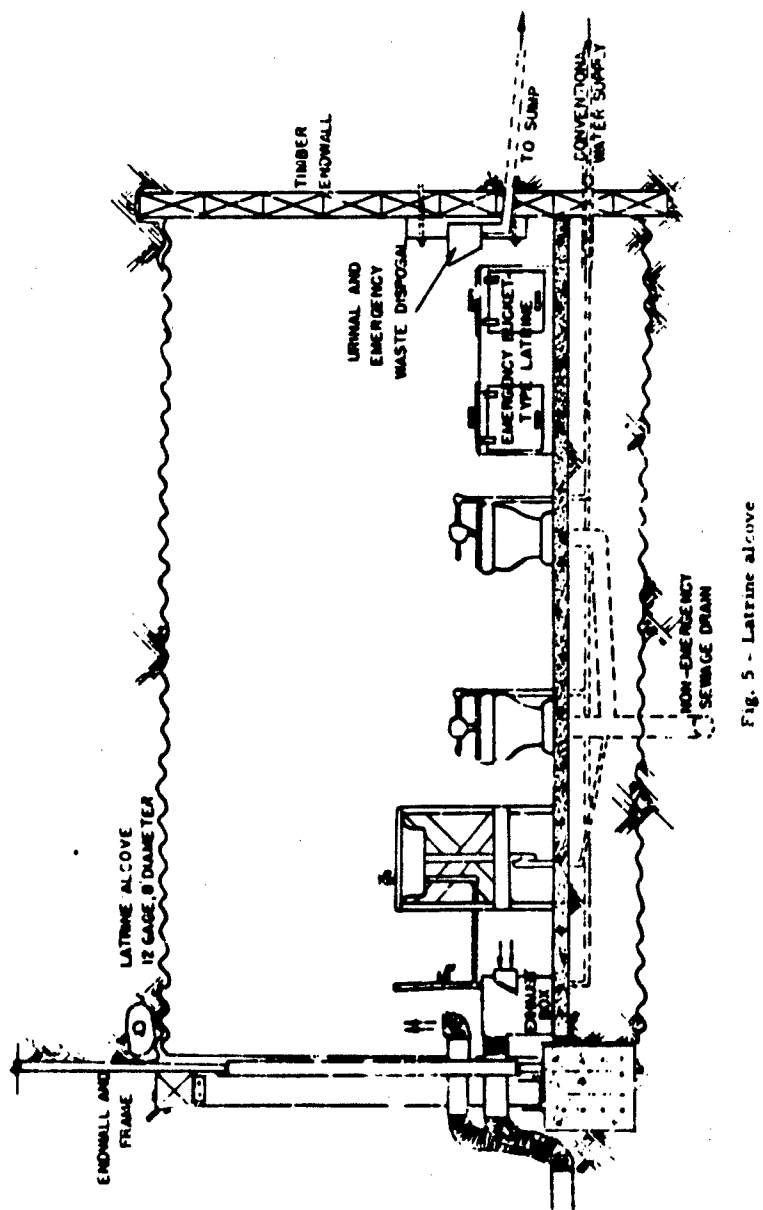


Fig. 5 - Latrine alcove

CONSIDERATION OF COSTS AND CAPABILITIES OF PROTECTIVE STRUCTURES*

R. B. Vaile, Jr.
Stanford Research Institute

The actual capability of a protective structure is impossible to determine, except by a test which destroys it, and even the design objectives are arrived at only with great difficulty, and commonly with important legitimate differences of opinion. One of the concerns in stating design objectives is the comparison of the importance of strength against a single shot with strength against multiple shots. This comparison is amenable to treatment on a very broad basis and leads to the conclusion that while it is appropriate to increase the cost of a structure 20 percent or more to achieve double strength against a single attack, less than a 5-percent increase is still to give it strength against two attacks rather than one.

Protective structures differ in two important respects from conventional structures. As a general rule, the methods of design and construction of standard structures have been tested and proved by actual experience. New trends or departures from proven procedures have been used with caution and their widespread application has ordinarily awaited confirmation of their validity by the test of time. The firm distinction of protective structures is that relatively large uncertainties of design (and loading) exist and that it is not possible to obtain confirmation of design by experience.

In most problems of structural design the direction of increased safety is obvious. Ordinarily this is accomplished simply by adding more concrete and steel. The structure is "beefed up." Notable exceptions include earthquake- and wind-resistant structures and airplanes and dirigibles. By and large, the exceptions are situations in which inertia forces involving components of the structure are important. In these cases mere beefing up does not necessarily improve safety and can even decrease it. Protective structures are generically in this class.

Thus in protective construction designed to withstand megaton weapons, it is not possible to check the validity of the design by subjecting the structure to the actual loads it is intended to withstand, and the direction of enhanced capability is by no means always clear. In addition, the total expenditure of effort and money in protective structures in this country during the next decade may well be a major drain on the economy of the country. In these circumstances it is particularly important to obtain the maximum of protection for every dollar and every man hour expended in the design and construction of structures. An aspect that further confuses the situation in protective construction is that civil and structural engineers commonly operate with factors of safety ranging roughly between 1.5 and 5. To the extent that a factor of safety is precisely known, it is entirely acceptable to the analyst and planner. However, that part of the factor of safety which represents real ignorance of the true strength of the structure represents a potentially serious loss of efficiency in the use of funds and effort. Thus a structure which, for example, begins to show distress at 400 psi can be described as having a factor of safety of 2 against 200-psi

*This paper was not presented at the Symposium.

situation or a factor of safety of 1.33 against a 300-psi input. On the other hand, if in a complex of structures designed to withstand an environment of 100 psi, some component structures will be damaged at 150 psi whereas others remain undamaged at 300 psi, then efficiency in the use of funds has suffered. A "one-hose shay" design is the ideal.*

The question of how many attacks a structure should be designed to withstand, and how the design should be modified for multiple attack compared with single attack, is very important and is intimately tied up with efficiency of our resource expenditure. Before entering a discussion directly bearing on this problem it is worthwhile first to cover some preliminary aspects.

The designer of protective structures which are intended to be effective against near-surface bursts of large weapons finds himself constrained very early in his deliberations to place his structures underground whenever possible, and, for those components which require surface exposure, to design them with smooth horizontal surfaces and with a minimum of vertical exposure above the surrounding level. He is forced to do this primarily because of wind forces or dynamic pressure due to air movement which are normally much more severe than the overpressure.

While the total regime of forces on an underground structure is complex and does not always stem directly from the pressure of the air at the surface above the structure, peak air overpressure is, for the purposes of this discussion, a satisfactory index of the severity of the input to a protective structure.

Nearly all protective structures are composed either entirely of steel or of a combination of steel and concrete. If structures or components of this type are subjected sequentially to loads or inputs of increasing magnitude, it is found that for loads below a certain magnitude, the entire structure remains within the elastic range, and that when the load is

*In deference to Dr. Herman Kahn of the RAND Corporation, it is agreed that the first units of any design may appropriately depart from the one-hose shay ideal; namely, those elements which can be designed for greater strength with very minor additional expense should be so designed, with the presumption that later construction will bring the remainder of the unit up to that increased strength. The one-hose shay design is ultimately the appropriate one.

removed the structure returns exactly to its original condition. Obviously, inputs within this range can be repeated indefinitely without damage to the structure.

As still larger loads are applied (and removed) the first thing that happens is that small permanent deflections occur; and as the loads are further increased, these deflections become larger and larger until at some stage the useful function of the structure is seriously impaired. While in some cases the first impairment is dramatically sudden, and coincides with collapse (in column buckling for example), it usually occurs at a load considerably less than that which causes complete collapse. Now the critical property of protective structures as a class is that the load required to seriously impair the function of the structure always is less than twice the maximum elastic load.

It is to be noted that the term load as used here can be either dynamic or static, that is, either time-varying or constant. For dynamic loads the only requirement is that in comparing the maximum elastic load with the minimum load causing impairment of function, the same time regime be used with only the amplitude at each instant being multiplied by a constant factor (in such case the factor is less than 2).

The next bit of ground work for the analysis is a consideration of some weapons characteristics. The peak air overpressure from a near-surface burst falls off as the inverse cube of the radius, R, for small R and as the inverse square for large R. All weapons delivery systems have inherent errors and, for our purposes, an elementary analysis of the probability situation is sufficient. In such an analysis the CEP is defined as the radius, within which half the burst points will fall.

Figure 1 shows a combination of the overpressure as a function of radius together with the probability that for any one shot the radius will be greater than the indicated value. It is to be noted that both of these curves are normalized to the CEP.[†] Now since the two curves on Fig. 1 have the same abscissa,

[†]While the precise values on the overpressure curve may be in some doubt because, as has been mentioned earlier, the profile in the close-in region varies as the inverse cube of R while farther out it varies as the inverse square, the general shape is as shown and the difference between inverse cube and inverse square is relatively minor.

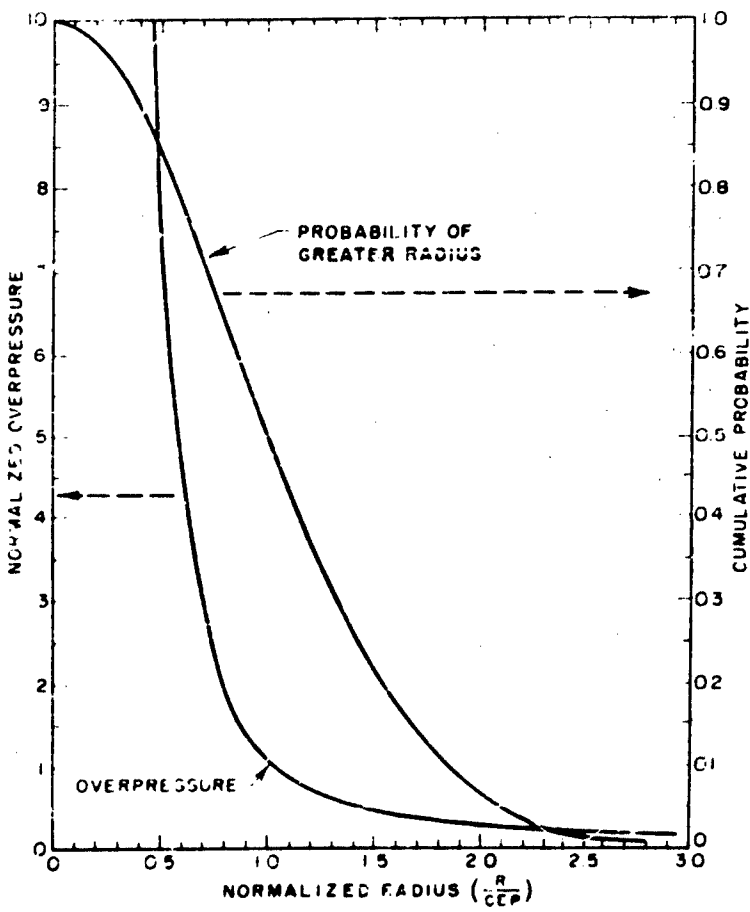


Fig. 1 - Overpressure and probability as a function of radius

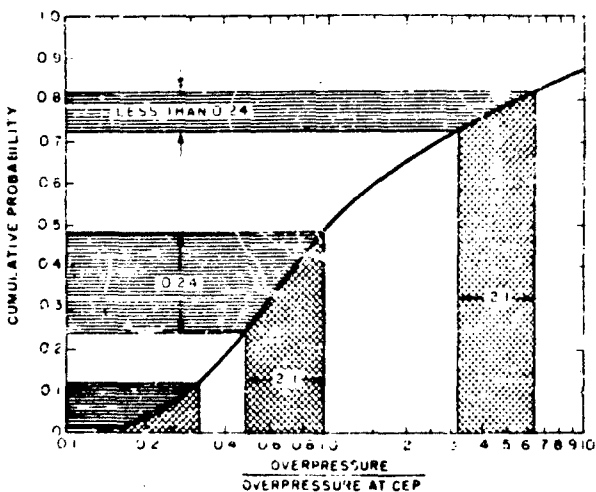


Fig. 2. Probability of lower pressure

namely, radius, this parameter can be eliminated and the normalized overpressure can be plotted against probability.

This has been done in Fig. 2 which shows the probability, for any one shot, that the actual overpressure will be smaller than the indicated value. For convenience in presentation a log scale of normalized overpressure has been used on the abscissa.

Now let us consider the significance of this characteristic of near-surface atomic explosions combined with the characteristic of protective structures that there is no more than a 2:1 range between the load for failure and the maximum elastic load. The curve of Fig. 2 shows that in the middle range of the curve the probability of the occurrence of an overpressure within a 2:1 range is 0.24 and that the corresponding probability at either end of the curve is still smaller. The significance of this figure is as follows:

In considering the capabilities of a structure in resisting attack by multiple shots it is clear that (1) for pressures lower than the maximum for elastic deflection, the structure can stand a large number of attacks and that (2) the structure can stand no attacks with an overpressure more than twice this large. Figure 2 shows, therefore, that the probability that a structure is damaged but not destroyed by a single shot is 0.24. Thus only in this 2:1 region, having a probability of 0.24, is the capability of the structure any different for

multiple shots than it is for single shots. Now the probability that two attacks will both fall within the same 2:1 pressure span is $(0.24)^2$ or 0.06.

Another way to view this situation is to consider that in an attack by multiple shots against a single structure some one of the multiple shots will produce a maximum pressure against the structure. The probability is 0.76 that this shot will either have destroyed the structure or will have left it undamaged. If it has destroyed the structure then there is no point in considering the other shots of the attack. If it has left the structure undamaged, since we postulated that this is the strongest of the multiple shots, then none of the others will damage the structure and hence they are of no interest. Only in the situation in which the strongest single attack has been in the 2:1 range of capabilities of the structure is there any interest in considering any other shot. In this case only, which has a probability 0.24, are we interested in the next strongest shot. The probability that it will lie within the same 2:1 pressure range is less than 0.24, and hence the probability that these two shots, namely, the most severe and the next most severe, will both fall in the 2:1 pressure range is less than 0.06.

The conclusion to be drawn from this analysis is that when a structure has been designed for a certain capability against a single attack, the additional expenditure justified to protect it against a second attack of

the same magnitude is no more than 6 percent. The corresponding figure for enhancement of the capability of the structure against single attack is that as much as a 24-percent increase in cost may be justified if the strength against single attack can be doubled.*

The range of validity of these conclusions is of some interest. In fact, they are essentially independent of the CEP of the attacking weapon or its yield and depend only on the exponent of the pressure versus distance curve. This exponent lies between -2 and -3 for a very wide range of pressures and distances, and within this range the conclusions are firm. In addition, to say that the pressure range between maximum elastic load and severe damage is two-to-one is quite conservative. In most cases the range is narrower than this. Finally, the S shape of the curve demonstrates that the probability of an attack with twice the pressure is generally smaller than the maximum value of 0.24 which occurs in the mid-range.

*By doubling the strength against single attack is meant increasing the strength to withstand an attack with twice the peak overpressure.

For all these reasons the cost justified to double the capability against single attack is less than the 0.24 indicated, and the cost justified for protection against multiple rather than single attack is less than the value of 0.06 given above. The precise mathematical statement is that the justified fractional increase in cost to double the strength of the structure against single attack (C_{2p}) is always less than 0.24, and the corresponding figure (C_m) for protection against multiple attack is less than the square of the actual value of the first.

That is:

$$C_{2p} < 0.24$$

and

$$C_m < C_{2p}^2$$

The pertinence of the conclusion that it is more valuable to double the strength against a single attack than to provide strength against a second attack, is enhanced because the costs are in the inverse relation. It costs less to double the strength against one attack than to provide for multiple attack. Sacrificial elements acquire very much greater interest if these conclusions stand the test of critical review.

Section 4

EFFECTS ON EQUIPMENT IN HARDSITES

NUCLEAR GROUND SHOCKS ENVIRONMENT

Ross W. Dowdy
Daniel, Mann, Johnson and
Mendenhall and Associates
Los Angeles 57, California

The ever increasing number of engineers engaged in the design of facilities which require some degree of resistance to ground shock, has dictated that some reliable and practical method of establishing ground shock information be developed. This method should use charts and simple formulas wherever possible.

This need resulted in the initiation of an independent study into the subject which is still in progress. Although the study cannot be considered even close to complete, it is believed that a sufficient number of useful results have been achieved to justify a report at this time.

In addition to some of the results of the study, this paper presents a resume of some methods of isolating an interior structure from ground shock including photographs of some typical installations.

BASIC STUDY APPROACH

Since the nuclear test observations available cover a very limited number of geological conditions, an empirical approach cannot be used. Instead, the basic approach of this study has been to use the fundamental dynamic soil characteristics as determined by numerous high explosive experiments and to build theoretically from that foundation to obtain the reaction resulting from a nuclear test. This theoretical reaction can then be compared with test results to determine the validity of the approach. The basic philosophy has been to start off with as few parameters as possible and add only those which from the theory seemed to have a significant effect on the results. Until recently practically all studies into the ground shock effects of nuclear weapons have been based on the assumption that soil behaves very much the same as an elastic medium. However, soil might better be

described as semiplastic. The plastic character of soil can be seen in Fig. 1, which shows a dynamic stress-strain curve for an average soil. This type of curve is obtained by exploding a charge of high explosive and recording an accurate pressure time curve at two different distances from the charge. The two curves are recorded on the same film or paper so that accurate time measurements can be made between each curve for the different pressure levels. With the distance between the charge and the gages being known, the velocity of propagation for each stress level can be calculated. This information when corrected for spherical spreading, can be used to plot a dynamic stress-strain curve such as the family of curves shown on Fig. 1 and it contains practically all the information necessary for determining the shock characteristics of the material. Dynamic stress-strain curves have not been developed for all of the different types of soil, but a great many

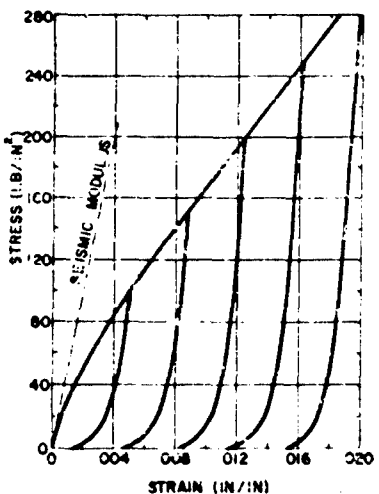


Fig. 1 - Dynamic stress-strain curves for average soil

high explosive loads have been instrumented and the pressures and displacements have been normalized with a single parameter reflecting the characteristics of the soil. This parameter called the soil constant, has been successfully correlated on the basis of the seismic velocity. This fact clearly indicates that the shape of the dynamic stress-strain curve is typical for a wide range of soil types. Logic might lead us to believe that this curve would apply only to clay, sand, silt and the like, but that rock would exhibit a somewhat more elastic character. This belief was not supported by tests which were conducted on a large mass of homogeneous limestone by the

Mason and Hanger-Silas Mason Company in 1955. The results of these tests correlated very well with computed values based on the empirical equations for soil, using, of course, the soil constant derived from the seismic velocity of the limestone.

The shape of this dynamic stress-strain curve is not entirely unfamiliar to most of us, since we have seen practically the same curve in static soil tests and also from concrete tests. When the basic similarity of all semi-plastic stress-strain curves is considered, it is not surprising that limestone should behave in a similar manner to soil, at least to a degree, and that degree is related to their relative seismic velocities.

One might question the use of the same curve shape for rock as for soil, on the grounds that we know from experience that solid rock transmits shock for greater distances than sand, loam, clay or silt. However, this reaction is easily explained by the relative seismic velocities alone, as demonstrated by the relative areas under the curves in Fig. 2, which shows the effects of changes in seismic velocity. Note the reduction in area within the curve as the seismic velocity increases which indicates far less energy attenuation in the pressure wave for any given distance. Each of the curves has the same basic slope relation with respect to the corresponding seismic slope for every stress level. Since this slope of the curve is virtually the modulus for the particular stress level, the velocity of the stress wave can be computed; it is simply the square root of the modulus divided by the square root of the mass per unit volume. With this information, the stress profile can be determined at any time as is shown plotted in the upper half

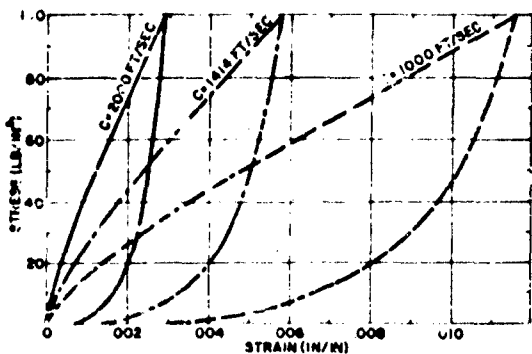


Fig. 2 - Effect of changes in seismic velocity

of Fig. 3. The corresponding strain profiles are shown in the lower half of the figure. Note that, as in any nonlinear medium, the strain profile is not proportional to the stress profile. This demonstrates the error in using the impulse to compute displacements. However, once the correct strain profile is known, the displacement of any point is simply the integral of the strain beyond the point. Accurate time displacement curves for soil at 1000 ft/sec seismic velocity are shown in Fig. 4, in which curves for the surface and for three scaled depths are given. Displacements for any other seismic velocity can be obtained simply by multiplying by 1000 and dividing by the seismic velocity. The curves apply only to the 100-psi range from a high yield surface burst and they will not work for any other combination.

Time displacement curves for any other weapon yield and pressure can be computed in the same manner by integrating the strain curve. The easiest method of accomplishing this is with a digital computer. The problem can be solved by numerical integration, but this method is not recommended since it is a long and laborious process.

Once a time displacement curve is computed, the "shock spectra" can be computed by the solution of an excursion problem for each frequency necessary to give enough points to plot a smooth curve. An example of such a spectra is shown in the triaxial plot of Fig. 5. The curves shown were computed on an IBM 704 digital computer and represent the displacements of single degree-of-freedom systems located at the surface and with their

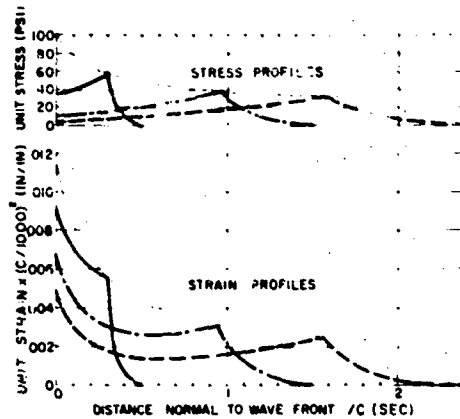


Fig. 3 - Stress-strain profiles

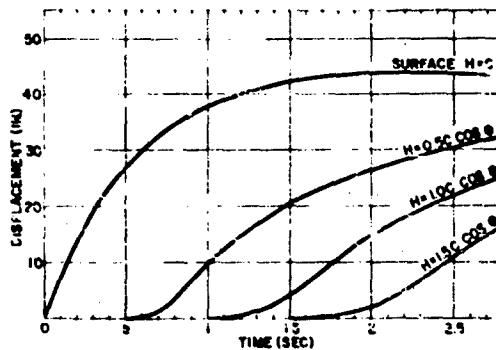


Fig. 4 - Time displacement curves ($C = 1000$ ft/sec; displacement normal to wave front)

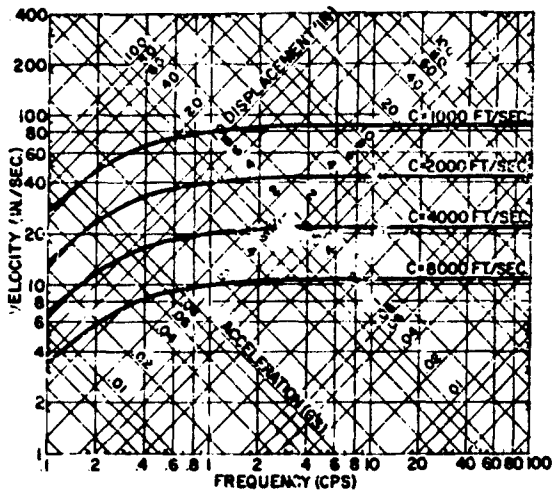


Fig. 5 - Surface shock spectra (average soil)

axis of motion oriented parallel with the ground motion. An average homogenous soil is assumed with a weight of 100 lbs/cu ft and the seismic velocities indicated. The air blast wave assumed is that associated with a high yield surface burst at the 100-psi range. These curves cannot be compared directly with test data for several reasons.

The assumption of homogenous soil will never be quite true for any site. The seismic velocity will normally increase in steps with depth. The reflections from these higher velocity layers tend to decrease the lower frequency displacements and to increase

displacements in certain of the middle frequencies. The major difference, however, is due to the fact that the curve applies to motion parallel with the ground wave motion and for comparison with a vertical spectra, the displacements must be multiplied by $\cos \theta$ where θ is the angle between the ground wave front and the ground surface as shown in Fig. 6.

This angle is approximately equal to $\text{arc sin } (2c/U)$ for values of P above 40 psi, in which c is the seismic velocity of the soil and U is the velocity of the air shock front. To change the curve to a horizontal spectra, the displacements must be multiplied by $\sin \theta$,

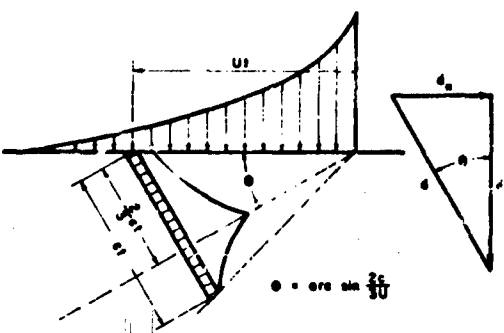


Fig. 6 - Stressed soil column, showing angle θ between the ground wave front and the ground surface

but since θ is similar to $\text{arc} \sin(2c/3U)$ the trigonometric functions cancel out and we multiply by $2c/3U$. However, since the original displacements are inversely proportional to the seismic velocity, c drops out and the horizontal spectra curve becomes a constant value being unaffected by the seismic velocity of the soil. The vertical and horizontal spectra at the surface for the 100-psi range from a high yield surface burst will be similar to those in Fig. 5.

Shock spectra for any range, weapon yield, and seismic velocity can be computed in the same manner provided c/U remains less than unity for a considerable depth. This depth should be such that the displacement caused by the overburden will be large enough to mask any effects caused by outrunning in the high velocity lower layer.

The high speed of the digital computer makes it possible to incorporate many factors in the problem about which information is needed; for example, the effects of reflections from hard lower strata. This problem is somewhat more complicated than the elastic solution, since the modulus changes as the pressure increases. By the use of the digital computer, the shock spectra can be solved to any desired degree of accuracy. However, many shock problems do not warrant the time or expense involved in programming; such as preliminary designs, siting problems, and simple designs in which some overdesign would involve little additional expense. For such problems simple formulae are needed to establish the envelope for a shock spectra curve. Such formulae are shown in the triaxial plot of Fig. 7, which shows the six basic formulas establishing the constant displacement line, the constant velocity line and the constant acceleration line for a homogeneous soil.

The vertical displacement is determined by the formula:

$$d_v = \frac{707 W^{2/3} \times 10^5}{rc} \cos \theta$$

in which

W = Weapon yield in megatons

r = Radial distance from charge in feet

c = Seismic velocity in ft/sec

$\theta = \text{arc} \sin(2c/3U)$

U = Air shock front velocity.

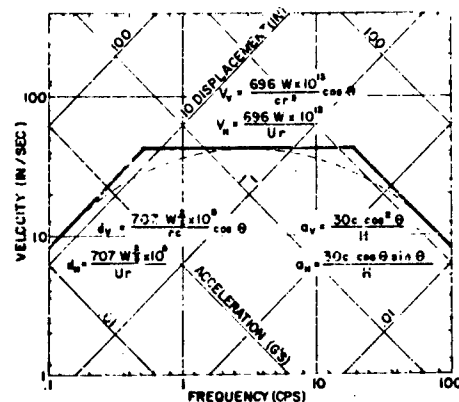


Fig. 7 - Sample formulae for establishing the shock spectra envelope

The horizontal displacement is determined by the formula:

$$d_h = \frac{707 W^{2/3} \times 10^5}{rc}$$

The vertical velocity is determined by the formula:

$$v_v = \frac{696 W \times 10^{13}}{U_r^3}$$

or

$$v_v = \frac{870 P}{c} \cos \theta$$

$$v_v = \frac{696 W \times 10^{13}}{U_r^3}$$

or

$$v_h = \frac{580 P}{U}$$

in which P is the peak side-on pressure.

The vertical acceleration is determined by the formula:

$$a_v = \frac{30 c \cos^2 \theta}{H}$$

in which H is the depth below the surface of the ground in feet.

The horizontal acceleration is determined by the formula:

$$a_R = \frac{30c \cos \theta \sin \beta}{H}$$

These are the six basic formulae upon which many others are based for handling special conditions.

EXAMPLES OF SHOCK ISOLATION SYSTEMS

The ground shock information, whether obtained from a digital computer or by the use of envelope formulas, can then be used to design shock isolation systems for the protection of equipment and personnel. Many articles have been published on methods for the design of shock isolation systems so there is no point in trying to go into the subject thoroughly in a paper of this length. In general, however, the object of shock isolation is to provide a flexible connection between the isolated object and the exterior structure or ground. The connection should provide for relative motion in all directions. A look at some typical solutions to the problem may be of interest.

Tunnels

Figure 8 is a typical tunnel section showing some methods of shock mounting pipes and

cable trays. Note the dark blocks which indicate rubber shock mounts.

Figure 9 shows a system of mounting a cluster of pipes with coil springs.

Figure 10 illustrates the soft coil spring mounting of the light fixtures in a tunnel.

Figure 11 is a good example of why rattle space sometimes is at a premium in tunnels.

Powerhouse

Figure 12 illustrates a type of shock isolation which is useful when the equipment on the lower level is sufficiently rugged to withstand the ground shock and only the upper level needs to be protected. The upper floor is isolated by means of spring beams located below the lower floor which take the vertical motion while the columns have sufficient flexibility to take the lateral motion.

Figure 13. When only one or two pieces of equipment on the lower floor need isolation, they may be handled separately as shown in Fig. 13, which is a water chiller that is resting on rubber sandwich-type shock mounts.

Figure 14 is a close-up of this same mounting showing the steel plates between the rubber pads.

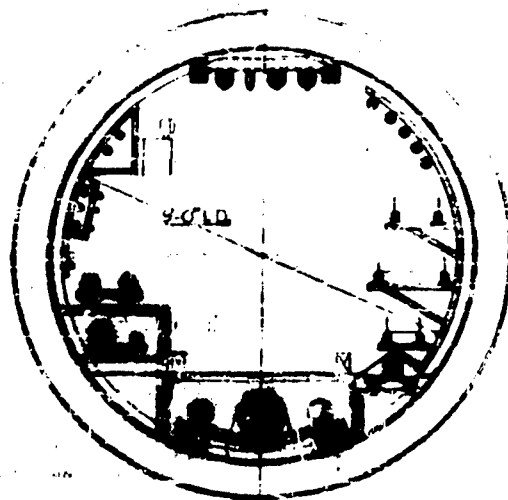


Fig. 8 - Type "A" tunnel section



Fig. 9 - C.H.I. spring pipe support



Fig. 10 - Stock mounted light fixture

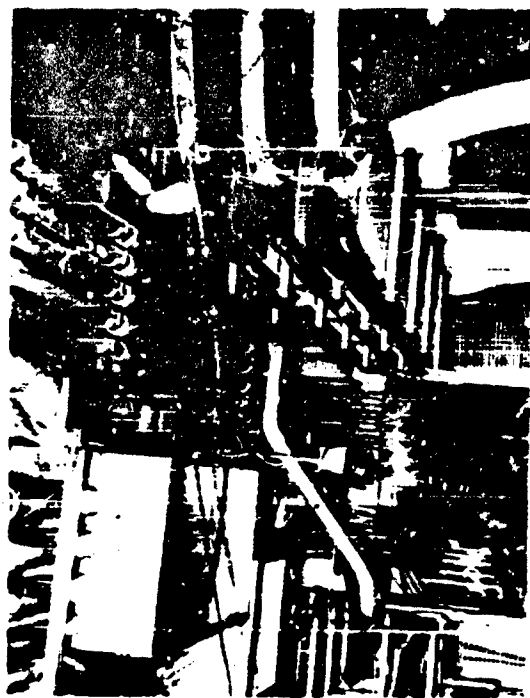


Fig. 11 - Ducts, cable trays, etc., entering tunnel

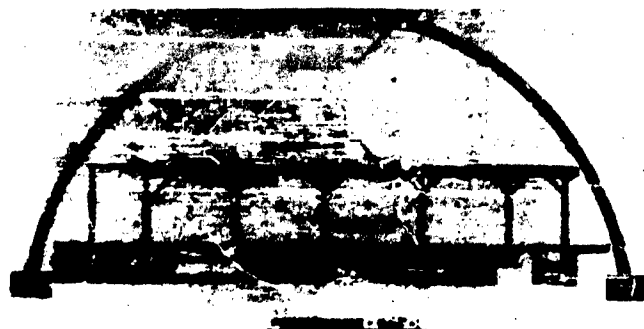


Fig. 12 - Typical single floor mounting

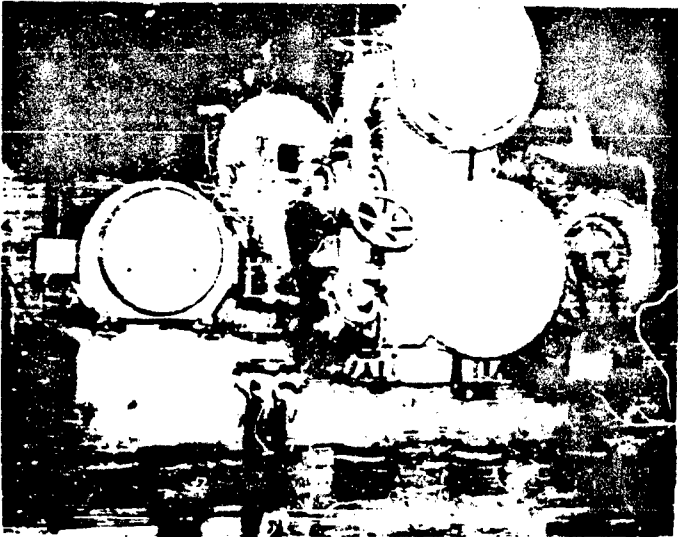


Fig. 13 - Rubber shock mounted chiller



Fig. 14 - Detail of rubber shock mounting

Figure 15 is a sulfuric acid tank which illustrates another type of individual mounting.

Powerhouse with Complete Shock Mounting

Figure 16 shows a system for shock mounting the complete interior structure by the use of spring beam units under the lower floor. The horizontal flexibility is accomplished by short 18-inch pendulums.

Figure 17 is a construction photograph showing the spring beam units in the process of installation.

Control Center

Figure 18 is an example of a structure with the major part of its delicate equipment located on the second floor, requiring only that floor to be shock mounted.

Figure 19. When both floors are required to be shock isolated, the solution shown in Fig. 19 may be used; the same type of spring beam units as shown previously are used.

Equipment Terminal

Figure 20 is an example of separately mounted floors in a silo type structure. When

there are only a few items such as pipes or conduits running between the floors and all of these can be made flexible, this system functions very well. However, if rigid items span between the floors, then the floors must be tied together with rigid bracing to form a crib, but the same shock mounting will serve just as well.

Figure 21 is a detail view of the spring beam for this silo system.

Figure 22 shows the base of the column which is a moment connection designed to utilize the bending stresses of the columns as a restoring force. This action holds the frequency high enough to avoid the possibility of extremely low frequency, but high amplitude ground motion from a high yield weapon.

Figure 23. Frequencies and amplification factors must be studied carefully when designing vibration isolators for equipment to be mounted on a shock mounted floor. Figure 23 is an example of such an isolator.

Figure 24 is an example of the use of coil springs to shock mount an interior structure. This method is justified only when the shock mounted equipment is extremely heavy with a high center of gravity and the space is limited.

Figure 25 shows the arrangement of the horizontal springs. The top of the columns are



Fig. 15 - Shock mounting of sulfuric acid tank

supported laterally by a steel frame floor which also ties into the large steel bottle clusters which are the reason for the shock mounting.

Figure 26 is a close-up of the horizontal springs. There is an interesting feature to this design; the spring is designed to function only in compression even

though the unit as a whole functions both in tension and compression.

Figure 27 is a view of the vertical springs which take all of the vertical load of the interior structures.

Figure 28 represents one of the more fragile but very important items of equipment.



Fig. 16 - Example of shock mounting of complete interior structure



Fig. 17 - Typical spring beam unit



Fig. 18 - Typical control center (top floor only mounted.)



Fig. 19 - Typical control center (both floors shock mounted)

Fig. 21 - Detail of spring beam and column connection



Fig. 20 - Typical silo structure with individual floor mounting

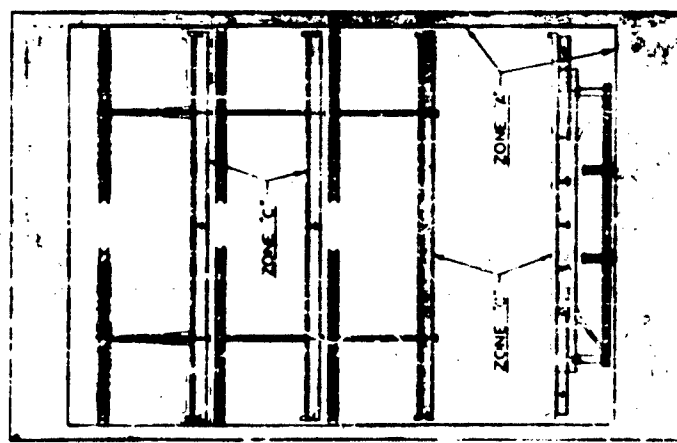




Fig. 24 - Detail of column showing fixed base

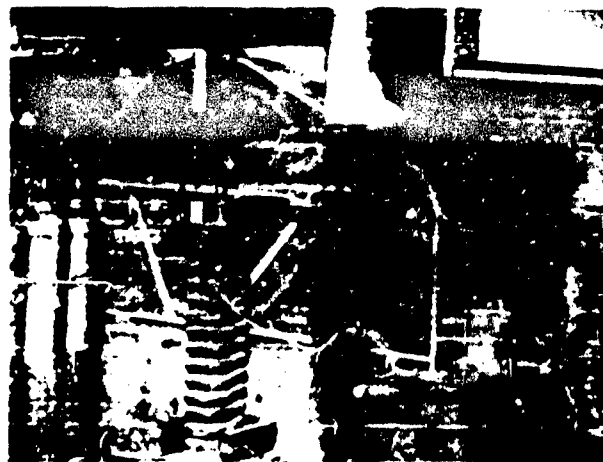


Fig. 23 - Vibration isolators on air compressor



Fig. 24 - Typical coil spring mounting of interior structure.

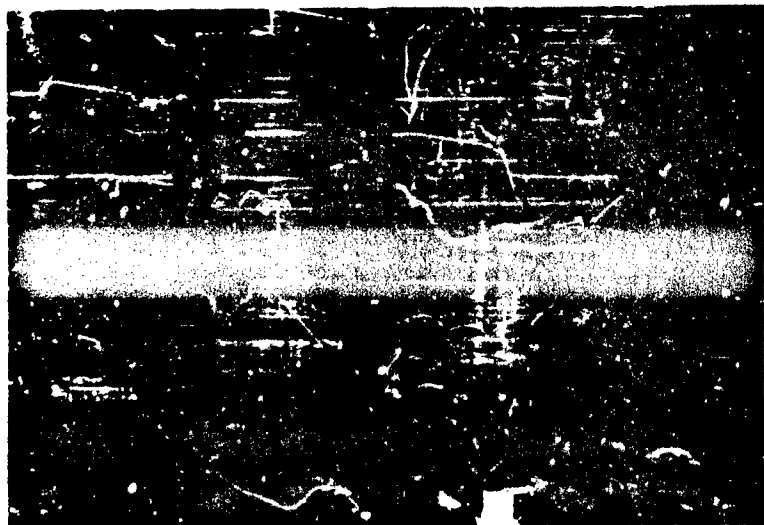


Fig. 25 - Horizontal spring arrangement.

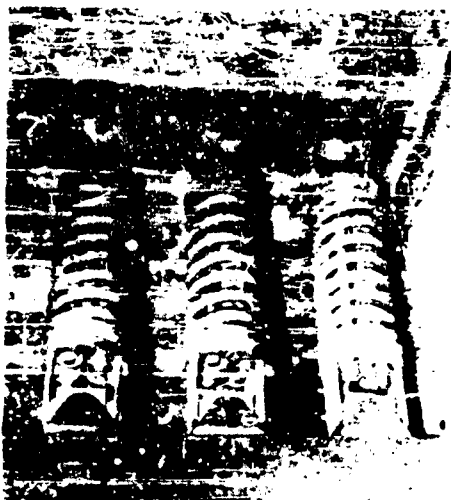


Fig. 26 - Detail of horizontal springs



Fig. 27 - Vertical springs



Fig. 28 - Important piece of shock
mounted equipment

CONCLUSIONS

Many conclusions may be drawn from this study, but the one most worthy of mention is that the nonlinear nature of soil has a definite effect on the shock spectra throughout its full range and especially in the high-frequency region where it is practically the only factor determining the free-field acceleration. The relative propagation velocities of the stress wave in the air and in the soil have a significant effect, and the resulting angle between the ground wave and the surface must be accounted for if accurate results are to be expected.

RECOMMENDATIONS

Wherever seismic testing is contemplated for site selection or other activities, it is recommended that slightly more sophisticated instrumentation be employed which will record pressure time curves as described previously, and that the resulting data be collected and analyzed to establish dynamic stress-strain curves for each type of soil. It is further recommended that the average curves shown here be used for predicting the inelastic behavior of all soils until such time as the test data indicates a trend away from the average for a particular type of soil.

BIBLIOGRAPHY

- Cook, Melvin A., "The Science of High Explosives," Reinhold Publishing Corp., New York (1958).
- Glasstone, Samuel, "The Effects of Nuclear Weapons," Supt. of Documents, U. S. Government Printing Office, Washington, D. C. (1957).

- Lampson, C. W., "Final Report on Effects of Underground Explosions" (Feb. 29, 1948), N.D.R.C. Report No. A-479.
- Crede, Chas. E., "Vibration and Shock Isolation," John Wiley & Sons, Inc., New York (1951).

DISCUSSION

Mr. Chasseyka (Armour Research Foundation): In your stress-strain curves where you show the steep rise for a hard rock and a gradual rise approaching the horizontal coordinate asymptotically for a porous medium, it indicates a greater attenuation of a seismic wave in the soft medium than in the hard rock. Do you have at least an approximate number giving the relative rates of attenuation of a seismic wave in the two different media?

Mr. Dowdy: No. Nothing other than the fact that it is related to the seismic velocity. If you trace out the stress wave based on this dynamic stress-strain curve, this gives you the attenuation as shown in that stress curve—the stress profile. Perhaps I should have dwelled on that a little longer. This actually gives you the peak pressure at each distance.

Mr. Chasseyka: That's what my question pertains to. How does this peak pressure vary from, say, the source of the explosion? How rapidly does the energy fall off in the two different media at, say, a given distance from the explosion? I thought you might have test data on that.

Mr. Dowdy: I don't have any available right here. There is quite a lot of test data on it, but I can't quote it.

Commander Christensen (Bureau of Yards & Docks): I notice in your shock spectra you have covered quite a wide range of frequencies from about 1/10 cps to about 1000 cps. Is this correct?

Mr. Dowdy: Yes.

Commander Christensen: It appears that at these lower frequencies your displacements get a little bit out of reason for this 100 psi which you quoted. For some of these lower seismic velocities you have displacements approaching 20 or 30 inches. This does not appear to be realistic. I'm wondering, are we covering too great a frequency range in these shock spectra?

Mr. Dowdy: I think the thing that makes this look high is the fact that this is an assumption of homogeneous soil. That is, if you take a soil that has 1000 ft/sec seismic velocity and assume this to continue on down to the depth of a wave of the size that we're talking of here, then you would get those displacements. But this is not a usual condition. You wouldn't

expect to get this type of displacement in normal test data because the seismic velocity increases and you get into something far above 1000 ft/sec. When you consider this, it drops back down to the order of 2 or 3 inches which is in keeping with the test data.

Commander Christensen: Then why do we use these values in design when they appear to be a little unrealistic? Does this not add appreciably to the cost of your shock mounting?

Mr. Dowdy: No. This is just a theoretical curve. You would not use this for design. You would use the particular seismic velocities that you have in a particular soil. Now if you did happen to run into a site that had a very low seismic velocity material for great depths, then you could expect to get this displacement. But you wouldn't pick a site like that to design a facility in.

Mr. Jeffrey (Formation Engineering, Montreal): Would you like to say a few words on what your approach is to furniture such as desks and things like that where you have fairly high shock spectra? Whether you tie them down or whether you let them bounce—what is your general approach to the problem?

Mr. Dowdy: Well, this would depend on the importance of the particular item I would think. If you felt that it didn't hurt anything to bounce around you could let it bounce. You can, unless you provide some special damping which you have in many cases, expect the vibration for quite some time on some of these shock mounted floors. This would cause quite a lot of movement of any loose articles on the floor. I think this is something you'd have to look into at the particular piece of equipment, to rate its importance. For instance, in missile base design we normally look at it from the point of view that if it doesn't keep you from getting the missile off, you don't worry about it too much.

Dr. Baron (Paul Weldinger Consultants, N.Y.C.): The frequency spectrum that you showed—the theoretical frequency spectrum—was it based on considering the soil to be elastic?

Mr. Dowdy: No. The entire curve is based on a nonelastic soil. Every thing is extrapolated from this dynamic stress-strain curve or the non-linear curve. But the frequencies are simply the frequencies of spring-mass systems.

Dr. Baron: No. What I'm thinking of is the particular diagram (Fig. 3) where you showed an air shock which was advancing over the surface and then you had two waves in the medium which were drawn at certain inclinations. This seems to conform to basic elastic theory. I was wondering, is this what you used?

Mr. Dowdy: The plot is a little different. I'll admit it looks very much like the linear elastic theory, but the two lines were indicating just the seismic wave and then the peak pressure level of the compression wave. Then, when you consider the nonelastic or nonlinear character of the soil, the peak pressure drops back and the seismic wave runs out ahead of it —

Dr. Baron: Yes, true, but the other thing I wanted to point out is this, that your frequency spectra are based on truly free field considerations. Whatever, for instance, a pressure gauge might read at the particular location. Now in some of these structures that you've shown, where you have components attached directly to the walls of the structure, particularly in the round tunnels, or even in cases where you showed square tunnels with sharp corners, the frequency spectra which

one will get in actuality may be tremendously altered by the effect of the structure. The fact that some of these square corners may serve as centers of diffraction and just completely change the peak accelerations and displacements to which your things are going to be subjected. I agree that if you take something and put a building in it and use relatively low frequency, the free field should be quite good, but I also think a note of warning should be mentioned that, for relatively high frequency components, one cannot and should not neglect the effect of the structure. The results may be quite erroneous.

Mr. Dowdy: Yes, this is quite true.

Mr. Wallerstein (Lord Mfg. Co.): Would you care to state the approximate order of magnitude of displacement that occurs across some of these large spring beam supports that you showed, for instance some in the typical silo suspension?

Mr. Dowdy: The static displacement on most of those were of the order of 1 inch, while the design dynamic displacement was approximately 3 inches — 3 to 4 possibly.

NUCLEAR WEAPON BLAST AND GROUND SHOCK EFFECTS

ON DYNAMIC RESPONSE OF INTERIOR COMPONENTS

AND EQUIPMENT IN UNDERGROUND STRUCTURES*

S. Weissman, E. Cohen and N. Dobbs
Ammann & Whitney, Consulting Engineers,
New York

This paper presents the procedures and significant results of studies of the dynamic responses of hardened underground rectangular and silo type structures subjected to reaction nuclear weapons blast and ground shock effects with particular attention to the transmission of shock and vibration to the interior structural components and contents of the structure. Included is a brief general discussion of the structure and soil interaction problem.

GENERAL INTERACTION PROBLEM

Underground structures experience motions which are a function of the free-field motions of the surrounding soil, the blast pressures applied directly to the structure, and the interaction between the soil and the structure.

It is important to note that free-field ground motions are obtained on the assumption that there is no structure or other large discontinuity of mass and stiffness present within the soil in the area of interest. The motion of a structure placed in the soil, shown schematically in Fig. 1, and its effect on the adjacent ground motions depends on the dimensions and mass of the structure. Generally, a small light structure tends to move with the surrounding soil, whereas a large structure will modify the free-field motions. The responses of a large underground structure may be estimated by evaluating the interaction of the structure and the surrounding soil during

the transient ground shock motions. Because the phenomena associated with these interaction effects are extremely complex and difficult to analyze simplified systems have been assumed in order to obtain even an approximate solution. In general, the many problems which are encountered in the analysis of underground structures are further complicated by the uncertainties associated with the prediction of free-field ground motions and corresponding shock spectra [1,2].

DESIGN REQUIREMENTS

For design purposes, it is necessary to evaluate the dynamic responses of both a hardened structure and its contents to the nuclear blast and shock environment. Of particular interest are the following:

1. Maximum stress, displacement and acceleration induced in the structural components.

*This paper is based in large measure on studies and reports prepared by Ammann & Whitney, Consulting Engineers, for The Office of the Chief of Engineers, Department of the Army, Contract No. DA-129-ENG-464; The Directorate of Civil Engineering, Headquarters, United States Air Force, Contract No. AF 49 (604)-2322; Ballistics Missiles Division (BMC), United States Air Force, and Bechtel Corporation, Contract No. AF 04 (647)-77; and the Canadian Department of National Defense in conjunction with the Foundation of Canada Engineering Corporation, Ltd.

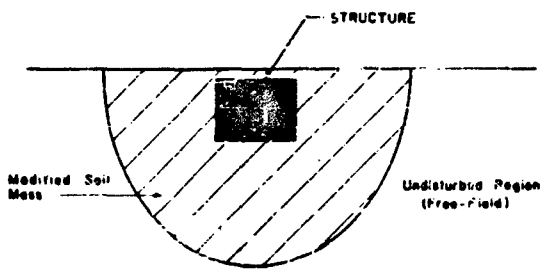


Fig. 1 - Schematic of structure in a ground shock field

2. Vibrational environment for shock sensitive equipment and personnel placed in the structure.

3. Design criteria for shock isolation systems.

In considering these design requirements as they relate to the structural analysis of ground shock effects, emphasis is placed on the transmission of shock and vibration to the interior structural components and contents of the structure, since for many hardened structures it appears adequate to consider the effect of the direct blast pressures only when analyzing and designing individual exterior portions of the structure, although ground motion effects should be considered for shear wall and deep beam action. However, for the design of the interior structural components, particularly in large multistory structures and structures which contain shock sensitive equipment, the vibrational effects resulting from the structure motions may be critical with respect to the design of interior floors and columns, etc., and the determination of the required shock isolation for equipment.

VELOCITY PULSE

In many cases only free-field ground shock spectra are specified as design criteria. A typical spectrum is shown in Fig. 2 where the solid line is an actual spectrum curve and the dashed line is an envelope to the spectrum. These cannot be applied directly to the analysis of many structures because of the interaction of the ground and the structure. Also, most shock spectra are based on elastic response and cannot be applied directly when elastoplastic, nonlinear, and discontinuous structural behavior exists. In these cases a

synthesized ground motion (time-history) curve consistent with the spectrum is useful. Such ground motions have been synthesized by approximating the ground motion as a single velocity pulse [7]. A velocity pulse of the form as shown in Fig. 3 has been found to agree with spectra within reasonable limits. The pulse is a rounded exponential curve with an exponential decay. This pulse when applied to a series of single degree-of-freedom oscillators will result in the peak responses given by the spectrum. Thus, a time-history ground motion, consistent with shock spectra previously specified or calculated, and which will have a wide range of applicability is established.

The velocity pulse is of the following form:

$$v(t) = v_0 e^{-t/\tau} - v_0 e^{-\alpha t/\tau} \quad (1)$$

where

$v(t)$ = the velocity of the base as a function of time (inches per second)

v_0 = parameter in units of velocity (constant for a particular spectrum) (inches per second)

t = Time (seconds)

τ = parameter in units of time (constant for a particular spectrum) (seconds)

α = dimensionless parameter (constant for a particular spectrum)

e = Base of natural logarithms.

The parameters v_0 , τ and α are a function of the shape of the spectrum curve.

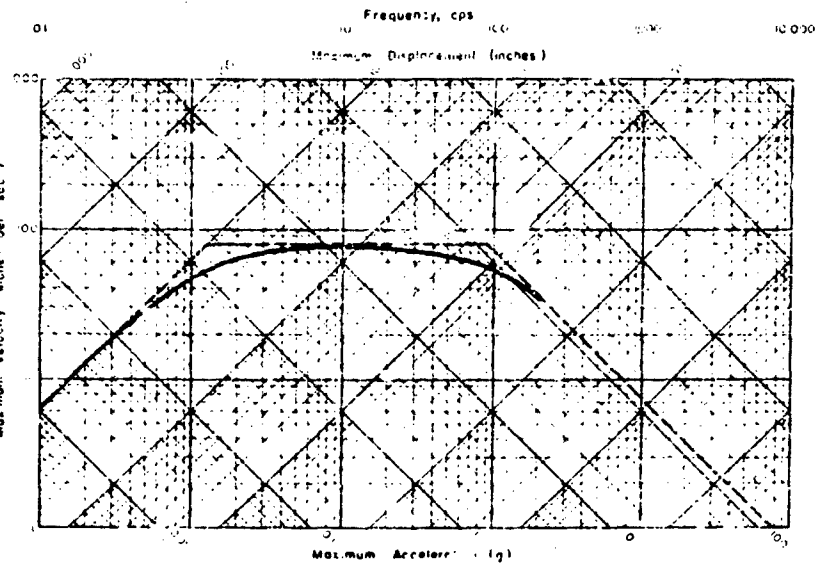


Fig. 2 - Free-field ground shock spectra

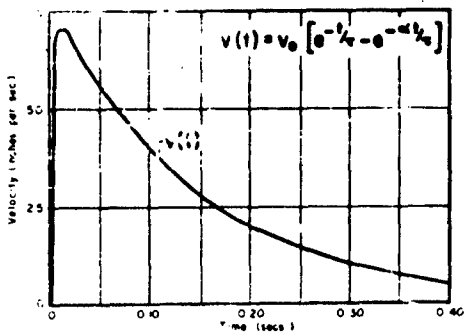


Fig. 3 - Velocity pulse

v_0 and τ are essentially dependent upon the low-frequency range of the spectrum and primarily affect the peak velocity and decay of the velocity pulse. ω is dependent upon the high-frequency range of the spectrum and primarily affects the rise time to the peak velocity of the velocity pulse. First trial values for v_0 and τ are obtained by neglecting the second term of Eq. (1) and substituting the displacement response values for two points from the given spectrum in the following equations:

$$\tau^2 = \frac{u_2^2 - u_1^2}{u_1^2 \omega_1^2 - u_2^2 \omega_2^2} \quad (2)$$

$$v_0 = \frac{u_1 \sqrt{1 + \omega_1^2 \tau^2}}{\tau} = \frac{u_2 \sqrt{1 + \omega_2^2 \tau^2}}{\tau} \quad (3)$$

where

u_1 = displacement response (inches) for frequency (ω_1)

u_2 = displacement response (inches) for frequency (ω_2)

ω = undamped natural circular frequency (radians per second).

Since Eqs. (2 and 3) are based on the low-frequency range of the spectrum, it is necessary to select the two points at frequencies below the frequency at which the peak acceleration response of the spectrum occurs, a point in the very low-frequency range of the spectrum curve and another at a higher frequency depending on the particular spectrum shape.

Once τ and v_0 have been estimated α is then computed. α is a function of the rise time as follows:

$$t_r = \frac{\tau}{\alpha - 1} \ln \alpha, \quad (4)$$

where t_r is the rise time. In most cases the rise time will not be accurately known and the following expression can be used:

$$\tau = \frac{A_p \tau}{v_0} + 1, \quad (5)$$

where A_p is the peak acceleration for a particular spectrum.

It is necessary to check several points on the spectrum since the shape of particular spectra may not exactly correspond to the velocity pulse at every frequency. This may be done by substituting values of the natural circular frequency in Eq. (6) below at various points throughout the spectrum with the previously determined values of v_0 , τ and α , comparing the displacement (u) so determined with the given spectrum. In general the two spectra will not exactly coincide at every frequency and it may be necessary to adjust v_0 , τ , or both taking into account the corresponding change in α , in order to obtain a velocity pulse resulting in responses approximately consistent with the entire spectrum curve. In some cases it may be necessary to use a velocity pulse which results in conservative responses at certain frequencies in order that other frequency responses are not too low compared to the given spectrum curve.

$$u_a = \frac{v_0 \tau (\alpha - 1)}{\sqrt{(1 + \tau^2 \omega^2)(\alpha^2 + \tau^2 \omega^2)}} \quad (6)$$

where u_a is the displacement response for a particular frequency (ω) from the response spectrum.

DYNAMIC ANALYSIS OF A SECTION OF A RECTANGULAR MULTI-STORY STRUCTURE

The dynamic responses of a typical interior bay of a multi-story, multi-bay, reinforced concrete, buried, flat slab type structure, subjected to 100-psf peak air overpressure, were analyzed with a digital computer after many simplifications had been made to achieve a feasible solution. To determine a practical solution, a simplified mathematical model was established which replaced an interior section of the structure and adjacent soil. The model was expected to have responses to the given input similar to those of the actual structure, consistent with the accuracy of the input data.

Figure 4 illustrates a mathematical model of the type utilized in the analysis. This model considers the motion of a typical interior bay in the vertical direction only. It does not consider the effects of relative transverse motion between adjacent bays and the coupling of vertical, horizontal and rotational motions. The model is composed of lumped masses for slabs, columns, and soil which are connected by compression, flexural and shear springs, and dashpots. Masses 1 to 3 represent column sections; mass 7 represents the roof slab; mass 10 the base slab. Mass 9 is an interior floor beam; and mass 8 an interior floor slab. The slab and beam masses correspond to a typical interior bay which is symmetrical with respect to the column, and the corresponding spring constants represent the resistance per unit displacement of the center of the bay, between adjacent columns with respect to the column. Masses 4, 5, 6, 11 and 12 represent the soil masses under the structure. The soil

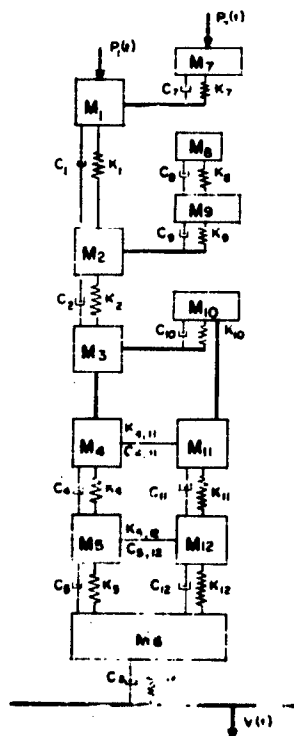


Fig. 4 - Vertical analysis.
Typical interior bay model.

masses are connected by compression and shear springs (Fig. 4).

In the analysis the time dependent blast loading $P(t)$ is applied to the roof masses, and a point in the soil far enough below the structure to move as the free-field, has motions corresponding to the vertical velocity pulse $V(t)$ determined from the free-field ground shock spectrum as previously described. The solution of the model involved solving equations of motion for the various masses simultaneously by numerical integration taking into account variable parameters, such as changes in spring constants corresponding to elastoplastic or plastic behavior.

Typical results of responses determined in the analysis are shown in the following figures. These figures pertain to the first run in the analysis which considered the responses due to the blast load on the roof only. Figure 5 is a plot of the dynamic resistance and acceleration of the roof slab versus time, the roof slab being subject to direct blast load. As shown, the peak acceleration is 14.4g down and the peak response of 6,900 kips represents an elastic response of 1.2 with respect to the blast load. Preliminary results of the responses due to combined blast and velocity pulse ground shock motion have indicated that the peak responses increased due to the combined effect of the direct blast load and the downward motion of the foundation.

Figure 6 is a plot of the resistance of a typical interior column due to the effect of

blast load only. The peak resistance of 10,000 kips represents a response of 1.5 with respect to the blast load. Preliminary results have indicated that the effect of the velocity pulse ground motion increases the peak column response due to the combined blast and ground shock effect and that the column goes plastic.

Figure 7 is a plot of the resistance and acceleration of a typical interior floor slab. As shown the slab experiences considerable reversed bending. As indicated by the peak accelerations, the dynamic resistance responses with respect to the dead load are 6.5 for downward deflection and 5.2 for reversed or upward deflection. Thus, it is important that these vibrational effects be considered even though the interior slabs are not subjected to direct blast loading. Preliminary results of the effect of the combined blast and velocity pulse motion has indicated that the reversed bending response of the slab increases.

It is important to note that many problems exist in an analysis of this type particularly with regard to dynamic soil properties and the time of onset of the ground motion. The methods of calculation of stiffness and damping coefficients in the elastic and elastoplastic ranges for the concrete and steel structural components of the building are well known. However, difficulties arise in expressing the approximate dynamic soil parameters to be used. In the dynamic analysis of structure and soil interaction it is important to consider the variations in the soil stress-strain

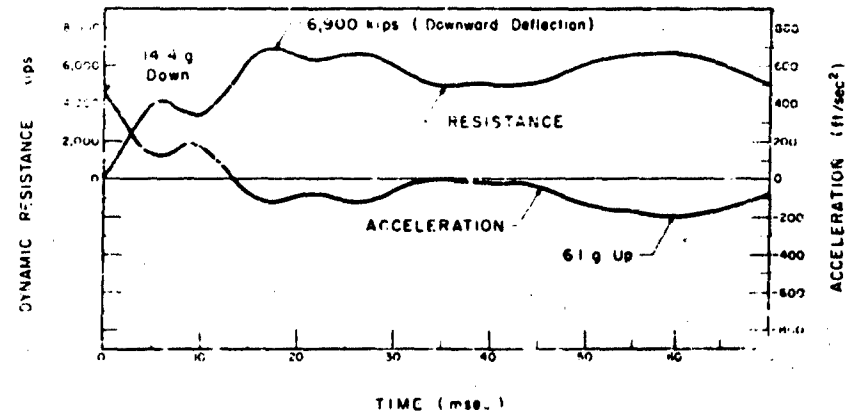


Fig. 5 - Dynamic resistance and acceleration of roof slab (vertical direction)

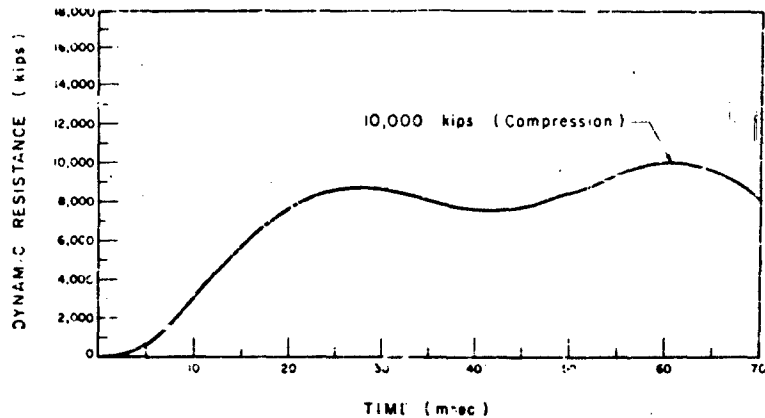


Fig. 6 - Dynamic resistance of interior column
(vertical direction)

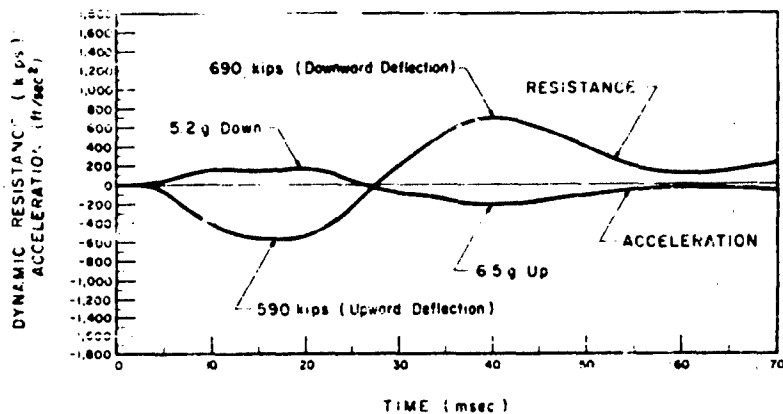


Fig. 7 - Dynamic resistance and acceleration of interior floor slab
(vertical direction)

curve and corresponding changes in stiffness. Although dynamic behavior of soils has been and is currently being investigated through laboratory tests and theoretical studies ([4,5,6] and many other current studies), the actual in situ behavior of soils under blast loadings is still uncertain. However, the particular type and intensity of loading which the soil will experience, depending on the proximity to the structure, should be evaluated and appropriate laboratory tests such as a confined compression test should be performed; and the results

evaluated based on judgment and theoretical knowledge of soil behavior.

The nature of nuclear blast loadings are such that a large expanse of soil is stressed effecting a condition of lateral confinement. This lateral restraint results in an increasing modulus of compression with increasing stress for many soils since the soil becomes extremely compacted and dense particularly under higher pressures. A general stress-strain curve indicating a constantly increasing

modulus is shown in Fig. 8(a). The stress range at which this type of stress-strain relationship occurs depends upon the particular soil, although it is generally associated with the higher stress ranges.

For different soil types or for different loadings applied to the same soil the corresponding stress-strain relationships vary. For example, a stress-strain curve for a granular soil would start elastically at a relatively high modulus due to shear between the grains resulting from friction. When the friction forces are overcome the modulus will decrease due to compaction of the soil and would then gradually increase with increasing stress. A stress-strain curve of this type is shown in Fig. 8(b). For extremely high stresses the modulus may decrease due to plastic deformation of the soil grains and thus a plateau would be reached on the stress-strain curve as indicated in Fig. 8(b).

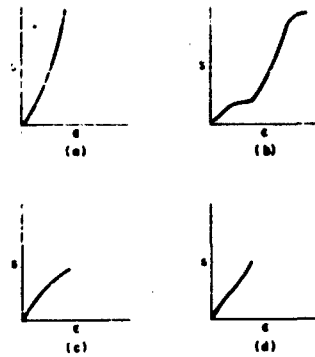


Fig. 8 - Typical soil stress-strain curves

Compression stress-strain curves determined in the laboratory by a standard triaxial soil test with constant lateral confining pressure are not usually representative of soil behavior under blast loading conditions, except, perhaps, for the low-stress range, as indicated in the typical triaxial test, compression, stress-strain curve shown in Fig. 8(c) where the modulus decreases with increasing stress, and failure of the specimen occurs at a relatively low compressive stress compared to expected blast load intensities. However, the results of constant-ratio-of-applied-stress triaxial tests, in which case the lateral confining pressure is

increased proportionally with the vertical pressure, indicate a more representative soil behavior [2], as shown in the stress-strain curve for a test of this type in Fig. 8(d) where the modulus does not sharply decrease with increasing stress and would tend to increase in the higher stress range.

Thus, in order to evaluate soil compression stress-strain relationships in the laboratory a type of confined compression test is required, and even this type of test results in an approximate estimate of the probable in situ stress-strain relationships under actual dynamic loading.

For the purpose of the dynamic analysis it may be suitable and convenient to approximate the variable soil stress-strain curves by a series of straight lines, each representing a constant compression spring constant, which approximates the actual stress-strain relationships. It may also be convenient for particular soils to approximate the soil stress-strain relationships by an elementary curve of known mathematical properties. Reference 1 describes an analysis in which the type of soil and loading were such that the stress-strain curve could be approximated by a hyperbola which mathematically expressed an increasing compression modulus.

Another important factor in the analysis is the time of onset of the ground motion, in terms of the velocity pulse, with respect to the blast wave arrival on the roof. The proper time is difficult to establish since it depends upon the shock wave transmission in the ground and the relative speeds of the air blast wave and the ground seismic velocity. However, the limits of time of onset should be estimated with due regard to the particular site conditions.

ANALYSIS OF AN EQUIPMENT SHOCK ISOLATION SYSTEM

A section of an existing structure was analyzed with respect to a shock isolation system for a heavy piece of equipment which was shock mounted to an interior beam as shown schematically in the mathematical model of Fig. 9. In the actual structure the beams and equipment were symmetrical with respect to the supporting intermediate column. The frequency of the column, roof slab above the column, and base slab below the column are such that these components could be considered rigid compared to the equipment and beam. Thus M_1 represents the combined mass of the

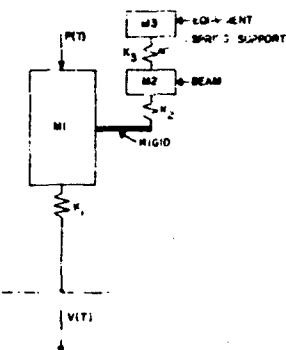


Fig. 9 - Model for analysis of equipment shock isolation system

entire system except the equipment and the equipment supporting members. Mass 3 represents the mass of the equipment and k_3 , the spring support for the equipment. Mass 2 represents the mass of the beam and k_2 , the flexural stiffness of the beam. k_1 represents

the stiffness of the soil below the structure base section. The time dependent blast load $P(t)$ with a peak of 25 psi, acts on the roof, and the ground motion at a point below the base is known in terms of the velocity pulse $V(t)$.

The purpose of the analysis was to make an approximate check of the adequacy of the existing spring length in isolating the shock mounted equipment. The equations of motion were numerically integrated assuming linear elastic action of the beam and linear elastic action of the equipment spring unless the solid height of the spring occurs.

The analysis was performed assuming blast pressure and ground motion acting simultaneously and also assuming only blast pressure acting, in order to determine the critical loading condition. Figure 10 is a plot of the beam resistance versus time where the solid line is for blast and ground motion and the dashed line represents blast only. For each loading two cases for the equipment spring were considered.

1. The actual spring length and the solid height of the spring were used.

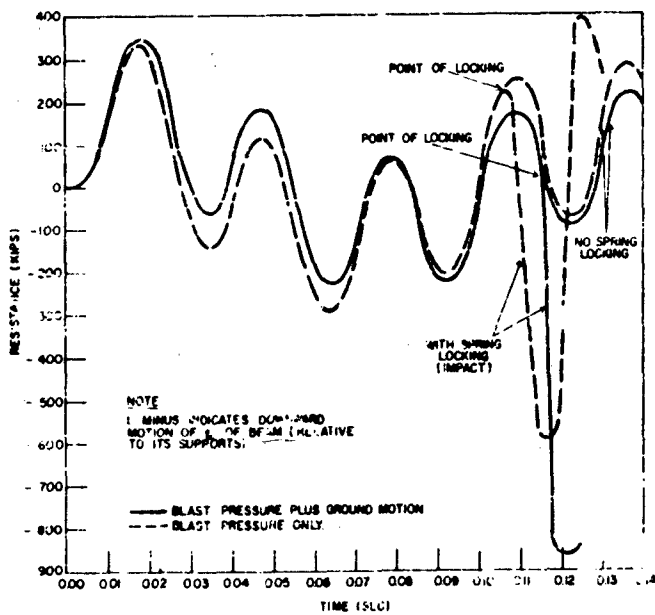


Fig. 10 - Beam resistance vs time

2. The spring was of the same stiffness but long enough to withstand the maximum relative displacement. This was used to estimate the required spring length if the existing spring was not adequate.

As shown in Fig. 10 the solid height of the existing spring was reached for both loading conditions and locking of the spring occurred. As shown the resulting elastic response of the beam without locking increased from about 200-300 kips to 600-900 kips due to equipment impact after spring locking.

From the response of the equipment spring the required length of the spring may be estimated and the shock isolation system modified to prevent the excess beam stress due to impact.

DYNAMIC ANALYSIS OF SILO OVERHEAD DOOR

The combined effects of blast loading and vertical ground shock on an overhead silo door were studied to determine the magnitudes of the relative motion between the door and the silo and stresses in the door system if tie-downs are not provided [8].

For the purposes of the analysis, the silo door was approximated by a single degree-of-freedom system. The silo motions caused by ground shock were defined by the velocity pulse corresponding to the average shock spectrum for the silo. The relative motions between the silo and the door were obtained by applying the velocity pulse to the silo and the blast load to the door and performing numerical integrations including the effects of damping since the relative arrival times were uncertain. Several combinations of blast overpressure and ground shock were assumed in the analysis, in order to evaluate a range of possible conditions of loading and to determine the critical condition.

The cases analyzed were:

Case 1. Blast pressure only at $t = 0$.

Case 2. Blast pressure at $t = 0$ with ground shock applied at time of maximum resistance in the door.

Case 3. Blast pressure at $t = 0$ with ground shock applied at time of minimum resistance in the door.

Case 4. Blast pressure and ground shock applied simultaneously at $t = 0$.

Case 5. Ground shock at $t = 0$ with blast pressure applied at time of maximum difference in displacement between the silo and the door.

The vertical plastic capacity of the door was taken as 7400 kips.

For case 1, with blast load (3700 kips) only, the peak response of the door was 6600 kips and no separation between the door and the silo occurred.

For case 2 where ground shock was applied at maximum resistance, the peak response of 6800 kips was not affected and no separation between the door and the silo occurred.

For case 3 where the ground shock was applied at minimum resistance the peak response of 6800 kips was not affected. This case was assumed to check any tendency for the door to lift off the silo when ground shock arrived after the blast. There was no separation between the door and the silo.

Thus, for the first three cases where only blast pressure existed or ground shock arrived after the blast, the door was found to remain elastic without any rebound or lifting of the door off the silo roof.

However, under cases 4 and 5, the door initially lifted off the silo roof as illustrated in the following figures. For case 4 (Fig. 11) where the blast and ground shock were applied simultaneously the door separated 0.05 inches and the maximum resistance increased to 6900 kips, thus still remaining elastic. Shown on Fig. 11 is a schematic model of the door and silo support where $P(t)$ is the blast overpressure applied to the door and $V(t)$ is the velocity pulse motion of the silo. Also shown for comparison is the response for blast load only and the applied blast load curve.

Case 5 (Fig. 12), where the blast was applied after the ground shock and a separation of 1.27 inches occurred, was found to be the worst case. Due to the impact effects the peak response increased to its maximum capacity and the door yielded plastically with a ductility ratio of 1.64.

However, it must be noted that the same ground motion was used for all cases. This appears unreasonable for case 5, since outrunning ground motions appear to be small compared to the peak effects at this pressure.

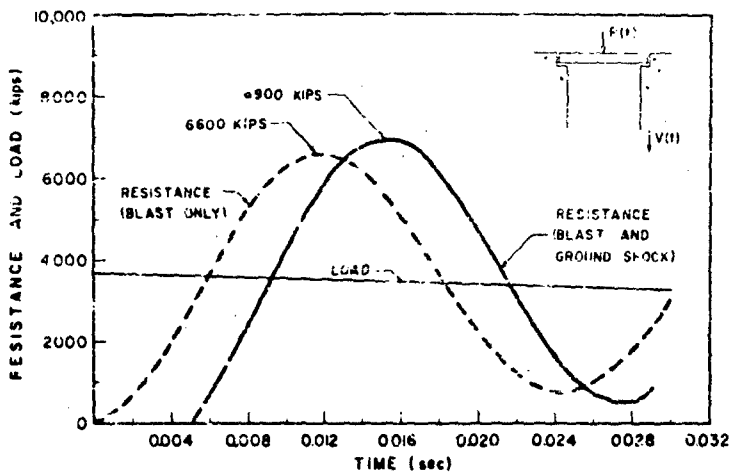


Fig. 11 - Resistance of door - blast and ground shock simultaneous

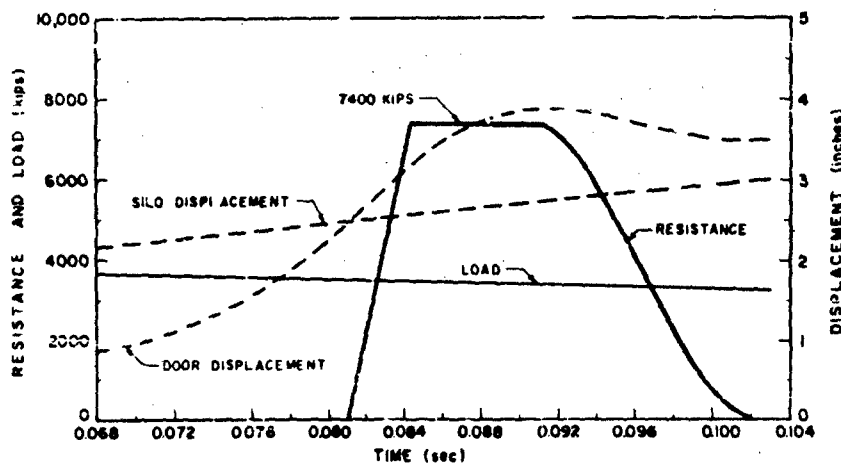


Fig. 12 - Resistance of door -- ground shock prior to blast

level. At higher pressure levels where the air blast is typically supersonic it appears that the problem disappears.

DYNAMIC ANALYSIS OF MISSILE CRIB SYSTEM

The dynamic responses of a missile crib system were analyzed for the effect of ground shock by using horizontal, vertical and rocking velocity pulses to represent the motion of

the support point of the suspension system [9]. The crib was suspended from a silo (Fig. 13). The pulses were of such magnitude and shape (exponential decay as previously shown) as to approximate the design shock spectra for systems attached to the silo. In the analysis of the suspended crib structure, the system was idealized as a suspended rigid body with a spring mounted second rigid body within it. This was possible as the frequencies of the free-free crib were much higher than the frequencies of the suspended assemblage

considered as a rigid body. Twelve coordinates were used to specify completely in space the position of two rigid bodies at any time. The structure was assumed to be linear and elastic.

Various analyses of the crib assemblage were performed to determine the effects of ground shock in two vertical planes at 90° to each other. Both planes passed through the center of the crib. One also passed through the center of the missile. Both were analyzed with the missile in 100 percent, and unloxed, conditions. Effect of tolerances in the location

of the center of gravity of the suspended system and of the elastic center of suspension springs was also considered.

For ground shock parallel to the YY direction the elastic center of the suspension springs and the center of gravity of crib, missile and launch platform lie in a vertical plane which is almost parallel to the plane of ground shock as shown on Fig. 10. Thus, plane motion of the crib for ground shock parallel to the YY plane, as shown in the mathematical model (Fig. 14), was assumed to give a good approximation to the resulting oscillation in this direction.

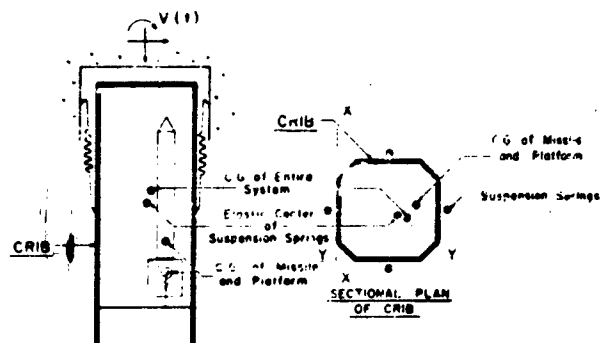


Fig. 13 - Suspended crib and missile

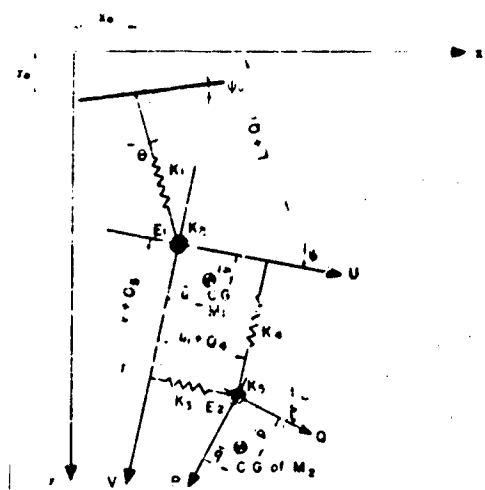


Fig. 14 - Plane motion of crib, missile and platform

For ground shock parallel to the XX direction the eccentricity of the center of gravity from the elastic center must be considered and is defined by the twelve coordinates shown in the mathematical model (Fig. 15).

The significant conclusions resulting from these two cases were as follows:

1. Linear differential equations of motion are adequate for determining dynamic displacements and accelerations.

2. The eccentricity between the elastic center of the suspension springs and center of gravity of the entire suspended crib system

is an important factor and has considerable effect on the maximum dynamic, horizontal and angular displacement and accelerations of the crib.

3. Maximum dynamic responses of the crib and of the launch platform with the 100-percent loxid missile were larger than those when the missile was not loxid.

4. The effect of coupling of dynamic responses was evaluated by assuming that the entire system acted as a single rigid body suspended from the silo, and that the elastic center of the suspension springs coincides with the center of gravity of the entire

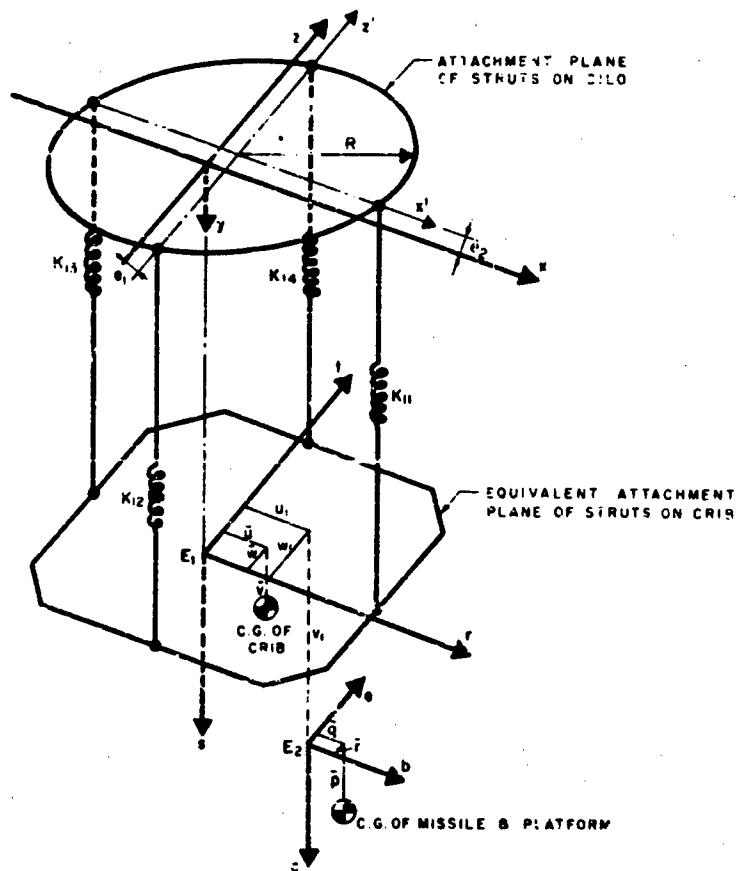


Fig. 15 Spatial motion of suspended crib, missile and launch platform

suspended rigid body. In this case the maximum dynamic responses of the crib were obtained directly from the design shock spectra. This gave good approximations to the horizontal and vertical displacements, and vertical acceleration at the elastic center of the suspension of the crib compared with responses for ground shock in the YY direction, but it gave very low values for the horizontal acceleration, angular displacement and acceleration at that point.

Other conclusions drawn from the results of the various analyses were:

- [1] Maximum dynamic responses of the crib to ground shock parallel to YY were either approximately equal to or greater than maximum dynamic responses to shock parallel to XX direction.

2. Maximum relative horizontal displacement, maximum relative vertical displacement, and maximum vertical acceleration of the crib at its elastic center of suspension springs were nearly independent of the direction of ground shock and of the percentage of fuel in the missile and in the storage tank of the crib. Maximum horizontal acceleration of the crib is greatest, among the cases studied, when the shock occurred in a plane parallel to YY and the missile was 100-percent loaded.

3. Ground shock parallel to XY caused dynamic angular displacement and acceleration about the vertical axis of the crib which are of the same order of magnitude as the dynamic angular displacements and accelerations of the crib about the horizontal axes.

REFERENCES

- [1] E. Cohen and S. Weissman, "Underground Shock Environment Data and Application to the Design of Underground Structures," Proceedings of the 28th Symposium on Shock, Vibration, and Associated Environments, Bulletin No. 26, Part III, Office of the Secretary of Defense, Research and Engineering, Washington, D. C., Sept. 1960.
- [2] E. Cohen and S. Weissman, "Nuclear Weapon Ground Shock Effects in Relation to Hardened Design," Symposium on Scientific Research in Protective Construction, Ernst-Mach Institut, Freiburg i. Br., Eckerstrasse 4, West Germany, Sept. 1960.
- [3] V. Chubotov, Space Technology Laboratories, Inc., Inglewood, California.
- [4] "The Response of Soils to Dynamic Loads," Report No. 3, First Interim Report on Dynamic Soil Tests, DASA-1162, Massachusetts Institute of Technology. Prepared for Waterways Experiment Station, U. S. Army Corps of Engineers, Contract No. DA-22-079-eng-224, Oct. 1959.
- [5] R. B. Parkin, "Impact Wave Propagation in Columns of Sand," RM-2468, Rand Corporation, Santa Monica, California, Nov. 1959.
- [6] "On the Application of the Theory of Locking Media to Ground Shock Phenomena," SR-18, Paul Weidlinger, Consulting Engineers, New York City, Prepared for The MITRE Corporation, Bedford, Massachusetts, Sept. 1960.
- [7] Goode, Shockley, Cunny and Strohm, "Soil Survey and Backfill Control in Frenchman Flat," Operation Plumbbob, Project 3.8, WT-1427, U. S. Army Waterways Experiment Station, Corps of Engineers, Oct. 1959.
- [8] "Design of Silo Overhead Door for Blast and Ground Shock Effects," Supplementary Report No. 13 to Basis for Hardened Design for SM-65 Complex 9x1 Unitary Silo, Prepared for Bechtel Corporation, Los Angeles, California by Ammann and Whitney, Consulting Engineers, New York City, Contract No. AF-04(647)-277 (Secret), Dec. 1959.
- [9] "Dynamic Analysis of Crib System," Supplementary Report No. 11 to Basis for Hardened Design for SM-65 Complex 9x1 Unitary Silo, Prepared for Bechtel Corporation, Los Angeles, California by Ammann and Whitney, Consulting Engineers, New York City, Contract No. AF-04(647)-277, Dec. 1959.

DISCUSSION

Mr. Flathau (U. S. Army Waterways Exp. Station): Regarding Fig. 4, I would like to know if you arbitrarily selected the reference plane for your mass from some particular free-field velocity. Did you just arbitrarily select a velocity and use that velocity at some depth for your reference plane?

Mr. Weissman: Well, it isn't arbitrary although it is difficult to establish the exact, proper point. The idea there is to go down far enough so that, assuming you know free-field ground shock motion, you are down to a point where these free-field motions will exist. In other words, so that they're not affected by the structure.

Mr. Flathau: Then you have selected some particular level where you will have a velocity. Did you then take into account the motion of this particular plane of the soil in your subsequent dynamic analysis of your system? The plane would be moving and therefore your mass would be referenced to this moving plane?

Mr. Weissman: That's right. That would actually be the reference point. In other words we're specifying the motion of that plane.

Mr. Flathau: It was included in your analysis?

Mr. Weissman: The ones that I showed on the response charts were not for that case. We don't really have final results on that but the preliminary results indicated, as I have pointed out, that responses tend to increase. The responses that I had shown in the first analysis of the multi-story building were without the velocity pulse. It included the stiffness of the soil. In other words, it was just a building resting on a foundation which has some stress-strain characteristics and applying a blast load to the roof.

Mr. Flathau: I was just wondering if you did use a reference plane and if you did take into account the motion?

Mr. Weissman: In the second analysis the motion of the soil was known in the analysis and that would be the reference plane.

Mr. Cavanaugh (Barry Controls): What is the physical meaning of this resistance parameter that you use?

Mr. Weissman: That was actually the responses of the structural members. In other words, for the slabs, that would just be the peak bending response or the resistance that was developed.

Mr. Cavanaugh: Is this the peak bending force?

Mr. Weissman: In bending, in the columns it would be for compression.

Captain Lycan (U. S. Army Waterways Exp. Station): In the first mathematical model of the structure you discussed the difficulties in determining the soil parameters, that is, the stiffness and damping coefficients. I wonder if you would discuss briefly the considerations involved in determining the magnitude of the soil mass that acts with the structure and how you determine the distribution of these soil masses.

Mr. Weissman: Well, as I pointed out, the model was for a typical interior bay, and the soil that would be considered would be the soil directly underneath a symmetrical section of the bay. We feel, although it's somewhat uncertain, that the masses would have to be broken up at least at a depth somewhat equal to the story heights in the buildings. In other words, you may have masses lumped together of ten feet depths and whatever widths the panel happens to be; in addition to lumping some of the mass directly underneath the building with the base layer. This is uncertain and it is the reason why we don't really have any good results for the interaction effects. It's just an approach, but the parameters are still uncertain.

A FREE-FIELD STRESS GAGE AND TEST RESULTS IN A NEW 1000-PSI DYNAMIC PRESSURE TANK

T. Winston and J. R. Stagner
United ElectroDynamics, Inc.
Pasadena, California

This paper is a report on a free-field stress gage currently under development for AFSC by the United Earth Sciences Division of United ElectroDynamics, Inc. The gage was tested under static and dynamic conditions to over 1000 psi in a pressure tank especially designed and fabricated for this purpose. Present test results indicate that the gage reads within 10 percent of the free-field stress up to somewhat beyond 200 psi. It is believed that future gages, developed along the same lines, will accurately measure free-field stresses up to 1000 psi.

An important side result was the design and fabrication of a dynamic pressure tank used in gage development and evaluation.

INTRODUCTION

The United Earth Sciences (UES) Division of United ElectroDynamics, Inc., was let a contract by the Air Force Special Weapons Center to develop a gage designed to measure blast-induced free-field stress in soil. Mason and Wolfe¹ discussed the problems of measuring soil stress under these conditions and described a gage designed to overcome some of these problems. This paper reviews some of the basic design concepts and presents the results of a series of static and dynamic tests conducted on this gage.

It is at best exceedingly difficult and probably impossible to mechanically match the stress-strain characteristics of soils with the traditional elastic elements such as springs, diaphragms, etc. The main reason for this being the wide variation in the stress-strain properties of soils. If the soil itself could somehow be incorporated as an active element of a gage, then it seems reasonable that the gage would have somewhat the same modulus

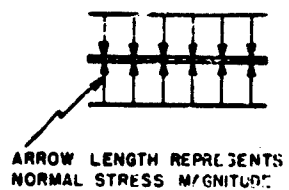
of deformation as that of the surrounding soil in which it is embedded.

SPOOL FREE-FIELD STRESS GAGE THEORY

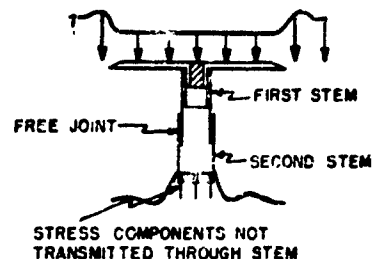
Figure 1 illustrates the steps in thinking which has led to the present UES free-field stress gage design. As indicated in Fig. 1(a), an extremely thin plate (e.g., a circular plate whose ratio of thickness to diameter is small) would be effective in free-field measurement. Any forces impinging on the top surface of the plate would be exactly balanced by equal and opposite reaction forces on the bottom surface. Measurement of the force over some accurately known area would then be a measure of stress. The main problem with a gage of this nature is to mount a transducer inside the plate to measure the force.

Consider next the effect of mounting a stem, stiff relative to the modulus of elasticity of the soil, on the underside of the thin plate suitable for housing a transducer or sensing element (Fig. 1(b)). If the gage and its surrounding soil were then subjected to a high pressure, the mismatch in modulus of deformation will cause the soil to arch onto the gage. This will result in the gage indicating a stress greater than that existing in the

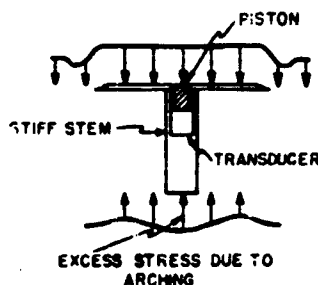
¹Harold Mason and C. M. Wolfe, "A Soil-Filled Soil Stress Gage," Bulletin No. 28, Shock, Vibration and Associated Environments, Part III, Sept. 1960, Office of the Secretary of Defense.



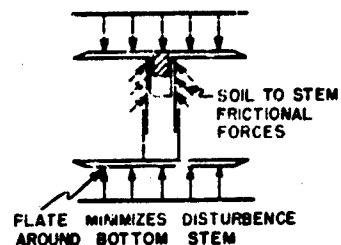
(a) - Thin flat plate does not disturb normal soil stress



(c) - Flat plate with "free" stem acts as "flexible" gage



(b) - Flat plate with stem acts as "stiff" gage



(d) - Soil to stem friction tends to offset the "flexible" gage effect

Fig. 1 - Diagram illustrating use of soil as an active gage element

free field. This effect can be minimized by making the cross sectional area of the stem small compared to the area of the plate.

Now, suppose the stem is inserted into a second stem such that a free sliding fit exists between them (Fig. 1(c)). The area of the top surface of the plate in contact with the soil is now greater than its lower surface. If pressure were now applied to this gage and its surrounding soil, there would be a net unbalance of force across the plate. This would cause the plate to move down until the soil pressure acting on its lower surface creates a force equal to that on the top surface. The movement of the plate unloads the soil above the gage but loads the soil below the plate. A pressure transducer on the upper surface would therefore indicate a stress lower than that in the free field. This may be eased but probably not completely compensated by friction between the stem and the soil.

The bottom stem, being free to move, cannot accept any load. The soil below it

would always be in an unloaded condition with the soil arching onto the lower surface of the plate. A plate may then be added to the lower stem (Fig. 1(d)) to reduce this disturbance of the stress pattern in the vicinity of the gage. Also the bottom plate minimizes the effects of transverse waves which would produce torques on the top plate, using the stem as a lever.

DESIGN

The UES free-field stress gage or "spool" gage as it has been nicknamed (Fig. 2), is essentially the gage represented in Fig. 1(d). It is made up of two sections, each consisting of a thin circular disc attached to a hollow stem. The stem of one fits inside the other, sliding freely on ground and lapped cylindrical surfaces.

The sensing element, consisting of a variable capacitance transducer, is actuated by a small piston, whose face is flush with the surface of the top plate. The piston load is

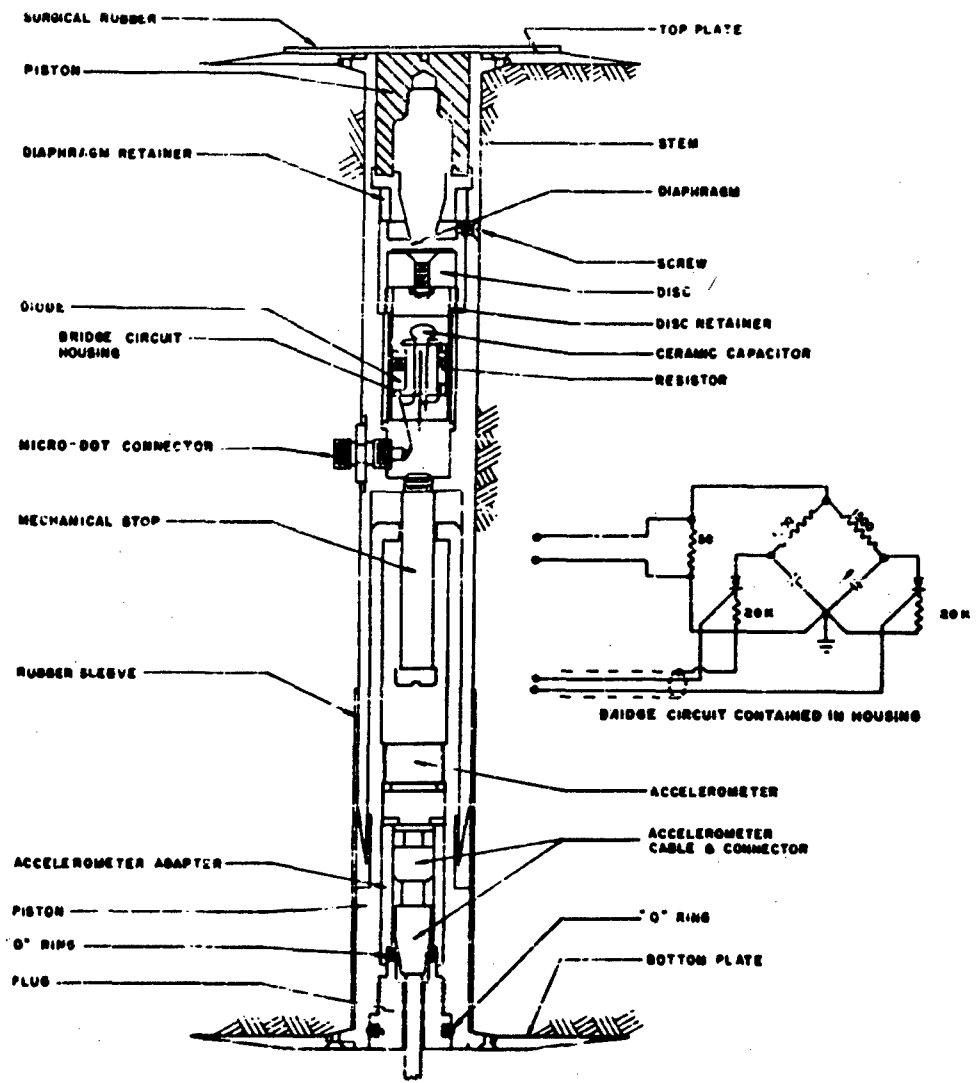


Fig. 2 - UES spool str. gage



Fig. 3 - UES spool gage assembled and disassembled

transmitted to a diaphragm, formed inside the top stem, which is one plate of the capacitor transducer. Full scale deflection of this diaphragm is 0.0002 inch at 1000 psi. The capacitor transducer is part of a bridge circuit built entirely within the gage.

A very thin surgical rubber membrane is cemented onto the end plate to keep dirt from the lapped joint between the plate and piston. Similarly a short piece of thin wall flexible rubber tubing is cemented to either concentric stem forming a cover for the lapped cylindrical joints. Figure 3 shows the stress gage assembled and disassembled. Figure 4 is a block diagram of the associated equipment required to complete the overall system.

UES DYNAMIC PRESSURE TANK

The dynamic pressure tank was developed in parallel with the spool stress gage. It was conceived as a simple, relatively inexpensive laboratory method of producing dynamic pressures needed for the free-field stress gage development. The principal design features of the dynamic pressure tank are illustrated in Fig. 5. The figure also serves to define various parts referred to throughout this paper.

Functionally the tank is composed of three basic elements: The high pressure tank, water chamber and soil chamber. Physically the tank consists of a base and lid which together comprise the test vessel, and the high pressure tank. The high pressure tank is used for storing compressed air. The water chamber is used to contain water and has as its physical boundaries the lid and a thin neoprene diaphragm. The soil chamber is used to contain soil and various instrumentation.

The tank is operated by filling the high pressure tank with compressed air to some selected pressure and activating a bursting mechanism which ruptures the burst diaphragm. This process rapidly applies a high pressure over the small area at the top of the water chamber which is transmitted hydraulically over the surface of the soil. The pressure wave, originating at the neck of the test vessel, thus becomes an input to the soil where instrumentation is located to measure its effect. The pressure waves are probably spherical in character since no attempt was made to alter the wave shape by means of baffling.

The time times (time to reach 63 percent of final pressure) of the pressure waves produced by the dynamic pressure tank, of the

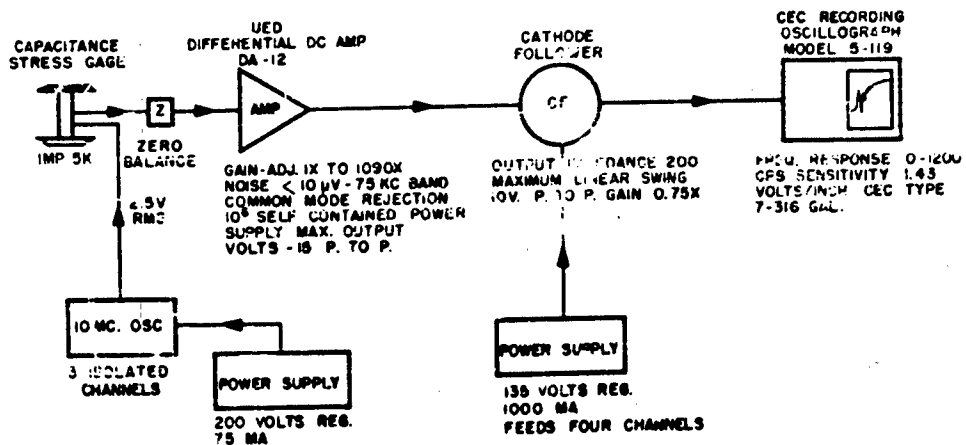


Fig. 4 - Complete stress measurement system

order of 15 to 50 milliseconds, are rather slow compared to the shock tube or similar devices. However, it is believed that these dynamic pressures are fast enough for gage development purposes. Methods for improving the rise time characteristics of the dynamic pressure tank are being considered at the present time.

Figure 6 shows the dynamic pressure tank set in a pit as a safety measure. An aluminum roof covers the equipment to protect it from the weather. The high pressure tank with its bourdon pressure gage is shown mounted on the lid of the test vessel.

Figure 7 shows the dynamic pressure tank with its lid removed and the neoprene diaphragma folded back to expose the test soil.

GENERAL TEST CONDITIONS

It was decided to use 20-30 Ottawa sand for the field gage development and evaluation since its properties are generally known. It was not practical to remove the tank lid and restore the sand to its initial conditions after every test. From three to four tests were conducted in succession before the lid was removed and the gages rearranged for another series of tests.

A CEC pressure gage was used in every test as a reference gage. It was always mounted flush with the surface of the sand in order to monitor the static and dynamic pressure inputs to the sand. The stress gage was to be tested under static and dynamic conditions

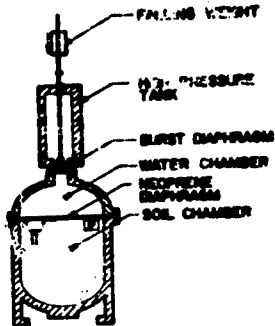


Fig. 5 - Principal features of UES dynamic pressure tank

at the surface and at various depths in the soil at pressures up to 1000 psi. Its performance was to be compared to a Carlson-Wiancko gage where possible.

CALIBRATION

The CEC pressure gage, the spool stress gage, and the Carlson-Wiancko gage were calibrated in the pressure tank itself. Instruments to be calibrated were mounted with their sensing areas flush with the surface of the sand. The calibration was accomplished by omitting the burst diaphragm, pressurizing the tank in discrete steps and recording the instrument outputs, using the precision Ascroft bourdon tube pressure gage mounted on the



Fig. 6 - UES dynamic pressure tank with high pressure tank, bourdon tube gage and test pit into which tank is situated, shown

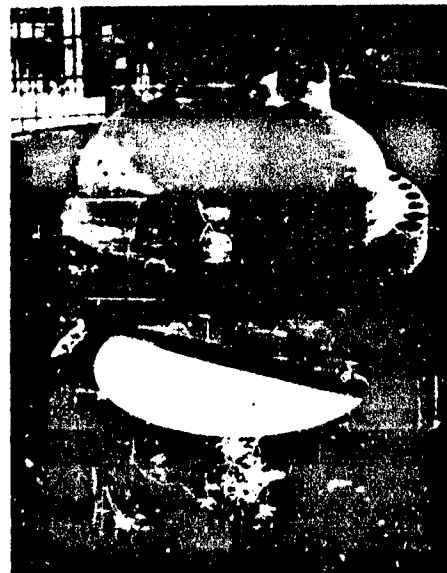


Fig. 7 - UES dynamic pressure tank with lid and base separated and neoprene diaphragm folded back

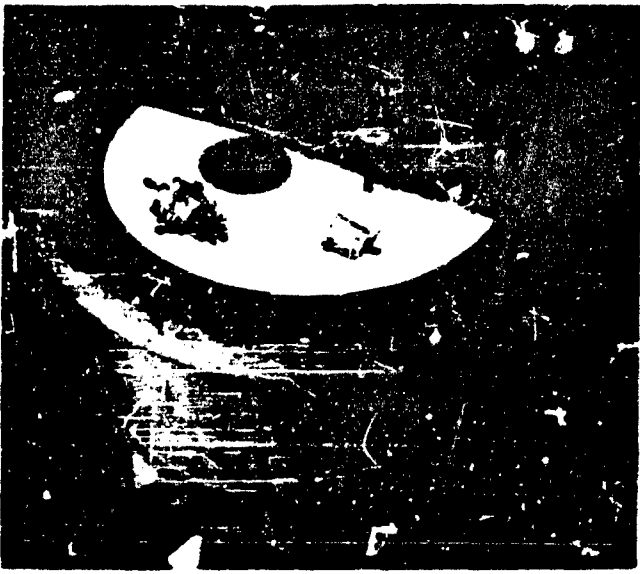


Fig. 8 - UES dynamic pressure tank with the neoprene diaphragm folded back exposing the Carlson-Wiancko, the UES spool gage, the CEC pressure gage, and the junction box on the surface of the sand

pressure tank at a reference gage. The instruments were calibrated with increasing and decreasing pressure to check hysteresis.

Figure 8 shows the Carlson-Wiancko gage, spool stress gage, and the CEC pressure gage lying on the surface of the soil in the tank. Short flexible leads were brought from the instruments to the junction box shown in the figure. This proved to be the most practical means of avoiding the laborious task of removing all the sand from the test vessel to remove or replace an instrument.

STATIC AND DYNAMIC EVALUATION TEST RESULTS

Evaluation tests were conducted in which both static and dynamic stresses in the sand were measured at various depths by the spool gage and compared to the CEC pressure gage at the surface as explained under general test conditions. Figures 9, 10, 11, and 12 summarize the static test results. Figure 13 is a sample dynamic test record which illustrates what is meant by first pressure peak, final surface pressure, etc. Figure 14 is a copy

of an actual record trace. Figures 15 and 16 summarize the dynamic test results.

Many of the curves were plotted from the data collected during just one test. The reliability of these curves must be questioned, especially when one considers the wide scatter shown by the test data. The major causes of these variations were probably amplifier drift and poor soil control.

Under static loading the spool gage behaves a little stiffly. When buried 4 inches in the soil, the gage read about 10 percent higher than the surface pressure up to 1000 psi. The points shown (Fig. 9) were each an average of 4 separate tests. With the gage at the 6-inch depth, it was about 10-percent hard up to 500 psi (Fig. 10), the result of only one test.

The test results with the gage at the 10 inch depth (Fig. 11) show a very wide variation. The data is not reliable above 250 psi because of an amplifier gain drift and because much of the data fell beyond the range of the calibration curves and had to be extrapolated. Below 250 psi the gage read within 10 percent of the static surface pressure.

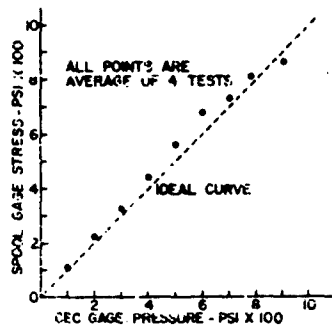


Fig. 9 - UES spool gage stress (at 4-inch depth) vs CEC gage pressure at surface under static loading

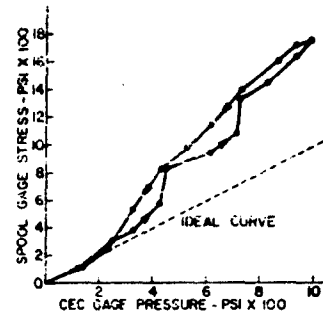


Fig. 11 - UES spool gage stress (at 10-inch depth) vs CEC gage pressure at surface under static loading

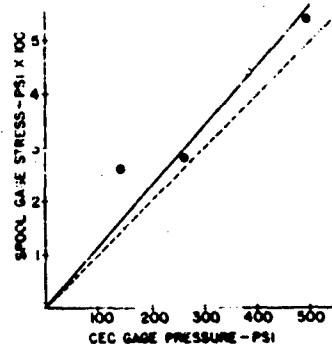


Fig. 10 - Comparison of UES spool gage stress (at 6-inch depth) vs CEC pressure at surface under static loading

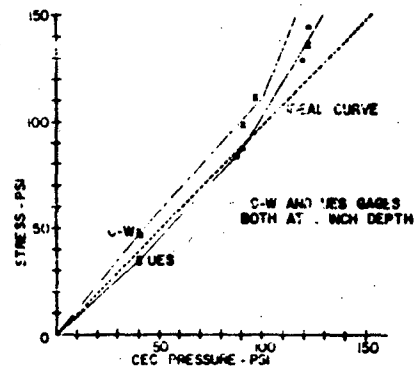


Fig. 12 - Comparison of C-W and UES gages under static loading

Figure 12 is a comparison between a Carlson-Wiancko and the spool gage buried 6 inches below the surface and subjected to pressures up to 150 psi. The curve showed that, for this particular soil type and depth, the spool gage read much closer to the surface pressure than did the Carlson-Wiancko gage and, in fact, was within 10 per cent of the surface pressure out to netter than 100 psi. The Carlson-Wiancko gage behaved like a stiff gage. The spool gage was soft.

In the recordings (Figs. 13 and 14) the paper moved from right to left through the oscillograph. At the bottom edge of the record appears a reference trace to compensate

for any shift which might have occurred as the paper passed through the oscillograph. A vertical timing line was placed on the records every 100 milliseconds. A sharp rise may be seen when the burst diaphragm ruptures subjecting the instruments to the pressure wave. Probably reflections off the sides or bottom of the tank or dynamic solubilities of the gas in the water cause the transients riding on the exponential pressure rise. Whenever the spool gage was buried, the spool gage record lagged behind the pressure record. This information was used to estimate the velocities of the pressure waves in the sand which varied between 400 and 1700 feet per second. Since the velocities are a kind of measure of

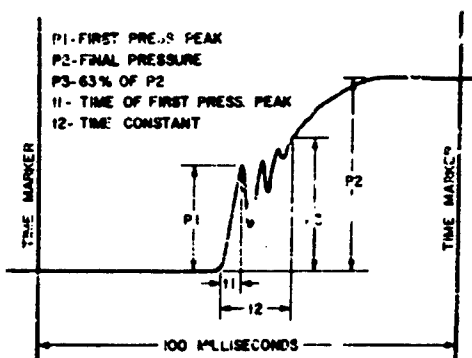


Fig. 13 - Definitions of certain terms on a sample dynamic test record

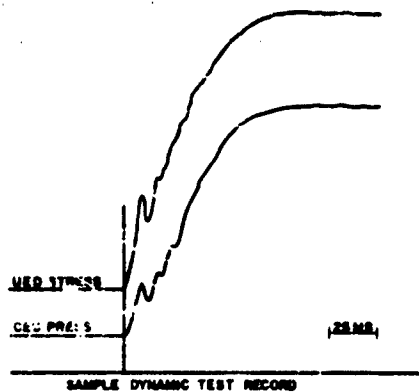


Fig. 14 - Sample dynamic test record

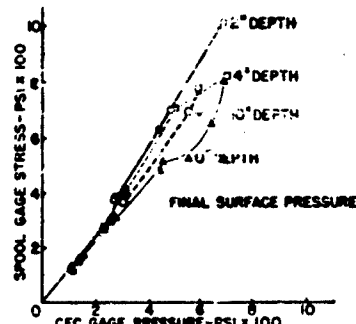


Fig. 15 - Comparison of UES spool gage stress (at various depths) vs CEC gage pressure at surface under dynamic conditions

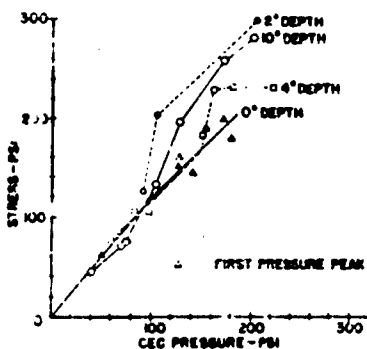


Fig. 16 - Comparison of UES gage stress (at various depths) vs CEC gage pressure under dynamic loading

the soil compaction, it points out the need for better soil control.

Figure 15 is a summary of dynamic tests, at various depths, for which only the final pressures of the spool gage and pressure gage have been plotted. Each point represents a separate test. The spool gage may be seen to consistently indicate higher pressures than that indicated by the CEC pressure gage at the surface in the sand. This occurred even when the spool gage was mounted at the surface with the CEC pressure gage. There was some evidence to show that the CEC pressure gage read as much as 10 percent lower than the air pressure in the tank. However, this correction factor was not applied to these test results.

Below 250 psi, the gage at all depths, read 25 percent high. Beyond this pressure, the depth at which the gage was buried had some effect. The gage at the surface had the lowest error. At the two inch depth, the gage read 50 percent higher with the error decreasing with the depth of burial.

We believe this error was caused either by a density mismatch between the soil and the spool gage or by the lubricant used between the two stems, or a combination of both. The gage is known to have a density of about twice that of the soil. It may thus react to the pressure waves more slowly than the soil, causing arching to occur. The viscous damping between the spool gage stems could have the same effect.

Figure 16 is a summary of dynamic tests, at various depths, for which the first pressure peaks of the spool gage and pressure gage have been plotted. This represents a true dynamic comparison of the gage because the various points were selected from a truly dynamic portion of the test data.

The spool gage reads, on the average, about 12 percent of the dynamic surface pressure, out to 100 psi, at all the various depths.

After 100 psi the spread of data is more pronounced, varying by about 20 to 30 percent of the surface pressure gage.

CONCLUSION

On the basis of the above test data, the UES spool stress gage can measure, with an average error of 10 percent, the static and dynamic free-field stresses over the range of 0-200 psi in this particular soil and at the various depths tested.

The data above 200 psi is too inconclusive to say, with certainty, what the average error should be. When the UES spool gage and a Carlson-Wiancko gage were tested together to 150 psi, the spool gage gave the better readings.

The high dynamic readings above 200 psi are attributed mainly to poor soil control, density mismatch and viscous friction between the stems of the gage.

The spool gage is being modified to include an accelerometer (Fig. 2) and a displacement transducer. Work is being done to vary the density of the gage relative to the soil to investigate this effect.

DISCUSSION

Mr. Flathau (U. S. Army Waterways Exp. Station): I was wondering how you were planning to use this gage in a cohesive soil; what problems that might be involved in placing the soil around the gage?

Mr. Winston: That's one of the problems we want to investigate. Right now we've been

using just the sand in our test tank. But, of course, it's designed to use almost any soil. The problem there would probably be trying to place the gage, trying to compact the soil around it, without affecting the free-field stresses.

TEST PLANNING FOR SHOCK TESTS OF A HARDENED WEAPON SYSTEM

Henry M. Suticbu,
Convair (Astronautics),
San Diego, California

To ensure that hardened silo-type sites can meet the requirements of withstanding an enemy attack, the first site built is to be tested under conditions closely simulating the environment of shock when subjected to an enemy atomic attack.

INTRODUCTION

Convair (Astronautics), a Division of General Dynamics Corporation is the integrating contractor for the activation of a large number of hardened silo-type sites.

To insure that these sites can meet the requirements of withstanding an enemy attack, the first site that is built will be tested under conditions which closely simulate the environment of shock when subjected to an enemy atomic attack.

The completeness and complexity of performing the tests described in this program require detailed test planning. This planning is accomplished as a part of an overall test program which is a part of this company's engineering evaluation of the operational silo design. This part of the test program is only a small part of the overall test planning carried out during the activation of the silo-type sites.

DESCRIPTION OF WEAPON SYSTEM

The General Layout

A typical Atlas silo-type operational site is shown in Figs. 1, 2, 3, 4, 5 and 6.

The site is a self-contained unit manned by approximately five personnel. The missile is stored within a concrete silo and shock-mounted crib in a condition which will permit a very short remote operated countdown to

launch. Figure 1 shows the site in a "hard" condition. Figure 2 shows the site configuration as missile launch occurs.

The crib structure within the silo is suspended on a shock absorbing system which protects the critical ground support equipment and the missile from ground shock resulting from an enemy attack. The site is designed to withstand an enemy attack and react as soon as possible after the debris has settled. Figure 6 provides detail of the crib and suspension system.

A launch operations building, buried near the silo structure, protects the crew. Launch operations are carried out from this location. Figure 5 provides detail of the launch operations building.

The Atlas missile is provided with an inertial guidance system which does not require control from the ground once the missile is launched.

Operational Philosophy

The site is designed to operate with a minimum crew and is serviced at regular intervals to check critical equipment and replace items as necessary. This work is performed by a mobile checkout team which services several sites. The checkout equipment is largely automatic to reduce checkout time to a minimum. The site is self sufficient, providing its own power and is able to operate for weeks without outside support. The missile

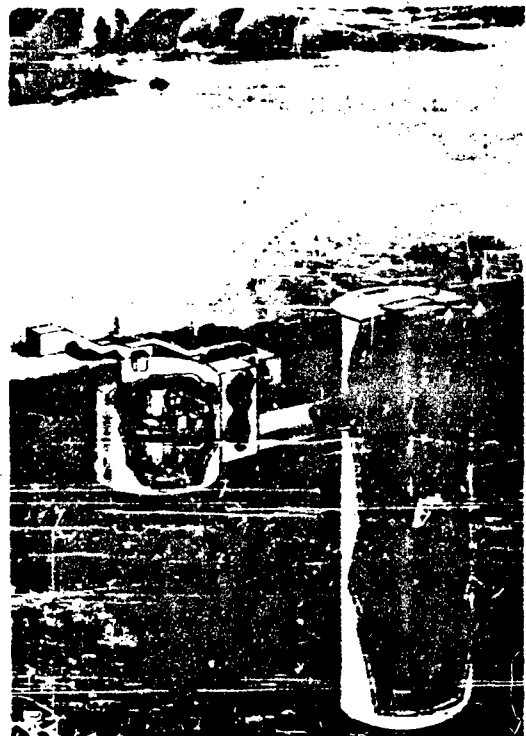


Fig. 1 - Site in hard condition



Fig. 2 - Site as missile is launched

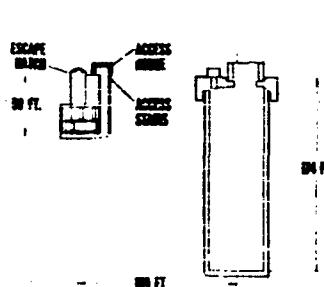


Fig. 3 - Sectional view of weapon system test site

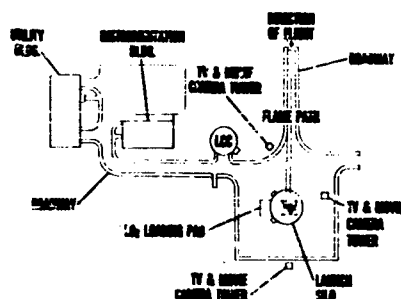


Fig. 4 - Plan view of test site

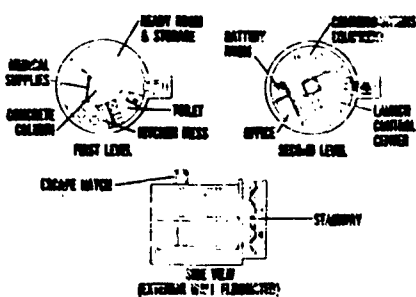


Fig. 7 - Detail view of launch control center

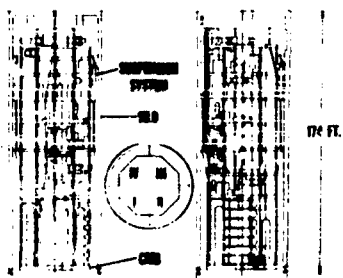


Fig. 8 - Detail view of silo and crib structure showing crib suspension system

is stored in a condition which permits very rapid reaction with a minimum requirement for additional preparation prior to launch. This fast reaction can permit missile launch prior to arrival of enemy weapons.

The site is also designed to withstand an enemy attack and react after the debris has settled. The cement silo structure and cap protects the site from blast overpressures. A suspension system isolates the crib structure within the silo from ground shock effects.

TEST PROGRAM

The test program will be carried out at Vandenberg Air Force Base. A complete Atlas silo-type weapon system is provided and there are additional facilities for evaluating the tests.

Test Objectives

The complete test program includes the following general objectives.

- (1) Evaluation of the ability of the weapon system to launch a missile after long periods of maintenance in a standby condition.
- (2) Evaluation of the ability of the weapon system to launch a missile in minimum time (before arrival of enemy weapons).
- (3) Evaluation of the ability of the weapon system to launch a missile after surviving an enemy atomic attack.

This report describes only the test program for accomplishing objective (1) above.

Test Philosophy and Test Limitations

It is impractical to attempt to create an actual ground shock to the concrete silo and launch control center structures. However, the equipment in each structure is shock mounted. The test program is accomplished by disturbing the shock mounted structures to simulate ground shock transmitted through the suspension system.

This method of test makes certain initial assumptions about the shock isolation system performance, but these assumptions are checked in performing the test.

The silo includes a crib structure which is isolated from the cement silo structure by 4 spring suspension systems (Fig. 8).

The crib, which includes most of the weapon system equipment, carries (1) the missile (2) cryogenic fuel storage (3) power supplies (4) missile elevator (5) missile support equipment and (6) gas and liquid supplies.

The large mass of the crib and its equipment results in a suspended system with a low natural frequency and a large attenuation of high frequency components of ground shock.

To shock test the crib structure the complete crib is hydraulically jacked to a deflected position which could occur at the instant of arrival of a ground shock at the silo structure. The crib is then released by explosive bolts, to be returned to its normal static position by action of the crib suspension system. Figure 7 shows details of shock creating equipment.

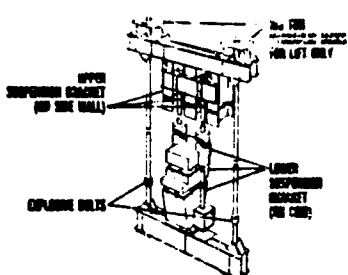


Fig. 7 - Detail of silo-crib shock-suspension system, showing detail of equipment used to simulate ground shock on crib structure, in white

The launch control center (Fig. 5) includes a suspension system which isolates the two floors. Most of the equipment within the center is mounted on the floors. The relatively small mass of the equipment in the launch control center, and the effect of many personnel moving about, and in and out, requires the use of a air cylinder type suspension system, which retains low frequency response, and provides automatic adjustment for changes in load due to personnel movement. This system is inactivated and the floors are deflected before a test (Fig. 8). The reactivation of the air cylinder and simultaneous explosive release of the floor from its deflected position results in a test of the launch control equipment under simulated ground shock. Initial deflection of the floor is adjusted to deflection values which correspond to ground shock effects to be tested.

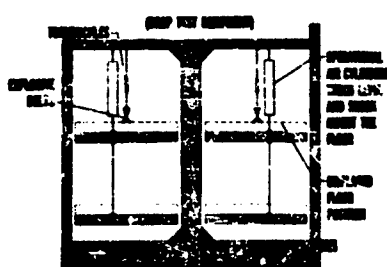


Fig. 8 - Detail of launch control center, showing detail of floor shock isolation system and method of simulating effect of ground shock.

The dynamic tests of the suspension system result in obtaining actual checks of suspension damping rates, natural frequencies, ability to return to the same static position, and relationship of center of gravity to center of suspension. The tests also check out ratline space provisions, structural stability, and plumbing security within the suspended structures. Of major importance is the demonstration that the weapon system can still effectively operate after being subjected to these deflections.

Instrumentation Equipment

The site includes an instrumentation building which is located nearby and is suitably built to protect operating personnel in case of a missile failure. The building is provided with monitoring instruments for recording and displaying the performance of the instrumented equipment in the site. All instrumentation is added to the site so that it is an addition, rather than a change to the site. In this way the basic site remains as close as possible to an operational configuration.

The instrumentation includes missile flight instrumentation, a landline instrumentation system, movie cameras with remote controls, and remote controlled TV cameras with suitable monitors located in the instrumentation building. Special controls for activating the shock producing equipment are also included in the instrumentation building.

Typical Shock Tests

Several shock tests will be performed. A typical test is described below.

The site will be put into a condition of first state readiness (ready to start a countdown at a moments notice) except that missile engine ignition will be prevented by suitable dummy ignitors. The operational crew will be instructed to perform as in an operational site. The floor to the Launch Control Center will be raised to the deflected position.

The instrumentation building for the site will be staffed with Convair-Astronautics and associate contractor test personnel who will initiate, terminate and monitor the test. The test conductor in the instrumentation building will start the test after all instrumentation is operating. The test will be started by sending a suitable signal into the site atomic blast sensors. This signal will initiate automatic

closure of all of the site openings, and will put the guidance system into inertial mode. A few seconds after the simulated atomic blast is sensed, hydraulic power will start moving the silo crib structure to a predetermined position above the normal static position. A few seconds after reaching the deflected position the silo and the launch operations building floor will be released by the detonation of explosive bolts to return to their original positions.

The release of the suspension systems, will permit them to operate as they would if subjected to ground shock created by an atomic blast. The launch crew will react, as in an operational situation, to carry out the launch procedure as required after enemy attack. The crew will carry out the complete countdown which will result in an aborted launch at the final point, due to the dummy missile engine ignitors. The crew will then return the site to the ready condition in preparation for correction of the fault. The test will then be halted. Throughout the test, the operational crew will react as in an operational site and, for added realism, will be isolated from the test crew.

The instrumentation systems will provide information to the test personnel for crew

safety, and will provide data for accomplishing test objectives. Initial tests will be simplified and at reduced shock values. These tests will "debug" system, and procedures, and determine critical areas where full value shock tests will need careful instrumentation. Later tests will be at operational shock values, and will include all details necessary to make the crews feel that they are in a tactical situation.

TEST PLANNING

Planning will be suitably documented many months before the start of these tests. It will include detailed documentation of all instrumentation requirements, details of each individual test and detailed descriptions of test objectives. The test planning documents will include the integrated test requirements and objectives from associate contractors in addition to Convair-Astronautics and Air Force requirements. This test planning aids in making sure that all equipment is available when necessary, and that each test provides maximum information. Coordination with the Air Force will insure that the tests are as realistic as possible. Final tests will include Air Force crew members as the operational crew.

DISCUSSION

Mr. Hansen (Martin Co., Denver): I have a question that I believe should be asked before every major systems test. With a system that's readily susceptible to analysis, why are you performing this test?

Mr. Salisbury: I think the best answer to that is to refer back to our second speaker at this Symposium, Herman Kahn. We have a real weapons system here. You can't very well perform an analysis on how crew members are going to perform, how well our procedures really work out, how a complicated

system such as this will really work. We have to know, for SAC commanders and people that are doing planning, either diplomatically or otherwise, just what they really have left over after we have been hit. By running tests of this sort, considering that we have a real, typical site, our own important people who are making decisions can get some kind of an evaluation of how many of these sites they're going to have left at any given time using a knowledge of what they expect to be hit by at any time.

GROUND SHOCK LOADS IMPOSED ON THE SILO STORED ICBM

Arlyn F. Winemiller
The Martin Company, Denver

The paper illustrates the method used in determining dynamic loads imposed on the silo stored ICBM due to nuclear blast induced ground shock and presents some of the more interesting results. The solution of the ground shock loads problem was sought via the passive analog computer.

INTRODUCTION

General

The ICBM Weapon Systems of the United States are built with two major points in mind. First, they are a deterrent and second, they must be capable of retaliation in the event of enemy attack. In order to be capable of retaliation, it is imperative that the weapon system be able to survive under enemy attack. Today, this means survival under nuclear blast. Nuclear blast implies severe ground shock, high radiation levels, strong surface winds, and high overpressure levels — to name a few. Survival under these conditions means designing and building a weapons system which after this form of hell is still capable of fighting back. Both men and machine must be adequately protected.

The first questions asked are, "How do we design a weapon system capable of high percentage survival? What should our weapon system distribution look like? What 'hardness' should each complex have?" These questions go on and on and require an extreme amount of system analysis before they are answered.

One question which must be answered is, "How, in terms the engineer can use, do you define a nuclear blast so that the system can be intelligently designed?" This question alone has been the subject of a considerable amount of work carried on in recent years.

The above statements are made only to impress upon the reader the fact that the dynamic loads imposed on the silo-stored ICBM are only one small facet of a very complex problem.

It is the intent herein to illustrate the method used by the Systems Dynamics Unit at Martin-Denver to determine the dynamic loads imposed upon a silo-stored ICBM due to nuclear blast induced ground shock, and to present some of the more interesting results.

Method of Solution

The solution of the ground shock loads problem was sought via the passive analog computer. The major reason for using this type of computer lies in the fact that system variations can be made, with a minimum of delay time, simply by changing the value of a particular lumped electrical element in the analog circuit. This makes the passive analog computer extremely well suited for studying dynamic systems wherein it is desired to follow system reaction with a minimum of

effort and determine resulting effects in a matter of seconds. Secondly, the passive analog eliminates the requirement of writing the equations of motion of the dynamic system and computing the multitude of coefficients involved in this set of equations since the analog circuits can be drawn directly from the idealized lumped spring-mass models. This cuts down the time that must be spent in preparing the problem for the computer. The obvious disadvantage, which must be mentioned, is that the final accuracy of the solution is not as high as is obtainable by digital techniques; however, it is well within engineering requirements. The author is aware that several arguments can be presented both for and against the passive analog and it is not the intent in this paper to stimulate such a discussion.

DYNAMIC MODELS

General

In simulating the dynamics of the overall system, longitudinal and lateral motions were assumed uncoupled and distinct models were derived for each. Beam-column effects due to gravity induced moments were simulated on the analog computer.

The effect of vertical acceleration due to ground shock on lateral bending was accounted for independently and the resulting bending moments added to those obtained from the passive analog. To accomplish this the maximum longitudinal acceleration due to vertical ground shock was determined from the uncoupled longitudinal study and the maximum relative base-tip deflection determined from the uncoupled lateral study. This combination of lateral position and vertical acceleration was utilized to obtain the additional bending moments due to vertical acceleration.

This method of accounting for the additional bending moments due to vertical acceleration is appropriate; however, the following points must be kept in mind. The maximum vertical acceleration from the longitudinal model was used. The maximum relative base-tip deflection was used and the missile assumed rotated into a straight line. The major omissions in this procedure are (a) secondary lateral deflections occurring due to the vertical acceleration and (b) the nonlinearities involving frequency reduction.

Longitudinal Model

The basic geometry of a large liquid propellant missile makes the system quite convenient for lumping into a longitudinal dynamic model. Figure 1(a) shows a typical upper stage of this type of missile, consisting of the re-entry vehicle, forward skirt, propellant tank, between tanks section,

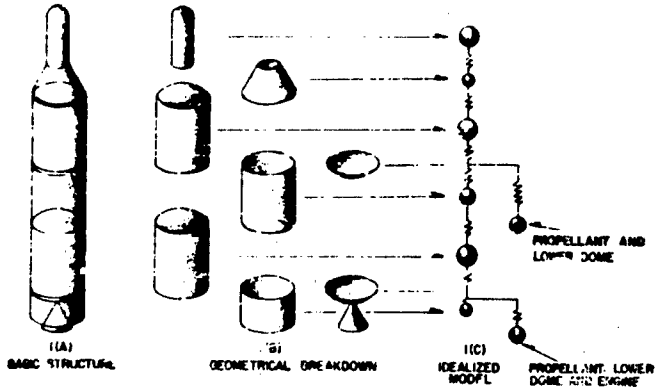


Fig. 1 - Derivation of longitudinal dynamic loads model

a second propellant tank with the engine affixed to the lower dome and a tail skirt. Figure 1(b) shows the same portion of the missile broken at natural geometrical splices. Figure 1(c) shows the lumped spring mass model which results from breaking the missile at these locations, determining the center-of-gravity of each segment, and deriving lumped longitudinal springs from accompanying AE data.

In the longitudinal model, the propellant masses were added to the mass of the lower domes and dome supported equipment, and the resulting masses suspended from the main structure as branches. The suspension springs were based entirely on the flexibility of the lower domes. The effect of added flexibility due to dilation or radial flexibility, of the barrel section of the tanks was omitted. In tanks with barrel section lengths which are small compared to the tank diameter this dilation effect is quite small. In tanks where the barrel length is of the same order of magnitude or larger than the tank diameter the effect becomes appreciable and the coupling of the propellant mass into the remainder of the system is not correctly defined without accounting for it. Studies concerning the overall effect of tank dilation on the dynamic loads for the large liquid propellant missile may or may not show that omitting the radial flexibility is important, depending on barrel length - radius relations and basic structural design.

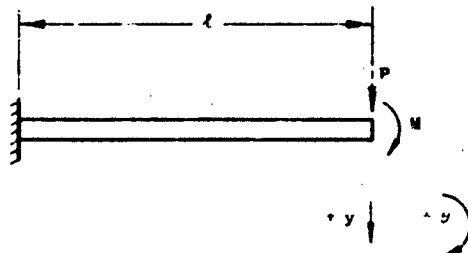
The scheme described above was followed for the development of the complete longitudinal dynamic model. In areas where long tank barrels existed, they were split and replaced by more than one mass in an attempt to keep the model as uniform as possible.

Lateral Model

Derivation of the lateral lumped spring-mass model was not as easy and straight forward as was the longitudinal model. Basically the lateral dynamics problem is that of solving a nonuniform beam problem. Lateral dynamics for the large liquid propellant missile is complicated by the motion of the liquid propellants, commonly referred to as propellant slosh. The influence of propellant slosh on the behavior of the system was taken into account by the addition of elastically attached slosh masses to the main body of the lateral model. This was accomplished by computing the magnitude, center-of-gravity location, and uncoupled natural frequencies of the sloshing propellant for each tank. Once these were known, the appropriate amount of propellant was removed for each total propellant mass distribution. A linear spring was determined for each slosh mass based on the magnitude of the mass and its uncoupled natural frequency. These springs were then used to couple the slosh masses to the lateral model.

The remaining propellant weight was apportioned along with the structural weight to form the lumped masses for the lateral model. Additional branches were added to the lateral model to account for the engines being cantilevered from the main structure.

Once the propellant, structure, and remaining equipment had been lumped the appropriate bending and shear springs connecting the mass lumps were determined. The procedure followed to develop these lumped springs is best illustrated by an example. Consider a cantilever beam of length l as shown below. To simplify the problem but yet illustrate the procedure let the beam be of uniform bending stiffness EI and uniform shear stiffness AG .



For this uniform beam the lateral deflection of the beam at the tip is given by

$$y = \frac{P\ell^3}{3EI} + \frac{P\ell}{EAG} + \frac{M\ell^2}{2EI} \quad (1)$$

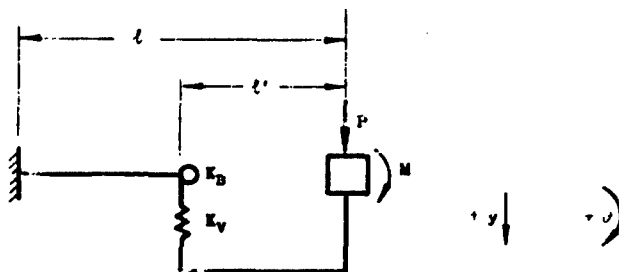
and the slope at the tip is given by

$$\theta = \frac{P\ell^2}{2EI} + \frac{M\ell}{EI} \quad (2)$$

Writing the matrix equation relating y and θ to P and M yields

$$\begin{bmatrix} y \\ \theta \end{bmatrix} = \begin{bmatrix} \left(\frac{\ell^3}{3EI} + \frac{P}{EAG} \right) & \frac{\ell^2}{2EI} \\ \frac{\ell^2}{2EI} & \frac{M}{EI} \end{bmatrix} \begin{bmatrix} P \\ M \end{bmatrix} \quad (3)$$

Next consider a lumped spring system as shown below.



For this lumped spring system the lateral deflection and slope at the tip are given by

$$y = \frac{P}{K_v} + \frac{P\ell'^2}{K_B} + \frac{M\ell'}{K_B} \quad (4)$$

$$\theta = \frac{P\ell'}{K_B} + \frac{M}{K_B} \quad (5)$$

or in the matrix form as

$$\begin{bmatrix} y \\ \theta \end{bmatrix} = \begin{bmatrix} \left(\frac{1}{K_v} + \frac{\ell'^2}{K_B} \right) & \frac{\ell'}{K_B} \\ \frac{\ell'}{K_B} & \frac{1}{K_B} \end{bmatrix} \begin{bmatrix} P \\ M \end{bmatrix} \quad (6)$$

Equating the elements of the square matrices of Eqs. (3) and (6) yields the following expressions for ℓ' , K_B , and K_v .

$$\ell' = \frac{l}{2} \quad (7)$$

$$\frac{1}{K_B} = \frac{l}{EI} \quad (8)$$

$$\frac{1}{K_V} = \frac{l^3}{12EI} \left[1 + \frac{1.27I}{l^{1/2} \cdot AG} \right] \quad (9)$$

Omission of the shear flexibility merely deletes the last term in the brackets of Eq. (9).

The above lumped spring system may be simulated directly or the passive analog by lumped electrical elements.

For nonuniform bending and shear stiffness as exist with missile structure, the expressions for ϵ' , K_B , and K_V are given by

$$\epsilon' = K_B \int_{0}^l \frac{dx}{EI(x)} \quad (10)$$

$$\frac{1}{K_B} = \int_{0}^l \frac{dx}{EI(x)} \quad (11)$$

$$\frac{1}{K_V} = \int_{0}^l \frac{x^2 dx}{EI(x)} + \frac{1}{K'} \int_{0}^l \frac{dx}{AG(x)} - \epsilon' \int_{0}^l \frac{xdx}{EI(x)} \quad (12)$$

where the integration is carried out over the interval for which the lumped stiffness is desired. A general idea of the derivation of the lateral model is given by Fig. 2.

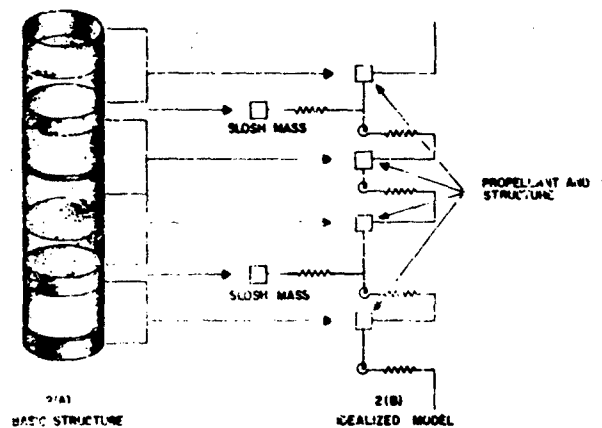


Fig. 2 - Derivation of lumped lateral model

FORCING FUNCTIONS

The ground shock design criteria is usually given in the form of a shock spectrum, i.e., as the peak displacement and velocity response of a linear oscillator to the projected ground shock as a function of oscillator frequency. A method utilizing the shock spectrum directly has been proposed by Fung and Burton* wherein a modal approach is used. In this method the peak response of each mode of a multi-degree-of-freedom system is added algebraically to obtain an upper bound for the dynamic response.

*"Some Shock Spectra Characteristics and Uses" by M. V. Burton and Y. C. Fung, ASME Paper No. 58-APM-5.

A somewhat more versatile method of specifying the ground shock forcing function was used in the series of studies herein described. Since the analyses were to be accomplished on the passive analog computer it was required that a forcing function be derived which was somehow definable as a function of time. The forcing function used was specified as an exponentially decaying velocity pulse, i.e., the ground was assumed to have a velocity of the form

$$V_{\text{Ground}} = Ae^{-\alpha t}$$

and thus a displacement time history given by

$$D = \frac{A}{\alpha} (1 - e^{-\alpha t}).$$

This motion of the ground is not what physically happens during ground shock; however, the shock spectrum derived from such an input can be made essentially identical to the specified shock spectrum design criteria by judicious selection of the constants A and α . It must be emphasized that these functions do not describe the actual ground motion and were used only as an artifice to adequately define ground shock.

SOME INTERESTING RESULTS

The series of studies conducted yielded several interesting results. The study was started utilizing a suspension stiffness equal to that set for the launch condition. This resulted in longitudinal load factors in the order of 10 to 15 as well as bending moments far in excess of structural allowables. This, of course, set the ground shock loads study into a full scale parameter study. By the time the parameter study was completed and the suspension system requirements were established, the design criteria was revised and became more demanding of the suspension system than originally anticipated. This resulted in considerable extrapolation of the data obtained to define new suspension system characteristics and eventually resulted in a second shock loads study to verify the various extrapolations.

The results presented herein are a part of the findings from two studies. No intent is made to define all the numbers, only generalities of some of the data obtained.

The answer to the basic question of how to reduce ground shock dynamic loads may be answered by two statements: (1) reduce the vertical suspension stiffness, (2) reduce the lateral suspension stiffness. A third answer is, of course, stay away from nuclear blasts. It was determined that essentially no reduction in loads was obtained by locating a lateral restraint between the upper stage and the silo wall. In fact, certain locations of such a spring actually magnified the resulting loads. Variation of the effective pitch and yaw rotational restraint at the missile base was found to have very little effect on the resulting loads. Consideration of the static stability of the missile on the suspension system fixed a lower limit for this spring constant. Probably the most important part played by the rotational restraint was that the actual silo diameter was in part dictated such that a satisfactory margin of static stability would be maintained. This restraint was obtained by a combination of the vertical suspension stiffness and the spacing of the vertical springs in a bifilar pendulum configuration.

Figures 3 and 4 show the variation of longitudinal load factors as functions of the vertical suspension stiffness. The data shown are the result of a typical ground shock input. The curves only indicate the general trend which might be anticipated. A rule of thumb resulting from the studies might be stated as follows: To keep longitudinal load factors in the order of one, the vertical suspension stiffness must be such that the static deflection of the missile is approximately equal to the peak anticipated ground displacement.

Figure 5 illustrates the variation of bending moment as a function of lateral suspension stiffness with the rotational (pitch and yaw) suspension stiffness held constant. The data shown are the result of a typical ground shock input. The major information depicted by Fig. 5 is an indication of the rates at which the bending moments may be reduced by variation in the lateral restraint.

Figures 6 and 7 indicate the effect on lateral loads of placing a second restraint towards the tip of the airframe. Successful load reduction is seemingly not attainable by this procedure.

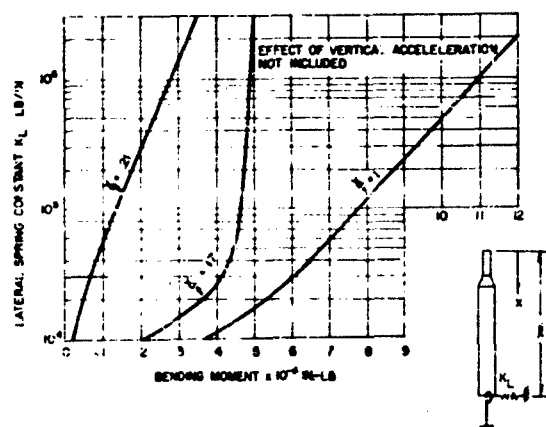
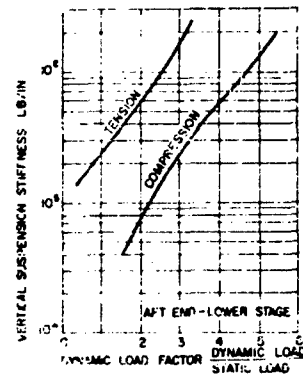
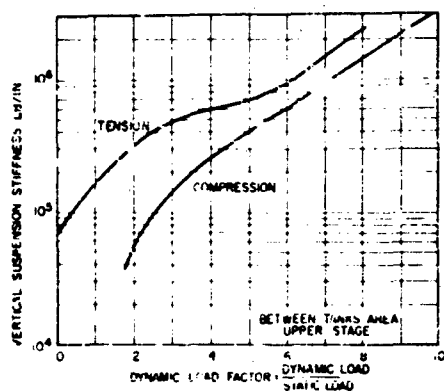


Fig. 5 - Bending moment as a function of lateral base restraint - torsional base restraint held constant - nondesign criteria input

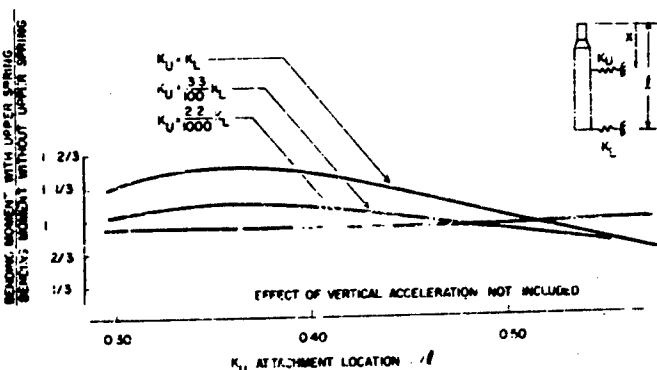


Fig. 6 - Bending moment at $x/l = 0.21$ nondesign criteria input

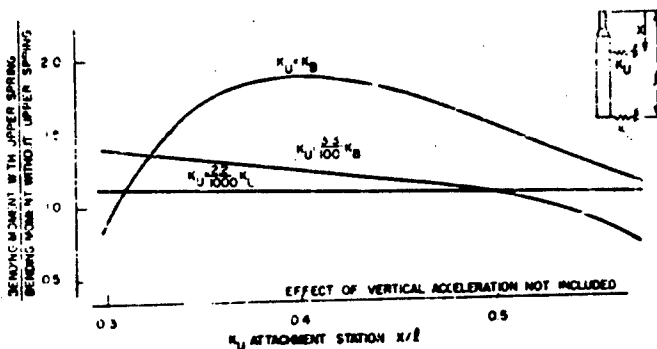


Fig. 7 - Bending moment at $x/l = 0.33$ nondesign criteria input

Note that in general the ratio of the load with the upper spring to the load without the upper spring is greater than one. When the load at a particular station was significantly reduced by this means, the load at several other stations was significantly increased.

Figure 8 shows one of the most interesting results obtained from the studies, at least from an academic point of view. This is the variation of bending moment distribution as a function of lateral viscous damping. In this instance, the response of the undamped system was essentially rigid body response. The inclusion of viscous damping resulted at first in reducing base moments and increasing the moments toward the tip of the missile. As more damping was placed in the system, the higher modes were excited; thus adding to the resulting bending moments. As the damping surpassed the 30 percent critical point, the undamped bending moment distribution was completely exceeded.

Figure 9 shows a comparison between the bending moment distribution resulting from an undamped suspension system and viscous and coulomb damped suspension systems. The viscous and coulomb damping shown resulted in approximately the same base motion decay times. Here it is shown theoretically that a definite advantage is offered by the frictional damping device when seeking a certain decay time without significantly intensifying the dynamic loads problem.

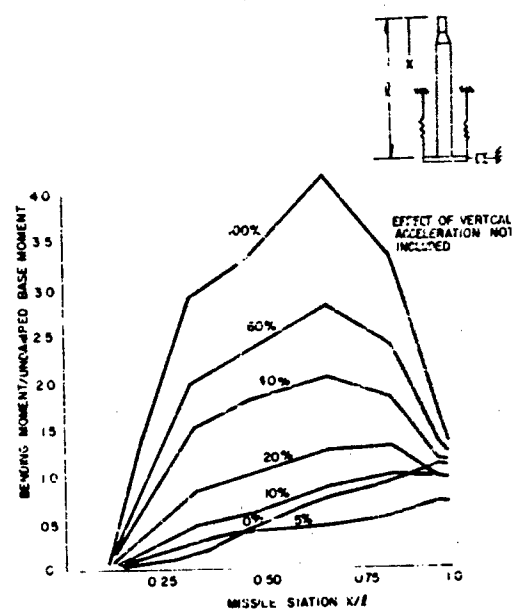


Fig. 8 - Bending moment as a function of lateral viscous damping in percent critical of the rigid body pendulum mode

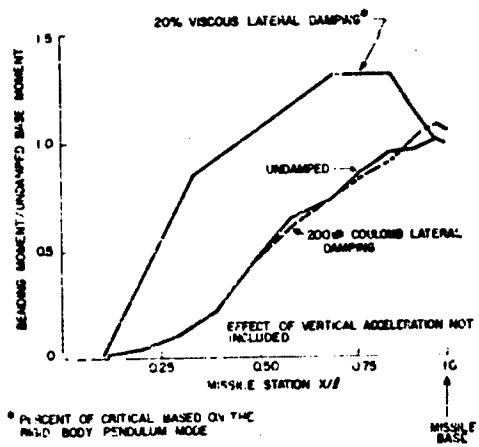


Fig. 9 - A comparison of the bending moment of the distribution resulting from an undamped suspension system and viscous and Coulomb damped suspension system

ACKNOWLEDGMENT

The author wishes to express his appreciation to Mr. Bernard Arrow, Unit Head of the Systems Dynamics Unit, for his continuous encouragement in the writing of this paper; to Mr. Jack Boxer for the helpful suggestions and proof reading; and Mr. Kenneth Burgess for drawing several of the figures.

DISCUSSION

Mr. Weissman (Ammann & Whitney): This is not a question but a comment. I'm equally gratified and reassured that you're also using a velocity pulse of the type that we're using. I'd like to state that the pulse is based on work also done by Fung and Barton, in addition to Chobotov at the Space Technology Laboratories. Perhaps I should have mentioned that in the paper. It is properly referenced in the written paper.

Mr. Wiesmiller: One comment I would like to make here. Please realize that in using this velocity pulse we're not saying that this is what happens. All we're saying is this is a way of describing the amount of energy which is available to excite the system. Please do not go away thinking that we are saying to ourselves that this is what the ground does. We realize that it is not what the ground does.

* * *